Alma Mater Studiorum – Università di Bologna

DOTTORATO DI RICERCA IN

MECCANICA E SCIENZE AVANZATE
DELL'INGEGNERIA

Ciclo XXXI

Settore Concorsuale: 09/G2

Settore Scientifico Disciplinare: ING-IND/34

ELECTROSPUN BIOMATERIALS AND STRUCTURES FOR THE REGENERATION OF TENDONS AND LIGAMENTS: DEVELOPMENT AND BIOMECHANICAL VALIDATION

Presentata da: Alberto Sensini

Coordinatore Dottorato

Prof. Marco Carricato

Supervisore

Prof. Luca Cristofolini

Co-Supervisore

Prof. Andrea Zucchelli

Prof. Maria Letizia Focarete

Esame finale anno 2019

Content

Sommario

La presente Tesi descrive i risultati ottenuti durante lo svolgimento del Dottorato di Ricerca in Meccanica e Scienze Avanzate dell'Ingegneria dal candidato Alberto Sensini. Il principale scopo della presente ricerca, era quello di progettare e sviluppare, attraverso la tecnologia dell'elettrofilatura, dispositivi bioriassorbibili o inerti per la rigenerazione o la simulazione tessutale, in grado di riprodurre la struttura gerarchica e le proprietà biomeccaniche, di tendini e legamenti. A tale proposito, la Tesi presenta la descrizione del processo sperimentale, produttivo e di industrializzazione che ha portato allo sviluppo di questi dispositivi. Il lavoro è stato prevalentemente svolto presso i Laboratori di Biomeccanica e di Elettrofilatura del Dipartimento di Ingegneria Industriale, ed il Laboratorio di Scienza dei Polimeri e Biomateriali del Dipartimento di Chimica "Giacomo Ciamician" dell'Università di Bologna. Parte del lavoro inoltre, è stato svolto presso lo Zeiss Global Centre dell'Università di Portsmouth (Regno Unito) e presso l'INSIGNEO – Institute for the In-Silico Medicine dell'Università di Sheffield (Regno Unito).

Gli infortuni a tendini e legamenti rappresentano oggigiorno un problema clinico irrisolto. Sono circa 30 milioni gli infortuni che si verificano annualmente al mondo a questi tessuti, con ricadute economiche di circa 140 miliardi di Euro l'anno, solo tra Europa e Stati Uniti. La principale criticità della rigenerazione o sostituzione del tessuto tendineo e legamentoso, risiede soprattutto nella difficoltà di riuscire a ripristinare la complessa struttura gerarchica delle fibrille di collagene che li compongono, mantenendo le proprietà meccaniche che li caratterizzano. Alle tecniche chirurgiche standard, nel corso degli anni sono stati affiancati approcci sia di sostituzione, attraverso dispositivi impiantabili inerti, sia di rigenerazione attraverso, ad esempio, strutture come allograft o autograft. Tuttavia queste soluzioni hanno riscontrato forti limitazioni e scarsa flessibilità nell'utilizzo. Inoltre ad oggi, risultano totalmente assenti dal mercato dispositivi bioriassorbibili, in grado di poter essere affidabilmente impiantati nell'uomo per rigenerare questi tessuti. A tal proposito, l'ingegneria tessutale ha cercato di rispondere a queste criticità producendo dei costrutti, chiamati scaffolds, i quali in maniera del tutto simile a delle impalcature, sono in grado di guidare la crescita delle cellule le quali,

trovando un ambiente del tutto simile al tessuto nativo, sono stimolate a proliferare e a rigenerare progressivamente il tessuto danneggiato. Inoltre questi scaffolds, essendo costituiti di materiali bioriassorbibili, vengono progressivamente degradati dalla componete cellulare del corpo, venendo completamente sostituiti da nuovo tessuto sano. Tra le varie tecnologie proposte per la produzione di scaffolds per tessuti molli, l'elettrofilatura risulta sicuramente essere la più promettente. Grazie alla sua capacità di produrre fibre del medesimo diametro delle fibrille di collagene nel tessuto corporeo, ha dimostrato di poter guidare la proliferazione cellulare e la rigenerazione di vari tessuti. Nella seguente Tesi grazie a questa tecnologia, sono state sviluppate strutture nanofibrose, chiamate bundles, di materiali riassorbibili sintetici e naturali, ed inerti, capaci di simulare fedelmente la morfologia e le proprietà meccaniche dei fascicoli di collagene di tendini e legamenti. Successivamente è stato messo a punto un processo ed una tecnologia industriale, in grado di poter unire un numero a piacere di questi bundles, attraverso una membrana di nanofibre, che simula le guaine che rivestono tendini e legamenti. Questi costrutti hanno dimostrato di essere morfologicamente e meccanicamente in grado di simulare la struttura gerarchica e le proprietà biomeccaniche di tendini e legamenti completi. Sono stati poi confermati *in vitro*, l'allineamento e la proliferazione delle cellule lungo la direzione delle nanofibre sia dei singoli bundles che sugli scaffolds multiscala. Inoltre è stata svolta anche una completa caratterizzazione morfologica degli scaffolds e dei dispositivi nanofibrosi, attraverso tomografie a raggi-X ad altissima risoluzione ottenenendo, per la prima volta in letteratura, risultati su materiali elettrofilati con questi livelli di risoluzione. Infine, tutte le tecnologie ed i processi produttivi descritti in questo lavoro di Tesi, sono stati oggetto di brevetto italiano e PCT da parte dell'Università di Bologna.

In conclusione, questa tesi propone promettenti dispositivi, e processi produttivi totalmente innovativi, in grado di configurarsi come un punto di svolta nel campo di ricerca dell'elettrofilatura per la produzione di scaffolds e dispositivi per la rigenerazione, sostituzione e simulazione non soltanto di tendini e legamenti, ma potenzialmente anche di altri tessuti quali quello nervoso e muscolare.

Abstract

The present Thesis describes the results reached by the candidate Alberto Sensini during is Ph.D. program in Mechanics and Advanced Sciences of Engineering. The main aim of this research was to design and develop, thanks to the electrospinning technology, both resorbable and inert devices, suitable for tissue regeneration and replacement respectively, able to reproduce the hierarchical structure and the biomechanical properties of tendons and ligaments. In particular the Thesis shows the description of the experimental, productive and industrialization process that permitted the development of these devices. The experimental work was performed in the Biomechanics and in the Electrospinning Laboratories of the Department of Industrial Engineering, and in the Polymer Science and Biomaterials Laboratory of the Department of Chemistry "Giacomo Ciamician" of the University of Bologna. Additional experimental sessions were also performed at the Zeiss Global Centre of the University of Portsmouth (United Kingdom) and at the INSIGNEO – Institute for the In-Silico Medicine of the University of Sheffield (United Kingdom).

Tendons and ligaments injuries are nowadays an unsolved clinical problem. Approximately 30 million of tendons and ligaments injuries are estimated every year worldwide, with economic outcomes of approximately 140 billion of Euro every year, only in Europe and United States. The main criticality of the regeneration or replacement of the tendon and ligament tissue, resides in the difficulty of being able to restore the complex hierarchical structure of collagen fibrils that compose them while maintaining their mechanical properties. Standard surgical techniques have been supported over the years with both replacement approaches, through inert implantable devices, and with regenerative ones, through structures such as allograft or autograft. However, these solutions have found strong limitations and lack of flexibility in their use. Moreover to date, resorbable devices able to be reliably implanted in humans to regenerate these tissues, are absent from the market.

Due to all these reasons, tissue engineering has attempted to answer to these problems producing constructs called scaffolds. Like proper scaffolds, they are able to guide the cells growth. The cells, finding such a biomimetic environment, are

stimulated to proliferate and progressively regenerate the damaged tissue. Furthermore, as they are made of bioresorbable materials, these scaffolds are progressively bioresorbed by the cells themselves, and they are replaced by healthy tissue.

Among the different technologies developed for the production of scaffolds for soft tissues, the electrospinning technique is the most promising. Thanks to its ability to produce fibers with the same diameter of the collagen fibrils in the human body, it has been proved to guide cells proliferation and regeneration of different tissues.

In the present Thesis at first, thanks to this technology, nanofibrous structures, called bundles, of both resorbable and inert materials, were developed. Such bundles demonstrated to faithfully simulate the morphology and mechanical properties of tendons and ligaments collagen fascicles.

Secondly, a dedicated process and an industrial technology, able to group a number of these bundles, through a nanofibrous membrane, was developed. These sheaths have demonstrated to mimic the membranes which cover tendons and ligaments. These constructs have shown to be morphologically and mechanically able to simulate the hierarchical structure and the biomechanical properties of whole tendons and ligaments. The alignment and proliferation of cells along the nanofibers direction, of both individual bundles and multiscale scaffolds, was confirmed *in vitro*. Furthermore, a complete morphological characterization of the nanofibrous scaffolds was also carried out by using a high-resolution x-ray tomography, obtaining for the first time in literature, results with these resolution levels.

Finally, all the technologies and the production processes described in this Thesis, were covered by an Italian and a PCT patent by the University of Bologna.

In conclusion, this Thesis proposes promising devices and totally innovative production techniques, able to be a turning point in the production of electrospun scaffolds and devices for the regeneration, the replacement and the simulation, not only of tendons and ligaments tissues, but also potentially for the nervous and muscular ones.

Chapter 1: Introduction

1.1 Tendons and ligaments: a general overview

1.1.1 Functions and composition

Locomotion is permitted by muscles that, during their contractions and relaxations, produce loads able to move the different bones of the body. The transmission of these forces from the muscles to the bones, is guaranteed by tendons [1]. Ligaments instead, are structures that unit two bones each other, stabilizing and guiding joints through their physiological range of motion [2]. Tendons attachments with muscles are called myotendinous junctions and the one with bones, the osteotendinous junctions (also called enthesis) [1]. The ligament connections with bones instead, are called insertions (or entheses) [2]. Depending on the muscles and bones they are linked to, the shape, the size and the orientation of the whole tendons and ligaments, and of their junctions and insertions, change a lot in the different anatomical sites (Figure 1.1(A)-(B)).

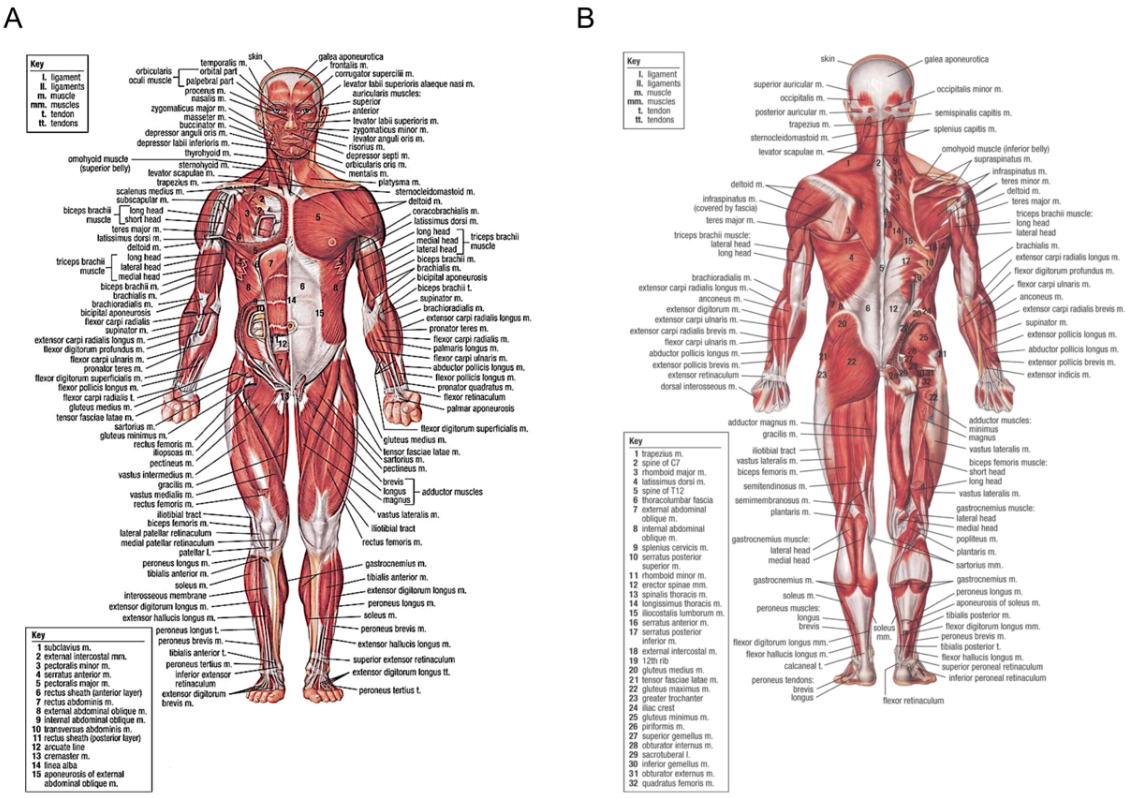

Figure 1.1 Tendons, ligaments and muscles of the human body. (A) Frontal view (www.anatomyscience.com). (B) Posterior view (www.humanbodyanatomy.com).

Macroscopically speaking, healthy tendons and ligaments appear as brilliant white structures, characterized by a fibrillar texture. This external morphology is consistent with their internal one, that is constituted by a complex hierarchical structure of collagen fibers, axially aligned with the tendon or ligament, and connected each other in different levels of aggregation [3,4]. The hierarchical rope-like structure of tendons and ligaments, confer them strength and non-linear mechanical properties [5]. Approximately 80% of their total composition, is made up by extracellular matrix and of this, the 70% is constituted by water. The remaining 30% of the extracellular matrix is composed by solids. Of these solids, the 75% is composed by collagen (most of all Type I and less amounts also of Types III, VI, V, XI and XIV), that confer mechanical resistance. The elastin instead (1-2%), is a protein that helps the elastic return of tendons and ligaments after a stretch. Finally, the ground substance (23-24%) is non-fibrous and constituted by hyaluronan, glycoproteins and proteoglycans (Figure 1.2). Its principal mechanical and physiological function is to produce a shock damping effect, reduce the friction between the fibers, and bind water to hydrate the tendon or ligament, conferring them also viscoelastic properties [6–8].

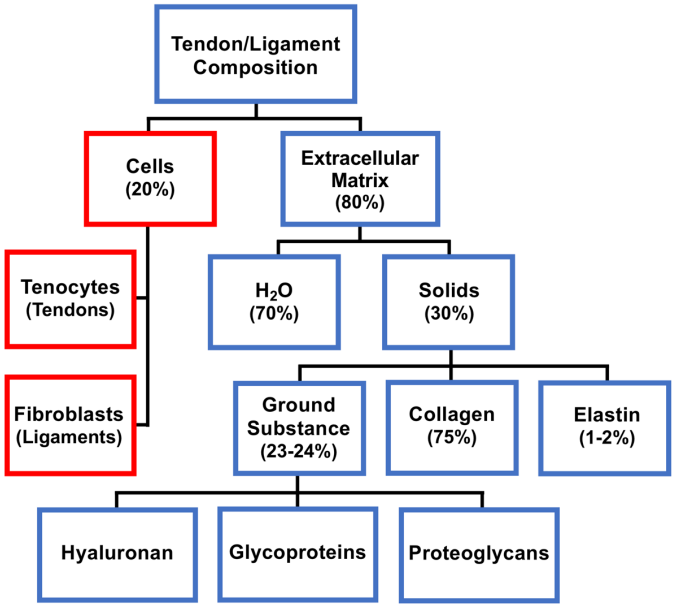

Figure 1.2 Composition of tendons and ligaments.

The cells component of tendons and ligaments is just about the 20% of their total composition [6]. The principal cells of tendons are the tenocytes, while the ones of ligaments are the fibroblasts [9].

Due to the hypovascularization of tendons and ligaments, the cellular activity is lower compared to the other tissues of the body [10]. These cells are differentiated from mesenchymal progenitor cells by specific chemical signals such as TGFb or FGF, from neighboring tissues and marked by the expression of Scx. This transcription factor is essential for tendons and ligaments maturation. The expression of Egr1 and Mkx follow soon after and support the differentiation of tenocytes into embryonic tendon tissue, and it is essential for tissue maintenance during adult life [9].

1.1.2 Cells mechanobiology

Tenocytes and fibroblasts have several ways to communicate each other and modify their activity, for example chemical signals and mechanical stimuli (Figure 1.3(A)) [11]. A relevant role in their activity is played by mechanical stimulations such as the physiological tendons and ligaments strains, the hydrostatic stresses of the water and fluids, and the shear stresses between the collagen fibrils and fascicles (Figure 1.3(B)) [12]. The mechanical stimulations are also involved in increasing collagen production and extracellular matrix modifications [13,14].

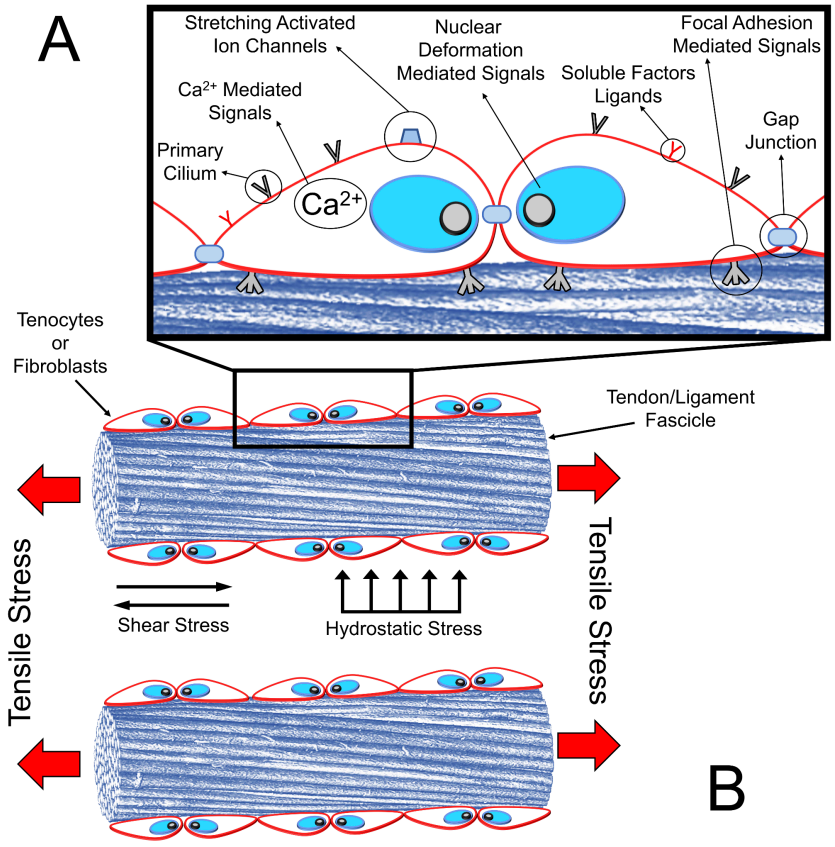

Figure 1.3 Signals and stimuli involved in tenocytes and fibroblasts activity. (A) Overview of the principal chemical and mechanical signals and transducers. (B) Main mechanical stimulations sensed by tenocytes and fibroblasts on tendon and ligament fascicles and fibrils.

One of the main second messengers utilized by cells to transduce mechanical signals is the ion calcium (Ca^{2+}), that can co-modulate multiple cell functions including gene transcription, cell growth and proliferation, contraction and apoptosis [15–17]. When a mechanical stretch occurs, tenocytes and fibroblasts communicate one another, passing fluxes of Ca^{2+} through channels called gap junctions (producing electrochemical currents), which allow cells to integrate and synchronize their activities [13]. In tenocytes, gap junctions can regulate load-induced DNA and collagen synthesis [18]. Another kind of channels activated by mechanical stresses, are the stress activated ion channels (i.e. mechanosensitive channels). These channels are triggered by membrane tensions, and may be activated not only by tissue elongation, but also during tissue shearing, compression, and/or intra/extracellular osmotic pressure gradients [13,19]. Healthy quiescent tenocytes and fibroblasts are attached to collagen fascicles. The stretch

of the fascicles plays a role in biological response of the tissue to mechanical loading. Loss of collagen fiber tension has been shown to trigger downstream consequences including tenocyte apoptosis and the collagen matrix protease secretion [20,21]. Focal adhesion mediated signals, connecting the cytoskeleton to the collagen fibrils, seem to play a key role in tendon mechanotransduction [11]. Despite a specific role of these sensors has not been clearly established, they seem to be involved in age-related tendon and ligament disorders [12]. An additional mechanical transducer is the primary cilium. Mechanosensory function of the primary cilia is related to stretch activated ion channels. Few informations are known concerning their function but they have been shown to deflect in response to applied mechanical tissue loads [22], and their length is apparently affected by mechanical signaling from the extracellular matrix [23,24].

1.1.3 Ageing

It has been demonstrated that mechanical deformations of cell nucleus induce a relative shift in nuclear envelope composition [25]. For this reason, age-related changes in the extracellular matrix, for example the loss of viscoelastic fibrils and fascicles movements and shear, or diminished tissue hydration and matrix compression, seem to modify the processes in which the nucleus deforms under mechanical stress [26,27]. Woo et al. evaluated the mechanical properties of the femur-anterior cruciate ligament (ACL)-tibia complex in younger (22-35 years), middle aged (40-50 years), and older (60- 97 years) knees and found that linear stiffness, ultimate load, and energy absorbed decreased significantly with specimen age [28,29]. Furthermore, some studies have showed that, with aging, tissue extracellular matrix volume increases and the relative number of cells per unit of tendon decreases. Cell proliferation, migration and response to mechanical stimuli is higher in skeletally immature animals [30]. An improved biomechanical response to healing was found in skeletally immature animals, due to a decrease in growth factor receptor number with age [31,32]. The tenocytes become longer and thinner and decrease protein synthesis [29]. The comparison between aged cells donors compared with younger ones, showed a decreased growth, stem cell potential and osteogenic differentiation [33]. Mature ligament fibroblast decreases in metabolic

activity, collagen production and response to platelet-rich plasma occur along with an increase in apoptosis [34]. Ligaments (and in particular the ACL) are subject to collagen fibril disorientation on increasing age [29,35].

1.1.4 Tissue healing and remodeling

All the mechanical, chemical and age-related signals and stimuli described above, are also particularly related to the regeneration and remodeling of the tendon and ligament tissue. Tenocytes and fibroblasts are practically always involved in the regenerative process, according to the microdamages which continuously occurs during the daily life activities or after an injury. Despite the severity of the lesion, the healing homeostatic process follows a similar workflow (Figure 1.4) [12,36,37]. When a lesion occurs, it produces a loss of the tissue continuity with a consequent production of several mechanical, chemical and inflammatory signals. These signals are transduced by cells waking up from their quiescent state [9,12]. The cells that participate in the early repair are thought to originate primarily from the extrinsic compartments of tendons and ligaments, because of the cells in the core of tendons and ligaments are understood to be limited in their reparative capacity, because of their lower number and metabolic rate [38]. Repair of larger tissue defects instead involves cells from the sheaths (i.e. epitenon/epiligament or endotenon/endoligament) that migrate into the wound [39]. Subsequently the process follows the general three steps of tissue healing: inflammation and hemorrhage, matrix and cellular proliferation and finally, remodeling and maturation. The first step starts retracting of the disrupted tendon or ligament ends by producing a blood clot, which is subsequently resorbed, and by replacing that with a cellular infiltrate. Then, a strong hypertrophic vascular response takes place in the gap, resulting in an increase in vascularity and blood flow, progressively decreasing in time. The proliferative phase is identified with the production of "scar tissue" (dense, cellular, collagenous connective tissue matrix bridging the torn ends) by hypertrophic fibroblastic cells. At first, the scar tissue is disorganized with the presence of inhomogeneities such as blood vessels, fat cells, fibroblastic/tenoblastic and inflammatory cells [2]. After a few weeks of healing, the collagen progressively increases its degree of alignment with the longitudinal

axis of the ligament or tendon. At this point, the types of collagen are abnormal (more Type III instead to Type I and an increase in Type V) and the collagen fibrils have smaller cross-sections compared to the healthy tissue. The third phase of tendon and ligament healing is matrix remodeling. Despite defects in the scar tissue are filled in, and the matrix becomes increasingly ligament/tendon-like with time, they continue persisting in the composition, architecture and function [2]. These differences include altered proteoglycan and collagen types, persistence of small collagen fibril diameters, altered cell connections, increased vascularity, abnormal innervation, increased cellularity and the incomplete resolution of matrix defects [40–43]. However, due to the low vascularization and cellular activity, the morphological and mechanical recovery and healing of tendons and ligaments in the long term, is often low. This also depends on a number of variables, as for instance the initial size of the lesion, whether contact exists between the torn ends, and the degree of joint movement which the particular tendon or ligament is subjected [2].

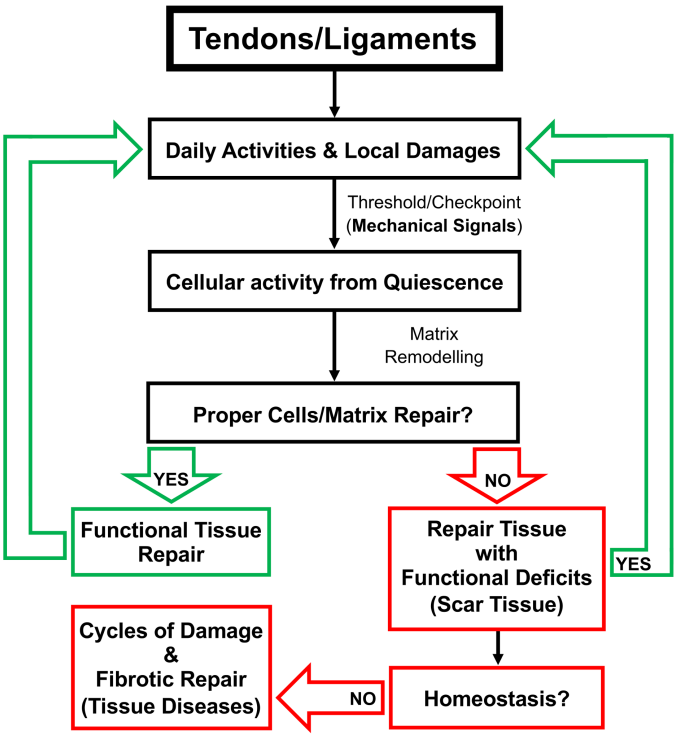

Figure 1.4 Typical workflow of the physiological regenerative process of tendon and ligament tissue. The black boxes show the common strategy adopted by fibroblasts and tenocytes to regenerate the extracellular matrix. The green boxes and arrows indicate the positive answer and the

proper tissue regeneration process. The red boxes and arrows explain the method adopted in case of an overproduction of fibrotic tissue.

For all the previously described reasons, tendons and ligaments injuries are particularly difficult to manage, and the research in the field of regeneration and replacement of these tissues is increased more and more during the last twenty years.

1.2 Tendons and ligaments injuries: causes and treatment options

The injuries of tendons and ligaments are today a clinical problem with unsatisfactory treatment options. Due to the complex hierarchical fibrous structure, the low vascularization and their non- linear mechanical behavior, the healing and regeneration of these tissues generally proceed slowly, as well as the recovery of the mechanical properties [44]. Moreover, is common that areas of scar tissue remain in the site of the lesion, after the tendon or ligament healing. These scar tissue portions contribute to the loss of the anisotropy of the fibrous collagen structure. This causes the loss of organization of the collagen fibrils, with the consequent onset of adhesions and chronic inflammatory phenomena. Is estimated that, every year, the worldwide incidence of tendons and ligaments injuries reaches a number of 30 million of cases [45]. Furthermore, the annual cost to manage these injuries, is estimated in the United States only at $30 billion (with an approximately 95000 new cases every year), whilst in Europe the healthcare expenditure exceeds €115 billion every year [46,47]. Tendon and ligament injuries are commonly categorized as chronic degenerative or acute ruptures. Degenerative inflammations usually precede acute ruptures, with the first considered as a failed healing response characterized by hypervascularity, mucoid degeneration, ectopic bone, cartilage nodules, and disorganized extracellular matrix [48]. Even after one year, the structure and function of the resulting tissue often remain inferior compared to uninjured one [49]. Examples of the most common tendon injuries are related to the rotator cuff and the Achilles tendon. The rotator cuff is composed by the interdigitating tendons of four muscles: subscapularis, supraspinatus, infraspinatus,

and teres minor. The attach on the lateral aspect of the humeral head plays an important role in both stabilizing and mobilizing the shoulder. Rotator cuff tears are a common cause of debilitating pain, reduced shoulder function, and weakness, that affect more than 40% of patients older than 60 years of age, and resulting in 30000 to 75000 repairs performed annually in the United States [49,50]. Despite the advances in surgical techniques and in the understanding of shoulder pathology, chronic tears fail to heal in 20–95% of cases [51,52]. In particular, the bone-to-tendon interface that forms following surgical repair fails to replicate the native enthesis, with a fibrovascular scar forming in place of the complex fibrocartilage transition seen between native tendon and bone [53]. The other most frequently injured tendon is Achilles one. Achilles tendon injuries are divided in chronic tendinopathies and ruptures. Achilles tendinopathies are accounting for 30–50% of all sports-related injuries [54]. Ruptures are commonly seen in men aged 30–50 [55]. Nevertheless, Achilles tendon ruptures also occur in elite athletes and, despite the research focus in this topic, this injury is well known due to its poor quality and slow rate of healing [56]. Just as full-thickness rotator cuff tears are frequently preceded by partial tears and tendon degeneration, tendinosis and chronic tendinopathy predispose the Achilles tendon to a complete rupture [57,58]. Because of the often occurrence of post- operative complications, the conservative approaches (i.e. reduced activity, cryotherapy, eccentric loading, deep friction massage, orthotics, and therapeutic ultrasounds) are generally preferable, producing also good outcomes in up to 75% of cases [49]. About the most injured ligaments instead, the ACL is for sure the most common and disabling one. ACL lesions are a typical consequence of sports participation [59]. These injuries often result in joint effusion, altered movement, muscle weakness, reduced functional performance [60]. ACL injuries are also associated with long-term clinical complications that include meniscal tears, chondral lesions and an increased risk of early onset post-traumatic osteoarthritis [61–66]. Moreover, ACL has a poor healing capacity, with a substantially high rate of failure (40-100%), even after surgical repair using suture [67–69]. The unsatisfactory outcomes of the ACL primary repair have led to unanimous abandonment of suture repair and widespread adoption of ACL reconstruction. ACL reconstruction has remained the gold standard of care for ACL

injuries, especially for young individuals and athletes who aim to return to sporting activities [59,60,70]. However, current surgical treatment of ACL injury is costly, with variable outcomes and is associated with high risk of post-traumatic osteoarthritis within two decades of injury [60,65,71]. While few athletes are able to resume sports at the same level without surgery, the surgical reconstruction is also not always successful at returning patients to their pre-injury activity level [60,72]. Furthermore, those athletes who successfully return to activity, are at high risk of a second knee injury with notably less favorable outcomes [59,73,74].

1.2.1 Conservative non-surgical approches

Due to the high risks related to the surgery of tendons and ligaments, a conservative approach is generally preferred to treat these pathologies. The primary goal of tendinopathy treatment is to reduce pain, mainly through the use of topical or systemic anti-inflammatory drugs, whereas surgical techniques aim to repair ruptured tendons [38,75–77]. The use of non-steroidal anti-inflammatory drugs (NSAIDs) in the treatment of tendinopathy remains controversial both in the acute stage and in the chronic stage. Corticosteroid injections are a commonly administered treatment for tendon and ligament disorders [38,78]. The use of autologous growth factors is another therapeutic approach that is gaining in popularity. Platelet rich plasma (PRP) is a blood derivative containing high levels of growth factors, known to promote tissue healing [79]. However, the benefits of PRP injection for tendon recovery remain controversial [77,80,81]. For both chronic and acute tendon and ligament injuries, exercise-based rehabilitation is indicated [82]. In fact, by decreasing drastically the loads on ligament and tendon tissue, alterations in matrix turnover occur. This causes that matrix degradation exceeds its formation and the newly synthesized matrix becomes less well organized, declining the tissue stiffness and strength [83]. Furthermore, prolonged limb immobilization decreases the content of water and glycosaminoglycans in the ligament or tendon, and alters the degree of orientation of the matrix collagen fibrils within the tissue [84]. Other methods explored and tested for tendon and ligament healing are the physical ones. Extracorporeal shock wave therapy, for example, has demonstrated effectiveness in calcified tendinitis of the shoulder [85]. However, if

not properly set, the shock wave therapy could produce several damages as fibrinoid necrosis, fibrosis, and inflammation [86,87]. Pulsed magnetic fields have shown to increase the collagen fibers alignment and load to failure of the lesioned tendon or ligament [87,88]. Finally, the laser therapy has shown some contributions in the reduction of the postoperative edema and in the improvement of the collagen production [89,90]. Despite non-surgical treatments are providing better and better results, the scientific evidence has stated that, in general, these approaches are less successful (only 60% of the restored tendons are functional) [38]. Up to 29% of patients need to be treated by surgery after failure of conservative therapies [58,91,92]. So, when the conservative non-invasive methods are insufficient, because of chronic inflammations or for the complete break of the tendon or ligament, the surgery is the only applicable solution. In these cases, there are two possible ways: a conservative approach, consisting in the suture of the lesion (or its augmentation), or the substitution of the tendon or ligament of interest, using resorbable structures, or the prosthetic replacement with inert devices. In these cases, one of the first parameter that must be considered, is the age of the patient. In fact, tendons and ligaments are subjected to several biological, cellular and mechanical modifications over time. Several studies on rotator cuff healing have noted that patient age is associated with increased healing complications [93–96]. An increase in the degradative enzyme production in aged tendons, for example the matrix metalloproteinase (MMP), is confirmed in several biochemical studies [29,97,98]. The increment in MMP production, could cause tendinosis resulting in irregular orientation of collagen, fibril disruption and change in diameter, decrease in density of collagen, upregulation of collagen type III production, and apoptosis [99–103]. Moreover, the increase in MMP production is associated with the reduction of the tendons mechanical properties [104].

For all these reasons is important for the surgeons chose the adequate surgical approach, evaluating both the severity of the lesion and the age of the specific patient.

1.2.2 Conservative surgery

When the tendon or ligament tissue loss its continuity because of a traumatic lesion or as a consequence of a chronic inflammation, the surgical approach is mandatory. If the fracture extremities are well defined, or the lesion is just partial, and the surrounding tissues are not strongly compromised or necrotic, the conservative surgery is the preferred option. Suture the ends of the injured tendon or ligament is a common conservative surgery technique. In the case of tendons, different suture strategies are applicable depending to the particular gravity of the injury (Figure 1.5A) [105–111]. Even if the suture techniques permit to restore faster the mobilization of the tendon to enhance healing, they have several related risks. The fast mobilization necessary to prevent the rise of adhesions and inflammations, is high related to a premature failure of the suture [112]. To prevent ruptures, surgeons often increase the amount of suture material, enhancing the risk of adhesions [105]. In the ligament conservative surgery suture techniques are suitable for a faster mobilization of the patients as well. For the ACL, examples of suturing techniques are the dynamic intraligamentary stabilization (Figure 1.5B), the internal braces and the anchors [113–116]. They basically consist in suture the site of the ligament lesion or passing through the ligament body, wires fixed in tibia and femur. Despite the faster mobilization of the patients, these techniques also increase the risk of inflammations and scar tissue formation [113].

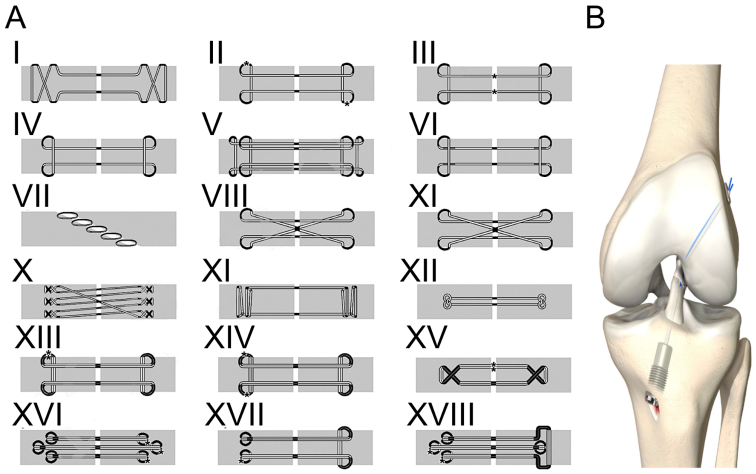

Figure 1.5 A) Some of the tendons joining techniques described in literature (adapted from Rawson et al. [105] reproduced with permission. Copyright 2013, CIC Edizioni Internazionali). Light Grey

= Tendon. White = Suture internal of tendon. Black = suture external of tendon. Dark Grey = Suture external of tendon, dorsally placed (Only shown on figures VI and XI). * = placement of knot (only shown on figures II, III and XIII to XVIII). Double strand suture used in repairs XIII to XVIII. I) Bunnell: 2 strand, non-grasping anchor. II) Grasping Kessler: 2 strands, grasping anchor. III) Tajima: 2 strands, grasping anchor. IV) Modified locking Kessler (aka. Pennington): 2 strand, locking anchor. V) Four strand double modified Kessler: 4 strands, locking anchor. VI) Modified Pennington: 2 strand, locking anchor. VII) Becker: interrupted stitch joining oblique tendon ends. VIII) Grasping Cruciate: 4 strand, grasping anchor. XI) Locking Cruciate: 4 strand, locking anchor. X) Savage: 6 strand, x-stitch anchor. XI) Locking Lee: 2 strand, locking anchor with large purchase. XII) Tsuge: 2 strand, anchor buried within tendon. XIII) Four strand Kessler repair. XIV) Four strand Kessler repair with knots on opposing sides. XV) Four strand cross-lock repair. XVI) Tang. XVII) U-shaped four strand repair XVIII) Six strand M-tang. B) Example of ACL repair with dynamic intraligamentary stabilization (www.mathysmedical.com).

According to the limitations above, surgeons in the last decades have decided to change the strategy to manage tendon and ligament injuries. In order to increase the biocompatibility and decrease the risk of inflammations and scar tissue formation, surgeons developed several techniques to repair injured tendons or ligaments with healthy portions of other ones of the patient's body. These particular kinds of autologous grafts are called autografts. Autografts surgery is currently a gold standard for managing tendon and ligament ruptures [117]. The principal advantage of autografts is high incorporative properties. Because of they are viable tissues, their cells can fast collaborate at damaged tissue healing [117,118]. However, reconstruction of such large defects requires massive tissue harvesting from the donor site and therefore the donor site morbidity and pain is a considerable challenge to autografts [118–121]. Another limitation is that there may not be enough autografts in the patient's body at the time of reconstruction. Moreover, this method is not cosmetically pleasant and a second surgery in the patient, increasing the surgical time and cost, is often necessary [117,120,122].

1.2.3 Regenerative surgery

To overcome the problems above, researchers have developed decellularized tendons and ligaments from different typologies of both human and animal donors, called respectively allografts and xenografts. The most positive issue regarding

allografts and xenografts is their availability and flexibility in shape [120–122]. However, because of allo- and xenografts are decellularized tissues, their main problem is the high risk of patient's contamination. In fact, they increase the chance of disease transmission of dangerous viruses and prions such as human immune deficiency virus, hepatitis type B and type C, and bovine spongiform encephalitis. Xenografts are more dangerous compared to the allografts, because of the possibility to be carrier for unknown zoonotic diseases [117–119]. For this reasons allografts and xenografts have this chance to be acutely or chronically rejected by the host [119]. Furthermore, to reduce the immunogenicity of the allo- and xenografts, several sterilizations and decellularizations processes have been made (e.g. sterilization, cell rinsing, freeze drying, etc.); these processes decrease the incorporative properties of grafts with the healing tissue, resulting in their rapid absorption during tendon or ligament healing [123].

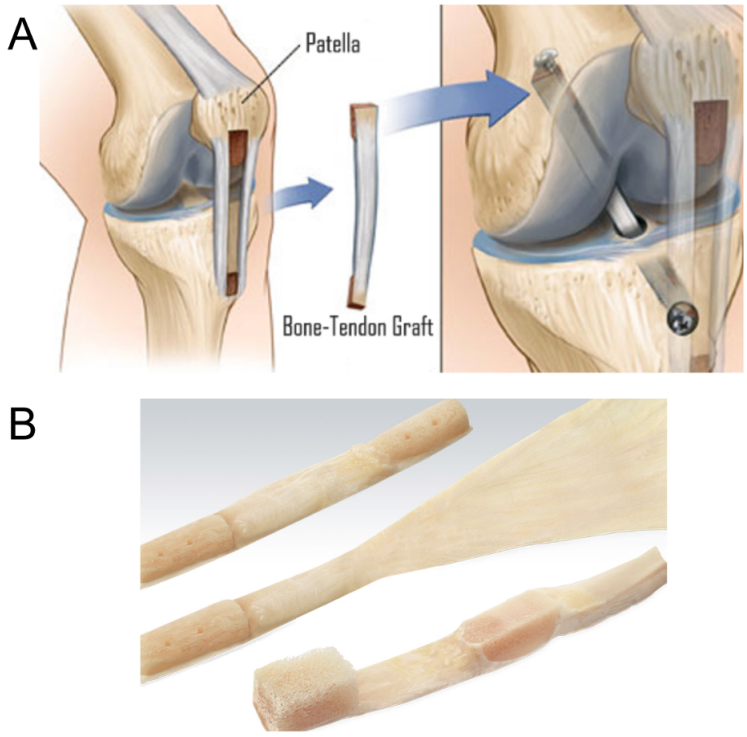

Figure 1.6 A) Schematic picture of Patella tendon autograft for ACL replacement (www.healthclues.net). B) different tendon and ligament allograft (www.conmed.com).

The different complications related to the biological scaffolds have suggested surgeons and researchers to develop different solutions to manage tendon and ligament injuries. For these reasons in the last two decades, the tissue engineering

has increased exponentially its importance. The key role in tissue engineering is played by the scaffolds, natural or synthetic resorbable polymer-based porous structures, able to be colonized by cells and guide their proliferation (Figure 1.7) [124]. To do this, it is strictly necessary that scaffolds mimic as much as possible the morphology and also the biomechanical properties of the tissue to regenerate.

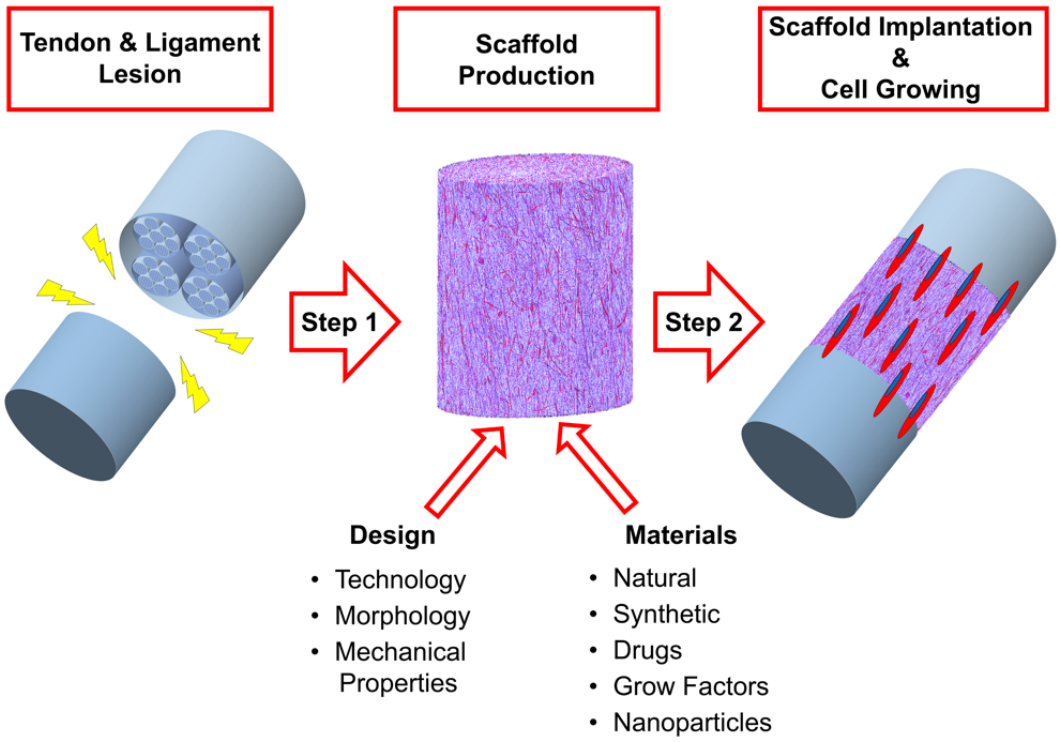

Figure 1.7 Schematic representation of the tissue engineering workflow applied to tendon and ligament regeneration and replacement.

Scaffolds are continuously improved in order to modulate their degradation rate, with the regeneration of the natural tissue. Morphologically speaking, in order to mimic the hierarchical structure of tendon and ligament tissue, scaffolds may unit porosity and a fiber-based shape. These scaffolds also need to reproduce strictly the mechanical properties of the tendon or ligament to be substituted. Several methods and techniques are proposed in literature to produce scaffolds for tendon and ligament tissue regeneration [125]. Among the others, thanks to its ability to generate fibers of micro- and nanometric dimensions, the electrospinning technology is currently the most promising technique to produce scaffolds for tendons and ligaments [126,127]. Even if nowadays no one is able to produce hierarchically structured electrospun scaffolds with mechanical properties in the

range of tendons or ligaments, encouraging purposes outcomes are present in literature [125–127]. The properties of scaffolds and of the electrospinning technique will be listed and explained in depth in the chapter 2. Moreover, all the literature about electrospun scaffolds for tendon and ligament tissue regeneration produced to date will be analyzed.

1.2.4 Replacement with prosthetic devices

Prosthetic devices started being developed in the 1980s and early 1990s. Especially focused on the surgery of elderly people (> 60 years old), according to the lower cellular activity, these devices are made of not resorbable materials. Several protheses for tendon and ligament replacement were produced with different inert materials such as polyester, polypropylene, polyarylamide, dacron, carbon, silicone and nylon [128–130]. These prosthetic devices have superior mechanical properties compared with biological scaffolds. However, they have poor biocompatibility and have caused numerous complications in the long-term application, which caused regulatory intervention. Several commercial synthetic ligaments were retired from the market in the past, because of the related complications in the short and long-term implantation [128]. Among their possible complications, implant degeneration, device failure, severe synovitis and inflammation response associated with foreign body reaction, were found [131–133]. However, the most relevant issues can be summarized mainly in three points: fiber abrasion resistance against osseous surfaces, flexo-rotational fatigue of the fibers, and loss of integrity caused by tissue infiltration during healing [134]. Nevertheless, some synthetic scaffolds are still frequently used in current medical practice. Gore-Tex materials are typically based on thermomechanically expanded polytetrafluoroethylene (PTFE) and other fluoropolymer products. Although it has been abandoned for ACL reconstruction due to severe complications, the results were controversial [132,135,136]. Satisfactory results using it for very large rotator cuff tear and patellar reconstruction were reported [137,138].

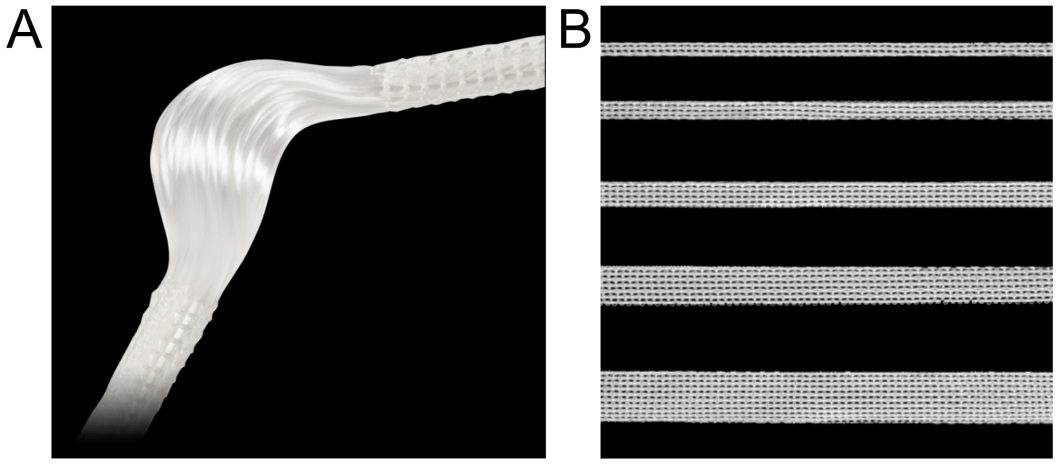

Figure 1.8 Examples of prosthetic devices for tendon and ligament repair. A) Lars Ligament (www.coringroup.com). B) Leeds-Keio device (www.neoligaments.com).

Lars Ligament is a, nonabsorbable synthetic ligament device made of terephthalic polyethylene polyester fibers (Figure 1.8A) [139]. It has been approved for a range of applications including cruciate reconstruction, and Achilles tendon and acromioclavicular repairs. Promising results have been reported in studies which used it for ACL and patellar reconstruction and collateral ligament repair [140–143]. Lars ligament causes minimum complications due to its very high biocompatibility [144]. It appears that Lars ligament has proper mechanical strength and biocompatibility suitable for long-term implantation [128]. Leeds-Keio graft, also known as Poly-Tapes is a popular nonabsorbable synthetic prosthesis for tendon and ligament reconstruction since the 1980s (Figure 1.8B). Made of polyester (ethylene terephthalate), is specifically designed for ACL [145]. Clinical results using Leeds-Keio ligament for ACL reconstruction were quite controversial, adverse events likes rerupture, tunnel enlargement, synovitis associated with polyester particles, greater pivot-shift and laxity were frequently reported in the 1990s-2000s [146–151]. However, positive results have also been constantly published and it seems that, along with the improvement of surgical technique, more favorable results have been achieved in the past 5 years [128,152,153]. Meanwhile, Leeds- Keio has also been used for other tendon repair such as rotator cuff, knee extensor, Achilles tendon, iliofemoral ligament, ankle lateral ligament, showing encouraging results [128,154–160].

1.3 Study aim

The aim of the present Thesis was to design, develop and characterize innovative, modular, nanofibrous, electrospun, hierarchically structured scaffolds and devices, made of bioresorbable and inert materials, able to replicate the hierarchical structure and the biomechanical properties of tendons and ligaments. To reach this goal, electrospun nanofibers of both resorbable and inert materials were optimized, mimicking the morphology of tendons and ligament fibrils. The mats of nanofibers were wrapped up producing bundles of nanofibers, that reproduced the structures and the properties of tendons and ligaments fascicles. Finally, an innovative electrospinning procedure was developed to group several bundles together with nanofibrous sheaths, simulating the whole tendons and ligaments structure.
The entire work is also focalized in the description of the procedures and methods developed to characterize each electrospun structure:

- their morphological similarities with the tendons and ligaments hierarchical structure were assessed by a scanning electron microscopy and a full volume high-resolution x-ray tomographic investigation.
- their biomimetic mechanical properties were confirmed by using tensile tests carried out with physiological parameters.

Furthermore, the cellular viability on the different hierarchical levels was also evaluated by culturing fibroblasts and tenocytes on the resorbable scaffolds.

1.4 Outline of the Thesis

The present work is organized in incremental steps, following a bottom-up approach to develop the final hierarchically structured scaffolds. In particular the work is divided in the steps described below:

- Chapter 2 presents an exhaustive literature review to describe and analyse the state of art about the electrospinning techniques applied to the regeneration and replacement of the tendon and ligament tissue.
- Chapter 3 reports a preliminary study of design and characterization of electrospun bundles made of Poly(L-lactic) acid (PLLA) and collagen

(Coll) blends, for tendon tissue regeneration. A particular focus also to the cells proliferation on the scaffolds is reported.

- Chapter 4 shows the design and characterization of bundles of PLLA/Coll crosslinked blends, able to maintain the collagen after ageing in physiological environment. Evaluation also of the effects of the crosslinking process on the morphology, the mechanical properties and the cells growing of the bundles is reported.
- Chapter 5 describes the validation of full-field high-resolution x-ray tomographic protocols to investigate the morphology and the nanofibers orientation on electrospun bundles of different materials.
- Chapter 6 reports the design, development, multiscale characterization and cell proliferation of resorbable PLLA, hierarchically structured, tendon/ligament-like scaffolds.
- Chapter 7 presents the design, development and characterization of different inert Nylon6.6 hierarchically structured assemblies for tendon and ligament replacement and simulation.
- Chapter 8 outlines general conclusions and future outcomes.

1.5 References

[1] Kannus P 2000 Structure of the tendon connective tissue Scand. J. Med. Sci. Sport. 10 312–20

[2] Frank C B 2004 Ligament structure, physiology and function J. Musculoskelet. Neuronal Interact. 4 199–201

[3] Santos M L, Rodrigues M T, Domingues R M A, Reis R L and Gomes M E 2017 Regenerative Strategies for the Treatment of Knee Joint Disabilities Regenerative Strategies for the Treatment of Knee Joint Disabilities vol 21, ed J M Oliveira and R L Ruis (Springer International Publishing) pp 349–71

[4] Benjamin M and Ralphs J R 1997 Tendon and ligaments-An overview.pdf Histol. Histopatology 12 1135–44

[5] Goh K L, Listrat A and Béchet D 2014 Hierarchical mechanics of connective tissues: Integrating insights from nano to macroscopic studies J. Biomed. Nanotechnol. 10 2464–507

[6] Murphy W, Black J and Hastings G 2016 Handbook of Biomaterial Properties ed W Murphy, J Black and G Hastings (Springer)

[7] Goh Y F, Shakir I and Hussain R 2013 Electrospun fibers for tissue engineering, drug delivery, and wound dressing J. Mater. Sci. 48 3027–54

[8] Kastelic J, Galeski A and Baer E 1978 The Multicomposite Structure of Tendon Connect. Tissue Res. 6 11–23

[9] Asahara H, Inui M and Lotz M K 2017 Tendons and Ligaments: Connecting Developmental Biology to Musculoskeletal Disease Pathogenesis J. Bone Miner. Res. 32 1773–82

[10] Woo S L Y, Almarza A J, Karaoglu S, Liang R and Fisher M B 2011 Functional Tissue Engineering of Ligament and Tendon Injuries Principles of Regenerative Medicine ed A Atala, R Lanza, A G Mikos and R Nerem (Elsevier Inc.) pp 997–1021

[11] Lavagnino M, Wall M E, Little D, Banes A J, Guilak F and Arnoczky S P 2015 Tendon mechanobiology: Current knowledge and future research opportunities J. Orthop. Res. 33 813–22

[12] Snedeker J G and Foolen J 2017 Tendon injury and repair – A perspective on the basic mechanisms of tendon disease and future clinical therapy Acta Biomater. 63 18–36

[13] Wall M E and Banes A J 2005 Early responses to mechanical load in tendon: Role for calcium signaling, gap junctions and intercellular communication J. Musculoskelet. Neuronal Interact. 5 70–84

[14] Yang G, Crawford R C and Wang J H C 2004 Proliferation and collagen production of human patellar tendon fibroblasts in response to cyclic uniaxial stretching in serum-free conditions J. Biomech. 37 1543–50

[15] Berridge M J, Lipp P and Bootman M D 2000 The Versatility and Universality of Calcium Signaling Nat. Rev. Mol. Cell Biol. 1 11–21

[16] Berridge M J, Bootman M D and Roderick H L 2003 Calcium signalling: Dynamics, homeostasis and remodelling Nat. Rev. Mol. Cell Biol. 4 517–29

[17] Bootman M D, Collins T J, Peppiatt C M, Prothero L S, Mackenzie L, Smet P De, Travers M, Tovey S C, Jeong T, Berridge M J, Ciccolini F and Lipp P 2001 Calcium signalling — an overview Semin. Cell Dev. Biol. 12 3–10

[18] Banes A J, Weinhold P and Yang X 1999 Gap Junctions Regulate Responses of Tendon Cells Ex Vivo to Mechanical Loading Clin. ORTOPAEDIC Relat. Res. 356–70

[19] O'Conor C J, Leddy H A, Benefield H C, Liedtke W B and Guilak F 2014 TRPV4-mediated mechanotransduction regulates the metabolic response of chondrocytes to dynamic loading PNAS 111 1–6

[20] Lavagnino M, Arnoczky S P, Tian T and Vaupel Z 2003 Effect of Amplitude and Frequency of Cyclic Tensile Strain on the Inhibition of MMP-1 mRNA Expression in Tendon Cells : An In Vitro Study Connect. Tissue Res. 44 181–7

[21] Lavagnino M, Arnoczky S P, Egerbacher M, Gardner K L and Burns M E 2006 Isolated fibrillar damage in tendons stimulates local collagenase mRNA expression and protein synthesis J. Biomech. 39 2355–62

[22] Lavagnino M, Arnoczky S P and Gardner K 2011 In situ deflection of tendon cell-cilia in response to tensile loading: An in vitro study J. Orthop. Res. 29 925–30

[23] Rowson D, Knight M M and Screen H R C 2016 Zonal variation in primary cilia elongation correlates with localized biomechanical degradation in stress deprived tendon J. Orthop. Res. 34 2146–53

[24] Gardner K, Arnoczky S P and Lavagnino M 2011 Effect of In vitro Stress-Deprivation and Cyclic Loading on the Length of Tendon Cell Cilia in situ J. Orthop. Res. 582–7

[25] Dahl K N, Booth-Gauthier E A and Ladoux B 2010 In the middle of it all: Mutual mechanical regulation between the nucleus and the cytoskeleton J. Biomech. 43 2–8

[26] Arnoczky S P, Lavagnino M, Whallon J H and Hoonjan A 2002 In situ cell nucleus deformation in tendons under tensile load; a morphological analysis using confocal laser microscopy J. Orthop. Res. 20 29–35

[27] Fessel G, Li Y, Diederich V, Guizar-Sicairos M, Schneider P, Sell D R, Monnier V M and Snedeker J G 2014 Advanced glycation end-products reduce collagen molecular sliding to affect collagen fibril damage mechanisms but not stiffness PLoS One 9

[28] Woo S L Y, Hollis J M, Adams D J, Lyon R M and Takai S 1991 Tensile properties of the human femur-anterior cruciate ligament-tibia complex: The effects of specimen age and orientation Am. J. Sports Med. 19 217–25

[29] McCarthy M M and Hannafin J A 2014 The Mature Athlete: Aging Tendon and Ligament Sports Health 6 41–8

[30] Mastrangelo A N, Magarian E M, Palmer M P, Vavken P and Murray M M 2010 The effect of skeletal maturity on the regenerative function of intrinsic ACL cells J. Orthop. Res. 28 644– 51

[31] Mihelic R, Pecina M, Jelic M, Zoricic S, Kusec V, Simic P, Bobinac D, Lah B, Legovic D and Vukicevic S 2004 Bone morphogenetic protein-7 (osteogenic protein-1) promotes tendon graft integration in anterior cruciate ligament reconstruction in sheep Am. J. Sports Med. 32 1619–25

[32] Vavken P, Saad F A and Murray M M 2010 Age dependence of expression of growth factor receptors in porcine ACL fibroblasts J. Orthop. Res. 28 1107–12

[33] Klatte-Schulz F, Pauly S, Scheibel M, Greiner S, Gerhardt C, Schmidmaier G and Wildemann B 2012 Influence of age on the cell biological characteristics and the stimulation potential of male human tenocyte-like cells Eur. Cells Mater. 24 74–89

[34] Cheng M, Johnson V M and Murray M M 2012 Effects of age and platelet-rich plasma on ACL cell viability and collagen gene expression J. Orthop. Res. 30 79–85

[35] Levy Y D, Hasegawa A, Patil S, Koziol J A, Lotz M K and D'Lima D D 2013 Histopathological changes in the human posterior cruciate ligament during aging and osteoarthritis: Correlations with anterior cruciate ligament and cartilage changes Ann. Rheum. Dis. 72 271– 7

[36] Arnoczky S P, Lavagnino M and Egerbacher M 2007 The mechanobiological aetiopathogenesis of tendinopathy: Is it the over-stimulation or the under-stimulation of tendon cells? Int. J. Exp. Pathol. 88 217–26

[37] Archambault J M, Wiley J P and Bray R C 1995 Exercise Loading of Tendons and the Development of Overuse Injuries: A Review of Current Literature Sport. Med. 20 77–89

[38] Rees J D, Wilson A M and Wolman R L 2006 Current concepts in the management of tendon disorders Rheumatology 45 508–21

[39] Manske P R and Lesker P A 1984 Biochemical evidence of flexor tendon repair in various experimental animals J. Hand Surg. Am. 9 117–20

[40] Plaas A H K, Wong-Palms S, Koob T, Hernandez D, Marchuk L and Frank C B 2000 Proteoglycan metabolism during repair of the ruptured medial collateral ligament in skeletally mature rabbits Arch. Biochem. Biophys. 374 35–41

[41] Amiel D, Frank C B, Harwood F L, Akeson W H and Kleiner J B 2009 Collagen Alteration in Medial Collateral Ligament Healing in a Rabbit Model Connect. Tissue Res. 16 357–66

[42] Bray R C, Rangayyan R M and Frank C B 1996 Normal and healing ligament vascularity: a quantitative histological assessment in the adult rabbit medial collateral ligament. J. Anat. 188 (1) pp. 87–95

[43] Frank C, McDonald D, Bray D, Rangayyan R, Chimich D and Shrvive N 1992 Collagen fibril diameters in the healing adult rabbit medial collateral ligament Connect. Tissue Res. 27 251–63

[44] Liu C-F, Aschbacher-Smith L, Barthelery N J, Dyment N, Butler D and Wylie C 2011 What We Should Know Before Using Tissue Engineering Techniques to Repair Injured Tendons: A Developmental Biology Perspective Tissue Eng. Part B Rev. 17 165–76

[45] Maffulli N, Wong J and Almekinders L C 2003 Types and epidemiology of tendinopathy Clin. Sports Med. 22 675–92

[46] Abbah S A, Spanoudes K, O'Brien T, Pandit A and Zeugolis D 2014 Assessment of stem cell carriers for tendon tissue engineering in pre-clinical models Stem Cell Res. Ther. 5 1–9 Zeugolis D I, Chan J C Y and Pandit A 2011 Tendons: Engineering of Functional Tissues

[47] Tissue Engineering: From Lab to Clinic ed N Pallua and C Suscheck (Springer Berlin Heidelberg) pp 1–634

[48] Riley G 2008 Tendinopathy - From basic science to treatment Nat. Clin. Pract. Rheumatol. 4 82–9

[49] Yang G, Rothrauff B B and Tuan R S 2013 Tendon and ligament regeneration and repair: Clinical relevance and developmental paradigm Birth Defects Res. Part C - Embryo Today Rev. 99 203–22

[50] Ricchetti E T, Aurora A, Iannotti J P and Derwin K A 2012 Scaffold devices for rotator cuff repair J. Shoulder Elb. Surg. 21 251–65

[51] Galatz L M, Ball C M, Teefey S A, Middleton W D and Yamaguchi K 2004 The Outcome and Repair Integrity of Completely Arthroscopically Repaired Large and Massive Rotator Cuff Tears J. Bone Jt. Surg. - Ser. A 86 219–24

[52] Derwin K A, Baker A R, Iannotti J P and McCarron J A 2010 Preclinical Models for Translating Regenerative Medicine Therapies for Rotator Cuff Repair Tissue Eng. Part B Rev. 16 21–30

[53] Newsham-West R, Nicholson H, Walton M and Milburn P 2007 Long-term morphology of a healing bone-tendon interface: A histological observation in the sheep model J. Anat. 210 318–27

[54] Sadoghi P, Rosso C, Valderrabano V, Leithner A and Vavken P 2013 The role of platelets in the treatment of Achilles tendon injuries J. Orthop. Res. 31 111–8

[55] Longo U G, Ronga M and Maffulli N 2009 Achilles Tendinopathy Sport. Med. Arthrosc. Rev. 17 112–126

[56] Maffulli N, Longo U G, Maffulli G D, Khanna A and Denaro V 2011 Achilles Tendon Ruptures in Elite Athletes Foot Ankle Int. 32 9–15

[57] Oh J H, Jun B J, McGarry M H and Lee T Q 2011 Does a Critical Rotator Cuff Tear Stage Exist? J. Bone Jt. Surgery-American Vol. 93 2100–9

[58] Hess G W 2015 Achilles Tendon Rupture: A Review of Etiology, Population, Anatomy, Risk Factors, and Injury Prevention Foot Ankle Spec. 3 29–32

[59] Kiapour A M and Murray M M 2014 Basic science of anterior cruciate ligament injury and repair. Bone Joint Res. 3 20–31

[60] Hewett T E, Di Stasi S L and Myer G D 2013 Current concepts for injury prevention in athletes after anterior cruciate ligament reconstruction Am. J. Sports Med. 41 216–24

[61] Levine J W, Kiapour A M, Quatman C E, Wordeman S C, Goel V K, Hewett T E and Demetropoulos C K 2013 Clinically relevant injury patterns after an anterior cruciate ligament injury provide insight into injury mechanisms Am. J. Sports Med. 41 385–95

[62] Chu C R, Beynnon B D, Buckwalter J A, Garrett W E, Katz J N, Rodeo S A, Spindler K P and Stanton R A 2011 Closing the gap between bench and bedside research for early arthritis therapies (earth): Report from the aossm/nih u-13 post-joint injury osteoarthritis conference II Am. J. Sports Med. 39 1569–78

[63] Lohmander L S, Östenberg A, Englund M and Roos H 2004 High prevalence of knee osteoarthritis, pain, and functional limitations in female soccer players twelve years after anterior cruciate ligament injury Arthritis Rheum. 50 3145–52

[64] Nebelung W and Wuschech H 2005 Thirty-five years of follow-up of anterior cruciate ligament - Deficient knees in high-level athletes Arthrosc. - J. Arthrosc. Relat. Surg. 21 696– 702

[65] Von Porat A, Roos E M and Roos H 2004 High prevalence of osteoarthritis 14 years after an anterior cruciate ligament tear in male soccer players: A study of radiographic and patient relevant outcomes Ann. Rheum. Dis. 63 269–73

[66] Quatman C E, Kiapour A, Myer G D, Ford K R, Demetropoulos C K, Goel V K and Hewett T E 2011 Cartilage pressure distributions provide a footprint to define female anterior cruciate ligament injury mechanisms Am. J. Sports Med. 39 1706–13

[67] Feagin J A and Curl W W 1976 Isolated tear of the anterior cruciate ligament: 5-year follow- up study. Am. J. Sports Med. 3 95–100

[68] Kaplan N, Wickiewicz T L and Warren R F 1990 Primary surgical treatment of anterior cruciate ligament ruptures: A long-term follow-up study Am. J. Sports Med. 18 354–8

[69] Strand T, Mølster A, Hordvik M and Krukhaug Y 2005 Long-term follow-up after primary repair of the anterior cruciate ligament: Clinical and radiological evaluation 15-23 years postoperatively Arch. Orthop. Trauma Surg. 125 217–21

[70] Musahl V, Becker R, Fu F H and Karlsson J 2011 New trends in ACL research Knee Surgery, Sport. Traumatol. Arthrosc. 19 19–21

[71] Murray J R D, Lindh A M, Hogan N A, Trezies A J, Hutchinson J W, Parish E, Read J W and Cross M V. 2012 Does anterior cruciate ligament reconstruction lead to degenerative disease?: Thirteen-year results after bone-patellar tendon-bone autograft Am. J. Sports Med. 40 404–13

[72] Ardern C L, Webster K E, Taylor N F and Feller J A 2011 Return to the preinjury level of competitive sport after anterior cruciate ligament reconstruction surgery: Two-thirds of patients have not returned by 12 months after surgery Am. J. Sports Med. 39 538–43

[73] Shelbourne K D, Gray T and Haro M 2009 Incidence of subsequent injury to either knee within 5 years after anterior cruciate ligament reconstruction with patellar tendon autograft Am. J. Sports Med. 37 246–51

[74] Spindler K P, Huston L J, Wright R W, Kaeding C C, Marx R G, Amendola A, Parker R D, Andrish J T, Reinke E K, Harrell F E, Pedroza A, An A Q, Schmitz L, McCarty E C, Wolf B R, Jones M H, Matava M J, Flanigan D C, Brophy R H, Vidal A F and Dunn W R 2011 The prognosis and predictors of sports function and activity at minimum 6 years after anterior cruciate ligament reconstruction: A population cohort study Am. J. Sports Med. 39 348–59

[75] Docheva D, Müller S A, Majewski M and Evans C H 2015 Biologics for tendon repair Adv. Drug Deliv. Rev. 84 222–39

[76] Childress M and Beutler A 2013 Management of chronic tendon injuries Am. Fam. Physician 87 486–90

[77] Nourissat G, Berenbaum F and Duprez D 2015 Tendon injury: From biology to tendon repair Nat. Rev. Rheumatol. 11 223–33

[78] Aslan A, Sofu H and Kirdemir V 2014 Ankle Ligament Injury: Current Concept OA Orthop. 2 1–6

[79] Jeong D U, Lee C-R, Lee J H, Pak J, Kang L-W, Jeong B C and Lee S H 2014 Clinical Applications of Platelet-Rich Plasma in Patellar Tendinopathy Biomed Res. Int. 2014 1–15

[80] Wang J H-C 2014 Can PRP effectively treat injured tendons? Muscles. Ligaments Tendons J. 4 35–7

[81] Guevara-Alvarez A, Schmitt A, Russell R P, Imhoff A B and Buchmann S 2014 Growth factor delivery vehicles for tendon injuries: Mesenchymal stem cells and Platelet Rich Plasma Muscles. Ligaments Tendons J. 4 378–85

[82] Khan K M and Scott A 2009 Mechanotherapy: How physical therapists' prescription of exercise promotes tissue repair Br. J. Sports Med. 43 247–52

[83] Hauser R A, Dolan E E, Phillips H J, Newlin A C, Moore R E and Woldin B A 2013 Ligament Injury and Healing: A Review of Current Clinical Diagnostics and Therapeutics Open Rehabil. J. 6 1–20

[84] Buckwalter J a 1995 Activity vs. rest in the treatment of bone, soft tissue and joint injuries. Iowa Orthop. J. 15 29–42

[85] Gerdesmeyer L, Wagenpfeil S, Haake M, Maier M, Loew M, Wortler K, Lampe R, Seil R, Handle G, Gassel S and Jan D. Rompe M 2003 Extracorporeal ShockWave Therapy for the Treatment of Chronic Calcifying Tendonitis of the Rotator Cuff Jama 290 7–10

[86] Rompe J D, Kirkpatrick C J, Küllmer K, Schwitalle M and Krischek O 1998 Dose-related effects of shock waves on rabbit tendo Achillis: A sonographic and histological study J. Bone Jt. Surg. 80 546–52

[87] Sharma P and Maffulli N 2005 Tendon Injury and Tendinopathy: Healing and Repair J. Bone Jt. Surg. 87 187

[88] Lee E W C, Maffulli N, Li C K and Chan K M 1997 Pulsed magnetic and electromagnetic fields in experimental Achilles tendonitis in the rat: A prospective randomized study Arch. Phys. Med. Rehabil. 78 399–404

[89] Ozkan N, Altan L, Bingol U, Akln S and Yurtkuran M 2004 Investigation of the Supplementary Effect of GaAs Laser Therapy on the Rehabilitation of Human Digital Flexor Tendons J. Clin. Laser Med. Surg. 22 105–10

[90] Reddy G K, Stehno-Bittel L and Enwemeka C S 1998 Laser photostimulation of collagen production in healing rabbit Achilles tendons Lasers Surg. Med. 22 281–7

[91] Alfredson H, Forsgren S, Thorsen K and Lorentzon R 2001 In vivo microdialysis and immunohistochemical analyses of tendon tissue demonstrated high amounts of free glutamate and glutamate NMDAR1 receptors, but no signs of inflammation, in Jumper's knee J. Orthop. Res. 19 881–6

[92] Wu F, Nerlich M and Docheva D 2017 Tendon injuries: basic science and new repair proposals EFORT Open Rev. 2 332–42

[93] Boileau P, Brassart N, Watkinson D J, Carles M, Hatzidakis A M and Krishnan S G 2005 Arthroscopic repair of full-thickness tears of the supraspinatus: Does the tendon really heal? J. Bone Jt. Surg. - Ser. A 87 1229–40

[94] Milgrom C, Schaffler M, Gilbert S and van Holsbeeck M 1995 Rotator-cuff changes in asymptomatic adults. The effect of age, hand dominance and gender. J. Bone Jt. Surg. 77 296–8

[95] Sørensen A K B, Bak K, Krarup A L, Thune C H, Nygaard M, Jørgensen U, Sloth C and Torp- Pedersen S 2007 Acute rotator cuff tear: Do we miss the early diagnosis? A prospective study showing a high incidence of rotator cuff tears after shoulder trauma J. Shoulder Elb. Surg. 16 174–80

[96] Yamaguchi K, Ditsios K, Middleton W D, Hildebolt C F, Galatz L M and Teefey S A 2006 The Demographic and Morphological Features of Rotator Cuff Disease. A Comparison of Asymptomatic and Symptomatic Shoulders J Bone Jt. Surg Am 88 1699–704

[97] Fu S C, Chan B P, Wang W, Pau H M, Chan K M and Rolf C G 2002 Increased expression of matrix metalloproteinase 1 (MMP1) in 11 patients with patellar tendinosis Acta Orthop. Scand. 73 658–62

[98] Riley G P, Curry V, DeGroot J, Van El B, Verzijl N, Hazleman B L and Bank R A 2002 Matrix metalloproteinase activities and their relationship with collagen remodelling in tendon pathology Matrix Biol. 21 185–95

[99] Järvinen M, Józsa L, Kannus P, Järvinen T L N, Kvist M and Leadbetter W 2007 Histopathological findings in chronic tendon disorders Scand. J. Med. Sci. Sports 7 86–95

[100] Józsa L, Réffy A, Kannus P, Demel S and Elek E 1990 Pathological alterations in human tendons Arch. Orthop. Trauma Surg. 110 15–21

[101] Tuoheti Y, Itoi E, Pradhan R L, Wakabayashi I, Takahashi S, Minagawa H, Kobayashi M, Okada K and Shimada Y 2005 Apoptosis in the supraspinatus tendon with stage II subacromial impingement J. Shoulder Elb. Surg. 14 535–41

[102] Yuan J, Murrell G A C, Wei A Q and Wang M X 2002 Apoptosis in rotator cuff tendonopathy J. Orthop. Res. 20 1372–9

[103] Yuan J, Wang M X and Murrell G A C 2003 Cell death and tendinopathy Clin. Sports Med. 22 693–701

[104] Lavagnino M and Arnoczky S P 2005 In vitro alterations in cytoskeletal tensional homeostasis control gene expression in tendon cells J. Orthop. Res. 23 1211–8

[105] Rawson S, Cartmell S and Wong J 2013 Suture techniques for tendon repair; a comparative review Muscles. Ligaments Tendons J. 3 220–8

[106] Cao Y and Tang J B 2010 A new variant of four-strand tendon repairs J. Hand Surg. (European Vol. 35 512–3

[107] Wada A, Kubota H, Miyanishi K, Hatanaka H, Miura H and Iwamoto Y 2001 Comparison of postoperative early active mobilization and immobilization in vivo utilising a four-strand flexor tendon repair J. Hand Surg. Am. 26 B 301–6

[108] Pennington D G 1979 The locking loop tendon suture Plast. Reconstr. Surg. 63 648–52

[109] Hatanaka H, Zhang J and Manske P R 2000 An in vivo study of locking and grasping techniques using a passive mobilization protocol in experimental animals J. Hand Surg. Am. 25 260–9

[110] Lee H 1990 Double loop locking suture: A technique of tendon repair for early active mobilization Part II: Clinical experience J. Hand Surg. Am. 15 953–8

[111] Wu Y F, Cao Y, Zhou Y L and Tang J B 2011 Biomechanical comparisons of four-strand tendon repairs with double-stranded sutures: Effects of different locks and suture geometry J. Hand Surg. Eur. Vol. 36 34–9

[112] Strickland J W 2000 Development of Flexor Tendon Surgery : Twenty-Five Years J. Hand Surg. Am. 25A 214–35

[113] Malahias M, Chytas D, Nakamura K, Raoulis V, Yokota M and Nikolaou V S 2018 A Narrative Review of Four Different New Techniques in Primary Anterior Cruciate Ligament Repair: " Back to the Future " or Another Trend ? Sport. Med. 4 1–12

[114] Achtnich A, Herbst E, Forkel P, Metzlaff S, Sprenker F, Imhoff A B and Petersen W 2016 Acute Proximal Anterior Cruciate Ligament Tears : Versus Anatomic Single-Bundle Reconstruction Arthrosc. J. Arthrosc. Relat. Surg. 1–8

[115] Bieri K S, Scholz S M, Kohl S, Aghayev E and Staub L P 2017 Dynamic intraligamentary stabilization versus conventional ACL reconstruction: A matched study on return to work Injury 48 1243–8

[116] Smith J O, Yasen S K, Palmer H C, Lord B R, Britton E M and Wilson A J 2016 Paediatric ACL repair reinforced with temporary internal bracing Knee Surgery, Sport. Traumatol. Arthrosc. 24 1845–51

[117] Moshiri A and Oryan A 2013 Tendon and Ligament Tissue Engineering, Healing and Regenerative Medicine J. Sports Med. Doping Stud. 3 1–18

[118] Oryan A, Moshiri A and Meimandi-Parizi A 2013 Graft selection in ACL reconstructive surgery: Past, present, and future Curr. Orthop. Pract. 24 321–33

[119] Moshiri A and Oryan A 2012 Role of tissue engineering in tendon reconstructive surgery and regenerative medicine: Current concepts, approaches and concerns Hard Tissue 1 1–11

[120] Beals T C, Severson E P, Kinikini D and Aoki S 2010 Complex achilles reconstruction for massive soft tissue loss: Allograft, autograft, and use of a temporary cement spacer J. Orthop. Trauma 24 e78–80

[121] Park Y-S and Sung K-S 2012 Surgical Reconstruction of Chronic Achilles Tendon Ruptures Using Various Methods Orthopedics 35 213–8

[122] Maffulli N, Spiezia F, Testa V, Capasso G, Longo U G and Denaro V 2012 Free gracilis tendon graft for reconstruction of chronic tears of the Achilles tendon J. Bone Jt. Surg. - Ser. A 94 906–10

[123] Cornwell K G, Landsman A and James K S 2009 Extracellular Matrix Biomaterials for Soft Tissue Repair Clin. Podiatr. Med. Surg. 26 507–23

[124] O'Brien F J 2011 Biomaterials & scaffolds for tissue engineering Mater. Today 14 88–95

[125] Beldjilali-Labro M, Garcia Garcia A, Farhat F, Bedoui F, Grosset J-F, Dufresne M and Legallais C 2018 Biomaterials in Tendon and Skeletal Muscle Tissue Engineering: Current Trends and Challenges Materials (Basel). 11 1116

[126] Brennan D A, Conte A A, Kanski G, Turkula S, Hu X, Kleiner M T and Beachley V 2018 Mechanical Considerations for Electrospun Nanofibers in Tendon and Ligament Repair Adv. Healthc. Mater. 1701277 1–31

[127] O'Connor R A and McGuinness G B 2016 Electrospun nanofibre bundles and yarns for tissue engineering applications: A review Proc. Inst. Mech. Eng. Part H J. Eng. Med. 230 987–98

[128] Chen J, Xu J, Wang A and Zheng M 2014 Scaffolds for tendon and ligament repair: review of the efficacy of commercial products Expert Rev. Med. Devices 6 61–73

[129] Hunter J M, Singer D I, Jaeger S H and Mackin E J 1988 Active tendon implants in flexor tendon reconstruction J. Hand Surg. Am. 13 849–59

[130] Kain C C, Manske P R, Reinsel T E, Rouse A M and Peterson W W 1988 Reconstruction of the digital pulley in the monkey using biologic and nonbiologic materials J. Orthop. Res. 6 871–7

[131] Wredmark T and Engström B 1993 Five-year results of anterior cruciate ligament reconstruction with the Stryker Dacron high-strength ligament Knee Surgery, Sport. Traumatol. Arthrosc. 1 71–5

[132] Miller M D, Peters C L and Allen B 2006 Early Aseptic Loosening of a Total Knee Arthroplasty Due to Gore-Tex Particle-Induced Osteolysis J. Arthroplasty 21 765–70

[133] Debnath U K, Fairclough J A and Williams R L 2004 Long-term local effects of carbon fibre in the knee Knee 11 259–64

[134] Guidoin M F, Marois Y, Bejui J, Poddevin N, King M W and Guidoin R 2000 Analysis of retrieved polymer fiber based replacements for the ACL Biomaterials 21 2461–74

[135] Muren O, Dahlstedt L, Brosjö E, Dahlborn M and Dalén N 2005 Gross osteolytic tibia tunnel widening with the use of Gore-Tex anterior cruciate ligament prosthesis: A radiological, arthrometric and clinical evaluation of 17 patients 13-15 years after surgery Acta Orthop. 76 270–4

[136] Sezhian N, Rimal D, Lawrence K and Suresh G 2007 Squamous cell carcinoma of the bladder following PTFE implantation Urol. Int. 79 90–1

[137] Hirooka A, Yoneda M, Wakaitani S, Isaka Y, Hayashida K, Fukushima S and Okamura K 2002 Augmentation with a Gore-Tex patch for repair of large rotator cuff tears that cannot be sutured J. Orthop. Sci. 7 451–6

[138] Kollender Y, Bender B, Weinbroum A A, Nirkin A, Meller I and Bickels J 2004 Secondary reconstruction of the extensor mechanism using part of the quadriceps tendon, patellar retinaculum, and gore-tex strips after proximal tibial resection J. Arthroplasty 19 354–60

[139] Ibrahim S A R, Ahmad F H F, Salah M, Al Misfer A R K, Ghaffer S A and Khirat S 2008 Surgical Management of Traumatic Knee Dislocation Arthrosc. - J. Arthrosc. Relat. Surg. 24 178–87

[140] Dominkus M, Sabeti M, Toma C, Abdolvahab F, Trieb K and Kotz R I 2006 Reconstructing the extensor apparatus with a new polyester ligament Clin. Orthop. Relat. Res. 328–34

[141] Talbot M, Berry G, Fernandes J and Ranger P 2004 Knee dislocations: Experience at the Hôpital du Sacré-Coeur de Montréal Can. J. Surg. 47 20–4

[142] Brunet P, Charrois O, Degeorges R, Boisrenoult P and Beaufils P 2005 [Reconstruction of acute posterior cruciate ligament tears using a synthetic ligament]. Rev. Chir. Orthop. Reparatrice Appar. Mot. 91 34

[143] Lavoie P, Fletcher J and Duval N 2000 Patient satisfaction needs as related to knee stability and objective findings after ACL reconstruction using the LARS artificial ligament Knee 7 157–63

[144] Trieb K, Blahovec H, Brand G, Sabeti M, Dominkus M and Kotz R 2004 In vivo and in vitro cellular ingrowth into a new generation of artificial ligaments Eur. Surg. Res. 36 148–51

[145] Matsumoto H and Fujikawa K 2001 Leeds–Keio artificial ligament: a new concept for the anterior cruciate ligament reconstruction of the knee. Keio J. Med. 50 161–6

[146] Engstrom B, Wredmark T and Westblad P 1993 Patellar tendon or Leeds-Keio graft in the surgical treatment of anterior cruciate ligament ruptures. Intermediate results. Clin. Orthop. Relat. Res. 190–7

[147] Denti M, Bigoni M, Dodaro G, Monteleone M and Arosio A 1995 Long-term results of the Leeds-Keio anterior cruciate ligament reconstruction. Knee Surg. Sports Traumatol. Arthrosc. 3 75–7

[148] Ochi M, Yamanaka T, Sumen Y and Ikuta Y 1993 Arthroscopic and histologic evaluation of anterior cruciate ligaments reconstructed with the Leeds-Keio ligament Arthrosc. J. Arthrosc. Relat. Surg. 9 387–93

[149] Rading J and Peterson L 1995 Clinical Experience with the Leeds-Keio Artificial Ligament in Anterior Cruciate Ligament Reconstruction: A Prospective Two-Year Follow-up Study Am. J. Sports Med. 23 316–9

[150] Macnicol M F, Penny D and Sheppard L 1991 Early results of the Leeds–Keio anterior cruciate ligament replacement. J. Bone Jt. Surg. 73–B 377–80

[151] Murray A W and Macnicol M F 2004 10–16 year results of Leeds-Keio anterior cruciate ligament reconstruction Knee 11 9–14

[152] Matsumoto H, Toyoda T, Kawakubo M, Otani T, Suda Y and Fujikawa K 1999 Anterior cruciate ligament reconstruction and physiological joint laxity: Earliest changes in joint stability and stiffness after reconstruction J. Orthop. Sci. 4 191–6

[153] Kobayashi M, Nakagawa Y, Suzuki T, Okudaira S and Nakamura T 2006 A Retrospective Review of Bone Tunnel Enlargement After Anterior Cruciate Ligament Reconstruction With

Hamstring Tendons Fixed With a Metal Round Cannulated Interference Screw in the Femur Arthrosc. - J. Arthrosc. Relat. Surg. 22 1093–9

[154] Tanaka N, Sakahashi H, Hirose K, Ishima T and Ishii S 2006 Augmented subscapularis muscle transposition for rotator cuff repair during shoulder arthroplasty in patients with rheumatoid arthritis J. Shoulder Elb. Surg. 15 2–6

[155] Toms A D, Smith A and White S H 2003 Analysis of the Leeds-Keio ligament for extensor mechanism repair: Favourable mechanical and functional outcome Knee 10 131–4

[156] Nomura E, Horiuchi Y and Kihara M 2000 A mid-term follow-up of medial patellofemoral ligament reconstruction using an artificial ligament for recurrent patellar dislocation Knee 7 211–5

[157] Sherief T I, Naguib A M and Sefton G K 2005 Use of Leeds-Keio Connective Tissue Prosthesis (L-K CTP) for reconstruction of deficient extensor mechanism with total knee replacement Knee 12 319–22

[158] Nomura E, Inoue M and Sugiura H 2005 Histological evaluation of medial patellofemoral ligament reconstructed using the Leeds-Keio ligament prosthesis Biomaterials 26 2663–70

[159] Akali A U and Niranjan N S 2008 Management of bilateral Achilles tendon rupture associated with ciprofloxacin: A review and case presentation J. Plast. Reconstr. Aesthetic Surg. 61 830–4

[160] Fujishiro T, Nishikawa T, Takikawa S, Saegusa Y, Yoshiya S and Kurosaka M 2003 Reconstruction of the iliofemoral ligament with an artificial ligament for recurrent anterior dislocation of total hip arthroplasty J. Arthroplasty 18 524–7

Chapter 2: Biofabrication of electrospun scaffolds for the regeneration of tendons and ligaments

Alberto Sensini[1], Luca Cristofolini[1, 2]

1 Department of Industrial Engineering, School of Engineering and Architecture, Alma Mater Studiorum—Università di Bologna, 40131 Bologna, Italy; alberto.sensini2@unibo.it

2 Health Sciences and Technologies—Interdepartmental Center for Industrial Research (HST-ICIR), Alma Mater Studiorum—Università di Bologna, 40064 Ozzano dell'Emilia, Bologna, Italy

Keywords: Electrospinning; Tendons and Ligaments; Scaffolds; Biofabrication; Hierarchical Structure; Non-Linear Mechanical Properties.

The candidate was the main investigator of the study. This work was published on MDPI Materials 2018, 11(10), 1963. Reproduced under the terms and conditions of the Creative Common Attribution (CC BY 4.0.)

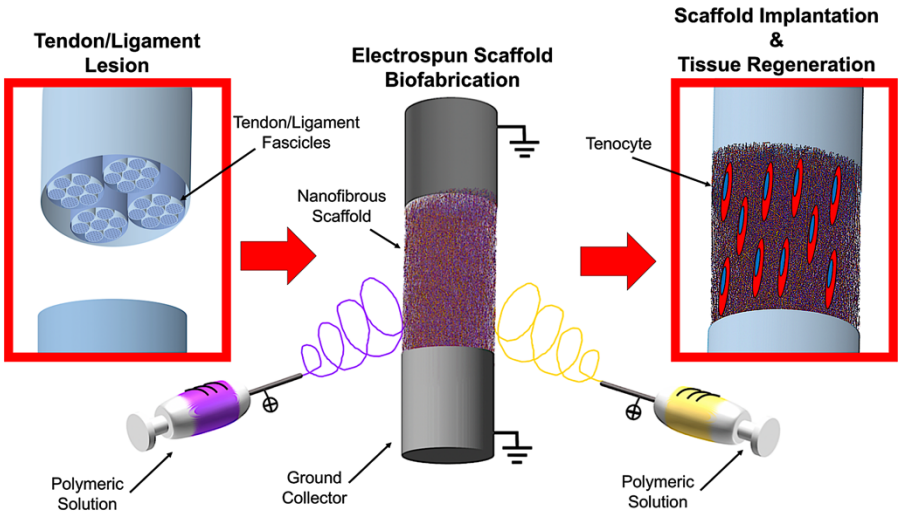

Graphical abstract of the work.

Published in: MDPI Materials 12 October 2018

2.1 Abstract

Tendon and ligament tissue regeneration and replacement are complex since scaffolds need to guarantee an adequate hierarchical structured morphology, and non-linear mechanical properties. Moreover, to guide the cells' proliferation and tissue re-growth, scaffolds must provide a fibrous texture mimicking the typical of the arrangement of the collagen in the extracellular matrix of these tissues. Among the different techniques to produce scaffolds, electrospinning is one of the most promising, thanks to its ability to produce fibers of nanometric size. This manuscript aims to provide an overview to researchers approaching the field of repair and regeneration of tendons and ligaments. To clarify the general requirements of electrospun scaffolds, the first part of this manuscript presents a general overview concerning tendons' and ligaments' structure and mechanical properties. The different types of polymers, blends and particles most frequently used for tendon and ligament tissue engineering are summarized. Furthermore, the focus of the review is on describing the different possible electrospinning setups and processes to obtain different nanofibrous structures, such as mats, bundles, yarns and more complex hierarchical assemblies. Finally, an overview concerning how these technologies are exploited to produce electrospun scaffolds for tendon and ligament tissue applications is reported together with the main findings and outcomes.

2.2 Introduction

In the last three decades the topic of tissue regeneration is getting extreme attention in the orthopedic research field [1–3]. The use of scaffolds allows driving cells to proliferate and regenerate tissues in specific directions [4]. This property is fundamental to produce devices able to guide cells to the regeneration of the collagen anisotropy in the musculoskeletal tissues, such as tendons or ligaments [5–7]. In fact, due to the low vascularization, the hypocellularity, the anisotropy and the non-linear mechanical properties of these tissues, natural tendon and ligament regeneration is particularly complex [8]. Among the various techniques proposed in the literature to produce scaffolds, electrospinning, and its ability to produce

nanofibers, is definitely one of the most promising for tendon and ligament tissue engineering. Several works are published annually on this topic, presenting electrospun scaffolds with increasingly improved biomimicry and enhanced cellular response [9–11].

The aim of this review is to analyze methods to build electrospun scaffolds for the regeneration of tendons and ligaments, and to illustrate the most promising applications. This review is conceived to give a general background of the main electrospinning setups to produce and collect nanofibers, and then to focus on the applications to produce scaffolds for tendon and ligament tissue engineering.

2.3 Methods of the literature search and review

A systematic search using ScienceDirect, Scopus, PubMed and Google Scholar and Google Patents databases was performed until March–July 2018. Papers relevant to the electrospinning methodologies to produce scaffolds and their applications related to tendons and ligaments regeneration and replacement, published between 1990 and 31 July 2018, were selected:

- The following search string was used to retrieve the manuscripts presenting equipment and techniques to produce electrospun scaffolds: "electrospinning AND (review OR technique OR setup OR production process OR equipment OR methods OR scaffold production OR scaffold manufacturing)".
- The following search string was used to retrieve the manuscripts presenting applications of electrospun scaffolds for regeneration and replacement of tendons and ligaments: "electrospinning AND (review OR regeneration OR repair OR tendon OR ligament OR bone OR muscle OR insertion)".

Moreover, to find additional papers possibly missed through the database searches, the list of citations from every paper was scanned. The title, abstract and main text of each work were examined, and only the papers truly relevant for this review were cited and incorporated. Inclusion criteria were manuscripts in English reporting electrospun scaffolds designed for tendon and ligament tissue regeneration and replacement applications.

The different electrospinning techniques listed in the Section 5 “Equipment and Techniques to Produce Electrospun Scaffolds” were divided into seven categories: mats of nanofibers and multilayered scaffolds, short and finite length bundles and yarns, continuous bundles, continuous yarns, tubes and conduits, textiles of nanofibers, multiscale hierarchical scaffolds.

For each paper of the Section 6 “Applications for Tendon and Ligament Regeneration and Replacement,” the materials used, the specific application, manufacturing methods and principal outcomes of the work are summarized. The papers are divided into six main categories and six subcategories: preliminary studies on electrospun materials (flat electrospun mats, multilayered and co-electrospun scaffolds), patches and augmentation grafts (patches, augmentation grafts), multiscale hierarchical scaffolds for massive replacement (fascicle inspired bundles and yarns, hierarchically structured scaffolds), bone insertion, muscle insertion, and tendon and ligament healing and anti- adhesion. Finally, in vitro studies are reported for each category and subcategory, followed by the in vivo applications.

2.4 Tendons and ligaments: properties and replacement

2.4.1 Morphological and mechanical properties of tendons and ligaments

To design scaffolds able to properly regenerate tendon and ligament tissues, it is mandatory to start by analyzing tendons and ligaments morphology and mechanical properties.

Despite the different physiological functions (connection and load transfer between a bone and a muscle (tendon) and between two bones (ligament)), and the different morphologies (depending also on the anatomical site), tendons and ligaments have similar composition and hierarchical structure [12,13].

Tendons and ligaments are filamentous collagen structures, composed approximately by an 80% of extracellular matrix. The remaining 20% are cells (fibroblasts or tenocytes), arranged in rows between the collagen fibers [14,15].

Approximately 70% of the total extracellular matrix is composed by water and the remaining 30% of solid material [15]. Collagen accounts for 70–80% of the dry weight of tendons and ligaments and Type I collagen accounts for 60–85% of the total collagen [12,14]. Type I collagen confers stiffness and strength to the tissue but other types of collagen exist in minor amounts, namely Type III, V, X, XI, XII and XIV collagens [12,14]. Type V collagen has been associated to Type I collagen in the regulation of the collagen fibril diameter while Type III collagen is functionalized in tendon repair. Type XII collagen is present in the surface of fibrils and bonds them with other matrix components such as decorin and fibromodulin [14]. The remaining part is composed by the ground substance (non-fibrous component of the matrix), basically comprised of hyaluronan, glycoproteins, and proteoglycans, and modulates tissue metabolism, provides shock absorption, decreases internal friction between collagen fibers, and binds water [15].

Morphologically speaking, tendons and ligaments are composed of a complex hierarchical structure of collagen fibrils, axially aligned with the tendon/ligament and connected to each other in different levels of aggregation (Figure 2.1). There is no standard nomenclature for aggregations of collagen fibrils within the tendon, perhaps due to their great variability depending on the function and the anatomical site [6]. The basic unit of tendons and ligaments is tropocollagen molecule, which is a long, thin protein produced inside a cell (e.g., fibroblast) and secreted into extracellular matrix as procollagen [16]. Tropocollagen molecules aggregation produce the collagen fibril, which is the smallest structural unit of the tendon and ligament tissue. The diameter of the fibrils ranges 10–500 nm, depending on species, age, and anatomical location [16]. A bunch of collagen fibrils forms a collagen fiber [6]. A bunch of collagen fibers forms a primary fiber bundle (sub-fascicle), and a group of primary fiber bundles forms a secondary fiber bundle (fascicle). A group of secondary fascicles, in turn, forms a tertiary bundle, and the tertiary bundles make up the tendon, which is surrounded by the epitenon/epiligament [6]. The structures from fibers to tertiary fiber bundles are surrounded by a thin collagen membrane called endotenon/endoligament, containing blood vessels, lymphatics and nerves [5,6,16].

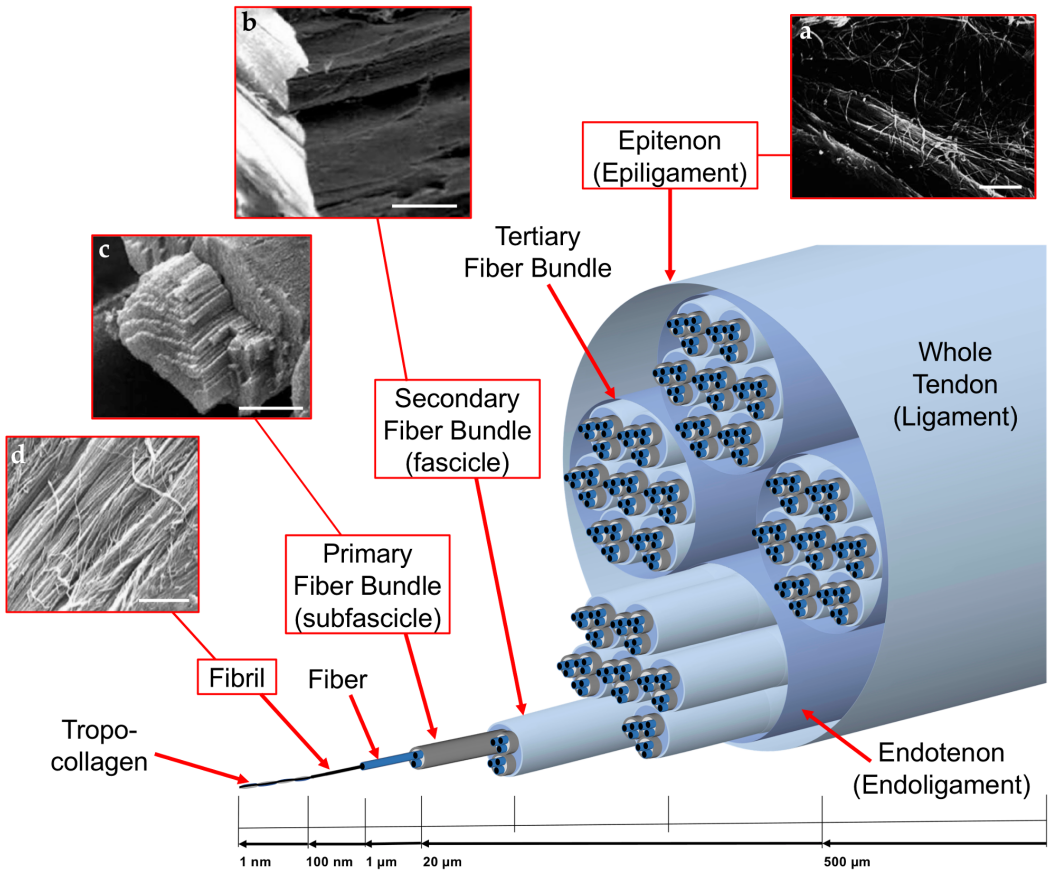

Figure 2.1. Hierarchical arrangement of the collagen of tendons and ligaments: (a) Scanning electron microscopy (SEM) of epitenon collagen fibrils (scale bar = 2 micrometers, adapted from Kannus et al. [6], reproduced with permission. Copyright 2008, John Wiley and Sons.); (b) SEM image of a collagen fascicle (scale bar = 100 micrometers); (c) SEM image of a collagen bundle (scale bar = 45 micrometers); and (d) SEM image of collagen fibrils (scale bar = 1.8 micrometers). (b–d) SEM images adapted from Moshiri et al. [17], reproduced with permission under the terms of the CC BY 4.0 license. Copyright 2013, OMICS Publishing Group.

This rope-like hierarchical structure confers to tendons and ligaments typical non-linear mechanical properties (Figure 2.2) [7,18,19]. When a load is applied to a tendon or ligament, the collagen fibers, which are crimped at rest (crimping angle depending on different tendons/ligaments), start to align with each other losing the crimped behavior until 2% of strain (toe region). Due to the load transfer function of the tendons, the toe region of their stress–strain plot is quite short (2–5%), and similar in each tendon of the human body. Conversely, ligaments must allow different range of motions in different joints, and consequently show wider ranges of strain for the toe region depending on the different anatomical sites (anterior

cruciate ligament: 4%; spine ligaments: 10–40% [15,20–22]). In the linear region of the stress–strain plots, the fibers of collagen are straightened and provide a quite ideal elastic recovery, if load is removed. After the linear region, the fibers progressively start sliding with respect to each other. This event is followed by progressive failure of the fibers, until complete failure of the tendon or ligament [14,16,18,19]. The mechanical properties are strongly related to the cross-section and function of the particular tendon or ligament of the body and from the strain rate with which the load is applied [7,15]. For example, the range of failure stresses may vary in tendons from the 24–69 MPa of the patellar to the 112 MPa of the gracilis, and in ligaments from the 1–15 MPa of the flavum to the 24–46 MPa of the lateral collateral [15]. Moreover, the nature of the weak bonds of collagen and the presence of water are responsible for the viscoelasticity of tendons and ligaments [7,15].

Considering these common morphological and mechanical characteristics, scaffolds for tendon and ligament tissue regeneration are often quite similar in their structure and properties.

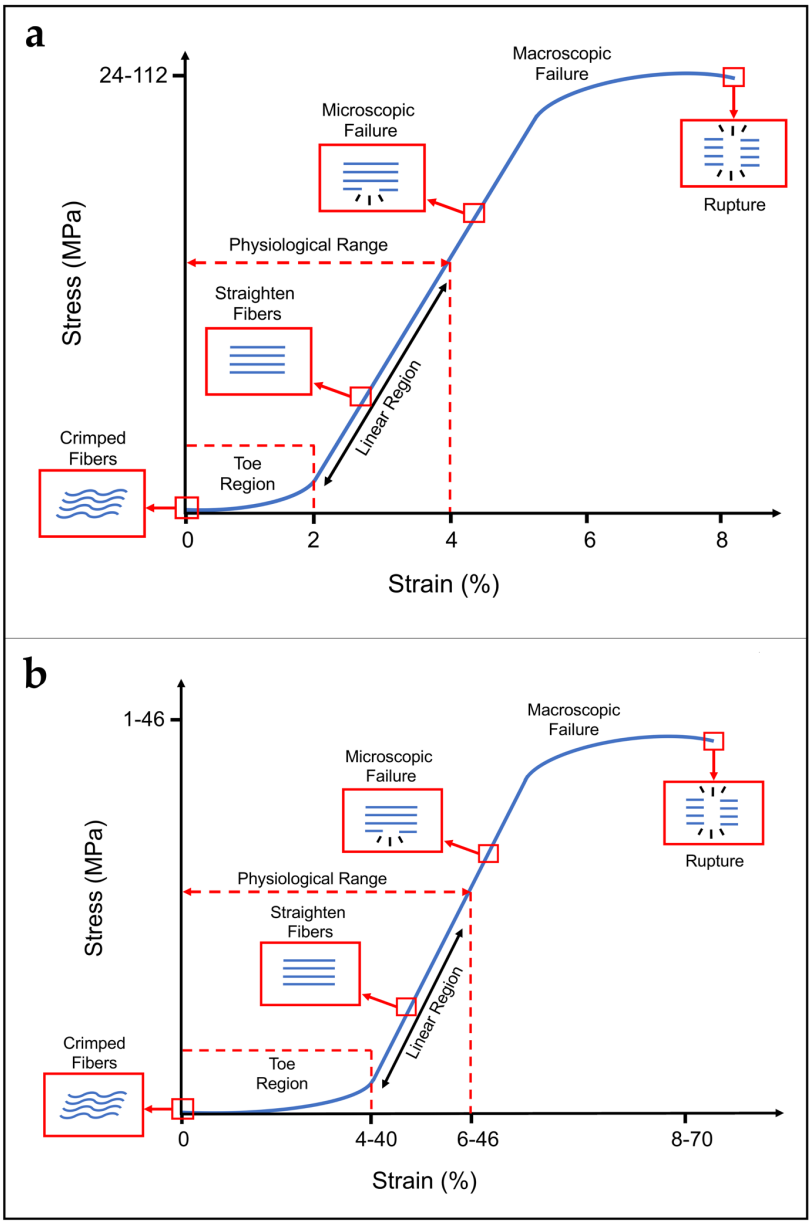

Figure 2.2. Typical stress–strain curve and schematization of the behavior of the collagen fibers for: (a) tendons; and (b) ligaments. Typical ranges of stress and strain are indicated on the x and y axes.

2.4.2 Generic requirements of scaffolds for tendon and ligament regeneration

Considering the morphology and the biomechanical properties of tendons and ligament previously described, the general requirements for a scaffold for the regeneration of these tissues are listed below [23,24]:

1. Biocompatibility: Scaffolds must be biocompatible and made of natural or synthetic materials. This encourages the cells to grow, infiltrate and proliferate on and into the scaffolds, reproducing the physiological collagen. Biocompatibility is also fundamental to prevent and minimize inflammatory phenomena which could compromise the regenerative process [17,23–25].
2. Biodegradability: Scaffolds need to be progressively degraded by cells and body fluids. Therefore, they must be properly engineered to permit that the degradation rate could allow cells to reproduce the natural collagen without being resorbed too fast. Moreover, the products of the degradation must not produce any inflammatory or toxic effects to cells and their surrounding tissues [17,23–25].
3. Mechanical Properties: To permit a correct replacement of the site of the lesion, cells have to feel the physiological stiffness of the substrate, and experience physiological levels of strain, and also have to be stimulated to reproduce collagen and proliferate [17,25,26]. For these reasons, the scaffolds need to be designed to provide mechanical properties in the range of the specific tendon or ligament. However, to prevent damages of the surrounding tissues after the suture in the site of the lesion, scaffolds must be less stiff and less strong compared with the host tendon or ligament. Finally, a degree of ductility before the nominal failure load is required to prevent an unexpected and abrupt failure of the scaffolds in case of an overload.
4. Morphology: Tendons and ligaments are composed of nanometric and axially aligned collagen fibrils connected in different hierarchical levels. A scaffold designed for tendon and ligament tissue regeneration needs to be produced with the same philosophy. In fact, fiber- like scaffolds permit cells to grow, attach and reproduce the collagen following the direction of alignment of the fibers, contributing to confer tendons' and ligaments' morphology and mechanical properties to the regenerated tissue.
5. Porosity: Scaffolds also need to be porous to allow the cells' infiltration [17,24–26]. Interconnected networks of porosities are essential for cell nutrition, proliferation, and migration for tissue vascularization and

formation of new tissues [27,28]. A porous network structure assists in guiding and promoting new tissue formation [29,30]. Materials with high porosity allow releasing biofactors such as proteins and genes, providing good substrates for nutrient exchange between the cells [31].

For these reasons, among the various techniques to regenerate and replace tendons and ligaments [14,26,32], electrospinning is one of the most promising techniques to develop scaffolds for tendon and ligament tissue engineering.

2.5 The electrospinning technique: an introduction

2.5.1 Electrospinning operating principles

Electrospinning technology is an electrically-driven method to produce fibers of nanometric or micrometric diameter. Electrospinning was invented in the early twentieth century [33], and it has attracted a lot of attention in the last three decades in the field of tissue engineering, thanks to its ability to mimic the extracellular matrix [34–37]. The formation of nanofibers through electrospinning is based on the uniaxial stretching of a viscoelastic solution [38]. The process requires only a few elements: a syringe charged with a polymeric solution provided with a metallic needle, a syringe pump, a high voltage power supply and a collector, generally at ground potential (Figure 2.3). In the electrospinning process, a high voltage is used to create an electrically charged jet of polymer micro- or nanofibers by the syringe [39]. When the solution is slowly pumped out of the needle tip through the spinneret, it forms a spherical droplet driven by surface tension. As the droplet is connected to the high voltage power supply, its surface will be quickly covered by charges of the same sign. The repulsion among these charges destabilizes the spherical shape. When the repulsion is strong enough to overcome the surface tension, the droplet deforms into a conical shape (called Taylor cone), and a jet will emanate from the apex of the cone [40]. The repulsive forces, generated by the charges on the surface of the fibers, cause the whipping of the liquid jet towards the collector. This whipping motion induces the polymer chains inside of the solution to stretch and slide past each other. The result of this process consists in the creation

of fibers with small enough diameters to be called nanofibers [41]. The distance between needle and collector is important to determine the morphology of the electrospun nanofiber, and depends on the polymeric solution. In general, large-diameter nanofibers are formed when the distance is small, whereas the diameter decreases as the distance is increased [41–44]. The solvent system plays a key role to prevent the formation of undesirable beads. Highly volatile solvents must be avoided because their low boiling points and high evaporation rates cause the drying of the jet at the needle tip, blocking the electrospinning process. Less volatile solvents must be avoided too, because their high boiling points prevents suitable drying of the nanofiber jet flight. The deposition of solvent-containing nanofibers on the collector will cause the formation of beaded nanofibers [45,46]. The conductivity and dipole moment of the solvents are also important [41,47].

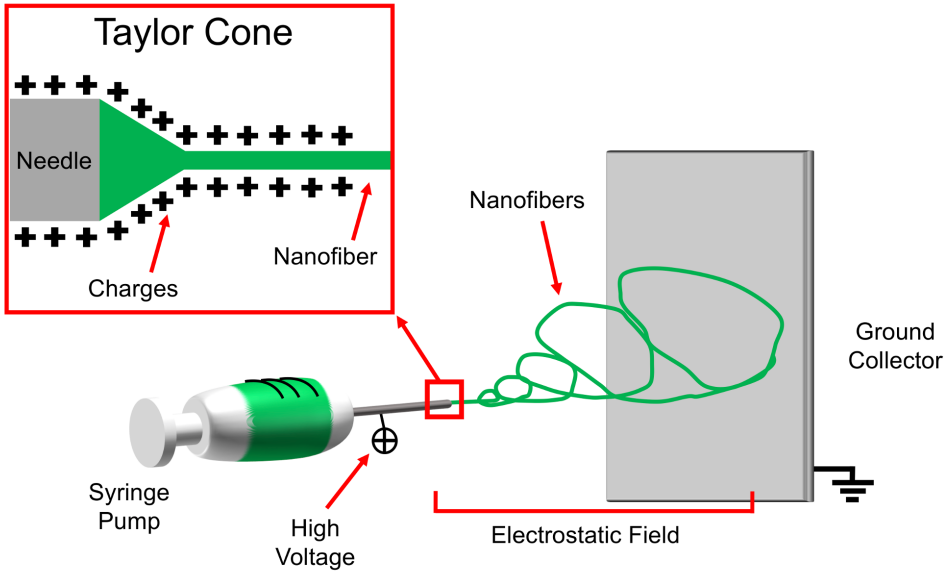

Figure 2.3. Electrospinning operating principle and Taylor cone formation.

The electrospinning process is strongly dependent on three families of parameters [41]:

1. Solution parameters: Polymers and solvents, viscosity, conductivity of solvents and polymers, and concentration of the polymers.

2. Electrospinning parameters: Flow rate of the pump, diameter and shape of the needle, applied voltage, distance between the needle and the collector, and shape and movement of the collector.
3. Environmental parameters: Temperature and relative humidity.

Tuning properly the combination of all these parameters, it is possible to tune the final morphology, cross-section and orientation of the nanofibers produced [38–41,48]. Due to its ability to produce nanofibers, even made of resorbable materials, with a morphology similar to the one of collagen fibrils of tendons and ligaments, electrospinning is very promising for the regeneration and replacement of these tissues [9,10]. Electrospinning is also suitable to produce scaffolds that are able to reproduce the typical non-linear toe region and the biomechanical properties of tendons and ligaments [10].

2.5.2 Materials for tendon and ligament tissue regeneration

The use of suitable materials is fundamental for scaffolds that have to regenerate and replace tendon and ligament tissue. A wide range of both resorbable and non-resorbable polymers, to produce electrospun nano- and microfibers for tendon and ligament applications, can be found [9,10,14]. In particular, natural or synthetic bioresorbable materials are indicated for young patients or sport athletes due to their faster cellular and metabolic activity [49]. Conversely, non-resorbable (inert) materials are preferred for tendon and ligament replacement in elderly patients, because of their lower cellular activity and metabolic responses [26]. In fact, it is well established that the mechanical properties of tendons and ligaments decrease according to the age of the patients and tend to become stiffer [50–52].

A wide range of natural or synthetic biopolymers is investigated for tendon and ligament tissue regeneration and replacement applications by means of electrospinning (Table 2.1). In some cases, nanofibers are also electrospun from polymers blends, or in a core–shell configuration (Table 2.2). Finally, even the possibility of loading nanofibers with different natural or synthetic nanoparticles or drugs is widely exploited (Table 2.3).

Table 2.1. Materials used in combination with electrospinning processes, in tendon and ligament tissue engineering.

Acronym	Extended Name	Application	References
P(LLA-CL)	Poly(L-lactide-co-ε-caprolactone)	Tendon/Ligament	[53]
		Ligament	[54]
		Tendon	[55,56]
PDLLA	Poly(D,L-lactic acid)	Ligament	[57]
PLDLA	Poly(L-lactide-co-D,L-lactic acid)	Ligament	[57]
PLLA	Poly(L-lactic acid)	Tendon/Ligament	[58–61]
		Ligament	[57]
		Tendon	[62–66]
		Ligament-to-Bone Interface	[67]
		Tendon-to-Muscle Interface	[68]
		Tendon Anti-Adhesion	[69–71]
PELA	Poly(L-lactic acid)-poly(ethylene glycol)	Tendon Anti-Adhesion	[72,73]
PDLLGA	Poly(D,L-lactide-co-glycolic acid)	Ligament	[74]
		Tendon	[75]
PLGA	Poly(lactic-co-glycolic acid)	Tendon/Ligament	[76,77]
		Ligament	[78–80]
		Tendon	[81,82]
		Tendon-to-Bone Interface	[83]
PLLGA	Poly(L-lactic-co-glycolic acid)	Tendon/Ligament	[84]
		Tendon-to-Bone Interface	[85,86]
		Bone-Ligament-Bone	[87]
PCL	Poly(ε-caprolactone)	Tendon/Ligament	[58,88]
		Ligament	[80,89–94]
		Tendon	[82,95–108]
		Tendon/Ligament-to-Bone Interface	[109]
		Ligament-to-Bone Interface	[110,111]
		Tendon-to-Bone Interface	[112]
		Tendon-to-Muscle Interface	[68]
		Tendon Anti-Adhesion	[71,113]
		Bone-Ligament-Bone	[87,114]
PCLDLLA	Poly(ε-caprolactone-co-D,L-lactic acid)	Ligament	[115]
PU	Poly(urethane)	Ligament	[79,116,117]
		Tendon	[118]
PEUR	Poly(ester urethane)	Ligament	[80]
PEUUR	Poly(ester urethane urea)	Tendon/Ligament	[119]
		Ligament	[74,78]
		Ligament-to-Bone Interface	[111]
PEUUR2000	Poly(ester urethane urea) elastomer	Ligament-to-Bone Interface	[110]
BPUR10	Biodegradable Poly(urethane urea) 10	Tendon-to-Bone Interface	[120]
BPUR50	Biodegradable Poly(urethane urea) 50	Tendon-to-Bone Interface	[120]
PEO	Poly(ethylene oxide)	Tendon/Ligament	[121,122]
		Tendon	[63,64,96]
PEGDA	Poly(ethylene glycol diacrylate)	Ligament	[78]
PEDOT	Poly(3,4-ethylenedioxythiophene)	Ligament	[123]
PDO	Poly(dioxanone)	Tendon	[106,124]
PAN	Poly(acrylonitrile)	Tendon	[105]
PVDF-TrFe	Poly(vinylidene fluoride-trifluoro ethylene)	Tendon	[105]
DP	Biodegradable Poly(ester urethane) block copolymer (DegraPol®)	Tendon Anti-Adhesion	[125–127]
P3HB	Poly(3-hydroxybutyrate)	Tendon/Ligament	[88]
Nylon6.6	Nylon 6.6	Tendon/Ligament	[60]
SE	Silk	Ligament	[123]
		Tendon	[128]
		Tendon-to-Bone Interface	[129]
SF	Silk Fibroin	Tendon	[56]
Fibrinogen	Fibrinogen	Tendon/Ligament	[121]
		Tendon/Ligament	[59,60]
Coll	Collagen	Tendon	[55,62,118]
		Tendon-to-Muscle Interface	[68]
CTS	Chitosan	Tendon/Ligament-to-Bone Interface	[109]
		Tendon	[63,97,104,108]
		Tendon Anti-Adhesion	[113]
GT	Gelatin	Tendon	[63]
HA	Hyaluronic acid	Tendon Anti-Adhesion	[70,73,113]
mGLT	Methacrylated Gelatin	Tendon	[100]
Carbothane™ 3575A	Poly(carbonate)-based thermoplastic poly(urethane)	Tendon/Ligament	[130]
MWCNTs	Multi Wallen Carbon Nanotubes	Tendon/Ligament	[130]

Table 2.2. Electrospun blends and core–shell fibers and their applications in tendon and ligament tissue engineering.

Acronym	Type	Application	References
P(LLA-CL)/Coll	Blend	Tendon	[55]
P(LLA-CL)/SF	Blend	Tendon	[56]
PLLA/PCL	Blend	Tendon Anti-Adhesion	[71]
PLLA/MMC	Core–Shell	Tendon Anti-Adhesion	[70]
PLLA/Coll	Blend	Tendon/Ligament	[59,60]
	Core–Shell	Tendon	[62]
	Blend	Tendon-to-Muscle Interface	[68]
PLLA/PEO	Blend	Tendon	[64]
PLLA/PEO/CTS/GT	Blend	Tendon	[63]
PEO/Fibrinogen	Blend	Tendon/Ligament	[121]
PCL/CTS	Blend	Tendon/Ligament-to-Bone Interface	[109]
		Tendon	[104,108]
PCL/Coll	Blend	Tendon-to-Muscle Interface	[68]
PCL/HA	Blend	Tendon Anti-Adhesion	[113]
PCL/PLGA	Blend	Tendon	[82]
PLGA/Coll	Blend	Ligament	[79]
PLGA/PEGDA	Blend	Ligament	[78]
PEUUR/PEGDA	Blend	Ligament	[78]
PEUUR/PCL	Blend	Ligament	[80]
PU/Coll	Blend	Tendon	[118]
PELA/HA	Blend	Tendon Anti-Adhesion	[73]

Table 2.3. Particles and drugs to load electrospun fibers and their applications in tendon and ligament tissue engineering.

Acronym	Extended Name	Application	References
bFGF	Basic Fibroblast Growth Factor	Tendon/Ligament	[76,84]
		Tendon Anti-Adhesion	[69]
		Tendon	[81]
DGNs	Dextran Glassy Nanoparticles	Tendon Anti-Adhesion	[69]
Celecoxib	Selective Non-Steroidal Anti-Inflammatory Drug	Tendon Anti-Adhesion	[72,73]
MMC	Mitomycin-C	Tendon Anti-Adhesion	[70]
TSA	Trichostatin-A	Tendon	[64]
HAp	Hydroxyapatite	Tendon/Ligament-to-Bone Interface	[109]
		Tendon-to-Bone Interface	[85]
		Ligament-to-Bone Interface	[110,111]
		Tendon	[66]
CNCs	Cellulose Nanocrystals	Tendon	[104,108]
CTGF	Connective Tissue Growth Factors	Ligament	[93]
PDGF-BB	Platelet Derived Growth Factor-BB	Tendon	[127]
TP	Tricalcium Phosphate	Tendon-to-Bone Interface	[83,131]
BLM	Biomimetically Prepared Bone-like Mineral	Bone-Ligament-Bone	[114]

2.6 Equipment and techniques to produce electrospun scaffolds for tendon and ligament

The complex multiscale structure composing tendons and ligaments suggests researchers investigate different electrospinning setups for mimicking these kinds of tissues as closely as possible [5–7]. Some of these setups, however, were applied in other research fields before being used for tissue engineering [9,132–134]. In this section, the most common setups and configurations are presented to produce electrospun nanofibers for tendon and ligament tissue regeneration.

2.6.1 Mats of nanofibers and multilayered scaffolds

Electrospun nanofibers are generally collected as nonwoven or randomly arranged structures, due to the "whipping instability" of the electrospinning jet [133]. By electrospinning on a flat ground plate (Figure 2.4a) or on a drum collector rotating at low speed (peripheral speed lower than 8 m/s) (Figure 2.4b), it is possible to obtain mats made by nanofibers with a random configuration [132–134]. Early studies concerning fiber deposition and assembly focus on controlling the fibers' alignment. Aligned nanofibers can be collected by using a dynamic mechanical collector such as a cylindrical drum [135–137]. When the collector rotates at a high peripheral speed, on the order of ≥8 m/s, fibers start to align circumferentially (Figure 2.4c) [133]. It is also possible to align nanofibers by using two split parallel flat plates, also called gap collectors, connected with grounded electrodes (Figure 2.4d) [136–146]. This final collector setup guarantees a high alignment of the nanofibers but is very limited in the final length and thickness of the mat and fibers [9,132–134].

Replacing a classical metal collector with a liquid bath to collect nanofibers is the operating principle of the so-called wet electrospinning (Figure 2.4e). This setup is particularly suitable to increase the pore sizes of the electrospun mats, and remove the residual charge on their surface [147]. Ki et al. and Yokoyama et al. proposed preliminary works to produce mats of nanofibers by electrospinning on liquid baths of methanol and a blend of water and tertiary-butyl alcohol [148,149].

Another method to produce mats of nanofibers, to guide the deposition of the electrospun nanofibers in specific directions, relies on the deposition of specific patterns, for example lines or grids, on the flat plate collector [150] (Figure 2.4f). Zhang et al. proposed different patterns on different metal collector setups producing nanofibrous mats with different patterns organizations [151]. More recently, Nedjari et al. studied different nanofibrous mats obtained by metal flat plate collectors with different superficial patterns on them [152].

Mats nanofibers also present some morphological limitations because, using these techniques, only the planar configuration is possible. The mechanical properties of the electrospun mats increase from a random to an aligned configuration. However,

mats of aligned nanofibers are not suitable to provide adequate yield and failure stress.

Different techniques have been proposed to increase the mechanical properties of the nanofibrous mats, and also to electrospin different materials in the same structure. Kidoaki et al. developed two new different approaches for electrospinning two polymers together. The first is mixing electrospinning (named co-electrospinning), in which two different polymers are simultaneously electrospun from different syringes under special conditions. The polymer fibers are mixed on the same target collector, resulting in the formation of a mixed fiber mesh [153] (Figure 2.4g). The second is multilayering electrospinning that consists of electrospinning layer by layer different polymers on the same collector [153] (Figure 2.4h).

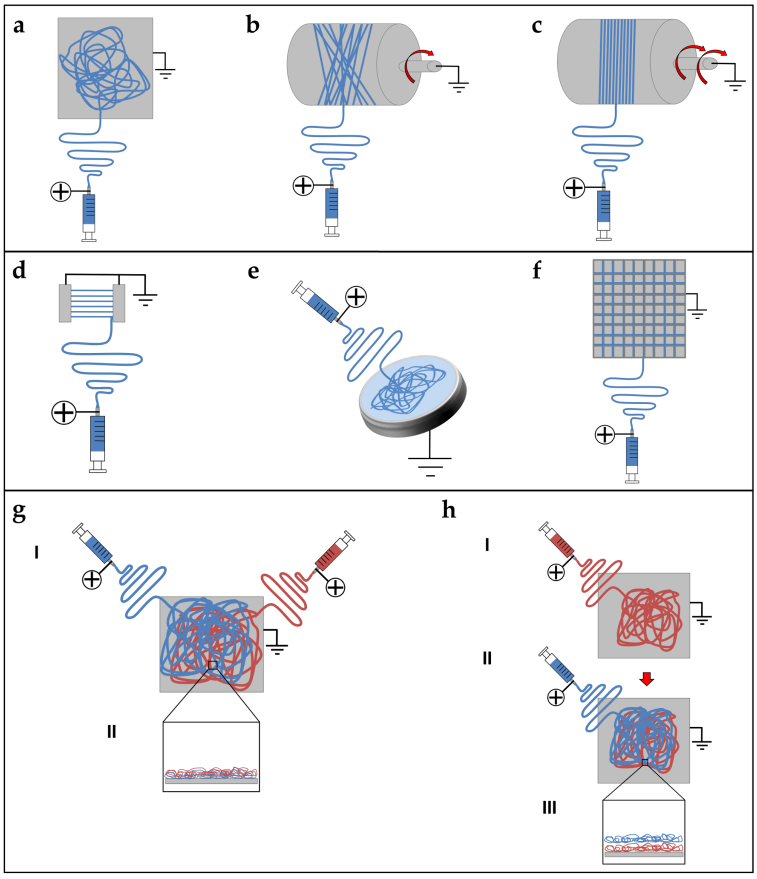

Figure 2.4. Different electrospinning setups to produce mats of nanofibers: (a) flat plate collector; (b) drum collector rotating at low speed, producing random nanofibers; (c) drum collector rotating at high speed, producing aligned nanofibers; (d) gap collector; (e) liquid bath collector; (f) flat plate collector with a grid pattern on the surface; (g) mixing electrospinning or co-electrospinning setup

((I) two syringes electrospin synchronously the solutions on a flat plate collector; and (II) section of the mat with the two different nanofibers mixed together; and (h) multilayering electrospinning setup ((I) one solution electrospins on a flat plate collector producing a random mat; (II) a second solution electrospins the previous random mat; and (III) section of the final mat shows two different layers of nanofibers overlapped).

2.6.2 Shorts and finite length bundles and yarns

To overcome the mechanical limitations of the electrospun mats, alternative electrospinning configurations have been developed to obtain bundles and yarns of nanofibers. A bundle is a filament composed of aligned electrospun nanofibers. A yarn is a filament of twisted electrospun nanofibers [9,132–134]. The firsts concepts and patents on electrospinning bundles and yarns were proposed by Formhals [9,133,143–146]. Deitzel et al. used a series of rings, charged as the polymeric solution and a flat plate collector connected to the ground, to align nanofibers on two wooden rods, passed between the rings and the collector. After a thin mat of aligned nanofibers was formed between the rods, the mat was twisted in a short yarn (Figure 2.5a) [154,155]. Later, Theron et al. used a rotating disk collector, with a tapered edge, to obtain short nanofibrous bundles of PEO (Figure 2.5b) [156]. Further studies on this technique show that the fibers are prone to necking due to the high rotational speed of the collector. This necking effect severely reduces the material strength [9,157]. Short yarns are produced by twisting groups of nanofibers or mats. Fennessey et al. produced mats of aligned electrospun nanofibers of PAN, using a rotating drum collector. Mats were cut in tows, linked together and then twisted with an electric spinner to obtain yarns [133,158]. Lui et al. used a high speed rotating annular collector, to obtain circular aligned nanofibers membranes, which were cut and twisted to obtain yarns [159]. Uddin et al. divided into continuous strips mats of aligned nanofibers of PAN, reinforced with carbon nanotubes (CNTs), which were obtained by a rotating drum collector. After the production of the strips, they were twisted to obtain yarns [132,133,160]. More recently, Pauly et al. and Sensini et al. developed a technique where mats of aligned nanofibers, electrospun on a high-speed rotating drum collector, were cut in strips and manually wrapped to obtain bundles (Figure 2.5c). As a result, the length of the

bundles produced with this method could be adjusted by changing the diameter of the collector [59,60,93].

Some groups designed automated methods to twist bundles and used some collector setups, modified from the gap collector shape, to obtain short bundles and yarns. Teo et al. produced bundles of aligned nanofibers using two close blade collectors, and then put into a water bath to compact the fibers [161]. A limitation of this approach is that, by increasing the distance between the collectors over 80 mm, a progressive reduction of deposition on the blades was observed [161]. Dalton et al. used two small discs as collectors: one could rotate and twist the aligned nanofibers to obtain a yarn (Figure 2.5d) [162]. Lui et al. produced yarns using a modified gap collector setup, based on the rotating ring collector and a rotating rod [159,163]. Later, Lotus et al. adopted the same philosophy of the modified gap collector proposed by Lui et al., but, by tuning the interaction between a rotating hollow hemisphere and a translating tapered metal rod, short nanofibrous yarns were obtained [163–165].

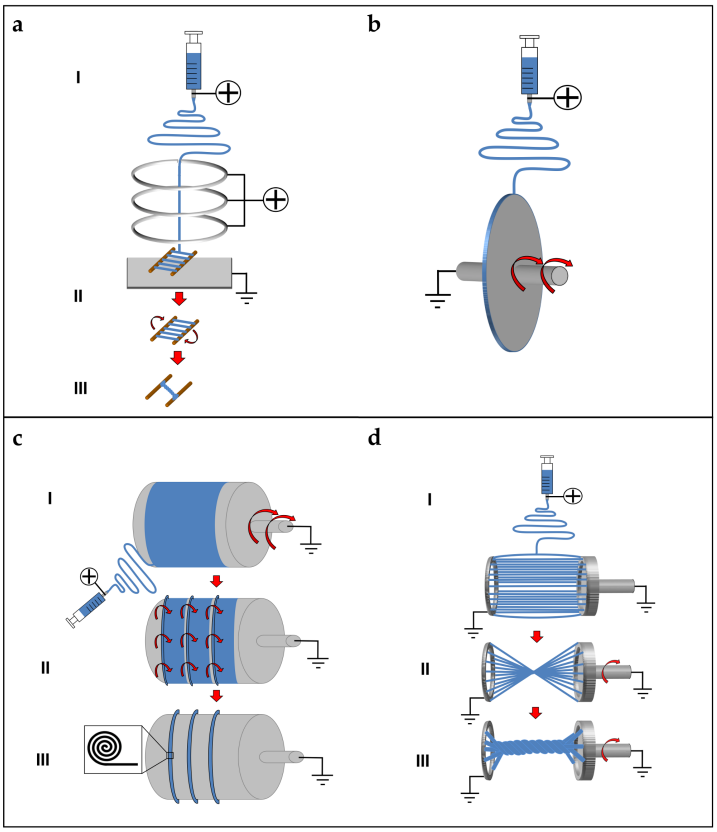

Figure 2.5. Different electrospinning setups to produce short yarns or bundles of nanofibers. (a) Short yarns production by three collimators rings: (I) the nanofibers travel through three metallic

rings charged with the same polarity of the needle; (II) the nanofibers are aligned on two parallel wooden rods placed between the last ring and a flat plate ground collector; and (III) the mat of aligned nanofibers is manually twisted to obtain a short yarn [154,155]. (b) Tapered edge disk collector to produce short bundles of nanofibers [156]. (c) Finite length bundles production setup: (I) Nanofibers electrospin on a high-speed rotating drum collector to obtain aligned nanofibers; (II) the mat cut in strips which are manually wrapped on the drum; and (III) final bundles on the drum before being cut (box: schematic of a cross-section of a bundle) [59,60,93]. (d) Finite length yarns production with small discs setup: (I) solution electrospins on two parallel small metallic ground discs to obtain aligned nanofibers; (II) after the electrospinning session, one of the discs is put in rotation to twist the nanofibers; and (III) final yarn produced between the discs [162].

2.6.3 Continuous bundles

While the methods described above can produce bundles/yarns of pre-defined length, other setups are developed to produce continuous and automatized bundles/yarns of nano- and microfibers. Smith et al., Kim et al. and Kim and Park utilized a setup, in which the polymeric solution was electrospun on a liquid collector with a high surface tension (distilled water or a blend with methanol) and collected on a rotating drum outside the solution (Figure 2.6a) [9,132,133,166–168]. Pan et al. developed a technique to produce bundles by co-electrospinning two polymers. Bundles are obtained by the attachment and alignment of electrospun nanofibers with opposite charges, in the air gap between the spinnerets and the drum collector (Figure 2.6b) [169]. Wang et al. produced continuous bundles, driving the alignment of the nanofibers, with a grounded needle and a rotating drum collector (Figure 2.6c) [170,171].

2.6.4 Continuous yarns

The first example of continuous electrospun yarn was presented by Ko et al. who electrospun poly(lactic acid) (PLA) and PAN filled with carbon nanotubes, imposing first a twisting degree and, then, collecting the yarn on a rotating drum [172]. Teo et al. demonstrated the feasibility of producing continuous electrospun bundles and yarns with a water vortex (Figure 2.6d) [173,174]. Dabirian et al., using a static negative charged plate and a static rod, obtained a triangular jet of nanofibers. This configuration allows producing a yarn helped by the collecting

system: a rotating drum, fixed on a rotating disk. The combination of the two rotations both permits the winding of the yarn and the modulation of its twisting degree [175]. Later, Dabirian et al. developed another setup to produce yarns, based on oppositely charged syringes posed on both sides of a charged collector. The nanofibers produced were then collected and twisted by the same rotating system [176]. Afifi et al. designed an electrospinning setup described for continuous aligning yarns. It comprises a slowly rotating grounded "funnel" target and a winder placed next to the funnel. A charged polymer jet was ejected from a needle. The electrospun fibers were first accumulated on the opening of the funnel to form a web. The web was then pulled upward and guided to a winder on which twisted fibers were continuously wound as a yarn [177]. Recently, Ali et al. developed a simple method to produce yarns. A rotating funnel was used to collect the nanofibers by two syringes opposite charged, on the edges of the funnel opening (Figure 2.6e) [178].

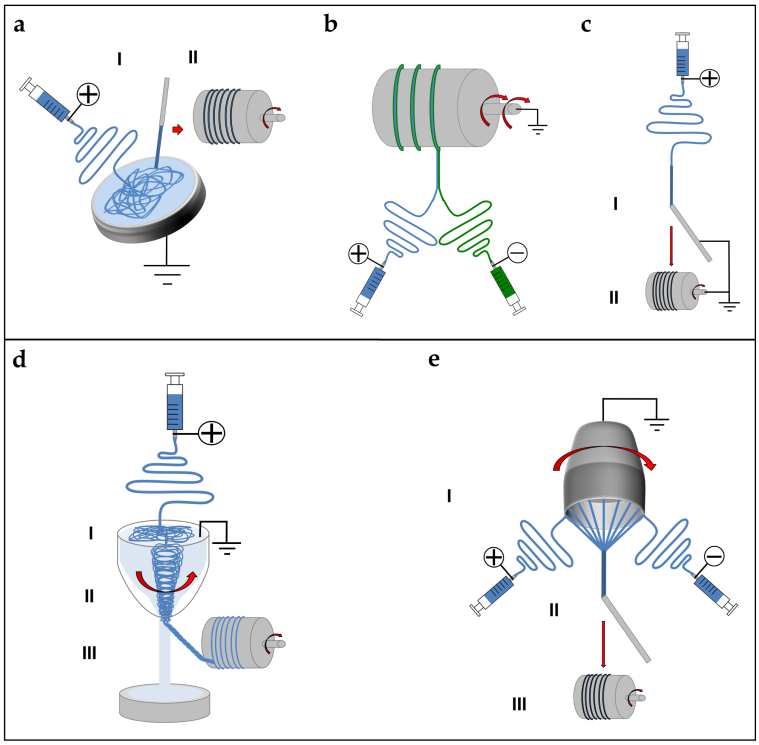

Figure 2.6. Different electrospinning setups to produce continuous bundles or yarns of nanofibers. (a) Continuous bundles production setup by a liquid bath collector: (I) solution electrospins on a liquid bath collector; and (II) nanofibers are taken by a glass rod and collected on a continuous rotating drum. (b) Continuous bundles obtained by co-electrospinning different solutions (oppositely charged) on a high-speed rotating drum collector. Nanofibers are attracted to each other

in air. (c) Continuous bundles obtained by a needle: (I) a solution is electrospun starting by a needle connected to the ground; and (II) the starting bundle is guided to a rotating drum collector producing a continuous bundle. (d) Continuous yarns production with liquid bath vortex setup: (I) solution electrospins on a liquid bath collector; (II) nanofibers are twisted by a liquid vortex producing a yarn; and (III) the yarns pass through a hole in the bottom of the bath and collected by a drum collector [173,174]. (e) Continuous yarn production with funnel collector setup: (I) two syringes, opposite charges, electrospin nanofibers on the mouth of the funnel collector, in rotation, producing a mat; (II) a glass rod bring the center of the mat producing the yarn; and (III) the yarn is collected on a rotating drum [178].

2.6.5 Tubes and conduits

By tuning the diameter of the drum collector, and pulling it off from the mat, at the end of the electrospinning process, it is possible to obtain tubular conduits (Figure 2.7a) [38,179]. This kind of configuration is widely applied in tissue engineering and especially in the production of vessels and nerve conduits [38,179–181]. Firsts examples of nanofibers conduits in nerve tissue engineering were obtained by Bini et al., who collected random nanofibers on a rotating Teflon mandrel placed above a negative collector grid [182]. In the field of research of vascular tissue engineering, Stitzel et al. developed a random electrospun nanofibrous conduit, on a slowly rotating drum collector [183]. Matsuda et al. studied the disposition of the nanofibers on conduits, electrospinning segmented poly(urethane) (SPU) on a rotating drum collector with the speeds of 150 and 3400 rpm. At 150 rpm, the nanofibers are random, on both the internal and the external sides of the conduits. However, at 3400 rpm, the nanofibers are aligned on the internal side and random on the external side [184]. Vaz et al. and Kidoaki et al. upgraded the production of tubes and conduits, co-electrospinning different polymers in different layers of the same conduit (Figure 2.7b) [38,153,185].

2.6.6 Textiles of nanofibers

To increase the mechanical properties of electrospun bundles and yarns and to unite these structures, different methods, derived from textiles production, are proposed. The methods most frequently used are knitting, waving and braiding [186]. Knitting is a well-established textile method to create complex two- and three-dimensional

porous structures, from bundles or yarns that are interlaced in a highly ordered arrangement of connected loops. In the knitting process, bundles or yarns are drawn to form interconnected loops (Figure 2.7c) [186]. In tissue engineering, knitting structures made of fibers obtained by different techniques, have found applications, for example in cartilage, skin ligaments/tendons and blood vessels [187–189]. Weaving is a textile technique where two distinct sets of warps or wefts are interlaced at right angles to form a fabric with controlled strength, porosity, morphology, and geometry. Woven structures are lightweight, strong, and flexible (Figure 2.7d) [187]. Moutos et al. proposed several works about woven scaffolds for cartilage tissue engineering [190–193]. Finally, braiding scaffolds are often applied to unite groups of bundles or yarns, reducing the diameter of the final scaffold and increasing their mechanical properties. In braiding, complex structures or patterns are formed by inter-twining three or more fiber strands, which allows making cylinders and rods suitable for engineering connective tissues (Figure 2.7e) [187]. A wide variety of three-dimensional geometrical shapes with fine-tuned stable properties can be obtained through varying the arrangements of diagonally intertwined strands [186]. For instance, Wu et al. produced woven, knitted and braided scaffolds starting by their electrospun nanofibrous yarns finding interesting results about cells proliferation and mechanical properties [194].

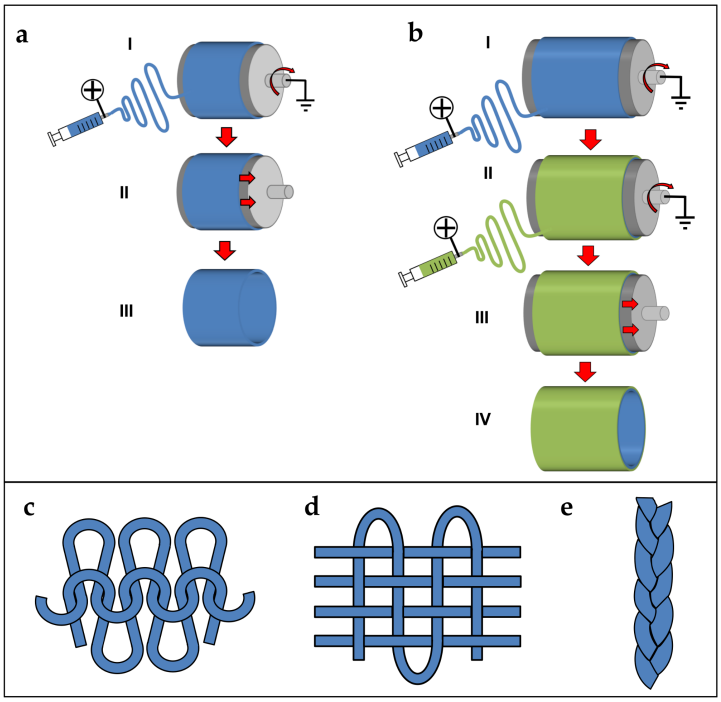

Figure 2.7. Different electrospinning setups and procedures to obtain tubes or conduits of nanofibers. (a) Tube of nanofibers obtained by a drum collector: (I) nanofibers are electrospun on a drum collector (by modulating the rotational speed, the nanofibers could be random or aligned); (II) the tube of nanofibers is removed from the drum; and (III) final tube of nanofibers. (b) Tube of different layers of nanofibers obtained by a drum collector: (I) the nanofibers of the first solution are electrospun on a drum collector (by modulating the rotational speed, the nanofibers could be random or aligned); (II) the nanofibers of the second solution are electrospun over the firs mat; (III) the mat of nanofibers is removed from the drum without cutting its side; and (IV) final tube of nanofibers with different nanofibers inside and outside. Different textile patterns to unit electrospun bundles or yarns of nanofibers: (c) Knitted; (d) Woven; and (e) Braided.

2.6.7 Multiscale hierarchical scaffolds

The structures presented so far can be used to build hierarchically organized super-structures. Some groups tried to extend the concept of electrospun nanofibrous conduits, filling their central hollows with nanofibers or bundles/yarns of nanofibers. Li et al. submitted a patent for producing different configurations of scaffolds, by an electrospinning setup inspired from the principle of the gap collector. Two rotating cylinders allowed producing aligned nanofibers between them. The rod of aligned nanofibers is inserted in a nanofibrous conduit. The random nanofibrous conduit is produced by electrospinning on a drum collector and

removed from it. Finally, the conduit is filled with the rod of aligned nanofibers (Figure 2.8a) [195]. Koh et al. assembled a nanofibrous scaffold for nerve regeneration matching conduits and bundles. First, a double layer conduit, with the inner part of aligned nanofibers and the external of random ones, is obtained by electrospinning the solution on a drum collector, rotating at different speeds. Then, the mat is axially cut and removed from the drum. The mat is rolled around a rod producing a conduit. After the removal of the nanofibrous conduit from the rod, the conduits central hollow is filled with nanofibers bundles of and nerve growth factor [173,196]. Recently, Li et al. presented a method for cover electrospun nanofibrous bundles with a random electrospun sheath, using a rotating drum collector. First, continuous bundles are produced. The bundles are cut in pieces and fixed on a drum collector rotating at low speed. Then, the nanofibers are electrospun on the bundles obtaining the final scaffold. Finally, the scaffold is removed from the drum collector, by sliding out the scaffold by the drum (Figure 2.8b) [178,197].

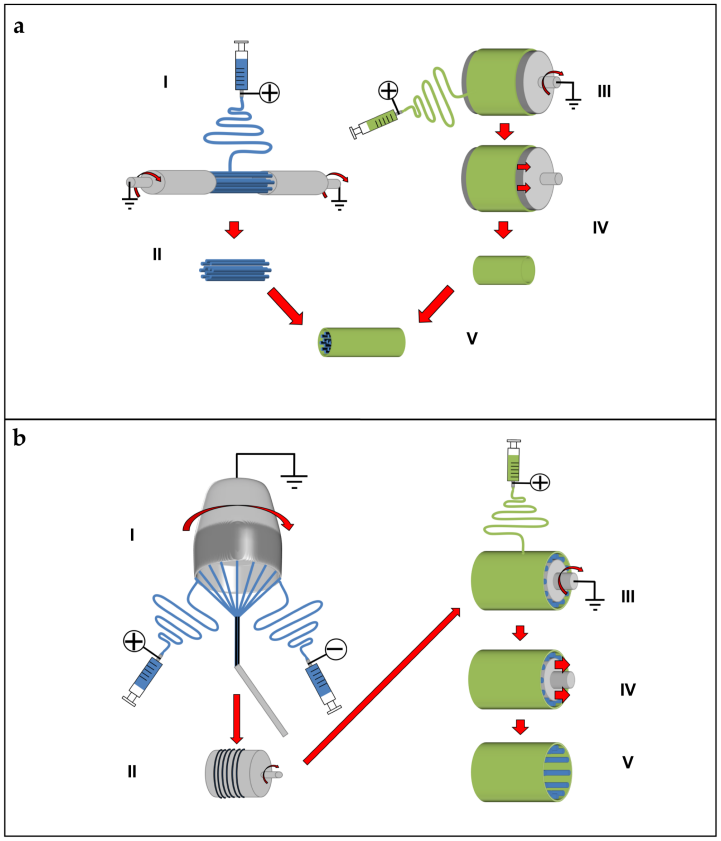

Figure 2.8. Different electrospinning procedures to obtain hierarchical multiscale scaffolds. (a) Nanofibers rod and conduit assembled in two steps: (I) nanofibers are electrospun on a rotating air gap collector; (II) the nanofibers rod is removed from the collector; (III) on a rotating drum collector,

a random mat is electrospun; (IV) the mat is removed from the drum obtaining a conduit; and (V) the conduit is filled with the nanofibers rod [195]. (b) Yarns covered with a nanofibrous sheath: (I) continuous yarn of nanofibers produced with a funnel setup; (II) the continuous yarn is collected on a rotating drum; (III) the continuous yarn is cut in multiple yarns, fixed on rotating drum collector and covered with a nanofibrous sheath; (IV) the drum is removed from the scaffold; and (V) final scaffold [178,197].

2.7 Applications for tendon and ligament regeneration and replacement

The previous section summarizes the most suitable electrospinning setups and methodologies to produce nanofibrous structures and scaffolds. In the present section, an overview of their applications in tendon and ligament tissue engineering is provided. The studies are divided according to the different clinical applications and the specific issues being solved.

2.7.1 Preliminary studies on electrospun materials

To start a preliminary investigation on the interactions between the cellular component and the electrospun nanofibers, the most suitable approach is on mats of random or aligned nanofibers. This is also useful to set the electrospinning parameters to obtain the desired morphology and arrangement of the fibers.

2.7.1.1 Flat electrospun mats

Lee et al. stimulated human ligament fibroblasts on electrospun mats of PU random and aligned nanofibers, with cyclic loads in a bioreactor. After seven days of dynamic culture, they found a statistically significant increment of the production of collagen Type I in the aligned mats compared to the random ones. They also found that fibroblasts were aligned in the direction of the aligned nanofibers [116]. In different studies for anterior cruciate ligament applications, Bashur et al. evaluated how the diameter and the orientation of electrospun PDLLGA and PEUUR fibers contributed to the morphology, orientation, and proliferation of NIH 3T3 fibroblasts and bone marrow stromal cells. Despite the growing capacity of fibroblasts on the different fiber meshes, they found that the aligned nanometric

fibers helped the cells in their orientation and growth, compared to the micrometric ones. Moreover, the production of collagen 1a1, decorin, tenomodulin and scleraxis was inhibited in the micrometric fibers [74,198].

Sahoo et al. evaluated bone marrow stem cell (BMSCs) proliferation, on random nanofibrous mats of PLGA, loaded with bFGF for tendon and ligament regeneration. The bioactive bFGF could activate tyrosine phosphorylation signaling within seeded BMSCs. The bFGF-releasing nanofibrous scaffolds facilitated BMSC proliferation, production and deposition of collagen and tenascin-C, and induced tendon/ligament-like fibroblastic differentiation [76]. Hayami et al. produced mats of aligned microfibers of PCLDLLA. They embedded the mats in a noncell-adherent photo-crosslinked N-methacrylated glycol chitosan hydrogel seeded with primary ligament fibroblasts. Ligament fibroblasts remained viable throughout the four-week culture period (72 ± 4%), and produced proteins such as collagen Types I and III, and decorin [115]. Surrao et al. produced aligned nanofibers of P(LLA-CL), PLDLA, PDLLA and PLLA for tendon and ligament applications. They compared the as-spun mats, with the crimped ones, obtained by immersing them in phosphate buffer saline (PBS). They investigated the effect of crimping both in terms of mechanical properties, and in terms of cell viability. They also found that the degree of crimping (amplitude and wavelength) was tunable by adjusting the difference between operating temperature and glass-transition temperature of the polymers. Crimping helped the nanofibers in recovery after the application of cyclic loads and increased the values of proliferation of the extracellular matrix production after 14 days and 8 weeks of culture with bovine fibroblasts [53,57].

Karchin et al. cultured with pig anterior cruciate ligament fibroblasts, different electrospun microfibrous mats of PU, obtained by electrospinning the nanofibers on flat plate collectors with different patterns (Figure 2.9a). The mechanical tests demonstrated tunable mechanical properties as a function of the templated architecture. Pig ligament fibroblast seeded scaffolds were subjected to periods of cyclic strains, of 1 h each, in a bioreactor. They found a statistically significant increment of collagen Type I gene expression, when stimulated at 3% strain at 0.5 Hz [117].

Tu et al. produced aligned PLLA and Coll core–shell nanofibers, aligned mats for tendon tissue regeneration. They used the PLLA as core polymer and the Coll as shell. The contact angle showed higher wettability of the core–shell nanofibers (47.93 ± 2.09°) compared to the native PLLA (104.52 ± 4.09°). Wide angle X-ray diffraction measurements confirmed the levels of crystalline orientation of 75.3% [62]. Chainani et al. electrospun PCL random microfibers mats on a saline bath, covered, respectively, by phosphate buffer saline (PBS), fibronectin or tendon-derived extracellular matrix. Scaffolds were maintained in culture with human adipose stem cells (hASCs). The collagen content was statistically greater by Day 28 in tendon-derived extracellular matrix scaffolds. The Young's modulus did not statistically change over time, but yield strain increased with time in the cultures on the fibronectin and tendon-derived extracellular matrix mats. Histology demonstrated cell infiltration through the full thickness of all scaffolds [95].

Cardwell et al. produced random and aligned mats of fibers of PEUUR in different concentrations and diameters (the fiber diameters divided into: small < 1 μm; medium = 1–2 μm; and large > 2 μm) as a tendon and ligament tissue engineering applications, and studied the mouse fibroblast viability. Their found that the fiber diameter affects cellular behavior more significantly than fiber alignment. Initially, the cell density was greater on the mats of small fibers, but similar cell densities were found on all mats after an additional week in culture. After two weeks, gene expression of collagen 1a1 and decorin was increased on all mats. Expression of the tendon/ligament transcription factor scleraxis was suppressed on all electrospun mats, but expression on the large- diameter fiber mats was consistently greater than on the medium-diameter ones [119].

Full et al. applied a co-axial electrospinning to produce random and aligned nanofibers with a core of PU and a shell of a blend of PLGA (50:50 and 85:15) and Coll for ligament tissue regeneration. Different typologies of PLGA in blend with the Coll were investigated. They studied the mats mechanical properties and human foreskin fibroblasts (HFF) proliferation until 14 days of culture. They found higher mechanical properties for the mats of aligned nanofibers of PLGA (50:50)/Coll-PU compared to the PLGA (85:15)/Coll-PU ones. Moreover, they found a statistically

significant increment of the cell adhesion in the aligned mats of PLGA (50:50)/Coll-PU compared to the other compositions and fiber organizations [79].
Sheikh et al. investigated random and aligned mats of nanofibers blends of CarbothaneTM and different percentages of MWCNTs (0.06%, 0.33%, and 0.66%), for tendon and ligament grafts. The biocompatibility and cell attachment of the mats were investigated while culturing them in the presence of NIH 3T3 fibroblasts. The results indicated a non-toxic behavior and significant attachment of cells towards nanofibers for all the different compositions after seven days of culture. Promising mechanical properties were found for the aligned mats, especially for the nanofibers with 0.33% of MWCNTs that reached a failure stress of 72.78 ± 5.5 MPa [130].
Zhang et al., as application for tendon tissue engineering, compared the mechanical properties and the cell proliferation, in an in vivo rat Achilles' tendon model, of random and aligned microfiber blends of PLLA, PEO and small molecule TSA. The in vivo implantation confirmed that TSA promoted the structural and mechanical properties of the regenerated Achilles tendon. However, the mechanical properties of the mats were weaker than the natural tendon [64].

2.7.1.2 Multilayered and co-electrospun scaffolds

Orr et al. used a modified liquid bath collector setup to obtain both random and aligned multilayer scaffolds of PCL microfibers for rotator cuff repair. For the random scaffolds, 70 layers of microfibers were overlapped. For the aligned scaffolds, 140 aligned layers were overlapped onto each other to obtain the final scaffold (Figure 2.9b). Then, scaffolds were cultured with hASCs for 0, 4, 7, 14 and 28 days. They evaluated that multilayered aligned scaffolds enhanced collagen alignment and tendon-related gene expression compared to multilayered nonaligned scaffolds. They also tested the mechanical properties of the scaffolds after 0 and 28 days of culture. Aligned scaffolds displayed increased expression of tenomodulin and exhibited aligned collagen fibrils throughout the full thickness, which increased yield stress and Young's modulus of cell-seeded aligned scaffolds along the axis of fiber alignment [99]. Deepthi et al. obtained a scaffold by combining co-electrospinning and multilayer electrospinning, for ligament tissue

regeneration. First, random and aligned nano/microfibrous mats were obtained, co-electrospinning PCL with different flow rates. The mats were then covered by a CTS/HA layer, and finally crosslinked. Better protein adsorption was found on the coated scaffolds, compared to the uncoated ones after 24 h of test. Moreover, the coated scaffolds improved the rabbit ligament fibroblast cell attachment and elongation along the aligned fibers after seven days of culture [91]. Yang et al. analyzed a multilayer electrospun scaffold, made by overlapping five co-electrospun microfibrous aligned mats of PCL and methacrylated gelatin, for tendon tissue regeneration. The scaffolds were then soaked with a photo-initiator and crosslinked by visible light. Photo-crosslinking was able to integrate stacked scaffold sheets to form multilayered constructs that mimic the structure of native tendon tissues. hASCs impregnated into the constructs remained responsive to topographical cues and exogenous tenogenic factors, such as TGF-b3. They also found statistically increased values of load to failure and Young's modulus on the crosslinked ones [100]. Thayer et al. obtained a scaffold electrospinning aligned nanofibrous mats of PEUUR and PCL blends (0/100, 75/25 and 100/0) and then immersed in Coll gels, for ligament tissue engineering. The mechanical testing of the mats showed Young's moduli of 15 ± 4.0 MPa (100/0 PEUUR/PCL), 31 ± 14 MPa (0/100 PEUUR/PCL) and 5.6 ± 2.5 MPa (75/25 PEUUR/PCL). Rat bone marrow mesenchymal stem cells (BMMSCs), seeded for 14 days in the collagen hydrogel phase, were oriented by the network. Systematic variation of fiber modulus affected expression of a-smooth muscle actin and Scleraxis [80]. Gurlek et al. electrospun PCL nanofiber random mats for anterior cruciate ligament regeneration, and studied their mechanical properties, which resulted lower than the ones of anterior cruciate ligament [89]. Dodel et al. produced a scaffold made of three different layers for ligament regeneration. First, a mat of aligned SE electrospun nanofibers was placed on a flat plate collector, and used to electrospun a random PEDOT nanofiber mat. Finally, the bilayer nanofibrous scaffold was embedded in a CTS sponge. Unrestricted somatic human stem cells (USSCs) were cultured. The effect of DC electric pulses to cells cultured on polymer was assessed. Cellular function was more active in scaffolds with electrical induction, where

collagen Type I, collagen Type III, decorin, biglycan and aggrecan genes were intensively expressed [123].

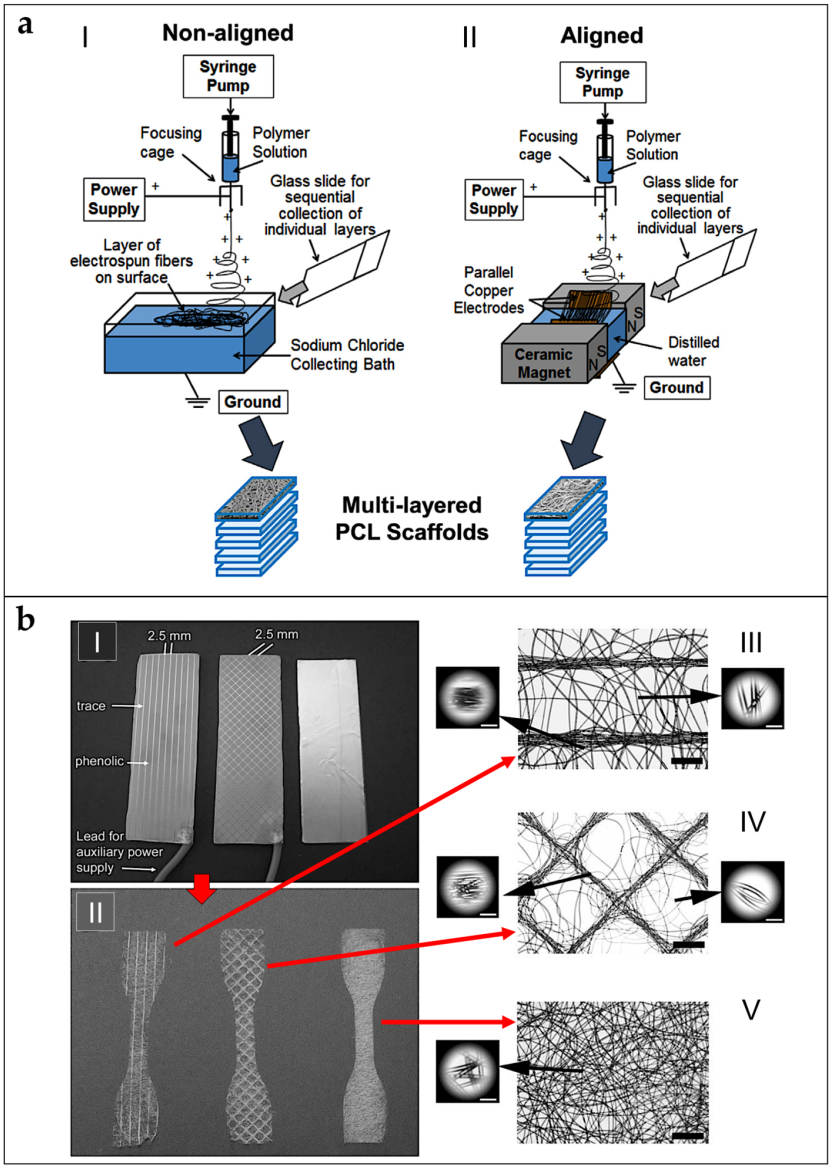

Figure 2.9. Different scaffolds produced as in vitro test bench for cell cultures. (a) Setup to produce PCL multi- layer scaffolds with liquid bath collectors for rotator cuff tissue engineering (adapted from Orr et al. [99], reproduced with permission. Copyright 2015, Elsevier): (I) setup to produce multilayer random nanofibrous scaffolds; and (II) setup to produce multilayer aligned nanofibrous scaffolds. (b) Nanofibrous mats of PU obtained by different pattern collectors (adapted from Karchin et al. [117], reproduced with permission. Copyright 2012, John Wiley and Sons): (I) mats of nanofibers are electrospun on a flat plate collector with different superficial patterns; (II) scaffolds prepared for tensile testing; and (III–V) SEM images of the different nanofibers scaffolds (scale bar: zoom out = 1 mm; zoom in = 100 micrometers).

2.7.2 Patches and augmentation grafts

Another way to try to increase the mechanical properties of the electrospun scaffolds, for tendon and ligament tissue engineering applications, is to apply different techniques derived from textiles. In some works, researchers have produced composite scaffolds, combining non-electrospun knitted structures, and electrospun nanofiber layers.

2.7.2.1 Patches

Sahoo et al. developed a scaffold for tendon/ligament tissue engineering applications, by covering with random electrospun nanofibers of PLGA, a knitted scaffold, composed by microfibers yarns of PLGA. Porcine bone marrow stromal cells were seeded onto the scaffolds. Cell proliferation was faster in these scaffolds compared to the only knitted ones. Moreover, cellular function was more active, with significant expression of the collagen Type I, decorin, and biglycan genes. However, the failure load of the nanofibrous coated scaffolds after ageing in PBS (7 days = 18.11 ± 3.53 N; 14 days = 2.26 ± 0.57 N) was lower than the tendons and ligaments [77]. To reproduce a tendon or a ligament, Sahoo et al. covered a knitted SE scaffold, mounted on a rotating drum collector, with random nanofibers of PLLGA loaded with bFGF. After this process, the scaffolds were twisted in yarns, and seeded with bone marrow stromal cells (BMStCs) (Figure 2.10a). The nanofibers coating sustained release of bFGF, initially stimulating mesenchymal progenitor cell (MPCs) proliferation, and, subsequently, their tenogenic differentiation. Up-regulated also gene expression of ligament/tendon- specific extracellular matrix proteins and increased collagen production. This contributed to enhancing the average failure load (83 N) of the construct after three weeks of cellular culture, reaching values similar to the rabbit medial collateral ligament (88 N). However, the average stiffness of the scaffolds (6.97 MPa) after cellular culture was lower than the natural ligaments (46–47 MPa) [84]. Vaquette et al. electrospun a microfibrous aligned mat of P(LLA-CL), on two different knitted structures of PLLGA and SE. The knitted scaffolds were fixed longitudinally on the surface of a high- speed rotating drum collector, and covered by a layer of nanofibers. The

mechanical tests exhibited an initial toe region and a Young's modulus similar to the ones of human ligaments. Rat BMMSCs proliferated on the composite scaffolds and orientated along the direction of microfibers alignment. Cells produced collagen Types I and III [54].

Beason et al. focused on rotator cuff repair: they produced mats of aligned nanofibers co- electrospinning PCL and PEO (as sacrificial fibers). A rat rotator cuff model was used to investigate the in vivo performance. The scaffolds remained in place, with more noticeable cellular infiltration and colonization lacking sacrificial fibers. Biomechanical testing revealed reduced mechanical properties in relation to the increased cross-sectional area, caused by the extra thickness of the implanted scaffold material [96].

2.7.2.2 Augmentation grafts

Sharifi-Aghdam et al. focused on tendon tissue engineering: they electrospun a random nanofibrous blend of PU/Coll on a knitted SE scaffold of non electrospun yarns. The tensile tests on samples including blend nanofiber and knitted SE indicated that PU/Coll-coated knitted SE had appropriate mechanical properties in terms of Young's modulus (525 ± 23 N). The Alamar Blue assay on the L929 fibroblast cell line demonstrated appropriate cell viability, with a significant proliferation on the scaffold containing more Coll content [118].

Ni et al. electrospun nanofibers of SE annealed in methanol for Achilles tendon augmentation. They compared, in an in vivo rabbit model, the different effects of healing of the SE patches, wrapped on the injured Achilles' tendons, and fixed with different suture techniques. After 28 days, they found that a surgical scenario, where the standard suture was augmented by the photobonded silk wrap, may provide optimal mechanical strength [128]. Inui et al. used an in vivo rabbit rotator cuff model, to test the behavior of PDLLGA random microfibers. They tested the mechanical and biological performances of the grafts at different time points until 16 weeks, finding progressively increment of the patch mechanical properties (failure load at: Week 0 = 5.4 ± 2.5 N; Week 16 = 75.3 ± 18.7 N), tissue regenerations and cells migration inside the patch [75]. Manning et al. tested in an in vivo canine model for tendon repair, a multi-layered scaffold made of aligned

nanofibrous mats of PCL in combination with fibrin/heparin-fibrin-based delivery system layers (filled also with mesenchymal stem cells). The in vitro study showed that the cells remained viable and that a sustained growth factor release was achieved. The in vivo study confirmed that cells remained viable in the tendon repair environment after nine days after implantation. No negative reaction was seen at dissection or based on the mRNA level. However, a mild immune response was detected histologically [98]. Zhao et al. developed random nanofibrous membranes of PLGA loaded with bFGF for rotator cuff repair. They tested the mats in an in vivo rat rotator cuff model. After surgery, the electrospun membranes increased the area of glycosaminoglycan staining at the tendon–bone interface compared with the control group, and bFGF–PLGA improved collagen organization. Biomechanical testing showed that the electrospun membrane had a greater ultimate load-to-failure and stiffness than the control group at four and eight weeks [81]. Zhao et al. embedded random nanofibers mats of PLLA in GT, and tested the scaffolds in an in vivo rat rotator cuff repair model. Histologic observations revealed that GT-PLLA membranes have proper biocompatibility and biodegradability. At eight weeks postoperatively, the area of glycosaminoglycan staining at the tendon–bone interface was increased compared to the control group and improved collagen organization. Biomechanical testing revealed that the GT-PLLA group had a greater average failure load (>30 N) and stiffness (>12.5 MPa) than the control group (failure load < 30 N; stiffness about 12.5 MPa) [65].

To obtain random nanofibers patches for rotator cuff repair, Zhao et al. co-electrospun PCL and CTS, and testing them in vivo in a rat model. The composite scaffolds had improved strength and failure strain compared to the control CTS scaffolds and increased stiffness compared to the control PCL scaffolds. Moreover, they demonstrated better fibroblast attachment and proliferation compared to the PCL scaffolds. Radiological and histological analysis revealed that the PCL-CTS scaffolds promoted new bone formation and collagen and glycosaminoglycan expression compared to the control [97]. Zhang et al. developed, for the regeneration for the Achilles tendon, random and aligned mats of nanofibers of a solution of CTS, GT, PLLA and PEO. The scaffolds were seeded with human-induced pluripotent stem cells (hiPSCs). The in vivo rat tendon repair study

confirmed that aligned fiber scaffold with hiPSCs improved the structural and mechanical properties of tendon injury repair [63]. Hakimi et al. developed a three-layers scaffold for tendon repair. The scaffold consisted of a woven layer of PCL monofilament, overlapped on a mat of random nanofibers of PCL, and an aligned mat of PDO nanofibers (Figure 2.10b). The mechanical properties were in the same range as the human rotator cuff. The in vivo rotator cuff rat model showed that all animals developed fibrous capsules around the repaired tendons. At 12 weeks post-operation, the fibrous tissue appeared more compact and tightly adhered to the material [106].

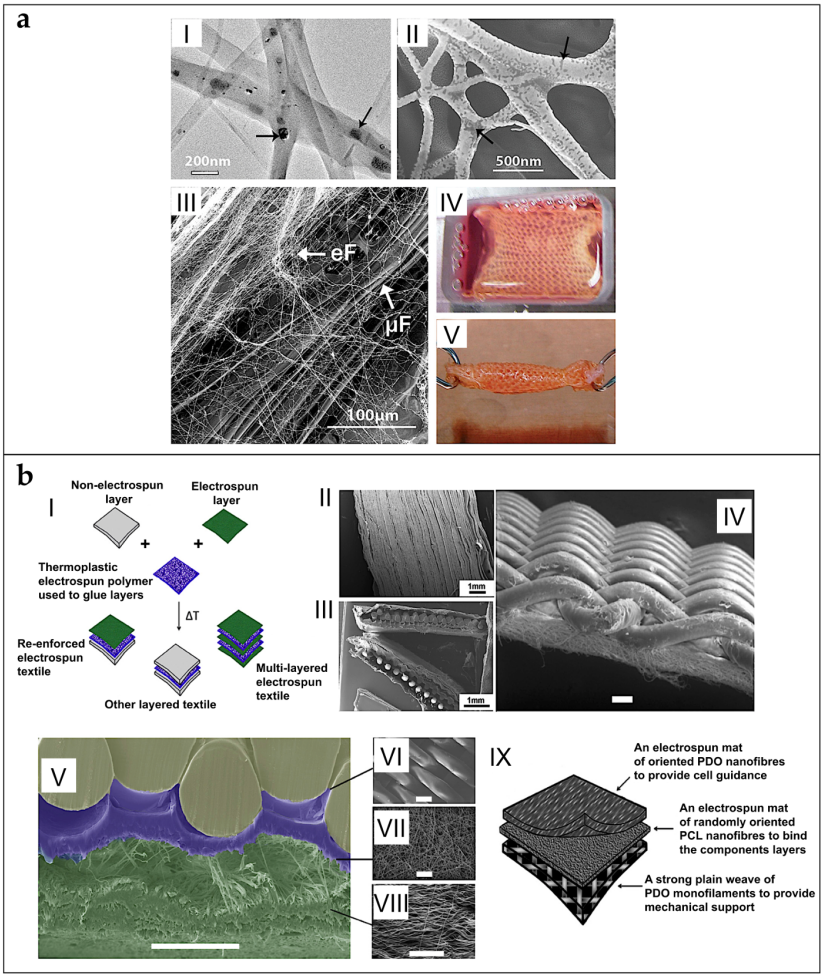

Figure 2.10. Different scaffolds used as *in vivo* patches or augmentations for tendon and ligament tissue engineering. (a) Microfiber SE knitted scaffolds, mounted on a drum collector, and covered by nanofibers of PLLGA loaded with bFGF (adapted from Sahoo et al. [84], reproduced with permission. Copyright 2010, Elsevier): (I–II) SEM images of nanofibers at different magnifications (arrows point bFGFs particles); (III) SEM image of nanofibers (eF) and SE microfibers (μF); and (IV–V) images of the complete scaffold before (IV) and after (V) twisting. (b) Multilayer scaffold

for tendon repair, made of a woven layer of PCL monofilament and electrospun nanofibers mats of random nanofibers of PCL and aligned PDO nanofibers, obtained using a drum collector at different rotation speeds (adapted from Hakimi et al. [106], reproduced with permission. Copyright 2015, Elsevier): (I) schematic assembly procedure; (II–VIII) SEM images of the scaffold and mats ((IV–VIII) scale bar = 100 micrometers); and (IX) explanation of the different mats functions.

2.7.3 Multiscale hierarchical scaffolds for massive replacement

Tendons and ligaments have a three-dimensional morphology and different shapes depending on the anatomical site. For this reason, some researchers have tried to develop scaffolds able to reproduce the entire hierarchical morphology of tendon and ligament tissue.

2.7.3.1 Fascicle-inspired bundles and yarns

A common approach is to use electrospun bundles and yarns as a basic "brick" to mimic the fascicles of tendons or ligaments [5–7,9].

Xu et al. produced aligned nanoyarns mats of P(LLA-CL) and Coll blends, for tendon tissue applications [173]. In this work, the nanofibers, twisted in nanoyarns by the vortex (adapted from Teo et al.), were collected on a rotating drum producing a mat of nanoyarns. Finally, the mats were cultured with rabbit tendon tenocytes, that showed increased values of proliferation after 14 days in static culture [55].

Bosworth et al. produced yarns of nanofibers of different polymers, such as PCL and PLGA for tendon tissue regeneration. The nanofibers were aligned on a rotating drum collector, producing mats which were cut in ribbons, and manually twisted to obtain the yarns (Figure 2.11a). The yarns showed mechanical properties in the range of tendon fascicles. The in vitro cell culture both with equine fibroblasts (static), and human stem cells (dynamic), showed increased values of proliferation and collagen production. After 21 days of dynamic cell culture, the bundles increased their mechanical properties (failure stress about 50 MPa; Young's modulus about 100 MPa) compared to the static culture at the same time point (failure stress about 20 MPa; Young's modulus 80–90 MPa) [82,101,102].

Thayer et al. focused on ligament regeneration: they electrospun blends of PLGA and PEGDA or PEUUR and PEGDA, obtaining random nanofiber mats. The mats

were then rolled up on a mandrel, and crosslinked with PEG hydrogel network. A single mesh was rolled and injected of PEGDA and phosphate buffer saline (PBS) solution loaded with a photoinitiator. The scaffold was finally crosslinked with ultraviolet light to form acellular composites. They tested the cell viability with mouse mesenchymal stem cells, finding decreased vitality after five days of culture [78]. Yang et al. adapted the setup proposed by Lotus et al. to produce mats of aligned micro-yarns of a blend of P(LLA-CL) and SF [164]. After its formation, the yarn was continuously wrapped on the drum and covered by the same random nanofibers, producing the final mat (Figure 2.11b). The mats of micro- yarns were then seeded with BMMSCs, finding increased values of viability after 28 days of culture, compared with the control mat of aligned and random nanofibers. However the mechanical properties of the micro-yarns (failure stress = 24.25 ± 0.76 MPa; Young's modulus = 288.95 ± 13.26 MPa) resulted lower compared to the aligned nanofibers (failure stress = 39.10 ± 2.89 MPa; Young's modulus = 433.6 ± 48.1 MPa) [56].

Mouthuy et al. developed an automated system, to produce continuous nanofiber bundles of PDO, electrospun on a metallic wire for tendon tissue engineering applications. After the coating with aligned nanofibers, a cutter wheel divided the wire collector from the bundle that was collected on a rotating drum (Figure 2.11c). The continuous bundle was cut in pieces that were twisted together. The average failure load of the single bundle was about 1 N. After eight days of culture in vitro with human tenocytes, the bundle showed cell attachment [124].

Cook et al. tested in a bioreactor hierarchical scaffolds for tendon and ligament applications: bundles of microfibers of PEO/fibrinogen loaded with adipose derived stem/stromal cells were investigated. The bundles, with different degrees of porosity, were obtained by electrospinning the solution in a liquid bath vortex collector containing $CaCl_2$, glucose and thrombin. They demonstrated that cells proliferation after 21 days was as higher as the bundle porosity was increased. They also monitored the strain distributions with fluorescent digital image correlation [121].

Domingues et al. produced nanofibrous bundles of a PCL/CTS blend, for tendon tissue regeneration, loaded with CNCs. They found that small CNC contents in the

bundles improved the limited tensile properties (strength and stiffness) while preserving their ductility [104]. Levitt et al. addressed tendon applications: they studied the changes in mechanical properties of nanofibrous yarns obtained by a funnel collector derived from Ali et al. [178]. PCL, PAN and PVDF-TrFe yarns were produced at different funnel rotational speed and mechanically characterized, finding that PVDF-TrFe and PCL yarns have a higher failure strain than PAN yarns [105]. Pauly et al. produced bundles of aligned and random nanofibers of PCL for ligament tissue engineering, by wrapping on a drum collector sections of the mats obtained. They also characterized the mechanical properties of the bundles, finding values close to human anterior cruciate ligament fascicles. Finally, they tested the cell proliferation with hASCs, finding increased values of proliferation after seven days of culture [92]. Sensini et al. developed a versatile method of production of bundles for tendon and ligament tissue regeneration and replacement. They characterized the morphology, the mechanical properties and the cells growing, of electrospun nanofibrous bundles of PLLA, PLLA/Coll blends and Nylon 6.6 (just morphologically characterized), obtained by wrapping the aligned mats on a drum collector (Figure 2.11d). They found that the resorbable bundles (PLLA and PLLA/Coll blends) had mechanical properties close to the human tendon fascicles. The internal morphology of the bundles and the directionality of the nanofibers (evaluated with high resolution X-ray tomography) was similar to the human fascicles one (Figure 2.11e). In addition, the cell viability tests with human tenocytes showed increased levels of proliferation on the PLLA/Coll blends after 14 days of culture [59,60].

Bhaskar et al. tested in an in vivo mouse model, the yarns previously developed by Bosworth et al. for tendon tissue regeneration [82,101,102]. To evaluate the effects of different sterilization approaches, different groups of scaffolds were sterilized using gamma irradiation and ethanol immersion before the implantation. Cell infiltration and proliferation were performed to determine the effect on cell response over a six-week period. Immunohistochemical analysis was performed to characterize inflammatory response, cell proliferation, collagen deposition, myofibroblast activity, and apoptosis. Both sterilization techniques did not significantly affect the cell response [103].

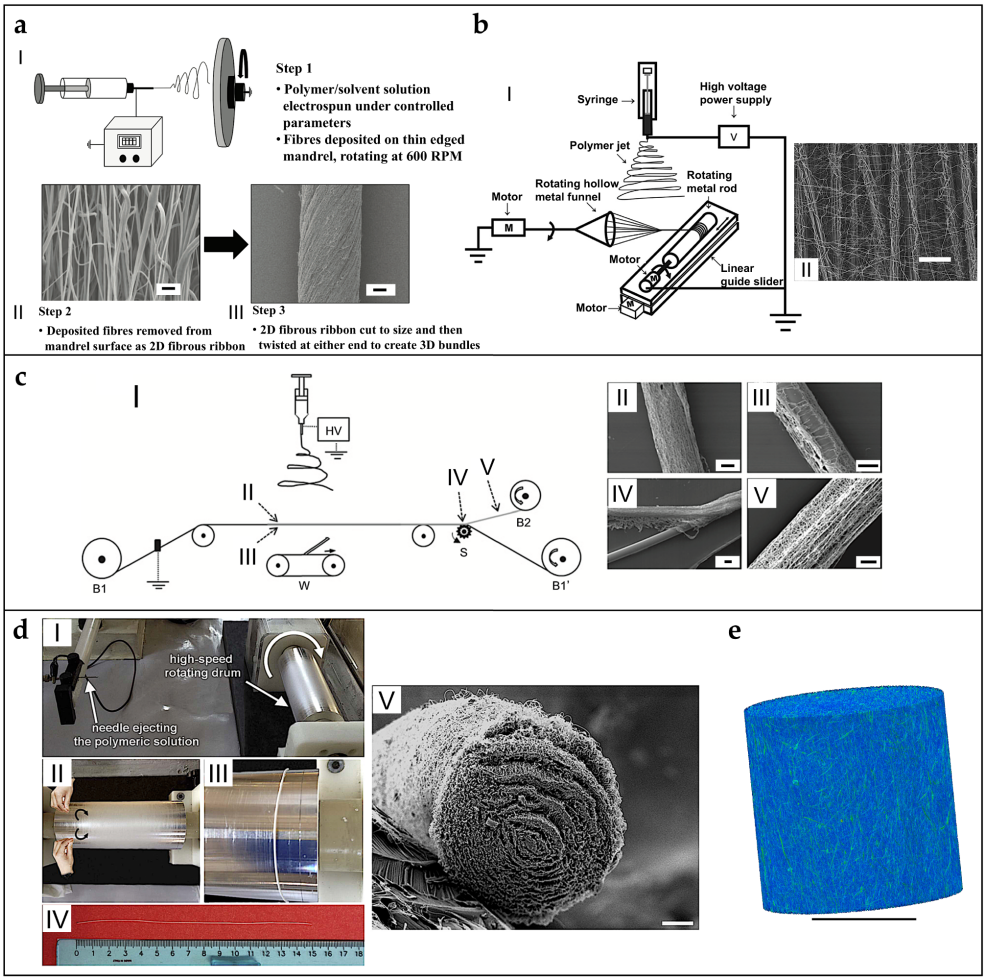

Figure 2.11. Different setups to produce nanofibrous bundles and yarns. (a) Yarns of PCL and PLGA, for tendon tissue regeneration (adapted from Bosworth et al. [82], reproduced with permission under the terms of the CC BY 3.0 license. Copyright 2014, Hindawi): (I) mats of nanofibers are electrospun on a high-speed rotating drum collector and then ribbons of the mat are cut and twisted to obtain the yarns; and (II–III) SEM images of the nanofibers and of a yarn (scale bar II = 2 micrometers; scale bar III = 50 micrometers). (b) Electrospinning setup to produce mats composed by micro-yarns of a blend of P(LLA-CL) and SF, for tendon tissue engineering (adapted from Yang et al. [56], reproduced with permission. Copyright 2014, Elsevier): (I) nanofibers are collected between the funnel collector and the rotating drum collector and the combination of the two rotating collectors allows producing a mat of micro-yarns and random nanofibers; and (II) SEM image of the micro-yarns (scale bar = 100 micrometers). (c) Automatic electrospinning setup to produce continuous bundles of PDO (adapted from Mouthuy et al. [124], reproduced with permission under the terms of the CC BY 3.0 license. Copyright 2014, IOP Publishing): (I) electrospinning machine, in which a metal rod is covered by nanofibers, and, in the final part, the electrospun mat is separated from the rod; and (II–IV) SEM images of a bundle during different points of the process (scale bars = 100 micrometers). (d) Process to produce finite length bundles of nanofibers of PLLA, PLLA/Coll blends (adapted from Sensini et al. [59], reproduced with

permission. Copyright 2017, IOP Publishing): (I) aligned nanofibers are collected on a high-speed rotating drum; (II–III) mats are manually wrapped on the drum to obtain bundles; (IV) the bundles are removed from the drum; and (V) SEM image of a section of a bundle (scale bar = 50 micrometers). (e) High resolution X-ray tomographic image at 0.4 micrometers voxel size of a PLLA bundle (adapted from Sensini et al. [60], reproduced with permission. Copyright 2018, John Wiley and Sons) (scale bar = 200 micrometers).

2.7.3.2 Hierarchically structured scaffolds

To increase the hierarchical organization and the mechanical properties of their scaffolds, some researchers tried to match multiple mats, bundles or yarns together by twisting or braiding them. Barber et al. focused on tendon and ligament tissue engineering: they braided a different number of electrospun bundles (3–5) of PLLA and tested their mechanical properties and cell viability with human mesenchymal stem cells (hMSCs) in a bioreactor. They tested the mechanical properties to measure the Young's modulus (three bundles = 55.0 ± 2.8 MPa; four bundles = 47.8 ± 7.5 MPa; five bundles = 47.6 ± 2.8 MPa) and failure stress (three bundles = 7.62 ± 0.2 MPa; four bundles = 6.57 ± 0.5 MPa; five bundles = 6.67 ± 0.4 MPa). They also found an up-regulation of the production of collagen Types I and III by the cells, during the cyclic stimulation in bioreactor [61]. Bosworth et al. used the yarns previously described [82,101,102], and produced a braided scaffolds for tendon regeneration [82]. Rothrauff et al. studied scaffolds made by dog-bone mats of aligned nanofibers of PLLA or PCL, for tendon and ligament tissue engineering. The mats were obtained electrospinning on a rotating drum collector, and finally braiding them together. They compared the mechanical properties and the BMMSCs infiltration of the braided structures, with multilayered scaffolds of the same materials. The failure load for the braided PCL scaffolds was 164.82 ± 11.13 N and for the stacked ones was 94.67 ± 6.7 MPa. The Young's modulus for the braided PCL scaffolds was 45.96 ± 10.03 MPa and for the stacked ones was 66.48 ± 11.29 MPa. The failure load of the braided PLLA scaffolds was 27.51 ± 4.40 MPa and for the stacked ones was 30.03 ± 1.57 MPa. The Young's modulus for braided PLLA was 45.57 ± 38.96 MPa and for the stacked ones was 118.47 ± 21.81 MPa. Cell proliferation was higher in the stacked scaffolds [58]. In another study on ligament tissue regeneration, Pauly et al. grouped in parallel bunches and

conjugated with CTGF the bundles previously described [92]. They studied the ovine bone-marrow derived mesenchymal stem cells (OBMSCs) proliferation. They found immediately increased values cell viability and collagen expression compared with the unconjugated control [93].

Other research groups developed scaffolds able to reproduce the hierarchical structure of tendons and ligaments by grouping the structures inside the scaffolds with electrospun sheaths, trying to mimic the epitenon or epiligament tissue. Zhou et al. morphologically characterized a scaffold, suitable as artificial tendon/ligament. First, a nanofibrous random sheath of PEO, was electrospun on a cardboard frame, in which were placed a parallel group of poly(amide) PA monofilaments. After the coverage, the monofilaments were twisted together to obtain a structure similar to a tendon or ligament. They also braided some of these structures to increase the hierarchical assembly (Figure 2.12a). However, they just briefly characterized the scaffold in terms of abrasion tests [122]. To mimic the tendon or ligament morphology, Naghashzargar et al. produced a random nanofibrous sheath of PCL or P3HB, on aligned SF yarns, fixed in a wooden structure, above the flat plate collector. After the deposition the SF yarns were twisted to obtain the final scaffold. They found that the nanofibrous sheath slightly increased the failure load of the scaffolds compared to the uncoated SF yarns (SF = 92.6 ± 8.2 N; SF-P3HB = 97.6 ± 11.4 N; SF-PCL = 110.5 ± 6.6 N). No cytotoxic effects on the murine fibroblast cells were found [88].

Some works aimed to replicate the hierarchical structure of the whole tendon, and the bone– ligament complex, electrospinning them with the gap collector technique. Samavedi et al. designed a nanofibrous scaffold that tried to morphologically reproduce a complete bone-ligament-bone complex (Figure 2.12b). Aligned PCL nanofibers were used to mimic the ligament tissue, instead PLLGA random nanofibers were used to reproduce the bone tissue. The scaffold was produced by alternating the electrospinning of the solutions on two drum collectors and on a gap between them. They tested the cell proliferation with BMStCs on the planar mats with gradients of random and aligned nanofibers, finding random orientations on the random PLGA regions, and high alignment on the aligned PCL regions. Finally, they tested the mechanical properties of both the mats and the three-dimensional

scaffolds. They found stress concentrations in the aligned PCL region of the three-dimensional scaffolds, and lower mechanical properties compared to the flat mats [87].

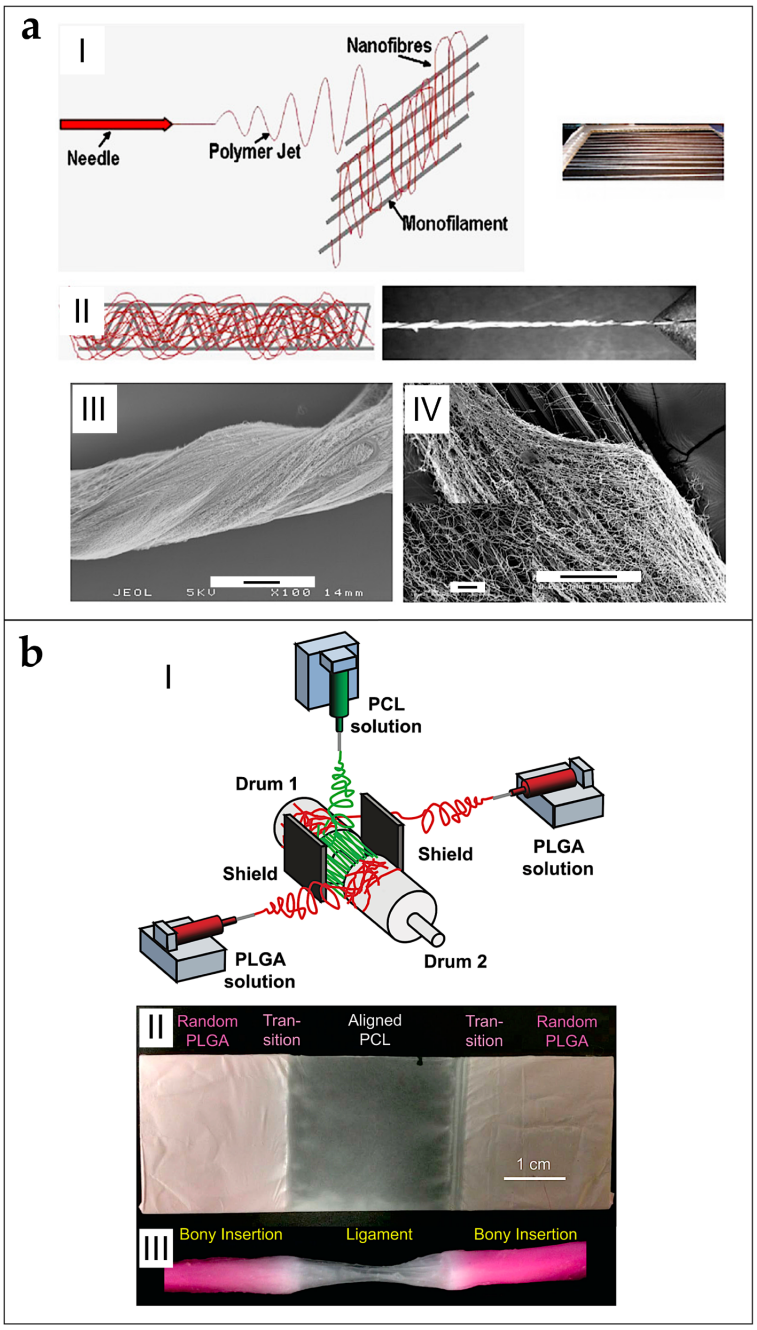

Figure 2.12. Schematic workflow to produce multiscale hierarchically structured scaffolds for tendon and ligament tissue engineering. (a) Microfilaments of PA covered by electrospun nanofibers of PEO, and manually twisted to obtain a scaffold for tendon and ligament applications (adapted from Zhou et al. [122], reproduced with permission. Copyright 2010, Elsevier): (I) the microfilaments are fixed parallel on a rectangular structure, and over pose to a flat plate collector.

Then, the nanofibers are electrospun on the microfilaments; (II) after the electrospinning session, the microfilaments are twisted to obtain a tendon/ligament like structure; and (III–IV) SEM images of the scaffold (scale bar III = 100 micrometers; scale bar IV = 100 micrometers, zoom-in = 10 micrometers). (b) Combination between air gap collector setup and co-electrospinning of PLLGA and PCL to produce a random/aligned nanofibrous scaffold for ligament tissue regeneration (adapted from Samavedi et al. [87], reproduced with permission. Copyright 2014, John Wiley and Sons): (I) schematic representation of the electrospinning setup; (II) image of the random–aligned–random nanofibrous mat after the removal from the collector; and (III) final scaffold after the wrap of the mat of nanofibers.

Banik et al. produced a scaffold to simulate the whole tendon. A gap collector was made by two cylindrical rods able to rotate synchronously. To enhance the deposition and alignment of the PCL nanofibers, magnets were placed near the gap. The final scaffold was a cylinder of aligned or random nanofibers, depending to the rotational speed of the two cylindrical collectors (Figure 2.13a). They found lower properties compared to the tendon tissue (average Young's modulus = 35.8 MPa; failure stress < 12 MPa). They also seeded hMSCs on the scaffolds, finding increased values of proliferation and no cytotoxic effects [107]. Lin et al. tried to reproduce the bone–ligament–bone complex, electrospinning PCL nanofibers on a motorized air gap conic collector setup (Figure 2.13b). As a result, they produced two random conic nanofibers mats on their surfaces, and an aligned nanofibrous region between the two tips of the cones. The conic nanofibrous ends were then mineralized with BLM. They tested the mechanical properties of the ligament-like bundle, finding values in the same range of the human ligament fascicles (failure stress = 38.7 ± 6.2 MPa; Young's modulus = 82.8 ± 11.6 MPa). They also evaluated the cell proliferation of human BMMSCs, finding up-regulation of the tendon or bone markers in the aligned and random sites [114]. Recently, Laranjeira et al. produced nanofibrous tendons starting from electrospun bundles of a blend of PCL/CTS, loaded with CNCs thanks to a liquid bath collector. After that, groups of bundles were twisted together and finally braided or woven to obtain the final scaffolds (Figure 2.13c). They tested the mechanical properties of the scaffolds finding increased values of the yield stress of the braided scaffolds (42 ± 8 MPa) compared to the woven ones (33 ± 2 MPa). They also found increased collagen

Types I and III after 7 and 21 days of culture with human tendon derived cells (hTDCs) and hASCs [108].

Mouthuy et al. manually twisted together the bundles previously described [124], and produced twisted structures for tendon replacement applications. They applied an annealing process at 65 °C to the twisted structures. The failure load of the twisted structure (of the order 20 N) was increased after the annealing process (average value > 20 N). They evaluated in vitro the changes in the mechanical properties after permanence in PBS, and found that, after 12 weeks, they were drastically reduced. They also found increased cell adhesion in the static culture compared with the single bundles. Finally they evaluated the performance of the twisted structure in an in vivo rat rotator cuff model, confirming the biocompatibility of the scaffold [124]. Vaquette et al. electrospun random nanofibrous mats of PCL for ligament tissue engineering applications. Three mats for each scaffold were wrapped and finally braided together. The mats were seeded with BMMSCs for four weeks and finally subcutaneously implanted in an in vivo rat model to evaluate the biocompatibility. While the biocompatibility and cell proliferation were promising, the mechanical properties after four weeks of static culture were significantly lower than the as-spun controls (average control failure load = 0.7 N; average four weeks scaffold failure load = 0.3 N) [94].

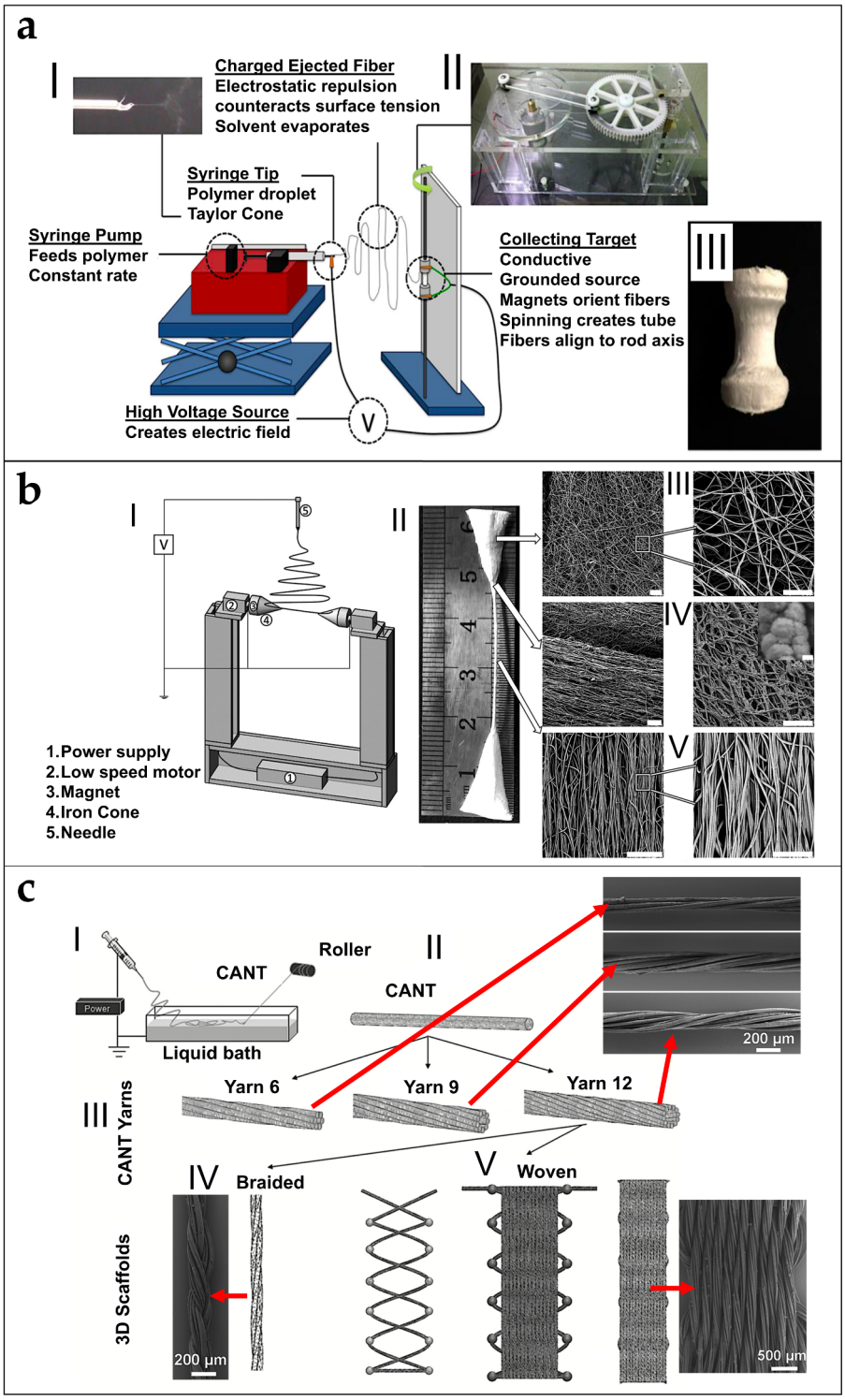

Figure 2.13. Schematic workflow to produce multiscale hierarchically structured scaffolds for tendon and ligament tissue engineering: (a) Modified gap collector setup to produce a scaffold for tendon tissue regeneration (adapted from Banik et al. [107], reproduced with permission. Copyright 2016, Springer Nature): (I) schematic representation of the electrospinning setup; (II) image of the motorized setup of the collector; and (III) image of the final scaffold. (b) Bone–ligament–bone nanofibrous scaffold of PCL, obtained by a modified air gap collector (adapted from Lin et al. [114],

reproduced by permission of The Royal Society of Chemistry. Copyright 2017); (I) picture of the electrospinning setup; (II) image of the final scaffold; (III–V) SEM images of the nanofibers in the different parts of the scaffold ((III–IV) scale bar = 10 micrometers; (V) scale bar = 10 micrometers (right image) and 5 micrometers (left image)). (c) Two different multiscale scaffolds made of braded or woven bundles blend of PCL/CTS, loaded with CNCs for tendon tissue engineering (adapted from Laranjeira et al. [108], reproduced with permission. Copyright 2017, John Wiley and Sons); (I–II) schematic picture of the process to obtain the continuous bundles by a liquid bath collector; (III) 6, 9 and 12 bundles are twisted together to obtain hierarchically structured yarns; (IV) SEM image and a schematic picture of the nanofibers hierarchically structured yarns braided together; and (V) SEM image and schematic picture of the woven multiscale scaffold.

2.7.4 Bone insertion

One of the critical points for clinical deployment is to provide adequate connection to the host bones (both for tendons and ligaments) or to the host muscle (tendons only). The insertion must provide enough strength, avoid stress concentrations, and promote tissue integration and growth. Some groups focalized their work on the mimicking and replacement of both the bone and the muscle insertion of tendons and ligaments.

Li et al. focused on the tendon-to-bone interface: they produced mats of PLGA and PCL nanofibers, mineralized with gradients of tricalcium phosphate. They found increased values of strain and decreased value of Young's modulus due to the reduction of the mineralization. They seeded the scaffolds with mouse preosteoblast cells (MPC3T3), finding increased values of proliferation in the sites with presence of tricalcium phosphate [131]. Samavedi et al., to simulate the bone-to-ligament interface, studied a random nanofibrous scaffold with a gradient of PEUUR2000 and PCL, loaded with nanohydroxyapatite (HAp). The two solutions were co-electrospun on the side of the drum with a central overlap zone (Figure 2.14a). The progressive mineralization of the mat induced a change of the mechanical properties in terms of Young's modulus (HAp-PCL = 2.4 MPa; PEUUR2000 = 0.23 MPa; mixed region = 0.55 MPa) and failure stress (HAp-PCL = 0.5 MPa; PEUUR2000 = 0.6 MPa; mixed region = 0.4 MPa). They obtained encouraging results in terms of MC3T3-31 osteoprogenitor cell metabolic activity [110]. In another work, Samavedi et al. applied the same principle to produce random

nanofibrous mats with a gradient of PCL, loaded with nanohydroxyapatite (HAp), and PEUUR. They cultured the mats with BMSCs, and found that the presence of mineral in the electrospun scaffolds promoted the elevation of morphogenic protein-2 and protein-like osteopontin mRNA, while suppressing the expression of alkaline phosphatase mRNA. Immunofluorescent staining confirmed the presence of proteins like osteopontin and bone sialoprotein, indicating osteoblastic maturation by day 28. Moreover the mineral gradients could promote a spatial gradient of osteoblastic phenotype in BMSCs [111]. Xie et al. focused on the tendon- to-bone insertion: they developed a machine able to modulate the gradient of the random electrospun nanofibers produced. They started aligning nanofibers of PCL, thanks to a gap collector setup. Subsequently, they collected the aligned fibers on a glass coverslip, and put the mat in the machine to produce the gradient. The flat plate collector of the machine was motorized and permitted to moving the scaffold to cover just sections of the mat with random nanofibers still of PCL. Finally they cultured adipose derived stem cells (ADSCs) finding a differentiation of the cells morphology depending on the orientation of the nanofibers [112]. Kolluru et al. focused on the tendon-to-bone insertion: they developed random mats of nanofibers of PLGA, with different degrees of mineralization (mineralized solution composed by calcium and phosphate). They found that the nanofibers morphology and mechanical properties were dependent from different degree of mineralization. The high toughness of this material was maintained without compromising the strength with the addition of hydroxyapatite mineral [83]. He et al. developed a solution for the tendon-to-bone insertion by co-electrospinning on a drum collector, a random (side) PLLGA mat of nanofibers loaded with nanohydroxyapatite (HAp), and aligned (center) PLLGA nanofibers, thus obtaining the desired gradient. They characterized the morphology and composition of the mats, addressing the gradient of alignment of the nanofibers [85]. Criscenti et al., to reproduce the ligament- to-bone interface, proposed an interesting method to combine the electrospinning and 3D printing. At first, PCL was 3D printed, obtaining a reticular structure (bone interface). Subsequently, a part of the 3D printed scaffold was covered by electrospun nanofibers of PLLGA. The nanofibers were aligned by the two collectors, producing a partial overlap on the 3D printed

scaffold (enthesis). In addition, the mat of aligned nanofibers (which were not overlapped), reproduced the ligament tissue. Different mechanical properties were measured in the different parts of the scaffolds (Young's modulus 3D print = 43.6 ± 8.1 MPa, mixed 50.6 ± 5.1 MPa electrospun = 88.9 6 ± 15.1 MPa; failure stress: 3D print = 1.62 ± 0.27 MPa; mixed = 2.57 ± 0.51 MPa; electrospun = 5.21 ± 1.11 MPa). They seeded the scaffolds with hMSCs, finding increased levels of proliferation and different orientation of the cells, depending on the side, after seven days of culture [86]. Kishan et al. to obtain patches for rotator cuff repair, developed random and aligned nanofibrous mats with a gradient of two different biodegradable BPUR10 and BPUR50. They found human BMMSCs differentiation in the different degrees of alignment of the fibers. They also reported different levels of strain depending on the disposition of the nanofibers [120]. Oliveira et al. studied the differentiation of bone marrow-derived porcine mesenchymal stem cells in ligament or bone/cartilage differentiation, using random and aligned microfibers of PCL. They added different growth factors to study the differentiation of cells in ligamentogenic, chondrogenic or fibrochondrogenic phenotype upon presentation of appropriate biochemical cues [90]. Wu et al. focused on the repair of the tendon-to-bone and ligament-to-bone insertions: they analyzed nanostructured HAp, loaded in random nanofibrous blends mats of PCL and CTS. They found increased osteoblast viability after 48 h of culture [109].

Zhu et al. conduced an in vivo study on a rabbit anterior cruciate ligament model, to investigate the cells growing on PLLA nanofibrous scaffolds, obtained by electrospinning on a flat plate collector with a copper grid on its surface. At the end of the animal trial, they found abundant extracellular matrix such as collagen (Types I–III) and fibrocartilage on the scaffolds [67]. Zhi et al. used random microfiber mats of SE, in culture with rabbit BMMSCs to evaluate the tendon-to-bone healing effects. After the cells test, they wrapped some mats on a resected rabbit Achilles' tendon, and implanted the assembly in a hole of the rabbit hindlimb. After 12 weeks, they found increased bone regeneration. Moreover, the electrospun mats could not be pulled out from the bones and showed a statistically significant increment of the mechanical properties compared to the control groups [129].

Li et al. designed a bilayer microfibrous scaffold made of a mat of PLLA, for rotator cuff repair. A second layer of PLLA microfibers loaded with nanohydroxyapatite (HAp). The in vivo rabbit model showed that the scaffolds significantly increased the area of glycosaminoglycan staining at the tendon-to-bone interface and improved collagen organization. Implanting the bipolar membrane also induced bone formation and fibrillogenesis, as assessed by micro-CT, and histological analysis. Biomechanical testing showed that the scaffolds had a greater failure load (181.5 ± 19.0 N), failure stress (4.6 ± 0.6 MPa) and stiffness (average value > 20 MPa) than the control group at 12 weeks after surgery [66].

2.7.5 Muscle insertion

The tendon-to-muscle interface was first addressed by Ladd et al. They co-electrospun random nanofibrous mats of a PCL and Coll blend and a PLLA and Coll blend. They obtained a gradient of the two solutions in the center of the mats and, the two distinct ones in the sides. The PCL side exhibited low Young's modulus (4.5 ± 1.6 MPa) and failure stress (1.07 ± 0.27 MPa). This section also demonstrated the largest failure strain (130.4 ± 44.56%). In contrast, the PLLA side had the highest Young's modulus (27.62 ± 6.06 MPa) and failure stress (3.74 ± 0.85 MPa), as well as low failure strain (35.3 ± 9.0%). The center region had the most variability in mechanical properties, but exhibited a Young's modulus (20.1 ± 7.8 MPa) and failure stress (2.38 ± 0.60 MPa) in between the values for the PLLA side and the PCL side. The failure strain (42.8 ± 17.7%) of the central region was similar to the PLLA side. They found also an increased viability of both myoblasts and fibroblasts [68].

2.7.6 Tendon and ligament healing and anti-adhesion

Preventing inflammation and adhesion is fundamental for a successful regeneration of the tissue. Such detrimental phenomena are due to excessive proliferation of fibroblasts on the injured surface of the treated tendon or ligament. For this reason, some researchers started to study how manage the anti-adhesion problem.

Lui et al. produced aligned nanofibers of PLLA and PCL in different percentages, charged with NPS to prevent tendon adhesion. They found that increasing the PCL content increased the failure strain but also the release rate of NPS. The failure stress was also enhanced with the addition of water as the co-solvent. This NPS-loaded scaffold showed no significant cytotoxicity, and L929 murine fibroblasts cultured on the scaffolds were able to proliferate and align along the fibers [71].

To prevent tendon adhesion, Jiang et al. investigated random nanofibrous mats of PELA loaded with the anti-inflammatory celecoxib (0%, 2%, 6%, and 10%). The mechanical tests showed a ductile behavior with different values of failure stresses depending to the percentage of celecoxib (PELA = 3.04 ± 0.32 MPa; PELA-2% = 2.87 ± 0.27 MPa; PELA-6% = 2.77 ± 0.34 MPa; PELA-10% = 2.72 ± 0.31 MPa). Cellular tests with rabbit tenocytes and dermal fibroblasts showed decreased viability, increasing the percentage of celecoxib. The in vivo rabbit model confirmed that the fibroblasts grew on the PELA mats. Moreover, the adhesions were inhibited by down-regulating the extracellular- regulated signal kinases 1/2 (ERK1/2) and small mother against decapentaplegic 2/3 (SMAD2/3) phosphorylation [72]. To promote the tendon healing and prevent adhesion, Liu et al. electrospun a random nanofibrous scaffold of PCL, as outer layer, and a blend of PCL/HA, as inner layer, to be wrapped on an injured tendon (Figure 2.14b). The cell viability (multipotent C3H10T1/2 cells) and in vivo chicken model, showed encouraging results in terms of anti-adhesion properties and release of HA [113]. Liu et al. electrospun random PLLA nanofibers, loaded with DGNs and bFGF, to prevent adhesions. The in vitro proliferation of the multipotent C3H10T1⁄2 (C3) cells showed the low affinity of these scaffolds to the cell adhesion. These results were confirmed by a rat in vivo study [69]. Zhao et al. loaded PLLA with a solution of HA and MMC, to obtain random core–shell nanofibrous mats to enhance anti-adhesion in tendon applications. The NIH/3T3 fibroblasts viability tests showed decreased cell adhesion and apoptotic effects, mediated by the release of MMC. In the in vivo rat model, the mats prevented adhesion surrounding the tendon lesion, without detrimental effect for the healing process of the injured tendon, by mediating fibroblast apoptosis and syntheses of collagen [70]. Buschmann et al. tested in vivo a DP nanofibrous random DP conduit in a rabbit Achilles tendon.

After the production, the conduits were pushed-out from the tube and inverted before implantation in a rat Achilles' tendon model. In the first study, they confirmed that DP tubes could be set around a sutured tendon rupture without any adverse effects: the cellular response of the healing tissue 12 weeks post-operation was the same as if no implant was set [125]. In the second study, the synthesis was modified to increase the elasticity. The new material was implanted in a similar rat model: the cellular response to the modified polymer, after 12 weeks, was similar to the classic DP [126]. Evrova et al. investigated a random nanofibrous bilayer tube for tendon tissue regeneration. A first layer of electrospun nanofibers of DP was electrospun on a rotating drum. A second layer of DP nanofibers, loaded with PDGF-BB, were obtained by emulsion electrospinning on the previous one (Figure 2.14c). The released PDGF-BB was shown to be bioactive, leading to increased proliferation of rabbit tenocytes in in vitro under serum free conditions [127].

To create a tendon healing and anti-adhesive scaffold, Li et al. designed a bilayer microfibrous mat, made by electrospinning first a solution of PELA and HA, and then a celecoxib-PELA solution. The in vivo data on a chicken model, confirmed that the celecoxib-loaded outer PELA layer can prevent adhesion and associated inflammation [73].

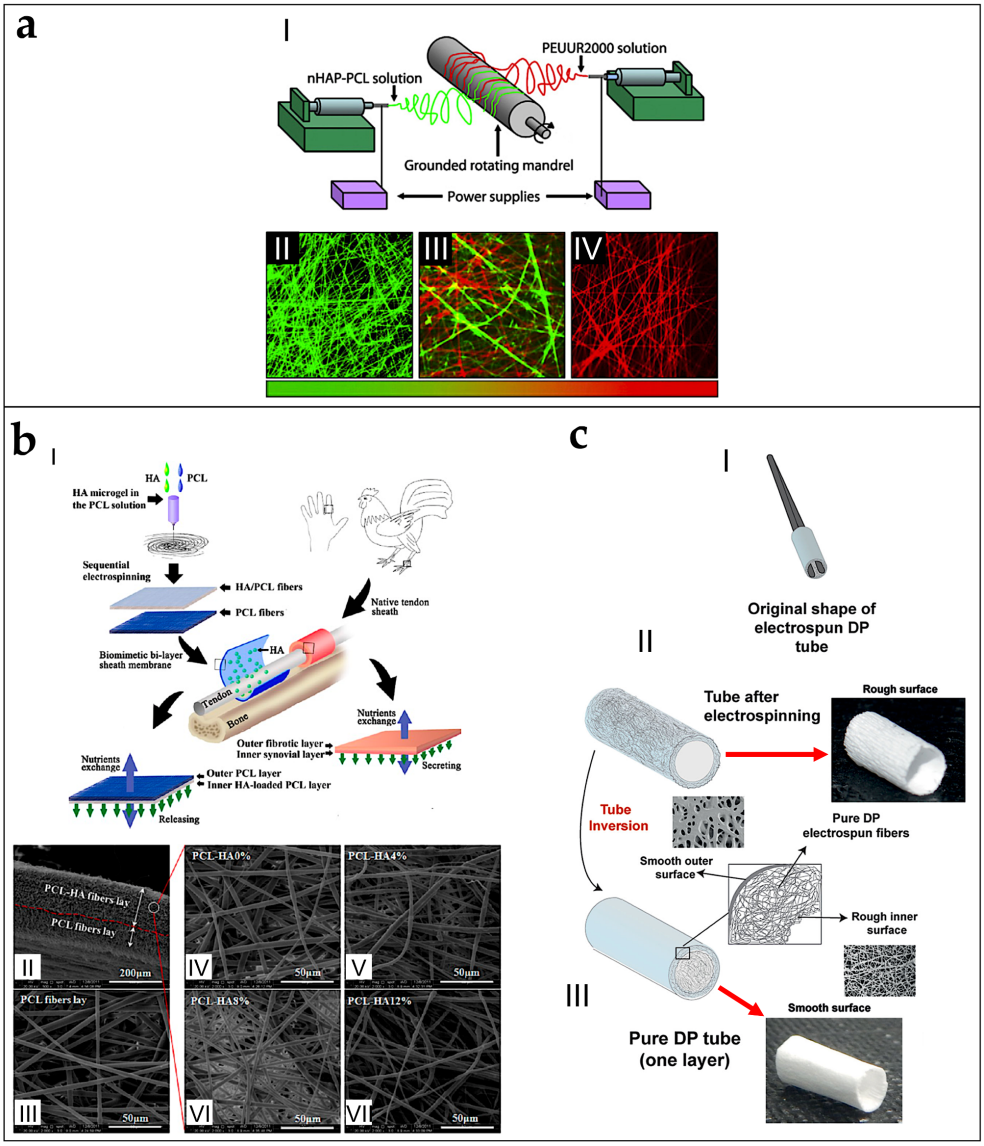

Figure 2.14. Schematic workflows to produce electrospun scaffolds suitable for tendon/ligament-to- bone attachment or for tendon and ligament healing and anti-adhesion applications. (a) Co-electrospun random mats with gradient of PEUUR2000 and PCL, loaded with nanohydroxyapatite (HAp) for ligament-to-bone regeneration (adapted from Samavedi et al. [110], reproduced with permission. Copyright 2011, Elsevier): (I) co-electrospinning setup to obtain nanofibrous mats with gradient on a rotating drum collector; (II) fluorescent image of the HAp-PCL nanofibers side; (III) fluorescent image of the transition region of the two nanofiber sides; and (IV) fluorescent image of the PEUUR2000 nanofibers side. (b) Double layer electrospun mat of random PCL and a blend of PCL/HA for tendon healing (adapted with permission from Liu et al. [113]. Copyright 2012, American Chemical Society): (I) electrospinning setup and in-situ application of the scaffold; (II) SEM section of the bilayer scaffold; (III) PCL nanofibers; and (IV–VII) layers of HA/PCL nanofibers with different percentages of HA. (c) Production process to obtain a nanofibrous tube or conduit of DP for tendon healing and anti-adhesion applications (adapted from Evrova et al. [127],

reproduced with permission. Copyright 2016, John Wiley and Sons); (I) after the nanofibers are electrospun on a rotating drum collector, the tube is removed from it; (II) structure and images of the tube immediately after the movement from the drum collector; and (III) structure and images of the tube after is inversion.

2.8 Conclusions and future perspective

Tendon and ligament regeneration and replacement is currently a hot topic for tissue engineering and orthopedic research. Among the various technologies explored for healing and regenerate these tissues, electrospinning is definitely one of the most promising since it combines biomimicry and manufacturing flexibility. In the last twenty years, more than one hundred scientific papers and several reviews have described different methodologies and the respective strengths and shortcomings of the electrospun nanofibers applied in the regeneration of tendons and ligaments. Researchers started investigating the effects of the nanofibers' morphology and orientation, on the cells proliferation and growing, testing different polymeric solutions. Several in vivo tests on small and large animal models are described, providing encouraging results in terms of integration with the host tissue, healing and biocompatibility. However, despite these promising outcomes, the limited mechanical properties are currently the principal constraint in the application of these scaffolds in human clinical trials. For these reasons, the new challenge of the next years will probably be the development of electrospun multiscale hierarchical scaffolds and devices, able to replicate as soon as possible not only the hierarchical structure, but also the biomechanical properties of tendons and ligaments. Moreover, scaffolds must be customizable so that the production can be adapted to the different tendons and ligaments requiring treatment. A further enhancement will consist in personalization to meet patient-specific needs in terms of anatomy as well as resorption rate. If these results are achieved, electrospun scaffolds and devices will be industrialized and potentially become a gold standard for the surgery and the tissue engineering of tendons and ligaments.

2.7 References

[161] Berthiaume, F.; Maguire, T.J.; Yarmush, M.L. 2011 Tissue Engineering and Regenerative Medicine: History, Progress, and Challenges. Annu. Rev. Chem. Biomol. Eng., 2, 403–430.

[162] Pećina, M.; Vukičević, S. 2014 Tissue engineering and regenerative orthopaedics (TERO). Int. Orthop., 38, 1757–1760.

[163] Guilak, F.; Baaijens, F.P.T. 2014 Functional tissue engineering: Ten more years of progress. J. Biomech., 47, 1931–1932.

[164] Abbah, S.A.; Delgado, L.M.; Azeem, A.; Fuller, K.; Shologu, N.; Keeney, M.; Biggs, M.J.; Pandit, A.; Zeugolis, D.I. 2015 Harnessing Hierarchical Nano- and Micro-Fabrication Technologies for Musculoskeletal Tissue Engineering. Adv. Healthc. Mater., 4, 2488–2499.

[165] Kastelic, J.; Galeski, A.; Baer, E. 1978 The Multicomposite Structure of Tendon. Connect. Tissue Res., 6, 11– 23.

[166] Kannus, P. 2000 Structure of the tendon connective tissue. Scand. J. Med. Sci. Sport., 10, 312–320.

[167] Goh, K.L.; Listrat, A.; Béchet, D. 2014 Hierarchical mechanics of connective tissues: Integrating insights from nano to macroscopic studies. J. Biomed. Nanotechnol., 10, 2464–2507.

[168] Rodrigues, M.T.; Reis, R.L.; Gomes, M.E. 2013 Engineering tendon and ligament tissues: Present developments towards successful clinical products. J. Tissue Eng. Regen. Med., 4,

[169] O'Connor, R.A.; McGuinness, G.B. 2016 Electrospun nanofibre bundles and yarns for tissue engineering applications: A review. Proc. Inst. Mech. Eng. Part H J. Eng. Med., 230, 987–998.

[170] Brennan, D.A.; Conte, A.A.; Kanski, G.; Turkula, S.; Hu, X.; Kleiner, M.T.; Beachley, V. 2018 Mechanical Considerations for Electrospun Nanofibers in Tendon and Ligament Repair. Adv. Healthc. Mater., 1701277, 1–31.

[171] James, R.; Laurencin, C.T. 2016 Nanofiber technology: Its transformative role in nanomedicine. Nanomedicine, 11, 1499–1501.

[172] Benjamin, M.; Ralphs, J.R. 1997 Tendon and ligaments-An overview.pdf. Histol. Histopatology, 12, 1135– 1144.

[173] Frank, C.B. 2004 Ligament structure, physiology and function. J. Musculoskelet. Neuronal Interact., 4, 199– 201.

[174] Santos, M.L.; Rodrigues, M.T.; Domingues, R.M.A.; Reis, R.L.; Gomes, M.E. 2017 Regenerative Strategies for the Treatment of Knee Joint Disabilities. In Regenerative Strategies for the Treatment of Knee Joint Disabilities; Oliveira, J.M., Ruis, R.L., Eds.; Springer: New York, NY, USA; Vol. 21, pp. 349–371

[175] Murphy, W.; Black, J.; Hastings, G. 2016 Handbook of Biomaterial Properties, 2nd ed.; Springer: New York, NY, USA

[176] Wang, J.H.C. 2006 Mechanobiology of tendon. J. Biomech., 39, 1563–1582.

[177] Moshiri, A.; Oryan, A. 2013 Tendon and Ligament Tissue Engineering, Healing and Regenerative Medicine. J. Sports Med. Doping Stud., 3, 1–18.

[178] Woo, S.L.Y.; Chan, S.S.; Yamaji, T. 1997 Biomechanics of knee ligament healing, repair and reconstruction. J. Biomech., 30, 431–439.

[179] Woo, S.L.Y.; Abramowitch, S.D.; Kilger, R.; Liang, R. 2006 Biomechanics of knee ligaments: Injury, healing, and repair. J. Biomech., 39, 1–20.

[180] Pioletti, D.; Rakotomanana, L.; Leyvraz, P. 1999 Strain rate effect on the mechanical behavior of the anterior cruciate ligament-bone complex. Med. Eng. Phys., 21, 95–100.

[181] Yoganandan, N.; Kumaresan, S.; Pintar, F.A. 2000 Geometric and Mechanical Properties of Human Cervical. J. Biomech. Eng., 122, 623–629.

[182] Mesfar, W.; Moglo, K. 2013 Effect of the transverse ligament rupture on the biomechanics of the cervical spine under a compressive loading. Clin. Biomech, 28, 846–852.

[183] Langer, R.; Vacanti, J.P. 1993 Tissue Engineering. Science (80), 260, 920–926.

[184] O'Brien, F.J. 2011 Biomaterials & scaffolds for tissue engineering. Mater. Today, 14, 88–95.

[185] Moshiri, A.; Oryan, A. 2012 Role of tissue engineering in tendon reconstructive surgery and regenerative medicine: Current concepts, approaches and concerns. Hard Tissue, 1, 1–11.

[186] Chen, J.; Xu, J.; Wang, A.; Zheng, M. 2014 Scaffolds for tendon and ligament repair: Review of the efficacy of commercial products. Expert Rev. Med. Devices, 6, 61–73.

[187] Hollister, S.J. Porous scaffold design for tissue engineering. Nat. Mater. 2005, 4, 518–524.

[188] Causa, F.; Netti, P.A.; Ambrosio, L. A multi-functional scaffold for tissue regeneration: The need to engineer a tissue analogue. Biomaterials 2007, 28, 5093–5099.

[189] Chevalier, E.; Chulia, D.; Pouget, C.; Viana, M. Fabrication of Porous Substrates: A Review of Processes Using Pore Forming Agents in the Biomaterial Field. J. Pharm. Sci. 2008, 97, 1135–1154.

[190] Sung, H.J.; Meredith, C.; Johnson, C.; Galis, Z.S. The effect of scaffold degradation rate on three- dimensional cell growth and angiogenesis. Biomaterials 2004, 25, 5735–5742.

[191] Loh, Q.L.; Choong, C. Three-Dimensional Scaffolds for Tissue Engineering Applications: Role of Porosity and Pore Size. Tissue Eng. Part B Rev. 2013, 19, 485–502.

[192] Walden, G.; Liao, X.; Donell, S.; Raxworthy, M.J.; Riley, G.P.; Saeed, A. A Clinical, Biological, and Biomaterials Perspective into Tendon Injuries and Regeneration. Tissue Eng. Part B Rev. 2017, 23, 44–58.

[193] Cooley, J.F. Electrical method of dispersing fluids. US745276A, 06 October 1899, 1–6.

[194] Agarwal, S.; Wendorff, J.H.; Greiner, A. Use of electrospinning technique for biomedical applications. Polymer (Guildf). 2008, 49, 5603–5621.

[195] Liu, W.; Thomopoulos, S.; Xia, Y. Electrospun nanofibers for regenerative medicine. Adv. Healthc. Mater. 2012, 1, 10–25.

[196] Sun, B.; Long, Y.Z.; Zhang, H.D.; Li, M.M.; Duvail, J.L.; Jiang, X.Y.; Yin, H.L. Advances in three-dimensional nanofibrous macrostructures via electrospinning. Prog. Polym. Sci. 2014, 39, 862–890.

[197] Jiang, T.; Carbone, E.J.; Lo, K.W.H.; Laurencin, C.T. Electrospinning of polymer nanofibers for tissue regeneration. Prog. Polym. Sci. 2015, 46, 1–24.

[198] Teo, W.E.; Ramakrishna, S. A review on electrospinning design and nanofibre assemblies. Nanotechnology 2006, 17, R89–R106.

[199] Huang, Z.M.; Zhang, Y.Z.; Kotaki, M.; Ramakrishna, S. A review on polymer nanofibers by electrospinning and their applications in nanocomposites. Compos. Sci. Technol. 2003, 63, 2223–2253.

[200] Xue, J.; Xie, J.; Liu, W.; Xia, Y. Electrospun Nanofibers: New Concepts, Materials, and Applications. Acc. Chem. Res. 2017, 50, 1976–1987.

[201] Haider, A.; Haider, S.; Kang, I.K. A comprehensive review summarizing the effect of electrospinning parameters and potential applications of nanofibers in biomedical and biotechnology. Arab. J. Chem. 2015.

[202] Baumgarten, P.K. Electrostatic spinning of acrylic microfibers. J. Colloid Interface Sci. 1971, 36, 71–79.

[203] Matabola, K.P.; Moutloali, R.M. The influence of electrospinning parameters on the morphology and diameter of poly(vinyledene fluoride) nanofibers- Effect of sodium chloride. J. Mater. Sci. 2013, 48, 5475– 5482.

[204] Wang, T.; Kumar, S. Electrospinning of polyacrylonitrile nanofibers. J. Appl. Polym. Sci. 2006, 102, 1023–1029.

[205] Lannutti, J.; Reneker, D.; Ma, T.; Tomasko, D.; Farson, D. Electrospinning for tissue engineering scaffolds. Mater. Sci. Eng. C 2007, 27, 504–509.

[206] Sill, T.J.; von Recum, H.A. Electrospinning: Applications in drug delivery and tissue engineering. Biomaterials 2008, 29, 1989–2006.

[207] Jarusuwannapoom, T.; Hongrojjanawiwat, W.; Jitjaicham, S.; Wannatong, L.; Nithitanakul, M.; Pattamaprom, C.; Koombhongse, P.; Rangkupan, R.; Supaphol, P. Effect of solvents on electro-spinnability of polystyrene solutions and morphological appearance of resulting electrospun polystyrene fibers. Eur. Polym. J. 2005, 41, 409–421.

[208] Reneker, D.H.; Yarin, A.L. Electrospinning jets and polymer nanofibers. Polymer (Guildf). 2008, 49, 2387– 2425.

[209] Woo, S.L.; Debski, R.E.; Zeminski, J.; Abramowitch, S.D.; Saw, S.S.C.; Fenwick, J.A. INJURY AND REPAIR OF LIGAMENTS AND TENDONS. Annu. Rev. Biomed. Eng. 2000, 2, 83–118.

[210] Kannus, P.; Paavola, M.; Józsa, L. Aging and degeneration of tendons. In Tendon Injuries; Maffulli, N., Renström, P., W.B., L., Eds.; Springer: New York, NY, USA, 2005; pp. 25–31 ISBN

[211] Clayton, R.A.E.; Court-Brown, C.M. The epidemiology of musculoskeletal tendinous and ligamentous injuries. Injury 2008, 39, 1338–1344.

[212] McCarthy, M.M.; Hannafin, J.A. The Mature Athlete: Aging Tendon and Ligament. Sports Health 2014, 6, 41–48.

[213] Surrao, D.C.; Hayami, J.W.S.; Waldman, S.D.; Amsden, B.G. Self-crimping, biodegradable, electrospun polymer microfibers. Biomacromolecules 2010, 11, 3624–3629.

[214] Vaquette, C.; Kahn, C.; Frochot, C.; Nouvel, C.; Six, J.L.; De Isla, N.; Luo, L.H.; Cooper-White, J.; Rahouadj, R.; Wang, X. Aligned poly(L-lactic-co-e-caprolactone) electrospun microfibers and knitted structure: A novel composite scaffold for ligament tissue engineering. J. Biomed. Mater. Res. - Part A 2010, 94, 1270–1282.

[215] Xu, Y.; Wu, J.; Wang, H.; Li, H.; Di, N.; Song, L.; Li, S.; Li, D.; Xiang, Y.; Liu, W.; Mo, X.; Zhou, Q. Fabrication of Electrospun Poly(L-Lactide-co-ε-Caprolactone)/Collagen Nanoyarn

Network as a Novel, Three- Dimensional, Macroporous, Aligned Scaffold for Tendon Tissue Engineering. Tissue Eng. Part C Methods 2013, 19, 925–936.

[216] Yang, C.; Deng, G.; Chen, W.; Ye, X.; Mo, X. A novel electrospun-aligned nanoyarn-reinforced nanofibrous scaffold for tendon tissue engineering. Colloids Surf. B Biointerfaces 2014, 122, 270–276.

[217] Surrao, D.C.; Waldman, S.D.; Amsden, B.G. Biomimetic poly(lactide) based fibrous scaffolds for ligament tissue engineering. Acta Biomater. 2012, 8, 3997–4006.

[218] Rothrauff, B.B.; Lauro, B.B.; Yang, G.; Debski, R.E.; Musahl, V.; Tuan, R.S. Braided and Stacked Electrospun Nanofibrous Scaffolds for Tendon and Ligament Tissue Engineering. Tissue Eng. Part A 2017, 23, 378–389.

[219] Sensini, A.; Gualandi, C.; Cristofolini, L.; Tozzi, G.; Dicarlo, M.; Teti, G.; Belmonte-Mattioli, M.; Focarete, M.L. Biofabrication of bundles of poly (lactic acid) collagen blends mimicking the fascicles of the human Achille tendon. Biofabrication 2017, 9, 1–13.

[220] Sensini, A.; Cristofolini, L.; Focarete, M.L.; Belcari, J.; Zucchelli, A.; Kao, A.; Tozzi, G. High-resolution x-ray tomographic morphological characterisation of electrospun nanofibrous bundles for tendon and ligament regeneration and replacement. J. Microsc. 2018.

[221] Barber, J.G.; Handorf, A.M.; Allee, T.J.; Li, W.-J. Braided Nanofibrous Scaffold for Tendon and Ligament Tissue Engineering. Tissue Eng. Part A 2013, 19, 1265–1274.

[222] Tu, H.; Bao, M.; Li, Q.; Li, B.; Yuan, H.; Zhang, Y. Aligned core–shell structured ultrafine composite fibers of PLLA–collagen for tendon scaffolding. J. Control. Release 2013, 172, e128.

[223] Zhang, C.; Yuan, H.; Liu, H.; Chen, X.; Lu, P.; Zhu, T.; Yang, L.; Yin, Z.; Heng, B.C.; Zhang, Y.; Ouyang, H. Well-aligned chitosan-based ultrafine fibers committed teno-lineage differentiation of human induced pluripotent stem cells for Achilles tendon regeneration. Biomaterials 2015, 53, 716–730.

[224] Zhang, C.; Wang, X.; Zhang, E.; Yang, L.; Yuan, H.; Tu, W.; Zhang, H.; Yin, Z.; Shen, W.; Chen, X.; Zhang, Y.; Ouyang, H. An epigenetic bioactive composite scaffold with well-aligned nanofibers for functional tendon tissue engineering. Acta Biomater. 2018, 66, 141–156.

[225] Zhao, S.; Xie, X.; Pan, G.; Shen, P.; Zhao, J.; Cui, W. Healing improvement after rotator cuff repair using gelatin-grafted poly(L-lactide) electrospun fibrous membranes. J. Surg. Res. 2015, 193, 33–42.

[226] Li, X.; Cheng, R.; Sun, Z.; Su, W.; Pan, G.; Zhao, S.; Zhao, J.; Cui, W. Flexible bipolar nanofibrous membranes for improving gradient microstructure in tendon-to-bone healing. Acta Biomater. 2017, 61, 204–216.

[227] Zhu, J.; Zhang, X.; Shao, Z.; Dai, L.; Li, L.; Hu, X.; Wang, X.; Zhou, C.; Ao, Y. In Vivo Study of Ligament-Bone Healing after Anterior Cruciate Ligament Reconstruction Using Autologous Tendons withMesenchymal Stem Cells Affinity Peptide Conjugated Electrospun Nanofibrous Scaffold Jingxian. J. Nanomater. 2013, 1–11.

[228] Ladd, M.R.; Lee, S.J.; Stitzel, J.D.; Atala, A.; Yoo, J.J. Co-electrospun dual scaffolding system with potential for muscle-tendon junction tissue engineering. Biomaterials 2011, 32, 1549–1559.

[229] Liu, S.; Qin, M.; Hu, C.; Wu, F.; Cui, W.; Jin, T.; Fan, C. Tendon healing and anti-adhesion properties of electrospun fibrous membranes containing bFGF loaded nanoparticles. Biomaterials 2013, 34, 4690–4701.

[230] Zhao, X.; Jiang, S.; Liu, S.; Chen, S.; Lin, Z.Y.W.; Pan, G.; He, F.; Li, F.; Fan, C.; Cui, W. Optimization of intrinsic and extrinsic tendon healing through controllable water-soluble mitomycin-C release from electrospun fibers by mediating adhesion-related gene expression. Biomaterials 2015, 61, 61–74.

[231] Lui, Y.S.; Lewis, M.P.; Loo, S.C.J. Sustained-release of naproxen sodium from electrospun-aligned PLLA– PCL scaffolds. J. Tissue Eng. Regen. Med. 2017, 11, 1011–1021.

[232] Jiang, S.; Zhao, X.; Chen, S.; Pan, G.; Song, J.; He, N.; Li, F.; Cui, W.; Fan, C. Down-regulating ERK1/2 and SMAD2/3 phosphorylation by physical barrier of celecoxib-loaded electrospun fibrous membranes prevents tendon adhesions. Biomaterials 2014, 35, 9920–9929.

[233] Li, L.; Zheng, X.; Fan, D.; Yu, S.; Wu, D.; Fan, C.; Cui, W.; Ruan, H. Release of celecoxib from a bi-layer biomimetic tendon sheath to prevent tissue adhesion. Mater. Sci. Eng. C 2016, 61, 220–226.

[234] Bashur, C.A.; Dahlgren, L.A.; Goldstein, A.S. Effect of fiber diameter and orientation on fibroblast morphology and proliferation on electrospun poly(d,l-lactic-co-glycolic acid) meshes. Biomaterials 2006, 27, 5681–5688.

[235] Inui, A.; Kokubu, T.; Mifune, Y.; Sakata, R.; Nishimoto, H.; Nishida, K.; Akisue, T.; Kuroda, R.; Satake, M.; Kaneko, H.; Fujioka, H. Regeneration of rotator cuff tear using electrospun poly(d,l-Lactide-Co-Glycolide) scaffolds in a rabbit model. Arthrosc. J. Arthrosc. Relat. Surg. 2012, 28, 1790–1799.

[236] Sahoo, S.; Ang, L.T.; Cho-Hong Goh, J.; Toh, S.L. Bioactive nanofibers for fibroblastic differentiation of mesenchymal precursor cells for ligament/tendon tissue engineering applications. Differentiation 2010, 79, 102–110.

[237] Sahoo, S.; Ouyang, H.; Goh, J.C.-H.; Tay, T.E.; Toh, S.L. Characterization of a Novel Polymeric Scaffold for Potential Application in Tendon/Ligament Tissue Engineering. Tissue Eng. 2006, 12, 91–99.

[238] Thayer, P.S.; Dimling, A.F.; Plessl, D.S.; Hahn, M.R.; Guelcher, S.A.; Dahlgren, L.A.; Goldstein, A.S. Cellularized Cylindrical Fiber / Hydrogel Composites for Ligament Tissue Engineering. Biomacromolecules 2014, 15, 75–83.

[239] Full, S.M.; Delman, C.; Gluck, J.M.; Abdmaulen, R.; Shemin, R.J.; Heydarkhan-Hagvall, S. Effect of fiber orientation of collagen-based electrospun meshes on human fibroblasts for ligament tissue engineering applications. J. Biomed. Mater. Res. Part B Appl. Biomater. 2015, 103, 39–46.

[240] Thayer, P.S.; Verbridge, S.S.; Dahlgren, L.A.; Kakar, S.; Guelcher, S.A.; Goldstein, A.S. Fiber/collagen composites for ligament tissue engineering: Influence of elastic moduli of sparse aligned fibers on mesenchymal stem cells. J. Biomed. Mater. Res. - Part A 2016, 104, 1894–1901.

[241] Zhao, S.; Zhao, J.; Dong, S.; Huangfu, X.; Li, B.; Yang, H.; Zhao, J.; Cui, W. Biological augmentation of rotator cuff repair using bFGF-loaded electrospun poly (lactide-co-glycolide) fibrous membranes. Int. J. Nanomedicine 2014, 9, 2373–2385.

[242] Bosworth, L.A. Travelling along the Clinical Roadmap: Developing Electrospun Scaffolds for Tendon Repair. Conf. Pap. Sci. 2014, 2014, 1–6.

[243] Kolluru, P.V.; Lipner, J.; Liu, W.; Xia, Y.; Thomopoulos, S.; Genin, G.M.; Chasiotis, I. Strong and tough mineralized PLGA nanofibers for tendon-to-bone scaffolds. Acta Biomater. 2013, 9, 9442–9450.

[244] Sahoo, S.; Toh, S.L.; Goh, J.C.H. A bFGF-releasing silk/PLGA-based biohybrid scaffold for ligament/tendon tissue engineering using mesenchymal progenitor cells. Biomaterials 2010, 31, 2990–2998.

[245] He, J.; Qin, T.; Liu, Y.; Li, X.; Li, D.; Jin, Z. Electrospinning of nanofibrous scaffolds with continuous structure and material gradients. Mater. Lett. 2014, 137, 393–397.

[246] Criscenti, G.; Longoni, A.; Di Luca, A.; De Maria, C.; van Blitterswijk, C.A.; Vozzi, G.; Moroni, L. Triphasic scaffolds for the regeneration of the bone-ligament interface. Biofabrication 2016, 8, 015009.

[247] Samavedi, S.; Vaidya, P.; Gaddam, P.; Whittington, A.R.; Goldstein, A.S. Electrospun meshes possessing region-wise differences in fiber orientation, diameter, chemistry and mechanical properties for engineering bone-ligament-bone tissues. Biotechnol. Bioeng. 2014, 111, 2549–2559.

[248] Naghashzargar, E.; Farè, S.; Catto, V.; Bertoldi, S.; Semnani, D.; Karbasi, S.; Tanzi, M.C. Nano/micro hybrid scaffold of PCL or P3HB nanofibers combined with silk fibroin for tendon and ligament tissue engineering. J. Appl. Biomater. Funct. Mater. 2015, 13, e156–e168.

[249] Gurlek, A.C.; Sevinc, B.; Bayrak, E.; Erisken, C. Synthesis and characterization of polycaprolactone for anterior cruciate ligament regeneration. Mater. Sci. Eng. C 2017, 71, 820–826.

[250] Olvera, D.; Sathy, B.N.; Carroll, S.F.; Kelly, D.J. Modulating microfibrillar alignment and growth factor stimulation to regulate mesenchymal stem cell differentiation. Acta Biomater. 2017, 64, 148–160.

[251] Deepthi, S.; Jeevitha, K.; Nivedhitha Sundaram, M.; Chennazhi, K.P.; Jayakumar, R. Chitosan-hyaluronic acid hydrogel coated poly(caprolactone) multiscale bilayer scaffold for ligament regeneration. Chem. Eng. J. 2015, 260, 478–485.

[252] Pauly, H.M.; Kelly, D.J.; Popat, K.C.; Trujillo, N.A.; Dunne, N.J.; McCarthy, H.O.; Haut Donahue, T.L. Mechanical properties and cellular response of novel electrospun nanofibers for ligament tissue engineering: Effects of orientation and geometry. J. Mech. Behav. Biomed. Mater. 2016, 61, 258–270.

[253] Pauly, H.M.; Sathy, B.N.; Olvera, D.; McCarthy, H.O.; Kelly, D.J.; Popat, K.C.; Dunne, N.J.; Haut Donahue, T.L. Hierarchically Structured Electrospun Scaffolds with Chemically Conjugated Growth Factor for Ligament Tissue Engineering. Tissue Eng. Part A 2017, 23, 823–836.

[254] Vaquette, C.; Sudheesh Kumar, P.T.; Petcu, E.B.; Ivanovski, S. Combining electrospinning and cell sheet technology for the development of a multiscale tissue engineered ligament construct (TELC). J. Biomed. Mater. Res. - Part B Appl. Biomater. 2017, 00B, 1–11.

[255] Chainani, A.; Hippensteel, K.J.; Kishan, A.; Garrigues, N.W.; Ruch, D.S.; Guilak, F.; Little, D. Multilayered Electrospun Scaffolds for Tendon Tissue Engineering. Tissue Eng. Part A 2013, 19, 2594–2604.

[256] Beason, D.P.; Connizzo, B.K.; Dourte, L.M.; Mauck, R.L.; Soslowsky, L.J.; Steinberg, D.R.; Bernstein, J. Fiber- aligned polymer scaffolds for rotator cuff repair in a rat model. J. Shoulder Elbow Surg. 2012, 21, 245250.

[257] Zhao, S.; Zhao, X.; Dong, S.; Yu, J.; Pan, G.; Zhang, Y.; Zhao, J.; Cui, W. A hierarchical, stretchable and stiff fibrous biotemplate engineered using stagger- electrospinning for augmentation of rotator cuff tendon- healing. J. Mater. Chem. B Mater. Biol. Med. 2015, 3, 990–1000.

[258] Manning, C.N.; Schwartz, A.G.; Liu, W.; Xie, J.; Havlioglu, N.; Sakiyama-Elbert, S.E.; Silva, M.J.; Xia, Y.; Gelberman, R.H.; Thomopoulos, S. Controlled delivery of mesenchymal stem

cells and growth factors using a nanofiber scaffold for tendon repair. Acta Biomater. 2013, 9, 6905–6914.

[259] Orr, S.B.; Chainani, A.; Hippensteel, K.J.; Kishan, A.; Gilchrist, C.; Garrigues, N.W.; Ruch, D.S.; Guilak, F.; Little, D. Aligned multilayered electrospun scaffolds for rotator cuff tendon tissue engineering. Acta Biomater. 2015, 24, 117–126.

[260] Yang, G.; Lin, H.; Rothrauff, B.B.; Yu, S.; Tuan, R.S. Multilayered polycaprolactone/gelatin fiber-hydrogel composite for tendon tissue engineering. Acta Biomater. 2016, 35, 68–76.

[261] Bosworth, L.A.; Alam, N.; Wong, J.K.; Downes, S. Investigation of 2D and 3D electrospun scaffolds intended for tendon repair. J. Mater. Sci. Mater. Med. 2013, 24, 1605–1614.

[262] Bosworth,L.A.;Rathbone,S.R.;Bradley,R.S.;Cartmell,S.H.Dynamicloadingofelectrospuny arnsguides mesenchymal stem cells towards a tendon lineage. J. Mech. Behav. Biomed. Mater. 2014, 39, 175–183.

[263] Bhaskar, P.; Bosworth, L.A.; Wong, R.; O'brien, M. A.; Kriel, H.; Smit, E.; McGrouther, D.A.; Wong, J.K.; Cartmell, S.H. Cell response to sterilized electrospun poly(Ɛ-caprolactone) scaffolds to aid tendon regeneration in vivo. J. Biomed. Mater. Res. Part A 2017, 105, 389–397.

[264] Domingues, R.M.A.; Chiera, S.; Gershovich, P.; Motta, A.; Reis, R.L.; Gomes, M.E. Enhancing the Biomechanical Performance of Anisotropic Nanofibrous Scaffolds in Tendon Tissue Engineering: Reinforcement with Cellulose Nanocrystals. Adv. Healthc. Mater. 2016, 5, 1364–1375.

[265] Levitt, A.S.; Knittel, C.E.; Vallett, R.; Koerner, M.; Dion, G.; Schauer, C.L. Investigation of nanoyarn preparation by modified electrospinning setup. J. Appl. Polym. Sci. 2017, 134, 1–7.

[266] Hakimi, O.; Mouthuy, P.A.; Zargar, N.; Lostis, E.; Morrey, M.; Carr, A. A layered electrospun and woven surgical scaffold to enhance endogenous tendon repair. Acta Biomater. 2015, 26, 124–135.

[267] Banik, B.L.; Lewis, G.S.; Brown, J.L. Multiscale Poly-(ε-caprolactone) Scaffold Mimicking Non-linearity in Tendon Tissue Mechanics. Regen. Eng. Transl. Med. 2016, 2, 1–9.

[268] Laranjeira, M.; Domingues, R.M.A.; Costa-Almeida, R.; Reis, R.L.; Gomes, M.E. 3D Mimicry of Native- Tissue-Fiber Architecture Guides Tendon-Derived Cells and Adipose Stem Cells into Artificial Tendon Constructs. Small 2017, 13, 1–13.

[269] Wu, G.; Deng, X.; Song, J.; Chen, F. Enhanced biological properties of biomimetic apatite fabricated polycaprolactone/chitosan nanofibrous bio-composite for tendon and ligament regeneration. J. Photochem. Photobiol. B Biol. 2018, 178, 27–32.

[270] Samavedi, S.; Olsen Horton, C.; Guelcher, S.A.; Goldstein, A.S.; Whittington, A.R. Fabrication of a model continuously graded co-electrospun mesh for regeneration of the ligament-bone interface. Acta Biomater. 2011, 7, 4131–4138.

[271] Samavedi,S.;Guelcher,S.A.;Goldstein,A.S.;Whittington,A.R.Responseofbonemarrowstro malcellsto graded co-electrospun scaffolds and its implications for engineering the ligament-bone interface. Biomaterials 2012, 33, 7727–7735.

[272] Xie, J.; Ma, B.; Michael, P.L.; Shuler, F.D. Fabrication of Nanofiber Scaffolds With Gradations in Fiber Organization and Their Potential Applications. Macromol. Biosci. 2012, 12, 1336–1341.

[273] Liu, S.; Zhao, J.; Ruan, H.; Tang, T.; Liu, G.; Yu, D.; Cui, W.; Fan, C. Biomimetic Sheath Membrane via Electrospinning for Antiadhesion of Repaired Tendon. Biomacromolecules 2012, 13, 3611–3619.

[274] Lin, Z.; Zhao, X.; Chen, S.; Du, C. Osteogenic and tenogenic induction of hBMSCs by an integrated nanofibrous scaffold with chemical and structural mimicry of the bone–ligament connection. J. Mater. Chem. B 2017, 5, 1015–1027.

[275] Hayami,J.W.S.;Surrao,D.C.;Waldman,S.D.;Amsden,B.G.Designandcharacterizationofabiodegradable composite scaffold for ligament tissue engineering. J. Biomed. Mater. Res. Part A 2010, 92, 1407–1420.

[276] Lee, C.H.; Shin, H.J.; Cho, I.H.; Kang, Y.M.; Kim, I.A.; Park, K.D.; Shin, J.W. Nanofiber alignment and direction of mechanical strain affect the ECM production of human ACL fibroblast. Biomaterials 2005, 26, 1261–1270.

[277] Karchin, a; Wang, Y.-N.; Sanders, J.E. Modulation of gene expression using electrospun scaffolds with templated architecture. J. Biomed. Mater. Res. A 2012, 100, 1605–1614.

[278] Sharifi-Aghdam, M.; Faridi-Majidi, R.; Derakhshan, M.A.; Chegeni, A.; Azami, M. Preparation of collagen/polyurethane/knitted silk as a composite scaffold for tendon tissue engineering. Proc. Inst. Mech. Eng. Part H J. Eng. Med. 2017, 231, 652–662.

[279] Cardwell, R.D.; Dahlgren, L.A.; Goldstein, A.S. Electrospun fibre diameter, not alignment, affects mesenchymal stem cell

[280] Kishan, A.P.; Robbins, A.B.; Mohiuddin, S.F.; Jiang, M.; Moreno, M.R.; Cosgriff-Hernandez, E.M. Fabrication of macromolecular gradients in aligned fiber scaffolds using a combination of in-line blending and air-gap electrospinning. Acta Biomater. 2017, 56, 118–128.

[281] Cook,C.A.;Huri,P.Y.;Ginn,B.P.;GilbertHonick,J.; Somers,S.M.; Temple,J.P.; Mao,H.Q.; Grayson,W.L. Characterization of a novel bioreactor system for 3D cellular mechanobiology studies. Biotechnol. Bioeng. 2016, 113, 1825–1837.

[282] Zhou, F.L.; Gong, R.-H.; Porat, I. Nano-coated hybrid yarns using electrospinning. Surf. Coatings Technol. 2010, 204, 3459–3463.

[283] Dodel, M.; Hemmati Nejad, N.; Bahrami, S.H.; Soleimani, M.; Mohammadi Amirabad, L.; Hanaee-Ahvaz, H.; Atashi, A. Electrical stimulation of somatic human stem cells mediated by composite containing conductive nanofibers for ligament regeneration. Biologicals 2017, 46, 99–107.

[284] Mouthuy,P.A.;Zargar,N.;Hakimi,O.;Lostis,E.;Carr,A.Fabricationofcontinuouselectrospun filaments with potential for use as medical fibres. Biofabrication 2015, 7, 025006.

[285] Buschmann, J.; Meier-Burgisser, G.; Bonavoglia, E.; Neuenschwander, P.; Milleret, V.; Giovanoli, P.; Calcagni, M. Cellular response of healing tissue to DegraPol tube implantation in rabbit Achilles tendon rupture repair: An in vivo histomorphometric study. J. Tissue Eng. Regen. Med. 2013, 7, 413–420.

[286] Buschmann, J.; Calcagni, M.; Meier Burgisser, G.; Bonavoglia, E.; Neuenschwander, P.; Milleret, V.; Giovanoli, P. Synthesis, characterization and histomorphometric analysis of cellular response to a new elastic DegraPolW polymer for rabbit Achilles tendon rupture repair. J. Tissue Eng. Regen. Med. 2015, 9, 584– 594.

[287] Evrova, O.; Houska, J.; Welti, M.; Bonavoglia, E.; Calcagni, M.; Giovanoli, P.; Vogel, V.; Buschmann, J. Bioactive, Elastic, and Biodegradable Emulsion Electrospun DegraPol Tube Delivering PDGF-BB for Tendon Rupture Repair. Macromol. Biosci. 2016, 1048–1063.

[288] Ni, T.; Senthil-Kumar, P.; Dubbin, K.; Aznar-Cervantes, S.D.; Datta, N.; Randolph, M.A.; Cenis, J.L.; Rutledge, G.C.; Kochevar, I.E.; Redmond, R.W. A photoactivated nanofiber graft material for augmented Achilles tendon repair. Lasers Surg. Med. 2012, 44, 645–652.

[289] Zhi,Y.;Liu,W.;Zhang,P.;Jiang,J.;Chen,S.Electrospunsilkfibroinmatenhancestendon-bonehealingin a rabbit extra-articular model. Biotechnol. Lett. 2016, 38, 1827–1835.

[290] Sheikh, F.A.; Macossay, J.; Cantu, T.; Zhang, X.; Shamshi Hassan, M.; Esther Salinas, M.; Farhangi, C.S.; Ahmad, H.; Kim, H.; Bowlin, G.L. Imaging, spectroscopy, mechanical, alignment and biocompatibility studies of electrospun medical grade polyurethane (Carbothane^{TM} 3575A) nanofibers and composite nanofibers containing multiwalled carbon nanotubes. J. Mech. Behav. Biomed. Mater. 2015, 41, 189–198.

[291] Li, X.; Xie, J.; Lipner, J.; Yuan, X.; Thomopoulos, S.; Xia, Y. Nanofiber scaffolds with gradations in mineral content for mimicking the tendon-to-bone insertion site. Nano Lett. 2009, 9, 2763–2768.

[292] Abbasipour, M.; Khajavi, R. Nanofiber bundles and yarns production by electrospinning: A review. Adv. Polym. Technol. 2013, 32, 1–9.

[293] Ali, U.; Zhou, Y.; Wang, X.; Lin, T. Electrospinning of Continuous Nanofiber Bundles and Twisted Nanofiber Yarns. Nanofibers - Prod. Prop. Funct. Appl. 2011, 153–174.

[294] Sahay, R.; Thavasi, V.; Ramakrishna, S. Design modifications in electrospinning setup for advanced applications. J. Nanomater. 2011.

[295] Ding, B.; Kim, H.Y.; Lee, S.C.; Shao, C.L.; Lee, D.R.; Park, S.J.; Kwag, G.B.; Choi, K.J. Preparation and characterization of a nanoscale poly(vinyl alcohol) fiber aggregate produced by an electrospinning method. J. Polym. Sci. Part B Polym. Phys. 2002, 40, 1261–1268.

[296] Li, D.; Wang, Y.; Xia, Y. Electrospinning Nanofibers as Uniaxially Aligned Arrays and Layer-by-Layer Stacked Films. Adv. Mater. 2004, 16, 361–366.

[297] Li, D.; Xia, Y. Electrospinning of nanofibers: Reinventing the wheel? Adv. Mater. 2004, 16, 1151–1170.

[298] Liu, L.; Dzenis, Y.A. Analysis of the effects of the residual charge and gap size on electrospun nanofiber alignment in a gap method. Nanotechnology 2008, 19.

[299] Li,D.;Wang,Y.;Xia,Y.Electrospinning of polymeric and ceramic nanofibers as uniaxially aligned arrays. Nano Lett. 2003, 3, 1167–1171.

[300] Bazbouz, M.B.; Stylios, G.K. Alignment and Optimization of Nylon 6 Nanofibers by Electrospinning. J. Appl. Polym. Sci. 2008, 107, 3023–3032.

[301] Kameoka, J.; Czaplewski, D.; Liu, H.; Craighead, H.G. Polymeric nanowire architecture. J. Mater. Chem. 2004, 14, 1503–1505.

[302] Ishii, Y.; Sakai, H.; Murata, H. A new electrospinning method to control the number and a diameter of uniaxially aligned polymer fibers. Mater. Lett. 2008, 62, 3370–3372. doi:10.1016/j.matlet.2008.03.038.

[303] Formhals,A.Process and apparatus for preparing artificial threads. US1975504A, 2 October 1934.

[304] Formhals,A. Artificial Fiber Construction. US2109333A, 4 March 1938.

[305] Formhals,A.Method and apparatus for the production of fibers. US2123992A, 19 July 1938.

[306] Formhals,A.Method and apparatus for spinning. US2349950A,30 May 1944.

[307] Wu, J.; Hong, Y. Enhancing cell infiltration of electrospun fibrous scaffolds in tissue regeneration. Bioact. Mater. 2016, 1, 56–64.

[308] Ki,C.S.;Park,S.Y.;Kim,H.J.;Jung,H.M.;Woo,K.M.;Lee,J.W.;Park,Y.H.Developmentof3-Dnanofibrous fibroin scaffold with high porosity by electrospinning: Implications for bone regeneration. Biotechnol. Lett. 2008, 30, 405–410.

[309] Yokoyama, Y.; Hattori, S.; Yoshikawa, C.; Yasuda, Y.; Koyama, H.; Takato, T.; Kobayashi, H. Novel wet electrospinning system for fabrication of spongiform nanofiber 3-dimensional fabric. Mater. Lett. 2009, 63, 754–756.

[310] Li, H.; Xu, Y.; Xu, H.; Chang, J. Electrospun membranes: Control of the structure and structure related applications in tissue regeneration and drug delivery. J. Mater. Chem. B 2014, 2, 5492–5510.

[311] Daming, Z.; Jiang, C. Electrospinning of three-dimensional nanofibrous tubes with controllable architectures. Nano Lett. 2008, 8, 3283–3287.

[312] Nedjari, S.; Hébraud, A.; Eap, S.; Siegwald, S.; Mélart, C.; Benkirane-Jessel, N.; Schlatter, G. Electrostatic template-assisted deposition of microparticles on electrospun nanofibers: Towards microstructured functional biochips for screening applications. RSC Adv. 2015, 5, 83600–83607.

[313] Kidoaki,S.;Kwon,I.K.;Matsuda,T.Mesoscopic spatial designs of nano-and microfiber meshes for tissue- engineering matrix and scaffold based on newly devised multilayering and mixing electrospinning techniques. Biomaterials 2005, 26, 37–46.

[314] Deitzel, J.M.; Kleinmeyer, J.D.; Hirvonen, J.K.; Tan, N.C.B. Controlled deposition of electrospun poly (ethylene oxide) fibers. Polymer (Guildf). 2001, 42, 8163–8170.

[315] Deitzel,J..;Kleinmeyer,J.;Harris,D.;BeckTan,N..Theeffectofprocessingvariablesonthemor phology of electrospun nanofibers and textiles. Polymer (Guildf). 2001, 42, 261–272.

[316] Theron, A.; Zussman, E.; Yarin, A.L. Electrostatic field-assisted alignment of electrospun nanofibres. Nanotechnology 2001, 12, 384–390.

[317] Zussman,E.;Rittel,D.;Yarin,A.L.Failuremodesofelectrospunnanofibers.Appl.Phys.Lett.20 03,82,3958–3960.

[318] Fennessey, S.F.; Farris, R.J. Fabrication of aligned and molecularly oriented electrospun polyacrylonitrile nanofibers and the mechanical behavior of their twisted yarns. Polymer (Guildf). 2004, 45, 4217–4225.

[319] Liu,C.K.;Sun,R.J.;Lai,K.;Sun,C.Q.;Wang,Y.W.Preparationofshortsubmicron-fiberyarnbyanannular collector through electrospinning. Mater. Lett. 2008, 62, 4467–4469.

[320] Uddin, N.M.; Ko, F.; Xiong, J.; Farouk, B.; Capaldi, F. Process, structure, and properties of electrospun carbon nanotube-reinforced nanocomposite yarns. Res. Lett. Mater. Sci. 2009, 2009.

[321] Teo, W.E.; Ramakrishna, S. Electrospun fibre bundle made of aligned nanofibres over two fixed points. Nanotechnology 2005, 16, 1878–1884.

[322] Dalton,P.D.;Klee,D.;Möller,M.Electrospinningwithdualcollectionrings.Polymer(Guildf).2 000,46,611– 614.

[323] Liu, L.Q.; Eder, M.; Burgert, I.; Tasis, D.; Prato, M.; Wagner, H.D. One-step electrospun nanofiber-based composite ropes. Appl. Phys. Lett. 2007, 90, 1–3.

[324] Lotus, A.F.; Bender, E.T.; Evans, E.A.; Ramsier, R.D.; Reneker, D.H.; Chase, G.G. Electrical, structural, and chemical properties of semiconducting metal oxide nanofiber yarns. J. Appl. Phys. 2008, 103, 1–6.

[325] Lotus, A.F.; Bhargava, S.; Bender, E.T.; Evans, E.A.; Ramsier, R.D.; Reneker, D.H.; Chase, G.G. Electrospinning route for the fabrication of p-n junction using nanofiber yarns. J. Appl. Phys. 2009, 106, 1–5.

[326] Smit,E.;Buttner,U.;Sanderson,R.D.Continuousyarnsfromelectrospunfibers.Polymer(Guildf).2005,46, 2419–2423.

[327] Khil, M.S.; Bhattarai, S.R.; Kim, H.Y.; Kim, S.Z.; Lee, K.H. Novel fabricated matrix via electrospinning for tissue engineering. J. Biomed. Mater. Res. Part B Appl. Biomater. 2005, 72, 117–124.

[328] Kim,H.-Y.;Park,J.-C.Process of preparing continuous filament composed of nanofibers 2010.

[329] Pan,H.;Li,L.;Hu,L.;Cui,X.Continuous aligned polymer fibers produced by a modified electrospinning method. Polymer (Guildf). 2006, 47, 4901–4904.

[330] Wang, X.; Zhang, K.; Zhu, M.; Hsiao, B.S.; Chu, B. Enhanced mechanical performance of self-bundled electrospun fiber yarns via post-treatments. Macromol. Rapid Commun. 2008, 29, 826–831.

[331] Wang,X.;Zhang,K.;Zhu,M.;Yu,H.;Zhou,Z.;Chen,Y.;Hsiao,B.S.Continuouspolymernanofiberyarns prepared by self-bundling electrospinning method. Polymer (Guildf). 2008, 49, 2755–2761.

[332] Ko, F.; Gogotsi, Y.; Ali, A.; Naguib, N.; Ye, H.; Yang, G.; Li, C.; Willis, P. Electrospinning of continuous carbon nanotube-filled nanofiber yarns. Adv. Mater. 2003, 15, 1161–1165.

[333] Teo, W.E.; Gopal, R.; Ramaseshan, R.; Fujihara, K.; Ramakrishna, S. A dynamic liquid support system for continuous electrospun yarn fabrication. Polymer (Guildf). 2007, 48, 3400–3405.

[334] Yousefzadeh, M.; Latifi, M.; Teo, W.-E.; Amani-Tehran, M.; Ramakrishna, S. Producing Continuous Twisted Yarn From Well-Aligned Nanofibers by Water Vortex. Polym. Eng. Sci. 2011, 51, 323–329.

[335] Dabirian, F.; Hosseini, Y.; Ravandi, S.A.H. Manipulation of the electric field of electrospinning system to produce polyacrylonitrile nanofiber yarn. J. Text. Inst. 2007, 98, 237–241.

[336] Dabirian, F.; Hosseini, S.A. Novel method for nanofibre yarn production using two differently charged nozzles. Fibres Text. East. Eur. 2009, 17, 45–47.

[337] Afifi, A.M.; Nakano, S.; Yamane, H.; Kimura, Y. Electrospinning of continuous aligning yarns with a funnel. Target. Macromol. Mater. Eng. 2010, 295, 660–665.

[338] Ali,U.;Zhou,Y.;Wang,X.;Lin,T.Directelectrospinningofhighlytwisted,continuousnanofiberyarns.J. Text. Inst. 2012, 103, 80–88.

[339] Kanani, A.G.; Bahrami, S.H. Review on Electrospun Nanofibers Scaffold and Biomedical Applications. Trends Biomater Artif Organs 2010, 24, 93–115.

[340] Sivolella, S.; Brunello, G.; Ferrarese, N.; Della Puppa, A.; D'Avella, D.; Bressan, E.; Zavan, B. Nanostructured guidance for peripheral nerve injuries: A review with a perspective in the oral and maxillofacial area. Int. J. Mol. Sci. 2014, 15, 3088–3117.

[341] Chiono, V.; Tonda-Turo, C. Trends in the design of nerve guidance channels in peripheral nerve tissue engineering. Prog. Neurobiol. 2015, 131, 87–104.

[342] Bini,T.B.;Gao,S.;Tan,T.C.;Wang,S.;Lim,A.;Hai,L.Ben;Ramakrishna,S.Electrospunpoly(L-lactide-co- glycolide) biodegradable polymer nanofibre tubes for peripheral nerve regeneration. Nanotechnology 2004, 15, 1459–1464.

[343] Stitzel,J.;Liu,J.;Lee,S.J.;Komura,M.;Berry,J.;Soker,S.;Lim,G.;VanDyke,M.;Czerw,R.;Yoo,J.J.;Atala, A. Controlled fabrication of a biological vascular substitute. Biomaterials 2006, 27, 1088–1094.

[344] Matsuda, T.; Ihara, M.; Inoguchi, H.; Kwon, I.K.; Takamizawa, K.; Kidoaki, S. Mechano-active scaffold design of small-diameter artificial graft made of electrospun segmented polyurethane fabrics. J. Biomed. Mater. Res. - Part A 2005, 73, 125–131.

[345] Vaz, C.M.; van Tuijl, S.; Bouten, C.V.C.; Baaijens, F.P.T. Design of scaffolds for blood vessel tissue engineering using a multi-layering electrospinning technique. Acta Biomater. 2005, 1, 575–582.

[346] Akbari, M.; Tamayol, A.; Bagherifard, S.; Serex, L.; Mostafalu, P.; Faramarzi, N.; Mohammadi, M.H.; Khademhosseini, A. Textile Technologies and Tissue Engineering : A Path Toward Organ Weaving. Adv. Healthc. Mater. 2016, 5, 751–766.

[347] Tamayol, A.; Akbari, M.; Annabi, N.; Paul, A.; Khademhosseini, A.; Juncker, D. Fiber-based tissue engineering: Progress, challenges, and opportunities. Biotechnol. Adv. 2013, 31, 669–687.

[348] Wang, X.; Han, C.; Hu, X.; Sun, H.; You, C.; Gao, C.; Haiyang, Y. Applications of knitted mesh fabrication techniques to scaffolds for tissue engineering and regenerative medicine. J. Mech. Behav. Biomed. Mater. 2011, 4, 922–932.

[349] Zhong, S.P.; Zhang, Y.Z.; Lim, C.T. Tissue scaffolds for skin wound healing and dermal reconstruction. Wiley Interdiscip. Rev. Nanomedicine Nanobiotechnology 2010, 2, 510–525.

[350] Moutos, F.T.; Freed, L.E.; Guilak, F. A biomimetic three-dimensional woven composite scaffold for functional tissue engineering of cartilage. Nat. Mater. 2007, 6, 162–167. doi:10.1038/nmat1822.

[351] Moutos, F.T.; Guilak, F. Composite scaffolds for cartilage tissue engineering. Biorheology 2008, 45, 501–12.

[352] Moutos, F.T.; Guilak, F. Functional properties of cell-seeded three-dimensionally woven poly(epsilon-caprolactone) scaffolds for cartilage tissue engineering. Tissue Eng. Part A 2010, 16, 1291–1301.

[353] Moutos, F.T.; Estes, B.T.; Guilak, F. Multifunctional Hybrid Three-dimensionally Woven Scaffolds for Cartilage Tissue Engineering. Macromol. Biosci. 2010, 10, 1355–1364.

[354] Wu,S.;Duan,B.;Liu,P.;Zhang,C.;Qin,X.;Butcher,J.T.FabricationofAlignedNanofiberPolymerYarn Networks for Anisotropic Soft Tissue Sca ff olds. ACS Appl. Mater. Interfaces 2016, 8, 16950–16960.

[355] Li,S.;Patel,S.;Hashi,C.;Huang,N.F.;Kurpinski,K. Biomimetic Scaffolds 2007.

[356] Koh, H.S.; Yong, T.; Teo, W.E.; Chan, C.K.; Puhaindran, M.E.; Tan, T.C.; Lim, A.; Lim, B.H.; Ramakrishna, S. In vivo study of novel nanofibrous intra-luminal guidance channels to promote nerve regeneration. J. Neural Eng. 2010, 7, 1–14.

[357] Li, D.; Pan, X.; Sun, B.; Wu, T.; Chen, W.; Huang, C.; Ke, Q.; EI-Hamshary, H.A.; Al-Deyab, S.S.; Mo, X. Nerve conduits constructed by electrospun P(LLA-CL) nanofibers and PLLA nanofiber yarns. J. Mater. Chem. B 2015, 3, 8823–8831.

[358] Bashur, C.A; Shaffer, R.D.; Dahlgren, L.A; Guelcher, S.A; Goldstein, A.S. Effect of fiber diameter and alignment of electrospun polyurethane meshes on mesenchymal progenitor cells. Tissue Eng. Part A 2009, 15, 2435–2445.

Chapter 3: Biofabrication of bundles of poly(lactic acid)-collagen blends mimicking the fascicles of the human Achille tendon

Alberto Sensini[1], Chiara Gualandi[2], Luca Cristofolini[1,3], Gianluca Tozzi[4], Manuela Dicarlo[5], Gabriella Teti[6], Monica Mattioli-Belmonte[5], Maria Letizia Focarete[2,3]

1 Department of Industrial Engineering, Alma Mater Studiorum—University of Bologna, I-40131 Bologna, Italy

2 Department of Chemistry 'G. Ciamician' and National Consortium of Materials Science and Technology (INSTM, Bologna RU), Alma Mater Studiorum—University of Bologna, I-40126 Bologna, Italy

3 Health Sciences and Technologies—Interdepartmental Center for Industrial Research (HST-ICIR), Alma Mater Studiorum—University of Bologna, I-40064 Ozzano dell'Emilia, Bologna, Italy

4 School of Engineering, University of Portsmouth, Portsmouth PO1 3DJ, United Kingdom

5 Department of Clinical and Molecular Sciences, Polytechnic University of Marche, School of Medicine, I-60126 Ancona, Italy

6 Department of Biomedical and Neuromotor Sciences, Alma Mater Studiorum—University of Bologna, I-40126 Bologna, Italy

Keywords: Human Achille Tendon; Electrospinning; Bundle; Poly(lactic acid); Collagen; Tissue Engineering; Tenocytes.

The candidate was the main investigator of the study. This work was published on Biofabrication 2017, 9(1), 015025. Reproduced with permission. Copyright 2017, IOP Publishing.

Published in: Biofabrication 8 March 2017

3.1 Abstract

Electrospinning is a promising technique for the production of scaffolds aimed at the regeneration of soft tissues. The aim of this work was to develop electrospun bundles mimicking the architecture and mechanical properties of the fascicles of the human Achille tendon. Two different blends of poly(L- lactic acid) (PLLA) and collagen (Coll) were tested, PLLA/Coll-75/25 and PLLA/Coll-50/50, and compared with bundles of pure PLLA. First, a complete physico-chemical characterization was performed on non-woven mats made of randomly arranged fibers. The presence of collagen in the fibers was assessed by thermogravimetric analysis, differential scanning calorimetry and water contact angle measurements. The collagen release in phosphate buffer solution (PBS) was evaluated for 14 days: results showed that collagen loss was about 50% for PLLA/Coll-75/25 and 70% for PLLA/ Coll-50/50. In the bundles, the individual fibers had a diameter of 0.48 ± 0.14 μm (PLLA), 0.31 ± 0.09 μm (PLLA/Coll-75/25), 0.33 ± 0.08 μm (PLLA/Coll-50/50), whereas bundle diameter was in the range 300–500 μm for all samples. Monotonic tensile tests were performed to measure the mechanical properties of PLLA bundles (as-spun) and of PLLA/Coll-75/25 and PLLA/Coll-50/50 bundles (as-spun, and after 48 h, 7 days and 14 days in PBS). The most promising material was the PLLA/Coll-75/25 blend with a Young modulus of 98.6 ± 12.4 MPa (as-spun) and 205.1 ± 73.0 MPa (after 14 days in PBS). Its failure stress was 14.2 ± 0.7 MPa (as-spun) and 6.8 ± 0.6 MPa (after 14 days in PBS). Pure PLLA withstood slightly lower stress than the PLLA/Coll-75/25 while PLLA/ Coll-50/50 had a brittle behavior. Human-derived tenocytes were used for cellular tests. A good cell adhesion and viability after 14 days culture was observed. This study has therefore demonstrated the feasibility of fabricating electrospun bundles with multiscale structure and mechanical properties similar to the human tendon.

3.2 Introduction

The reconstruction of the tendon tissue is a current problem in medicine and orthopedic surgery. Over 30 million human tendon-related procedures take place annually worldwide [1]. However, due to the anatomical and physiological

complexity of the hierarchical structure of this tissue, it is very difficult to obtain satisfactory results [2–4]. Often, the formation of scar tissue generates morphological discontinuities which impair the mechanical properties and the proper work of the tendon [5]. Moreover, since tendon responds to mechanical forces by adapting its metabolism and its mechanical properties [6], its immobilization for long periods decreases its mass and reduces its stiffness and strength [7]. Surgical intervention is frequently considered in serious injuries and when damage is extensive tendon grafts may be required [8]. The grafts can be (i) prosthetic devices made of synthetic materials, (ii) allografts, (iii) autografts and (iv) resorbable devices. The choice of the most suitable option encompasses considerations of the type and site of injury and of the patient but, in a way, all the options above present some drawbacks. For instance prosthetic devices, besides developing inflammatory process, can encounter mechanical damage over time [9]. Autografts are better immunologically suitable, but their success is associated to morbidity of the donor site [10–15]. Alternatively, with autografts the risk of rejection exists [16–19]. Tendon reconstruction through tissue engineering is an additional option that encompasses the use of a biocompatible and bioresorbable scaffold capable of promoting tissue healing and of withstanding mechanical stresses. The design of a scaffold for tendon reconstruction must take into account the complex hierarchical structure of native tendon which is constituted by Collagen Type I (Coll) filaments aggregated in fascicles, with increasing diameters, orientated in the directions of applied loads [20, 21].

One promising technique for the production of scaffolds for tendon tissue is electrospinning. Thanks to its ability to produce filaments of both natural and synthetic polymers with nano- and micrometric diameters and oriented in specific directions, electrospinning grants the potential of producing scaffolds morphologically very similar to the hierarchical structure of the tendon collagen fascicles. Several technical approaches have been developed for producing electrospun bundles of highly aligned fibers [22–24] that have been proposed for tendon tissue engineering [23, 25–27]. Bosworth et al in particular, developed electrospun bundles of poly(ε-caprolactone), they carried out in vitro cell culture under dynamic tensile loading [27] and assessed the in vivo performance of the

bundles [26], gaining encouraging results. Recently, Zhang et al demonstrated that the unidirectional alignment of electrospun fibers helps enabling tenogenic differentiation of human-induced pluripotent stem cells in vitro and in vivo [28]. Mouthuy et al. developed a robust and automated method to manufacture continuous electrospun filaments that can be stretched and used to create multifilament yarns that imitate the hierarchical architecture of ten- dons and ligaments [23]. Besides morphological features of the scaffold, it is well-established that chemical properties are also extremely important in ensuring cell adhesion and proliferation. Because of their inherent properties of biological recognition, natural polymers have therefore been proposed in combination with synthetic polymers for tendon reconstruction: for instance poly(L-lactide-co-ε-caprolactone) copolymer has been blended with either collagen [29] or silk [30] and chitosan and gelatin have been used in combination with poly(L-lactic acid) (PLLA) [28].

While blends of collagen and PLLA have been investigated in the past [31–34] they have never been manufactured to produce bundles for tendon reconstruction. Moreover, the effect of the amount of the natural component on the mechanical properties of the bundle and on cell behavior, as well the stability of bundle composition under physiological condition have never been deeply investigated.

The aim of this study was to design, manufacture and characterize bioresorbable electrospun bundles made of highly aligned fibers of PLLA-collagen blends, to mimic the morphology and mechanical properties of the bundles composing the human Achilles tendon (300–500 μm in diameter). The two polymers were selected in order to seek an optimal compromise in terms of biocompatibility, stiffness, hydrolytic degradation and toughness. Bundles of PLLA containing different amounts of collagen have been prepared and characterized to determine the effect of collagen on scaffold wettability, thermal and mechanical proper- ties. The compositional stability of the scaffold and its mechanical performances have been evaluated over 14 days. Human tenocytes were cultured over the same time range on the bundles and cell morphology was assessed by scanning and transmission electron microscopy (TEM).

3.3 Materials and methods

In a first phase, flat mats were prepared to allow physico-chemical characterization of the material, bundles were then prepared to assess the mechanical properties and to perform cell culture experiments.

3.3.1 Materials

Acid soluble collagen type I (Coll), extracted from bovine skin was kindly provided by Kensey Nash Corporation d/ b/a DSM Biomedical (Exton, USA). Poly-L-lactic acid (PLLA) (Lacea H.100-E, Mw = 8.4 × 104 g mol−1, PDI = 1.7) was purchased from Mitsui Fine Chemicals (Dusseldorf, Germany). 2,2,2-trifluoroethanol (TFE), 1,1,1,3,3,3-hexafluoro-2-propanol (HFIP), dichloromethane (DCM) and dimethylformamide (DMF) were purchased from Sigma-Aldrich and used as received. The following polymeric solutions were used: (i) PLLA samples were produced from a 13% (w/v) solution of PLLA dissolved in DCM:DMF = 65:35 (v/v); (ii) PLLA/ Coll-75/25 (w/w) samples were prepared from a 15% (w/v) solution of PLLA and Coll dissolved in TFE: HFIP = 50:50 (v/v) (1.125 g of PLLA and 0.375 g of Coll were dissolved in 10 ml); PLLA/Coll-50/50 (w/w) samples were prepared from a 15% (w/v) solution of PLLA and Coll dissolved in TFE:HFIP = 50:50 (v/v) (0.75 g of PLLA and 0.75 g of Coll were dissolved in 10 ml).

3.3.2 Electrospinning and imaging

The home-made electrospinning apparatus consisted of a high-voltage power supply (Spellman SL 50 P 10/ CE/230), a syringe pump (KD Scientific 200 series), a glass syringe containing the polymer solution and connected to a stainless-steel blunt-ended needle through a Teflon tube. Electrospinning was performed at room temperature (RT) and relative humidity 40–50%. PLLA solution was electrospun by applying the following processing conditions: applied voltage = 18 kV, feed rate = 1.2 ml h^{-1}, needle inner diameter = 0.84 mm. PLLA/Coll solutions were electrospun by applying the following processing conditions: applied voltage = 22 kV, feed rate = 0.5 ml h^{-1}, needle inner diameter = 0.51 mm.

The grounded collector was positioned 200 mm away from the tip of the needle. The non-woven mats made of randomly arranged fibers were electrospun on an aluminum flat plate (100 mm × 100 mm). A high-speed rotating collector (length = 120 mm, diameter = 50 mm, 6000 rpm, peripheral speed = 16.2 m s^{-1}) was used to produce mats made of fibers preferentially aligned in the direction of drum rotation as previously described [35, 36] (Figure 3.1(A)). The central part of the sleeve (about 75 mm long) was manually rolled up transversely to the length of the roller, from end to end (Figure 3.1(B)). To remove it from the collector, the rolled-up scaffold was incised axially with a cutter (Figure 3.1(C)). Thus, the final bundle was as long as the circumference of the rotating collector (approximately 150 mm), and was made of fibers predominantly aligned axially (Figure 3.1(D)).

Scanning electron microscopy (SEM) observations were carried out using a Philips 515 SEM at an accelerating voltage of 15 kV, on samples sputter-coated with gold both of flat mats and bundles. The distribution of fiber diameters (average and standard deviation) was measured on the SEM images of about 200 fibers, by means of an acquisition and image analysis software (EDAX Genesis). The one-way ANOVA was used to test the statistical significance of the differences between averages.

The diameter of each bundle depended on the amount of fibers deposited in the central part of the collector, that in turn was affected by polymeric solution concentration, flow rate and jet deposition diameter. For each blend, the deposition time was optimized to produce bundles with a diameter of 300–500 μm (Figures 3.1(E) and 3.1 (F)).

In addition, to investigate the three-dimensional structure high-resolution images of one bundle was acquired with a micro-computed tomography scanner (micro-CT) (ZEISS Xradia 520 Versa) (Figure 3.1(G)) with the following settings: 40 kV/3 W Power, 149 μA tube current, 10–12 s exposure time. Images were collected at rotational steps of 0.09–0.11 over 360°, for a scanning time of 10–15 h. The reconstructed micro-CT images had an isotropic voxel size of 0.4 μm. To quantify directionality and scatter, the scans were analyzed with ImageJ [37], using a dedicated plugin called Directionality [38, 39]. Directionality histogram reports the amount of fibers as a function of the fiber orientation. The fiber alignment followed

a gaussian distribution (goodness > 0.90) with a narrow scatter (standard deviation < 15°, Figure 3.1(F)). The 3D reconstruction video of the bundle is available as supporting information.

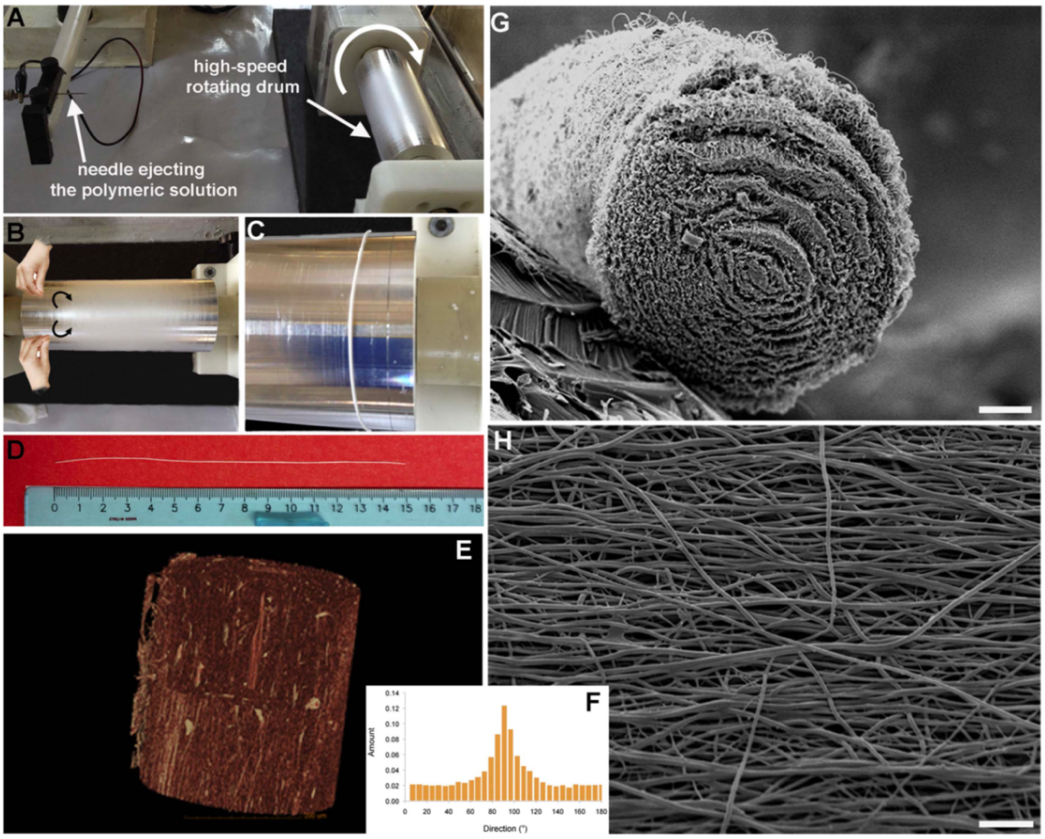

Figure 3.1 Procedure for the fabrication of the bundles: polymeric fibers were collected on a high-speed rotating drum (A), the mat made of aligned fibers was manually rolled up (B) and (C) to produce a bundle (D). The three-dimensional organization from the micro-CT images is reported as an example for a typical PLLA/Coll-50/50 specimen ((E), scale bar = 200 μm). The Directionality histogram is also reported for the same specimen ((F), in degrees). The real histogram values are used for the summation, not the gaussian fit. SEM images of a bundle are reported for a section ((G), scale bar = 50 μm) and for the external surface ((H), scale bar = 5 μm).

3.3.3 Release of collagen from the electrospun mats

Specimens of non-woven mats made of randomly arranged fibers (about 25 mg) were dried over P2O5 under vacuum at RT and weighed to obtain the sample initial mass. The specimens were individually immersed in 3 ml of phosphate buffer solution (PBS) (0.1 M, pH = 7.4) with sodium azide (Sigma-Aldrich) and incubated in a SW22 Julabo water bath at 37 °C with shaking at 80 rpm. At different time

intervals, triplicate specimens for each sample were recovered from the bath, gently washed with deionized water and dried over P2O5 under vacuum.

The amount of collagen released in PBS (collagen loss %) was determined using Biuret assay [40]. The Biuret reagent was prepared by dissolving 0.375 g of copper sulphate (Sigma-Aldrich) and 1.69 g of sodium tartrate hemihydrate (Sigma-Aldrich) in 100 ml distilled water. Subsequently, 100 ml of 10.5% (w/v) NaOH was added to the solution. The resulting solution was then diluted up to 250 ml and stored at 2 °C– 8 °C. 0.5 ml of the retrieved PBS which previously contained the mat specimen was mixed with 2.25 ml of Biuret assay solution and kept at RT for 10 min. UV absorbance at 545 nm was measured with a Cary 1E (Varian) spectrophotometer, and converted to collagen concentration through a calibration curve obtained by measuring the absorbance of collagen standard solutions. Collagen loss % was calculated (Equation (3.1)):

$$\text{Collagen loss } \% = \frac{m_{Coll}}{m_{in} \times w_{coll}} \times 100 \quad (3.1)$$

where m_{Coll} is the mass of collagen released in PBS determined by Biuret assay, m_{in} is the initial dry sample weight and w_{coll} is the collagen weight fraction in the flat mats (i.e. w_{coll} = 0.25 for PLLA/Coll-75/25 and w_{coll} = 0.5 for PLLA/Coll-50/50). The same analysis was also carried out on PBS medium containing PLLA mats, demonstrating that substances interfering with the Biuret method were absent. In parallel, the collagen loss % was also evaluated gravimetrically by comparing the sample dry weight remaining at a specific time with the initial sample weight (Equation (3.2)) and by assuming that the weight loss was only ascribable to collagen dissolution. This assumption was supported by the fact that PLLA mat incubated in PBS did not show any weight loss in the time range investigated (up to 14 days).

$$\text{Collagen loss } \% = \frac{m_{in} - m_{fin}}{m_{in} \times w_{coll}} \times 100 \quad (3.2)$$

where m_{in} is the initial dry sample weight, m_{fin} is the dry sample weight after PBS immersion and w_{coll} is the Collagen weight fraction in the flat mats sample (i.e. w_{coll} = 0.25 for PLLA/Coll-75/25 and w_{coll} = 0.5 for PLLA/Coll-50/50).

3.3.4 Physico-chemical characterization techniques

Thermogravimetric analysis (TGA) were performed with a TA Instruments TGA2950 analyzer from RT to 600 °C (heating rate 10 °C min^{-1}, nitrogen gas).
Differential scanning calorimetry (DSC) measurements were carried out using a TA Instruments Q100 DSC equipped with the liquid nitrogen cooling system accessory. DSC scans were performed in helium atmosphere from −60°C to 190°C. The heating rate was 20 °C min^{-1} and the cooling rate was 10 °C min^{-1}.
The static water contact angle (WCA) was measured under ambient conditions with a KSV CAM 101 instrument. Milli-Q water was used for measurements. The side profiles of water drops laying on the surface of non-woven mats made of randomly arranged fibers were recorded in a time range 0–30 s. At least six drops were observed for each mat.

3.3.5 Mechanical Characterization of bundles

Stress–strain measurements were carried out with a material testing machine (Mod. 4465, Instron, Canton, MA) on electrospun bundles of the three compositions. In order to evaluate the variation of mechanical properties in relation to collagen loss, bundles of PLLA/Coll-75/25 and PLLA/Coll-50/50 were also immersed in PBS at 37 °C for 48 h, 7 days and 14 days. After these time intervals, the bundles were retrieved from PBS and dried before mechanical testing. Six specimens were tested for each composition and each type of ageing. To measure the diameter of each bundle, a polarized light optical microscope (Axioskop Zeiss,) equipped with a camera (AxioCam MRc Zeiss) was used (average of 5 measurements). The section was measured (average of 5 measurements) immediately after preparation of the bundles, and also after permanence in PBS (where applicable).
'Ad hoc' designed capstan grips were used to limit the stress concentrations at sample ends. The gauge length was 20 mm. The actuator speed was 5 mm min^{-1}.

Load–displacement curves were converted to stress– strain curves using the cross-section area measured in the dry specimens as-spun. The following indicators were considered: Young modulus, yield stress, failure stress, failure strain, and work to yield and failure. The stress– strain curves were analyzed as described in Figure 3.2.

The significance of differences between bundle compositions was assessed with the one-way ANOVA; the effect of PBS immersion on the two blends was assessed with the two-way ANOVA.

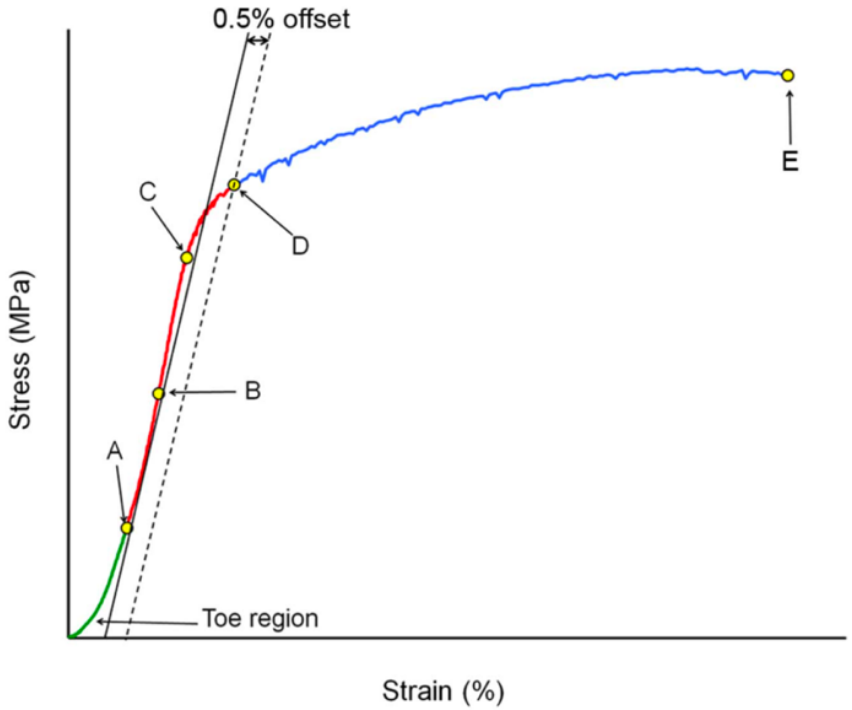

Figure 3.2 Sketch of the method used to analyze the stress– strain curves. The initial toe region was disregarded; the failure stress (E) was identified as the highest stress in the entire curve; the starting point of the linear region (A) was univocally identified as 20% of failure stress; an initial guess for the yield strain was visually identified (C); the initial linear regression (solid line) was applied to the first 50% of the linear region, between points A and B (which was half-way between A and C); a second line parallel to the initial regression was drawn, with an offset of 0.5% strain (dashed line); the limit of proportionality was defined with the 0.5%-strain offset criterion as the intersection (D) between the latter line and the stress–strain curve; the Young modulus was calculated as the slope of a new regression line between A and D. The work to yield and to failure were calculated as the integrals under the curves (with the method of trapezoids).

3.3.6 Biological assessment

3.3.6.1 Cell isolation

Human tenocytes were isolated from anterior cruciate ligament of healthy subjects undergoing surgery for orthopedic trauma (mean age 60 years). In accordance with the Local Ethical Committee guidelines and with the 1964 Helsinki declaration an informed consent was obtained from all individual participants included in the study. Briefly, ligament explants were aseptically rinsed three times with Dulbecco's phosphate-buffered saline (D-PBS) lacking in Ca^{2+} and Mg^{2+}, then cut into small pieces and incubated with 1 mg ml^{-1} type I collagenase (Collagenase NB 4G Proved Grade, Serva Electrophoresis GmbH) in Dulbecco's modified Eagle's medium (DMEM; Sigma- Aldrich, Milan, Italy) supplemented with 2% foetal bovine serum (FBS) and 1% antibiotics (penicillin-streptomycin; Gibco-Life Technologies, Milan, Italy) for approximately 18 h at 37 °C in controlled atmosphere.

After digestion, the suspension was passed through a sterile cell strainer (70 μm in diameter) to remove debris and the filtrate centrifuged at 1200 rpm for 10 min. The cell pellet was then resuspended in DMEM supplemented with 10% FBS and 1% anti- biotics, and placed in sterile vented cell culture flasks.

The medium was changed twice a week. Confluent cells were detached with 0.25% trypsin in 1 mM ethylenediaminetetraacetic acid (EDTA) (Gibco-Life Technologies) and split 1:2.

3.3.6.2 Cell characterization

Tenocytes at the 3rd passage were seeded in chamber- slides (NuncTM, Rochester, NY) at a density of 5×10^3 cells cm^{-2}. At confluence, cells were fixed in 4% paraformaldehyde in PBS for 15 min at RT, permeabilized using 0.1% Triton-X-100 in D-PBS for 15 min at RT, and then incubated with anti-fibronectin (dil. 1:600; clone IST-4, Sigma Aldrich), anti-collagen Type I (dil. 1:1000; clone COL-1, Abcam Cambridge, UK), anti-collagen Type III (dil. 1:100; clone Col-29, Abcam) or anti-vimentin (ready to use, Clone V9, Dako Cytomation, Milan, Italy) mouse

monoclonal antibodies. Cells were incubated over-night at 4 °C with primary antibodies and then washed in D-PBS. The immuno-complexes were visualized using the streptavidin–biotin peroxidase technique (Envision peroxidase kit, Dako). After the incubation with 0.05% 3, 3′-diaminobenzidine (Sigma–Aldrich) in 0.05 M Tris buffer, pH 7.6 with 0.01% hydrogen peroxide, cells were counterstained with Mayer's haematoxylin (BioOptica, Milan, Italy), dehydrated in ethanol and coverslipped with Eukitt mounting medium (Electron Microscopy Sciences, PA, USA). For negative controls, the primary antibody was replaced with non-immune serum. The immunohistochemical expression of the before mentioned antigens was evaluated under a Nikon Eclipse E600 light microscope (Nikon, Milan, Italy). Images were captured with a Nikon DSVi1 digital camera (Nikon Instruments) and NIS Elements BR 3.22 imaging software (Nikon Instruments) was used. Stained cells were counted in at least 10 fields per sample (field's area: 0.7 mm^2, magnification: 400X) and quantified as a percentage of the total counted cells. The fields were randomly selected evaluating the most positive, moderate and less positive areas. Average ± standard deviation (SD) was considered for each value.

3.3.6.3 Cell cultures

Before seeding, PLLA/Coll-75/25 and PLLA/Coll- 50/50 bundles were sterilized with 70% ethanol for 30 min, washed twice in D-PBS, and then incubated with DMEM supplemented with 10% FBS and 1% penicillin–streptomycin (100 U ml^{-1}) at 37 °C. After one hour, the bundles were cut into 1 cm pieces and placed in 24-well polystyrene plates (Corning® ultra-low attachment) and fixed with CellCrownTM (Scaffdex, Tampere, Finland). Tenocytes were detached from culture flasks using 0.25% trypsin in 1 mM EDTA and seeded on the samples at a density of 1×10^5 cells/sample in a volume of 50 µl. After one hour incubation at 37°C, necessary to allow cell adhesion and prevent sliding off and falling in the wells, 1 ml of DMEM was added in each well, and samples were further cultured for 7 and 14 days. Medium was changed twice a week. 32.3.6.4 Scanning electron microscopy

For SEM analysis, the cell-material constructs were fixed in 2% v/v glutaraldehyde in 0.1 M cacodylate buffer (pH 7.4) for 1 h at 4 °C, post-fixed in 1% v/v osmium

tetroxide for 1h at 4°C, dehydrated for 15min at 4°C in a series of increasing ethanol concentrations (from 25% to absolute ethanol), critical point dried using CPD 010 Balzers Instruments (FL-9496 Balzers, Liechtenstein) according to the manufacturer's instructions, mounted on aluminium stubs and gold-sputtered (Edwards Sputter Coater B150S). Samples were observed with a Philips XL 20 SEM (FEI Italia SRL, Milan, Italy) using the secondary electron detector.

3.3.6.4 Transmission electron microscopy

Samples were fixed in 2.5% glutaraldehyde in 0.1 M cacodylate buffer for 2 h at 4 °C and post-fixed in 1%. Osmium tetroxide in 0.1M cacodylate buffer for 30 min at RT. Samples were dehydrated in graded ethanol and finally infiltrated and embedded in RL London White (Fluka, Sigma Aldrich, St. Louis, Missouri, USA). 100 nm ultra-thin sections were cut using a Diatome (Diatome, Hatfield, PA, USA) diamond knife on a NOVA LKB Ultratome. Sections were picked up on nickel grids and stained with alcoholic uranyl acetate and Reynold's lead citrate. Ultrastructural examination was performed using the Philips CM10 Transmission Microscope (FEI Company, Eindhoven, The Netherlands). Images were recorded by Megaview III digital camera (FEI Company, Eindhoven, The Netherlands).

3.4 Results

3.4.1 Morphology of the electrospun mats

Electrospun mats made of randomly oriented continuous fibers were produced by collecting fibers on an aluminium plate target (Figure 3.3). PLLA bead-free fibers with diameters of (0.48 ± 0.14) μm were obtained as previously reported [41–43] by dissolving the polymer in a mixture of DCM (to dissolve the polymer) and DMF (to improve the electrical proper- ties of the solution). PLLA/Coll-75/25 fibers had diameters of (0.31 ± 0.09) μm and PLLA/Coll-50/50 fibers had diameters of (0.33 ± 0.08) μm (Figure 3.3).

The behavior of a representative water drop for each sample is reported in figure 3(E). PLLA mat dis- played a WCA of 110° ± 6° that remained constant during the

measurement. Conversely, for PLLA/Coll samples the WCA values significantly decreased with time: the water drop was completely absorbed after 30 and 10 s by PLLA/Coll-75/25 and PLLA/Coll-50/50 mat, respectively.

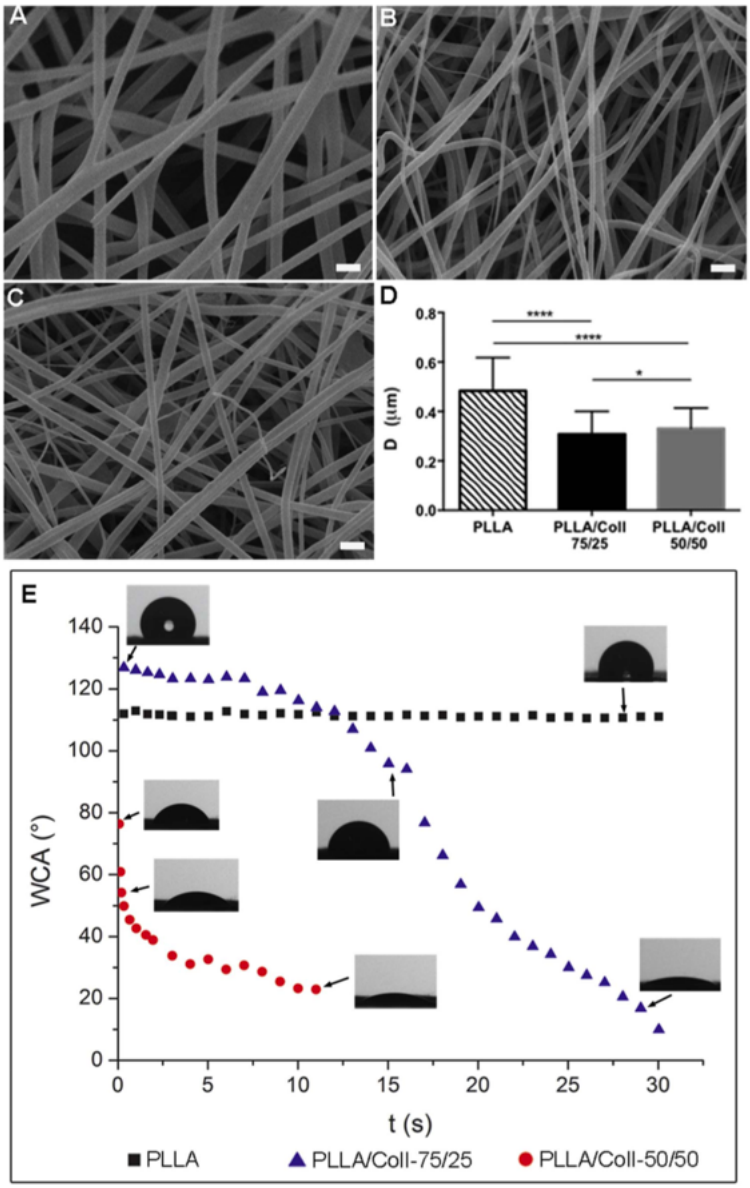

Figure 3.3 Representative SEM micrographs of PLLA (A), PLLA/Coll-75/25 (B) and PLLA/Coll-50/50 (C) non-woven mats of randomly arranged fibers. Scale bar = 1 µm. The diameter (average and standard deviation) of the fibers is plotted for the three compositions (D), together with statistical significance of post-hoc comparisons (Tuckey multiple comparisons, * $P \leq 0.05$, ** $P \leq 0.01$, *** $P \leq 0.001$, **** $P \leq 0.0001$). (E) WCA as a function of time of a representative drop for each electrospun mat.

3.4.2 Thermal characterization of the electrospun mats

TGA curves of electrospun mats are reported in Figure 3.4(A). For sake of comparison, TGA of collagen powder is also shown. PLLA sample started losing weight above 250 °C and degraded in a single-step process that leaded to an almost negligible residue (4%) above 350 °C. Thermal degradation of collagen powder proceeded via a multistep process that started at RT with a residual weight of about 27% at 600 °C. Collagen weight loss at low temperature (RT-150 °C) has been attributed to the removal of bound water [44, 45]. Similarly, to collagen powder, PLLA/Coll samples displayed an initial weight loss in the range RT-150 °C, ascribable to water evaporation from the Coll component. Subsequently, the samples showed a weight decrement in the range 200 °C–500 °C, due to the concomitant degradation of Coll and PLLA fractions, and weight residues at 600 °C of 18% and 10% for PLLA/Coll-50/50 and PLLA/Coll-75/25, respectively. The residual weights at 600 °C of blends were in line with the theoretical ones, the latter being calculated by considering the feed of PLLA and Coll in the starting polymeric solutions. Indeed, the theoretical residual weight values—calculated by taking into account the weight residues of pure components—of PLLA/Coll-50/50 and PLLA/Coll-75/25 are 15.5% and 9.75%, respectively, which are close to the experimental ones, within the accuracy of TGA quantification.

The DSC curve of collagen powder showed a broad and intense endothermic peak in the range 0°C–150 °C in the first heating scan (Figure 3.4(B)), due to the evaporation of water [44], whereas no appreciable thermal transitions where observed in the second heating scan (figure 3.4(C)). The first heating scan of PLLA showed a glass transition (T_g) at a temperature around 61 °C and a cold crystallization exothermic peak (T_c = 87 °C) followed by a melting endothermic peak (T_m = 163 °C) of the same entity ($\Delta H_c = \Delta H_m$ = 33 J g^{-1} (Figure 3.4(B)). This result indicates that the melting phenomena that follows the cold crystallization concerns only the PLLA crystal phase developed during the heating scan, thus demonstrating that completely amorphous PLLA mats were obtained through the electrospinning process, as previously reported [46]. The first heating scans of PLLA/ Coll-75/25 and PLLA/Coll-50/50 samples displayed the above described PLLA thermal transitions whose entity correlated with the PLLA weight fraction in

the blends. In addition, the endothermic peak of water evaporation from the Coll fraction was also visible (Figure 3.4(B)). Since the second heating scan of the blends displayed only the thermal transitions associated to the PLLA component, it was possible to calculate the effective PLLA/Coll composition in the blends by comparing the PLLA ΔC_p and ΔH_m of the blends with those of pure PLLA. In Table 2.1 calorimetric data of the second heating scans are reported together with the value of PLLA content in the blend, calculated on the basis of either ΔC_p or ΔH_m:

$$\text{PLLAwt \%}_{\Delta Cp} = \frac{\Delta C_p^{PLLA/Coll}}{\Delta C_p^{PLLA}} \times 100 \quad (3.3)$$

$$\text{PLLAwt \%}_{\Delta Hm} = \frac{\Delta H_m^{PLLA/Coll}}{\Delta H_m^{PLLA}} \times 100 \quad (3.4)$$

Mat composition calculated according to DSC data agrees with the starting solution composition in terms of PLLA/Coll ratio, within the accuracy of DSC quantification.

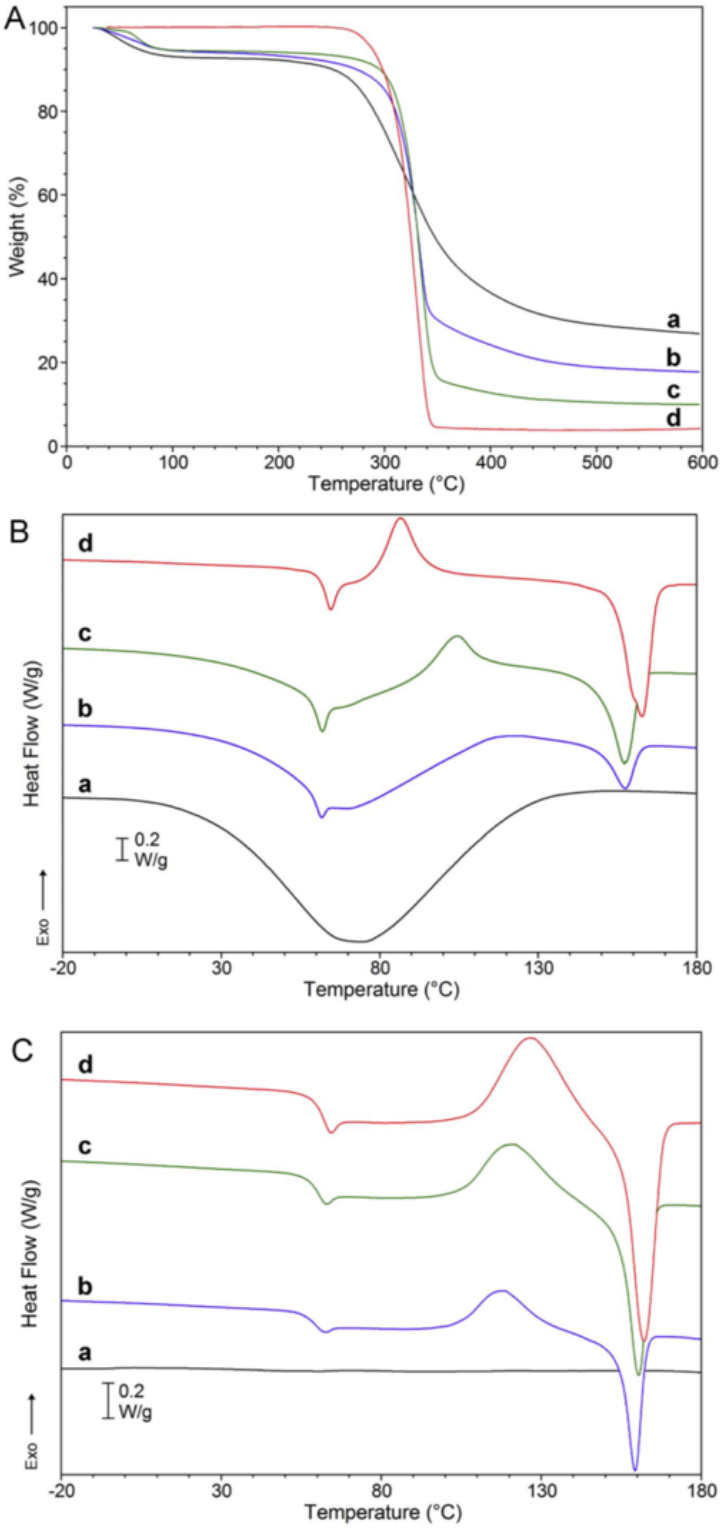

Figure 3.4 Thermal characterization of collagen powder (a), PLLA/Coll-50/50 (b), PLLA/Coll-75/25 (c) and PLLA (d). (A) TGA curves; (B) DSC first heating scans; (C) DSC second heating scans after controlled cooling at 10 °C min^{-1}.

Table 3.1 Calorimetric data of collagen, PLLA, and PLLA/Coll blends (heating run at 20 °C min^{-1} following the cooling run).

Sample	T_g (°C)	ΔC_p (J g^{-1} $°C^{-1}$)	T_c (°C)	ΔH_c (J g^{-1})	T_m (°C)	ΔH_m (J g^{-1})	PLLA (wt%)[a]	PLLA (wt%)[b]
Collagen powder	n.a.	n.a.	n.a.	n.a.	n.a.	n.a.	-	-
PLLA	60	0.53	126	31	162	32	-	-
PLLA/Coll-75/25	59	0.39	122	20	160	23	74	72
PLLA/Coll-50/50	58	0.27	119	13	159	14	51	44

[a] PLLA wt% in the blend calculated by using Equation (3.3)

[b] PLLA wt% in the blend calculated by using Equation (3.4)

3.4.3 Release of collagen from the electrospun mats

Figures 3.5(A) and (B) show the collagen percentage loss (collagen loss %) calculated for PLLA/Coll-50/50 and PLLA/Coll-75/25. Data obtained from Biuret assay (using Equation (3.1)) showed a significant collagen loss at the very beginning of the experiment: after 30 min PLLA/Coll-75/25 and PLLA/Coll-50/50 lost about 40% and 50% of their initial collagen content, respectively. At the end of the experiment (14 days) the collagen loss was about 50% and 70% for PLLA/Coll- 75/25 and PLLA/Coll-50/50, respectively, corresponding to a final composition of PLLA/Coll-86/14 for the former, and PLLA/Coll-77/23 for the latter. Data obtained from gravimetric analysis had a similar trend but a higher collagen loss was always determined. According to gravimetric measurements (Equation (3.2)) the collagen loss after 14 days in PBS was about 80% and 90% for PLLA/Coll-75/25 and PLLA/Coll-50/50, respectively. This discrepancy between the results of gravimetric method and Biuret assay can be explained considering that electrospun samples retrieved from the buffer were fragile and might have undergone a further loss during sample washing with fresh water.

As expected, PLLA fibers did not show any evident change of fiber morphology during 14 days of permanence on PBS (Figure 3.5(C)). PLLA/Coll-75/25 fibers appeared slightly swollen (compare Figure 3.5(D) with Figure 3.3(B)) and PLLA/Coll-50/50 fibers were welded at contact points after 14 days in PBS (compare Figure 3.5(E) with Figure 3.3(C)).

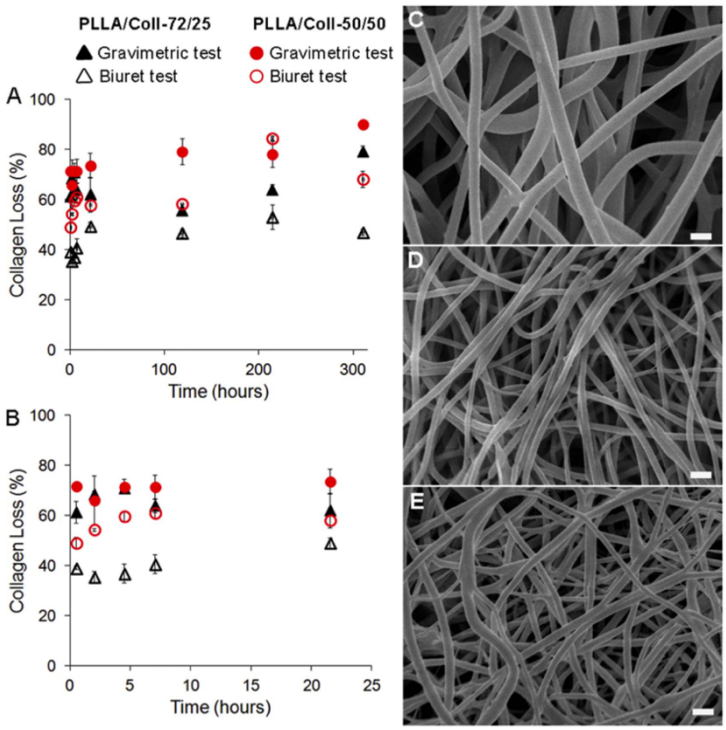

Figure 3.5 (A) Percentage of collagen loss during immersion of PLLA/Coll-75/25 (black triangles) and PLLA/Coll-50/50 (red circles) in PBS at different times; (B) an enlarged view in the range 0–25 h. The collagen loss was determined both gravimetrically (full markers) and throughout Biuret assay (empty markers). Representative SEM micrographs of PLLA (C), PLLA/Coll-75/25 (D) and PLLA/Coll-50/50 (E) samples after 14 days of immersion in PBS. Scale bar = 1 μm.

3.4.4 Mechanical properties of the electrospun bundles

Stress–strain curves of the three types of bundles (i.e. PLLA, PLLA/Coll-75/25, and PLLA/Coll-50/50) presented a similar nonlinear behavior at the foot of the curve (toe region), but different trends and different magnitudes were found for the three as-spun compositions at higher stress (Figure 3.6(A)). The PLLA bundles had a ductile behavior, with large plastic deformation; the PLLA/Coll-75/25 bundles had a ductile behavior, but with a higher Young modulus, higher yield and failure stress, and lower failure strain than PLLA; finally the PLLA/Coll-50/50 bundles showed an elastic and brittle behavior, with lower Young modulus and failure stress than the other two types. Such differences were statistically significant (Figures 3.6(B)– (E); one-way ANOVA p-value < 0.05).

After the electrospun bundles of the two blends (i.e. PLLA/Coll-75/25 and PLLA/Coll-50/50) were maintained in PBS they still consistently exhibited the

initial nonlinear toe-region, independent of the time in PBS, but showed some variation of mechanical properties over time (Figure 3.7). In particular, the PLLA/Coll-75/25 bundles after 48 h demonstrated a ductile behavior and values similar to the as-spun ones (Figure 3.7(A)). After 7 days in PBS, the bundles were still ductile, and stiffer, with lower yield and failure stress and strain. At 14 days PLLA/Coll-75/25 bundles showed an elastic-brittle behavior, with failure stress and strain lower than the previous ones. The PLLA/ Coll-50/50 bundles always showed an elastic-brittle behavior (Figure 3.7(B)) with values of stiffness that increased over time while the failure stress and strain decreased. Such differences were statistically significant (Figures 3.7(C)–(F); two-way ANOVA p-value < 0.05).

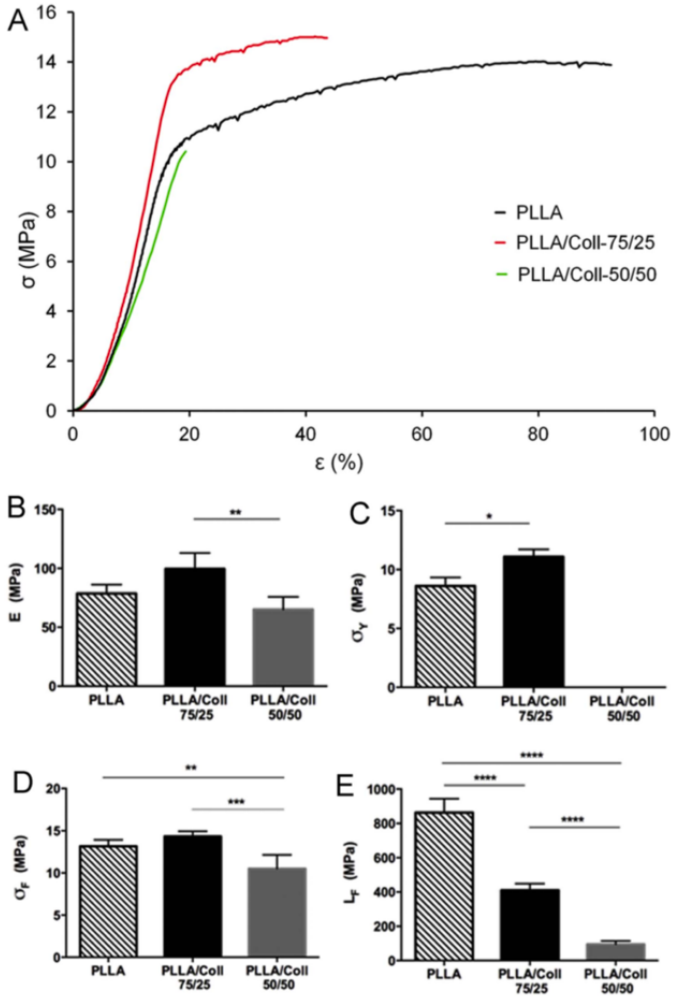

Figure 3.6 (A) Typical stress–strain curves for as-spun PLLA, PLLA/Coll-75/25, PLLA/Coll-50/50 bundles tested. Comparison of the mechanical properties of the as-spun bundles: (B) Young modulus (E); (C) yield stress (σ_Y); (D) failure stress (σ_F); (E) work to failure (L_F). The average and standard

deviation is plotted for the three compositions, together with statistical significance of post-hoc comparisons (Tuckey multiple comparisons, * P ≤ 0.05, ** P ≤ 0.01, *** P ≤ 0.001, **** P ≤ 0.0001). The yield stress is missing for the PLLA/Coll-50/50 composition as it had a brittle behavior.

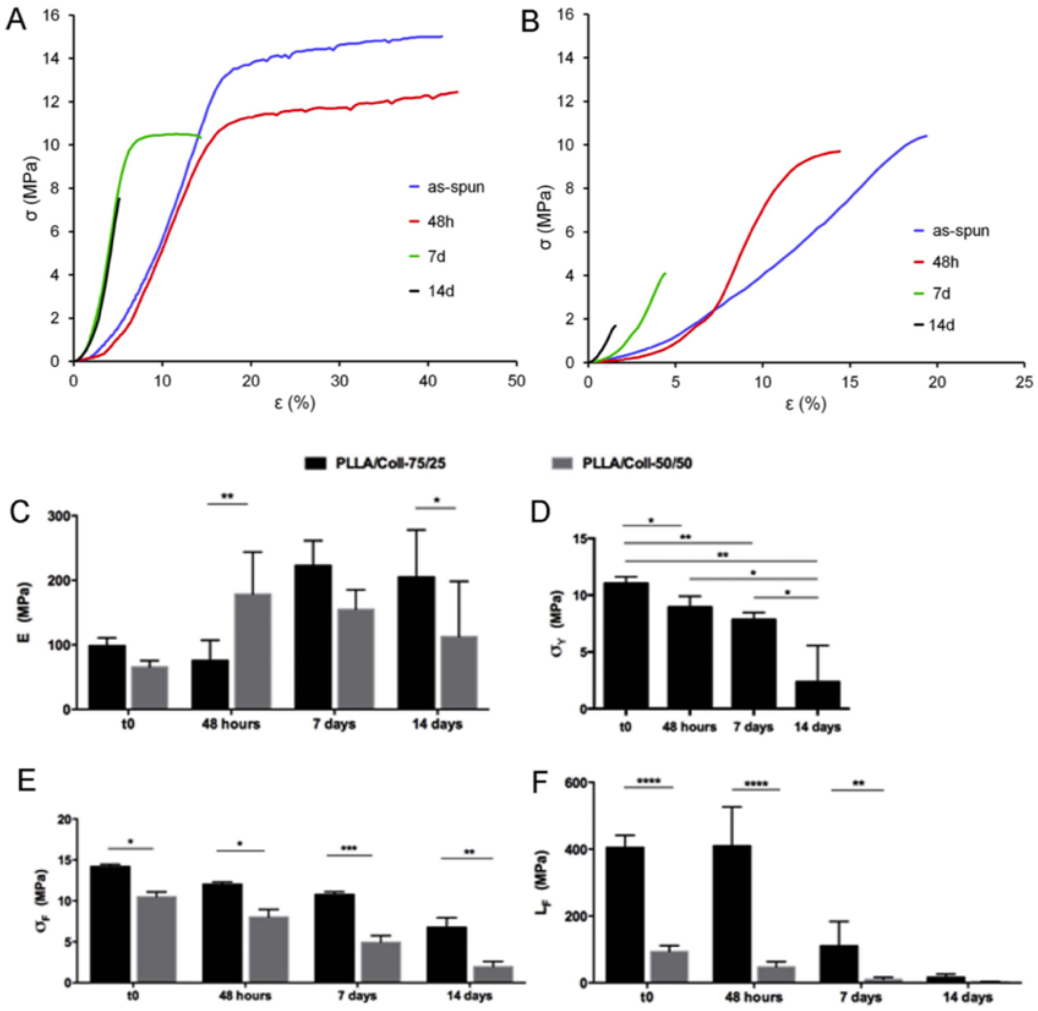

Figure 3.7 Typical stress–strain curves for PLLA/Coll-75/25 (A) and PLLA/Coll-50/50 (B) bundles after ageing in PBS solution (as- spun bundles (as-spun), after 48 h (48 h), 7 days (7d) and 14 days (14d) in PBS). Comparison of the mechanical properties: (C) Young modulus (E), (D) yield stress (σ_Y), (E) failure stress (σ_F), (F) work to failure (L_F) of the bundles PLLA/Coll-75/25 and PLLA/Coll-50/ 50 as-spun and after immersion in PBS. The average and standard deviation is plotted for the three compositions, together with statistical significance of post-hoc comparisons (Tuckey multiple comparisons, * P ≤ 0.05, ** P ≤ 0.01, *** P ≤ 0.001, **** P ≤ 0.0001). The yield stress is missing for the PLLA/Coll-50/50 composition as it had a brittle behavior. Similarly, the yield stress is missing for PLLA/Coll-50/50 at 14 days, as 3 specimens out of 6 had a brittle behavior.

3.4.5 Biological assessment

First, to confirm the identity of tenocytes the immuno-cytochemical detection of collagen Type I and Type III, fibronectin and vimentin was performed. The majority of cells were positive for vimentin and fibronectin (Figures 3.8(A) and (B)). Vimentin is an intermediate filament that is characteristically found in cells of mesenchymal origin and usually used as a tenocyte marker [47, 48]. The expression of this marker was so high that counterstaining with haema-toxylin and eosin was not perceptible (Figure 3.8(A)). The production of collagen type I and a low expression of collagen type III were also detected (Figures 3.8(C) and (D)), indicating the fibroblastic phenotype (tenocytes) of selected population, as previously described for this model [47, 49, 50].

Morphological analyses showed a different adhesion of tenocytes onto the PLLA/Coll bundles. Overall adhesion seems better on PLLA/Coll-50/50 samples in comparison to PLLA/Coll-75/25 one (Figure 3.9). Light microscopy and SEM observations evidenced that cells were present only on bundle surface with a more elongated morphology on PLLA/Coll-50/50 (Figures 3.9(B) and (D)) and more spread features on PLLA/Coll-75/25 at both time analyzed (Figures 3.9(F) and (H)). TEM ultrastructural assessment demonstrated cells in good condition. Nuclei and the relative envelops were well preserved and the quite rare mitochondria maintained a correct morphology, with well evident cristae. The rough endoplasmic reticulum (RER) cisternae were always dilated and some rare vacuole autophagocytosis were visible (Figure 3.10). This well preserved cell ultrastructure is suggestive of a good compatibility of the proposed bundles. Cells adhered to the bundles only in small points (Figure 3.10) and not in the extended areas and this is probably responsible for the detected low proliferation.

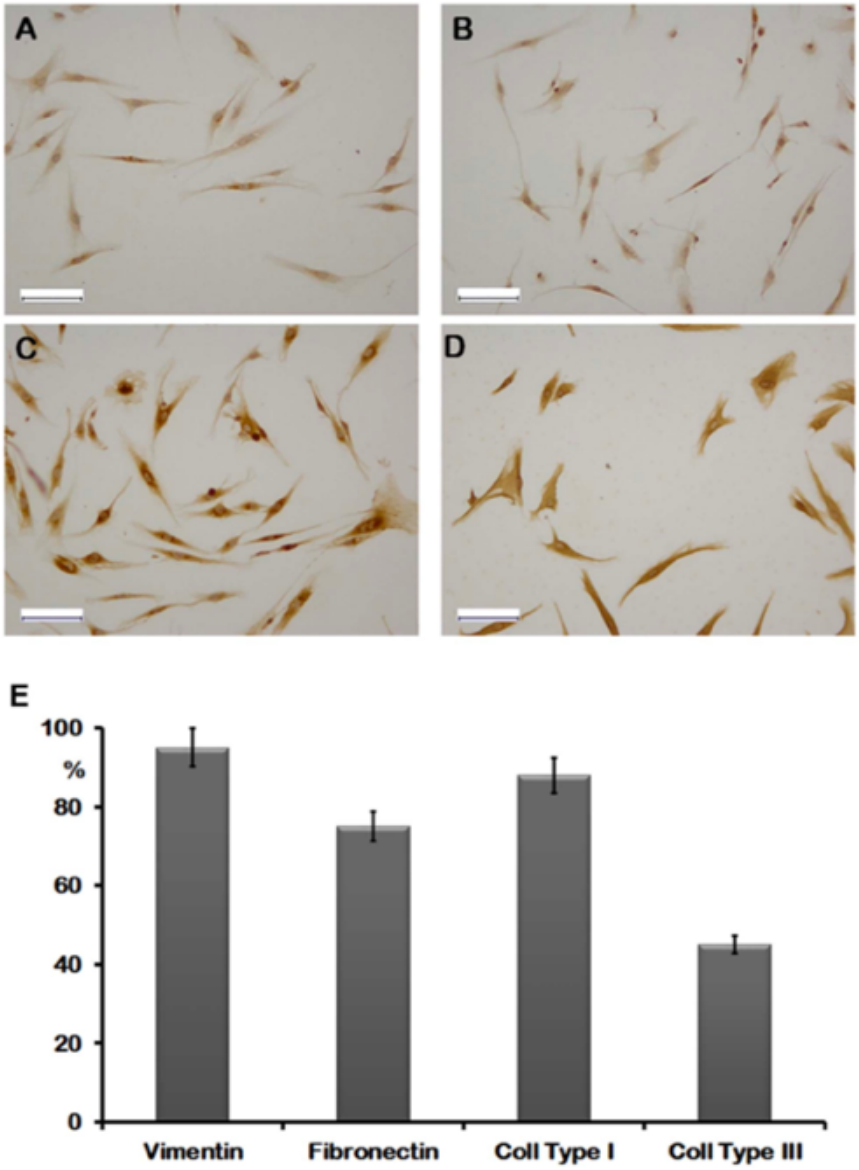

Figure 3.8 Tenocytes characterization. Tenocytes were characterized through vimentin (A), fibronectin (B), and Collagen Type I (C) and III (D) immunostaining. Scale bars = 50 μm; original magnification 200x. Histogram depicts percentage of positive cells (E).

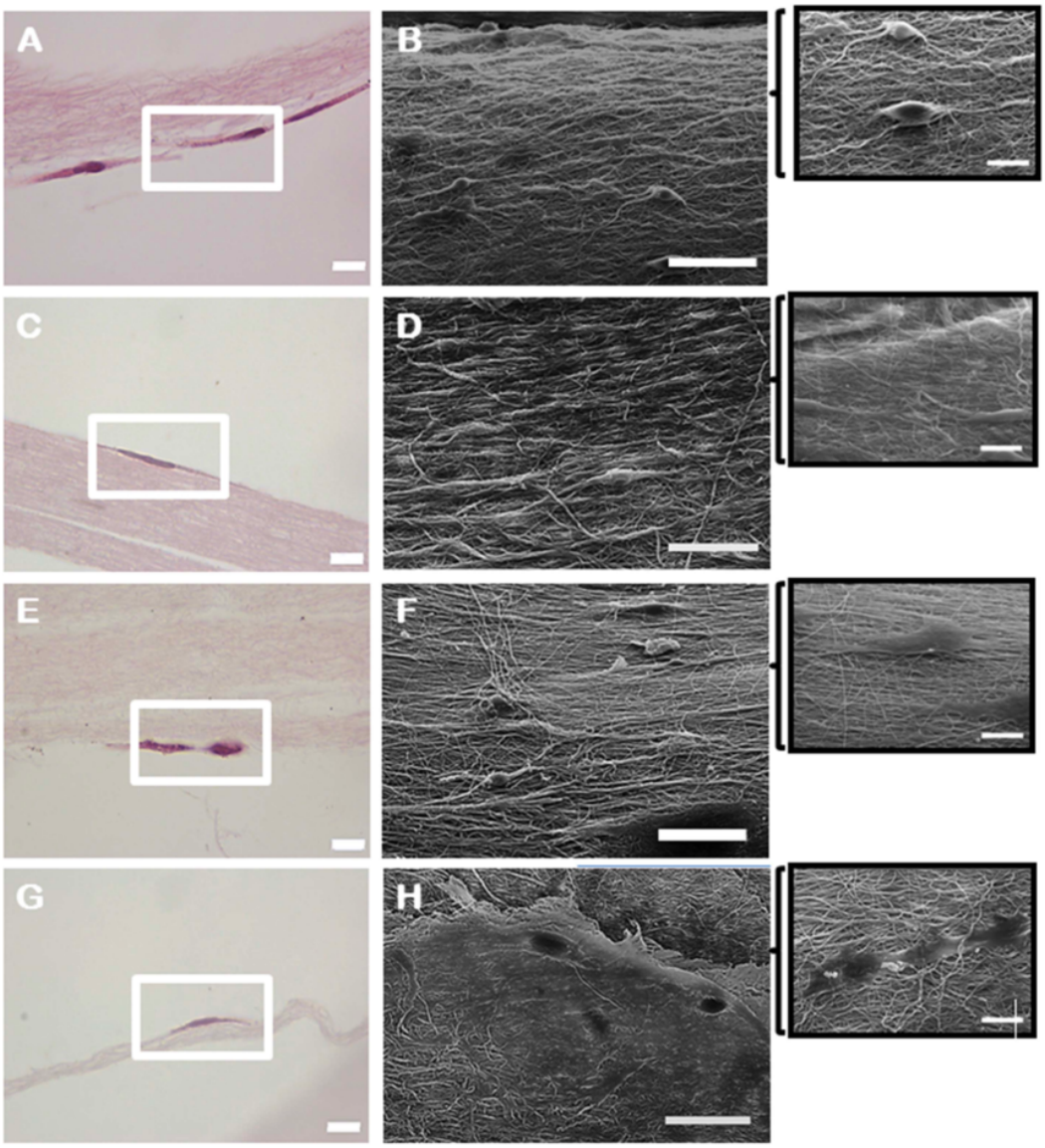

Figure 3.9 Light and scanning electron microscopy of tenocytes cultured onto PLLA/Coll-50/50 (A)–(D) and PLLA/Coll-75/25 (E)– (H) bundles for 7 (A), (B), (E), (F) and 14 (C), (D), (G), (H) days. Elongated cells were detectable on the surface of fibers. Scale bar (A), (C), (E), (G) = 20 μm; scale bar (B), (D), (F), (H) = 50 μm; insets scale bar = 10 μm.

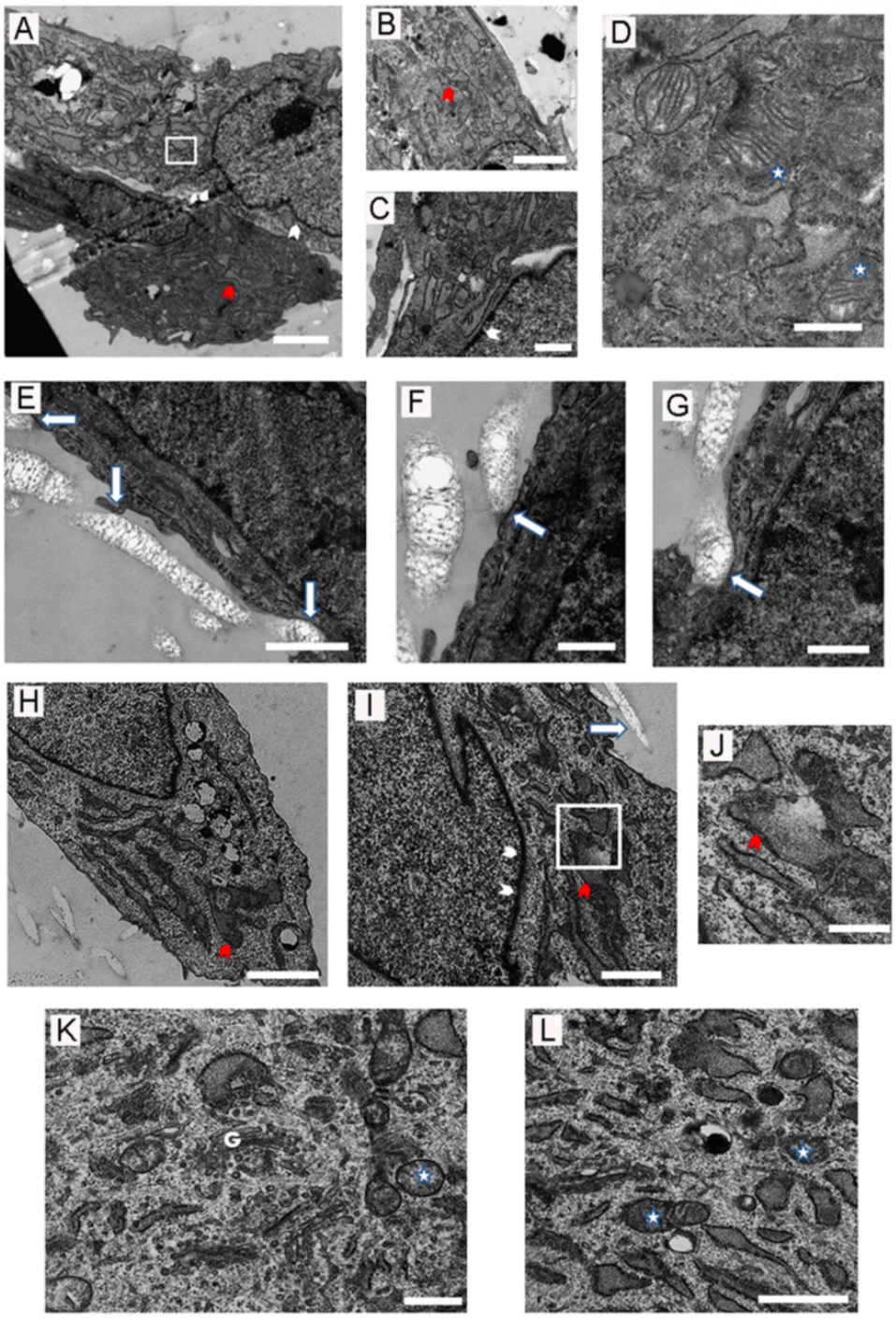

Figure 3.10 Transmission electron microscopy of tenocytes cultured onto PLLA/Coll-50/50 (A)–(G) and PLLA/Coll-75/25 (H)–(L) after 14 days. Cells showed a preserved cell ultrastructure as well as adhesion to bundles (E)–(G). Square indicates area enlarged in B and I, respectively. Note the well conserved nuclear envelop (white pointed arrows), the enlarged RER cisternae (red pointed arrows) and well conserved mitochondria (asterisks). Small bundle adhesion points are also evident (white arrows). G = Golgi apparatus. Scale bars (A), (B), (D), (H) = 0.2 µm; Scale bars (E), (I), (L) = 0.1 µm; scale bars (C), (F), (G), (J), (K) = 500 nm.

3.5 Discussion

In the design of a biomimetic scaffold for tendon tissue repair it is mandatory to consider the high complexity of the natural tendon hierarchical structure both from a morphological and from a chemical point of view, in order to achieve the mechanical properties required to restore function while allowing regeneration. The aim of this study was to develop and characterize bundles of PLLA-Coll blends, to be used as bioresorbable scaffolds for the repair of tendon tissue. In this work we focused on the chemical composition, cellular response and mechanical properties. Electrospinning has been used to reproduce the morphology of a subfascicle, having a diameter in the range 300–500 μm, similar to that of native human Achille's tendon [51]. To manufacture the bundles, PLLA was used in combination with collagen. The expected advantages of this formulation were long-term degradation, plasticity and toughness (provided by PLLA) and high biocompatibility and stiffness (provided by Collagen). Two different compositions were investigated and tested against tenocytes culture: PLLA/Coll- 75/25, and PLLA/Coll-50/50, while pure PLLA was characterized as a reference to assess the effect of collagen addition on scaffold properties. Collagen content in the fibers was not further increased to ensure long-term degradability of the scaffolds.

Flat mats and bundles made of sub-micrometric fibers were successfully spun (figures 3.1 and 3.2): the diameter of the fibers developed in our study (PLLA/ Coll-75/25: 0.31 ± 0.09 μm; and PLLA/Coll-50/50: 0.33 ± 0.08 μm) were in the same range of the diameter of the fibrils of the Achille tendon (i.e. 0.3 μm [52]). Moreover, the bundles diameters for the two blends were in the same range proposed in the literature for Achille tendon fascicles [21, 51, 53]. TGA and DSC analyses (Figure 3.3) enabled to quantitatively con- firm that the effective Coll content in the blend corresponded to the initial feeding, for both compositions.

The wettability (measured as drop WCA, Figure 3.2) indicated that increasing the collagen content led to an improved scaffold wettability, a positive aspect for the intended application. In nature, collagen molecules are arranged in a triple-helix structure [4, 21], which guarantees stability in a watery environment, while electrospun collagen normally requires a crosslinking treatment to reduce its

dissolution upon water contact [54], However, in previous literature studies cross-linking was not performed when collagen was blended with a synthetic polymer [55–57]. In these cases, although the effective stability of electrospun fiber composition upon water contact was not verified, the addition of the natural polymer had positive effects on cell culture [55–57]. In another study it was demonstrated that collagen release from weakly crosslinked poly(lactide-co-glycolide)/collagen blends occurred and had a remarkable effect on fiber morphology at high collagen content [58]. In the present study, cross- linking was not performed in order to avoid the use of toxic agents and possible contaminants. For both PLLA/Coll compositions we found that a portion of collagen was lost after very short time of water immersion (30 min); the PLLA/Coll-75/25 and PLLA/Coll- 50/50 scaffolds after 14 days in PBS had respectively an effective composition of 86/14 and 77/23 (determined by Biuret Assay, Figure 2.4). These results suggest that part of collagen in our electrospun fibers is promptly dissolved by water, reasonably the portion at fiber surface, while the remaining collagen is in intimate contact with the PLLA component and is not susceptible of rapid dissolution. Similar results were found by Yang et al on electrospun blends of PLLA/gelatin [59].

The mechanical tests confirmed that, in general, all the tested compositions showed an initial highly-compliant toe-region similar to that of natural tendon fascicles. The initial properties of the PLLA/Coll-75/25 were most promising: in fact this composition had the highest Young modulus (about 100 MPa), which was closest to the values reported for tendon collagen (about 200 MPa [51]), and a higher failure stress than both pure PLLA and PLLA/Coll-50/50. Furthermore, PLLA/Coll-75/25 had a ductile behavior, with higher yield stress than pure PLLA which can guarantee some safety factor in case of overload. It must be noted that the toughness of PLLA/Coll-75/25 was half of that of pure PLLA. PLLA/Coll-50/50 exhibited the worst properties in terms of brittleness. The PLLA/Coll-75/ 25 blend showed a significant increase of the Young modulus after permanence in PBS, whereas for PLLA/ Coll-50/50 the Young modulus first increased and then decreased over time. For both blends, a significant reduction of the yield stress, failure stress and work to failure was observed due to collagen loss during immersion in PBS. The Young

modulus and failure stress of our PLLA/ Coll-75/25 bundles (Figure 3.6) were in the same range as the human Achille tendon. The failure stress of fascicles from the Achille's tendon of Afro-Americans was 21.9 ± 9.9 MPa, and for Caucasians was 28.1 ± 9.8 MPa, with a Young's modulus of 316.8 ± 110 MPa and 222.8 ± 84.6 MPa respectively [51]. This data con- firms the suitability of the Young modulus of the PLLA/Coll-75/25 bundles, especially after 7 and 14 days in PBS (about 200 MPa, figure 3.7). The failure stress of PLLA/Coll-75/25 as-spun bundles is however lower than that of human tendons, and it further decreased due to permanence in PBS. A possible explanation for this progressive embrittlement and stiffening of the bundles is related to the loss of collagen from the bundles. Collagen component may be responsible of water absorption in PBS, that is expected to act as plasticizer and thus to promote material plasticity; the decrease of the amount of collagen in the fibers after 14 days in PBS may thus contribute to promoting material stiffening. This suggests that crosslinking the collagen might make it more stable after ageing in PBS. No other study reported the mechanical properties of electrospun PLLA-Coll bundles in the literature, rather mechanical properties were reported for: bundles of poly(ε-capro-lactone) (PCL) (E = 12.44 ± 4.96 MPa, σ_F = 4.12 ± 2.00 MPa [26]; bundles of poly(lactide-co-glicolide) (85:15) (E = 138.20 ± 16.98 MPa, σ_F = 9.48 ± 0.82 MPa [26]); non-woven scaffolds made of PCL/Chit-osan/Cellulose nanocrystals aligned fibers (E = 540.5 ± 83.7 MPa, σ_F = 39.3 ± 1.9 MPa) [60] and non-woven scaffolds made of chitosan/PLLA/gelatin/ PEO aligned fibers (E = 325.01 ± 25.05 MPa, σ_F = 14.23 ± 1.08 MPa) [28].

Cells biological tests confirm that fibers orientation represents an instructive pattern for the alignment of tenocytes [50]. SEM ultrastructural analysis suggested that the presence of collagen is of outmost importance for the adhesion and proliferation of human cells. TEM investigation demonstrated, how- ever, that tenocyte metabolic activity is not impaired by the presence of PLLA. Overall, this investigation support the hypothesis that the proposed bundles may prospectively provide a clinical option for tendon tissue augmentation. The present findings about cell viability are in agreement with previous works on electrospun PLLA/Coll scaffolds. Schofer et al described the good osteoblastic differentiation of mesenchymal stem cells on random fiber electrospun scaffolds mats of PLLA/Coll in ratio 4:1 [31, 32]. Theisen

et al tested the same blend in electrospun scaffolds, and demonstrated a good proliferation of human tenoblasts from long biceps tendons [33]. Conçalves et al studied the morphology, mechanical properties and osteoblastic differentiation of random electrospun fiber scaffolds mats made by five different kinds of PLLA/Coll blends and solvents systems, confirming their good biocompatibility [34].

One limitation of the present findings is certainly the fast loss of collagen, which resulted in a significant loss of the mechanical properties of the two blends within 14 days in PBS that can be reasonably limited by treating the electrospun bundles to crosslink the collagen. It is pointed out that after permanence in PBS, some of the bundles had shrunk to the point that their length was no more sufficient to roll them around the pins of the capstan grips for the tensile tests. In these cases, standard clamps were used: this might have resulted in a slight under-estimate of the failure properties. However, as no specimen failed in the clamp, such effects, if present at all, must have been negligible. Hansen et al used an actuator speed of 2 mm min^{-1}, with a specimen free length of 10 mm [48], which results in a strain rate slightly lower than the present study.

It must be noted that our bundles were produced with an operator-dependent approach. In the future, a more automated electrospinning configuration should be defined to standardize the manufacturing process. In fact, it has been shown that bundle production can be standardized [22].

From a biological point of view, it will be necessary to improve cell adhesion on the proposed bundles by limiting the loss of collagen and possibly tests other kind of cells involved in tendon regeneration (i.e. mesenchymal stem cells).

3.6 Conclusions

This study has demonstrated the feasibility of manufacturing bundles of a blend of bioresorbable polymers (PLLA and collagen). The use of electrospinning resulted in an arrangement of the fibers that mimicked that of tendon collagen. In fact, bundles with a cross section of 300–500 mm and a length of 150 mm were fabricated with different blends. The mechanical properties (stiffness and strength) achieved are similar to those of natural tendon. The cellular culture tests confirmed that the electrospun bundles of the selected blends promoted tenocyte adhesion and

proliferation. In this study single bundles were manufactured and tested. The future steps will include assembling multiple bundles in a multiscale arrangement mimicking the hierarchical structure of collagen in the human tendon.

3.7 References

[1] Abbah S A, Spanoudes K, O'Brien T, Pandit A and Zeugolis D I 2014 Assessment of stem cell carriers for tendon tissue engineering in pre-clinical models Stem Cell Res. Ther. 5 1–9

[2] Dy C J, Daluiski A, Do H T, Hernandez-Soria A, Marx R and Lyman S 2012 The epidemiology of reoperation after flexor tendon repair J. Hand Surg. 37 919–24

[3] Soroceanu A, Sidhwa F, Aarabi S, Kaufman A and Glazebrook M 2012 Surgical versus nonsurgical treatment of acute achilles tendon rupture: a meta-analysis of randomized trials J. Bone Joint Surg. 94 2136–43

[4] Lomas A J et al 2015 The past, present and future in scaffold- based tendon treatments Adv. Drug Deliv. Rev. 84 257–77

[5] Sharma P and Maffulli N 2005 Tendon injury and tendinopathy: healing and repair J. Bone Joint Surg. 87 187–202

[6] Wang J H C 2006 Mechanobiology of tendon J. Biomech. 39 1563–82

[7] Woo S L, Gomez M A, Woo Y K and Akeson W H 1982 Mechanical properties of tendons and ligaments: II. The relationships of immobilization and exercise on tissue remodeling Biorheology 19 397–408

[8] Miller D, Waterston R J, Barrass V and Muffulli N 2005 Conservative management, percutaneous or open repair of acute achilles tendon rupture: a retrospective study Scottish Med. J. 50 160–5

[9] Bagnaninchi P O, Yang Y, El Haj A J and Maffulli N 2007 Tissue engineering for tendon repair Br. J. Sports Med. 41 e10

[10] Ichioka S, Harii K, Yamada A and Sugiura Y 1994 Tendinocutaneous free flap transfer to cover an extensive skin- tendon defect of the dorsum of the hand: case report J. Trauma-Injury Infection Crit. Care 36 901–3

[11] Wang S, Zinderman C, Wise R and Braun M 2007 Infections and human tissue transplants: review of FDA MedWatch reports 2001–2004 Cell Tissue Bank. 8 211–9

[12] Adani R, Marcoccio I and Tarallo L 2003 Flap coverage of dorsum of hand associated with extensor tendons injuries: a completely vascularized single-stage reconstruction Microsurgery 23 32–9

[13] Kim S W, Hong J P, Lee W J,Chung Y K and Tark K C 2003 Single-stage achilles tendon reconstruction using a composite sensate free flap of dorsalis pedis and tendon strips of the extensor digitorum longus in a complex wound Ann. Plast. Surg. 50 653–7

[14] McGuire D A and Hendricks S D 2007 Allografts in sports medicine Operative Tech. Sports Med. 15 46–52

[15] Hampson K, Forsyth N R, El Haj A and Maffulli N 2008 Topics in Tissue Engineering vol. 4

[16] Kim C and Pedowitz R 2007 Daniel's Knee Injuires: Ligament and Cartilage Structure, Function, Injury, and Repair ed R Pedowitz et al (Philadelphia: Lippincott Williams & Wilkins)

[17] de Vos R J, Weir A and van Schie H M 2010 Platelet-rich plasma injection for chronic achilles tendinopathy: a randomized controlled trial J. Am. Med. Assoc. 303 144–9

[18] Schepull T, Kvist J, Norrman H, Trinks M, Berlin G and Aspenberg P 2011 Autologous platelets have no effect on the healing of human achilles tendon ruptures: a randomized single-blind study Am. J. Sports Med. 39 38–47

[19] Bowman K F, Muller B, Middleton K, Fink C, Harner C D and Fu F H 2013 Progression of patellar tendinitis following treatment with platelet-rich plasma: case reports Knee Surg. Sports Traumatol. Arthrosc. 21 2035–9

[20] Kannus P 2000 Structure of the tendon connective tissue Scand. J. Med. Sci. Sports 10 312–20

[21] Goh K L, Listrat A and Béchet D 2014 Hierarchical mechanics of connective tissues: integrating insghts from nano to macroscopic studies J. Biomed. Nanotechnol. 10 2464–507

[22] Ali U, Zhou Y,Wang X and LinT 2011 Nanofibers-Production, Properties & Functional Applications ed T Lin (Rijeka: InTech) ch8

[23] Mouthuy P A, Zargar N, Hakimi O, Lostis E and Carr A 2015 Fabrication of continuous electrospun filaments with potential for use as medical fibres Biofabrication 7 025006

[24] Sun B, Jiang X J, Zhang S, Zhang J C, Li Y F, You Q Z and Long Y Z 2015 Electrospun anisotropic architectures and porous structures for tissue engineering J. Mater. Chem. B 3 5389–410

[25] Bosworth L A, Rathbone S R, Bradley R S and Cartmell S H 2014 Dynamic loading of electrospun yarns guides mesenchymal stem cells towards a tendon lineage J. Mech. Behav. Biomed. Mater. 39 175–83

[26] Bosworth L A 2014 Travelling along the clinical roadmap: developing electrospun scaffolds for tendon repair Conference Papers in Science 2014 304974

[27] Bosworth L A, Alam N, Wong J K and Downes S 2013 Investigation of 2D and 3D electrospun scaffolds intended for tendon repair J. Mater. Sci., Mater. Med. 24 1605–14

[28] Zhang C et al 2015 Well-aligned chitosan-based ultrafine fibers committed teno-lineage differentiation of human induced pluripotent stem cells for Achilles tendon regeneration Biomaterials 53 716–30

[29] Xu Y et al 2013 Fabrication of electrospun poly(L-lactide-co-ε- caprolactone)/collagen nanoyarn network as a novel, three- dimensional, macroporous, aligned scaffold for tendon tissue engineering Tissue Eng. C 19 925–36

[30] Yang C, Deng G, Chen W, Ye X and Mo X 2014 Anovel electrospun-aligned nanoyarn-reinforced nanofibrous scaffold for tendon tissue engineering Colloids Surf. B 122 270–6

[31] Schofer M D, Boudriot U, Leifeld I, Sutterlin R I, Rudisile M, Wendorff J H, Greiner A, Paletta J R J and Fuchs-Winkelmann S 2009 Characterization of a PLLA- collagen I blend nanofiber scaffold with respect to growth and osteogenic differentiation of human mesenchymal stem cells Sci. World J. 9 118–29

[32] Schofer M D, Veltum A, Theisen C, Chen F, Agarwal S, Fuchs-Winkelmann S and Paletta J R J 2011 Functionalisation of PLLA nanofiber scaffolds using a possible cooperative effect between collagen type I and BMP-2: impact on growth and osteogenic differentiation of human mesenchymal stem cells J. Mater. Sci., Mater. Med. 22 1753–62

[33] Theisen C, Fuchs-Winkelmann S, Knappstein K, Efe T, Schmitt J, Paletta J R and Schofer M D 2010 Influence of nanofibers on growth and gene expression of human tendon derived fibroblast BioMed. Eng. OnLine 9 1–12

[34] Gonçalves F, Bentini R, Burrows C M, Carreira C A, Kossugue M P, Sogayar C M and Catalani H L 2015 Hybrid membranes of plla/collagen for bone tissue engineering: a comparative study of scaffold production techniques for optimal mechanical properties and osteoinduction ability Materials 8 408–23

[35] Saino E, Focarete M L, Gualandi C, Emanuele E, Cornaglia A I, Imbriani M and Visai L 2011 Effect of electrospun fiber diameter and alignment on macrophage activation and secretion of proinflammatory cytokines and chemokines Biomacromolecules 12 1900–11

[36] Gazzano M, Gualandi C, Zucchelli A, Sui T, Korsunsky A M, Reinhard C and Focarete M L 2015 Structure-morphology correlation in electrospun fibers of semicrystalline polymers by simultaneous synchrotron SAXS-WAXD Polymer 63 154–63

[37] Liu Z Q 1991 Scale space approach to directional analysis of images Appl. Opt. 30 1369–73

[38] Schindelin J et al 2012 Fiji: an open-source platform for biological-image analysis Nat. Methods 9 676–82

[39] Schneider C A, Rasband W S and Eliceiri K W 2012 NIH Image to ImageJ: 25 years of image analysis Nat. Methods 9 671–5

[40] Janairo G, Linley S M, Yap L, LIanos-Lazaro N and Robles J 2011 Determination of the sensivity range of biuret test for undergraduate biochemestry experiments e-J. Sci. Technol. 6 77–83

[41] Colombo V, Fabiani D, Focarete M L, Gherardi M, Gualandi C, Laurita R and Zaccaria M 2014 atmospheric pressure non- equilibrium plasma treatment to improve the electrospinnability of poly(l-lactic acid) polymeric solution Plasma Process. Polym. 11 247–55

[42] Torricelli P, Gioffrè M, Fiorani A, Panzavolta S, Gualandi C, Fini M, Focarete M L and Bigi A 2014 Co-electrospun gelatin-poly(l-lactic acid) scaffolds: Modulation of mechanical properties and chondrocyte response as a function of composition Mater. Sci. Eng. C 36 130–8

[43] Gualandi C, Govoni M, Foroni L, Valente S, Bianchi M, Giordano E, Pasquinelli G, Biscarini F and Focarete M L 2012 Ethanol disinfection affects physical properties and cell response of electrospun poly(l-lactic acid) scaffolds Eur. Polym. J. 48 2008–18

[44] Puett D 1967 DTA and heals of hydration of some polypeptides Biopolymers 5 327–30

[45] Lim J J and Shamos M H 1974 Evaluation of kinetic parameters of thermal decomposition of native collagen by thermogravimetric analysis Biopolymers 13 1791–807

[46] Mukherjee S, Gualandi C, Focarete M L, Ravichandran R, Venugopal J R, Raghunath M and Ramakrishna S 2011 Elastomeric electrospun scaffolds of poly(l-lactide-co- trimethylene carbonate) for myocardial tissue engineering J. Mater. Sci., Mater. Med. 22 1689–99

[47] Fong G, Backman L J, Andersson G, Scott A and Danielson P 2013 Human tenocytes are stimulated to proliferate by acetylcholine through an EGFR signalling pathway Cell Tissue Res. 351 465–75

[48] Giusti I, D'Ascenzo S, Mancò A, Di Stefano G, Di Francesco M, Rughetti A, Dal Mas A, Properzi G, Clvisi V and Dolo V 2014 Platelet concentration in platelet-rich plasma affects tenocytes behaviour in vitro BioMed Res. Int. 2014 630870

[49] Backman L J, Fong G, Andersson G, Scott A and Danielson P 2011 Substance p is a mechanoresponsive, autocrine regulator of human tenocyte proliferation PloS One 6 e27209

[50] Gigante A, Cesari E, Busilacchi A, Manzotti S, Kyriakidou K, Greco F, Primio R D and Mattioli-Belmonte M 2009 Collagen I membranes for tendon repair: effect of collagen fiber orientation on cell behavior J. Orthopaedic Res. 27 826–32

[51] Hanson P, Aagaard P and Magnusson S P 2012 Biomechanical properties of isolated fascicles of the iliopsoas and achilles tendons in african american and caucasian men Ann. Anat. 194 457–60

[52] Pingel J, Lu Y, Starborg T, Fredberg U, Langberg H, Nedergaard A, Weis M, Eyre D, Kjaer M and Kadler K E 2014 3D ultrastructure and collagen composition of healthy and overloaded human tendon: evidence of tenocyte and matrix buckling J. Anat. 224 548–55

[53] Hansen P, Kovanen V, Holmich P, Krogsgaard M, Hansson P, Dahl M, Hald M, Aagaard P, Kjaer M and Magnusson S P 2013 Micromechanical properties and collagen composition of ruptured human achilles tendon Am. J. Sports Med. 41 437–43

[54] Fiorani A, Gualandi C, Panseri S, Montesi M, Marcacci M, Focarete M L and Bigi A 2014 Comparative performance of collagen nanofibers electrospun from different solvents and stabilized by different crosslinkers J. Mater. Sci., Mater. Med. 25 2313–21

[55] Xue J, Shi R, Niu Y, Gong M, Coates P, Crawford A, Chen D, Tian W and Zhang L 2015 Fabrication of drug-loaded anti- infective guided tissue regeneration membrane with adjustable biodegradation property Colloids Surf. B 135 846–54

[56] Kijenska E, Prabhakaran M P, Swieszkowski W, Kurzydlowski K J and Ramakrishna S 2012 Electrospun bio- composite P(LLA-CL)/collagen I/collagen III scaffolds for nerve tissue engineering J. Biomed. Mater. Res. B 100B 1093–102

[57] Li M, Mondrinos M J, Chen X, Gandhi M R, Ko F K and Lelkes P I 2006 Co-electrospun poly(lactide-co-glycolide), gelatin, and elastin blends for tissue engineering scaffolds J. Biomed. Mater. Res. A 79A 963–73

[58] Jose M V, Thomas V, Dean D R and Nyairo E 2009 Fabrication and characterization of aligned nanofibrous PLGA/Collagen blends as bone tissue scaffolds Polymer 50 3778–85

[59] Yang X, Xu Q, Yan N, Sui G, Cai Q and Deng X 2011 Structure and wettability relationship of coelectrospun poly (L-lactic acid)/gelatin composite fibrous mats Polym. Adv. Technol. 22 2222–30

[60] Domingues R M A, Chiera S, Gershovich P, Motta A, Reis R L and Gomes M E 2016 Enhancing the biomechanical performance of anisotropic nanofibrous scaffolds in tendon tissue engineering: reinforcement with cellulose nanocrystals Adv. Healthc. Mater. 5 1364–75

Chapter 4: Tendon fascicle-inspired nanofibrous scaffold of polylactic acid/collagen with enhanced 3d-structure and biomechanical properties

Alberto Sensini[1], Chiara Gualandi[2,3], Andrea Zucchelli[1], Liam Boyle[4], Alexander P. Kao[5], Gwendolen C. Reilly[4], Gianluca Tozzi[5], Luca Cristofolini[1,3], Maria Letizia Focarete[2,3]

1 Department of Industrial Engineering, Alma Mater Studiorum - Università di Bologna, 40131 Bologna, Italy

2 Department of Chemistry "G. Ciamician" and National Consortium of Materials Science and Technology (INSTM, Bologna RU), Alma Mater Studiorum - Università di Bologna, 40126 Bologna, Italy

3 Health Sciences and Technologies – Interdepartmental Center for Industrial Research (HST-ICIR), Alma Mater Studiorum - Università di Bologna, 40064 Ozzano dell'Emilia, Bologna, Italy

4 INSIGNEO Institute for in silico Medicine, University of Sheffield, Sheffield S10 2TN, United Kingdom

5 ZEISS Global Centre, School of Engineering, University of Portsmouth, Portsmouth PO13DJ, United Kingdom

Keywords: Tendon; Electrospun Bundles; High Resolution X-Ray Tomography; Mechanical Characterization, Poly(lactic acid)/Collagen Blends.

The candidate was the main investigator of the study. This work was published on Scientific Reports 2018, 8, 17167. Reproduced under the terms and conditions of the Creative Common Attribution (CC BY 4.0.).

Published in: Scientific Reports 21 November 2018

4.1 Abstract

Surgical treatment of tendon lesions still yields unsatisfactory clinical outcomes. The use of bioresorbable scaffolds represents a way forward to improve tissue repair. Scaffolds for tendon reconstruction should have a structure mimicking that of the natural tendon, while providing adequate mechanical strength and stiffness. In this paper, electrospun nanofibers of two crosslinked PLLA/Collagen blends (PLLA/Coll-75/25, PLLA/Coll-50/50) were developed and then wrapped in bundles, where the nanofibers are predominantly aligned along the bundles. Bundle morphology was assessed via SEM and high-resolution x-ray computed tomography (XCT). The 0.4-micron resolution in XCT demonstrated a biomimetic morphology of the bundles for all compositions, with a predominant nanofiber alignment and some scatter (50–60% were within 12° from the axis of the bundle), similar to the tendon microstructure. Human fibroblasts seeded on the bundles had increased metabolic activity from day 7 to day 21 of culture. The stiffness, strength and toughness of the bundles are comparable to tendon fascicles, both in the as-spun condition and after crosslinking, with moderate loss of mechanical properties after ageing in PBS (7 and 14 days). PLLA/Coll-75/25 has more desirable mechanical properties such as stiffness and ductility, compared to the PLLA/Coll-50/50. This study confirms the potential to bioengineer tendon fascicles with enhanced 3D structure and biomechanical properties.

4.2 Introduction

Ruptures and lesions of tendons are very common in elderly people, but also in athletes and young adults, deriving from chronic tendinopathies, acute injuries due to inflammatory processes, or trauma [1-3]. Frequently injured tendons are, for example, the shoulder rotator cuff, the flexor, the Achilles and the patellar [4,5]. Among others, Achilles tendon rupture is a common sports-related injury, with the highest incidence observed in 30- to 50-years old males, that often results in disability with degeneration occurring in an estimated 11% of runners [6-8]. Surgical treatment is the standard therapy for the majority of patients and includes minimally invasive, percutaneous or open repair strategies, depending on the extent

of the injury. Unfortunately, postoperative complications often occur, with associated re-rupture risk: for example the Achilles tendon re-fracture occurs in 8–13% cases and for the flexor/extensor tendon in 4–18% cases [7-10]. Furthermore, the formation of scar tissue generates morphological discontinuities, which impair the mechanical properties and the proper biomechanical functionality of the tendon11. In order to avoid this complication, often surgeons tailor the use of autografts, allografts, xenografts, or tendon prostheses and/or sutures, depending on the site and severity of the injury [12]. Autologous grafts are immunologically suitable, but are often associated with some degree of donor morbidity, whereas allografts are not widely available, can be expensive and carry the risk of rejection and transmission of disease. Implants made of inert synthetic materials, typically made from non-resorbable polymers such as polytetrafluoroethylene (PTFE), polythiophene (PTP), polyethylene (PE) or silicone, are relatively successful in reconstructive surgery since they initially have good postoperative mechanical properties. However, inert synthetic implants have poor long-term effectiveness as their mechanical properties degrade over time due to wear, while the residual tendon tissue can be compromised due to stress shielding [2,3,13-15]. Other drawbacks with artificial tendon prostheses are inflammatory responses, failure at the fixation sites, and lack of long-term biocompatibility [13-16]. For these reasons, a tissue engineering (TE) approach represents a promising solution for tendon reconstruction, prompted also by the increasing development of biocompatible and resorbable scaffolds. The primary role of scaffolds in tendon TE is to provide temporary structural and mechanical support to promote tissue healing. Scaffolds can uptake the loads during the initial phase of repair of the injured tendon. By accurately tuning the rate of bioresorption with respect to the time needed for native tissue formation, they aim to encourage regeneration through tissue remodeling [2]. Among the various techniques to produce scaffolds for tendon tissue regeneration, electrospinning is one of the most versatile. Thanks to its ability to produce filaments of both natural and synthetic polymers with nano- and micrometric diameters oriented in specific directions, electrospinning enables the production of scaffolds morphologically similar to the hierarchical structure of the tendon collagen fascicles and fibrils [17-20]. By wrapping an electrospun mat of aligned

fibers, or by mechanically rolling groups of fibers, it is possible to produce electrospun units, called bundles, composed of aligned nanofibers that resemble tendon fascicles [17,21,22].

These scaffolds can be pre-seeded with tendon derived fibroblasts, commonly referred to as tenocytes, dermal derived fibroblasts or even stem cells. Dermal fibroblasts may be beneficial as a seeding cell compared to stem cells, as they are not able to differentiate into bone or cartilage cell lineages, which can lead to ectopic bone or cartilage formation [23]. Dermal fibroblasts also have similar characteristics to tendon derived fibroblasts and have the added benefit that they can be harvested from a simple skin biopsy [24]. Alternatively, scaffolds can be implanted directly and allow the hosts cells to migrate into and populate the scaffold.

Published literature confirms fibroblasts can proliferate on electrospun scaffolds made of resorbable materials, and their attachment and growth can be guided by the direction of fibers, both for tendon and ligament applications [17,21,25-35]. It is also well established that a combination of resorbable synthetic polymers such as poly(L-lactic acid) (PLLA), poly(lactic-co-glycolic acid) (PLGA), poly(ε-caprolactone) and natural polymers such as collagen, silk, chitosan or gelatin, are able to increase the biocompatibility and cell adhesion to these scaffolds [2,17,25,32,35]. Among the various combinations of synthetic and natural polymers proposed for producing electrospun fibers mats for tendon TE, the system composed of PLLA and collagen (Coll) represents a promising choice, since it combines the good mechanical and processing properties of a synthetic component with the bioactivity of a natural polymer [17,35]. Some groups have investigated blends of PLLA and Coll [17,35-39]. The two polymers have also been electrospun as separate phases by means of a coaxial electrospinning process40. The two main challenges that scaffolds for tendon TE face at present are: (i) providing adequate mechanical strength to meet the in vivo requirements, with a stiffness matching that of the natural tendon, and (ii) having a 3D structure and architecture that closely resemble the complex multiscale organization of native tendon tissue. An important aspect in the development of scaffolds for tendon TE, in addition to assessing their

biomechanical properties, is accurately evaluating the 3D structure and morphology.

In the present work, crosslinked PLLA/Coll electrospun bundles were developed, with a 3D structure suitable to mimic the tendon hierarchical structure (Fig. 1A), and with enhanced mechanical properties, in the range of human tendon fascicles. The biomechanical properties of the scaffolds were evaluated in detail, and in vitro tests were performed to assess cell adhesion and metabolic activity. High-resolution x-ray computed tomography (XCT) was also used to undertake a detailed evaluation of the bundle internal morphology and the effects of the crosslinking process on nanofiber morphology, distribution and alignment.

4.3 Results

4.3.1 Morphology of Fibers and Bundles

Electrospun bundles of the two compositions PLLA/Coll-75/25 and PLLA/Coll-50/50 were produced as previously reported, by means of a high-speed rotating drum collector (Figure S1) that allowed the production of nanofibers preferentially aligned in the direction of the drum rotation [17]. By rolling up the electrospun mat along the axis of the drum (Figure 4.1(B)), bundles of several centimeters in length were obtained (Figure 4.1(C)). The individual electrospun nanofibers mimicked the natural collagen fibrils. The bundle containing a number of nanofibers mimicked the fascicles of collagen in the natural tendon.

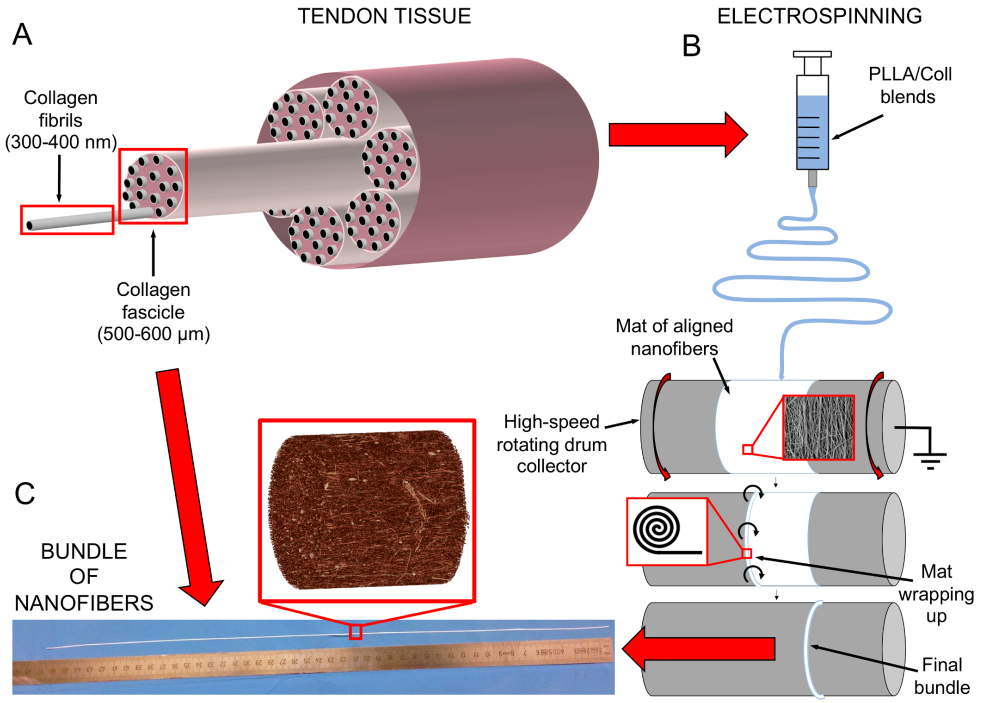

Figure 4.1. Multiscale structure of a tendon highlighting the main three hierarchical levels of aggregation (nomenclature derived from Kastelic et al. [18]) (A), schematic of the fabrication process (B) and photograph of the final bundle resembling the structure of tendon fascicle (C). The individual electrospun nanofibers mimic the natural collagen fibrils. The bundle containing a number of nanofibers mimics the fascicles of collagen in the natural tendon.

Bundles consisted of bead-free nanometric fibers (Figure 4.2). Alteration of nanofiber morphology, as a consequence of the crosslinking treatment (which was performed as described in the Experimental Section to delay collagen loss), and the ageing process in phosphate buffered saline (PBS) for different time intervals, were assessed by SEM observations (Figure 4.2). As-spun PLLA/Coll-75/25 and PLLA/Coll-50/50 nanofibers had similar diameters of 0.36 ± 0.07 µm and 0.39 ± 0.09 µm (mean ± standard deviation) respectively (Figure 4.2(E)). Nanofibers retained the same morphology and similar diameter after the crosslinking treatment and after 7 days of immersion in PBS, while both compositions showed a slight swelling of the nanofibers leading to higher nanofiber diameters after 14 days (Figure 4.2: this difference, even if relatively small, was statistically significant due to the large sample size). Moreover, after PBS immersion there were no visible cracks, welds or loss of material (Figure 4.2(B),

4.2(C), 4.2(D)). However, after crosslinking the nanofibers assumed a slightly wavy appearance, especially in the case of the PLLA/Coll-50/50 blend.

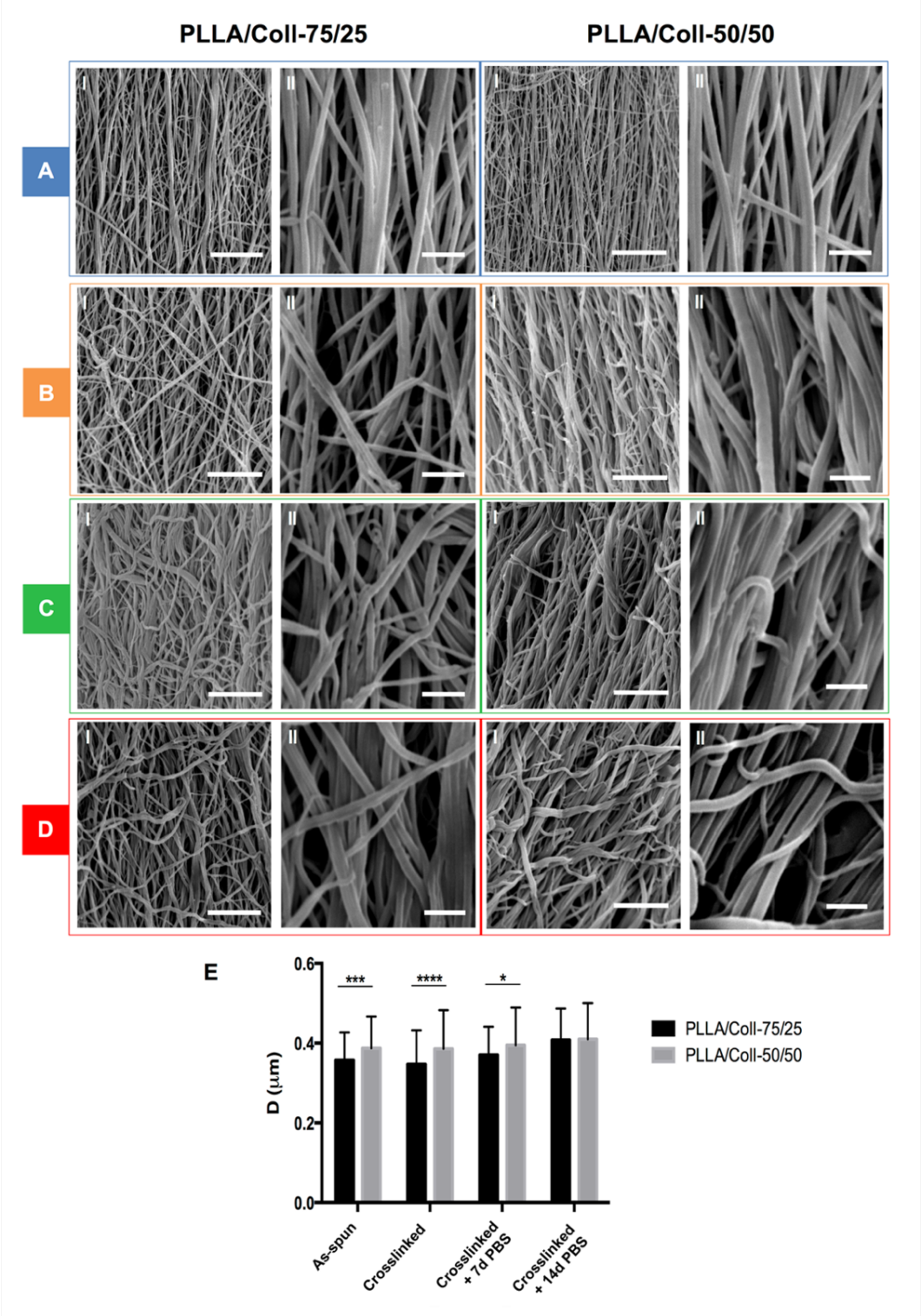

Figure 4.2. SEM images of PLLA/Coll-75/25 and PLLA/Coll-50/50 as-spun (A), immediately after cross-linking (B), after 7 days in PBS (C) and after 14 days in PBS (D). For each case, images at

two different magnifications are presented (Scale bars: I = 10 μm; II = 2 μm). The mean and standard deviation of nanofibers diameters (E) is plotted for the two compositions together with statistical significance of post-hoc comparisons (Tukey multiple comparisons, * P≤ 0.05, ** P≤ 0.01, *** P≤ 0.001, **** P≤ 0.0001).

The PLLA/Coll-75/25 bundles as-spun had a diameter of 624.9 ± 38.8 μm; the PLLA/Coll-50/50 bundles as-spun had a diameter of 643.1 ± 29.2 μm. Bundles as-spun of both compositions appeared flexible in handling in the dry state. After crosslinking the PLLA/Coll-75/25 and PLLA/Coll-50/50 bundles had a diameter of 575.1 ± 43.9 μm and 433.8 ± 37.3 μm, respectively. After crosslinking, the dry bundles were more brittle to handle.

The bundle did not have a measurable change in diameter after 7 and 14 days immersion in PBS, but became more brittle in handling. However, when re-immersed in PBS, all bundles regained flexibility. It is worth mentioning that immediately after crosslinking both PLLA/Coll-75/25 and PLLA/Coll-50/50 bundles shrunk in length with a decrease of about 21.5 ± 1.1% of the original length, as a consequence of PLLA chain relaxation occurring when macromolecules in the amorphous state acquire mobility [41].

High-resolution x-ray computed tomography (XCT) investigation with 1 μm (Figure 4.3) and 0.4 μm (Figure 4.4) voxel sizes, confirmed the aligned morphology of the nanofibers for the PLLA/Coll-75/25 and PLLA/Coll-50/50 blends both for the as-spun and crosslinked bundles. Scans with 1 μm voxel size did not enable clear discernment of the nanofibers (Figure 4.3). However, at 0.4 μm voxel size the nanofibers were clearly visible and very well defined (Figure 4.4). Negligible loss of material was observed in the XCT images within the crosslinked bundles.

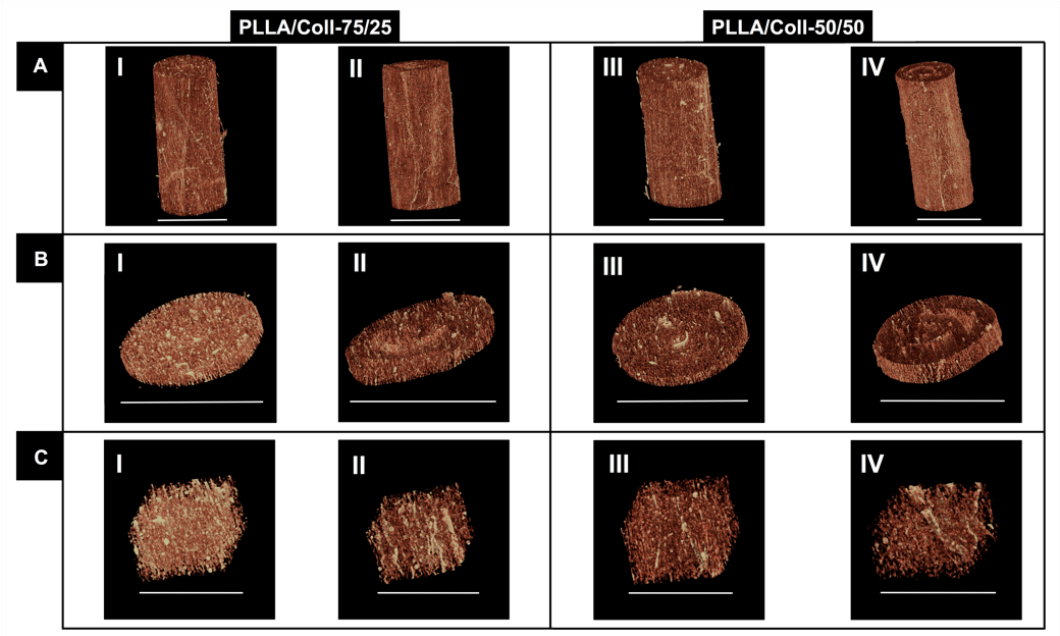

Figure 4.3. High-resolution x-ray computed tomography (XCT) images of the bundles at 1 μm voxel size: bundle segment (A), slice of a bundle (B) and magnification of cropped internal sub-volume (C) (A and B scale bar = 500 μm, C scale bar = 200 μm). PLLA/Coll-75/25 as-spun (I) and after crosslinking (II). PLLA/Coll-50/50 as-spun (III) and after crosslinking (IV).

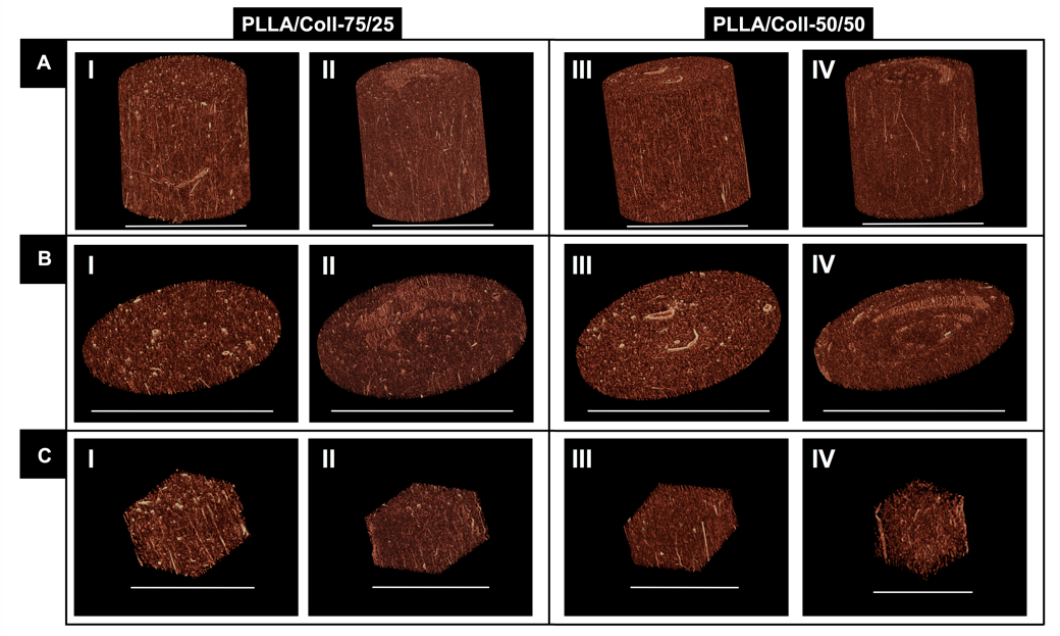

Figure 4.4. High-resolution x-ray computed tomography (XCT) images of the bundles at 0.4 μm voxel size: bundle segment (A), slice of a bundle (B) and magnification of cropped internal sub-volume(C)(A and B scalebar = 500 μm, C scalebar = 200 μm). PLLA/Coll-75/25 as-spun (I) and after crosslinking (II). PLLA/Coll-50/50 as- spun (III) and after crosslinking (IV).

The uniaxial alignment of the nanofibers, both on the surface and in the body of the samples, as well as the retention of morphology after crosslinking and PBS immersion, were confirmed by the "Directionality analysis" on the 0.4 µm voxel size scans (Figure 5.4).

The XCT morphological analysis showed that the PLLA/Coll-75/25 bundles as-spun had 56.9 ± 3.1% of the nanofibers aligned within ±12° from the longitudinal axis of the bundle, whereas the PLLA/Coll-75/25 crosslinked had 52.4 ± 1.8% of the nanofibers aligned within ±12° from the axis of the bundle (Figure 5(I)), with a mean reduction of alignment of 4.5%. The PLLA/Coll-50/50 as-spun had 59.9 ± 2.8% of the nanofibers aligned within ±12° from the axis of the bundle, whereas the PLLA/Coll-50/50 crosslinked had 56.6 ± 2.1% of the nanofibers aligned within ±12° from the axis of the bundle (Figure 5(II)), with a mean reduction of alignment of 3.3%.

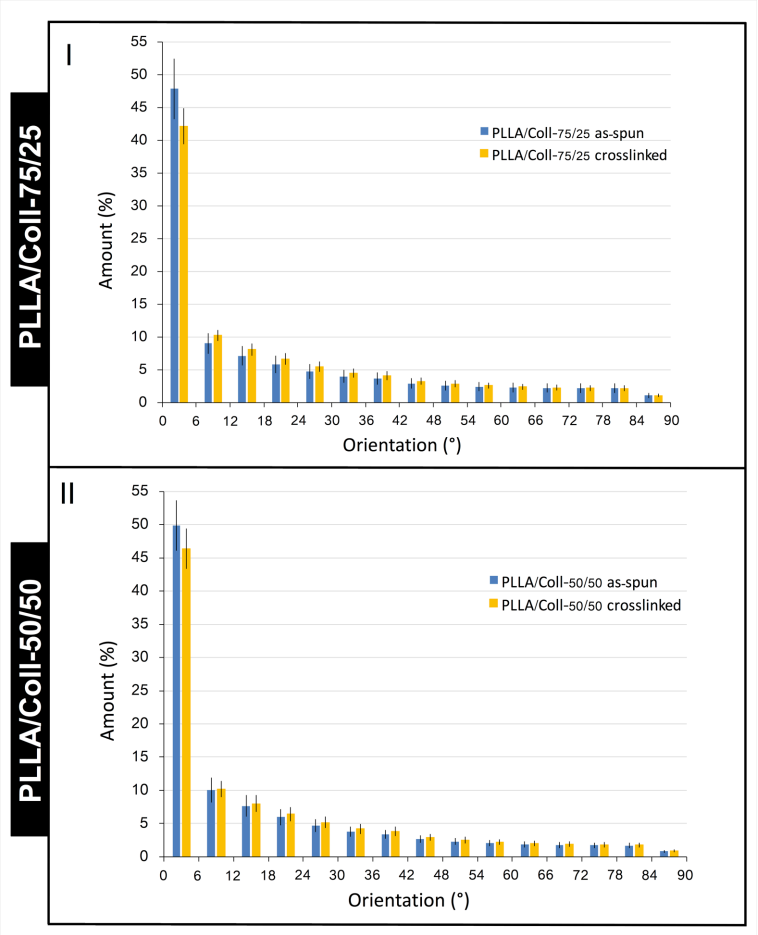

Figure 4.5. Orientation of the nanofibers measured in the XCT scans at 0.4 µm voxel size for the PLLA/Coll-75/25 (I) and PLLA/Coll-50/50 (II) bundles. The histograms report the percentage of

nanofibers aligned within a specific orientation from the longitudinal direction. An orientation of the nanofibers parallel to the axis of the bundle corresponds to 0°. An orientation of the nanofibers in a transverse plane corresponds to 90°. For each orientation, the mean and standard deviation are reported among all the axial slices that were obtained reslicing each scan.

4.3.2 Bundles Chemical Composition

TGA analysis was carried out on the bundles as-spun to verify their composition (Figure 4.S3). To this aim, the residual weight of the bundle at the end of the analysis was compared to that of the pure blend components (PLLA and Coll) and the actual composition of the bundles was determined by applying Equation 4.1. The results showed that the chemical composition of the bundles as-spun was close to the nominal one (Table 4.1). After crosslinking, the collagen content slightly decreased from 25 to 19 wt% in the PLLA/Coll-75/25 bundles, and from 49 to 45 wt% in the PLLA/Coll-50/50. In other words, PLLA/Coll-75/25 lost about 30% of their collagen, while PLLA/Coll-50/50 only 15%. When the crosslinked bundles were maintained in PBS at 37 °C for 7 and 14 days, the chemical composition showed a very low reduction in collagen content.

Table 4.1. Chemical composition of the bundles as-spun, after crosslinking, and after ageing in PBS at 37°C for different times.

	Sample	PLLA:Coll [wt:wt]
PLLA/Coll-75/25	As-spun	75:25[a]
	Crosslinked	(80.9±0.8):(19.1±0.8)[b]
	Crosslinked + 7d PBS	(80.6±0.6):(19.4±0.6)[b]
	Crosslinked + 14d PBS	(81.4±0.1):(18.6±0.1)[b]
PLLA/Coll-50/50	As-spun	51:49[a]
	Crosslinked	(54.6±0.1):(45.4±0.1)[b]
	Crosslinked + 7d PBS	(56.0±0.2):(44.0±0.2)[b]
	Crosslinked + 14d PBS	(57.3±0.1):(42.7±0.1)[b]

[a)]Determined by TGA analysis by applying Equation 4.1; [b)]Determined by gravimetric method by applying Equation 4.2 and 4.3.

4.3.3 Mechanical Properties of the Bundles

After hydration in PBS for 2 minutes, the stress–strain curves of the bundles as-spun for both blends showed a similar nonlinear behavior with an initial toe region, and a ductile behavior (Figure 4.6A and 4.6B). Such ductility was maintained also after the crosslinking treatment and after ageing in PBS for 7 and 14 days.

After crosslinking, both blends showed a visible increase in mechanical properties, especially of the yield and failure stress. The mechanical properties progressively decreased after ageing in PBS with respect to the condition immediately after crosslinking, but even after 14 days they remained in the same range as the bundles as-spun (Figure 4.6).

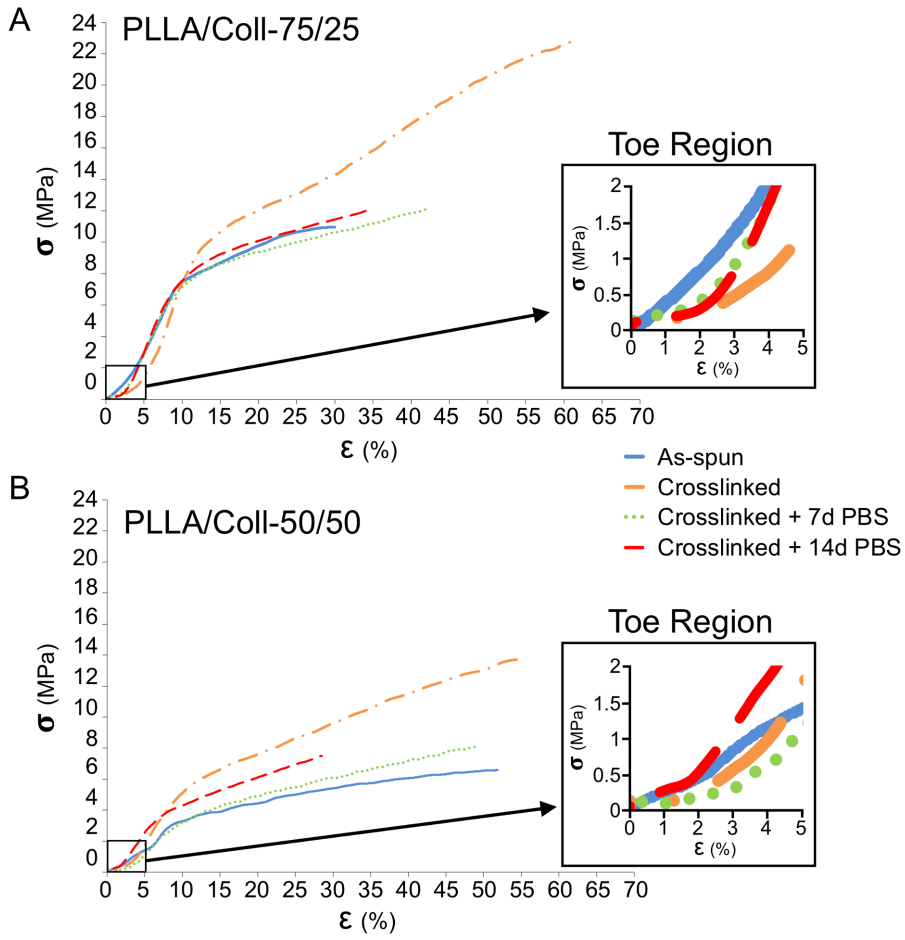

Figure 4.6. Representative stress-strain curves of the PLLA/Coll-75/25 (A) and PLLA/Coll-50/50 (B) in four different conditions: as-spun, immediately after crosslinking (crosslinked), after crosslinking and immersion in PBS at 37°C for 7 days (crosslinked + 7d PBS) and 14 days (crosslinked + 14d PBS). For both plots a zoom is provided of the initial toe region.

The PLLA/Coll-75/25 bundles showed an increase in failure stress from 11.3 ± 0.6 MPa (as-spun) to 18.8 ± 3.8 MPa (immediately after crosslinking) and maintained a failure stress of 10.2 ± 1.1 MPa after 14 days in PBS. The PLLA/Coll-50/50 bundles showed an increase in failure stress from 6.0 ± 0.6 MPa (as-spun) to 14.2 ± 2.4 MPa (immediately after crosslinking) and after 14 days of ageing in PBS the failure stress was 6.6 ± 1.1 MPa. Moreover, as the crosslinking increased, the failure stress and failure strain also increased, and the crosslinked bundles displayed a higher work to failure. The PLLA/Coll-75/25 bundles had a work to failure of 0.225 ± 0.021 J/mm^3 (as-spun), which increased to 0.647 ± 0.185 J/mm^3 (immediately after crosslinking), and then decreased to 0.213 ± 0.045 J/mm^3 after 14 days in PBS. For the PLLA/Coll-50/50 bundles the work to failure was 0.208 ± 0.022 J/mm^3 (as-spun), and increased to 0.588 ± 0.195 J/mm^3 (immediately after crosslinking) then decreasing to 0.137 ± 0.052 J/mm^3 after 14 days in PBS. Some variations due to treatment were statistically significant (one-way ANOVA, Figure 4.7). The highest yield and failure stress values were found for the PLLA/Coll-75/25 crosslinked bundles. In addition, the PLLA/Coll-75/25 showed higher values than the PLLA/Coll-50/50 also for the other mechanical properties (yield strain, Young's modulus and work to yield) (Figure 4.7). Conversely, the PLLA/Coll-50/50 had larger failure strain than the PLLA/Coll-75/25. Some differences between compositions were statistically significant (two-way ANOVA, Table 4.S1).

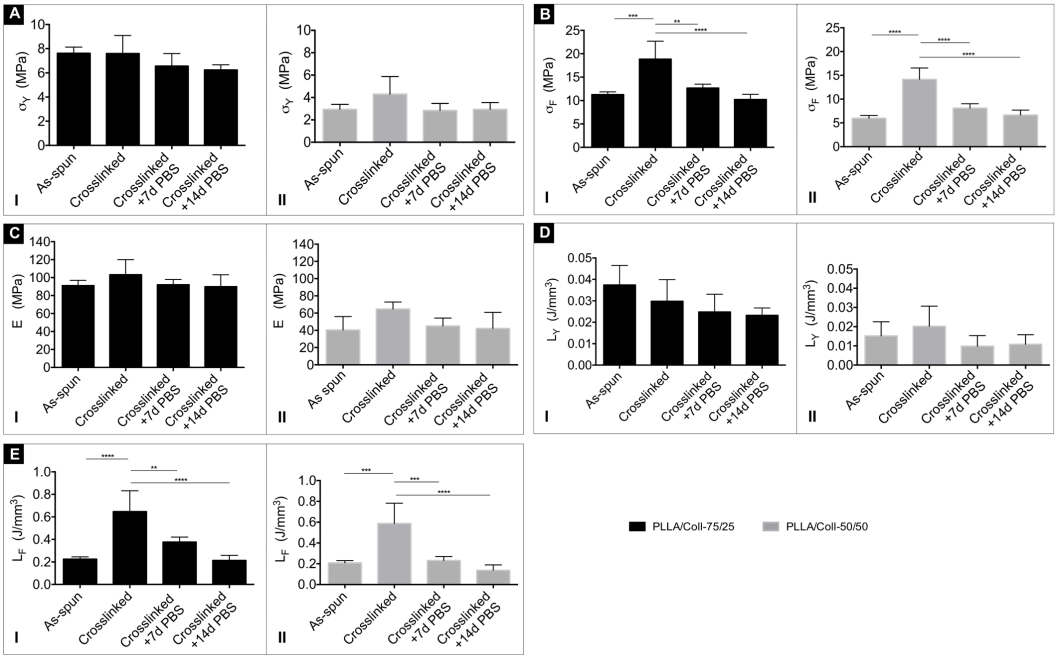

Figure 4.7. Mechanical properties of the bundles of PLLA/Coll-75/25 and PLLA/Coll-50/50 for the different conditions (as-spun, crosslinked, and after ageing in PBS). The following mechanical properties are reported: (A) yield stress (σ_Y), (B) failure stress (σ_F), (C) Young modulus, (D) work to yield (L_Y), (E) work to failure (L_F). The mean and standard deviation is plotted for the 5 specimens tested for each condition. Statistical significance was assessed with a one-way analysis of variance (ANOVA), followed by post-hoc comparisons (Tukey multiple comparisons, * $P \leq 0.05$, ** $P \leq 0.01$, *** $P \leq 0.001$, **** $P \leq 0.0001$).

4.3.4 Cell Methabolic Activity and Morphology

Cell attachment was higher on crosslinked bundles compared to non-crosslinked bundles of the same composition (Figure 4.8). By day 7, cell metabolic activity, assessed by resazurin reduction, was similar in the PLLA/Coll-75/25 bundles (both as-spun and crosslinked) and in the PLLA/Coll-50/50 bundles crosslinked; only the PLLA/Coll-50/50 as-spun had significantly lower cell metabolic activity. By day 21, all bundle compositions supported similar cell metabolic activity. Only viable cells can exhibit metabolic activity, therefore this indicates that cells were viable on the bundles after 21 days of culture. The fluorescent images show that the cells were distributed over the length of the scaffolds and, after day 21, they were predominantly aligned with the nanofibers (Figure 4.8(A)–(D)).

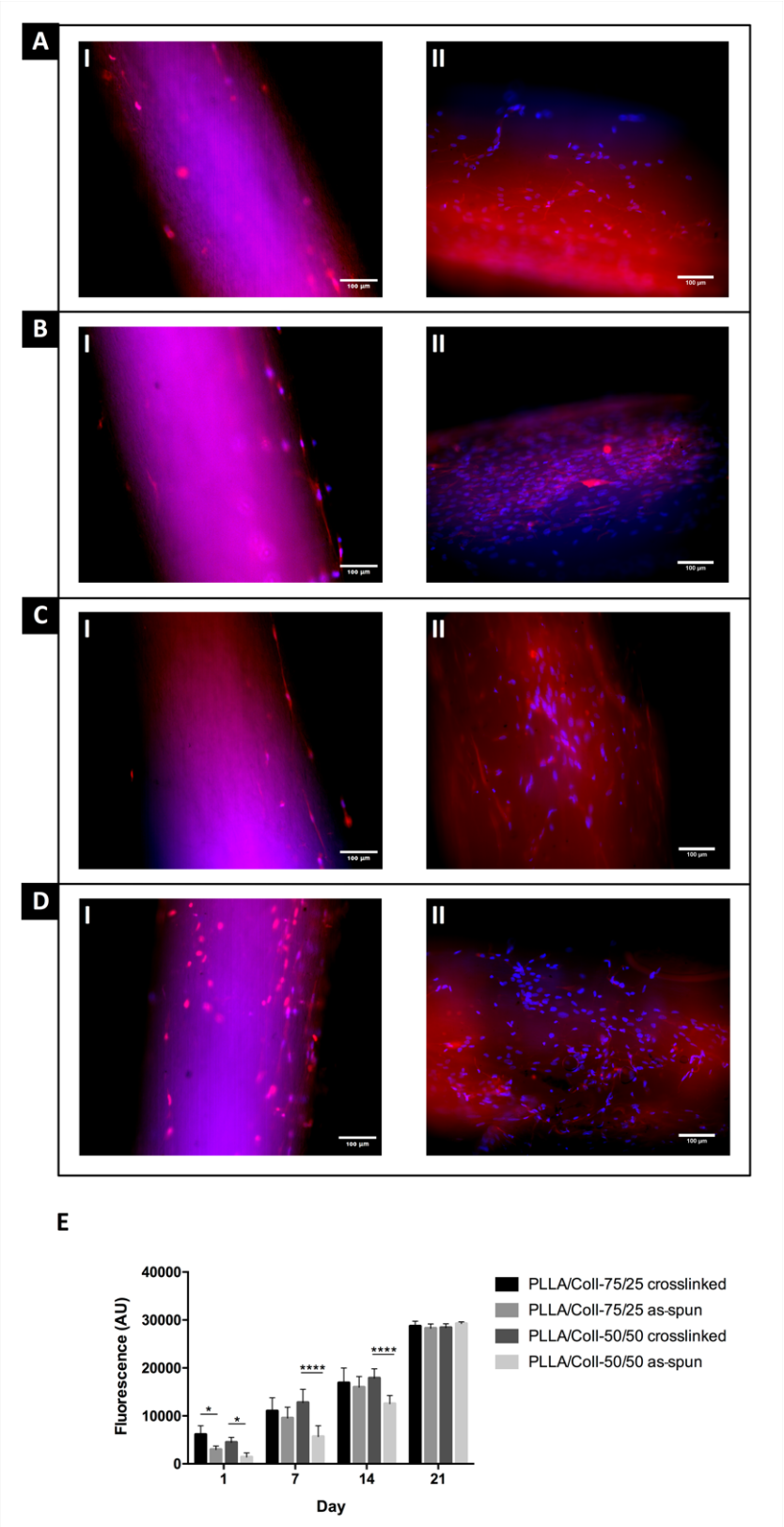

Figure 4.8. Fluorescence microscopy of NTF-322s with DAPI (cell nuclei, blue) and phalloidin-TRITC (actin, red) after (I) 14 days and (II) 21 days of NTF-322 culture on (A) PLLA/Coll-75/25 as-spun, (B) PLLA/Coll-75/25 crosslinked, (C) PLLA/Coll-50/50 as-spun and (D) PLLA/Coll-

50/50 crosslinked bundles. The fibers exhibited some autofluorescence; however the cell nuclei could be clearly identified as discrete ellipses. (E) Comparison of NTF-322 cell viability assessed using a resazurin reduction assay after 1, 7, 14 and 21 days of culture. Initial attachment of the NTF-322s to the scaffolds was significantly lower in the scaffolds as-spun, compared to their crosslinked counterparts. Mean and standard deviation for 6 samples is reported. Statistical analysis was performed using two-way analysis of variance (ANOVA) followed by Tukey post-hoc test (* $P \leq 0.05$, **** $P \leq 0.0001$).

4.4 Discussion

Tendon injuries still constitute an unsolved clinical need and are a major clinical problem for healthcare systems worldwide [2,3]. Recent advances in materials chemistry, biology and bioengineering have made 3D scaffolds available as a promising method to reinforce and replace tendons, providing structural support and a path for cells and new tissue formation. Synthetic scaffolds have been manufactured using a variety of polymers and fabrication methods from inert and resorbable polymers. In designing scaffolds for tendon tissue engineering, it is fundamental that the scaffold presents an appropriate 3D morphology and structure in order to mimic the complex hierarchical structures and mechanical properties of the tissue to replace [18-20].

To face these challenges, in the present work bundles of axially aligned electrospun nanofibers were fabricated, with the aim of mimicking the fascicles of the human tendons. Among other fabrication methods, electrospinning appears to be an optimal technique, since aligned nano- and microfibrous mats, as well as fibrous bundles, can be produced with mechanical and morphological features similar to the tissue to be replaced. As a model material for the present study, blends of PLLA/Coll in two different compositions - PLLA/Coll-75/25 and PLLA/Coll-50/50 - were chosen, since it was previously shown that such materials allowed human-derived fibroblast adhesion and proliferation [17]. In order to prevent the collagen loss from the bundles, as well as to maintain the mechanical properties after ageing in PBS, in this paper a crosslinking treatment was carried out, by using the EDC/NHS reagents [42,43]. This chemical method has been largely employed in the literature to crosslink electrospun collagen scaffolds [28,44-46]. In particular, Barnes et al. have crosslinked electrospun collagen with EDC by immersion in

ethanol instead of aqueous solution during the crosslinking treatment, to better preserve the fibrous morphology [46,47]. EDC enables activation of the carboxylic acids of the aspartic and glutamic acid residues present along the chains of collagen, which subsequently react with the amine functions of lysine residues of other chains. To maximize the effectiveness of EDC, it is also necessary to introduce NHS that converts the O-acylisourea group of EDC into an NHS-activated carboxylic acid group, which is reactive towards amine groups of lysine48. At the end of the reaction, EDC is not linked between the collagen residues, but it leaves the process as a 1-ethyl-3-(3-dimethyl- aminopropyl) urea by-product. Commonly, EDC and NHS are used in water based solutions, but Barnes et al. showed that when ethanol is used the fibrous morphology is better preserved [42,46,47,49,50]. In the present work measures of weight loss demonstrated that this collagen crosslinking procedure successfully maintained the collagen component in the bundles, since uncrosslinked collagen chains are expected to quickly dissolve upon water contact. It can be noted that the crosslinking procedure is less effective on PLLA/Coll-75/25 compared to PLLA/Coll-50/50 (the former lost 30% of collagen while the latter only 15%), probably due to the increased number of PLLA chains leading to a reduced amount of collagen crosslinking sites.

In order to evaluate the 3D-structure and morphology of the produced scaffolds and to make comparison with the architecture of the native tendon fascicles, a thorough morphological analysis was performed by means of SEM and XCT [18-20,51]. These imaging techniques were also useful to assess the effect of the crosslinking treatment and of the immersion in PBS for 7 and 14 days on the morphology of the nanofibers. Interestingly, the mean diameters of the nanofibers of both blends (in the range 0.35–0.40 μm, measured by SEM) were in line with the range of the fibrils in the human tendons, such as in the Achilles [52]. The crosslinking process did not modify the average diameter and the morphology of the nanofibers. The nanofibers also remained in the same dimensional range even after 7 days in PBS, whereas a slight increase in fiber diameter was observed after 14 days in PBS.

The manufacturing process proposed in this paper enabled highly aligned electrospun nanofibers arranged in bundles with length of several centimeters to be fabricated. The versatility of the proposed fabrication workflow allows the diameter

of the bundles to be tailored to the required structure by adjusting the mat thickness and the wrapping process. Bundles of both PLLA/Coll blends were produced with a diameter in the same range of tendon fascicles, such as Achilles, reported in the literature, even after the slight collagen loss occurring during the crosslinking process that caused a slight narrowing of the bundles [18-20].

While SEM analysis allowed investigation of the morphology of the nanofibers on the outer surface of the bundles, XCT analysis was used to evaluate detailed morphology of fiber distribution within the bundles at submicron resolution. The XCT analysis confirmed that the internal morphology and alignment of the nanofibers were in agreement with those obtained through SEM on the surface of the bundles. It was found that, while the nanofibers were mainly aligned within the bundles, a fraction of nanofibers exhibited a range of alignments (Figures 4.3–4.5): this represents a desirable feature to mimic the morphology of the human tendon [18-20]. This morphology was maintained also after the crosslinking process. Producing XCT images with such voxel size is critical to minimize partial volume effects, but is very challenging. Only a few studies so far were able to produce sub-micron imaging of electrospun nanofibers. Farrugia et al. produced high-resolution tomographic images of poly(ε-caprolactone) (PCL) electrospun microfibers (mean fiber diameter 7.5 ± 1.6 μm) with a voxel size of 0.79 μm [53]. Later Bosworth et al. imaged PCL electrospun nanofibers yarns (mean diameter 0.4 μm) with a resolution of 0.61 μm [29,31]. Kogikoski et al. obtained XCT images of PCL/Polyaniline blends electrospun nanofibers (mean diameter 0.6–0.3 μm) with a voxel size of 3.37 μm [54]. Finally, Bradley et al. performed XCT on electrospun mats of poly(lactide-co-glicolide) (PLGA) microfibers (mean diameter 4.0 μm) with a voxel size of 0.13 μm [55]. However, to the best of our knowledge we were the first group to obtain high quality XCT images of electrospun PLLA/Coll nanofibers and we were able to have a complete characterization of the bundles' nanostructure. In fact, obtaining XCT images of such bundles and nanofibers is very challenging because: (i) it is very difficult to resolve the collagen due to its low radiographic density, without using contrast agents; (ii) the mean diameter of the nanofibers was close to the pixel size resolution of the scan [56].

The mechanical tests (Figure 4.6) confirmed that both blends in all the tested conditions had an initial highly compliant toe region similar to that of the natural tendon fascicles [57]. The two bundles' compositions, as-spun and after crosslinking and ageing in PBS for 7 and 14 days, showed a ductile behavior (Figure 4.6). As expected, hydration in PBS before the test increased the ductility of the bundles of both compositions, compared to dry samples [17]. The crosslinking process significantly improved the mechanical performance (especially the failure stress and work to failure) of the bundles of both compositions (Figure 4.7). In addition, crosslinking preserved the mechanical properties after ageing compared to the non-crosslinked version [17]. The ductile behavior of the hydrated bundles guarantees a safety factor in case of overload, which is an essential requirement for a strenuously loaded orthopedic device.

The mechanical tests indicate that the PLLA/Coll-75/25 bundles are superior to the PLLA/Coll-50/50 in terms of yield stress, failure stress and of Young's modulus (Figure 4.7) (all values of the bundles' mechanical properties, alongside the values for human tendon fascicles [57], are listed with mean and standard deviation in Table 4.S2). Furthermore, the failure stress of the PLLA/Coll-75/25 bundles (also after 14 days of ageing in PBS) was slightly lower, but in the same range as the fascicles of different human tendon (range: 6.8–28.1 MPa, Table 4.S2) [57]. It must be noted that while the fascicles of the natural tendon exhibits a rather sudden failure (at a higher stress than the bundles of the present study), the bundles exhibit a pronounced post-yield region. The different mechanical properties of the two tested compositions can be ascribable to the specific contribution provided by each component: after crosslinking, electrospun collagen behaves as a rigid and fragile material [46] while the PLLA component, being more ductile, provides higher elongation and plasticity. The fact that the artificial scaffold is weaker than the natural tendon is desirable in terms of patient safety: in fact, to avoid damage in the patient's repaired site in case of overload, failure should start in the implanted device, rather than in the host tissue.

The Young's modulus of both blends was slightly lower than that of the Achilles tendon fascicles (i.e. 222.8 ± 84.6 MPa (Afro-American) and 316.8 ± 110.0 (Caucasian)), but in the same range of iliopsoas tendon fascicles (i.e.

165.3 ± 67.3 MPa (Afro-American) and 63.5 ± 23.6 (Caucasian)) reported in literature [17,57]. However, this discrepancy might not be critical since these kinds of resorbable electrospun scaffolds are meant to serve as a temporary replacement and allow tenocyte proliferation while the limb is only partially loaded to prevent damage. Progressive replacement of the electrospun nanofibers with the physiological triple helix collagen expects to progressively increase the stiffness of the regenerated tendon.

Comparisons with previous studies are difficult, as no other research groups have investigated the mechanical properties of electrospun bundles of PLLA/Coll blends, apart from our previous work [17]. Among others, some works reported the mechanical properties of bundles and yarns for tendon tissue regeneration. Bosworth et al. tested nanofibrous yarns of poly(ε-capro-lactone) (PCL) finding a Young's modulus of 14.11 ± 3.76 MPa and a failure stress of 4.74 ± 1.64 MPa [31]. Pauly et al. tested bundles of aligned nanofibers of PCL with a Young's modulus of about 40 MPa and a failure stress of about 14 MPa [33]. Domingues et al. investigated the mechanical properties of aligned bundles of nanofibers, made of PCL/Chitosan/Cellulose nanocrystals, finding a Young's modulus of 540.5 ± 83.7 MPa and a failure stress of 39.3 ± 1.9 MPa [58].

Biological evaluation showed that both bundle compositions supported cell attachment and growth both crosslinked and as-spun. Crosslinking collagen via EDC has been previously shown by Haugh et al. to reduce cellular attachment when used at high concentrations (>6 mM) [59]. This was theorized to happen due to the cytotoxic effects of urea - a by-product formed by the crosslinking reaction that remained trapped within the scaffold at higher EDC concentrations, which is in contrast to the increased attachment found here. However, it should also be noted that the study by Haugh et al. used collagen-glycosaminoglycan scaffolds and the increased cellular attachment found here could be due to the retention of the Coll within the bundles due to the crosslinking, as previously shown [17,59]. Other studies have also shown that improved Coll retention in the PLLA/Coll bundles improved attachment and cytocompatibility in comparison to unmodified PLLA [60]. The improved attachment can be attributed to increased hydrophilicity of the PLLA/Coll in comparison to unmodified PLLA and to the introduction of bioactive

factors [60,61], that are maintained in the natural polymeric chains, although the triple helix collagen structure is lost after electrospinning, as extensively demonstrated in other works [46,62,63].

This study focused on the suitability of the mechanical properties, morphology and cell metabolic activity of the bundles to be used as a scaffold for tendon regeneration. With respect to our previous work [17] this study demonstrates that electrospun bundle of aligned fibers with a proper and controlled collagen content and tested under physiological conditions possess unprecedented stable mechanical and biological properties. In future it would be important to address a possible means of attachment of the scaffold at the extremities, either to the residual tendon, or to the bone insertion, or to the muscle extremity.

4.5 Conclusion

This study proposed a technique for fabricating electrospun bundles made of PLLA/Collagen blends for tendon repair. The analysis of the directionality of the fibers obtained via high-resolution x-ray computed tomography (XCT) indicated a satisfactory alignment and the scatter of the nanofibers, so as to allow mimicking the natural tendons. The mechanical properties of the bundles after crosslinking were comparable to those required to replace/regenerate tendinous tissue, and were well-preserved even after ageing in PBS. The most promising composition in terms of mechanical properties was the PLLA/Coll-75/25 blend. Finally, the crosslinked bundles supported good cell viability when seeded with fibroblasts. While this study focused on the use of PLLA/Coll electrospun scaffolds for tendon regeneration, possible future applications could include repair of the ligaments, which have similar composition and microstructural arrangement of the collagen nanofibers in the tendon.

4.6 Experimental Section

4.6.1 Materials

Acid soluble collagen type I (Coll), extracted from bovine skin (Kensey Nash Corporation d/b/a DSM Biomedical, Exton, USA) and Poly(L-lactic acid) (PLLA) (Lacea H.100-E, Mw = 8.4 × 10^4 g mol^{-1}, PDI = 1.7, Mitsui Fine Chemicals, Dusseldorf, Germany) were used. 2,2,2- Trifluoroethanol (TFE), 1,1,1,3,3,3-Hexafluoro-2-propanol (HFIP), Dichloromethane (DCM), Dimethylformamide (DMF), N-(3-Dimethylaminopropyl)-N′-ethylcarbodiimide hydrochloride (EDC) and N-Hydroxysuccinimide (NHS) (Sigma-Aldrich, Staint Louis, USA) were used as received. The following polymeric solutions were used: (i) PLLA/Coll-75/25 (w/w) prepared from a 15% (w/v) solution of PLLA and Coll dissolved in TFE:HFIP=50:50 (v/v) (1.125 g of PLLA and 0.375 g of Coll were dissolved in 10 mL); (ii) PLLA/Coll-50/50 (w/w) prepared from a 15% (w/v) solution of PLLA and Coll dissolved in TFE:HFIP=50:50 (v/v) (0.75 g of PLLA and 0.75 g of Coll were dissolved in 10 mL).

4.6.2 Electrospinning

Bundles were fabricated using a laboratory electrospinning machine (Spinbow Lab Unit, Spinbow S.r.1., Bologna, Italy), equipped with a linear sliding spinneret (carrying two syringes ejecting the same polymer solution) and a rotating drum collector (diameter = 150 mm; length = 500 mm) (Figure 4.S1). To electrospin each the solutions, a syringe pump (KD Scientific 200 series, Hillinois, USA) and two glass syringes containing the same polymer solution and connected to two stainless-steel blunt-ended needles (inner diameter = 0.51 mm) with PTFE tubes, were used. Electrospinning was performed at room temperature (RT) and relative humidity 20-30%. Both blends were electrospun in the following conditions: applied voltage = 22 kV, feed rate = 0.5 mL h^{-1}, electrospinning time = 2 hours. A high-speed rotating aluminum drum collector (peripheral speed = 22.8 m s^{-1}), positioned 200 mm away from the needle tips, was used to produce mats made of nanofibers preferentially aligned in the direction of drum rotation. The sliding spinneret with the two needles

had an excursion of 120 mm, with a sliding speed of 1200 mm min^{-1}. The mats made of aligned nanofibers were cut circumferentially into strips, and manually wrapped to produce the bundles (Figure 4.1). By fixing the time of electrospinning and the width of the strips to be wrapped, bundles of approximately 550-650 μm in diameter were obtained. Thus, the final bundles were as long as the circumference of the rotating drum collector (i.e. about 470 mm), and were made of nanofibers aligned axially (Figure 4.1B).

4.6.3 Crosslinking Treatment

Bundles of PLLA/Coll-75/25 and PLLA/Coll-50/50 were immersed for 24 hours at RT under mild agitation in a crosslinking solution of EDC and NHS 0.02 M in 95% ethanol, adapted from a previously reported procedure [64]. The specimens were then immersed in phosphate buffer saline (PBS, 0.1 M, pH = 7.4) for 30 min, thoroughly washed in distilled water for 2 hours (by changing water every 15 min) and dried over P_2O_5 under vacuum at RT.

4.6.4 Imaging and Morphological Analysis

Scanning Electron Microscopy (SEM) (Philips 515 SEM, Amsterdam, Netherlands) observations were carried out using an accelerating voltage of 15 kV, on specimens sputter-coated with gold. The distribution of nanofiber diameters was measured on the SEM images of approximately 200 nanofibers, by using the software ImageJ [65]. The two-way ANOVA followed by the Tukey post-hoc test was used to test the statistical significance of the differences between means.

High-resolution images of both compositions as-spun and immediately after crosslinking were acquired with a high-resolution x-ray computed tomography (XCT, Xradia Versa 510, ZEISS, Pleasanton, CA, USA), with two different isotropic voxel sizes. (i) Images with 1 μm voxel size were collected at rotational steps of 0.18 over 360° (scanning time: 6 h); (ii) Images with 0.4 μm voxel size were collected at rotational steps of 0.18 over 360° (scanning time: 10 h). For both voxels sizes the same settings were used: 40 kV Voltage, 3 W Power, 75.5 μA tube current. The images were reconstructed using ZEISS Scout-and-Scan

Reconstructor software and were visualizedXM3DViewer1.2.8 software. To measure the nanofiber orientation, the scans at 0.4 μm voxel size were analyzed with ImageJ: first the scans were resliced for an axial view of the nanofibers, then the Directionality plugin of ImageJ was used, which exploits the Local Gradients orientation method [65–67].

4.6.5 Instrumental Characterization

Thermogravimetric analysis (TGA) was performed (TGAQ500 analyzer, TA Instruments, New Castle, USA) from RT to 700 °C (heating rate 10 °C min^{-1}, nitrogen gas). TGA was performed on the as-spun bundles of both blends, and on pure PLLA and collagen powders. Since pure collagen shows a considerable residual weight at 700°C while PLLA residual weight is very low, it can be assumed that the weight residues of the bundles are proportional to the amount of collagen. Therefore, by comparing the residual weights at 700°C, the real composition of the bundles was determined by applying the following linear system:

$$Wt\%_{res}^{Coll} \cdot x + Wt\%_{res}^{PLLA} \cdot y = Wt\%_{res}^{Blend}$$

$$x + y = 1 \qquad (4.1)$$

Where $Wt\%_{res}^{Coll}$ is the residual weight percentage of pure collagen (26.7%); $Wt\%_{res}^{PLLA}$ is the residual weight percentage of pure PLLA (1.6%); is the residual weight percentage of PLLA/Coll bundles (7.8% for PLLA/Coll-75/25 and 14.9% for PLLA/Coll-50/50); x and y are the weight fractions of Collagen and PLLA in the bundles, respectively.

4.6.6 Collagen Loss from the Crosslinked Bundles

In order to determine collagen loss after the crosslinking treatment and after immersion in PBS for 7 and 14 days at 37°C after the crosslinking treatment, triplicate samples of as-spun bundles (about 40 mg each) were dried over P2O5 under vacuum at RT and weighed to obtain the initial mass. The specimens were crosslinked, washed and dried, as described above. The specimens were

individually immersed in 3 mL of PBS with sodium azide (Sigma-Aldrich, Saint Louis, USA) and incubated in a water bath (SW22, Julabo, Milan, Italy) at 37°C with shaking at 80 rpm. At 7 and 14 days, the specimens were recovered from the bath, gently washed with distilled water for 2 hours and a half, dried over P2O5 under vacuum and weighted. The weight loss was entirely ascribed to the dissolution of not-crosslinked collagen. This assumption is supported by the fact that PLLA mat incubated in PBS do not show any weight loss in the time range investigated (up to 14 days) [17].

The bundle composition in terms of weight content of PLLA (wt%PLLA) and of Collagen (wt%Coll) after crosslinking, immersion in PBS for 7 days and immersion in PBS for 14 days, was calculated by applying Equation 4.2 and 4.3:

$$wt\%_{PLLA} = \frac{m_{in} \cdot w_{PLLA}}{m_{fin}} \cdot 100 \quad (4.2)$$

$$wt\%_{Coll} = 100 - wt\%_{PLLA} \quad (4.3)$$

Where m_{in} is the initial dry weight, m_{fin} is the dry weight after treatment and w_{PLLA} is the initial PLLA weight fraction (i.e. w_{PLLA} = 0.75 for PLLA/Coll-75/25 and w_{PLLA} = 0.5 for PLLA/Coll- 50/50).

4.6.7 Mechanical Characterization of the Bundles

In order to evaluate the mechanical properties, also in relation to collagen crosslinking and to ageing in PBS, destructive tensile tests were performed on bundles of both blends as-spun, after crosslinking, and on the crosslinked bundles aged in PBS for 7 and 14 days. To measure the diameter of each bundle, a light optical microscope (Axioskop, ZEISS, Oberkochen, Germany) equipped with a camera (AxioCam MRc, ZEISS, Oberkochen, Germany) was used (mean and standard deviation of 10 measurements). The section was measured on dried specimens, immediately after preparation of the bundles, and also after crosslinking and immersion in PBS. The specimens were immersed in PBS for two minutes before the tensile test. The mechanical tests (5 specimens per treatment group) were carried out with a servo-hydraulic testing machine (8032, Instron, High Wycombe,

UK), with a ±1kN dynamic cell (Instron, precision class 0.5, High Wycombe, UK). Selection of the appropriate range and signal filtering allowed measuring the force with a precision of 0.02N. Dedicated capstan grips (Fig. S2) were used to limit the stress concentrations at the extremities. The gauge length was 47.42 mm (consistently with similar to the BS EN 12562:1999 and the ASTM D2256/D2256M-10(2015) Standards, this included the free length and the portion of specimen wrapped around the capstans). The test machine was operated in displacement control, with an actuator speed of 16 mm sec^{-1} (resulting in a strain rate of 33 % sec^{-1}: this is in the range of strain rates experienced by the tendon during a variety of physiological tasks [68,69]). The load-displacement curves were converted to stress-strain curves using the cross-section area measured in the dry specimens. The following indicators were extracted: yield stress (σ_Y), yield strain (e_Y), failure stress (σ_F), failure strain (e_F), Young modulus (E), work to yield (L_Y), work to failure (L_F). The significance of the effect of the crosslinking and the ageing in PBS on the two blends was assessed with the two-way ANOVA followed by the Tukey post-hoc, while the effect of the crosslinking and the ageing in PBS on the same composition was assessed with one-way ANOVA, followed by the Tukey post-hoc.

4.6.8 Biological Evaluation

Non-tumoral human fibroblasts (NTFs), obtained from waste tissue collected under ethical approval 09/H1308/66 from the NRES Committee Yorkshire and The Humber, Sheffield (Informed consent was provided for the collection and use of surgical waste tissue for research), were cultured in basal medium (BM) consisting of α-MEM culture medium (Lonza®, Slough, UK), 10% foetal bovine serum (FBS, Labtech, Heathfield, UK), 2 mM L-glutamine (Sigma Aldrich, Saint Louis, USA) and 100 mg mL^{-1} penicillin/streptomycin (Sigma Aldrich, Saint Louis, UK). NTFs were cultured in 75 cm^2 tissue-culture flasks at 37 °C in 5% CO_2 in a humidified atmosphere with media changes every 2–3 days. Cells were used between passage 4 and 6. The electrospun bundles were cut to 1 cm in length and sterilized by soaking in 70 vol% ethanol for 1 h before being washed 3 times in PBS (Sigma Aldrich, Saint Louis, USA). The bundles were seeded with 50,000 cells at a density

of 1,000,000 cells mL^{-1} in a 24 well plate. The cells were left for 45 minutes to attach, after which 1 mL of BM was added to each well to submerge the bundles. Resazurin reduction (RR) assay was used to measure the metabolic activity of the cells attached to the bundles. A RR was performed at 4 time points (day 1, 7, 14 and 21). Before each RR the bundles were transferred into a new 24 well plate to ensure the metabolic activity of only the cells attached to the bundles was measured. 1 mL of 0.1 mM resazurin salt solution in BM was added to each well and incubated in the dark for 4 hours at 37 °C. During this period, the non-fluorescent blue resazurin solution is reduced by the cells to resorufin, a highly fluorescent pink solution. 200 µL of the reduced solution was transferred to a 96 well plate and measured using a spectrofluorometer (FLX800, BIO-TEK Instruments Inc., Winooski, USA) at an excitation wavelength of 540 nm and an emission wavelength of 630 nm. The bundles were washed twice with PBS before fresh BM was added.

To assess the distribution of cells on the bundles, the samples were stained for cell nuclei on day 7 of culture. The bundles were fixed in 3.7% formaldehyde (Sigma Aldrich, Saint Louis, USA) for 15 minutes before permeabilization with 0.1% v/v Triton X-100 (Sigma Aldrich, Saint Louis, USA) in PBS for 10 minutes. 5 uM phalloidin-TRITC (Sigma Aldrich, Saint Louis, USA) in PBS was applied for 30 minutes to stain actin followed by 3 PBS washes. 1 µg/mL 4′-6-diamidino-2-phenylindole (DAPI, Sigma Aldrich, Saint Louis, USA) was applied for 15 minutes to stain the nuclei. The samples were visualized with a microscope (Eclipse Ti, Nikon, Tokyo, Japan) equipped with a camera (Intensilight C-HGFI, Nikon, Tokyo, Japan). Cell metabolic activity was compared using a two-way analysis of variance (ANOVA) followed by the Tukey post-hoc test.

4.7 Supporting Informations

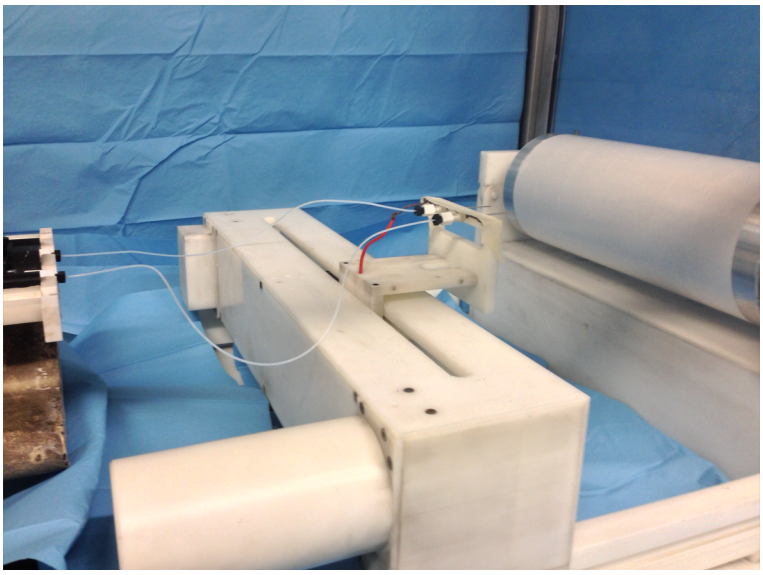

Figure 4.S1. Electrospinning setup. The pump-driven syringes are visible on the left. The two needles were mounted on a motorized sliding spinneret (at the center of the picture) and were connected to a positive high voltage. The high-speed rotating drum collector (visible on the right) was connected to the ground.

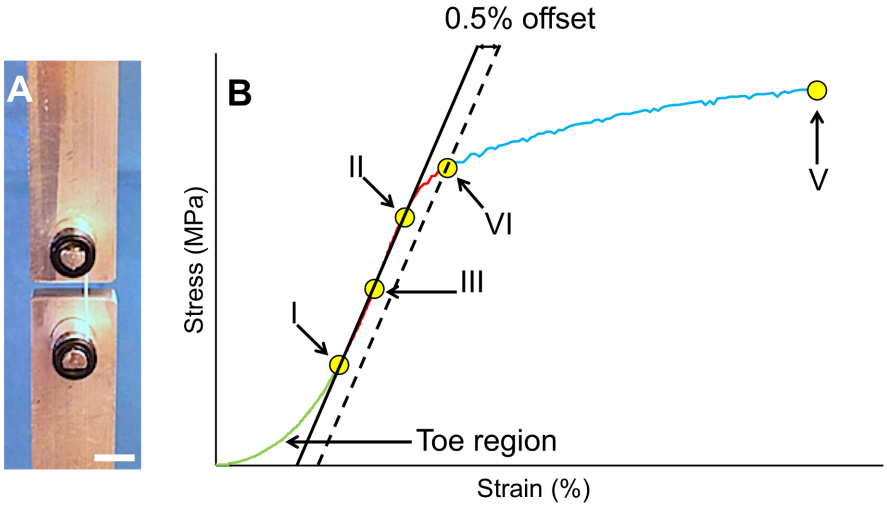

Figure 4.S2. Capstan grips designed to perform the tensile test on the bundles (A, scale bar = 10 mm). Typical stress-strain plot (B): the initial toe region was disregarded; the failure stress (V) was identified as the highest stress in the entire curve; the starting point of the linear region (I) was univocally identified as 20% of failure stress; an initial guess for the yield strain was visually identified (III); the initial linear regression (solid line) was applied to the first 50% of the linear region, between points I and II (which was half-way between I and III); a second line parallel to the initial regression was drawn, with an offset of 0.5% strain (dashed line); the limit of proportionality was defined with the 0.5%-strain offset criterion as the intersection (IV) between the latter line and

the stress-strain curve; the Young modulus was calculated as the slope of a new regression line between I and IV. The work to yield and to failure were calculated as the integrals under the curves (with the method of trapezoids).

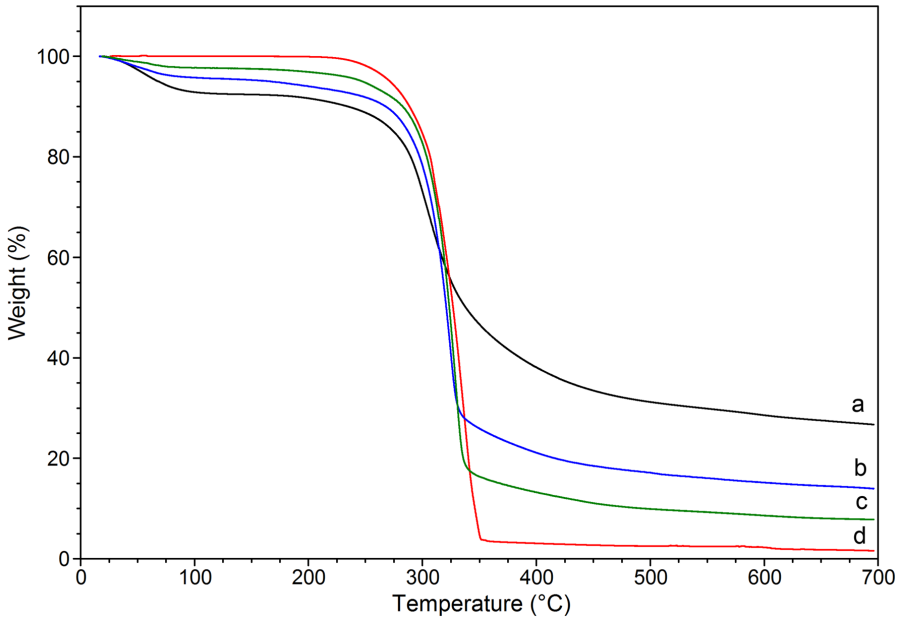

Figure 4.S3. TGA analysis of collagen powder (a), of the as-spun bundles of PLLA/Coll-50/50 (b), and PLLA/Coll-75/25 (c) and of PLLA pellets (d).

Table 4.S1. Comparison of mechanical properties of PLLA/Coll-75/25 and PLLA/Coll-50/50 exposed to the same treatment (as-spun, crosslinking) and ageing in PBS for the same periods, using two way ANOVA. The mean and standard deviation are plotted for the two compositions, together with statistical significance of post-hoc comparisons (Tukey multiple comparisons, * P≤ 0.05, ** P≤ 0.01, *** P≤ 0.001, **** P≤ 0.0001, ns = not significant).

	Yield stress	Failure stress	Yield strain	Failure strain	Young modulus	Work to yield	Work to failure
As-spun	****	**	ns	**	***	**	ns
Crosslinked	**	**	ns	ns	**	ns	ns
Crosslinked + 7d PBS	***	**	ns	ns	***	ns	ns
Crosslinked + 14d PBS	***	*	ns	ns	***	ns	ns

Table 4.S2. Mechanical properties of PLLA/Coll-75/25 and PLLA/Coll-50/50 exposed to the same treatment (as-spun, crosslinking) and ageing in PBS for the same periods, and the mechanical properties of human tendon fascicles reported by Hanson et al. (i.e. AA=Afro-American man; CC=Caucasian man) [57]. The mean and standard deviation are plotted for each value.

PLLA/Coll-75/25	**Yield stress (MPa)**	**Failure stress (MPa)**	**Yield strain (%)**	**Failure strain (%)**	**Young modulus (MPa)**	**Work to yield (J/mm^3)**	**Work to failure (J/mm^3)**
As-spun	7.6±0.5	11.3±0.6	10.5±1.8	29.6±2.3	91.1±5.9	0.038±0.0092	0.225±0.021
Crosslinked	7.6±1.5	18.8±3.8	11.2±1.6	54.6±5.5	103.2±16.8	0.030±0.010	0.647±0.185
Crosslinked+7d PBS	6.6±1.0	12.7±0.8	9.9±1.3	44.6±4.8	92.0±5.9	0.025±0.0081	0.377±0.044
Crosslinked+14d PBS	6.2±0.4	10.2±1.1	11.5±2.2	32.0±4.9	89.9±13.3	0.023±0.0036	0.213±0.045
PLLA/Coll-50/50							
As-spun	2.9±0.4	6.0±0.6	9.8±1.9	50.1±1.7	40.4±15.6	0.015±0.0072	0.208±0.022
Crosslinked	4.8±1.2	14.2±2.4	9.1±2.2	63.8±12.5	64.7±8.1	0.020±0.011	0.588±0.195
Crosslinked+7d PBS	2.8±0.6	8.1±0.9	8.8±3.4	46.7±5.4	45.0±9.2	0.010±0.0055	0.231±0.038
Crosslinked+14d PBS	3.0±0.6	6.6±1.1	8.9±2.5	34.4±12.8	42.1±18.7	0.011±0.0049	0.137±0.052
Human collagen fascicles [57]							
Achilles' tendon (AA)	-	21.9±9.9	-	16.3±3.5	222.8±84.6	-	-
Achilles' tendon (CC)	-	28.1±9.8	-	13.8±4.4	316.8±110.0	-	-
Iliopsoas tendon (AA)	-	22.5±7.3	-	19.7±5.2	165.3±67.3	-	-
Iliopsoas tendon (CC)	-	6.8±2.1	-	18.3±3.5	63.5±23.6	-	-

4.8 References

[1] Cheng X, Tsao C, Sylvia V L, Cornet D, Nicolella D P, Bredbenner T L and Christy R J 2014 Platelet-derived growth-factor-releasing aligned collagen-nanoparticle fibers promote the proliferation and tenogenic differentiation of adipose-derived stem cells Acta Biomater. 10 1360–9

[2] Verdiyeva G, Koshy K, Glibbery N, Mann H and Seifalian A M 2015 Tendon reconstruction with tissue engineering approach - A review J. Biomed. Nanotechnol. 11 1495–523

[3] Butler D L, Juncosa-Melvin N, Boivin G P, Galloway M T, Shearn J T, Gooch C and Awad H 2008 Functional tissue engineering for tendon repair: A multidisciplinary strategy using mesenchymal stem cells, bioscaffolds, and mechanical stimulation J. Orthop. Res. 26 1–9

[4] Noyes F R, Mooar P A, Matthews D S and Butler D L 1983 The symptomatic anterior cruciate-deficient knee. Part I J. Bone Jt. Surg. 65 154–62

[5] Roos H, Ornell M, Gärdsell P, Lohmander Ls and Lindstrand A 1995 Soccer after anterior cruciate ligament injury— an incompatible combination? A national survey of incidence and risk factors and a 7-year follow-up of 310 players Acta Orthop. Scand. 66 107–12

[6] Wu Y, Lin L, Li H, Zhao Y, Liu L, Jia Z, Wang D, He Q and Ruan D 2016 Is surgical intervention more effective than non-surgical treatment for acute Achilles tendon rupture? A systematic review of overlapping meta-analyses Int. J. Surg. 36 305–11

[7] James S L, Bates B T, Osternig L R and Oregon E 1978 Injuries to runners Am. J. Sports Med. 6 40–50

[8] Chesney A, Chauhan A, Kattan A, Farrokhyar F and Thoma A 2011 Systematic Review of Flexor Tendon Rehabilitation Protocols in Zone II of the Hand Plast. Reconstr. Surg. 127 1583–92

[9] Dy C J, Daluiski A, Do H, Hernandez-Soria A, Marx R and Lyman S 2012 The Epidemiology of Reoperation After Flexor Tendon Repair J. Hand Surg. Am. 37A 919–24

[10] Lomas A J, Ryan C N M, Sorushanova A, Shologu N, Sideri A I, Tsioli V, Fthenakis G C, Tzora A, Skoufos I, Quinlan L R, O'Laighin G, Mullen A M, Kelly J L, Kearns S, Biggs M, Pandit A and Zeugolis D I 2015 The past, present and future in scaffold-based tendon treatments Adv. Drug Deliv. Rev. 84 257–77

[11] Sharma P and Maffulli N 2005 Tendon Injury and Tendinopathy: Healing and Repair J. Bone Jt. Surg. 87 187

[12] Longo U G, Lamberti A, Maffulli N and Denaro V 2010 Tendon augmentation grafts: A systematic review Br. Med. Bull. 94 165–88

[13] Bader F F and Curtin J W 1968 A successful silicone tendon prosthesis Arch. Surg. 97 406–11

[14] Mahoney J, Farkas L and Lindsay W 1976 Quality of tendon graft healing in silastic pseudosheaths: breaking-strength studies Surg. Forum 27 572–3

[15] Beris A E, Darlis N A, Korompilias A V., Vekris M D, Mitsionis G I and Soucacos P N 2003 Two-stage flexor tendon reconstruction in zone II using a silicone rod and a pedicled intrasynovial graft J. Hand Surg. Am. 28 652–60

[16] Hampson K, Forsyth N R, El Haj A and Maffulli N 2008 Tendon Tissue Engineering Topics in Tissue Engineering vol 4, ed N Ashammakhi, R Reis and F Chiellini pp 1–21

[17] Sensini A, Gualandi C, Cristofolini L, Tozzi G, Dicarlo M, Teti G, Belmonte-Mattioli M and Focarete M L 2017 Biofabrication of bundles of poly (lactic acid) -collagen blends mimicking the fascicles of the human Achille tendon Biofabrication 9 1–13

[18] Kastelic J, Galeski A and Baer E 1978 The Multicomposite Structure of Tendon Connect. Tissue Res. 6 11–23

[19] Kannus P 2000 Structure of the tendon connective tissue Sca. J. Me. Sci. Spor. 10 312- 20

[20] Goh K L, Listrat A and Béchet D 2014 Hierarchical mechanics of connective tissues: Integrating insights from nano to macroscopic studies J. Biomed. Nanotechnol. 10 2464–507

[21] Mouthuy P-A, Zargar N, Hakimi O, Lostis E and Carr A 2015 Fabrication of continuous electrospun filaments with potential for use as medical fibres. Biofabrication 7 25006

[22] Ali U, Zhou Y, Wang X and Lin T 2011 Electrospinning of Continuous Nanofiber Bundles and Twisted Nanofiber Yarns Nanofibers - Prod. Prop. Funct. Appl. 153–74

[23] Young M 2012 Stem cell applications in tendon disorders: A clinical perspective Stem Cells Int. 2012 1–10

[24] Liu W, Chen B, Deng D, Xu F, Cui L and Cao Y 2006 Repair of tendon defect with dermal fibroblast engineered tendon in a porcine model. Tissue Eng. 12 775–88

[25] Yang C, Deng G, Chen W, Ye X and Mo X 2014 A novel electrospun-aligned nanoyarn-reinforced nanofibrous scaffold for tendon tissue engineering, Coll Surf B Biointerfaces 122 270–6

[26] Deepthi S, Nivedhitha Sundaram M, Deepti Kadavan J and Jayakumar R 2016 Layered chitosan-collagen hydrogel/aligned PLLA nanofiber construct for flexor tendon regeneration Carbohydr. Polym. 153 492–500

[27] O'Connor R A and McGuinness G B 2016 Electrospun nanofibre bundles and yarns for tissue engineering applications: A review Proc. Inst. Mech. Eng. Part H J. Eng. Med. 230 987–98

[28] Sun B, Jiang X-J, Zhang S, Zhang J-C, Li Y-F, You Q-Z and Long Y-Z 2015 Electrospun anisotropic architectures and porous structures for tissue engineering J. Mater. Chem. B 3 5389–410

[29] Bosworth L A, Rathbone S R, Bradley R S and Cartmell S H 2014 Dynamic loading of electrospun yarns guides mesenchymal stem cells towards a tendon lineage J. Mech. Behav. Biomed. Mater. 39 175–83

[30] Bosworth L A 2014 Travelling along the Clinical Roadmap: Developing Electrospun Scaffolds for Tendon Repair Conf. Pap. Sci. 2014 1–6

[31] Bosworth L A, Alam N, Wong J K and Downes S 2013 Investigation of 2D and 3D electrospun scaffolds intended for tendon repair J. Mater. Sci. Mater. Med. 24 1605–14

[32] Zhang C, Yuan H, Liu H, Chen X, Lu P, Zhu T, Yang L, Yin Z, Heng B C, Zhang Y and Ouyang H 2015 Well-aligned chitosan-based ultrafine fibers committed teno-lineage differentiation of human induced pluripotent stem cells for Achilles tendon regeneration Biomaterials 53 716–30

[33] Pauly H M, Kelly D J, Popat K C, Trujillo N A, Dunne N J, McCarthy H O and Haut Donahue T L 2016 Mechanical properties and cellular response of novel electrospun nanofibers for ligament tissue engineering: Effects of orientation and geometry J. Mech. Behav. Biomed. Mater. 61 258–70

[34] Bhaskar P, Bosworth L A, Wong R, O'brien M A, Kriel H, Smit E, McGrouther D A, Wong J K and Cartmell S H 2017 Cell response to sterilized electrospun poly(Ɛ-caprolactone) scaffolds to aid tendon regeneration in vivo J. Biomed. Mater. Res. - Part A 105 389–97

[35] Xu Y, Wu J,Wang H, Li H, Di N, Song L, Li S, Li D, Xiang Y,Liu W, Mo X and Zhou Q 2013 Fabrication of Electrospun Poly(L-Lactide-co-ε-Caprolactone)/Collagen Nanoyarn Network as a Novel, Three-Dimensional, Macroporous, Aligned Scaffold for Tendon Tissue Engineering Tissue Eng. Part C Methods 19 925–36

[36] Schofer M D, Boudriot U, Leifeld I, Sütterlin R I, Rudisile M, Wendorff J H, Greiner A, Paletta J R J and Fuchs-Winkelmann S 2009 Characterization of a PLLA-Collagen I Blend Nanofiber Scaffold with Respect to Growth and Osteogenic Differentiation of Human Mesenchymal Stem Cells Sci. World J. 9 118–29

[37] Schofer M D, Veltrum A, Theisen C, Chen F, Agarwal S, Fuchs-Winkelmann S and Paletta J R J 2012 Functionalisation of PLLA nanofiber scaffolds using a possible cooperative effect between collagen type I and BMP-2: Impact on colonization and bone formation in vivo J. Mater. Sci. Mater. Med. 23 2227–33

[38] Theisen C, Fuchs-Winkelmann S, Knappstein K, Efe T, Schmitt J, Paletta J R J and Schofer M D 2010 Influence of nanofibers on growth and gene expression of human tendon derived fibroblast. Biomed. Eng. Online 9 9

[39] Gonçalves F, Bentini R, Burrows M C, Carreira A C O, Kossugue P M, Sogayar M C and Catalani L H 2015 Hybrid Membranes of PLLA/Collagen for Bone Tissue Engineering: A Comparative Study of Scaffold Production Techniques for Optimal Mechanical Properties and Osteoinduction Ability Materials (Basel). 8 408–23

[40] Tu H, Bao M, Li Q, Li B, Yuan H and Zhang Y 2013 Aligned core–shell structured ultrafine composite fibers of PLLA–collagen for tendon scaffolding J. Control. Release 172 e128

[41] Gualandi C, Govoni M, Foroni L, Valente S, Bianchi M, Giordano E, Pasquinelli G, Biscarini F and Focarete M L 2012 Ethanol disinfection affects physical properties and cell response of electrospun poly(l-lactic acid) scaffolds Eur. Polym. J. 48 2008–18

[42] Torres-Giner S, Gimeno-Alcañiz J V., Ocio M J and Lagaron J M 2009 Comparative performance of electrospun collagen nanofibers cross-linked by means of different methods ACS Appl. Mater. Interfaces 1 218–23

[43] Sinz A 2006 Chemical cross-linking and mass spectrometry to map three-dimensional protein structures and protein-protein interactions Mass Spectrom. Rev. 25 663–82

[44] Matthews J A, Wnek G E, Simpson D G and Bowlin G L 2002 Electrospinning of core-shell collagen nanofibers Biomacromolecules 3 232–8

[45] Casper C L, Yang W, Farach-Carson M C and Rabolt J F 2007 Coating electrospun collagen and gelatin fibers with perlecan domain I for increased growth factor binding Biomacromolecules 8 1116–23

[46] Fiorani A, Gualandi C, Panseri S, Montesi M, Marcacci M, Focarete M L and Bigi A 2014 Comparative performance of collagen nanofibers electrospun from different solvents and stabilized by different crosslinkers J. Mater. Sci. Mater. Med. 25 2313–21

[47] Barnes C P, Pemble C W, Brand D D, Simpson D G and Bowlin G L 2007 Cross-Linking Electrospun Type II Collagen Tissue Engineering Scaffolds with Carbodiimide in Ethanol Tissue Eng. 13 1593–605

[48] Grabarek Z and Gergely J 1990 Zero-length crosslinking procedure with the use of active esters Anal. Biochem. 185 131–5

[49] Buttafoco L, Kolkman N G, Engbers-Buijtenhuijs P, Poot A A, Dijkstra P J, Vermes I and Feijen J 2006 Electrospinning of collagen and elastin for tissue engineering applications Biomaterials 27 724–34

[50] Meng L, Arnoult O, Smith M and Wnek G E 2012 Electrospinning of in situ crosslinked collagen nanofibers J. Mater. Chem. 22 19412–7

[51] Radaelli F, D'Alfonso L, Collini M, Mingozzi F, Marongiu L, Granucci F, Zanoni I, Chirico G and Sironi L 2017 μMAPPS: a novel phasor approach to second harmonic analysis for in vitro-in vivo investigation of collagen microstructure Sci. Rep. 7 17468

[52] Pingel J, Lu Y, Starborg T, Fredberg U, Langberg H, Nedergaard A, Weis M, Eyre D, Kjaer M and Kadler K E 2014 3-D ultrastructure and collagen composition of healthy and overloaded human tendon: Evidence of tenocyte and matrix buckling J. Anat. 224 548–55

[53] Farrugia B L, Brown T D, Upton Z, Hutmacher D W, Dalton P D and Dargaville T R 2013 Dermal fibroblast infiltration of poly(ε-caprolactone) scaffolds fabricated by melt electrospinning in a direct writing mode Biofabrication 5 025001

[54] Kogikoski S, Liberato M S, Factori I M, da Silva E R, Oliveira C L P, Ando R A and Alves W A 2017 Polycaprolactone–Polyaniline Blend: Effects of the Addition of Cysteine on the Structural and Molecular Properties J. Phys. Chem. C 121 863–77

[55] Bradley R S, Robinson I K and Yusuf M 2017 3D X-Ray Nanotomography of Cells Grown on Electrospun Scaffolds Macromol. Biosci. 17 1–8

[56] Zidek J, Vojtova L, Abdel-Mohsen A M, Chmelik J, Zikmund T, Brtnikova J, Jakubicek R, Zubal L, Jan J and Kaiser J 2016 Accurate micro-computed tomography imaging of pore spaces in collagen-based scaffold J. Mater. Sci. Mater. Med. 27 1–18

[57] Hanson P, Aagaard P and Magnusson S P 2012 Biomechanical properties of isolated fascicles of the Iliopsoas and Achilles tendons in African American and Caucasian men Ann. Anat. 194 457–60

[58] Domingues R M A, Chiera S, Gershovich P, Motta A, Reis R L and Gomes M E 2016 Enhancing the Biomechanical Performance of Anisotropic Nanofibrous Scaffolds in Tendon Tissue Engineering: Reinforcement with Cellulose Nanocrystals Adv. Healthc. Mater. 5 1364–75

[59] Haugh M G, Murphy C M, McKiernan R C, Altenbuchner C and O'Brien F J 2011 Crosslinking and Mechanical Properties Significantly Influence Cell Attachment, Proliferation, and Migration Within Collagen Glycosaminoglycan Scaffolds Tissue Eng. Part A 17 1201–8

[60] Ma Z, Gao C, Gong Y, Ji J and Shen J 2002 Immobilization of natural macromolecules on poly-L-lactic acid membrane surface in order to improve its cytocompatibility J. Biomed. Mater. Res. 63 838–47

[61] Van Wachem P B, Beugeling T, Feijen J, Bantjes A, Detmers J P and Van Aken W G 1985 Interaction of Cultured Human-Endothelial Cells With Polymeric Surfaces of Different Wettabilities Biomaterials 6 403–8

[62] Yang L, Fitié C F C, van der Werf K O, Bennink M L, Dijkstra P J and Feijen J 2008 Mechanical properties of single electrospun collagen type I fibers Biomaterials 29 955–62

[63] Bürck J, Heissler S, Geckle U, Ardakani M F, Schneider R, Ulrich A S and Kazanci M 2013 Resemblance of electrospun collagen nanofibers to their native structure Langmuir 29 1562–72

[64] Kim H W, Song J H and Kim H E 2005 Nanofiber generation of gelatin-hydroxyapatite biomimetics for guided tissue regeneration Adv. Funct. Mater. 15 1988–94

[65] Schneider C A, Rasband W S and Eliceiri K W 2012 NIH Image to ImageJ: 25 years of image analysis Nat. Methods 9 671–5

[66] Liu Z 1991 Scale space approach to directional analysis of images Appl. Opt. 30 1369–73

[67] Schindelin J, Arganda-Carreras I, Frise E, Kaynig V, Longair M, Pietzsch T, Preibisch S, Rueden C, Saalfeld S, Schmid B, Tinevez JY, White D J, Hartenstein V, Eliceiri K, Tomancak P and Cardona A 2012 Fiji: an open-source platform for biological-image analysis. Nat. Meth. 9 676–82

[68] Thermann H, Frerichs O, Biewener A, Krettek C and Schandelmaier P 1995 Biomechanical studies of human Achilles tendon rupture. Unfallchirurg 98 570–5

[69] Lyght M, Nockerts M, Kernozek T W and Ragan R 2016 Effects of foot strike and step frequency on Achilles tendon stress during running J. Appl. Biomech. 32 365–72

Chapter 5: High-resolution x-ray tomographic morphological characterisation of electrospun nanofibrous bundles for tendon and ligament regeneration and replacement

Alberto Sensini[1], Luca Cristofolini[1, 2], Maria Letizia Focarete[2, 3], Juri Belcari[1], Andrea Zucchelli[1], Alexander P. Kao[4], Gianluca Tozzi[4]

1 Department of Industrial Engineering, Alma Mater Studiorum – Università di Bologna, Bologna, Italy

2 Health Sciences and Technologies – Interdepartmental Center for Industrial Research (HST-ICIR), Alma Mater Studiorum – Università di Bologna, Ozzano dell'Emilia, Bologna, Italy

3 Department of Chemistry 'G. Ciamician' and National Consortium of Materials Science and Technology (INSTM, Bologna RU), Alma Mater Studiorum – Università di Bologna, Bologna, Italy

4 Zeiss Global Centre, School of Engineering, University of Portsmouth, Portsmouth PO1 3DJ, U.K.

Keywords: Electrospinning; Nanofibres; Tendon and Ligament Repair and Replacement, Tissue Engineering, X-Ray Tomography.

The candidate was the main investigator of the study. This work was published on Journal of Microscopy 2018, 272(3), pp. 196-206. Reproduced with permission.

Published in: Journal of Microscopy 25 May 2018

5.1 Summary

Repair of ligaments and tendons requires scaffolds mimicking the spatial organisation of collagen in the natural tissue. Electrospinning is a promising technique to produce nanofibres of both resorbable and biostable polymers with desired structural and morphological features. The aim of this study was to perform high-resolution x-ray tomography (XCT) scans of bundles of Nylon6.6, pure PLLA and PLLA-Collagen blends, where the nanofibres were meant to have a predominant direction. Characterisation was carried out via a dedicated methodology to firmly hold the specimen during the scan and a workflow to quantify the directionality of the nanofibres in the bundle. XCT scans with 0.4 and 1.0 μm voxel size were successfully collected for all bundle compositions. Better image quality was achieved for those bundles formed by thicker nanofibres (i.e. 0.59 μm for pure PLLA), whereas partial volume effect was more pronounced for thinner nanofibres (i.e. 0.26 μm for Nylon6.6). As expected, the nanofibres had a predominant orientation along the axis of the bundles (more than 20% of the nanofibres within 3° and more than 60% within 18° from the bundle axis), with a Gaussian-like dispersion in the other directions. The directionality assessment was validated by comparison against a similar analysis performed on SEM images: the XCT analysis overestimated the amount of nanofibres very close to the bundle axis, especially for the materials with thinnest nanofibres, but adequately identified the amount of nanofibres within 12°.

5.2 Introduction

Injuries of tendons and ligaments are still an unsolved clinical problem, and surgical treatments are far from satisfactory [1]. Tendon and ligaments such as the rotator cuff, the anterior cruciate ligament and the Achilles tendon are among the most commonly injured tissues in relation to both sporting activities and degenerative process associated with chronic inflammation [2–5]. The repair of these tissues is particularly difficult since their complex hierarchical structure, composed of predominantly aligned collagen fibers at different levels of aggregation [6–8], is difficult to replicate. Another critical aspect is given by the difficulty in restoring

the natural mechanical properties, which are intrinsically non-linear [1,8] after an injury. Among all the strategies to manage these kind of injuries tissue engineering is very promising, as it allows regeneration of the native tissue [1]. Thanks to its capability to produce nanofibers from polymeric solutions of both resorbable and biostable materials, electrospinning, is one of the most promising technologies in the field of regenerative medicine [9]. In fact, electrospinning technology allows to fabricate scaffolds that reproduce the structure of collagen fibrils [10]. In order to increase the mechanical properties of the nanofibrous mats, 3D scaffolds of both aligned and twisted nanofibers (called respectively bundles and yarns) were proposed [11]. In particular the multiscale morphology of the bundles is also suitable to mimic the multiscale morphology of tendon and ligament fascicles [11]. Generally, the morphological investigation of electrospun mats, bundles and yarns is performed using scanning electron microscopy (SEM) [10,11]. This characterization technique, however, only produces information related to the morphology of the surface, and does not allow examining the internal volume of the scaffolds. To overcome this limitation, x-ray computed tomography was employed to study electrospun polymeric fibers. Micro–computed tomography (micro-CT) is available from the late Eighties with a resolution down to few micrometers [12,13]. More recently, high-resolution x-ray tomography systems with a sub-micrometer resolution have become available, and are referred to as XCT in this paper. However, XCT imaging of electrospun fibers poses a number of technical issues: (i) the low attenuation of the polymeric fibers; (ii) the difficulty in avoiding micro-movements of the specimens (which are highly deformable) during imaging, which would produce artifacts; and (iii) the difficulty to conjugate nanometric dimension of the fibers and high-resolution in terms of voxel size of the scans. For these reasons, only few studies employed high-resolution XCT imaging of electrospun nanofibers, mostly referring to random nano/microfibrous electrospun mats. [14] produced tomographic images with a voxel size of 0.79 micrometers of a poly(ε-caprolactone) electrospun scaffold made of random microfibers with a mean diameter of 7 micrometers, estimating the porosity of the scaffolds. The composition of the scaffolds and the micrometric diameter of the fibers allowed to clearly distinguish the fibers' contours. [15] used tomographic

images with a voxel size of 3.37 micrometers to visualize mats of random nanofibers (mean diameters 0.6-0.3 micrometers) of poly(ε)-caprolactone (PCL) with polyaniline (PANI) doped with the amino acid N-acetyl-L-cysteine (NAC) blends. Also in that work the porosity was investigated. However, as the voxel size exceeded the fibers diameter visualization of the individual fibers was not possible, but just an overview of the density of the scaffolds was showed. [16] acquired tomographic images with sub- micrometer resolution (0.13 micrometers of voxel size) to investigate the cells' infiltration on electrospun microfibrous (mean fiber diameters 4 micrometers) mats of poly(lactide-co-glycolide) (PLGA). Thanks to the segmentation and the post processing methods, but also to the voxel size being one order of magnitude lower than

the diameters of the fibers, the fibers' contours and the cells were highly defined. However, due to the small voxel size selected, just a short portion of the samples was scanned.

Moving from mats of electrospun fibers to more complex configurations, such as bundles or yarns, the difficulties related to centring the specimen in the scanner x-ray microscope, and to micro-movements during the scans increase dramatically. Just two works were presented in the literature about tomographic scans on electrospun bundles and yarns for tendon and ligament regeneration. [17,18] showed tomographic images, with a voxel size of 0.61 micrometers, of electrospun nanofibrous yarns of PCL (mean fiber diameters 0.4 micrometers) as-spun and after cell culture. Their tomograms allowed showing the bundles surface and the regenerated tissue on their surfaces. However the fibers' contours were not clearly distinguishable, due to a significant partial volume effect. Very recently, tomographic scans with a resolution of 0.33 micrometers were produced using synchrotron x-ray phase contrast imaging of mats of biodegradable polyester nanofibers with diameters between 1.9 and 3.7 micrometers [19].

One limitation of most of the works mentioned above is that the electrospun samples (either mats, or yarns or bundles) were placed inside a plastic tube for the scans to avoid micro-movements due to the flexibility of the scaffolds. The outer diameter of the tube forces to enlarge the volume of interest, thus reducing the resolution of the scan. Furthermore, the tube adds a shielding effect to the

electrospun samples: even if the tube is made of a similar material, it adds significant absorption because its walls are much thicker, and because the tube material does not have significant porosity. This can result in a loss of image quality. Recently, [20] investigated electrospun bundles of aligned nanofibers of PLLA and collagen blends (mean fiber diameters of 0.3 micrometers), including a XCT feasibility study with a voxel size of 0.4 micrometers. In that study, the individual fibers were well-defined, and no artefacts due to micro-movements were observed.

The aims of the present study were: 1) to acquire high-resolution x-ray tomography scans of electrospun nanofibrous bundles made of pure PLLA, Nylon6.6 and PLLA/Coll blends in different percentages; and 2) to define a post processing workflow on the XCT scans to evaluate the alignment of the nanofibers in all the bundles' volume. In order to validate the alignment based on XCT, a similar investigation was performed on scanning electron microscopy (SEM) images.

5.3 Materials and Methods

5.3.1 Electrospun bundles preparation

Polymeric solutions were obtained using the reported materials: acid soluble collagen type I (Coll) from bovine skin kindly provided by Kensey Nash Corporation d/ b/a DSM Biomedical (Exton, USA); Poly-L-lactic acid (PLLA) (Lacea H.100-E, Mw = 8.4 × 104 g mol^{-1}, PDI = 1.7) was purchased from Mitsui Fine Chemicals (Dusseldorf, Germany); Nylon6.6 kindly provided by DuPont (Wilmington, USA); trifluoroacetic acid (TFA) was purchased by Carlo Erba (Milan, Italy), 2,2,2-trifluoroethanol (TFE), 1,1,1,3,3,3-hexafluoro-2-propanol (HFIP), dichloromethane (DCM), dimethylformamide (DMF), acetone (AC), N-(3-Dimethylaminopropyl)-N′-ethylcarbodiimide hydrochloride (EDC) and N-Hydroxysuccinimide (NHS) were purchased by Sigma-Aldrich (Saint Louis, USA) and used as received. The PLLA samples were produced from PLLA dissolved in a solution of DCM and DMF. The PLLA/Coll-75/25 and PLLA/Coll-50/50 blends were dissolved in a solution of TFE and HFIP. The Nylon6.6 was dissolved in a

solution of TFA and AC. For more details, the reader is referred to our previous work [20].

A laboratory electrospinning machine (Spinbow Lab Unit, Spinbow S.r.1., Bologna, Italy), equipped with a linear sliding spinneret (two syringes for PLLA and PLLA/Coll blends; four syringes for Nylon6.6) and a high-speed rotating drum collector (diameter = 150 mm; length = 500 mm; rotational speed = 2900 rpm) was used to produce mats of aligned nanofibers as shown in Figure 5.1(A). To electrospin the solutions a syringe pump (KD Scientific 200 series, Holliston, USA) and glass syringes connected to stainless steel blunt-ended needles with Teflon tubes were used. Electrospinning was performed at room temperature and relative humidity 20-30%. The pure PLLA, PLLA/Coll-75/25 and PLLA/Coll-50/50 blends were electrospun with the parameters previously reported [20]. Nylon6.6 was electrospun with 20 kV voltage, 0.5 mL/hour flow rate per syringe and 160 mm needle-collector distance. After the spinning sessions, the mats of electrospun aligned nanofibers were cut in strips and manually wrapped to obtain bundles with mean diameters of 550-650 micrometers as shown in Figure 5.1(B) – (C) – (D). This diameter is in the same range as tendon and ligament fascicles [6–8]. The bundles of PLLA/Coll-75/25 and PLLA/Coll-50/50 were crosslinked by immersion for 24 hours at room temperature in a crosslinking solution of EDC and NHS 0.02 M in ethanol and distilled water (adapted from [21]).

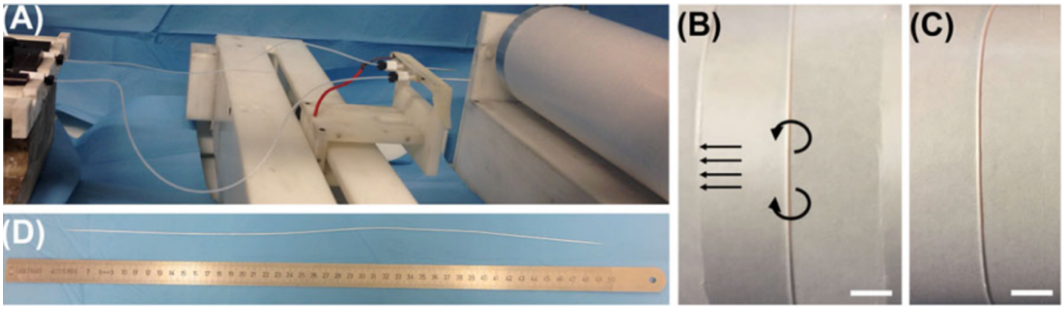

Fig. 5.1 (A) Electrospinning machine setup. (B) Image of an electrospun mat during the procedure of wrapping on the drum (scale bar = 20 mm). (C) Image of a final bundle wrapped on the drum (scale bar = 20 mm). (D) Overview of a bundle.

5.3.2 XCT Imaging

The three-dimensional high-resolution scans were acquired using a XCT (Versa 510, ZEISS, Pleasanton, CA, USA), with two different isotropic voxel sizes for the reconstructed images. XCT scans of one specimen for each composition (Nylon6.6, pure PLLA, PLLA/Coll-75/25 and PLLA/Coll-50/50 as-spun and immediately after crosslinking) were acquired. In order to eliminate artefacts caused by micro-movements, custom made rectangular masks (31×8×0.5 mm) made of polyethylene terephthalate (PET), with a central rectangular window (13×5 mm), were used to stabilize the bundles in the XCT chamber. Specimens of 36 mm in length were mounted vertically in the centre of the windows, with the extremities fixed on the masks with bi-component glue as shown in Figure 5.2(AI). This solution was adapted from a first prototype previously applied in a feasibility study of XCT on PLLA/Coll bundles [20].

Settings used for each voxel size were as follows:

(i) Voxel size of 1.0 micrometer: 40 kV Voltage, 3 W Power, 75.5 microAmpere tube current, 8 sec exposure time, images collected at rotational steps of 0.18° over 360°, for a scanning time of approximately 6 hours;

(ii) Voxel size of 0.4 micrometers: 40 kV Voltage, 3 W Power, 75.5 microAmpere tube current, 14 sec exposure time, images collected at rotational steps of 0.18° over 360°, for a scanning time of approximately 10 hours.

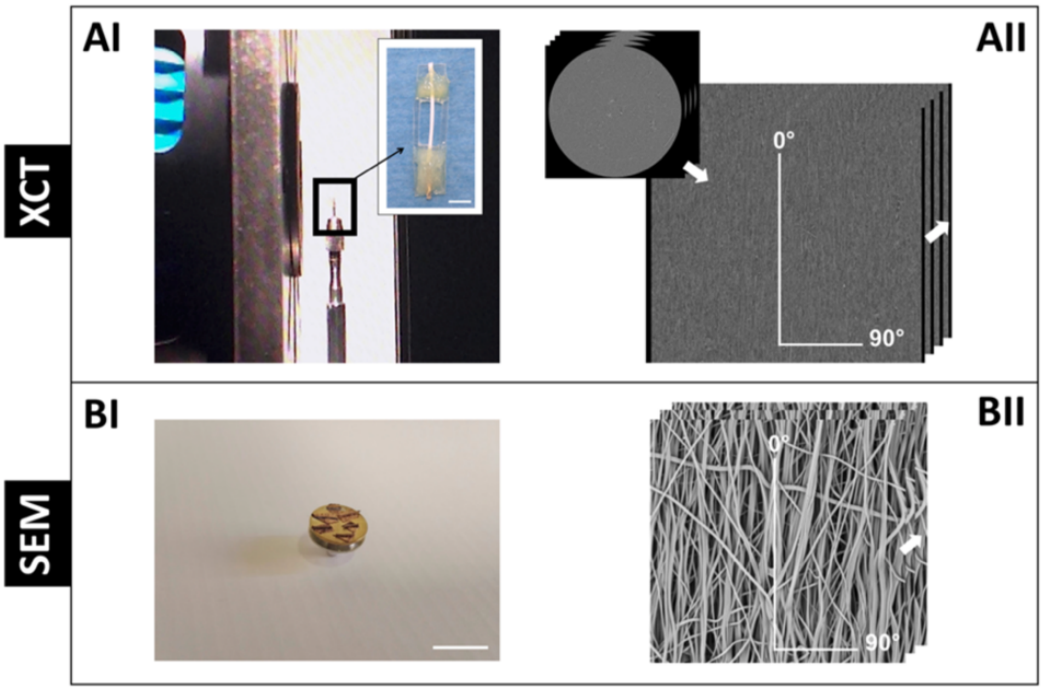

Fig.5.2 Workflow of the Directionality analysis applied to the XCT and SEM images. (AI)Bundle mounted on the mask and ready for XCT scanning (scale bar = 10 mm). (AII) Simplified representation of the Directionality procedure for the XCT images: the XCT stack consisting of cross-sections of the bundle at 0.4 μm voxel size was resliced in an axial stack by ImageJ. Then Directionality was applied to all the axial slices and angles were measured as indicated. (BI) Stub with five pieces of bundle, gold-sputtered and ready for SEM imaging (scale bar = 10 mm). (BII) Simplified representation of the Directionality procedure for SEM images: 10 SEM images were acquired on different points of the surface of each bundle with a magnification of 8000×. The SEM images were investigated with Directionality with the same parameters of the XCT stacks.

5.3.3 Post processing: analysis of directionality from XCT images

The images were reconstructed using the Scout-and-Scan Reconstructor software (ZEISS), and were visualised using XM3DViewer1.2.8 software (ZEISS). Before the Directionality analysis, the XCT stack of cross-sectional slices of each bundle were axially resliced using the command Reslice of ImageJ Figure 5.2(AII). In order to quantify the directionality of the nanofibers, the scans at 0.4 micrometers of voxel size of all compositions were analysed with ImageJ [22], using a dedicated plugin called Directionality [23,24]. The Directionality histogram reported the amount of nanofibers as a function of the fiber orientation using a Local Gradients

orientation method applied to each slice. The mean and standard deviation between slices was then computed.

5.3.4 SEM imaging

Scanning electron microscopy (SEM) observations were carried out using a Phenom ProX (Eindhoven, Netherlands) at an accelerating voltage of 15 kV, on samples sputter-coated with gold Figure 5.2(BI). For each of the bundle compositions (i.e. Nylon6.6, pure PLLA, PLLA/Coll-75/25 and PLLA/Coll-50/50 both as-spun and crosslinked) ten images were acquired with a magnification of 8000x. The diameter of the nanofibers was measured on the SEM images using the software ImageJ [22]. The distribution of diameters (mean and standard deviation) was measured for about 200 nanofibers, for each bundle composition.

5.3.5 Validation of XCT imaging based on SEM images

In order to validate the Directionality investigation on the XCT scans of the bundles, the same directionality investigation was performed as a comparison, on 10 SEM images for each of the compositions, as shown in Figure 5.2(BII).

5.4 Results

5.4.1 Bundles nanofibers morphology from SEM and XCT imaging

All the bundles in the different compositions had a mean diameter in the range of 550–650 μm as measured in the SEM images. Furthermore, the SEM investigation revealed that the nanofibres for each composition and each treatment condition had a well-defined morphology with no defects such as beads, as shown in Figure 5.3. The nanofibres had comparable diameters (mean and standard deviation) for all compositions and all treatments: Nylon6.6 0.26 ± 0.04 μm; pure PLLA 0.59 ± 0.14 μm; PLLA/Coll-75/25 as-spun 0.33 ± 0.08 μm; PLLA/Coll-75/25 crosslinked 0.30 ± 0.06 μm; PLLA/Coll-50/50 as-spun 0.39 ± 0.13 μm; PLLA/Coll-50/50 crosslinked 0.40 ± 0.08 μm.

The specimen mounting setup for the XCT scans successfully prevented the artefacts of micromovements, while permitting to centre the bundle in the scanning window of the XCT as shown in Figure 5.2(AI). After the three-dimensional re-construction at both voxel sizes, sharp high-resolution images were successfully obtained, as shown in Figures 5.4 and 5.5. The reconstructions with 1.0 μm voxel size provided an overview of each specimen. At 0.4 μm voxel size, the nanofibres were clearly distinguishable. Such high-resolution images allowed zooming-in a section of the specimens, both on its surface and inside the volume of the bundles. The XCT images highlighted some loss of material inside the bundles of the two PLLA/Coll blends, due to the crosslinking process, as shown in Figure 5.5.

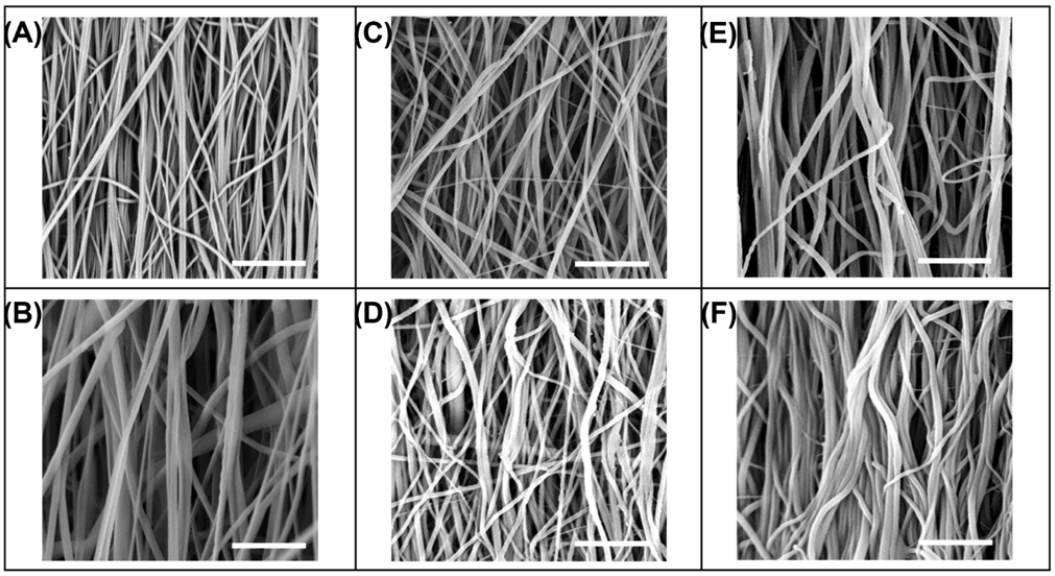

Figure 5.3 SEM images of the nanofibre distribution within the bundles (magnification = 8000×, scale bar = 5 μm). (A) Nylon 6.6. (B) PLLA. (C) PLLA/Coll-75/25 as-spun. (D) PLLA/Coll-75/25 crosslinked. (E) PLLA/Coll-50/50 as-spun. (F) PLLA/Coll-50/50 crosslinked.

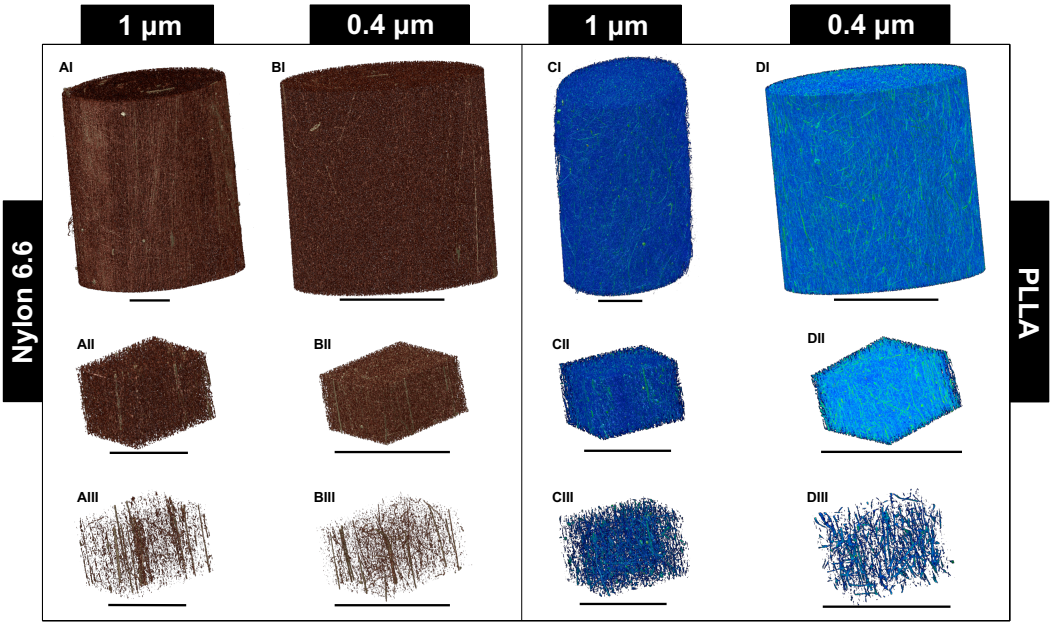

Figure 5.4 XCT images of (A, B) the Nylon 6.6 and (C, D) PLLA bundles at (A, C) 1.0 µm voxel size, and (B, D) 0.4 µm voxel size (scale bars = 200 µm). (I) Overview of the bundles for the two different voxel sizes showing all the nanofibres. (II), (III) Crop of an internal volume of the bundles with different thresholding.

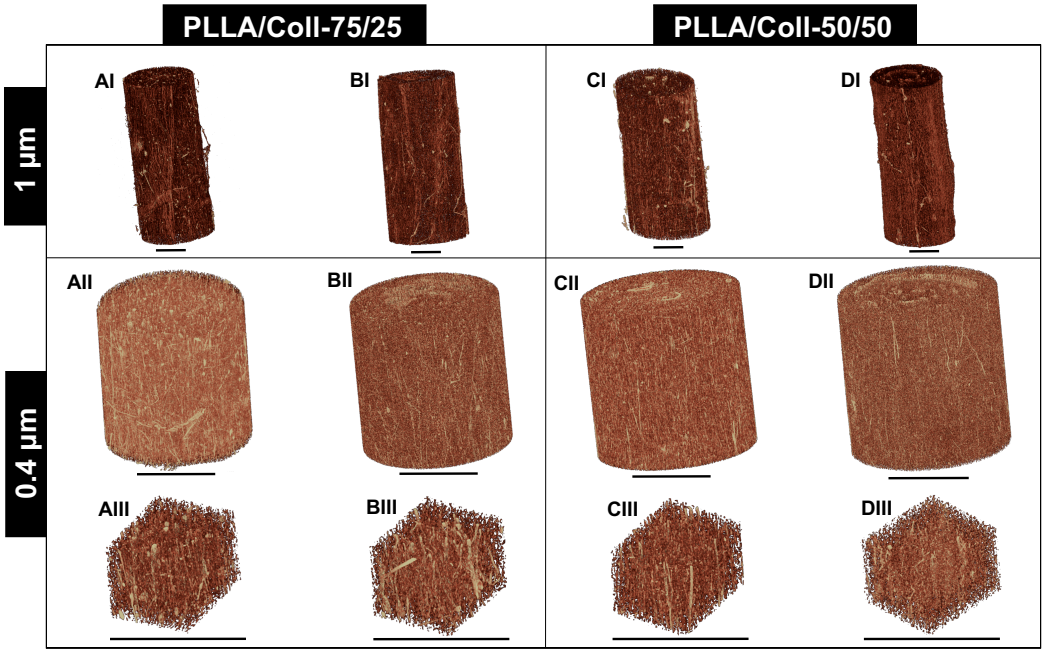

Figure 5.5 XCT images of the PLLA/Coll-75/25 bundles (A) as-spun and (B) crosslinked, and of the PLLA/Coll-50/50 bundles (C) as-spun, and (D) crosslinked (scale bar = 200 µm). Two voxel sizes are shown: (I) the 1.0 µm scan shows the nanofibres of the bundles for the different compositions; the 0.4 µm scan is shown as (II) an overview of the entire bundle, and (III) as a crop of an internal volume, showing the nanofibres.

5.4.2 Directionality of the nanofibers from XCT images

For all the bundles, the Directionality analysis on the XCT stacks confirmed a preferential alignment of the nanofibres, which were predominantly close to the axis of the bundle, and with a progressive Gaussian-like dispersion (Figs. 5.6–5.8). The single-polymer bundles presented lower peaks in the range of 0°–3° (Nylon6.6 29.5% ± 2.4% and PLLA 21.5% ± 1.8%) compared to the PLLA/Coll blends, both as-spun (PLLA/Coll- 75/25 as-spun 38.4% ± 4.3% and PLLA/Coll-50/50 as-spun 39.4% ± 3.5%) and crosslinked (PLLA/Coll-75/25 crosslinked 31.4% ± 2.5% and PLLA/Coll-50/50 crosslinked 35.3% ± 2.7%). A small fraction of nanofibres were oriented in the range of 87°–90° for the single-polymer bundles (Nylon6.6 0.4% ± 0.1% and PLLA 0.6% ± 0.1%), the PLLA/Coll blends, both as-spun (PLLA/Coll-75/25 as-spun 0.5% ± 0.2% and PLLA/Coll-50/50 as-spun 0.4% ± 0.1%) and crosslinked (PLLA/Coll-75/25 crosslinked 0.5% ± 0.1% and PLLA/Coll- 50/50 crosslinked 0.4% ± 0.1%).

5.4.3 Validation of XCT imaging against SEM images

The comparison between the XCT and SEM images focused on the analysis of Directionality. The analysis of the XCT stacks resulted in a higher estimation of the axial alignment of the nanofibres: for all the compositions, the amount of nanofibres in the 0°–3° range was systematically higher when estimated from the XCT scans than from the SEM images (Figure .6–3.8). In the range from 3° to 21° (for Nylon6.6) or 24° for the other compositions, the XCT underestimated the amount of nanofibres, compared to the SEM images (the discrepancy was smaller compared to the 0°–3° range). The discrepancy be- tween the amount of nanofibres between 21° and 90° estimated from the XCT scans and SEM images was well below 1%, for all the compositions.

The largest amount of nanofibres in the 0°–3° range were measured in the XCT scans of the PLLA/Coll blends. The differences between the XCT and SEM amount histograms in the 0°–3° range were relatively small for the Nylon6.6 (3.2% discrepancy) and the PLLA (0.8%). The differences between the XCT and SEM were larger for the blends containing collagen (15.6% for the PLLA/Coll-75/25 as-

spun, 12.6% for the PLLA/Coll-75/25 crosslinked and 13.6% for the PLLA/Coll-50/50 as-spun, 14.9% for the PLLA/Coll-50/50 crosslinked).

The discrepancy between the amount of nanofibres estimated based on the XCT scans and SEM images was smaller if a larger range of angles was considered (0°–12°): the difference for the PLLA/Coll blends did not exceed 2%; the largest difference was found for the Nylon6.6 (10% difference) and pure PLLA (6% difference).

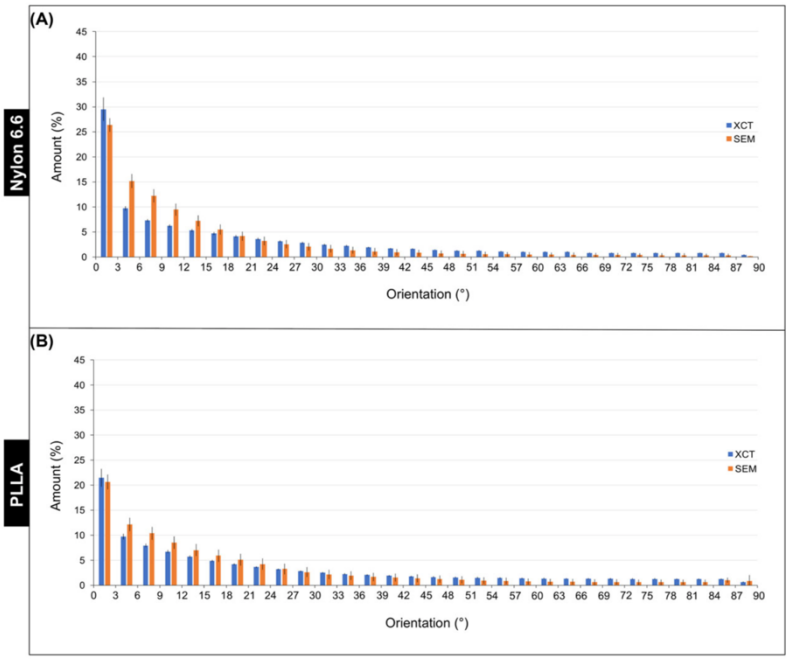

Figure 5.6 Comparison between the Directionality measured on the XCT at 0.4 µm voxel size (blue bars) and SEM images at 8000× magnification (orange bars) for two compositions: (A) Nylon 6.6 bundles and (B) pure PLLA bundles. An angle of 0° means that the nanofibres were aligned with the axis of the bundles, an angle of 90° means that the nanofibres were perpendicular to the bundle. Mean and standard deviation between images of the same specimen are plotted.

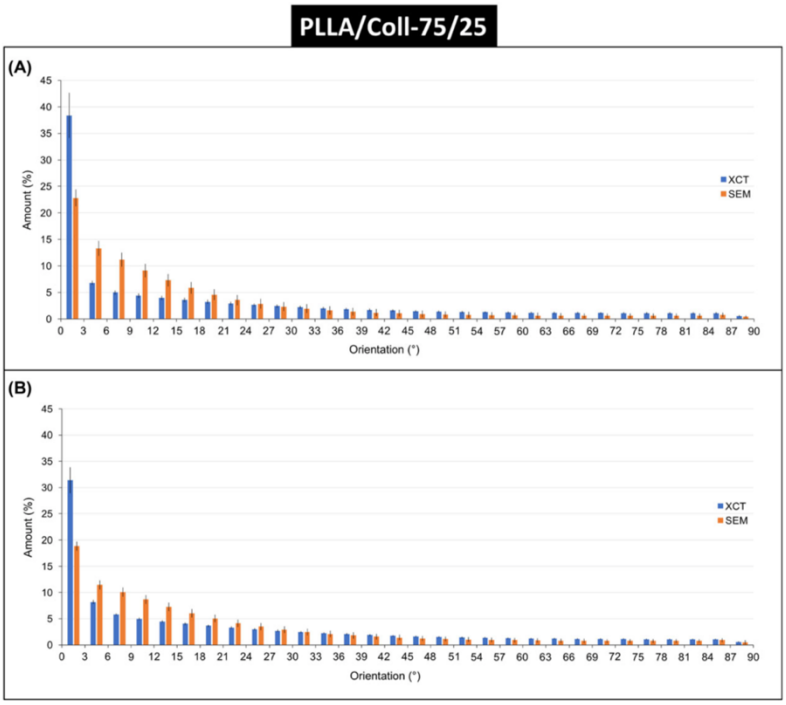

Figure 5.7 Comparison between the Directionality measured on the XCT at 0.4 µm voxel size (blue bars) and SEM images at 8000× magnification (orange bars) for the PLLA/Coll-75/25 bundles (A) as-spun bundles and (B) crosslinked. An angle of 0° means that the nanofibres were aligned with the axis of the bundles, an angle of 90° means that the nanofibres were perpendicular to the bundle. Mean and standard deviation between images of the same specimen are plotted.

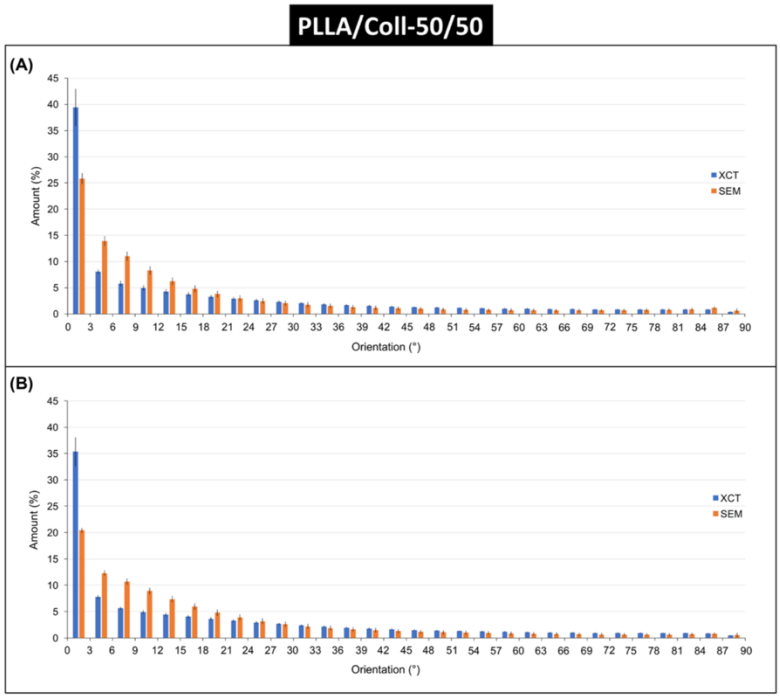

Figure 5.8 Comparison between the Directionality measured on the XCT at 0.4 µm voxel size (blue bars) and SEM images at 8000× magnification (orange bars) for the PLLA/Coll-50/50 bundles (A)

as-spun bundles and (B) crosslinked. An angle of 0° means that the nanofibres were aligned with the axis of the bundles, an angle of 90° means that the nanofibres were perpendicular to the bundle. Mean and standard deviation between images of the same specimen are plotted.

5.5 Discussion

The first aim of the present study was to obtain XCT scans of electrospun bundles of different materials in order to compare their morphology with the multiscale structure of tendon and ligament fascicles and fibrils [6–8]. For this reason, we developed a setup to avoid micro-movements during the XCT scans, and we defined a post processing workflow on the XCT scans to evaluate the alignment of the nanofibers in all the bundles' volume. To validate the alignment measured from the XCT, a comparison was performed against a similar investigation with SEM images (SEM).

We produced bundles of nanofibers of biostable and resorbable materials, morphologically and hierarchically similar, in terms of diameters and fiber alignment to the fascicles and fibrils of the human tendons and ligaments [6–8,25,26]. The surface morphology and alignment of the nanofibers were assessed through SEM investigation (Figure 5.3). In order to analyse the 3D-morphology of the bundles and verify the alignment of the nanofibers even in their internal part, an XCT characterization with two different voxel sizes (1.0 and 0.4 micrometers) was performed on all the different compositions (Figure 5.4 and 5.5). For all the compositions, sharp XCT scans were obtained, for both voxel sizes (Figures 5.4 and 5.5). The two different voxel sizes were chosen to have an overview of the bundles (1.0 micrometer) and a zoom-in on the fibers (0.4 micrometers). Because of the nanofibers diameters (550–250 nm), increasing the resolution of the scan resulted in a better detection of the fibers contours (Figure 5.4 and 5.5), basically because a 0.4 micrometer voxel is more likely contains just one nanofiber. In fact, when increasing the dimension of the voxel more than one fiber could be contained in the same voxel, thus making it impossible to identify the nanofibers individually. No images were affected by artefacts caused by micro-movements, and were sufficiently sharp to allow identification of the individual nanofibers. The main element to prevent micro-movements of such slender specimens was the fixture

developed to hold the bundle during XCT imaging (Figure 5.2). This dedicated setup allowed placing the x-ray source and detector of the XCT as close as few millimeters to the specimen surface. Furthermore, the design of the support fixture did not enclose the specimen into any additional material, which could compromise the scan quality. Other works on electrospun materials used polyamide tubing [17] or Kapton tubing [16] as a support for the specimen during XCT imaging. With this configuration it is difficult to obtain a correct contrast between the walls of the tubing and the bundles, because of the low absorption of the electrospun polymers, as well as additional attenuation due to the tube itself.

The Directionality analysis on the XCT scans, confirmed a preferential axial alignment in the range of 0°-3° for all the bundles, and a progressive dispersion of the nanofibers in the range of 3°-90°. This is similar to the physiological dispersion of collagen fibrils in the tendons and ligaments [8,26,27]. The fact that most (but not 100%) of the fibers are aligned with the bundle axis is important to mimic the arrangement of the collagen in the tendons and ligaments. In fact, this structure of the bundles is expected to be bio-mimetic, to promote tissue regeneration, and to provide a non-linear mechanical response similar to that of the natural tissue [8]. A related study has shown that three-dimensional multiscale morphology of scaffolds similar to those in the current study, as well as the particular use of PLLA/Coll blends permitted the bundles to better reproduce the biomechanical properties of human tendon and ligament fascicles [8,20].

The comparison between the Directionality analyses performed on the XCT scans and SEM images showed generally a good agreement. It must be noted that the SEM inspection was assumed as a ground truth: however, SEM inspection only addresses the specimen's surface, whereas it cannot access the inner volume. The Directionality tests were performed on all the XCT stacks for each specimen (about 900 slices), while for the SEM the analysis relied on 10 images from the surface of each bundle. This can partially explain the difference between XCT and SEM assessment of directionality. The largest discrepancy between the two examination methods was found in the estimation of the amount of nanofibers aligned within 3° from the axis of the bundle, where the XCT scan provided a considerable overestimation. While this discrepancy was within 3% for the bundles of Nylon6.6

and the PLLA, larger discrepancies were observed for the PLLA/Coll blends (between 12.6% and 15.6%). However, if a larger range of directionality was considered (i.e. 0°-12°) better agreement was found between directionality assessed form XCT scans and SEM images (2% discrepancy for the PLLA/Coll blends, 6% for pure PLLA and 10% for Nylon6.6). This seems to indicate that XCT scans are less suited to assess the amount of nanofibers in a very narrow range of angles, whereas they can reliably quantify the amount of nanofibers in a range of 12°. The reason of this behavior is probably the partial volume effect. The nanofibers of pure PLLA had a mean diameter (0.59 micrometers) larger than the voxel size (0.4 micrometers). Thus, most of the nanofibers were clearly distinguishable, and consequently their direction was more accurately captured. Conversely, PLLA nanofibers thinner than the voxel size were not clearly recognised in the XCT scan and therefore they contributed to overestimate the amount in the range of 0°-21°. The partial volume effect was more pronounced for the XCT scans of the Nylon6.6 bundles, where the mean diameter of the nanofibers (0.26 micrometers) was smaller than the voxel size. This effect was further increased for the PLLA/Coll blends as the collagen: in fact it is well well-know that it is difficult to obtain tomographic images of the collagen due to its low absorption of x-ray radiation [28,29].

In our study on electrospun bundles, the XCT scans had a greyscale similar to the background, because of the space between nanofibers, and because the nanofibers dimensions. This made the detection of the nanofibers direction even more difficult. To obtain tomographic scans with a resolution of 0.33 micrometers, synchrotron X-ray phase contrast was used [19]: while this allowed identifying the individual polyester nanofibers (diameter between 1.9 and 3.7 micrometers), it also caused significant material modification due to the high radiation dose. Some works used contrast agents to enhance radiopacity during CT scans of portions of anterior cruciate ligaments and patellar tendons where the effects of phosphotungstig acid (PTA) and iodine solution (IKI) staining were compared, in order to increase the visualization of the tissues, down to the fascicle level [30,31]. Unstained rat common carotid artery embedded in paraffin, was successfully XCT scanned using a voxel size of 0.5 micrometers, showing collagen fibrils [32].

5.6 Conclusions

We have shown the feasibility of assessing the morphology of electrospun polymeric bundles by means of high-resolution computed tomography (XCT). We were able to quantify the directionality of the nanofibres in bundles with different biostable and bioresorbable compositions that produced a 3D multiscale scaffold able to replicate the morphology of the human tendon and ligament fascicles.

5.7 References

[1] Santos M L, Rodrigues M T, Domingues R M A, Reis R L and Gomes M E 2017 Regenerative Strategies for the Treatment of Knee Joint Disabilities Regenerative Strategies for the Treatment of Knee Joint Disabilities vol 21, ed J M Oliveira and R L Ruis (Springer International Publishing) pp 349–71

[2] Harvie P, Ostlere S J, Teh J, McNally E G, Clipsham K, Burston B J, Pollard T C B and Carr A J 2004 Genetic influences in the aetiology of tears of the rotator cuff. Sibling risk of a full-thickness tear. J. Bone Joint Surg. Br. 86–B 696–700

[3] Woo S L Y, Abramowitch S D, Kilger R and Liang R 2006 Biomechanics of knee ligaments: Injury, healing, and repair J. Biomech. 39 1–20

[4] Rees J D, Wilson A M and Wolman R L 2006 Current concepts in the management of tendon disorders Rheumatology 45 508–21

[5] September A V, Schwellnus M P, Collins M and Gibson W 2007 Tendon and ligament injuries: the genetic component Br. J. Sports Med. 41 241–6

[6] Kastelic J, Galeski A and Baer E 1978 The Multicomposite Structure of Tendon Connect. Tissue Res. 6 11–23

[7] Kannus P 2000 Structure of the tendon connective tissue Scand. J. Med. Sci. Sport. 10 312–20

[8] Goh K L, Listrat A and Béchet D 2014 Hierarchical mechanics of connective tissues: Integrating insights from nano to macroscopic studies J. Biomed. Nanotechnol. 10 2464–507

[9] Uquillas J A, Pacelli S, Kobayashi S and Uquillas S 2017 Musculoskeletal Tissue Engineering : Tendon, Ligament, and Skeletal Muscle Replacement and Repair Tissue Engineering for Artificial Organs: RegenerativeMedicine, Smart Diagnostics and PersonalizedMedicine ed A Hasan (Wiley) pp 465–523

[10] Verdiyeva G, Koshy K, Glibbery N, Mann H and Seifalian A M 2015 Tendon reconstruction with tissue engineering approach - A review J. Biomed. Nanotechnol. 11 1495–523

[11] O'Connor R A and McGuinness G B 2016 Electrospun nanofibre bundles and yarns for tissue engineering applications: A review Proc. Inst. Mech. Eng. Part H J. Eng. Med. 230 987–98

[12] Flannery B P, Deckman H W, Roberge W G, Amico K L D, Flannery B P, Deckman H W, Roberge W G and Amico K L D 1987 Three -Dimensional X- ray Microtomography Science (80-.). 237 1439–44

[13] Dover S D, Elliott J C, Boakes R and Bowen D K 1989 Three-dimensional X- ray microscopy with accurate registration of tomographic sections J. Microsc. 153 187–91

[14] Farrugia B L, Brown T D, Upton Z, Hutmacher D W, Dalton P D and Dargaville T R 2013 Dermal fibroblast infiltration of poly(ε-caprolactone) scaffolds fabricated by melt electrospinning in a direct writing mode Biofabrication 5 025001

[15] Kogikoski S, Liberato M S, Factori I M, da Silva E R, Oliveira C L P, Ando R A and Alves W A 2017 Polycaprolactone–Polyaniline Blend: Effects of the Addition of Cysteine on the Structural and Molecular Properties J. Phys. Chem. C 121 863–77

[16] Bradley R S, Robinson I K and Yusuf M 2017 3D X-Ray Nanotomography of Cells Grown on Electrospun Scaffolds Macromol. Biosci. 17 1–8

[17] Bosworth L A, Rathbone S R, Bradley R S and Cartmell S H 2014 Dynamic loading of electrospun yarns guides mesenchymal stem cells towards a tendon lineage J. Mech. Behav. Biomed. Mater. 39 175–83

[18] Bosworth L A, Alam N, Wong J K and Downes S 2013 Investigation of 2D and 3D electrospun scaffolds intended for tendon repair J. Mater. Sci. Mater. Med. 24 1605–14

[19] Maksimcuka J, Obata A, Sampson W W, Blanc R, Gao C, Withers P J, Tsigkou O, Kasuga T, Lee P D and Poologasundarampillai G 2017 X-ray Tomographic Imaging of Tensile Deformation Modes of Electrospun Biodegradable Polyester Fibers Front. Mater. 4 1–11

[20] Sensini A, Gualandi C, Cristofolini L, Tozzi G, Dicarlo M, Teti G, Belmonte- Mattioli M and Focarete M L 2017 Biofabrication of bundles of poly (lactic acid) -collagen blends mimicking the fascicles of the human Achille tendon Biofabrication 9 1–13

[21] Kim H W, Song J H and Kim H E 2005 Nanofiber generation of gelatin- hydroxyapatite biomimetics for guided tissue regeneration Adv. Funct. Mater. 15 1988–94

[22] Liu Z 1991 Scale space approach to directional analysis of images Appl. Opt. 30 1369–73

[23] Schindelin J, Arganda-Carreras I, Frise E, Kaynig V, Longair M, Pietzsch T, Preibisch S, Rueden C, Saalfeld S, Schmid B, Tinevez J-Y, White D J, Hartenstein V, Eliceiri K, Tomancak P and Cardona A 2012 Fiji: an open- source platform for biological-image analysis. Nat. Methods 9 676–82

[24] Schneider C A, Rasband W S and Eliceiri K W 2012 NIH Image to ImageJ: 25 years of image analysis Nat. Methods 9 671–5

[25] Fang F and Lake S P 2016 Modelling approaches for evaluating multiscale tendon mechanics Interface Focus 6 20150044

[26] Radaelli F, D'Alfonso L, Collini M, Mingozzi F, Marongiu L, Granucci F, Zanoni I, Chirico G and Sironi L 2017 μMAPPS: a novel phasor approach to second harmonic analysis for in vitro-in vivo investigation of collagen microstructure Sci. Rep. 7 17468

[27] Franchi M, Trirè A, Quaranta M, Orsini E and Ottani V 2007 Collagen Structure of Tendon Relates to Function Sci. World J. 7 404–20

[28] Zidek J, Vojtova L, Abdel-Mohsen A M, Chmelik J, Zikmund T, Brtnikova J, Jakubicek R, Zubal L, Jan J and Kaiser J 2016 Accurate micro-computed tomography imaging of pore spaces in collagen-based scaffold J. Mater. Sci. Mater. Med. 27 1–18

[29] Balint R, Lowe T and Shearer T 2016 Optimal contrast agent staining of ligaments and tendons for X-ray computed tomography PLoS One 11

[30] Shearer T, Rawson S, Castro S J, Ballint R, Bradley R S, Lowe T, Vila-Comamala J, Lee P D and Cartmell S H 2014 X-ray computed tomography of the anterior cruciate ligament and patellar tendon Muscles. Ligaments Tendons J. 4 238–44

[31] Shearer T, Bradley R S, Hidalgo-Bastida L A, Sherratt M J and Cartmell S H 2016 Three-dimensional visualisation of soft biological structures by X-ray computed micro-tomography J. Cell Sci. 129 2483–92

[32] Walton L A, Bradley R S, Withers P J, Newton V L, Watson R E B, Austin C and Sherratt M J 2015 Morphological characterisation of unstained and intact tissue micro-architecture by X-ray computed micro- and nano-tomography Sci. Rep. 5 1–14

Chapter 6: Multiscale hierarchical bioresorbable scaffolds for the regeneration of tendons and ligaments

Alberto Sensini[1], Chiara Gualandi[2,3], Maria Letizia Focarete[2,3], Juri Belcari[1], Andrea Zucchelli[1], Liam Boyle[4], Gwendolen C. Reilly[5], Alexander P. Kao[6], Gianluca Tozzi[6], Luca Cristofolini[1,3]

1 Department of Industrial Engineering, Alma Mater Studiorum - Università di Bologna, 40131 Bologna, Italy.

2 Department of Chemistry "G. Ciamician" and National Consortium of Materials Science and Technology (INSTM, Bologna RU), Alma Mater Studiorum - Università di Bologna, 40126 Bologna, Italy.

3 Health Sciences and Technologies – Interdepartmental Center for Industrial Research (HST-ICIR), Alma Mater Studiorum - Università di Bologna, 40064 Ozzano dell'Emilia, Bologna, Italy.

4 Department of Materials Science and Engineering, University of Sheffield, Sheffield S31 3JD, UK.

5 INSIGNEO Institute for in silico Medicine, University of Sheffield, Sheffield S31 3JD, UK.

6 School of Engineering, University of Portsmouth, Portsmouth PO1 3DJ, UK.

Keywords: Tissue Engineering; Tendon and Ligament Tissue; Electrospinning; Multiscale Hierarchical Scaffolds; Multiscale Assembly.

The candidate is the main author of the study. The work is under revision at Biofabrication.

Under revision at Biofabrication 2019

6.1 Abstract

Lesions of tendons and ligaments account for over 40% of the musculoskeletal lesions. Surgical techniques and materials for repair and regeneration are currently not satisfactory. The high rate of post-operative complications and failures mainly relates to the technical difficulties in replicating the complex multiscale hierarchical structure of the native tendons and ligaments. Here we mimicked the hierarchical structure of tendons and ligaments by fabricating scaffolds made of resorbable electrospun nanofibers of Poly-L-Lactic acid (PLLA). The scaffold consists of multiple bundles having tailored dimensions, wrapped in a sheath of non-aligned nanofibers able to compact the construct. The bundles in turn consist of electrospun nanofibers with a preferential direction. High-resolution x-ray tomographic investigation at nanometer resolution confirmed that the morphology of the single bundles and of the entire scaffold replicated the hierarchical arrangement in the natural tendons and ligaments. The stiffness, strength and toughness, measured with dedicated tensile tests, were in the range required to replace and repair tendons and ligaments. Human fibroblasts were able to attach and spread along the scaffolds, with increasing viability over time. These results demonstrate the potential for these scaffolds to be utilized in the regeneration of tendons and ligaments.

6.2 Introduction

Tendon and ligament reconstructions still represent an unsolved clinical problem in orthopedics. In the United States, about 45% of the 32.8 million musculoskeletal injuries each year involve tendons and ligaments [1–3]. However, because current clinical techniques are unable to restore the complex hierarchical structure of the tendon and ligament and their excellent mechanical properties [4–6], post-operative complications and failures are common [7–9]. Furthermore, at the site of the lesion or fracture, scar tissue created after healing from the surgical treatment, may create morphological discontinuities which impair the mechanical properties and functionality [10]. The research field of tissue engineering aims to provide tools that enable reconstruction of these tissues using resorbable scaffolds. Different techniques are used to produce scaffolds [6,8,9,11,12], but probably the most

promising for tendon and ligament regeneration or substitution is electrospinning [13]. Due to its ability to produce fibers of both natural and synthetic polymers with nanometric diameters, electrospinning has the potential to produce scaffolds morphologically very similar to the hierarchical structure of the tendon and ligament collagen fascicles and fibrils [4–6,14–16]. Specific arrangement of the electrospinning setup allows alignment of the nanofibers in desired directions.

Researchers have approached tendon and ligament regeneration using electrospinning either by using singular units or building hierarchical multiscale assemblies [11–13,17,18]. Focusing on singular units, electrospun bundles and yarns [19,20] are the scaffolds which can better mimic the morphological structure and mechanical properties of tendon and ligament fascicles. For example, Bosworth et al. demonstrated that electrospun yarns of different resorbable materials provided basic mechanical properties and cell proliferation [21–23]. Xu et al. produced Poly (L-Lactide-co-e- Caprolactone)/Collagen nanoyarns for tendon regeneration [24]. Pauly et al. produced very promising bundles of Poly (e-Caprolactone) (PCL) for ligament regeneration [25]. More recently Sensini et al. produced bundles of Poly-L-Lactic acid (PLLA) and Collagen blends with promising mechanical properties and cell viability for tendon tissue reconstruction [14,15]. Banik et al. developed an electrospun scaffold of a high number of PCL nanofibers with a ‘Chinese-finger trap’ configuration [26]. These approaches allow production of nanofibers similar to collagen fibrils, and with adequate composition, but the proposed constructs did not provide adequate strength and stiffness to replace or regenerate the tendon or ligament.

The alternative approach uses hierarchical assemblies that aim to reproduce the multiscale structure of a complete tendon or ligament, and provide adequate strength by joining several bundles or yarns in different configurations [11,13,17,18]. Xu et al. produced a multiscale scaffold by twisting some yarns as a scaffold for tendon regeneration with encouraging mechanical properties and cell proliferation [24,27]. Several approaches which involved twisting yarns of nanofibers have been tested using polydioxanone [28] and PCL/Chitosan blends reinforced with cellulose nanocrystals [29] to replace tendons and ligaments.

Assembling multiple bundles or yarns is certainly a promising approach to mimic the hierarchical structure of tendons and ligaments, but adequate mechanical strength and stiffness are achieved only if the bundles or yarns are densely arranged, otherwise significant cavities and a critical reduction of structural properties results. Therefore, a key point is to include in the multiscale production a method for compacting the bundles and yarns together. The outer surface of natural tendons and ligaments is wrapped in a epitenon/epiligament sheath [4–6]. Replicating this natural morphology would allow compaction of the bundles/yarns inside the scaffold, and higher mechanical properties. In conjunction an ideal sheath should be engineered so as to permit to cells to cross it, or at least to allow to biological fluids to bring the nutrients to the cells inside the scaffold structure. For example, Zhou at al. electrospun a Poly(ethylene oxide) coating on a group of aligned monofilaments of Polyamide which were twisted during the coating [30]. Naghashzargar et al. coated yarns of monofilaments of silk with PCL and P3HB, for possible tendon and ligament regeneration [31]. Padmakumar et al. coated electrospun yarns of PLLA with an electrospun sheath of Poly(lactic-co-glycolic) acid fibers loaded with drugs, as a suture wire [32]. Recently Li et al., produced an electrospun scaffold for nerve conduit, made of a coating of Poly (L-lactide-co-caprolactone) on electrospun yarns of PLLA, and studied the cell proliferation and ability to cross the membrane [33].

While promising steps have been taken both in the production of single bundles and yarns, and in possible methods for assembling a hierarchical structure, none of the developed solutions was able to mimic the hierarchical structure of tendons and ligaments, and at the same time, to provide adequate mechanical properties.

We report here our bottom-up method to produce an innovative multiscale hierarchical electrospun nanofibrous scaffold able to mimic both the hierarchical structure and the biomechanical properties of a tendon or a ligament. With this method, we were able to manufacture resorbable scaffolds with suitable morphology, mechanical properties and cell viability to regenerate tendons and ligaments.

6.3 Materials and Methods

6.3.1 Materials

Poly-L-lactic acid (PLLA) (Lacea H.100-E, Mw = 8.4×10^4 g/mol, PDI = 1.7) was purchased from Mitsui Fine Chemicals (Dusseldorf, Germany). Dichloromethane (DCM) and Dimethylformamide (DMF) were purchased from Sigma-Aldrich (Sigma-Aldrich, Saint Louis, USA) and used as received. The following polymeric solution was prepared for electrospinning: 13% (w/v) solution of PLLA dissolved in DCM:DMF=65:35 (v/v).

To embed the extremities of the PLLA multiscale hierarchical scaffolds for the mechanical tests, an acrylic cement (Restray, Salmoiraghi Mulazzano, Italy), was used. For the hydration of both the PLLA single bundles and multiscale hierarchical scaffolds before the mechanical tests, 0.9% NaCl solution, purchased by S.A.L.F. (Cenate Sotto, Italy), was used.

6.3.2 Electrospinning and assembling the PLLA multiscale hierarchical scaffold

In this work, the complete hierarchical structure of a tendon or ligament (Figure 6.1A) was reproduced by using two different electrospinning set-ups: a commercial electrospinning unit (Spinbow srl, Bologna, Italy) (Figure 6.S1A) was employed to produce PLLA single bundles while a custom-made electrospinning apparatus was used to produce the sheath wrapping the multiscale hierarchical scaffold. Electrospinning was performed at room temperature (RT) and relative humidity 30-40%. The commercial electrospinning unit is equipped with a linear sliding spinneret with two syringes configuration (40 mm apart), and a rotating drum collector. To control the flux of the solution, a syringe pump (KD Scientific 200 series, Illinois, USA), two glass syringes containing the polymer solution and connected to two stainless-steel blunt-ended needles through two Teflon tubes, were used. The sliding spinneret with the two needles had a linear excursion of 120 mm along the collector, with a speed of 1500 mm/min. PLLA solution was electrospun by applying the following processing conditions: applied voltage = 18

kV, feed rate = 1.2 mL/hour, needles inner diameter = 0.84 mm, electrospinning time = 1 hour. A rotating aluminum collector (length = 405 mm, diameter = 150 mm) turning at 2900 rpm (resulting in a peripheral speed of 22.8 m/sec.) was used to produce mats made of fibers preferentially aligned in the direction of drum rotation. The rotating collector was positioned 200 mm away from the tip needles. To detach the electrospun mats, the collector was covered with a sheet of paper with a Polyethylene layer. To obtain the PLLA single bundles, the mat was cut in rectangular strips and manually wrapped along the collector (Figure 6.1B). To remove the PLLA single bundles from the collector, they were incised axially with a cutter. Thus, the final PLLA single bundles were as long as the circumference of the rotating collector (approximately 471 mm), and were made of fibers predominantly axially aligned. The bundles obtained with this process had a diameter of 550-600 micrometers.

To produce the PLLA multiscale hierarchical scaffold, the single bundles were cut into segments with a length of 100 mm each. To obtain a PLLA multiscale hierarchical scaffold with a mean diameter of 6.5 mm, 100 bundles were used. The extremities were tied together at first with Parafilm (Pechiney Plastic Packaging, Chicago, USA) and then were covered with paper tape. After this operation, a PLLA sheath of randomly aligned nanofibers was electrospun on the group of bundles for 3 hours. To electrospin the sheath, a custom-made electrospinning apparatus was used, consisting of a high- voltage power supply (FuG Elektronik GmbH, Schechen, Germany), a syringe pump (KD Scientific Legato 100, Illinois, USA), a glass syringe containing the polymer solution and connected to a stainless-steel blunt-ended needle. In order to concentrate the fibers on the PLLA multiscale hierarchical scaffold, the scaffold was placed in front of a flat aluminum collector plate (200 mm high and 50 mm wide) (Figure 6.S1B). To pre-strain the nanofibers of the sheath on the scaffold surface, the scaffold itself was in a static position, and was intermittently put in rotation (approximately 20 rpm for 1 minute every 5 minutes) while the sheath was being electrospun (Figure 6.1C). The PLLA solution and the electrospinning parameters were the same previously described.

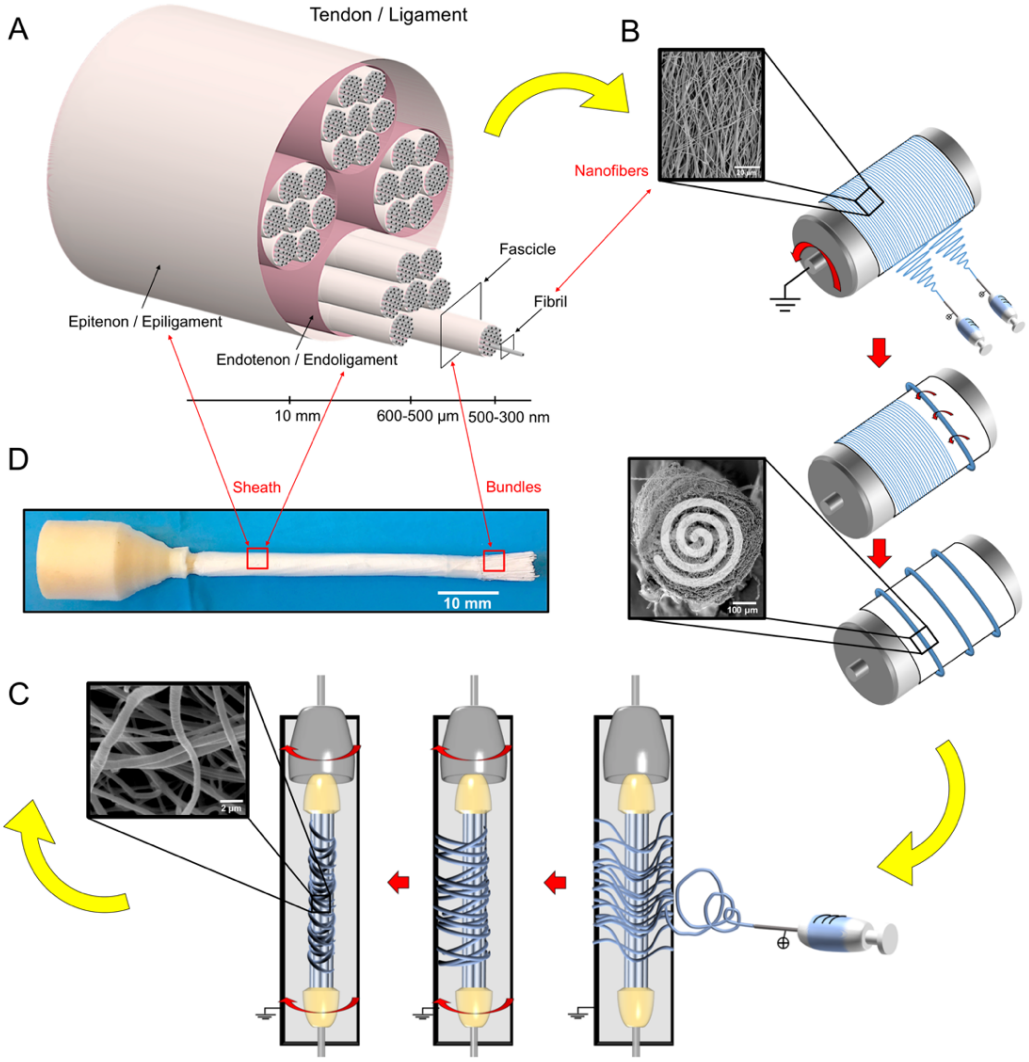

Figure 6.1. Electrospun PLLA multiscale hierarchical scaffold production process. (A) Tendon/ligament tissue hierarchical structure. (B) Representation of the electrospinning workflow to produce bundles. (C) Schematic representation of the random nanofibrous sheath production process on a group of PLLA single bundles. (D) Final PLLA multiscale hierarchical scaffold after the random sheath production process, with the left end cemented and the right end exposed, with the internal single bundles visible.

6.3.3 Imaging: scanning electron microscopy and high-resolution x-ray tomography

To examine the surface morphology of both PLLA single bundles and multiscale hierarchical scaffold, a Scanning Electron Microscopy (SEM) analysis was performed. A commercial SEM (Philips 515 SEM, Amsterdam, Netherlands) was

used with an accelerating voltage of 15 kV, on samples sputter-coated with gold. The distribution of fiber diameters (average and standard deviation) was measured on the SEM images of about 200 fibers, by means of an image analysis software ImageJ [34].

To investigate the three-dimensional structure of the PLLA single bundles, high-resolution x-ray tomographic scans were acquired with a high-resolution x-ray tomograph (Xradia 510 Versa, ZEISS, Pleasanton, CA, USA). For all the scans, the following settings were used: 40 kV Voltage, 3 W Power, 75.5 microAmpere tube current. Images were collected at rotational steps of 0.18° over 360°. Two different isotropic voxel sizes were obtained: (i) Voxel size 1 micrometer, using 8 second exposure time (scanning time of approximately 6 hours); (ii) Voxel size 0.4 micrometers, using 14 second exposure time (scanning time of approximately 10 hours).

To investigate the three-dimensional structure of the PLLA multiscale hierarchical scaffold, high- resolution x-ray tomographic scans were acquired with another high-resolution x-ray tomograph (Xradia 520 Versa, ZEISS, Pleasanton, CA, USA). The following parameters were used: 40 kV Voltage, 3 W Power, 75 microAmpere tube current. Two different isotropic voxel sizes were obtained: (i) 20 micrometers of voxel size to obtain a full view of the PLLA multiscale hierarchical scaffold for a length of 35 mm, by acquiring three consecutive scans, which were later assembled (this was obtained using 5 second exposure time, rotational steps of 0.22° over 360°, for a total scanning time of 9 hours); and (ii) 8.5 micrometers of voxel size to visualize the internal PLLA single bundles and the random sheath on a shorter portion (this was achieved with 7 second exposure time, rotational steps of 0.12° over 360°, for a scanning time of 7.5 hours).

All the XCT images, were reconstructed using the Scout-and-Scan Reconstructor software (ZEISS), and were visualized using XM3DViewer1.2.8 software (ZEISS).

To measure the alignment of the nanofibers in the PLLA single bundles, the XCT scans at the highest resolution (0.4 micrometer of voxel size) were analyzed with the Directionality plugin of ImageJ [34– 36]. This approach allowed to quantify the number of nanofibers within a given angle from the axis of the PLLA single bundle.

6.3.4 Machanical characterization of the PLLA single bundles and multiscale hierarchical scaffolds

The mechanical properties of the PLLA single bundles and multiscale hierarchical scaffolds were measured with a servo-hydraulic testing machine (8032, Instron, High Wycombe, UK), with a ±1kN dynamic cell (Instron, High Wycombe, UK). The testing machine was in class of accuracy 0.5. The force signals had an accuracy of 0.01 N after filtering. All the specimens were immersed in saline for two minutes before the mechanical test.

To measure the diameter of each PLLA single bundle before the test, a polarized light optical microscope (Axioskop, ZEISS, Pleasanton, CA, USA) equipped with a camera (AxioCam MRc, ZEISS, Pleasanton, CA, USA) was used by means of an acquisition and image analysis software ImageJ [34]. For each PLLA single bundle, the mean and standard deviation of 10 measurements was computed.

Ten specimens of PLLA single bundles were tested. Dedicated capstan grips (Figure 6.4A) were used to minimize the stress concentrations at sample ends. The gauge length was 47.42 mm (consistently with similar to the BS EN 12562:1999 and the ASTM D2256/D2256M-10 (2015) Standards, this included the free length and the portion of specimen wrapped around the capstans). The test machine was operated in displacement control, with an actuator speed of 16 mm/sec. (resulting in a strain rate of 33 %/sec.).

Five PLLA multiscale hierarchical scaffolds were tested. To measure the diameter of each PLLA multiscale hierarchical scaffold, six images were acquired (at three positions along the specimen, rotating the scaffold by 90°), and analyzed with ImageJ [34]. The diameter was measured ten times in each image. The diameter of each PLLA multiscale hierarchical scaffold was obtained as mean and standard deviation of 60 measurements. To minimize the stress concentrations, the extremities of the PLLA multiscale hierarchical scaffolds were potted in stumps of acrylic cement having a cylindrical shape and ending with a 30° taper. The stumps were fixed in the grips of the machine (Figure 6.4B). As the length of the PLLA multiscale hierarchical scaffold varied slightly between specimens, in order to perform the test with the same strain rate (100%/sec.), the gauge length of each

scaffold's specimen was measured with a caliper (mean and standard deviation of 5 measurements). The actuator rate was consequently adjusted for each specimen. The load-displacement curves were converted to stress-strain curves using the cross-section area measured before the test respectively for the PLLA single bundles and for the multiscale hierarchical scaffolds (Figure 6.4C and D). The following indicators were considered: Young Modulus, Yield Stress, Yield Strain, Failure Load, Failure Stress, Failure Strain, Work to Yield, Work to Failure (Figure 6.4 and Supporting Information Table 6.S1). The stress-strain curves were analyzed as described in the Supporting Information (Figure 6.S2).

6.3.5 Cell testing

Human non-tumoral fibroblasts (NTFs) from a single donor were kindly provided by Dr Vanessa Hearnden, University of Sheffield. These were obtained from waste tissue under informed consent, the procedure for which was approved by the National Health Service (NHS) Research Ethics committee (REC, 09/h1308/66). They were maintained in α-MEM culture medium (LonzaR, UK),
10% foetal bovine serum (FBS, Labtech, UK), 2 mM L-glutamine (Sigma Aldrich, UK) and 100mg/mL penicillin/streptomycin (Sigma Aldrich, UK). NTFs were cultured at 37°C in 5% CO2 in a humidified incubator. The cells were passaged in 75 cm2 tissue-culture flasks with media changes every 2-3 days. The cells were used between passage 4 and 6.

The PLLA multiscale hierarchical scaffolds were cut to 1 cm lengths and sterilized in 70 vol% ethanol for 1 hour. Before seeding the PLLA multiscale hierarchical scaffolds were rinsed 3 times in phosphate buffered saline (PBS) (Sigma Aldrich, UK) to remove any remaining ethanol. The PLLA multiscale hierarchical scaffolds were seeded with 200,000 cells at a density of 1,000,000 cells/mL in a 24 well plate. The PLLA multiscale hierarchical scaffolds were seeded with half of the 200,000 cells on the top surface then rotated and seeded with the remaining 100,000 cells on the bottom surface. The cells were left to attach to the scaffold for 45 minutes after which they were submerged in 1 mL of media.

On days 1, 7, 14 and 16 a resazurin reduction (RR) assay was performed to measure the cell viability as previously described [37]. The scaffolds were transferred to new

24 well plates before the assay was performed to ensure only the viability of cells attached to the PLLA multiscale hierarchical scaffold was measured. 1 mL of resazurin salt solution (0.1 mM in α-MEM) was added to each well and incubated for 4 hours. 200 microLiters of the reduced resazurin solution was transferred into a 96 well plate and the fluorescence measured at 540 nm excitation and 630 nm emission using a spectrofluorometer (FLX800, BIO-TEK instruments Inc., Winooski, VT, USA). The PLLA multiscale hierarchical scaffolds were then washed twice in PBS before 1 microliter of new media was added to the wells.

On day 14 of culture samples were fixed in 4 vol% formaldehyde for 30 minutes for histological analysis. The PLLA multiscale hierarchical scaffolds were placed in cassettes and ran through a tissue processor (Leica TP 1020, Wetzlar, GER), passing the samples though 70% industrial methylated spirits (IMS) for 1 hour twice followed by a sequential dehydration at 80%, 85%, 90%, 95% and 100% twice for 1.5 hours each. This was followed by clearing in Xylene twice for 1.5 hours then infiltrating with paraffin wax for 2 hours twice. The samples were then embedded in molten paraffin wax using an embedding center (Leica EG 1160, Wetzlar, Germany). The samples were then sectioned longitudinally at a thickness of 10 micrometers with a microtome (Leica RM2145, Wetzlar, Germany) and mounted onto glass slides. Following sectioning the samples were stained with haematoxylin and eosin.

6.4 Results and Discussion

6.4.1 Production process of the PLLA multiscale hierarchical salffold

In order to reproduce the complex hierarchical structure of the tendons and ligaments [4,5] (Figure 6.1A), we first produced PLLA single bundles mimicking the natural collagen fascicles, by means of electrospinning on a high-speed rotating drum collector (Figure 6.S1A). This process allowed production of bundles of aligned nanofibers of PLLA, similar to the fascicles composing tendons and ligaments [4–6] (Figure 6.1B). To produce a scaffold with a relevant section (e.g.

comparable to the antero-posterior thickness of the human Achille's tendon [38] or to the diameter of the anterior cruciate ligament [39]), we prepared groups of 100 bundles each with a length of 100 mm, aligned to each other and fixed at the extremities (Figure 6.S1B). To replicate the membrane wrapping the tendons and ligaments (respectively named epitenon and epiligament [4]), a non-aligned nanofibrous sheath was electrospun on the group of bundles (Figure 6.1C). Alternating rotations and stops while electrospinning the sheath allowed to stretch and wrap the nanofibers around the group of bundles. As a result, the sheath was able to reduce the multiscale hierarchical scaffolds' external diameter. This is a highly innovative method compared to previously developed sheaths [26,30,31,33,40] is expected to improve the overall mechanical properties of the structure. The final PLLA multiscale hierarchical scaffold had similar macroscopic dimensions, but also micro- and nano-structure and hierarchical organization similar to natural tendons and ligaments (Figure 6.1D).

6.4.2 Morphology of the PLLA bundles and multiscale hierarchical scaffold

In order to assess the morphology of the nanofibers, of the single bundles and of the entire PLLA multiscale hierarchical scaffold, we performed a scanning electron microscopy (SEM) (Figure 6.2). The SEM investigation showed that the PLLA single bundles and the sheaths were produced without significant defects. The nanofibers in the bundles showed a preferential direction, as desired to replicate the arrangement of the fibrils in the tendons and ligaments [41]. Conversely the nanofibers in the sheath were randomly arranged, similar to the natural epitenon and epiligament [4]. The nanofibers forming the single bundles and the sheath had similar diameters of 0.59±0.14 micrometers (Figure 6.2D-F). The single bundles had diameters of 586.5±38.0 micrometers (Figure 6.2C). The PLLA multiscale hierarchical scaffolds, had a mean diameter of 6.5±0.8 millimeters (Figure 6.2A and B). These dimensions are comparable to those found in the hierarchical organization of the fibrils and fascicles in the tendons and ligaments [4,5,38,39].

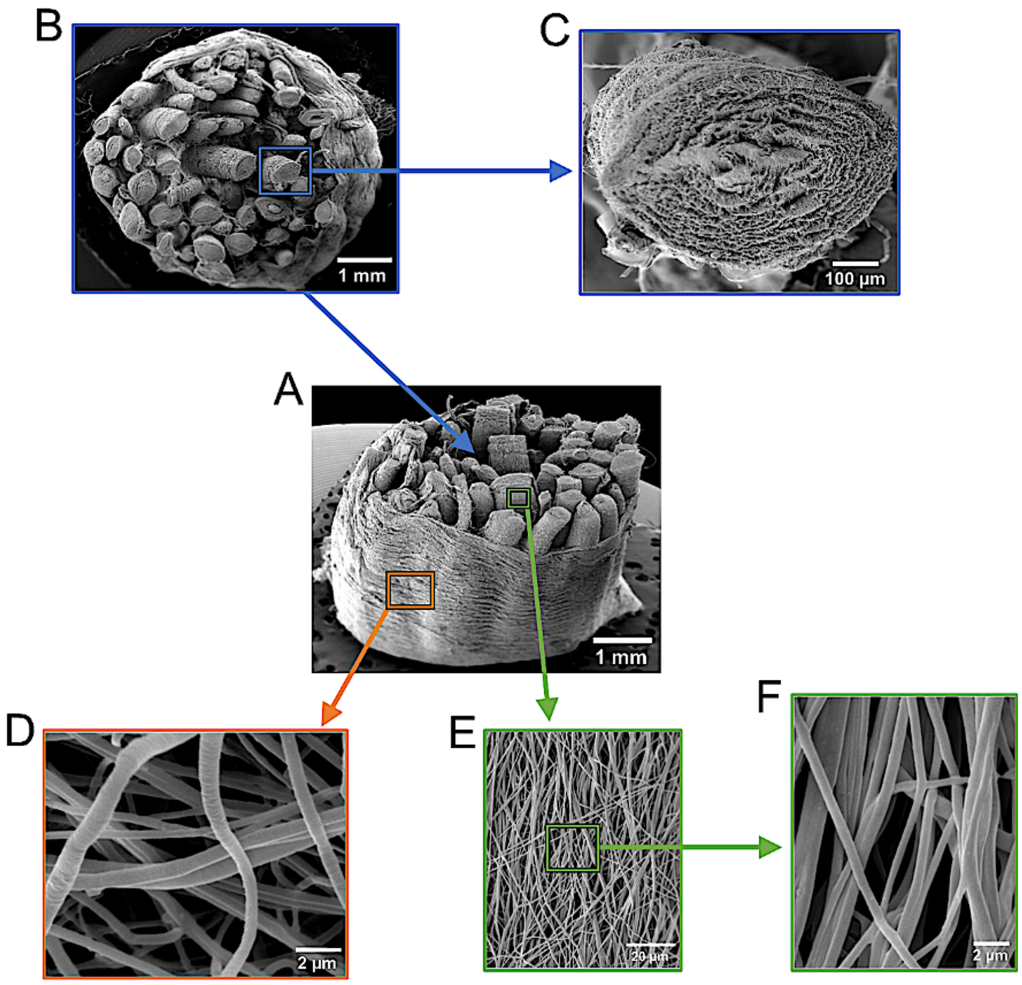

Figure 6.2. SEM images of the PLLA multiscale hierarchical scaffold. (A, B) Section of the PLLA multiscale hierarchical scaffold made of PLLA single bundles of aligned nanofibers with the random sheath epitenon/epiligament-like. (C) Section of a PLLA single bundle. (E, F) Aligned nanofibers on the surface of a PLLA single bundle at different magnifications. (G) PLLA nanofibers of the random sheath.

To investigate the arrangement of the nanofibers of the PLLA single bundles and of the multiscale hierarchical scaffold in the entire volume (rather than just on the surface, as with the SEM), we performed a high-resolution x-ray tomography (XCT) investigation (Figure 6.3). This technique has only recently become available at sub-micrometer resolution; it is extremely difficult to implement in on low-density materials such as the electrospun polymer fibers [15,22,42,43].

The XCT analysis showed that the internal multiscale morphology of the scaffolds was similar to that of tendon and ligament tissue [4,5]. This analysis confirmed a

preferential alignment of the nanofibers, which were predominantly close to the axis of the bundle, and with a Gaussian-like dispersion (Figure 6.3): 51.5% of the nanofibers lay within 15° from the axis of the bundle, while fewer than 7% were between 75° and 90° from the axis. This distribution of alignments resembles the natural alignment of collagen in tendons and ligaments [41]. Analyzing the PLLA multiscale hierarchical scaffolds with the XCT, we were able to confirm that all the bundles were tightly placed side by side, and were aligned along the axis of the scaffold. The twist angle was less than 3°. The external sheath was visible in the XCT images, it completely wrapped the PLLA multiscale hierarchical scaffold, and showed a porous structure.

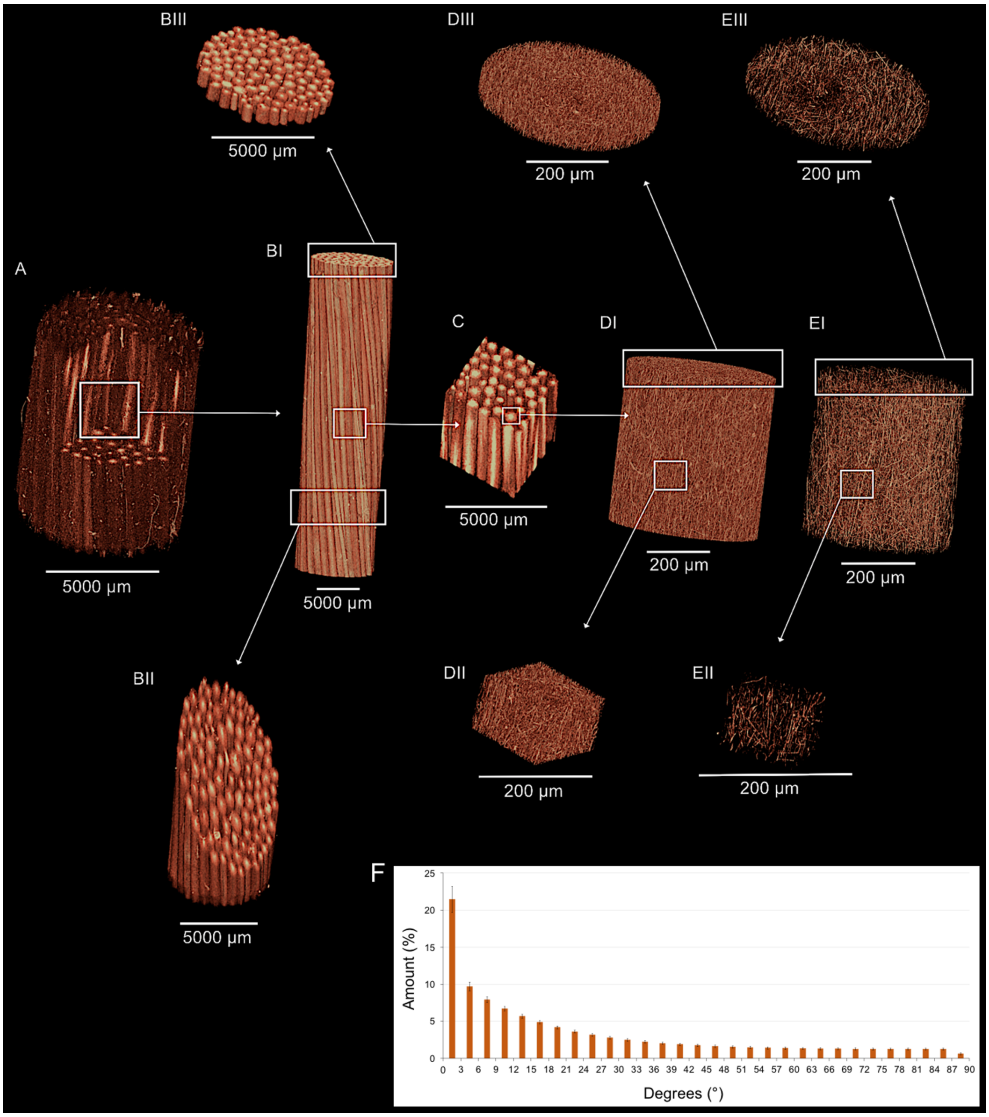

Figure 6.3. High-resolution x-ray tomographic images of the hierarchical structure of the PLLA multiscale hierarchical scaffold. (A) Section of a PLLA multiscale hierarchical scaffold in which

the random nanofibrous sheath and the internal single bundles are visible (voxel size: 8.5 micrometers). (BI) Section of a PLLA multiscale hierarchical scaffold in which the axially aligned single bundles are visible (voxel size: 20 micrometers). (BII, BIII) Crop of the PLLA multiscale hierarchical scaffolds showing a section of the internal single bundles (voxel size: 20 micrometers). (C) Crop of the internal part of the PLLA multiscale hierarchical scaffold with the single axially aligned bundles (voxel size: 20 micrometers). (DI) Section of a PLLA single bundle of axially aligned nanofibers (voxel size: 0.4 micrometers). (DII) Cubic crop of the PLLA single bundle showing also all the internal nanofibers axially aligned across the section (voxel size: 0.4 micrometers). (DIII) Circular slice of the PLLA single bundle with all the nanofibers (voxel size 0.4 micrometers). (EI, EII, EIII) By tuning the thresholding it is possible to display just the internal nanofibers of the PLLA single bundle (voxel size: 0.4 micrometers). (F) Percentage amount of nanofibers, in the PLLA single bundles, oriented in a specific range of angles (i.e. 0° = aligned with the axis of the PLLA single bundle; 90° represents the radial orientation).

6.4.3 Mechanical properties of the PLLA single bundles and of the multiscale hierarchical scaffold

To measure the mechanical properties of the PLLA single bundles and of the multiscale hierarchical scaffold, we performed tensile testing (Figure 6.4). To minimize stress concentrations at the extremities we designed a dedicated test including specific capstan fixtures for the PLLA single bundles and potted extremities for the multiscale hierarchical scaffolds. To replicate a relevant loading condition, we applied a monotonic stretch at a strain rate of 30%/second on the PLLA single bundles and of 100%/second on the multiscale hierarchical scaffold. These strain rates are in the range of those experienced by tendons and ligaments during strenuous physiological activities [44–47].

Both the PLLA single bundles and the multiscale hierarchical scaffolds showed a nonlinear toe region up to 2 - 5% strain, similar to the nonlinear behavior of natural fascicles of tendons and ligaments [3– 5]. After the toe region, both the PLLA single bundles and the multiscale hierarchical scaffolds exhibited an extensive linear elastic behavior (again, similar to the behavior of the natural tendons and ligaments). The modulus of elasticity of the PLLA single bundles was 157±39 MPa, whereas for the multiscale hierarchical scaffolds the modulus was 119±19MPa. The PLLA single bundles started yielding at 15.6±2.7 MPa, while the multiscale hierarchical scaffolds 5.8±0.9 MPa. After yield, both the PLLA single bundles and

the multiscale hierarchical scaffolds exhibited a ductile behavior, reaching high deformations (up to 30% strain) before failing. This provides a wide safety factor in case of partial damage, before catastrophic failure occurs. In fact, high energy was required to induce failure in both the PLLA single bundles and the multiscale hierarchical scaffolds (Supplementary Information Table 6.S1). Final failure of the PLLA single bundles occurred at 18.1±2.4 MPa and of the multiscale hierarchical scaffolds at 7.6±1.4 MPa.

For the PLLA single bundles, the stiffness was comparable to those of the fascicles of natural tendon (range: 40-400 MPa [5,48]) and ligament (range: 320-345 MPa [49]). The maximum stress of the PLLA single bundles was also comparable to the fascicles of natural tendons (range: 6-40 MPa [5,48]) and ligaments (range: 34-36 MPa [49]). The maximum deformation of the PLLA single bundles exceeded that of fascicles of natural tendon (range: 9-25 MPa [5,48]) and ligament (range: 14-15 MPa [49]). Therefore, the energy absorbed before failure of the PLLA single bundles (i.e. the work to failure) was also greater than for the natural fascicles. The PLLA multiscale hierarchical scaffold exhibited a similar stiffness to natural tendon (range: 65-3000 MPa [5,50]) and ligament (range: 20- 700 MPa [5,50]). The yield stress and failure stress of the PLLA multiscale hierarchical scaffold was lower that of natural tendon (range: 20-116 MPa [5,50]) and ligament (range: 1-46 MPa [5,50]). The maximum deformation of the PLLA multiscale hierarchical scaffolds was in the same range of the natural tendons (range: 14-59 MPa [5,50]) and ligaments (range: 8-120 MPa [5,50]). Considering the planned applications in reconstructive surgery, it is important that the PLLA multiscale scaffold has lower strength than natural tendons and ligaments; to avoid damage in the patient's repaired site in a case of overload, failure should initiate in the implanted device, rather than in the host tissue. As expected, the modulus of elasticity and the yield and failure stress in the multiscale scaffold was lower than for the single bundles. This has a simple explanation: the stress in the multiscale scaffold is calculated over the total cross-sectional area (which includes the actual cross section of the bundles, but also some unavoidable empty space). Furthermore, the system used for clamping the extremities of the multiscale scaffold caused some stress concentration (in fact the scaffolds started failing at the one of the extremities)

whereas loading on the single bundles prevented such artifact (in fact all the single bundles failed in the central portion of the specimen).

In the destructive tests on the multiscale scaffolds the external sheath contained and kept together the bundles after the individual ones began to fail. This effect provided better structural behavior of the scaffold. Most previous scaffolds for tendon and ligament replacements consist of braided, twisted or knitted fibers [23,26–29], which do not replicate the morphology of natural tissue. Compared to previous solutions featuring a multiscale structure, our approach allowed a better compaction of the single bundles in the multiscale hierarchical scaffold [23,26–29], thus providing optimal compromise between morphology and mechanical properties. Not surprisingly, most of the scaffolds developed in the past focused on the regeneration of peripheral nerves, where mechanical strength is not a critical requirement [33]. The porous sheath of random nanofibers also allowed cell growth, and in the long term can allow cell migration inside the scaffold.

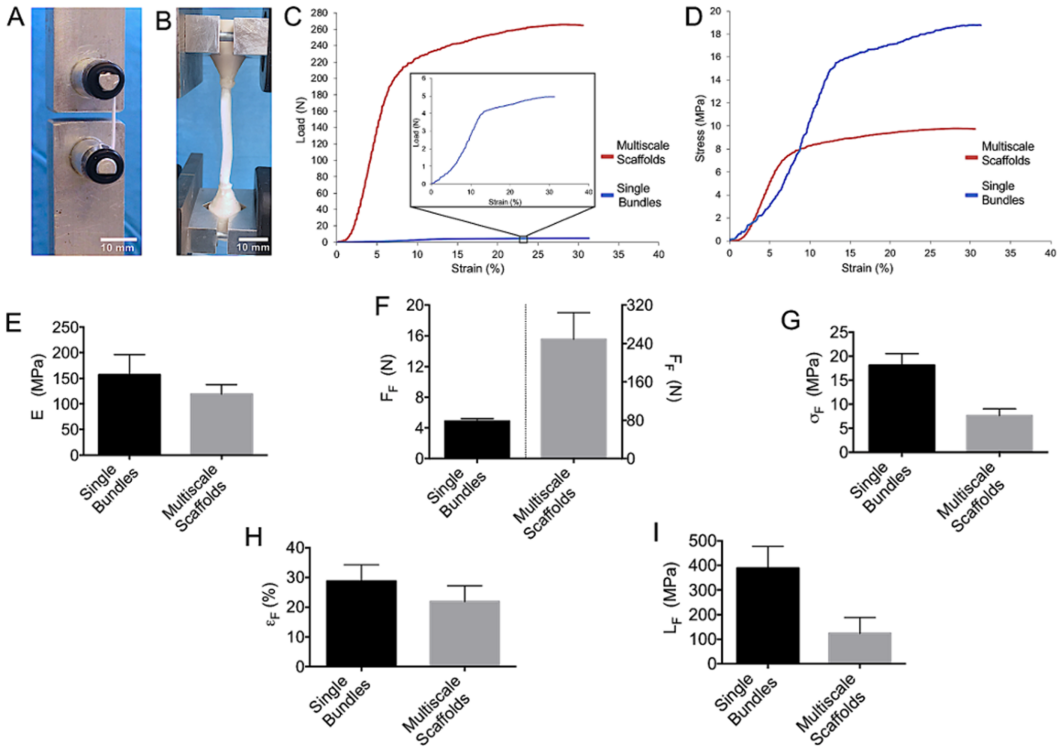

Figure 6.4. Mechanical characterization of the PLLA single bundles and the multiscale hierarchical scaffolds. (A) Capstan grips designed for testing the PLLA single bundles. (B) Setup for the mechanical tests on the PLLA multiscale hierarchical scaffolds. (C) Example load-strain curves of the PLLA multiscale hierarchical scaffold and the PLLA single bundles (square: zoom-in of the

PLLA single bundle curve). (D) Example stress-strain curves of the PLLA multiscale hierarchical scaffold and the PLLA single bundle. Comparison of the mechanical properties between PLLA single bundles and multiscale hierarchical scaffolds: (E) Young modulus (E); (F) load to failure (F_F) (left axis refers to the PLLA single bundles, right axis to the PLLA multiscale hierarchical scaffolds); (G) failure stress (σ_F); (H) failure strain (e_F) and (I) work to failure (L_F).

6.4.4 Cell viability

To evaluate the suitability of the PLLA multiscale hierarchical scaffolds for cell culture, resazurin reduction assays were performed on days 1, 7, 14 and 16 (Figure 6.5). The PLLA multiscale hierarchical scaffolds showed an increase in cell viability between day 1 and 16, suggesting an increase in the number of cells present on the scaffolds by day 16. To assess the cells spatial distribution and morphology within the PLLA multiscale hierarchical scaffolds, histological sectioning with haematoxylin and eosin staining was performed (Figure 6.5). Sections were analyzed at the seeded surfaces, the side 'walls' and the core of the PLLA multiscale hierarchical scaffolds. Cells were present in all regions of the PLLA multiscale hierarchical scaffold, suggesting cells were capable of penetrating into the interior region of the scaffold from the upper and lower seeded surfaces. Cells can be seen growing into the fibers of the PLLA multiscale hierarchical scaffolds in the sections taken from the side of the scaffolds. However, within the core of the PLLA multiscale hierarchical scaffold cells were densely packed between the individual fibers of the scaffold imitating the interfascicular matrix of native tendon, which had been shown to play an important role in the sliding mechanisms of tendon [51–53].

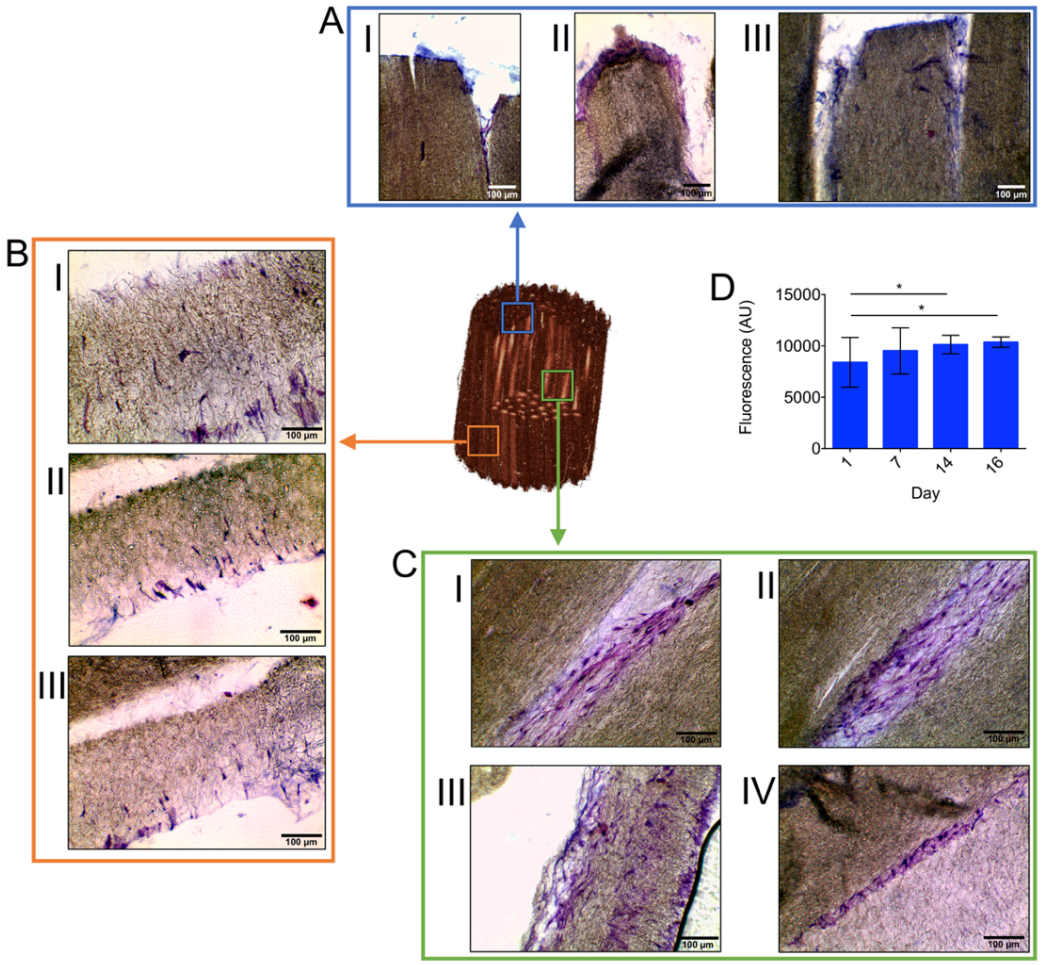

Figure 6.5. Cell viability test. Haematoxylin and eosin stained sections of different regions of the PLLA multiscale hierarchical scaffolds after 14 days of culture. (AI, AII, AIII) The upper surface of the specimens showing cells on the exterior surface. (BI, BII, BIII) Cells can be seen penetrating into the multiscale hierarchical scaffold structure (top of the images: interior region of the multiscale hierarchical scaffold; bottom of the images: external region). (CI, CII, CIII, CIV) Internal core section of the PLLA multiscale hierarchical scaffold, highlighting the cells aligning between the internal single bundles. (D) Resazurin reduction assay at different time points. Statistical analysis was performed using one-way analysis of variance (ANOVA) followed by Tukey post-hoc test (* $P \leq 0.05$).

6.5 Conclusion

We have developed an innovative method to produce a scaffold for the repair and regeneration of tendons and ligaments. We used high-resolution x-ray tomography to investigate the morphology of the PLLA single bundles and of the PLLA multiscale hierarchical scaffold, from nano- to micrometric resolution. Our

hierarchical approach allowed mimicking of the multiscale arrangement of the collagen fibrils and fascicles in the ligaments and tendons. Moreover, the developed scaffold provided comparable stiffness to the natural tendons and ligaments. As required by safety criteria for implantable materials and devices, the strength of our multiscale scaffold was slightly lower than that of the natural tissues where it would be hosted. We demonstrated that the porous sheath of random nanofibers allowed cell growth and migration in the interior of the scaffold after 14 days of cell culture in static conditions, thus providing an ideal environment for cell proliferation. While so far we focused on pure PLLA constructs, this technological platform can be applied to a broad spectrum of synthetic and natural polymers to customize scaffold properties for specific patients and applications.

6.6 Supplementary informations

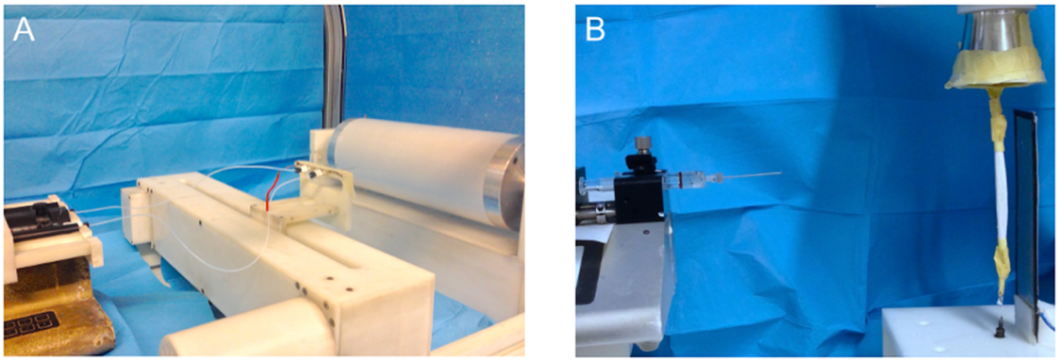

Figure 6.S1. Electrospinning machine for nanofibrous bundles production and sheath setup. (A) Electrospinning machine for bundles production. The pump-driven syringes are visible on the left. The two needles were mounted on a motorized sliding spinneret (at the center of the picture) and were connected to a positive high-voltage source. The high-speed rotating drum collector (visible on the right) was connected to the ground. (B) Electrospinning setup for the sheath production. A syringe pump electrospun the nanofibers towards a plate ground collector behind the scaffold. The multiscale scaffold is put in rotation by the upper cup.

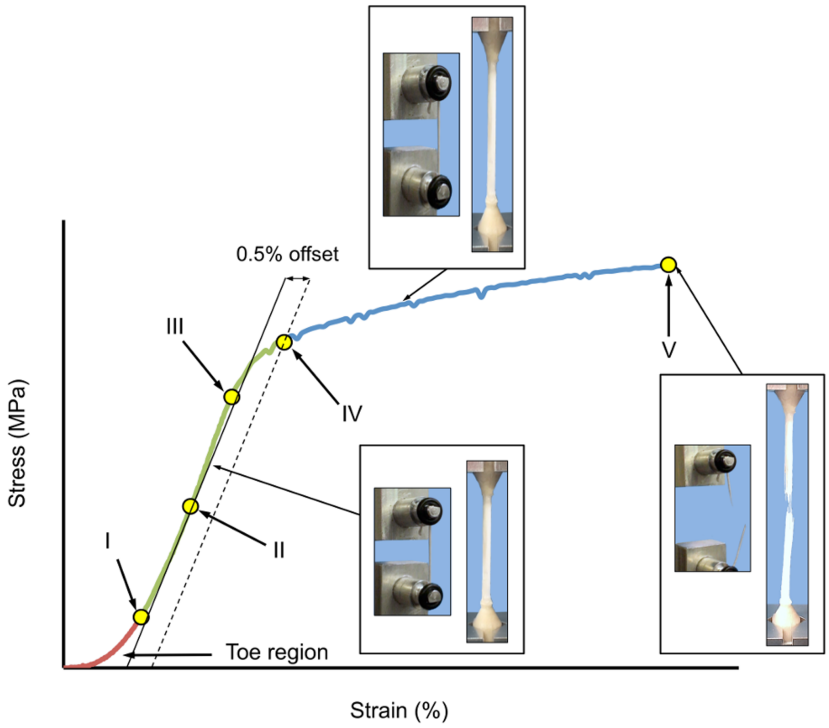

Figure 6.S2. Post processing of the stress-strain curves. The initial toe region was disregarded; the failure stress (V) was identified as the highest stress in the entire curve; the starting point of the linear region (I) was univocally identified as 20% of failure stress; an initial guess for the yield strain was visually identified (III); the initial linear regression (solid line) was applied to the first 50% of the linear region, between points (I) and (II) (which was half-way between I and III); a second line parallel to the initial regression was drawn with an offset of 0.5% strain (dashed line); the limit of proportionality was defined with the 0.5%-strain offset criterion as the intersection (IV) between the latter line and the stress-strain curve; the Young modulus was calculated as the slope of a new regression line between (I) and (IV). The work to yield and to failure were calculated as the integrals under the curves (with the method of trapezoids). The three squares show a bundle and a PLLA multiscale scaffold during the test (from left to right: linear line; yield; failure).

Table 6.S1. Comparison of the mechanical properties between the PLLA single bundles and the multiscale hierarchical scaffolds.

	Diameter (mm)	Young Modulus (MPa)	Yield Stress (MPa)	Yield Strain (%)	Failure Load (N)	Failure Stress (MPa)	Failure Strain (%)	Work to Yield (J/mm^3)	Work to Failure (J/mm^3)
Single Bundles	0.58±0.04	156.9±39.4	15.6±2.7	13.9±1.4	4.9±0.3	18.1±2.4	28.8±5.5	0.1±0.02	0.39±0.09
Multiscale Scaffolds	6.5±0.8	118.7±18.8	5.8±0.9	7.6±2.3	248.5±56.1	7.6±1.4	21.9±5.4	0.02±0.003	0.12±0.06

6.7 References

[1] Liu C F, Aschbacher-Smith L, Barthelery N J, Dyment N, Butler D and Wylie C 2011 What We Should Know Before Using Tissue Engineering Techniques to Repair Injured Tendons: A Developmental Biology Perspective Tissue Eng. Part B Rev. 17 165–76

[2] Rees J D, Wilson A M and Wolman R L 2006 Current concepts in the management of tendon disorders Rheumatology 45 508–21

[3] Woo S L Y, Abramowitch S D, Kilger R and Liang R 2006 Biomechanics of knee ligaments: Injury, healing, and repair J. Biomech. 39 1–20

[4] Kannus P 2000 Structure of the tendon connective tissue Scand. J. Med. Sci. Sport. 10 312–20

[5] Goh K L, Listrat A and Béchet D 2014 Hierarchical mechanics of connective tissues: Integrating insights from nano to macroscopic studies J. Biomed. Nanotechnol. 10 2464–507

[6] Hampson K, Forsyth N R, El Haj A and Maffulli N 2008 Tendon Tissue Engineering Topics in Tissue Engineering vol 4, ed N Ashammakhi, R Reis and F Chiellini pp 1–21

[7] James S L, Bates B T, Osternig L R and Oregon E 1978 Injuries to runners Am. J. Sports Med. 6 40–50

[8] Dy C J, Daluiski A, Do H, Hernandez-Soria A, Marx R and Lyman S 2012 The Epidemiology of Reoperation After Flexor Tendon Repair J. Hand Surg. Am. 37A 919–24

[9] Lomas A J, Ryan C N M, Sorushanova A, Shologu N, Sideri A I, Tsioli V, Fthenakis G C, Tzora A, Skoufos I, Quinlan L R, O'Laighin G, Mullen A M, Kelly J L, Kearns S, Biggs M, Pandit A and Zeugolis D I 2015 The past, present and future in scaffold-based tendon treatments Adv. Drug Deliv. Rev. 84 257–77

[10] Sharma P and Maffulli N 2005 Tendon Injury and Tendinopathy: Healing and Repair J. Bone Jt. Surg. 87 187

[11] Verdiyeva G, Koshy K, Glibbery N, Mann H and Seifalian A M 2015 Tendon reconstruction with tissue engineering approach - A review J. Biomed. Nanotechnol. 11 1495–523

[12] Liu Y, Ramanath H S and Wang D A 2008 Tendon tissue engineering using scaffold enhancing strategies Trends Biotechnol. 26 201–9

[13] Mo X, Wu T, Sun B and El-Hamshary H 2017 Nanofiber composites in tendon tissue engineering Nanofiber Composites for Biomedical Applications ed M Ramalingam and S Ramakrishna (Elsevier) pp 345–67

[14] Sensini A, Gualandi C, Cristofolini L, Tozzi G, Dicarlo M, Teti G, Belmonte-Mattioli M and Focarete M L 2017 Biofabrication of bundles of poly (lactic acid) -collagen blends mimicking the fascicles of the human Achille tendon Biofabrication 9 1–13

[15] Sensini A, Cristofolini L, Focarete M L, Belcari J, Zucchelli A, Kao A and Tozzi G 2018 High-resolution x-ray tomographic morphological characterisation of electrospun nanofibrous bundles for tendon and ligament regeneration and replacement J. Microsc.

[16] Sensini A and Cristofolini L 2018 Biofabrication of Electrospun Scaffolds for the Regeneration of Tendons and Ligaments Materials (Basel). 11 1963

[17] Pedde R D, Mirani B, Navaei A, Styan T, Wong S, Mehrali M, Thakur A, Mohtaram N K, Bayati A, Dolatshahi-Pirouz A, Nikkhah M, Willerth S M and Akbari M 2017 Emerging Biofabrication Strategies for Engineering Complex Tissue Constructs Adv. Mater. 29 1–27

[18] Santos M L, Rodrigues M T, Domingues R M A, Reis R L and Gomes M E 2017 Regenerative Strategies for the Treatment of Knee Joint Disabilities Regenerative Strategies for the Treatment of Knee Joint Disabilities vol 21, ed J M Oliveira and R L Ruis (Springer International Publishing) pp 349–71

[19] Ali U, Zhou Y, Wang X and Lin T 2011 Electrospinning of Continuous Nanofiber Bundles and Twisted Nanofiber Yarns Nanofibers - Prod. Prop. Funct. Appl. 153–74

[20] O'Connor R A and McGuinness G B 2016 Electrospun nanofibre bundles and yarns for tissue engineering applications: A review Proc. Inst. Mech. Eng. Part H J. Eng. Med. 230 987–98

[21] Bosworth L A, Alam N, Wong J K and Downes S 2013 Investigation of 2D and 3D electrospun scaffolds intended for tendon repair J. Mater. Sci. Mater. Med. 24 1605–14 Bosworth L A, Rathbone S R, Bradley R S and Cartmell S H 2014 Dynamic loading of

[22] electrospun yarns guides mesenchymal stem cells towards a tendon lineage J. Mech. Behav. Biomed. Mater. 39 175–83

[23] Bosworth L A 2014 Travelling along the Clinical Roadmap: Developing Electrospun Scaffolds for Tendon Repair Conf. Pap. Sci. 2014 1–6

[24] Xu Y, Wu J, Wang H, Li H, Di N, Song L, Li S, Li D, Xiang Y, Liu W, Mo X and Zhou Q 2013 Fabrication of Electrospun Poly(L-Lactide-co-ε-Caprolactone)/Collagen Nanoyarn Network as a Novel, Three-Dimensional, Macroporous, Aligned Scaffold for Tendon Tissue Engineering Tissue Eng. Part C Methods 19 925–36

[25] Pauly H M, Kelly D J, Popat K C, Trujillo N A, Dunne N J, McCarthy H O and Haut Donahue T L 2016 Mechanical properties and cellular response of novel electrospun nanofibers for ligament tissue engineering: Effects of orientation and geometry J. Mech. Behav. Biomed. Mater. 61 258–70

[26] Banik B L, Lewis G S and Brown J L 2016 Multiscale Poly-(ε-caprolactone) Scaffold Mimicking Non-linearity in Tendon Tissue Mechanics Regen. Eng. Transl. Med. 2 1–9

[27] Xu Y, Dong S, Zhou Q, Mo X, Song L, Hou T, Wu J, Li S, Li Y, Li P, Gan Y and Xu J 2014 The effect of mechanical stimulation on the maturation of TDSCs-poly(L-lactide-co-e-caprolactone)/collagen scaffold constructs for tendon tissue engineering Biomaterials 35 2760–72

[28] Mouthuy P-A, Zargar N, Hakimi O, Lostis E and Carr A 2015 Fabrication of continuous electrospun filaments with potential for use as medical fibres. Biofabrication 7 25006

[29] Laranjeira M, Domingues R M A, Costa-Almeida R, Reis R L and Gomes M E 2017 3D Mimicry of Native-Tissue-Fiber Architecture Guides Tendon-Derived Cells and Adipose Stem Cells into Artificial Tendon Constructs Small 13 1–13

[30] Zhou F L, Gong R-H and Porat I 2010 Nano-coated hybrid yarns using electrospinning Surf. Coatings Technol. 204 3459–63

[31] Naghashzargar E, Farè S, Catto V, Bertoldi S, Semnani D, Karbasi S and Tanzi M C 2015 Nano/micro hybrid scaffold of PCL or P3HB nanofibers combined with silk fibroin for tendon and ligament tissue engineering J. Appl. Biomater. Funct. Mater. 13 e156–68

[32] Padmakumar S, Joseph J, Neppalli M H, Mathew S E, Nair S V., Shankarappa S A and Menon D 2016 Electrospun Polymeric Core-sheath Yarns as Drug Eluting Surgical Sutures ACS Appl. Mater. Interfaces 8 6925–34

[33] Li D, Pan X, Sun B, Wu T, Chen W, Huang C, Ke Q, EI-Hamshary H A, Al-Deyab S S and Mo X 2015 Nerve conduits constructed by electrospun P(LLA-CL) nanofibers and PLLA nanofiber yarns J. Mater. Chem. B 3 8823–31

[34] Liu Z 1991 Scale space approach to directional analysis of images Appl. Opt. 30 1369–73

[35] Schindelin J, Arganda-Carreras I, Frise E, Kaynig V, Longair M, Pietzsch T, Preibisch S, Rueden C, Saalfeld S, Schmid B, Tinevez J-Y, White D J, Hartenstein V, Eliceiri K, Tomancak P and Cardona A 2012 Fiji: an open-source platform for biological-image analysis. Nat. Methods 9 676–82

[36] Schneider C A, Rasband W S and Eliceiri K W 2012 NIH Image to ImageJ: 25 years of image analysis Nat. Methods 9 671–5

[37] O'Brien J, Wilson I, Orton T and Pognan F 2000 Investigation of the Alamar Blue (resazurin) fluorescent dye for the assessment of mammalian cell cytotoxicity Eur. J. Biochem. 267 5421–6

[38] Pang B S and Ying M 2006 Sonographic measurement of Achilles tendons in asymptomatic subjects. J. ultrasound Med. 25 1291–6

[39] Triantafyllidi E, Paschos N K, Goussia A, Barkoula N M, Exarchos D A, Matikas T E, Malamou-Mitsi V and Georgoulis A D 2013 The shape and the thickness of the anterior cruciate ligament along its length in relation to the posterior cruciate ligament: A cadaveric study Arthrosc. - J. Arthrosc. Relat. Surg. 29 1963–73

[40] Kohlman L W and Roberts G D 2015 Method for coating tow with an electrospun nanofiber 12–5

[41] Radaelli F, D'Alfonso L, Collini M, Mingozzi F, Marongiu L, Granucci F, Zanoni I, Chirico G and Sironi L 2017 μMAPPS: a novel phasor approach to second harmonic analysis for in vitro-in vivo investigation of collagen microstructure Sci. Rep. 7 17468

[42] Bradley R S, Robinson I K and Yusuf M 2017 3D X-Ray Nanotomography of Cells Grown on Electrospun Scaffolds Macromol. Biosci. 17 1–8

[43] Maksimcuka J, Obata A, Sampson W W, Blanc R, Gao C, Withers P J, Tsigkou O, Kasuga T, Lee P D and Poologasundarampillai G 2017 X-ray Tomographic Imaging of Tensile Deformation Modes of Electrospun Biodegradable Polyester Fibers Front. Mater. 4 1–11

[44] Butler D L 1989 Anterior cruciate ligament: its normal response and replacement J. Orthop. Res. 7 910–21

[45] Lewis G and Shaw K M 1997 Tensile properties of human tendo Achillis: effect of donor age and strain rate. J. Foot Ankle Surg. 36 435–45

[46] Wren T A ., Yerby S A, Beaupré G S and Carter D R 2001 Mechanical properties of the human achilles tendon Clin. Biomech. 16 245–51

[47] Lee M and Hyman W 2002 Modeling of failure mode in knee ligaments depending on the strain rate BMC Musculoskelet. Disord. 3 1–8

[48] Hanson P, Aagaard P and Magnusson S P 2012 Biomechanical properties of isolated fascicles of the Iliopsoas and Achilles tendons in African American and Caucasian men Ann. Anat. 194 457–60

[49] Butler D L, Kay M D and Stouffer D C 1986 Fascicle-Bone Units From Human Patellar Tendon and Knee Ligaments J. Biomech. 19 425–32

[50] Murphy W, Black J and Hastings G 2016 Handbook of Biomaterial Properties ed W Murphy, J Black and G Hastings (Springer)

[51] Spiesz E M, Thorpe C T, Chaudhry S, Riley G P, Birch H L, Clegg P D and Screen H R C 2015 Tendon extracellular matrix damage, degradation and inflammation in response to in vitro overload exercise J. Orthop. Res. 33 889–97

[52] Spiesz E M, Thorpe C T, Thurner P J and Screen H R C 2018 Structure and collagen crimp patterns of functionally distinct equine tendons, revealed by quantitative polarised light microscopy (qPLM) Acta Biomater. 70 281–92

[53] Thorpe C T and Screen H R C 2016 Metabolic Influences on Risk for Tendon Disorders 920 3–10

Chapter 7: Morphologically bioinspired hierarchical Nylon 6,6 electrospun assembly recreating the structure and performance of tendons and ligaments

Alberto Sensini[1], Carlo Gotti[1], Juri Belcari[1], Andrea Zucchelli[1], Maria Letizia Focarete[2,3], Chiara Gualandi[2,4], Ivan Todaro[1], Alexander P. Kao[5], Gianluca Tozzi[5], Luca Cristofolini[1,3]

1 Department of Industrial Engineering, Alma Mater Studiorum—University of Bologna, I-40131 Bologna, Italy

2 Department of Chemistry 'G. Ciamician' and National Consortium of Materials Science and Technology (INSTM, Bologna RU), Alma Mater Studiorum—University of Bologna, I-40126 Bologna, Italy

3 Health Sciences and Technologies—Interdepartmental Center for Industrial Research (CIRI-HST), Alma Mater Studiorum—University of Bologna, I-40064 Ozzano dell'Emilia, Bologna, Italy

4 Advanced Mechanics and Materials – Interdepartmental Center for Industrial Research (CIRI-MAM), Alma Mater Studiorum—University of Bologna, I-40123 Bologna, Italy

5 Zeiss Global Centre, School of Mechanical and Design Engineering, University of Portsmouth, Portsmouth PO1 3DJ, United Kingdom

Keywords: Bioinspired Structures; Electrospinning; Hierarchical Devices; Tendons and Ligaments.

The candidate is the main author of the study. The work is under revision at Medical Engineering &Physics.

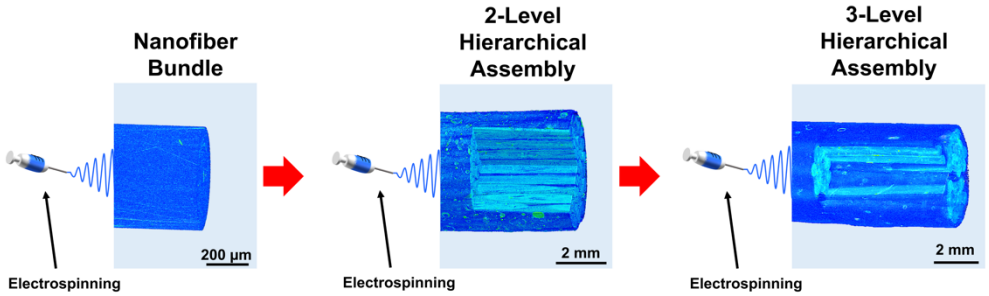

Graphical abstract of the work.

Under revision at Medical Engineering & Physics

7.1 Abstract

Reconstructions of ruptured tendons and ligaments currently have dissatisfactory failure rate. Failures are mainly due to the mechanical mismatch of commercial implants with respect to the host tissue. In fact, it is crucial to replicate the morphology (hierarchical in nature) and mechanical response (highly-nonlinear) of natural tendons and ligaments. The aim of this study was to develop morphologically bioinspired hierarchical Nylon 6,6 electrospun assemblies recreating the structure and performance of tendons and ligaments. First, we built different electrospun bundles to find the optimal orientation of the nanofibers. A 2-level hierarchical assembly was fabricated with a dedicated process that allowed tightly joining the bundles one next to the other with an electrospun sheath, so as to improve the mechanical performance. Finally, a further hierarchical 3- level assembly was constructed by grouping several 2-level assemblies. The morphology of the different structures was assessed with scanning electron microscopy and high-resolution X-ray tomography, which allowed measuring the directionality of the nanofibers in the bundles and in the sheaths. The mechanical properties of the single bundles and of the 2-level assemblies were measured with tensile tests. The single bundles and the hierarchical assemblies showed morphology and directionality of the nanofibers similar to the tendons and ligaments. The strength and stiffness were comparable to that of tendons and ligaments. In conclusion this work showed an innovative electrospinning production process to build nanofibrous Nylon 6,6 hierarchical assemblies, suitable as future implantable devices, able to mimic the multiscale morphology and the biomechanical properties of tendons and ligaments.

7.2 Introduction

The design and development of innovative solutions to repair or substitute injured tendons and ligaments is one of extreme interest in orthopaedic research. In fact, approximately 30 million new cases of tendon and ligament injuries are diagnosed worldwide annually [1]. From over 33 million musculoskeletal injuries per year in the United States alone, almost 50% of them are tendon and ligament related, with

about 95,000 new cases annually [2]. The difficulty in healing these tissues is mainly related to their non-linear mechanical properties and complex hierarchical structure, composed of collagen fibers that are axially aligned and organized in different levels of aggregation [3–5]. Above all, due to low cellular activity, the injuries of elderly people, generally require the use of permanent inert prosthetic devices [6–8].

The most popular examples of inert devices for tendon and ligament are Lars® Ligament, Leeds-Keio® (i.e. Poly-tape®) and Gore-Tex® [9]. In the last two decades, several studies published in literature have assessed the clinical quality of these devices [8]. However, even if they have adequate mechanical behavior, compared to the native tendon or ligament tissue, they have a different morphology and are not hierarchically structured. The Lars® Ligament is composed of aligned microfibers grouped together by an external knitted membrane; Leeds-Keio® (i.e. Poly-tape®) is a totally knitted/waved microfibrous device; while Gore-Tex® is made of groups of aligned microfibers braided together to obtain the final device. However, all these textile patterns produce implantable devices have a very different morphology when compared to a natural tendon or ligament [10]. In fact, tendon or ligament tissue is composed of collagen nanofibers preferentially axially aligned, organized in different levels of aggregation and covered by membranes of randomly arranged collagen nanofibers [3,4,11]. The lack of bioinspired hierarchical organization of these implantable devices, is often cause inflammatory outcomes and post-operative complications [8,9]. Furthermore, several clinical follow-ups of such devices, have shown controversial outcomes, in terms of failure or success over a long-term period. Among the others, Lars® Ligament showed the most promising results for long term positive outcomes of the implants and low incidence of revision surgery in Anterior Cruciate Ligament (ACL) applications [12]. However minor episodes of knee stiffness and synovitis were documented in the past [8,12,13]. The published studies about the clinical performances in ACL reconstruction using the Leeds-Keio®, despite several positive results, showed frequent events of re-rupture, tunnel enlargement, synovitis associated with polyester particles, greater pivot-shift and laxity, especially until the early 2000ies [14–17]. Moreover different applications of this device were explored to repair

other tendons and ligaments such as rotator cuff, knee extensor, Achilles tendon, iliofemoral ligament and ankle lateral ligament [8]. Gore-Tex® devices showed satisfactory results to treat very large rotator cuff tears and patellar reconstructions [18,19] but, due to severe osteolytic complications, were completely abandoned for ACL applications [8,20,21].

A promising approach to overcome the morphological and mechanical limitations of these devices is offered by the electrospinning technology. Producing polymeric nanofibers, by stretching solutions in high electrostatic fields, the electrospinning technique has demonstrated the ability to fabricate scaffolds that mimic the tendon and ligament tissue [22,23]. However, so far no one have demonstrated the possibility to obtain electrospun complex assemblies that reproduce the hierarchical structure and mechanical properties of a whole tendon or ligament yet [24].

The aim of this study was to develop morphologically bioinspired hierarchical assemblies (made of inert Nylon 6,6) to replicate the biomechanical response of natural tendon and ligament. For this reason, three levels of aggregation were investigated: (i) bundles of random and aligned electrospun nanofibers; (ii) a 2-level hierarchical assembly built using the most promising type of bundles (aligned nanofibers); (iii) a 3-level hierarchical assembly containing several 2-levels hierarchical assemblies. For all of these structures, the morphology and the associated mechanical properties were investigated.

7.3 Materials and methods

In order to develop a complex hierarchical structure, in the first phase two different methods for producing electrospun bundles were developed: in one instance, the nanofibers were randomly aligned, while in the second instance a high alignment of the nanofibers was achieved. The morphology of the Bundles was characterized with Scanning Electron Microscopy (SEM) and High-Resolution X-ray Computed Tomography (XCT); mechanical tests were performed to assess the strength and modulus of elasticity of the constructs. The most promising candidates (bundles of aligned nanofibers) were used to produce the 2-level hierarchical assemblies, which were again characterized in terms of morphology and mechanical properties. The

3-level hierarchical assembly was built by joining three 2-level hierarchical assemblies, and its morphology was fully characterized.

7.3.1 Materials

Nylon 6,6 pellets, kindly provided by DuPont (Wilmington, USA), were dissolved in a trifluoroacetic acid (TFA) (Carlo Erba, Milan, Italy) and acetone (AC) (Sigma Aldrich, Saint-Louis, USA) mixture, in order to obtain the following solution: 15% (w/v) solution of Nylon 6,6 dissolved in TFA:AC = 50:50 (v/v).

7.3.2 Identification of optimal electrospun bundle preparation

7.3.2.1 Electrospun bundles production

Electrospun bundles were produced using a laboratory electrospinning machine (Spinbow Lab Unit, Spinbow S.r.1., Bologna, Italy), equipped with a linear sliding spinneret (carrying four syringes ejecting the same polymeric solution) and a rotating drum collector (diameter = 150 mm; length = 500 mm). A syringe pump (KD Scientific 200 series, Illinois, USA) and four glass syringes were used to electrospin the solution. Each syringe was connected to a stainless-steel blunt-ended needle (inner diameter = 0.84 mm) with a PTFE tube. The electrospinning was performed at room temperature (RT) and relative humidity 20-30%. The solution was electrospun with an applied voltage of 20 kV and a feed rate of 0.50 mL h^{-1}. The drum collector was positioned 160 mm away from the needle tips. The sliding spinneret with the four needles had an excursion of 100 mm, with a sliding speed of 1200 mm min^{-1}. The mats of nanofibers were cut circumferentially into strips.

In order to reach the best configuration in terms of fiber orientation and mechanical properties, different electrospun bundles were produced. Bundles made of random fibers were obtained by rotating the drum collector with a low peripheral speed of 0.78 m s^{-1} and for an electrospinning time of 1.5 hours (Figure 7.1A). The mats of random nanofibers were cut into 70 mm wide strips, and manually wrapped to produce bundles, with a cross-sectional diameter of approximately 550-650

micrometers. At the end of the procedure, the bundles (about 470 mm in length) were cut in an extremity and removed from the collector (Figure 7.1A).

However, in order to improve the mechanical properties of the random bundles (see results section), bundles of aligned nanofibers were produced. To obtain mats of nanofibers preferentially aligned in the direction of drum rotation, the drum collector was rotated with a higher peripheral speed of 22.8 m s^{-1} during an electrospinning time of 3 hours. The mats of aligned nanofibers were cut into 50 mm wide strips, and rolled on the drum as previously described.

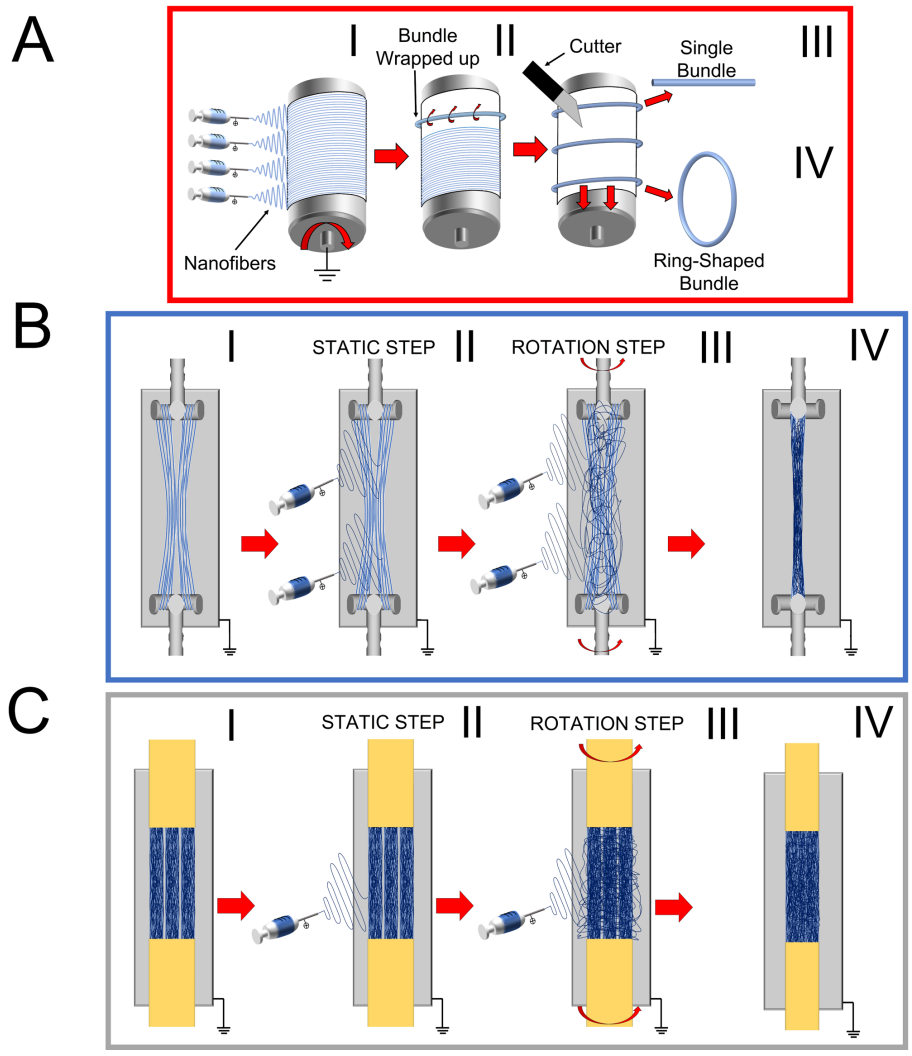

Figure. 7.1 Electrospinning setups and procedures to produce the bundles and the hierarchical devices. A) Bundles production: I) random or aligned nanofibers were electrospun on the rotating drum collector; II) mats of nanofibers cut in strips and manually wrapped to obtain the bundles; III) Some bundles were cut for remove them from the drum (single bundles); IV) other bundles were removed from the drum without cutting (ring-shaped bundles). B) 2-level hierarchical assembly

production: I) ring- shaped bundles of aligned nanofiber were hooked on the 6-arms capstan grip; II) electrospun sheath production during the static step; III) during the rotation step the mat of nanofibers was torn from one side of the collector and wrapped around the group of bundles; IV) final 2-level hierarchical assembly ready to be tested. B) 3-level hierarchical assembly production: I) three 2-level hierarchical assembly grouped together; II) electrospun sheath production during the static step; III) during the rotation step the mat of nanofibers was torn from one side of the collector and wrapped around the group of 2-level hierarchical assembly; IV) final 3-level hierarchical assembly ready to be characterized.

7.3.2.2 Morphological investigation of the bundles

To examine the surface morphology of the Nylon 6,6 bundles, Scanning Electron Microscopy (SEM) analysis was performed. A commercial SEM (Philips 515 SEM, Amsterdam, Netherlands) was used with a voltage of 15 kV, on samples sputter-coated with gold. The distribution of fiber diameters (mean and SD) was measured on the SEM images of about 200 fibers, by means of an image analysis software ImageJ [25].

In order to investigate also the three-dimensional structure of the Nylon 6,6 bundles, high-resolution x-ray tomographic scans were acquired with a laboratory XCT (Versa 510, Zeiss, Pleasanton, CA, USA). For the XCT scans, the following settings were used: 40 kV Voltage, 3 W Power, 75.5 microAmpere tube current. Projections were collected at rotational steps of 0.18° over 360°, with a voxel size 0.4 micrometers, using 14 second exposure time (scanning time of approximately 10 hours).

All the XCT images, were reconstructed using the Scout-and-Scan Reconstructor software (Zeiss), and were visualized using XM3DViewer1.2.8 software (Zeiss).

7.3.2.3 Directionality of the nanofibers in the bundles

In order to quantify the distribution of orientation of the nanofibers in the bundles, the Directionality plugin of ImageJ was used [25–27]. This approach allowed to quantify the amount of nanofibers within a given angle from the axis. The analysis was performed using a Local Gradient Orientation method following a procedure previously validated [28]. For the random nanofiber bundles the Directionality analysis was performed on stacks of five SEM images (magnification = 8000x). For

the aligned nanofiber bundle a full volume investigation was performed applying the same procedure to all the slices of the XCT stacks, after reslicing.

7.3.2.4 Mechanical characterization of the bundles

The mechanical properties of the random and aligned nanofiber bundles were measured with a servo-hydraulic testing machine (8032, Instron, High Wycombe, UK), with a ±1 kN dynamic cell (Instron, High Wycombe, UK). The force signals had a noise of 0.01 N after filtering. All the specimens were immersed in saline for two minutes before the mechanical test. The test machine was operated in displacement control, adjusting the actuator speed according to the actual specimen length, to obtain a strain rate of 70 % $sec.^{-1}$. This strain rate is in the range of those experienced by tendons and ligaments during strenuous physiological activities [29–32].

To measure the diameter of each specimen before the test, a light optical microscope (Axioskop, Zeiss, Pleasanton, CA, USA) equipped with a camera (AxioCam MRc, Zeiss, Pleasanton, CA, USA) was used and image analysis was conducted using ImageJ [25]. For each bundle, the mean and standard deviation (SD) of ten measurements was computed. To measure the weight of each specimen before the test (mean and SD of three measures), a precision balance was used (MC 210 P, capacity resolution: 210 g x 0.01 mg, Sartorius, Göttingen, Germany).

Ten specimens of both random and aligned nanofiber bundles were tested. Dedicated capstan grips (Figure 7.5) were used to minimize the stress concentration at the specimens ends. The gauge length was 47.42 mm (this included the free length and the portion of specimen wrapped around the capstans, consistently with the BS EN 12562:1999 and the ASTM D2256/D2256M-10 (2015) Standards).

The mechanical characterization of the random and aligned bundles was performed to identify the most biomimetic candidate, so just the typical load-strain curves and the force and stress data were analyzed (see 7.3.3.4 section and Figure 7.2).

7.3.3 Optimization of the hierarchical assemblies

Based on the most promising configuration from section 7.3.2 (see Results), aligned bundles were adopted for the following steps. In order to allow easier handling and

stretching of the bundles in the subsequent steps of preparation of the hierarchical structures, the bundles were removed from the collector without any cut, thus obtaining ring-shaped bundles (Figure 7.1).

7.3.3.1 Fabrication of the hierarchical assemblies

In order to reproduce the whole morphology of a tendon or ligament [4,11,24], two different electrospun bioinspired assembly were produced. To group together different numbers of bundles, an innovative electrospinning procedure to electrospin nanofibrous sheaths was developed (Figure 7.1B). These sheaths were designed to reproduce the morphology of the natural membranes of tendons (endotenon, epitenon) or ligaments (endoligament, epiligament) [4,24]. The same electrospinning parameters previously described were used.

Two custom made stainless-steel 6-arms capstan grips (6 cylindrical arms of 8 mm of diameter each) were fixed in a custom-made rotating electrospinning machine. Then, 24 bundles were hooked on the grips, 4 for each arm (Figure 7.1B). After this operation, a Nylon 6,6 sheath of nanofibers was electrospun on the group of bundles for 12 hours. The custom-made electrospinning apparatus was composed of a high-voltage power supply (FuG Elektronik GmbH, Schechen, Germany), two syringe pumps (KD Scientific Legato 100, Illinois, USA), and two glass syringes containing the polymeric solution, connected to stainless-steel blunt-ended needles (inner diameter = 0.84 mm) by PTFE tubes. In order to concentrate the nanofibers on the group of bundles, a flat aluminum collector plate (200 mm high and 50 mm wide) was placed behind the bundles (Figure 7.1). To pre-strain the nanofibers of the sheath on the final assembly surface, the group of bundles was in a static position, and intermittently put in rotation (approximately 20 rpm for 1 minute every 5 minutes), while the sheath was being electrospun (Figure 7.1B). Finally, in order to produce a hierarchical assembly to completely simulate the structure of a whole tendon or ligament [4,24], including the endotenon/endoligament sheaths and the tertiary fiber bundles inside, a 3-level hierarchical assembly was produced. First, three Nylon 6,6 2-level hierarchical assemblies, with five ring-shaped bundles each, were produced as previously described (with an electrospinning session of 10 hours each). Then, the extremities of the three 2-level hierarchical assemblies were tied

together with paper tape, and fixed in the machine (Figure 7.1C). To produce the epitenon/epiligament-like sheath, the same procedure and methods previously described were used, with and electrospinning session of 10 hours (Figure 7.1C).

7.3.3.2 Morphological investigation of the hierarchical assemblies

The SEM investigation on the 2-level and 3-level hierarchical assemblies were performed with the same parameters previously described in the 7.3.2.2 section.

To investigate the three-dimensional structure of the Nylon 6,6 hierarchical assemblies, the XCT scans were acquired with a different high-resolution x-ray tomography system (Versa 520, Zeiss, Pleasanton, CA, USA). The following parameters were used (depending on the shape and thickness of the specimens): (i) 2-level hierarchical assembly: 50 kV Voltage, 4 W Power, 80 microAmpere tube current, 5.27 micrometers voxel size, 1.75 second exposure time, rotational steps of 0.12° over 360°, for a scanning time of 7.5 hours; (ii) 3-level hierarchical assembly: 50 kV Voltage, 3 W Power, 60 microAmpere tube current, 5.27 micrometers voxel size, 1.75 second exposure time, rotational steps of 0.12° over 360°, for a scanning time of 7.5 hours. All the XCT images, were reconstructed using the Scout-and-Scan Reconstructor software (Zeiss), and were visualized using XM3DViewer1.2.8 software (Zeiss).

7.3.3.3 Directionality of the nanofibers of the sheath and of the internal bundles

In order to quantify the orientation of the nanofibers in the electrospun sheaths and in the bundles inside the assemblies, the Directionality plugin of ImageJ was used [25–27], as described above in the bundles section. The Directionality analysis was performed with two different approaches derived from [28].

For the external sheaths, the Directionality analysis was performed on stacks of 5 SEM surface images (magnification = 8000x). To assess the orientation of the bundles inside the hierarchical assemblies, a full volume investigation was performed applying the procedure to all the slices of the XCT stacks, after a reslice.

7.3.3.4 Mechanical characterization of the hierarchical assemblies

The mechanical characterization was performed both on the ring-shaped bundles and on the 2-level hierarchical assemblies (due to limited availability of specimens, the mechanical tests were not performed on the 3-level hierarchical assembly).

As the hierarchical assemblies were built with ring-shaped bundles (as opposed to the straight bundles tested before, see 7.3.2.4) the mechanical test was performed starting from the single ring-shaped bundles. Ten specimens of ring-shaped bundles were tested using capstan grips with the same strain rate as before (Figure 7.9). The gauge length was 220 mm (consistently to the ASTM D1414 Standard).

Finally, three specimens of 2-level hierarchical assembly were tested. The cross-sectional diameter of each specimen was measured as above (mean and SD between 30 measures in three different sections). The specimens were weighted with the same precision balance. In order to minimize the stress concentration, the specimens were tested directly on the stainless-steel 6-arms capstan grips, mounted on the Instron testing machine (Figure 7.9).

The following indicators were considered: Yield Stress (σ_Y), Yield Strain (ε_Y), Modulus of Elasticity (E), Failure Force (F_F), Failure Stress (σ_F), Failure Strain (ε_F), Unit Work

to Yield (L_Y), Unit Work to Failure (L_F) (Figure 7.2). The force-displacement curves were converted to stress-strain curves using two different approaches:

- To describe the macroscopic mechanical behavior of the specimen, the apparent stress was computed dividing the force by the cross-sectional area measured before the test.
- To quantify the net mechanical properties, the net stress was also computed dividing the apparent stresses by the volume fraction (v) of the specimens.
- The apparent and the net modulus of elasticity (E), and unit works to failure were computed (L_Y, L_F)

The volume fraction (v) was calculated by using the equation:

$$v = w/(L \times A \times r) \quad (7.1)$$

Where:

- w is the weight of the specimen
- L is length of the specimen,
- A is the cross-sectional area of the specimen
- r is the density of the raw material (Nylon 6,6 = 1.14 g/cm^3)

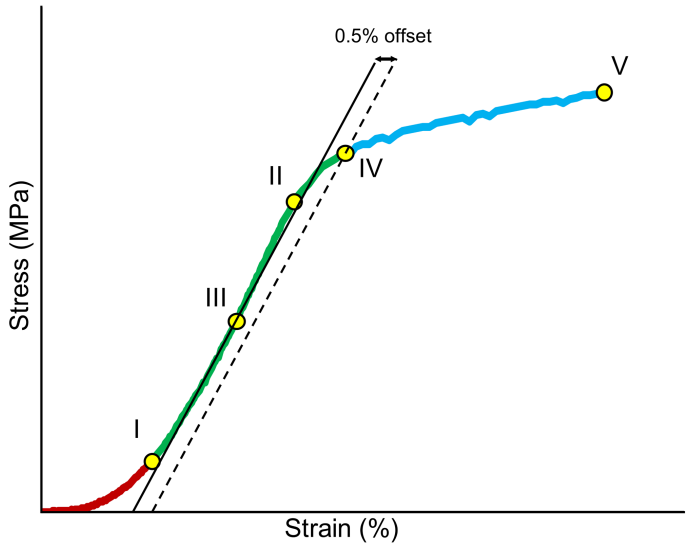

Figure 7.2 Post processing of the stress-strain curves. The failure stress (σ_F) (V) was identified as the highest stress in the entire curve. The starting point of the linear region (I) was identified as 20% of the failure stress (σ_F) for the bundles of aligned nanofibers and the 2-level hierarchical assembly, and as 5% of the failure stress (σ_F) for the bundles of random nanofibers (the different threshold was required due to the different behaviour of the two types of bundle). The initial toe region (from 0 N to I) was disregarded. An initial guess for the yield strain was visually identified (II). A first linear regression (solid line) was applied to the first 50% of the linear region, between points (I) and (III) (III was half-way between I and II). A second line parallel to the first regression was drawn with an offset of 0.5% strain (dashed line). The limit of proportionality was defined with the 0.5%-strain offset criterion as the intersection (IV) between the latter line and the stress-strain curve. The modulus of elasticity (E) was calculated as the slope of a new regression line between (I) and (IV). The unit work to yield (L_Y) and to failure (L_F) were calculated as the integrals under the curves (with the method of trapezoids). Two plots were obtained for each specimen: one reporting the apparent stress, the other one with the net stress.

7.4 Results

7.4.1 Comparison between random and aligned bundles

The electrospun bundles of random and aligned Nylon 6,6 nanofibers were compared. The random bundles had a cross-sectional diameter of 0.52±0.050 mm, and the aligned bundles of 0.52±0.062 mm. The volume fraction (v) for the random bundles was 0.21±0.03 and 0.30±0.04 for the aligned bundles.

7.4.1.1 Morphological investigation of the bundles

The SEM investigation showed that the Nylon 6,6 nanofibers of both the random bundles and the aligned bundles were homogeneous, with no defects such as beads (Figure 7.3A, B). The mean cross-sectional diameter of the nanofibers was of 0.23±0.025 micrometers. The different orientation of the nanofibers in the random and in the aligned bundles was clearly visible.

The XCT investigation of the random bundles showed that nanofibers were randomly arranged both on the surface and inside the bundle (Figure 7.3C). Few wrapping defects were noted in the internal body of random bundles (Figure 7.3C).

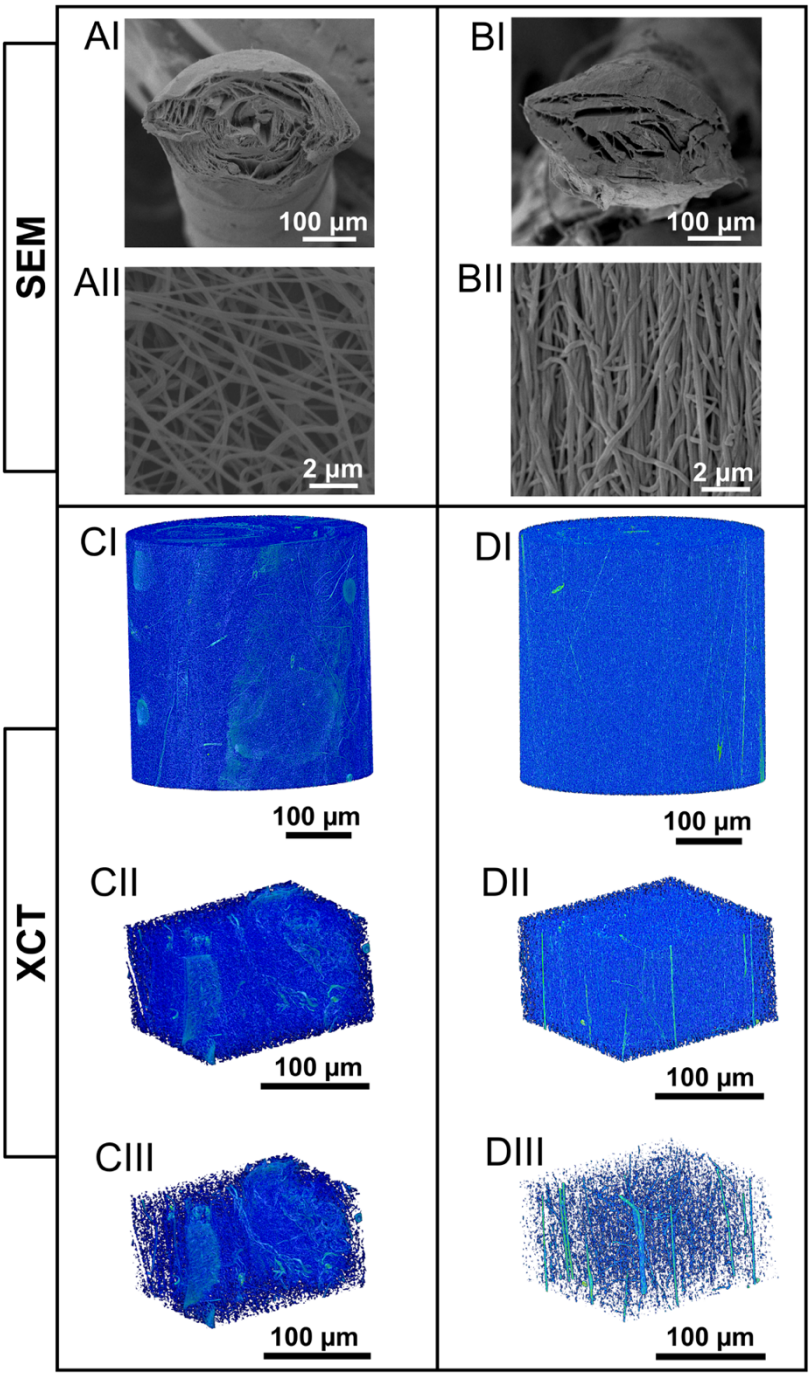

Figure 7.3 Imaging of the random and of the aligned bundles. A) SEM images of a random nanofiber bundle. B) SEM images of an aligned nanofiber bundle. The sections of the bundles (magnification = 100x) are visible in part I; the surface of the bundle (magnification = 8000x) are visible in part II. C) XCT images of a random nanofiber bundle; D) XCT images of an aligned nanofiber bundle (0.4 micrometers of voxel size). The sections of the bundles are visible in part I; an internal crop showing the alignment of the nanofibers inside the bundle is reported in part II; tuning the thresholding the most internal nanofibers become visible in part III.

7.4.1.2 Directionality of the nanofibers

The Directionality analysis confirmed the different preferential orientation of the nanofibers in the aligned bundles as opposed to the random ones (Figure 7.4). The random bundles showed a dispersion of the orientation of the nanofibers so that about 7% of nanofibers fell in each bin. The aligned bundles had a predominant peak in the range of 0°-6° from the bundle axis (42.7% ± 3.08% of the total), and a Gaussian-like distribution. A small amount of nanofibers of 0.78% ± 0.15% was perpendicular to the bundle (84°-90°).

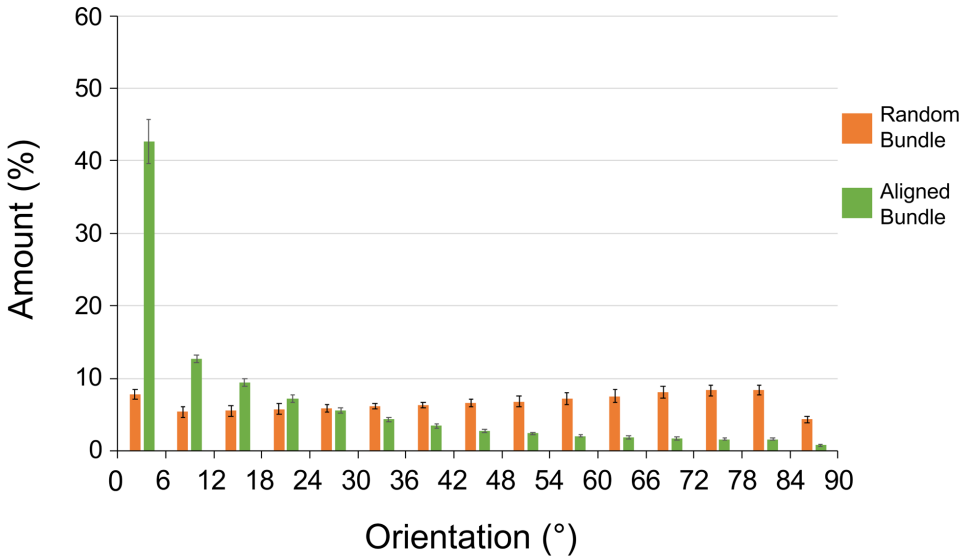

Figure 7.4 Directionality of the nanofibers in the random and in the aligned bundles. The directionality histograms show the distribution of the nanofibers in the different directions for the two types of bundles. An angle of 0° means that the nanofibers were aligned with the axis of the bundle, an angle of 90° means that the nanofibers were perpendicular to the bundle.

7.4.1.3 Mechanical properties of the bundles

The load-strain curves revealed a more deformable behavior for the random bundles and a stiffer behavior for the aligned bundles (Figure 7.5). Both types of bundles showed a nonlinear toe region up to 1-4% strain (Figure 7.5). The random bundles had a failure force of F_F = 3.27±0.61 N, and were weaker than the aligned ones (F_F = 14.38±2.74 N). After the toe region, the random bundles showed a short elastic region up to an apparent yield stress of σ_Y = 3.28±0.90 MPa and a final ductile region up to an apparent failure stress of σ_F = 15.60±2.81 MPa (Figure 7.5). The

aligned bundles also showed higher apparent failure stress (σ_F = 68.70±15.06 MPa) compared to the random bundles (Figure 7.5). For both of the bundle types, the net mechanical properties were 3-5 times higher than the apparent ones (Table 7.1).

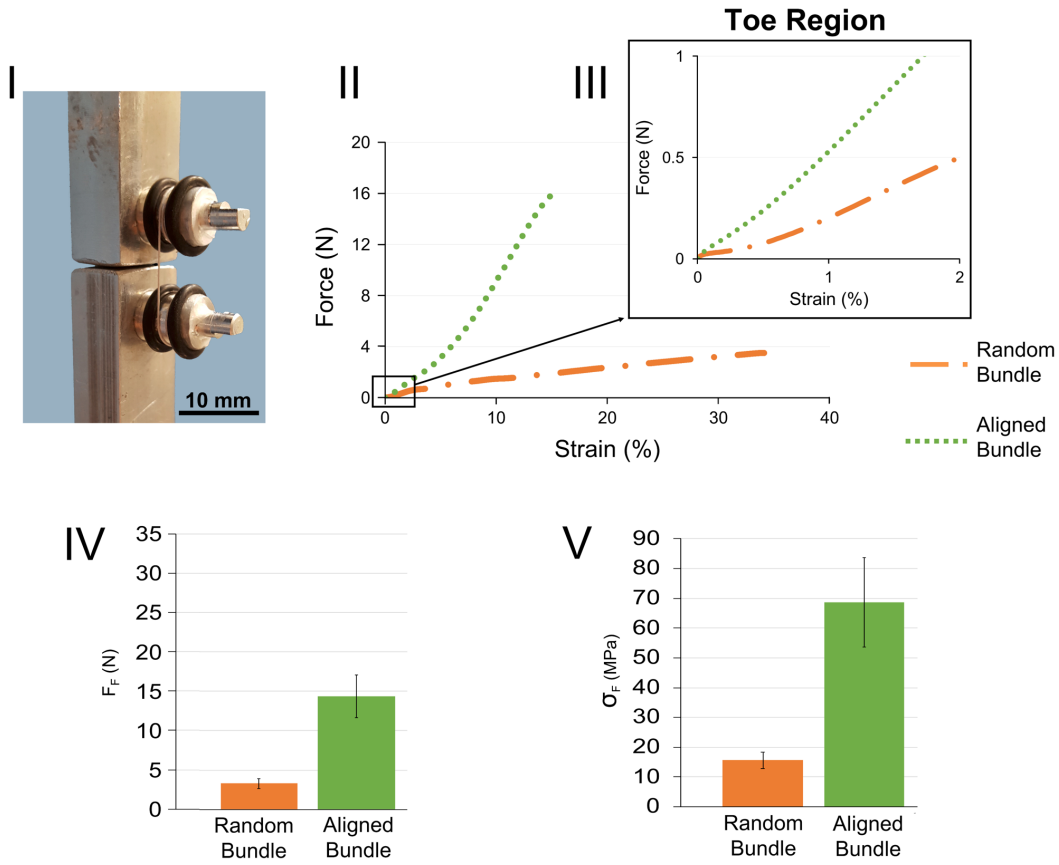

Figure 7.5 Mechanical characterization of the bundles of random nanofiber bundles and of aligned nanofibers. I) Tensile test setup with custom-made capstan grips. II) typical load-strain curves of the random bundles and the aligned bundles; III) zoom-in of the nonlinear toe region. Comparison between the mechanical properties of the random and of the aligned bundles: IV) failure force (F_F); V) apparent failure stress (σ_F). The corresponding net mechanical properties are reported in Table 7.1.

7.4.2 Properties of the hierarchical assemblies

The ring-shaped bundles and the hierarchical assemblies made of such bundles were compared. The bundles used for the assemblies were homogeneous, and had a cross-sectional diameter of 0.47±0.038 mm. Three 2-level hierarchical assemblies were prepared, each with 24 ring-shaped bundles. The 2-level assemblies had a final cross-sectional diameter of 4.3±0.57 mm, and a length of 220 mm (Figure 7.6II).

The bundles inside the assemblies were tightly grouped together and covered with a homogeneous nanofibrous sheath (Figure 7.6). The volume fraction (v) for the single bundles was $v = 0.33 \pm 0.02$. The 2-level hierarchical assemblies had a lower volume fraction $v = 0.22 \pm 0.05$, due to the free-volume between the single bundles. The 3-level hierarchical assembly had a cross-sectional diameter of 4.6±0.17 mm with a length of 220 mm. Observing the 3-level hierarchical assembly, the original 2-level hierarchical assemblies were still distinguishable; they were tightly compacted inside the external nanofibrous sheath (Figure 7.6III). The volume fraction of the 3-level hierarchical assembly was $v = 0.175$.

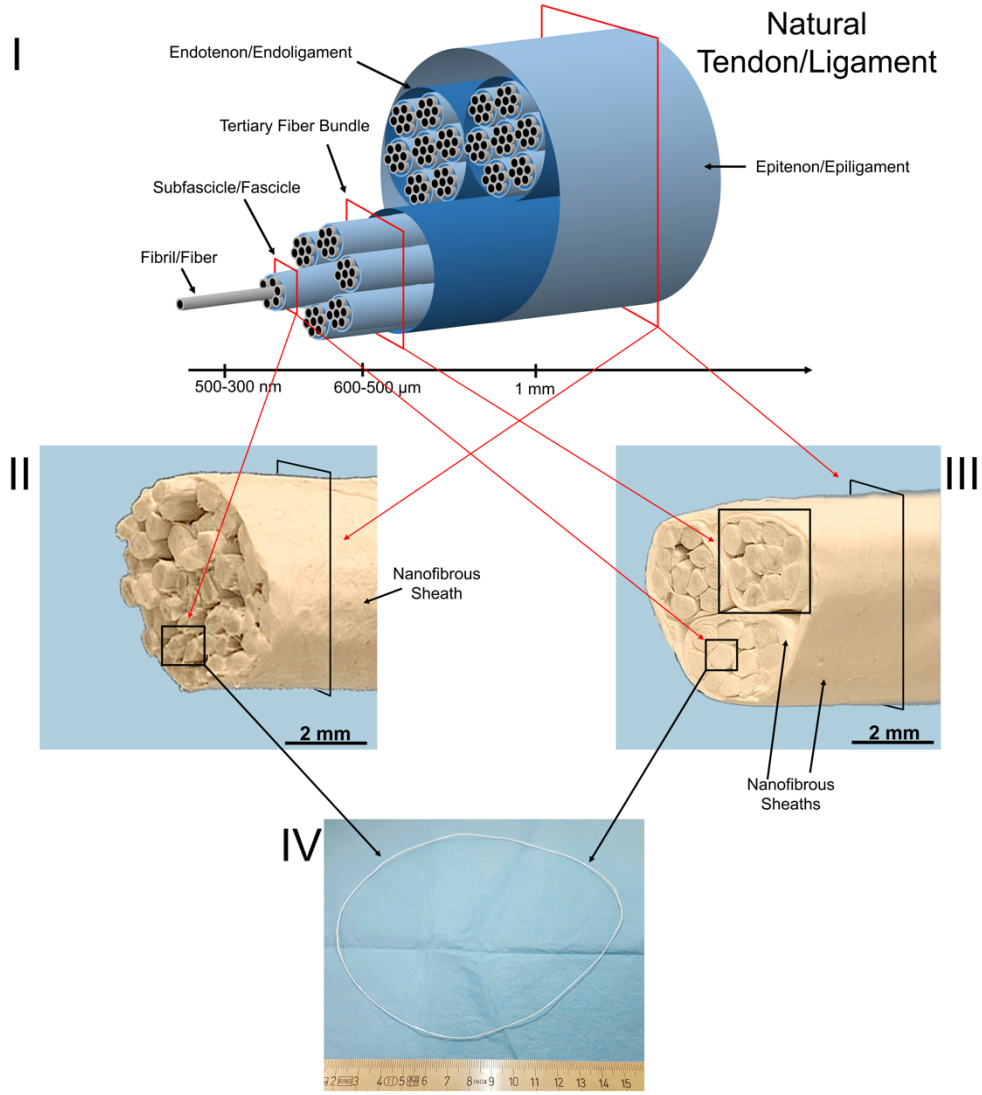

Figure 7.6 Comparison between a natural tendon or ligament and the electrospun hierarchical assemblies. I) Hierarchical structure of a tendon or ligament [4]. II) Image of the cross-section of a

2-level hierarchical assembly. III) Image of the cross-section of a 3-level hierarchical assembly. IV) Image of a ring-shaped bundle used to build the hierarchical assemblies.

7.4.2.1 Morphology of the hierarchical assemblies

The SEM investigation showed that the nanofibers in the hierarchical assemblies were homogeneous, without the presence of defects such as beads (Figure 7.7A, B). The cross- sectional diameter of the nanofibers within the electrospun sheaths was of 0.23±0.025 micrometers. The bundles were strongly grouped inside the nanofibrous sheaths (Figure 7.7A, B). The XCT investigation on the 2-level hierarchical assemblies revealed that the sheath was homogeneous across the surface of the hierarchical assembly, with the presence of some circular defects. In the internal volume of the 2-level hierarchical assemblies, the bundles were axially aligned (Figure 7.7C). The XCT reconstructions of the 3-level hierarchical assembly showed that: (i) the nanofibrous sheaths were homogeneous, both the external and the internal with the presence of a few circular defects (Figure 7.7D) and (ii) the 2-level hierarchical assemblies forming the 3-level assembly were axially aligned, as well as the single bundles they were made of (Figure 7.7C, D).

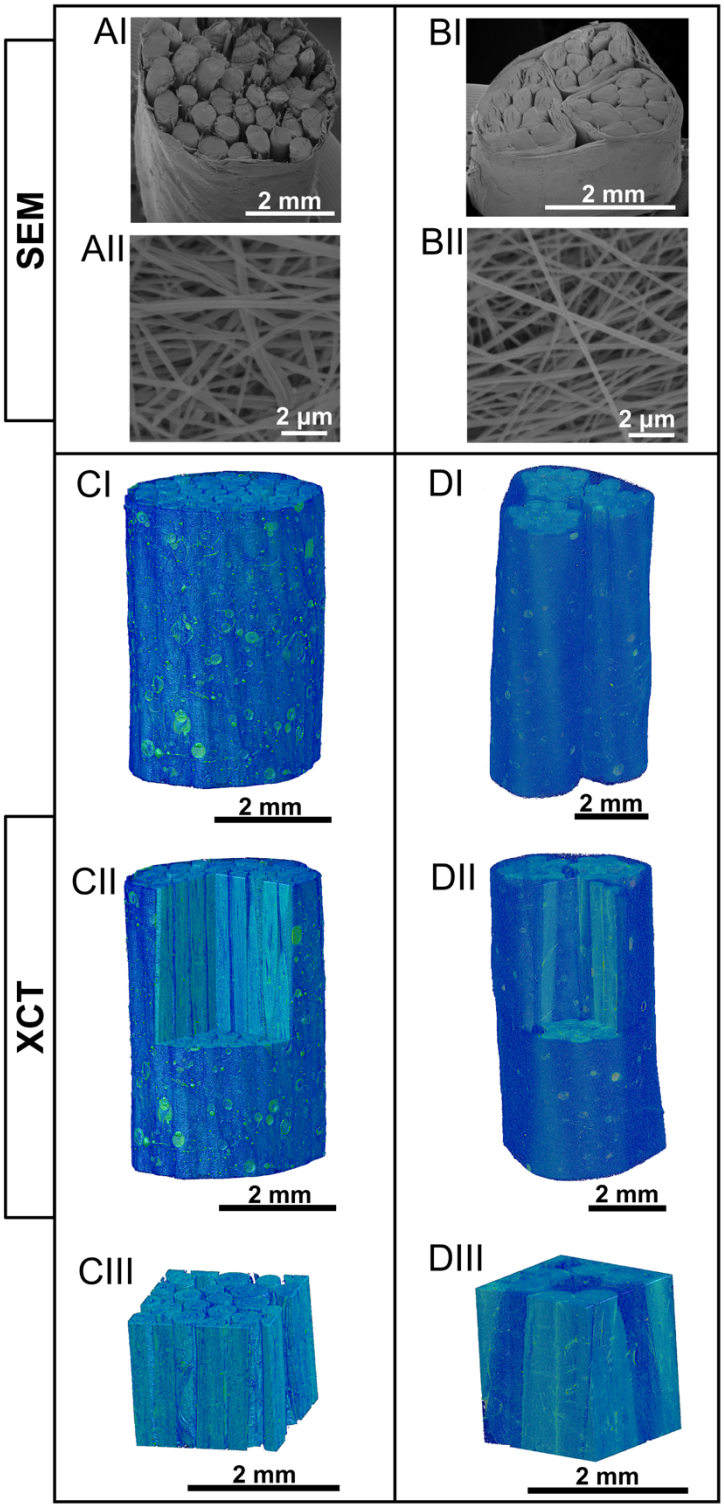

Figure 7.7 Imaging of the of the 2-level and 3-level hierarchical assemblies. A) SEM images of a 2-level hierarchical assembly. B) SEM images of a 3-level hierarchical assembly. The sections of the hierarchical assemblies (magnification = 25x) are visible in part I; the nanofibers on the surface of the electrospun sheaths (magnification = 8000x) are visible in part II. C) XCT images of a 2-level

hierarchical assembly (5.27 micrometers voxel size). D) XCT images of a 3-level hierarchical assembly (5.27 micrometers voxel size). An external section showing the external electrospun sheath is visible in part I; an external crop showing the internal axially aligned bundles is reported in part II; an internal crop showing the most internal axially aligned bundles are visible in part III.

7.4.2.2 Alignment of the nanofibers of the sheath and of the internal bundles

The Directionality investigation showed that the nanofibers of the sheaths for the hierarchical assemblies had a slight preferential circumferential orientation (Figure 7.8): more than 45% of the nanofibers fell in the range of 66°-90° for the 2-level hierarchical assembly; more than 48% of the nanofibers fell in the range of 66°-90° for the 3-level assembly.

The preferential axial of alignment of the bundles and the nanofibers inside the bundles was confirmed by the XCT-based Directionality investigation (Figure 7.8). All the specimens had a predominant peak in the range of 0°-6° and a Gaussian-like dispersion. The 2-level hierarchical assembly showed strong axial alignment, with 52.0% ± 5.09% in the range 0°-6°. Similarly, the 3-level hierarchical assembly had a strong axial alignment (47.3% ± 5.71% of the nanofibers were peak in the range of 0°-6° from the axis).

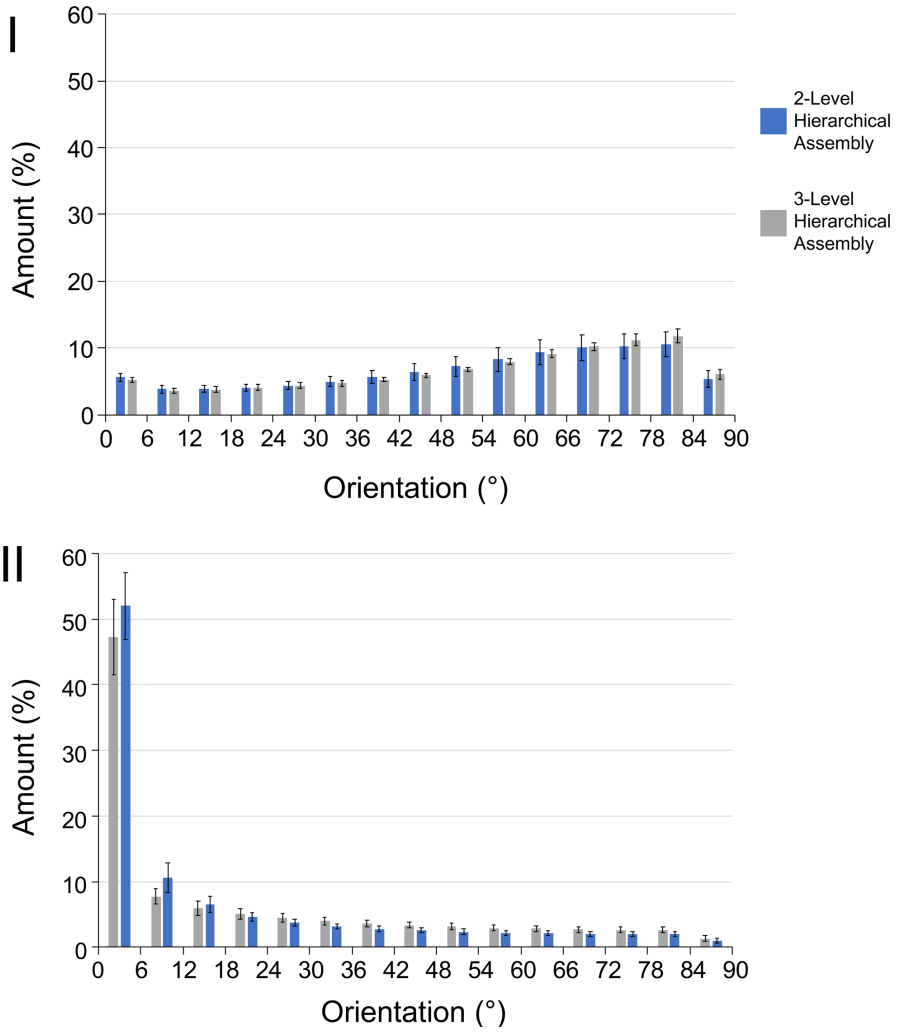

Figure 7.8 Comparison between the alignment of the nanofibers in the outer sheaths (I) and inside the assemblies (II) for the 2-level and the 3-level hierarchical assemblies. An angle of 0° means that the nanofibers were aligned with the axis of the bundle, 90° means that the nanofibers were perpendicular to the bundle.

7.4.2.3 Comparison of the mechanical properties of the single bundlesand of the hierarchical assemblies

The typical load-strain curves of the single ring-shaped bundles and 2-level hierarchical assembly confirmed a brittle behavior with a nonlinear toe region up to 1 – 4% of strain (Figure 7.9). The single ring-shaped bundles showed a failure force of F_F = 21.82±1.75 N (mean and SD of ten specimens) and the 2-level hierarchical assemblies of F_F = 330.6±11.02 N (mean and SD of three specimens) (Figure 7.9). The bundles had values of apparent failure stress σ_F = 63.48±10.98 MPa (ε_F = 9.29±1.02%) and the hierarchical assemblies of σ_F = 22.93±4.99 MPa

(ε_F = 8.58±0.20%) respectively (Figure 7.9). The modulus of elasticity of the single bundles was E = 877.9 ±83.19 MPa and for the hierarchical assembly E = 343.0±87.02 MPa (Figure 7.9). The unit work to failure for the bundles was L_F = 0.253±0.08 J/mm3 and L_F = 0.080±0.021 J/mm3 for the 2-level hierarchical assemblies (Figure 7.9).

The net mechanical properties (computed considering the volume fraction *v*) were 4-6 times higher than apparent ones (Table. 7.1).

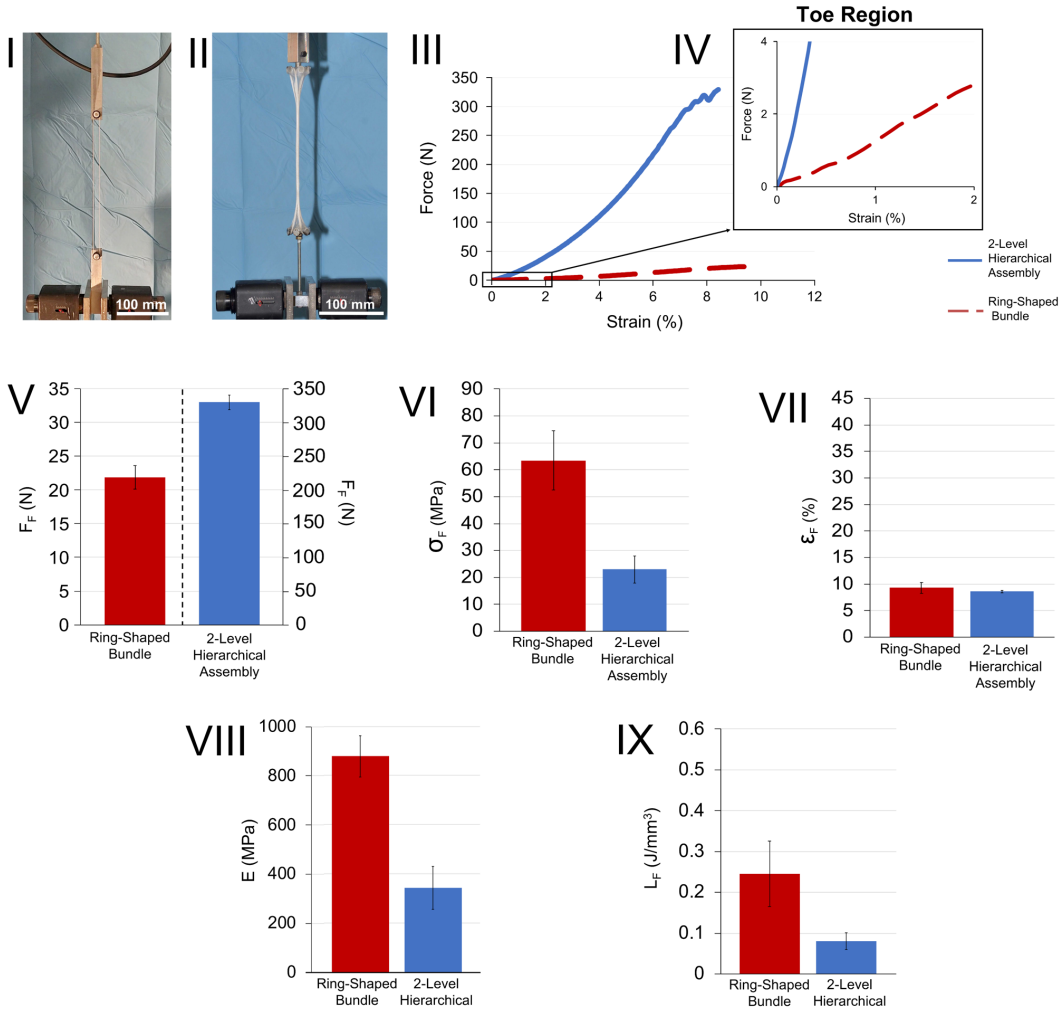

Figure 7.9 Mechanical characterization of the ring-shaped bundles and of the 2-level hierarchical assembly. I) tensile testing of the ring-shaped bundles using custom-made capstan grips; II) tensile testing of the 2-level hierarchical assembly using the 6-arms capstan grips. III) typical load-strain curves of the ring aligned nanofiber bundles and of the 2-level hierarchical assemblies; IV) zoom-in the nonlinear toe regions. Comparison between the mechanical properties of the bundles and the 2-level hierarchical assemblies: V) failure force (F_F); VI) apparent failure stress (σ_F); VII) failure

strain (ε_F); VIII) apparent modulus of elasticity (E); IX) apparent unit work to failure (L_F). The corresponding net mechanical properties are reported in Table 7.1.

Table 7.1 Net mechanical properties of the bundles and the 2-level hierarchical assemblies obtained from the apparent ones, considering the fraction of volume (v) actually taken by the nanofibers.

	Yield stress (MPa)	Failure stress (MPa)	Modulus of Elasticity (MPa)	Unit work to failure (J/mm^3)
Random Bundle	15.63±3.12	75.58±13.13	-	-
Aligned Bundle	-	235.4±28.62	-	-
Ring-shaped Bundle	-	389.6±65.31*	5390.8±421.1	1.56±0.48
2-level Hierarchical Assembly	-	106.7±4.04*	1589±41.20	0.37±0.02

Note*: a slightly lower failure stress was found for the aligned bundles compared to the ring-shaped ones, in relation to the different gripping system (the gripping system used in the first case induced a higher stress concentration than with the ring-shaped bundles)

7.5 Discussion

The aim of the present study was to develop an innovative morphologically bioinspired electrospun nanofibrous assembly, by using non-resorbable Nylon 6,6, to replicate the hierarchical structure and the mechanical properties of a whole tendon or ligament. Nylon 6,6 was selected for its wide range of clinical applications, such as for suture wires and implantable non-resorbable devices [33]. In order to replicate every single hierarchical level of aggregation of the collagen fibrils inside the tendon and ligament tissue [3,4,11] (Figure 7.6), different electrospun bundles were produced.

Firstly, random and aligned nanofiber bundles were obtained by means electrospinning Nylon 6,6 on a drum collector, rotating at different speed. In both cases, the nanofibers had the same diameter of the collagen fibrils [3,4,11] observed within tendons and ligaments. The random bundles were not satisfactory, because they had a morphology and an arrangement of the nanofibers, assessed with SEM

and XCT imaging (Figure 7.3) far from the tendon and ligament fascicles [34]. Furthermore, their mechanical properties were lower than the human tendon and ligament fascicle [11,35] (Figure 7.5). For all these reasons the random bundles were discarded as candidates. The aligned bundles were selected as best fascicle-inspired candidates. Firstly, the SEM and the XCT images (Fig.
3) confirmed that the morphology was similar to the collagen fascicles [3,11,34,36]. The Directionality analysis on the XCT scan of the aligned bundle (Figure 7.4) confirmed that the alignment of the Nylon 6,6 nanofibers was similar to that of the tendon and ligament collagen fibrils [37]. Finally, the mechanical properties were in the same range of the human tendon and ligament fascicles [11,35] (Figure 7.5). These findings are consistent with previous studies on electrospun bundles [22,24,38,39].

Subsequently, in order to reproduce the whole structure of a tendon or ligament [3,4,11], several ring-shaped bundles were grouped together, obtaining the 2-level hierarchical assembly (Figure 7.6). To do this, a dedicated procedure to electrospin sheath was developed (Figure 7.1) in order to mimic the morphology of the epitenon/epiligament membranes of tendons and ligaments [3,4,11]. The Directionality analysis on XCT scans confirmed a pronounced axial alignment of the nanofibers inside the 2-level assembly, and a slight circumferential alignment of the nanofibers in the outer sheath. Compared to previous similar processes [40–44], our method allowed a finer tuning of the level of compaction of the bundles. In fact, the degree of circumferential orientation can be controlled through the electrospinning procedure by matching the process parameters (i.e. static/rotational time and the rotational speed of the device) during the production of the sheaths (Figure 7.8). Thus, it was also possible to adjust the final cross-section of the assemblies themselves, improving their overall mechanical properties (Figure 7.9). As this procedure was particularly flexible, we were able to produce 3-level hierarchical assemblies by grouping a number of 2-level hierarchical assemblies (Figure 7.6). The 3- level assemblies incorporate sheaths that mimicked the tendon and ligament endotenon/endoligament membranes [3,4,11]. The Directionality analysis confirmed a pronounced axial alignment of the nanofibers inside the 3-

level assembly. The slightly lower values of alignment for the 3-level assembly compared to the 2-level assemblies

were caused by the higher percentage of nanofibers in the different sheaths forming the 3-level assembly. These hierarchical assemblies showed and unprecedented morphology, biomimicking every single collagen structure that compose a whole natural tendon or ligament [3,4,11].

Both the ring-shaped bundles and the 2-level hierarchical assemblies showed a nonlinear toe region up to 2 - 4% strain, similar to the behavior of the natural fascicles, tendons and ligaments [5,11,35]. After the toe region, both the bundles and the 2-level hierarchical assemblies exhibited a linear elastic behavior, up to 9% strain, before failing (again, similar to the behavior of the natural tendons and ligaments) (Figure 7.9). The single bundles had a modulus of elasticity higher than the fascicles of tendons and ligaments [5,11,35]. The hierarchical assembly had a similar modulus of elasticity to natural tendons and ligaments (range: 20-3000 MPa [5,11]). The maximum strain of the bundles was in the same range of collagen fascicles and of natural tendons and ligaments (range: 9-25 % [5,35,45]). The failure strain of the hierarchical assemblies was in the range of the natural tendons and ligaments (range: 8-120 MPa [5,11]). The apparent failure stress of the bundles was σ_F = 63.48±10.98 MPa. These values were higher than the fascicles of natural tendons and ligaments (range: 6-40 MPa [5,35,45]). The apparent failure stress for the hierarchical assemblies was σ_F = 22.93±4.99 MPa, which is in the same range observed in natural tendons and ligaments (range: 1-116 MPa [5,11]). As expected, the modulus of elasticity and the failure stress of the 2-level hierarchical assembly was lower than that of the single bundles. This may be due to the fact that the apparent stress in the hierarchical assembly is calculated over the total cross-sectional area (which includes the actual cross-section of the bundles, but also some unavoidable empty space). Similarly, the values of net stress (i.e. computed considering the volume fraction actually filled by nanofibers) were significantly higher (4-6 times) than the apparent ones.

Altogether, these properties can grant excellent mechanical performance, and a biomimetic behavior of the hierarchical assembly. Considering that the Nylon 6,6 is an inert material, the possible applications in reconstructive surgery could include

replacement of injured tendons or ligaments for the elderly patients (i.e. age higher than 60 years). In fact, due to the low metabolic activity in the elderly, regenerative medicine (i.e. resorbable scaffolds) is not recommended.

Most of the previous electrospun scaffolds reported for tendon and ligament replacements consist of braided, twisted or knitted fibers [44,46–50] which do not replicate the morphology of natural tissues. Compared to previous literature results, the method herein proposed to produce electrospun sheaths confers a better compaction of the single bundles in the multiscale hierarchical scaffold [44,46–50]; thus, providing optimal compromise between morphology and mechanical properties.

Moreover, such high biofidelic hierarchical assemblies will also be suitable as artificial tendons or ligaments for in vitro biomechanical validations tests or surgical training. In fact, to the best of our knowledge, there are no specific devices available on the market for such applications. The previous attempts in this field were absolutely trivial and not biomimetic [51–53].

A limitation of this study should be mentioned: some droplets were created during deposition of the electrospun sheaths (Figure 7.7). Such defects might have reduced the ability of the sheath to tightly bind the bundles together: this might have reduced the improvement in mechanical properties deriving from the compaction of the bundles. In the future, these defects can be avoided optimizing the flow rate of the Nylon 6,6 solution, thus possibly further improving the mechanical strength of the assemblies.

The XCT investigation was extremely challenging because of the small diameter of the electrospun nanofibers, and of the low attenuation of the polymer [28,39,49,50,57,58]. Additional images and videos of the XCT scans of the single bundles and of the 2-level and 3-level hierarchical structures are available through Figshare (aligned bundle: https://doi.org/10.6084/m9.figshare.7636580.v4; 2-level hierarchical assembly: https://doi.org/10.6084/m9.figshare.7636592.v3; 3-level hierarchical assembly: https://doi.org/10.6084/m9.figshare.7636595.v3).

In conclusion this work showed an innovative electrospinning production process to design and build nanofibrous Nylon 6,6 hierarchical assemblies, suitable as

future implantable devices, able to mimic the multiscale morphology and the biomechanical properties of tendons and ligaments.

7.6 References

[1] Abbah SA, Spanoudes K, O'Brien T, Pandit A, Zeugolis D. 2014 Assessment of stem cell carriers for tendon tissue engineering in pre-clinical models. Stem Cell Res Ther 5:1–9.

[2] Zeugolis DI, Chan JCY, Pandit A. 2011 Tendons: Engineering of Functional Tissues. In: Pallua N, Suscheck C, editors. Tissue Eng. From Lab to Clin. Tissue Eng, Springer Berlin Heidelberg p. 1–634.

[3] Kastelic J, Galeski A, Baer E. 1978 The Multicomposite Structure of Tendon. Connect Tissue Res 6:11–23.

[4] Kannus P. 2000 Structure of the tendon connective tissue. Scand J Med Sci Sport 10:312–20.

[5] Goh KL, Listrat A, Béchet D. 2014 Hierarchical mechanics of connective tissues: Integrating insights from nano to macroscopic studies. J Biomed Nanotechnol 10:2464–507.

[6] McCarthy MM, Hannafin JA. The Mature Athlete: Aging Tendon and Ligament. Sports Health 2014;6:41–8.

[7] Woo SLY, Hollis JM, Adams DJ, Lyon RM, Takai S. 1991 Tensile properties of the human femur-anterior cruciate ligament-tibia complex: The effects of specimen age and orientation. Am J Sports Med 19:217–25.

[8] Chen J, Xu J, Wang A, Zheng M. 2014 Scaffolds for tendon and ligament repair: review of the efficacy of commercial products. Expert Rev Med Devices 6:61–73.

[9] Longo UG, Lamberti A, Maffulli N, Denaro V. 2010 Tendon augmentation grafts: A systematic review. Br Med Bull 94:165–88.

[10] Jackson DW, Heinrich JT, Simon TM. 1994 Biologic and synthetic implants to replace the anterior cruciate ligament. Arthrosc J Arthrosc Relat Surg 10:442–52.

[11] Murphy W, Black J, Hastings G. 2016 Handbook of Biomaterial Properties. Second. Springer.

[12] Batty LM, Norsworthy CJ, Lash NJ, Wasiak J, Richmond AK, Feller JA. 2015 Synthetic devices for reconstructive surgery of the cruciate ligaments: A systematic review. Arthrosc - J Arthrosc Relat Surg 31:957–68.

[13] Brunet P, Charrois O, Degeorges R, Boisrenoult P, Beaufils P. 2005 Reconstruction of acute posterior cruciate ligament tears using a synthetic ligament. Rev Chir Orthop Reparatrice Appar Mot 91:34–43.

[14] Engstrom B, Wredmark T, Westblad P. 1993 Patellar tendon or Leeds-Keio graft in the surgical treatment of anterior cruciate ligament ruptures. Intermediate results. Clin Orthop Relat Res 190–7.

[15] Ochi M, Yamanaka T, Sumen Y, Ikuta Y. 1993 Arthroscopic and histologic evaluation of anterior cruciate ligaments reconstructed with the Leeds-Keio ligament. Arthrosc J Arthrosc Relat Surg 9:387–93.

[16] Rading J, Peterson L. 1995 Clinical Experience with the Leeds-Keio Artificial Ligament in Anterior Cruciate Ligament Reconstruction: A Prospective Two-Year Follow-up Study. Am J Sports Med 23:316–9.

[17] Murray AW, Macnicol MF. 2004 10–16 year results of Leeds-Keio anterior cruciate ligament reconstruction. Knee 11:9–14.

[18] Hirooka A, Yoneda M, Wakaitani S, Isaka Y, Hayashida K, Fukushima S, et al. 2002 Augmentation with a Gore-Tex patch for repair of large rotator cuff tears that cannot be sutured. J Orthop Sci 7:451–6.

[19] Kollender Y, Bender B, Weinbroum AA, Nirkin A, Meller I, Bickels J. 2004 Secondary reconstruction of the extensor mechanism using part of the quadriceps tendon, patellar retinaculum, and gore-tex strips after proximal tibial resection. J Arthroplasty 19:354–60.

[20] Muren O, Dahlstedt L, Brosjö E, Dahlborn M, Dalén N. 2005 Gross osteolytic tibia tunnel widening with the use of Gore-Tex anterior cruciate ligament prosthesis: A radiological, arthrometric and clinical evaluation of 17 patients 13-15 years after surgery. Acta Orthop 76:270–4.

[21] Miller MD, Peters CL, Allen B. 2006 Early Aseptic Loosening of a Total Knee Arthroplasty Due to Gore-Tex Particle-Induced Osteolysis. J Arthroplasty 21:765–70.

[22] O'Connor RA, McGuinness GB. 2016 Electrospun nanofibre bundles and yarns for tissue engineering applications: A review. Proc Inst Mech Eng Part H J Eng Med 230:987–98.

[23] Brennan DA, Conte AA, Kanski G, Turkula S, Hu X, Kleiner MT, et al. 2018 Mechanical Considerations for Electrospun Nanofibers in Tendon and Ligament Repair. Adv Healthc Mater 1701277:1–31.

[24] Sensini A, Cristofolini L. 2018 Biofabrication of Electrospun Scaffolds for the Regeneration of Tendons and Ligaments. Materials (Basel) 11:1963.

[25] Liu Z. 1991 Scale space approach to directional analysis of images. Appl Opt 30:1369–73.

[26] Schindelin J, Arganda-Carreras I, Frise E, Kaynig V, Longair M, Pietzsch T, et al. 2012 Fiji: an open-source platform for biological-image analysis. Nat Methods 9:676–82.

[27] Schneider CA, Rasband WS, Eliceiri KW. 2012 NIH Image to ImageJ: 25 years of image analysis. Nat Methods 9:671–5.

[28] Sensini A, Cristofolini L, Focarete ML, Belcari J, Zucchelli A, Kao A, et al. 2018 High-resolution x-ray tomographic morphological characterisation of electrospun nanofibrous bundles for tendon and ligament regeneration and replacement. J Microsc 272(3):196–206.

[29] Butler DL. 1989 Anterior cruciate ligament: its normal response and replacement. J Orthop Res 7:910–21.

[30] Lewis G, Shaw KM. 1997 Tensile properties of human tendo Achillis: effect of donor age and strain rate. J Foot Ankle Surg 36:435–45.

[31] Wren TA., Yerby SA, Beaupré GS, Carter DR. 2001 Mechanical properties of the human achilles tendon. Clin Biomech 16:245–51.

[32] Lee M, Hyman W. 2002 Modeling of failure mode in knee ligaments depending on the strain rate. BMC Musculoskelet Disord 3:1–8.

[33] Maitz MF. 2015 Applications of synthetic polymers in clinical medicine. Biosurface and Biotribology 1:161–76.

[34] Moshiri A, Oryan A. 2013 Tendon and Ligament Tissue Engineering, Healing and Regenerative Medicine. J Sports Med Doping Stud 3:1–18.

[35] Hanson P, Aagaard P, Magnusson SP. 2012 Biomechanical properties of isolated fascicles of the Iliopsoas and Achilles tendons in African American and Caucasian men. Ann Anat 194:457–60.

[36] Kannus P, Paavola M, Józsa L. 2005 Aging and degeneration of tendons. In: Maffulli N, Renström P, W.B. L, editors. Tendon Inj., London: Springer p. 25–31.

[37] Provenzano PP, Vanderby R. 2006 Collagen fibril morphology and organization: Implications for force transmission in ligament and tendon. Matrix Biol 25:71–84.

[38] Sensini A, Gualandi C, Cristofolini L, Tozzi G, Dicarlo M, Teti G, et al. 2017 Biofabrication of bundles of poly(lactic acid)-collagen blends mimicking the fascicles of the human Achille tendon. Biofabrication 9.

[39] Sensini A, Gualandi C, Zucchelli A, Boyle L, Kao AP, Reilly GC, et al. 2018 Tendon Fascicle-Inspired Nanofibrous Scaffold of Polylactic acid/Collagen with Enhanced 3D-Structure and Biomechanical Properties. Sci Rep 8:1–15.

[40] Zhou FL, Gong R-H, Porat I. 2010 Nano-coated hybrid yarns using electrospinning. Surf Coatings Technol 204:3459–63.

[41] Kohlman LW, Roberts GD. 2015 Method for coating tow with an electrospun nanofiber. US8932683B1.

[42] Naghashzargar E, Farè S, Catto V, Bertoldi S, Semnani D, Karbasi S, et al. 2015 Nano/micro hybrid scaffold of PCL or P3HB nanofibers combined with silk fibroin for tendon and ligament tissue engineering. J Appl Biomater Funct Mater 13:e156–68.

[43] Li D, Pan X, Sun B, Wu T, Chen W, Huang C, et al. 2015 Nerve conduits constructed by electrospun P(LLA-CL) nanofibers and PLLA nanofiber yarns. J Mater Chem B 3:8823–31.

[44] Banik BL, Lewis GS, Brown JL. 2016 Multiscale Poly-(ε-caprolactone) Scaffold Mimicking Non-linearity in Tendon Tissue Mechanics. Regen Eng Transl Med 2:1–9.

[45] Butler DL, Kay MD, Stouffer DC. 1986 Fascicle-Bone Units From Human Patellar Tendon and Knee Ligaments. J Biomech 19:425–32.

[46] Xu Y, Dong S, Zhou Q, Mo X, Song L, Hou T, et al. 2014 The effect of mechanical stimulation on the maturation of TDSCs-poly(L-lactide-co-e- caprolactone)/collagen scaffold constructs for tendon tissue engineering. Biomaterials 35:2760–72.

[47] Bosworth LA. 2014 Travelling along the Clinical Roadmap: Developing Electrospun Scaffolds for Tendon Repair. Conf Pap Sci 2014:1–6.

[48] Mouthuy P-A, Zargar N, Hakimi O, Lostis E, Carr A. 2015 Fabrication of continuous electrospun filaments with potential for use as medical fibres. Biofabrication 7:25006.

[49] Laranjeira M, Domingues RMA, Costa-Almeida R, Reis RL, Gomes ME. 2017 3D Mimicry of Native-Tissue-Fiber Architecture Guides Tendon-Derived Cells and Adipose Stem Cells into Artificial Tendon Constructs. Small 13:1–13.

[50] Abhari RE, Mouthuy PA, Vernet A, Schneider JE, Brown CP, Carr AJ. 2018 Using an industrial braiding machine to upscale the production and modulate the design of electrospun medical yarns. Polym Test 69:188–98.

[51] Tare M. 2004 Dental rolls: A suitable model for practising tendon repair techniques. J Hand Surg Am 29:506–7.

[52] Ingraham JM, Weber RA, Weber RA. 2009 Utilizing a simulated tendon to teach tendon repair technique. Hand 4:150–5.

[53] Abdulal S, Onyekwelu O. 2016 An alternative model for teaching tendon repair and surgical skills in plastic surgery. JPRAS Open 7:12–5.

[54] Jordan MC, Schmitt V, Jansen H, Meffert RH, Hoelscher-Doht S. 2015 Biomechanical Analysis of the Modified Kessler, Lahey, Adelaide, and Becker Sutures for Flexor Tendon Repair. J Hand Surg Am 40:1812–7.

[55] Sherman SL, Copeland ME, Milles JL, Flood DA, Pfeiffer FM. 2016 Biomechanical Evaluation of Suture Anchor Versus Transosseous Tunnel Quadriceps Tendon Repair Techniques. Arthrosc - J Arthrosc Relat Surg 32:1117–24.

[56] Yang W, Qiao D, Ren Y, Dong Y, Shang Y, Zhang T. 2017 A Biomechanical Analysis of the Interlock Suture and a Modified Kessler-Loop Lock Flexor Tendon Suture. Clinics (Sao Paulo) 72:582–7.

[57] Bosworth LA, Rathbone SR, Bradley RS, Cartmell SH. 2014 Dynamic loading of electrospun yarns guides mesenchymal stem cells towards a tendon lineage. J Mech Behav Biomed Mater 39:175–83.

[58] Bradley RS, Robinson IK, Yusuf M. 2017 3D X-Ray Nanotomography of Cells Grown on Electrospun Scaffolds. Macromol Biosci 17:1–8.

Chapter 8: General Conclusions

The present Ph.D. project originated with the main aim to try to produce an innovative answer to the orthopaedic unsolved clinical problem of the regeneration and replacement of tendons and ligaments. This ambitious topic was reached by developing a new generation of electrospun hierarchically structured scaffolds for tendon and ligament tissue regeneration and replacement. The scaffolds were completely designed and characterized from the chemical, physical, morphological, biomechanical and cell viability point of view. To produce these outcomes, every step of the work was organized following a bottom-up approach.

In the first part of the research, a new strategy to produce bioresorbable electrospun bundles of aligned nanofibers of PLLA and Collagen was proposed. The PLLA/Coll fascicle inspired bundles showed biomimetic morphological and mechanical properties. However, the fast loss of collagen from the bundles, after the incubation in physiological environment, needed to be solved in order to preserve the mechanical performances of the scaffolds for long time. This limitation was overpassed by applying a proper crosslinking process to the scaffolds, that permitted not only to preserve the long-term morphology and resistence, but also to increase the mechanical properties of the scaffolds themselves. The cell viability test performed, showed that fibroblasts and tenocytes were able to proliferate and elongate their shape in a phisiologiac way.

Moreover, in order to reach a complete biomimetic reproduction of a whole tendon or ligament, for the first time a method to produce an electrospun sheath epitenon/epiligament-like was described. The electrospun sheath had demonstrated to be able to group any number of bundles, tuning also the internal porosity of the scaffolds. The PLLA multiscale hierarchical scaffolds obtained by using this methodology, showed mechanical properties comparable to the human and animal tendons and ligaments ones, with a biomimetic morphology without precedents in literature. Furthermore, human fibroblasts demonstrated to be able to infiltrate inside the scaffolds and growth in them in an excellent biomimetic way.

In the last part of the work, in order to offer also an answer for the topic of the complete tendon and ligament prosthetic replacement and simulation, different shapes of Nylon6.6 hierarcally structerd assemblies were developed. The Nylon6.6 assemblies not only demonstrated to have the ability of perfectly replicating the

mechanical properties of the tendons and ligaments, but also the possibility to be grouped together in higher hierarchical levels too, simulating perfectly all the hierarchical levels of aggregation of the collagen in the native tissue. Moreover, the limitation of the surgical suturing and fixation in the site of the lesion were also overcome by developing in the assemblies ends, fixing loops suitable to reduce the mechanical stress contentrations.

In addition, during the whole project, custom-made protocols were described and validated to develop the first multiscale morphological characterization of electrospun materials by using high-resolution x-ray tomography. The levels of resolution reached permitted a full field morphological assessment of the scaffolds object of the present Thesis, from the nanofiber, to the whole hierarchical scaffold level.

Once completed the *in vitro* assessment of the scaffolds during this Thesis, the future outcomes of the work will be various and multidisciplinary. In fact, from one side, the regenerative one, the hierarchical tendon/ligament-like scaffolds are ready for a large *in vivo* animal trial before a future chilincal applications. This step will be carried out in the next few months. Moreover, thanks to the similar hierarchical structure of muscles and nerves with tendons and ligaments, these scaffolds will also be used for the regeneration of muscle and nerve tissue.

Finally, the inert hierarchical assemblies will be applied in the next months for soft robotic applications, to develop a new generation of bioinspired actuators and sensors.

Appendix A: Scaffold multiscala elettrofilato per la rigenerazione e/o sostituzione del tessuto tendineo/legamentoso e metodo di produzione

Alberto Sensini[1], Luca Cristofolini[1,3], Chiara Gualandi[2], Maria Letizia Focarete[2,3], Juri Belcari[1], Andrea Zucchelli[1]

1 Department of Industrial Engineering, Alma Mater Studiorum—University of Bologna, I-40131 Bologna, Italy

2 Department of Chemistry 'G. Ciamician' and National Consortium of Materials Science and Technology (INSTM, Bologna RU), Alma Mater Studiorum—University of Bologna, I-40126 Bologna, Italy

3 Health Sciences and Technologies—Interdepartmental Center for Industrial Research (HST-ICIR), Alma Mater Studiorum—University of Bologna, I-40064 Ozzano dell'Emilia, Bologna, Italy

Patent application number: 102017000064613

The candidate was the first name of the Italian patent.

Patent filed 12 June 2017

A.1 Riassunto

La presente invenzione si riferisce ad un supporto multiscala per la rigenerazione tissutale, in particolare per la rigenerazione o sostituzione del tessuto tendineo e/o legamentoso. La presente invenzione si riferisce inoltre ai procedimenti per ottenere tale supporto ed ai suoi usi.

A.2 Descrizione

A.2.1 Campo tecnico dell'invenzione

La presente invenzione si riferisce ad un supporto *(scaffold)* multiscala per la rigenerazione tissutale, in particolare per la rigenerazione o sostituzione del tessuto tendineo e/o legamentoso. La presente invenzione si riferisce inoltre ai procedimenti per ottenere tale supporto ed ai suoi usi.

A.2.2 Stato della tecnica

Nel campo dell'ingegneria dei tessuti, lo scaffold svolge un ruolo importante nel fornire un ambiente ideale per l'adesione, proliferazione e migrazione delle cellule. La morfologia e la struttura dei supporti per ingegneria tissutale sono fondamentali per la forma e la struttura definitiva dei tessuti e degli organi da ricostruire o sostituire. Pertanto, ci sono alcuni requisiti specifici nella struttura, nella morfologia ed in altri aspetti delle proprietà fisiche e chimiche dello scaffold che lo rendono ideale per la ricostruzione o sostituzione dei tessuti.

In particolare gli scaffold per la ricostruzione del legamento o del tendine dovrebbero essere biodegradabili, porosi, biocompatibili, presentare una sufficiente resistenza e rigidezza meccanica, e favorire la formazione di tessuti del legamento o del tendine.

Dawei et al. in J. Mater. Chem B 2015, 3, 8823 descrivono un supporto *(scaffold)* per la rigenerazione di lesioni nervose periferiche preparato mediante elettrofilatura di nanofibre di poli(L-lattide-co-caprolattone) (P(LLA-CL)) e acido polilattico (PLLA). Tale scaffold presenta una camicia esterna formata da nanofibre

elettrofilate senza una orientazione preferenziale con evidenti limiti di applicabilità nel campo della ingegneria tissutale del tessuto tendineo e/o legamentoso. In primo luogo, per la filatura della camicia esterna viene utilizzato un collettore di terra a rullo attorno al quale vengono fissati manualmente i fasci che comporranno lo scaffold. Tale soluzione tecnologica non consente di compattare i fasci elettrofilati nello scaffold completo, limitandone evidentemente le proprietà meccaniche finali, inoltre richiede una successiva rimozione del collettore di terra dal costrutto finale, operazione che potrebbe compromettere la struttura dello scaffold stesso. Inoltre la soluzione tecnologica adottata da Dawei at al. consente di rivestire un numero limitato di fasci elettrofilati con la camicia esterna. Aumentando infatti il numero di fasci e/o il diametro dei fasci, o eventualmente riducendo il diametro del collettore a rullo, vi è il forte rischio che l'effetto di terra del collettore venga drasticamente indebolito, rendendo impossibile la deposizione delle fibre elettrofilate che costituiscono la camicia esterna.
Lo stato della tecnica come sopra ricostruito indica quindi la necessità di fornire nuovi supporti e metodi per la loro produzione che non presentino gli svantaggi di quelli della tecnica nota.

A.2.3 Sommario dell'invenzione

Gli inventori sono riusciti ad ottenere un supporto *(scaffold)* che permette di sostituire e/o ricostruire il tessuto tendineo e/o legamentoso attraverso un costrutto multiscala in grado di riprodurre le caratteristiche meccaniche, morfologiche e fisiologiche di tendini e legamenti. La tecnologia usata per la produzione di tale scaffold permette di produrre una camicia esterna elettrofilata, che può anche essere utilizzata per compattare sottogruppi di fasci all'interno dello scaffold, senza l'utilizzo di collettori di terra interni al corpo dello scaffold. Inoltre tale camicia conferisce protezione, e compattamento meccanico dei fasci al suo interno, permettendo al contempo il passaggio delle cellule. Lo scaffold multiscala ottenuto dagli inventori riesce a replicare vari livelli di aggregazione del tessuto tendineo/legamentoso, dalle fibrille di collagene, ai fascicoli tendineo/legamentosi, fino a raggiungere il tendine/legamento completo. Inoltre gli inventori sono riusciti a sviluppare un procedimento per poter elettrofilare una camicia di nanofibre

secondo un allineamento casuale (random) sulla superficie dei fasci di filamenti, simile per morfologia alla guaina che riveste i tendini/legamenti (epitenon), riuscendo eventualmente a rivestirne anche sottogruppi (endotenon), in modo tale da permettere il compattamento dei fasci e favorirne la resistenza meccanica da un lato, ma permettere anche il passaggio delle cellule attraverso la camicia e la colonizzazione dei fasci.

Un ulteriore vantaggio dello scaffold qui descritto risiede nella possibilità di includere al proprio interno un numero qualsiasi di fasci di qualsiasi diametro, compattati e riuniti attraverso una camicia elettrofilata porosa in grado di garantire da un lato protezione ai fasci al suo interno, dall'altro il passaggio delle cellule attraverso di essa al fine di potersi depositare sui fasci e ricostruire la matrice extracellulare tendineo/legamentosa. La camicia elettrofilata viene prodotta senza l'utilizzo di collettori interni allo scaffold ed è in grado di compattare ed eventualmente attorcigliare (twisting) i fasci al proprio interno. Tale camicia può anche essere utilizzata per rivestire sottogruppi di fasci all'interno dello scaffold incrementando ulteriormente le proprietà meccaniche.

E' quindi un primo oggetto della presente invenzione uno scaffold multiscala per la sostituzione, riparazione, ricostruzione o simulazione di un tessuto, in particolare del tessuto tendineo e legamentoso comprendente:

-una pluralità di fasci ottenuti per elettrofilatura costituiti da nanofibre allineate assialmente e in cui detta pluralità di fasci sono disposti in modo da formare un singolo fascio;

-una camicia porosa ottenuta per elettrofilatura costituita da nanofibre disposte in modo casuale, in cui detta camicia riveste esternamente e compatta detta pluralità di fasci mantenendoli allineati tra loro.

Detta camicia quindi riesce a compattare i fasci mantenendoli contemporaneamente allineati tra loro, senza la necessità doverli intrecciare, attorcigliare e senza l'eventuale utilizzo di riempitivi compattanti per ottenere il medesimo effetto, a differenza del caso dei costrutti precedentemente sviluppati, garantendo di conseguenza proprietà meccaniche simili a quelle proprie del tessuto tendineo e legamentoso corporeo, consentendo contemporaneamente di mimare in maniera

assolutamente fedele l'organizzazione gerarchica del tessuto tendineo e legamentoso stesso.

Tale caratteristica risulta di fondamentale importanza per uno scaffold pensato per la rigenerazione del tessuto tendineo e legamentoso: variando infatti la struttura morfologica dello scaffold da quella del tessuto nativo, è forte il rischio dell'insorgere di tessuto cicatriziale con conseguente impoverimento delle proprietà meccaniche finali del tessuto rigenerato. Detta camicia permette inoltre il passaggio delle cellule che dovranno colonizzare l'intera struttura multiscala; altresì permette la corretta vascolarizzazione della componente cellulare e l'eliminazione delle componenti di scarto prodotte dalle cellule durante la ricostruzione del tessuto in oggetto. Il costrutto che ne consegue ha caratteristiche meccaniche (resistenza e rigidezza) elevate, dello stesso ordine di grandezza dei tessuti tendinei e legamentosi umani.

Un secondo oggetto della presente invenzione è un procedimento per la preparazione di uno scaffold multiscala per la sostituzione, riparazione o ricostruzione di un tessuto, in particolare del tessuto tendineo e legamentoso, comprendente i seguenti passaggi:

a) preparare mediante elettrofilatura una pluralità di fasci costituiti da nanofibre allineate assialmente;

b) elettrofilare nanofibre in modo da rivestire detti fasci con una camicia porosa costituta da nanofibre disposte secondo un allineamento casuale in modo tale da fornire un rivestimento esterno e compattare la pluralità di fasci preparati con il passaggio a).

In particolare secondo una forma di realizzazione tale procedimento prevede i seguenti passaggi:

a) preparare mediante elettrofilatura una pluralità di fasci (bundles) costituiti da nanofibre allineate assialmente;

b) posizionare detta pluralità di fasci preparati al punto a) in modo da formare un singolo fascio;

c) afferrare il fascio ottenuto al passaggio b) su afferraggio capace di ruotare rigidamente e in asse mantenendo così il fascio afferrato in posizione idonea per il processo di rivestimento con camicia elettrofilata;

d) realizzare una camicia esterna del fascio afferrato al punto c) mediante elettrofilatura, in particolare controllando i parametri di rotazione del fascio afferrato, i parametri geometrici del setup, e parametri di processo.
La camicia che si genera ha l'effetto di compattare i fasci di fibre, minimizzando gli spazi vuoti tra un fascio e l'altro e minimizzando quindi la sezione globale del costrutto. Tale effetto permette di ottenere un costrutto dalle proprietà meccaniche migliori.
Altri vantaggi, caratteristiche e le modalità di impiego della presente invenzione risulteranno evidenti dalla seguente descrizione dettagliata di alcune forme di realizzazione, presentate a scopo esemplificativo e non limitativo.

A.2.4 Descrizione breve delle figure

-La Figura 1 è una fotografia di un singolo fascio dello scaffold multiscala secondo una forma di realizzazione preferita della presente invenzione.
-la Figura 2 è una fotografia che mostra lo scaffold multiscala per intero, costituito da una pluralità di fasci (Figura 1) tenuti insieme da una camicia esterna di fibre disposte in modo casuale secondo una forma di realizzazione preferita della presente invenzione.
-la Figura 3 è una fotografia del set-up sperimentale che consente di fissare i fasci parallelamente uno all'altro e uno di fianco all'altro nella fase precedente alla filatura della camicia secondo una forma di realizzazione preferita della presente invenzione.
-la Figura 4 è una fotografia del set-up sperimentale che consente di rivestire i fasci con una camicia esterna di fibre disposte in modo casuale secondo una forma di realizzazione preferita della presente invenzione.
- la Figura 5 è una immagine tomografica delle nanofibre di un fascio (bundle) singolo in PLLA.
- la Figura 6 è una immagine SEM della sezione di uno scaffold multiscala in PLLA composto da 100 bundles e con camicia esterna elettrofilata.

A.2.5 Descrizione dettagliata dell'invenzione

La presente invenzione si riferisce ad uno scaffold multiscala, ai procedimenti per la sua produzione e ai suoi usi.

Nella presente descrizione con l'espressione "supporto o scaffold multiscala" s'intende: un costrutto tridimensionale anisotropo poroso composto da biomateriali assemblati a livello morfologico a diversi livelli di scala dimensionale (da nanometrica a micrometrica e millimetrica) per mimare il più fedelmente possibile la matrice extracellulare del tessuto che si vuole ricostruire nel suo stato nativo. Gli scaffold sono tipicamente progettati per eseguire le seguenti funzioni: (i) promuovere l'interazione cellula-biomateriale, l'adesione cellulare e la proliferazione cellulare, (ii) consentire il trasporto di gas e nutrienti, (iii) se bioassorbibili, biodegradare ad una velocità che approssimi il tasso di rigenerazione tissutale sotto le condizioni di coltura di interesse, (iv) provocare un grado minimo di infiammazione o di tossicità in vivo e (v) avere proprietà meccaniche simili al tessuto che si vuole ricostruire.

Lo scaffold secondo la presente invenzione comprende una pluralità di fasci ottenuti per elettrofilatura costituiti da nanofibre allineate assialmente. Nella presente descrizione con l'espressione nanofibre allineate assialmente s'intende che le nanofibre che costituiscono i fasci sono disposte parallelamente lungo l'asse di sviluppo longitudinale dello scaffold.

Lo scaffold secondo la presente invenzione comprende inoltre una camicia porosa ottenuta per elettrofilatura che riveste esternamente i fasci di nanofibre. Detta camicia esterna (involucro) è costituita anch'essa da nanofibre che presentano una disposizione casuale (random). La porosità della camicia viene generata dalla sovrapposizione di strati di fibre continue disposte su uno stesso piano ma senza una direzione preferenziale a formare un tessuto-non-tessuto. La porosità della camicia è quindi interconnessa, nel senso che i pori mettono in comunicazione lo strato esterno della camicia di fibre con lo strato più interno (a contatto con i fasci). L'interconnessione tra i pori consente alle cellule di filtrare attraverso la camicia esterna per raggiungere gli strati interni dello scaffold multiscala.

La lunghezza dello scaffold potrà essere compresa tra 10 e 500 mm, preferibilmente 20-200 mm e avrà un diametro medio compreso tra 1 e 100 mm, preferibilmente

compreso tra 2 e 50 mm. Secondo una forma di realizzazione lo scaffold sarà in materiale bioriassorbibile o biostabile e/o inerte.

Esempi di materiali bioassorbibili o biostabili di origine sintetica sono poliesteri, poliuretani, poliammidi, poliolefine e polimeri fluorurati. Esempi di materiali bioassorbibili o biostabili di origine naturale sono polisaccaridi, proteine, poliesteri, poliammidi, polipeptidi. Esempi preferiti di materiali per la preparazione delle nanofibre sono acido poli-(L)-lattico (PLLA) e/o nylon 6,6.

Secondo una forma di realizzazione lo scaffold multiscala e/o le nanofibre di cui esso si compone, potranno essere caricate e/o funzionalizzate con componenti di natura organica e/o inorganica che svolgano un'azione biologica e/o di cambiamento delle proprietà chimico-fisiche e/o meccaniche del tessuto in cui potrà essere usato lo scaffold. Ad esempio componenti di natura organica e/o inorganica che potranno essere usati sono farmaci, fattori di crescita, sostanze antibatteriche, peptidi, idrossiapatiti, fosfati, biovetri, ossidi metallici, grafene, nanotubi di carbonio. Le procedure di caricamento e/o funzionalizzazione sono note al tecnico del settore.

Le nanofibre che costituiscono i fasci e/o la camicia avranno un diametro medio compreso tra 10 e 10000 nm, preferibilmente compreso tra 300 e 1000 nm, mentre il diametro medio dei fasci potrà essere compreso tra 20 e 10000 μm, preferibilmente tra 500 e 650 μm. Il numero di fasci dello scaffold sarà ad esempio compreso tra 2 e 1000, preferibilmente tra 40 e 200, ad esempio 100.

Gli scaffold multiscala secondo la presente invenzione avranno vantaggiosamente un valore di resistenza meccanica compreso tra 10 e 5000 N preferibilmente tra 200 e 500 N e/o un modulo elastico compreso tra 20 e 100000 MPa, preferibilmente di circa 30-20000 MPa. Tali caratteristiche meccaniche sono state misurate tramite prova a trazione monoassiale con afferraggi a cabestano (capstan grips) per i singoli fasci, e cementando le estremità per gli scaffold multiscala, come descritto negli esempi.

Un secondo oggetto della presente invenzione è un procedimento per la preparazione di uno scaffold multiscala per la sostituzione, riparazione o ricostruzione di un tessuto, in particolare del tessuto tendineo e/o legamentoso, comprendente i seguenti passaggi:

a) preparare mediante elettrofilatura una pluralità di fasci costituiti da nanofibre allineate assialmente;
b) elettrofilare nanofibre in modo da rivestire detti fasci con una camicia porosa costituta da nanofibre disposte secondo un orientamento casuale in modo tale da fornire un rivestimento esterno e compattare la pluralità di fasci preparati con il passaggio a).
In particolare il procedimento prevedrà i seguenti passaggi:
a) preparare mediante elettrofilatura una pluralità di fasci (bundles) costituiti da nanofibre allineate assialmente, cioè secondo l'asse longitudinale di sviluppo dello scaffold;
b) posizionare detta pluralità di fasci preparati al punto a) in modo da formare un singolo fascio;
c) afferrare il fascio ottenuto al passaggio b) su afferraggio capace di ruotare rigidamente e in asse mantenendo così il fascio afferrato in posizione idonea per il processo di rivestimento con camicia elettrofilata;
d) realizzare una camicia esterna del fascio afferrato al punto c) mediante elettrofilatura, in particolare controllando i parametri di rotazione del fascio afferrato, i parametri geometrici del setup, e parametri di processo.
Secondo una forma di realizzazione le nanofibre dei fasci e/o della camicia potranno essere preparate elettrofilando una soluzione di PLLA sciolto in idoneo solvente, ad esempio in diclorometano (DCM) e N,N-dimetilformammide (DMF). La soluzione potrà essere preparata ad esempio con 10-30% (w/v) di PLLA in ad esempio 65/35 (v/v) (DCM/DMF).
Secondo una forma di realizzazione le condizioni di filatura dei fasci prevedono l'applicazione di un campo elettrico con un voltaggio compreso tra 10 e 30 kV, preferibilmente 18 kV per un tempo di elettrofilatura di almeno 15 min, preferibilmente di un'ora, depositando le fibre su un collettore rotante ad alta velocità che consenta l'allineamento delle fibre. Le fibre depositate sul collettore vengono successivamente raccolte insieme per formare un fascio di fibre allineate.
Secondo una forma di realizzazione le condizioni di elettrofilatura sulla macchina rotante per la produzione della camicia esterna di fibre random prevedono

l'applicazione di un campo elettrico con un voltaggio compreso tra 10 e 30 kV , per un tempo di elettrofilatura di almeno 2 ore, preferibilmente di 3 ore.

Vantaggiosamente per la preparazione della camicia saranno applicati i seguenti paramenti di processo:

- distanza tra i fasci e il collettore piano minore di 5 mm;
- una velocità rotazione dei fasci di circa 20-25 rpm;
- periodi di immobilità dei fasci di circa 3-5 min;
- periodi di rotazione dei fasci 1-2 min.

Il procedimento per la preparazione dello scaffold secondo la presente invenzione ha importanti vantaggi, in particolare lo sviluppo della camicia attorno ai fasci, che viene prodotta senza inserire nulla nel corpo dello scaffold per guidare la deposizione delle fibre.

Tale risultato è ottenuto modulando la forma, le dimensioni e la posizione del collettore posto nelle vicinanze, ma non a contatto con il gruppo di fasci da rivestire e modulando i tempi di rotazione e di stasi degli stessi, ad esempio potrà essere posizionato ad una distanza compresa tra 1 e 50 mm.

Così facendo durante i tempi di stasi i fasci saranno circondati, da uno strato di nanofibre random che avrà le proprie estremità depositate sul collettore. Mettendo in rotazione il gruppo di fasci, si verificherà il distaccamento di una estremità dello strato di nanofibre dal collettore piano, avvolgendo il gruppo di fasci e favorendone il compattamento e pretensionamento. Una volta arrotolato tutto lo strato di nanofibre random attorno al gruppo di fasci, l'estremità ancora adesa al collettore piano si staccherà a sua volta. A distacco avvenuto, grazie all'azione combinata di rotazione e di campo elettrostatico anche la parte restante dello strato di nanofibre random si depositerà sulla superficie dei fasci. La ripetizione di questo processo porta progressivamente alla compattazione con conseguente riduzione della sezione del gruppo di fasci ed alla completa formazione della camicia per ottenere lo scaffold multiscala completo.

Allo stato dell'arte infatti, sono state realizzate con un tale livello di omogeneità, 1) solamente camicie elettrofilate su fasci fissati attorno ad un rullo messo in rotazione, oppure 2) camicie prodotte a parte, al cui interno in un secondo momento vengono inseriti i fasci oppure 3) camicie prodotte su gruppi di fasci fissati tra loro

da un riempitivo come ad esempio resine. Questi procedimenti non permettono alti livelli di compattamento dello scaffold finale, fondamentale per aumentare le proprietà meccaniche del costrutto, e pone seri vincoli progettuali sul numero di fasci utilizzabili.

È anche oggetto della presente invenzione lo scaffold multiscala ottenibile secondo una qualsiasi delle forme di realizzazione del procedimento qui descritto.

Lo scaffold multiscala qui descritto potrà essere usato in diverse applicazioni ad esempio nel settore biomedicale in ambito ortopedico o veterinario come dispositivo protesico impiantabile, in particolare quando preparato in materiale biostabile, o per la proliferazione cellulare e la rigenerazione tissutale, in particolare quando preparato in materiale bioriassorbibile.

Quando preparato in materiale sintetico potrà inoltre essere applicato anche in robotica e nella produzione di attuatori e guide o nella produzione di tendini e/o legamenti sintetici per la simulazione di pratiche chirurgiche in vitro.

È anche qui descritto un metodo per la rigenerazione o sostituzione di tessuti, in particolare del tessuto tendineo e/o legamentoso comprendente un passaggio d'impiantare in un soggetto che necessita di uno scaffold multiscala secondo una qualsiasi delle forme di realizzazione qui descritte.

Lo scaffold qui descritto potrà essere usato in un metodo ex vivo per la produzione di tendini e/o legamenti in vitro, ad esempio un metodo in cui cellule sono coltivate in vitro con lo scaffold.

* * *

A.3 Esempi

A.3.1 Esempio 1

Sono stati sviluppati 8 prototipi di tendini in Acido poli-(L)-lattico (PLLA) di lunghezza 100 mm (diametro medio 5-6 mm) composti da 100 fasci costituiti da nanofibre allineate nella direzione del fascio (diametro medio fasci 550-650 μm, diametro medio nanofibre 500-600 nm).

Su di essi la camicia è stata prodotta elettrofilando la medesima soluzione di PLLA utilizzata per produrre i fasci. La composizione è preparata con il 13%(p/v) di PLLA disciolto in un sistema solvente di Diclorometano (DCM) e Dimetilformammide (DMF) in percentuale 65/35 (v/v). La camicia è stata prodotta elettrofilando per 3 ore ed intervallando periodi di stasi del gruppo di fasci con periodi di rotazione.

Condizioni di filatura per la produzione di un singolo fascio:

- filatura con 2 aghi metallici Gauge 20;
- portata pompa a siringa 1,2 ml/h;
- voltaggio campo elettrico 18 kV;
- velocità rotazione collettore rotante 2900 rpm;
- distanza ago-collettore 200 mm;
- spessore utile scaffold prodotto 550-650 μm

Una volta tagliati i fasci in campioni da 100 mm di lunghezza ciascuno sono stati allineati e fissati sulla macchina rotante per la produzione della camicia esterna di fibre random, applicando le seguenti condizioni:

- filatura con ago Gauge 20;
- portata pompa a siringa 1,2 ml/h;
- voltaggio campo elettrico 18 kV;
- collettore metallico;
- distanza collettore-ago/i 200 mm;
- distanza gruppo di fasci-collettore piano minore di 5 mm;
- velocità rotazione del gruppo di fasci circa 20-25 rpm;
- periodi di immobilità del gruppo di fasci 2-5 min;
- periodi di rotazione del gruppo di fasci 1-2 min;
- spessore utile della camicia: 5-10 μm

A.3.2 Esempio 2: test meccanici dei fasci prodotti ottenuti nell'esempio 1

Sono stati poi testati meccanicamente i fasci singoli con un test a trazione.

Sinteticamente il test è stato eseguito utilizzando un test a trazione a rottura con velocità di deformazione del 100% sec-1 per simulare condizioni fisiologiche di velocità di deformazione compatibili a rottura del tessuto tendineo:

- campioni testati: 10
- tratto utile 16 mm

velocità traversa 16 mm/sec (velocità di deformazione: 1/sec);

- rampa monotona a rottura;
- controllo di spostamento;
- idratazione dei campioni prima della prova per 2 min in soluzione salina allo 0,9% NaCl;
- i singoli fasci hanno resistito a rottura fino a 4-5 N con un comportamento duttile e deformazioni nell'ordine del 90%, con un modulo elastico di circa 80 MPa.

A.3.3 Esempio 3: test meccanici su scaffolds multiscala prodotti ottenuti nell'esempio1

Gli *scaffold multiscala* completi sono anche essi stati testati meccanicamente con una prova a trazione anche in questo caso con velocità di deformazione del 100% sec-1 per simulare condizioni fisiologiche di rottura del tessuto tendineo:

- tratto utile 50 mm per 5 campioni testati;
- le estremità dei campioni prima della prova erano state cementate in polimetilmetacrilato (PMMA) per un migliore afferraggio. Tali colate avevano forma rastremata per minimizzare la concentrazione di tensioni.
- velocità traversa 50 mm/sec (velocità di deformazione: 1/sec);
- rampa monotona a rottura;
- controllo di spostamento;
- idratazione dei campioni prima della prova per 2 min in soluzione salina allo 0,9% NaCl;
- i cinque tendini hanno raggiunto valori di forza compresi tra i 230-380 N, con deformazioni circa del 30% ed un modulo elastico di circa 130 MPa.
- La rottura dei campioni è avvenuta all'interfaccia tra scaffold e cemento: ciò implica l'insorgere di una concentrazione di tensioni a causa degli afferraggi che ha comportato una notevole sottostima del valore di forza a rottura dello scaffold.

* * *

La presente invenzione è stata fin qui descritta con riferimento ad alcune forme preferite di realizzazione. È da intendersi che possano esistere altre forme di realizzazione che afferiscono al medesimo nucleo inventivo, come definito dall'ambito di protezione delle rivendicazioni qui di seguito riportate.

A.4 Rivendicazioni

1. Scaffold multiscala per la sostituzione, riparazione, ricostruzione o simulazione di un tessuto, in particolare del tessuto tendineo e legamentoso comprendente:
-una pluralità di fasci ottenuti per elettrofilatura costituiti da nanofibre allineate assialmente e in cui detta pluralità di fasci sono disposti in modo da formare un singolo fascio;
-una camicia porosa ottenuta per elettrofilatura costituita da nanofibre disposte in modo casuale, in cui detta camicia riveste esternamente e compatta detta pluralità di fasci mantenendoli allineati tra loro.
2. Scaffold secondo la rivendicazione 1 avente una resistenza meccanica compresa tra 10 e 5000 N e un modulo elastico compreso tra 20 e 100000 MPa.
3. Scaffold secondo la rivendicazione 1 o 2 avente una resistenza meccanica compresa tra 200 e 500 N e/o un modulo elastico compreso tra 30 e 20000 MPa.
4. Scaffold secondo una qualsiasi delle rivendicazioni precedenti in cui detto scaffold ha una lunghezza compresa tra 10 e 500 mm ed un diametro medio compreso tra 1 e 100 mm.
5. Scaffold secondo una qualsiasi delle rivendicazioni precedenti in cui detto scaffold ha una lunghezza compresa tra 20 e 200 mm ed un diametro medio compreso tra 5 e 50 mm.
6. Scaffold secondo una qualsiasi delle rivendicazioni precedenti in cui dette nanofibre che costituiscono detti fasci o detta camicia hanno un diametro medio compreso tra 10 e 10000 nm.
7. Scaffold secondo una qualsiasi delle rivendicazioni precedenti in cui dette nanofibre che costituiscono detti fasci o detta camicia hanno un diametro medio compreso tra 300 e 1000 nm.

8. Scaffold secondo una qualsiasi delle rivendicazioni precedenti in cui il diametro medio di detti fasci è compreso tra 20 e 10000 μm.

9. Scaffold secondo una qualsiasi delle rivendicazioni precedenti in cui il diametro medio di detti fasci è compreso tra 500 e 650 μm.

10. Scaffold secondo una qualsiasi delle rivendicazioni precedenti in cui il numero di detti fasci in detto scaffold è compreso tra 40 e 1000.

11. Scaffold secondo una qualsiasi delle rivendicazioni precedenti in cui detto scaffold è realizzato in materiale bioriassorbibile o biostabile e/o inerte.

12. Scaffold secondo una qualsiasi delle rivendicazioni precedenti in cui detto scaffold è realizzato in un materiale di origine sintetica scelto tra poliesteri, poliuretani, poliammidi, poliolefine e polimeri fluorurati o di origine naturale scelto tra polisaccaridi, proteine, poliesteri, poliammidi, polipeptidi.

13. Scaffold secondo una qualsiasi delle rivendicazioni precedenti in cui per la preparazione delle nanofibre è usato acido poli-(L)-lattico (PLLA) e/o nylon 6,6.

14. Scaffold secondo una qualsiasi delle rivendicazioni precedenti in cui detto scaffold multiscala e/o dette nanofibre sono caricate e/o funzionalizzate con componenti di natura organica e/o inorganica atte a svolgere un'azione biologica e/o di cambiamento delle proprietà chimico-fisiche e/o meccaniche di detto tessuto.

15. Scaffold secondo una qualsiasi delle rivendicazioni precedenti in cui detti componenti di natura organica e/o inorganica sono scelti tra farmaci, fattori di crescita, sostanze antibatteriche, peptidi, idrossiapatiti, fosfati, biovetri, ossidi metallici, grafene, nanotubi di carbonio o loro miscele.

16. Scaffold secondo una qualsiasi delle rivendicazioni precedenti ottenibile secondo una qualsiasi delle rivendicazioni da 16 a 22.

17. Dispositivo protesico impiantabile comprendente uno scaffold secondo una qualsiasi delle rivendicazioni da 1 a 15.

18. Tendine e/o legamento sintetico comprendente uno scaffold secondo una qualsiasi delle rivendicazioni da 1 a 15.

19. Procedimento per la preparazione di un supporto multiscala secondo una qualsiasi delle rivendicazioni da 1 a 15 comprendente i seguenti passaggi:

a) preparare mediante elettrofilatura una pluralità di fasci costituiti da nanofibre allineate assialmente;

b) elettrofilare nanofibre in modo da rivestire detti fasci con una camicia porosa costituta da nanofibre disposte secondo un orientamento casuale in modo tale da fornire un rivestimento esterno e compattare la pluralità di fasci preparati con il passaggio a).

20. Procedimento per la preparazione di un supporto multiscala secondo una qualsiasi delle rivendicazioni da 1 a 15 comprendente i seguenti passaggi:

a) preparare mediante elettrofilatura una pluralità di fasci (bundles) costituiti da nanofibre allineate assialmente;

b) posizionare detta pluralità di fasci preparati al punto a) in modo da formare un singolo fascio;

c) afferrare il fascio ottenuto al passaggio b) su afferraggio capace di ruotare rigidamente e in asse mantenendo così il fascio afferrato in posizione idonea per il processo di rivestimento con camicia elettrofilata;

d) realizzare una camicia esterna del fascio afferrato al punto c) mediante elettrofilatura, in particolare controllando i parametri di rotazione del fascio afferrato, i parametri geometrici del setup, e parametri di processo.

21. Procedimento secondo la rivendicazione 16 o 17 in cui le nanofibre dei fasci e/o della camicia sono preparate elettrofilando una soluzione di PLLA sciolto in diclorometano (DCM) e/o N,N-dimetilformammide (DMF).

22. Procedimento secondo una qualsiasi delle rivendicazioni da 16 a 18 in cui durante il passaggio di elettrofilatura delle nanofibre a) è applicato un campo elettrico con un voltaggio compreso tra 10 e 30, preferibilmente 18 kV, per un tempo di almeno 15 min.

23. Procedimento secondo una qualsiasi delle rivendicazioni da 16 a 19 in cui durante il passaggio di elettrofilatura delle nanofibre a), dette nanofibre sono depositate su un collettore in modo da consentirne l'allineamento.

24. Procedimento secondo la rivendicazione 23 in cui detto collettore, è posto in prossimità dei fasci da rivestire ma senza alcun contatto con detti fasci, in particolare è posto a circa 2-5 mm dai fasci da rivestire.

25. Procedimento secondo una qualsiasi delle rivendicazioni da 17 a 24 in cui in detto passaggio d) per la preparazione della camicia sono applicati i seguenti paramenti di processo:

- distanza tra i fasci e il collettore minore di 5 mm;
- velocità rotazione dei fasci compresa tra circa 20-25 rpm;
- periodi di immobilità dei fasci compreso tra circa 3-5 min;
-periodi di rotazione dei fasci compreso tra 1-2 min.

A.5 Figure

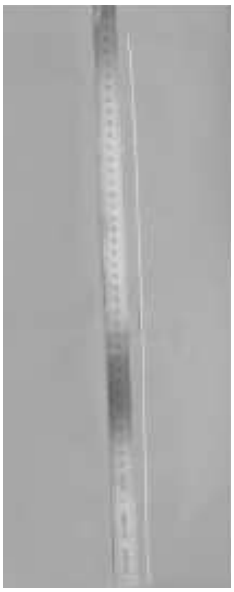

Figura 1

Figura 2

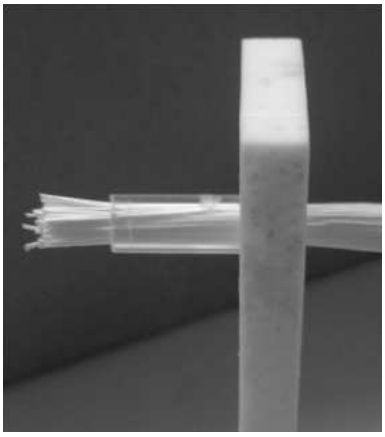

Figura 3

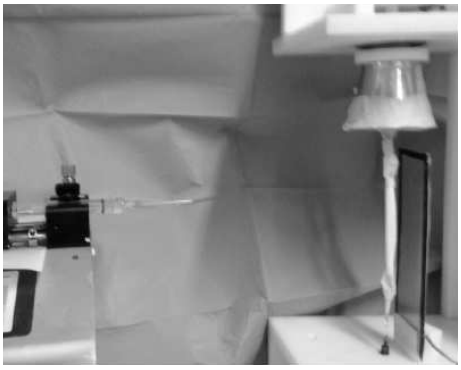

Figura 4

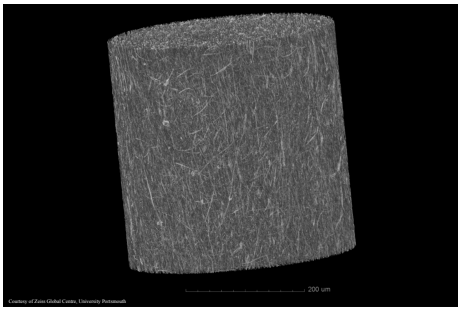

Figura 5

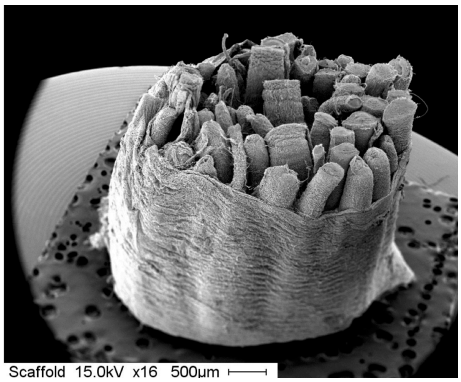

Figura 6

Appendix B: Hierarchical multiscale electrospun scaffold for the regeneration and/or replacement of the tendinous/ligamentous tissue and a method for its production

Alberto Sensini[1], Luca Cristofolini[1,3], Chiara Gualandi[2], Maria Letizia Focarete[2,3], Juri Belcari[1], Andrea Zucchelli[1]

1 Department of Industrial Engineering, Alma Mater Studiorum—University of Bologna, I-40131 Bologna, Italy

2 Department of Chemistry 'G. Ciamician' and National Consortium of Materials Science and Technology (INSTM, Bologna RU), Alma Mater Studiorum—University of Bologna, I-40126 Bologna, Italy

3 Health Sciences and Technologies—Interdepartmental Center for Industrial Research (HST-ICIR), Alma Mater Studiorum—University of Bologna, I-40064 Ozzano dell'Emilia, Bologna, Italy

International publication number: WO2018/229615 A1

The candidate was the first name of the PCT patent. This appendix is the English version of the patent.

Patent filed 8 June 2018

B.1 Abstract

The present invention relates to a support or a multiscale hierarchical scaffold for the tissue regeneration, in particular for the regeneration or replacement of the tendinous and/or ligamentous and/or muscular and/or nervous tissue. The present invention further relates to the processes for obtaining such support and the uses thereof.

B.2 Description

B.2.1 Technical field of the invention

The present invention relates to a support (scaffold) characterized by a hierarchical and multiscale three-dimensional structure for the tissue regeneration, in particular for the regeneration or replacement of the tendinous and/or ligamentous tissue.
The present invention can also be applied for the regeneration and/or replacement and/or simulation of the muscular and/or nervous tissue.
The present invention further relates to the processes to obtain such support and uses thereof.

B.2.2 State of art

In the field of tissue engineering, the scaffold plays an important role in providing an ideal environment for the adhesion, proliferation and migration of cells. The morphology and the structure of the supports for tissue engineering are fundamental for the shape and definite structure of the tissues and the organs to be reconstructed or replaced. Therefore, there are some specific requirements in structure, in morphology and in other aspects of the physical and chemical properties of the scaffold which make it ideal for the tissue reconstruction and/or replacement.
In particular the scaffolds for the reconstruction of the ligament or tendon should be biodegradable, porous, biocompatible, they should have a sufficient resistance and mechanical stiffness, and favour the formation of tissues of ligament or tendon.

Dawei et al. in J. Mater. Chem B 2015, 3, 8823 describe a support (scaffold) for the regeneration of peripheral nervous lesions prepared by electrospinning nanofibers di poly(L-lactide-co-caprolactone) (P(LLA-CL)) and polylactic acid (PLLA). Such scaffold has an outer sheath formed by electrospun nanofibers without a preferential orientation, which coats a certain number of clusters of previously implemented twisted nanofibers (yarns). The applicability limitations of this construct in the field of tissue engineering of tendinous and/or ligamentous and/or muscular and/or nervous tissue appear evident.

First of all, in fact, if for the spinning of the outer sheath a drum ground collector is used, around which the clusters of twisted nanofibers (yarns), which will constitute the complete scaffold, are fastened manually, such technological solution does not allow good compaction of such clusters of twisted nanofibers (yarns) in the complete scaffold, by limiting evidently the final mechanical properties thereof; moreover, this approach requires a subsequent removal of the ground collector from the final construct, a procedure which could compromise the integrity of the scaffold itself. At last, the technological solution adopted by Dawei at al. allows to coat a limited number of clusters of twisted nanofibers (yarns) electrospun with the outer sheath: upon increasing the number of clusters of twisted nanofibers (yarns) and/or the diameter of the clusters of twisted nanofibers (yarns), or in case upon reducing the diameter of the drum collector, there is great risk that the ground effect of the collector is drastically weakened, making impossible the deposition of the electrospun fibers constituting the outer sheath.

Furthermore, in literature up to know no valid solutions are provided capable of being able to effectively suture and/or fix such clusters of twisted nanofibers (yarns) and/or clusters of axially aligned nanofibers (bundles) to the interface with the damaged tissue and/or with muscular and/or bone interface.

Jackson et al. (WO 2010/062297 A1) describe a support (scaffold), for the regeneration di some tissues such as the nervous one, obtained through the electrospinning technology, constituted by a porous sheath of randomly arranged nanofibers (random), which includes an inner portion constituted by single nanofibers, obtained through electrospinning technology too, axially aligned with respect to the scaffold itself. According to the description of the authors, in order to

electrospin the scaffold two synchronous rotating cylinders, and having a gap therebetween (gap), are used as ground collectors. During the initial phase of the electrospinning process the nanofibers, attracted by the two ground collectors, adhere on the two faced sides of the rollers, filling-up the gap between the rollers themselves and by aligning. Once coated the inner faces of the rollers with aligned nanofibers, by continuing the process, the nanofibers arrange randomly, by constituting a sheath which coats the aligned nanofibers (attracted by the axial area of the two rollers). At the end of the process a porous scaffold is obtained, constituted by single nanofibers axially aligned inside thereof, coated by a sheath of nanofibers arranged randomly. The first limitation lies in the impossibility of being able to modulate the final length of the scaffold. In fact, it is known that upon increasing the distance between the rollers, progressively the ground effect between the two rollers decreases until it disappears completely, by allowing the nanofibers to deposit only on the two rollers separately, by making impossible the production of the scaffold and/or the alignment of the nanofibers. Moreover, morphologically such scaffold has a quite different structure with respect to the nervous tissue, which is characterized by a complex, compact, hierarchical and multiscale fibrous structure, organized in substructures which join in different levels to create the complete tissue. In the multiscale hierarchical structure of the nerves, the fundamental elements of such tissues lie in the mielinized neuronal axons. The neuronal axons align and join in groups, the neuronal fascicles; groups of neuronal fascicles are joined and compacted with one another by a fibrous sleeve called epineurium to obtain the complete nerve. Moreover in some nerves, single sub-groups of neuronal fascicles are joined therebetween by sleeves called perineurium, and in turn, these structures are tied up together by the epineurium sleeve. All the just mentioned structures are not reproduced morphologically by the scaffold proposed by the authors which, on the contrary, appears with nor hierarchical nor multiscale three-dimensional structure. Such lack in hierarchical organization in the scaffold proposed by the authors further compromises the mechanical properties of the scaffold itself which, since it includes inside thereof only aligned nanofibers, but having no organization in substructures and no level of compaction, are not able

to offer satisfying mechanical resistance to support the physiological loads thereto such tissues are in vivo subjected.

Sensini et al. (Biofabrication. 2017 Mar 8;9(1):015025) describe a method for producing, through the electrospinning technology, clusters of axially aligned nanofibers (bundles). For their implementation, polymeric nanofibers are electrospun on a drum collector, rotating at high speed. At the end of the electrospinning process circumferential strips of membrane of nanofibers are cut on the drum, and they are rolled up by forming the clusters of axially aligned nanofibers (bundles) (each one having diameter of about 500 micrometers) which are then cut and removed from the drum. However, the authors show these clusters of axially aligned nanofibers (bundles) as scaffolds which mimic the morphology and mechanical properties of single tendinous fascicles of collagen, without proposing any method in order to produce a multiscale hierarchical scaffold capable of reproducing a complete tendon.

What above said shows a huge lack in the literature for reproducing multiscale hierarchical scaffolds capable of reproducing in each element the hierarchical structure of tendons and/or ligaments and/or muscles and/or nerves.

The state of art as above summarized shows then the need for providing new supports and methods for their production not having the disadvantages of those of state of art.

B.2.3 Summary of the invention

The inventors have succeeded in obtaining a support (scaffold) allowing to replace and/or reconstruct the tendinous and/or ligamentous and/or muscular and/or nervous tissue through a construct with hierarchical and multiscale three-dimensional structure (multiscale hierarchical scaffold) capable of reproducing the mechanical, morphological and physiological features of tendons and ligaments and/or muscles and/or nerves.

In the present description under construct and/or multiscale hierarchical scaffold each device or structure is meant, constituted by sub-structures, with different dimensional scales, mutually joining in a hierarchical order. This configuration is typical of the connective tissues such as tendons and/or ligaments, and also of the

muscles and nerves. In fact, the tendinous and/or ligamentous and/or muscular and/or nervous tissues are constituted by a multiscale hierarchical structure constituted by different features (enlisted hereinafter starting from the molecular level as far as the whole tendon and/or ligament and/or muscle and/or nerve):

In the multiscale hierarchical structure of tendons and/or ligaments, the fundamental elements of such tissues lie in the tropocollagen molecules which are joined with one another by producing a collagen fibril; the collagen fibrils are aligned in different groups, called fascicles; groups of fascicles are joined and compacted with each other by a sleeve of collagen fibrils, called epitenon/epiligament, to form the whole tendon or ligament. Moreover in some tendons and/or ligaments, single sub-groups of fascicles are joined therebetween by sleeves called endotenon/endoligament and, in turn, these structures are tied up together by the epitenon/epiligament sleeve.

The natural multiscale hierarchical structure of tendons and/or ligaments is perfectly mimiked by the multiscale hierarchical scaffold the present invention relates to: the electrospun nanofibers (fibers having diameter of nanometers, comparable to the collagen fibrils of tendons and/or ligaments) consist of polymer macromolecules (at a dimensional scale similar to the tropocollagen); a plurality of electrospun nanofibers are aligned to form a cluster of axially aligned nanofibers (bundle) and/or twisted to form a cluster of twisted nanofibers (yarn) (similar to the fascicle of tendons and/or ligaments); the plurality of clusters of axially aligned nanofibers (bundles), and/or the plurality of clusters of twisted nanofibers (yarns), are joined and compacted with each other by an electrospun sheath of nanofibers (imitating the epitenon/epiligament sleeve of tendons and/or ligaments) which forms the multiscale hierarchical scaffold the present invention relates to. Moreover, several multiscale hierarchical scaffolds, the invention relates to, can be joined, in turn, therebetween in an additional hierarchical level, by an additional electrospun sheath produced similarly to the previous one. In this case the sheath coating the single multiscale hierarchical scaffolds will simulate the endotenon/endoligament sleeves of tendons and/or ligaments, whereas the outer sheath joining it will simulate the epitenon/epiligament of tendons and/or ligaments.

In the hierarchical and multiscale structure of the muscles, the fundamental elements of such tissues lie in the molecules of actin and myosin, joined with each other by producing filamentous structures called muscle fibres. The muscle fibres align and join in groups, the muscle fascicles; groups of muscle fascicles are joined and compacted with each other by a fibrous sleeve called epimysium, by forming the complete muscle. Moreover, in some muscles, sub-groups of muscle fascicles are joined therebetween by sleeves called perimysium, and in turn these structures are tied up together by epimysium.

The natural multiscale hierarchical structure of the muscles is perfectly mimiked by the multiscale hierarchical scaffold the present invention relates to: the polymer macromolecules (at a dimensional scale comparable to actin and myosin of the muscles), form the electrospun nanofibers (comparable to the muscular fibrils); a plurality of electrospun nanofibers are aligned to form a cluster of axially aligned nanofibers (bundle), and/or twisted to form a cluster of twisted nanofibers (yarn) (similar to the muscle fascicle); the plurality of clusters of axially aligned nanofibers (bundles), and/or the plurality of clusters of twisted nanofibers (yarns), are joined and compacted with each other by an electrospun sheath of nanofibers (imitating the epimysium sleeve) which forms the multiscale hierarchical scaffold, the present invention relates to. Moreover, several multiscale hierarchical scaffolds the invention relates to, can be joined, in turn, therebetween in an additional hierarchical level by an additional electrospun sheath produced similarly to the previous one. In this case the sheath coating the single multiscale hierarchical scaffolds, will simulate the perimysium sleeves of the muscles, whereas the outer sheath joining them will simulate the epimysium sleeve of the muscle tissue.

In the multiscale structure of the nerves, all fundamental elements of such tissues lie in the mielinized neuron axons. The neuron axons align and join in groups, the neuron fascicles; groups of neuron fascicles are joined and compacted with each other by a fibrous sleeve called epineurium in order to obtain the complete nerve. Moreover, in some nerves, single sub-groups of neuron fascicles are joined therebetween by sleeves called perineurium, and in turn, these structures are tied up together by the epineurium sleeve.

The natural multiscale hierarchical structure of the nerves is perfectly mimiked by the multiscale hierarchical scaffold the present invention relates to: a plurality of electrospun nanofibers (for guiding the growth of the neuron sprouts and cells of Schwann) are aligned and grouped in clusters of axially aligned nanofibers (bundles) and/or twisted in clusters of nanofibers (yarns) (similar to the fascicles of the nerves); the plurality of clusters of nanofibers axially aligned (bundles) and/or the plurality of clusters of twisted nanofibers (yarns), are joined and compacted with each other by an electrospun sheath of nanofibers (imitating the epineurium sleeve of the nerves) which forms the multiscale hierarchical scaffold, the present invention relates to. Moreover, several multiscale hierarchical scaffolds, the invention relates to, can be joined, in turn, therebetween in an additional hierarchical level by an additional electrospun sheath produced similarly to the previous one. In this case the sheath coating the single multiscale hierarchical scaffolds will simulate the perineurium sleeves of the nerves, whereas the outer sheath joining them will simulate the epineurium sleeve of nervous tissue.

The process used for producing such multiscale hierarchical scaffold allows to produce an outer electrospun sheath, which can also be used to compact sub-groups of clusters of axially aligned nanofibers (bundles) and/or of clusters of twisted nanofibers (yarns) inside the multiscale hierarchical scaffold, without using ground collectors inside the body of the multiscale hierarchical scaffold. Moreover, such sheath provides protection and mechanical compaction of the clusters of axially aligned nanofibers (bundles) and/or clusters of twisted nanofibers (yarns) inside thereof, by allowing the passage of cells at the same time.

The multiscale hierarchical scaffold obtained by the inventors succeeds in repeating various aggregation levels of the tendinous /ligamentous tissue, from collagen fibrils to the tendinous/ligamentous fascicles, until reaching the complete tendon/ligament. Moreover, the inventors have succeeded in developing a process in order to be able to electrospin a sheath of nanofibers on the surface of the clusters of axially aligned nanofibers (bundles) and/or clusters of twisted nanofibers (yarns), similar by morphology to the sleeve coating the tendons/ligaments (epitenon), in case by succeeding in coating also sub-groups thereof (endotenon), so as to allow the compaction of the clusters of axially aligned nanofibers (bundles) and/or

clusters of twisted nanofibers (yarns) and to favour the mechanical resistance thereof on one side, but even to allow the passage of the cells through the sheath and the colonization of the clusters of axially aligned nanofibers (bundles) and/or clusters of twisted nanofibers (yarns).

An additional advantage of the herein described multiscale hierarchical scaffold lies in the possibility of including inside thereof any number of clusters of axially aligned nanofibers (bundles) and/or clusters of twisted nanofibers (yarns) having any diameter, compacted and joined through a porous electrospun sheath capable of guaranteeing on one side protection to the clusters of axially aligned nanofibers (bundles) and/or clusters of twisted nanofibers (yarns) inside thereof, on the other side the passage of the cells therethrough with the purpose of being able to deposit on the clusters of axially aligned nanofibers (bundles) and/or clusters of twisted nanofibers (yarns) and to reconstruct the tendinous/ligamentous and/or muscular and/or nervous extracellular matrix. The electrospun sheath is produced without using collectors inside to the multiscale hierarchical scaffold and it is capable of compacting and in case twisting (twisting) the clusters of axially aligned nanofibers (bundles) and/or clusters of twisted nanofibers (yarns) inside thereof. Such sheath can also be used to coat sub-groups of clusters of axially aligned nanofibers (bundles) and/or clusters of twisted nanofibers (yarns) inside the multiscale hierarchical scaffold by further increasing the mechanical properties and the aggregation hierarchical level.

Therefore, firstly the present invention relates to a multiscale hierarchical scaffold for the replacement and/or repair and/or regeneration and/or reconstruction and/or simulation of a tissue, in particular of the tendinous and/or ligamentous and/or muscular and/or nervous tissue comprising:

- a plurality of clusters obtained by electrospinning, each one consisting of nanofibers, wherein said plurality of clusters are arranged in order to form one single group;
- a porous sheath obtained by electrospinning consisting of nanofibers, wherein said sheath externally coats and compacts said plurality of clusters by keeping them aligned with each other.

Such sheath is also capable of joining groups of multiscale hierarchical scaffolds with each other, by increasing the aggregation hierarchical level.

Said sheath then succeeds in compacting the clusters of axially aligned nanofibers (bundles) and/or twisted nanofibers (yarns) by keeping them aligned with each other at the same time, without the need of having to interlace them, to twist them and without the possible use of compacting fillers to obtain the same effect, differently from the case of the previously developed constructs, by consequently guaranteeing mechanical properties similar to those typical of the tendinous and/or ligamentous and/or muscular and/or nervous body tissue, allowing at the same time to mimic absolutely fidelic the hierarchical organization of the tendinous and/or ligamentous and/or muscular and/or nervous tissue itself.

Such feature results to be substantially important for a scaffold devised for the regeneration of the tendinous and/or ligamentous and/or muscular and/or nervous tissue: in fact, by varying the morphological structure of the scaffold from that of the native tissue, the risk that scar tissue arises is very strong, with consequent depletion of the final mechanical and morphological properties of the regenerated tissue. Said sheath further allows the passage of the cells which should colonize the whole multiscale hierarchical structure; moreover, it allows the correct vascularization of the cell component and the removal of the waste components produced by the cells during the reconstruction of the subject tissues. The resulting scaffold has high mechanical features (resistance and stiffness), of the same order of magnitude of the tendinous and/or ligamentous and/or muscular and/or nervous human tissues.

Secondly, the present invention relates to a process for preparing a multiscale hierarchical scaffold for the replacement, repair or reconstruction of a tissue, in particular of the tendinous and/or ligamentous and/or muscular and/or nervous tissue, comprising the following steps:

a) preparing by electrospinning a plurality of clusters of axially aligned nanofibers (bundles) and/or clusters of twisted nanofibers (yarns);

b) electrospinning nanofibers so as to coat said plurality of clusters of axially aligned nanofibers (bundles) and/or clusters of twisted nanofibers (yarns) with a porous sheath which consists of nanofibers so as to provide an external coating and

to compact the plurality of clusters of axially aligned nanofibers (bundles) and/or clusters of twisted nanofibers (yarns) prepared according to step a).

In particular according to an embodiment such process provides the following steps:

a) preparing by electrospinning a plurality of clusters each one consisting of axially aligned nanofibers (bundles) and/or clusters of twisted nanofibers (yarns);

b) positioning said plurality of clusters of axially aligned nanofibers (bundles) and/or clusters of twisted nanofibers (yarns) prepared at step a) so as to form one single group;

c) clamping the group of clusters of axially aligned nanofibers (bundles) and/or clusters of twisted nanofibers (yarns) obtained at step b) on a grip capable of axially rigidly rotating and in line, thus by keeping the clamped group of clusters of axially aligned nanofibers (bundles) and/or clusters of twisted nanofibers (yarns) in suitable position for the coating process with electrospun sheath;

d) implementing an outer sheath of the group of clusters of axially aligned nanofibers (bundles) and/or clusters of twisted nanofibers (yarns) clamped at step c) by electrospinning, in particular by controlling the rotation parameters of the clamped group of clusters of axially aligned nanofibers (bundles) and/or clusters of twisted nanofibers (yarns), the geometrical parameters of the setup, and process parameters.

The sheath which is produced has the effect to compact the clusters of axially aligned nanofibers (bundles) and/or twisted nanofibers (yarns), by reducing to minimum the gaps between the different clusters and thus by reducing to minimum the global section of the multiscale hierarchical scaffold. Such effect allows to obtain a construct capable of expressing mechanical properties comparable to those of the natural tissues which it has to mimic, and homogeneous for the whole section thereof.

By replacing the group of clusters of axially aligned nanofibers (bundles) and/or clusters of twisted nanofibers (yarns), according to step b), with a group of multiscale hierarchical scaffolds, and by repeating the steps c) and d), it will be further possible to obtain a multiscale hierarchical scaffold with a further increased

aggregation hierarchical level, as in turn constituted by a plurality of multiscale hierarchical scaffolds.

Thirdly, the invention relates to a new electrospun construct called ring-like cluster of nanofibers (ring bundle). Such construct is configurated morphologically like a closed ring, consisting of randomly arranged nanofibers (random) and/or with an alignment degree along the axial direction of the ring. Such ring-like clusters of nanofibers (ring bundles) will be not necessarily used in the original circular shape, but they could be stretched according to a direction to obtain a closed elongated shape. In particular such ring-like clusters of nanofibers (ring bundle), if used singularly and/or placed side by side to a plurality of ring-like clusters of nanofibers similar to this one, could be used to construct multiscale hierarchical electrospun scaffolds similar to tendons and/or ligaments and/or muscles and/or nerves. In particular if replaced, the clusters of axially aligned nanofibers (bundles) and/or clusters of twisted nanofibers (yarns), at step a), with a single ring-like cluster of nanofibers (ring bundle) and/or with a plurality of ring-like clusters of nanofibers (ring bundles), and by repeating the procedure for the production of the sheath from step b) to step d), the electrospun sheath will compact the central area of the ring-like clusters of electrospun nanofibers (ring bundles), by providing thereto an elongated shape, and by generating loops at the end of the multiscale hierarchical scaffold. Such loops for example will result to be useful to suturing and/or fixing the so-obtained multiscale hierarchical scaffold, to the interface with the tendon and/or ligament and/or muscle and/or nerve and/or bone of interest. Moreover, such ring-like clusters of nanofibers (ring bundles) could be arranged inside the multiscale hierarchical scaffolds, both axially aligned with each other and/or twisted (twisted) with each other and/or singularly twisted and axially placed side by side to each other and/or twisted (twisted) singularly and in turn twisted (twisted) with each other and/or placed in the same scaffold together with one or more clusters of axially aligned nanofibers (bundles) and/or one or more clusters of twisted nanofibers (yarns).

Such ring-like clusters of electrospun nanofibers (ring bundles) in turn could consist of randomly arranged (random) and/or axially aligned and/or twisted nanofibers.

Other advantages, features and use modes of the present invention will result evident from the following detailed description of some embodiments, shown by way of example and not for limitative purposes.

B.2.4 Brief description of the figures

- Figure 1 is a picture of one single cluster of axially aligned nanofibers (bundle) of the multiscale hierarchical scaffold according to a preferred embodiment of the present invention.
- Figure 2 is a picture showing the multiscale hierarchical scaffold fully, which consists of a plurality of clusters of axially aligned nanofibers (bundles) (Figure 1) kept together by an outer sheath of randomly arranged fibers according to a preferred embodiment of the present invention.
- Figure 3 is a picture of the experimental set-up allowing to fix the clusters of axially aligned nanofibers (bundles) and/or clusters of twisted nanofibers (yarns) parallelly to each other and one placed side by side in the phase preceding the spinning of the sheath according to a preferred embodiment of the present invention.
- Figure 4 is a picture of the experimental set-up allowing to coat the clusters of axially aligned nanofibers (bundles) and/or clusters of twisted nanofibers (yarns) with an outer sheath of nanofibers according to a preferred embodiment of the present invention.
- Figure 5 is a tomographic image of the nanofibers of one single cluster of axially aligned nanofibers (bundle) in poly(L)lactic acid (PLLA).
- Figure 6 is a SEM image of the section of a multiscale hierarchical scaffold in PLLA constituted by 100 clusters of axially aligned nanofibers (bundles) and with electrospun outer sheath.
- Figure 7 is a picture of one single ring-like cluster of nanofibers (ring bundle) according to a preferred embodiment of the present invention.
- Figure 8 is a picture showing the multiscale hierarchical scaffold fully, which consists of a plurality of ring-like clusters of nanofibers (ring bundles) (Figure 7) kept together by an outer sheath of randomly arranged nanofibers according to a

preferred embodiment of the present invention, by showing the loops for suturing and/or fixing at their own ends.

- Figure 9 is a schematic representation of the multiscale hierarchical levels of aggregation of the tendinous and/or ligamentous, muscular and nervous tissue, compared with the hierarchical structure of the multiscale hierarchical scaffold the present invention relates to. In particular: a) Multiscale hierarchical structure of tendons and/or ligaments; b) Multiscale hierarchical structure of muscles; c) Multiscale hierarchical structure of nerves; d) Multiscale hierarchical scaffold structure.

- Figure 10 is a schematic representation of the multiscale hierarchical levels of aggregation of the tendinous and/or ligamentous, muscular and nervous tissue according thereto further down hierarchical units of the same tissue join together by increasing the multiscale hierarchical level of the same. Such levels are compared with the hierarchical structure of the multiscale hierarchical scaffold, the present invention relates to, according to the embodiment wherein groups of multiscale hierarchical scaffolds are joined together by an additional sheath of electrospun nanofibers, by forming a multiscale hierarchical scaffold with a higher level of hierarchical organization. In particular: a) Multiscale hierarchical structure of tendons and/or ligaments; b) Multiscale hierarchical structure of muscles; c) Multiscale hierarchical structure of nerves; d) Multiscale hierarchical scaffold structure in turn constituted by groups of multiscale hierarchical scaffolds.

B.2.5 Detailed description of the invention

The present invention relates to a multiscale hierarchical scaffold, to the processes for the production thereof and the uses thereof.

In the present description under hierarchical and multiscale it is meant: each device or structure, constituted by sub-structures, having different dimensional scales, which join in a hierarchical order.

In the present description under the expression “support or a multiscale hierarchical scaffold” it is meant: a porous anisotropic three-dimensional construct constituted by biomaterials assembled at morphological level at different levels of dimensional scale (from nanometric to micrometric and millimetric), hierarchically organized in

a multiscale structure (as defined previously), to mimic as exactly as possible the extracellular matrix of the tissue which one wants to reconstruct in its native state. The scaffolds are typically designed to perform the following functions: (i) promoting the cell-biomaterial interaction, the cell adhesion and the cell proliferation, (ii) allowing the transportation of oxygen, carbon dioxide and nutrients, (iii) if bioresorbable, biodegrading at a speed approximating the tissue regeneration rate under the culture conditions of interest, (iv) not causing in vivo inflammation or toxicity and (v) having mechanical properties similar to the tissue which one wants to reconstruct.

Even a not bioresorbable material could be selected, but in this case it should not cause in vivo inflammation or toxicity and have mechanical and morphological properties similar to the tissue which one wants to reconstruct and/or simulate and/or replace.

In the present description under "cluster of axially aligned nanofibers (bundle)" an electrospun structure is meant, with variable extension and/or section, consisting of nanofibers which arrange with a level of alignment according to the axis of the cluster itself, that is along the greater development direction of these constructs.

In the present description under "cluster of twisted nanofibers (yarn)" an electrospun structure is meant, with variable extension and/or section, consisting of nanofibers which arrange with a level of twisting according to the axis of the yarn itself, that is along the longitudinal direction of these constructs.

In the present description under "ring-like cluster of nanofibers (ring bundle)" a ring-shaped electrospun structure is meant, with variable extension and section, consisting of nanofibers, with a level of alignment according to the axis of the ring-like cluster or ring bundle itself.

In the present description under the expression "forming one single group" the fact of forming one single cluster is meant.

In an additional embodiment the nanofibers constituting the ring-like cluster could be arranged randomly (random) and/or in a twisted way (twisted) and/or with a level of axial alignment inside the body of the ring-like cluster or ring bundle itself.

The multiscale hierarchical scaffold according to the present invention further comprises a porous sheath obtained by electrospinning which coats externally the

clusters of axially aligned nanofibers (bundles) and/or clusters of twisted nanofibers (yarns) and/or ring-like clusters of nanofibers (ring bundles), obtained by electrospinning. Said outer sheath (casing) is constituted by nanofibers too. The porosity of the sheath is produced by the superimposition of layers of continuous nanofibers which deposit in the process period of time on a same plane, by forming a three-dimensional structure like the one of a tissue-non-tissue. The porosity of the sheath is then interconnected, in the sense that the pores put into communication the outer layer of the sheath of fibers with the innermost layer, in contact with the clusters of axially aligned nanofibers (bundles) and/or clusters of twisted nanofibers (yarns) and/or ring-like clusters of nanofibers (ring bundles) and/or sub-groups of multiscale hierarchical scaffolds. The interconnection between the pores allows the cells to filtrate through the outer sheath to reach the inner layers of the multiscale hierarchical scaffold.

The nanofibers of the sheath could be arranged randomly and/or with a level of axial alignment and/or level of peripheral alignment.

The average diameter of the nanofibers constituting the multiscale hierarchical scaffold could be comprised between 10 and 100000 nm.

The length of the multiscale hierarchical scaffold could be comprised between 10 and 1000 mm, in particular between 10 and 500 mm, preferably 20 and 200 mm and it will have an average diameter comprised between 1 and 100 mm, preferably comprised between 2 and 50 mm. According to an embodiment the multiscale hierarchical scaffold will be made of bioresorbable or biostable and/or inert material.

Examples of bioresorbable or biostable materials of synthetic origin are polyesters, polyurethanes, polyamides, polyolefins, fluorinated polymers and copolymers thereof. Examples of bioresorbable or biostable materials of natural origin are polysaccharides, proteins, polyesters, polypeptides and copolymers thereof. Preferred examples of materials for preparing the nanofibers are poly-(L)-lactic acid (PLLA) and/or collagen and/or nylon 6,6, also other biocompatible polyamides known to the person skilled in the art could be used.

According to an embodiment the multiscale hierarchical scaffold and/or the nanofibers it consists of, could be loaded and/or functionalized with components of

organic and/or inorganic nature which play a biological action and/or change in the chemical-physical and/or mechanical properties of the tissue wherein the multiscale hierarchical scaffold could be used. For example components of organic and/or inorganic nature which could be used are drugs, growth factors, antibacterial agents, peptides, hydroxyapatites, phosphates, bio-glasses, metal oxides, graphene, carbon nanotubes.

In an embodiment of the nanofibers constituting the multiscale hierarchical scaffold and/or the sheath and/or the clusters of axially aligned nanofibers (bundles) and/or the clusters of twisted nanofibers (yarns) and/or the ring-like clusters of nanofibers (ring bundles) they could be, from the point of view of morphology, classic nanofibers constituted by one single phase (made of one single material and/or by a mixture of materials and/or loaded and/or functionalized materials) and/or nanofibers constituted by two or more phases (for example core-shell nanofibers, wherein, under core-shell, nanofibers are meant made of different materials between central portion and outer portion of the nanofiber itself) and/or hollow-shell nanofibers (wherein, under hollow-shell, nanofibers are meant constituted by an inner central cavity along the axis of the nanofibers themselves) and/or porous nanofibers (under porous nanofibers nanofibers are meant having pores along their surface and/or in their inner volume).

The procedures for loading and/or functionalizing and/or producing nanofibers with different morphology are known to the person skilled in the art.

The nanofibers constituting the single clusters of axially aligned nanofibers (bundles) and/or clusters of twisted nanofibers (yarns) and/or ring-like clusters of nanofibers (ring bundles) and/or the sheath and/or the sheaths will have an average diameter comprised between 10 and 10000 nm, preferably comprised between 200 and 1000 nm, and in particular between 300 and 1000 nm, whereas the average diameter of the clusters of axially aligned nanofibers (bundles) and/or clusters of twisted nanofibers (yarns) and/or ring-like clusters of nanofibers (ring bundles) could be comprised between 10 and 10000 μm, in particular comprised between 20 and 10000 μm, preferably between 500 and 650 μm. The number of clusters of axially aligned nanofibers (bundles) and/or clusters of twisted nanofibers (yarns)

and/or ring-like clusters of nanofibers (ring bundles) will be for example comprised between 2 and 1000, preferably between 40 and 200, for example 100.

The multiscale hierarchical scaffolds according to the present invention advantageously will have a value of mechanical resistance comprised between 10 and 5000 N preferably between 200 and 500 N and/or an elastic modulus comprised between 20 and 100000 MPa, preferably of about 30-20000 MPa. Such mechanical features were measured by means of monoaxial tensile test with capstan grips (capstan grips) and by cementing the ends as described in the examples.

The present invention further relates to a process for preparing a multiscale hierarchical scaffold for the replacement and/or repair and/or regeneration and/or reconstruction and/or simulation of a tissue, in particular of the tendinous and/or ligamentous and/or muscular and/or nervous tissue comprising the following steps:

a) preparing by electrospinning a plurality of clusters of axially aligned nanofibers (bundles) and/or of clusters of twisted nanofibers (yarns)

b) electrospinning nanofibers so as to coat a plurality of said clusters of axially aligned nanofibers (bundles) and/or clusters of twisted nanofibers (yarns) with a porous sheath consisting of nanofibers so as to provide an external coating and to compact the plurality of clusters of axially aligned nanofibers (bundles) and/or clusters of twisted nanofibers (yarns) prepared according to step a) by obtaining a support or a multiscale hierarchical scaffold;

c) electrospinning nanofibers so as to coat a plurality of said supports or multiscale hierarchical scaffolds according to step b) with an additional porous sheath consisting of nanofibers so as to provide an external coating and to compact the plurality of clusters of axially aligned nanofibers (bundles) and/or clusters of twisted nanofibers (yarns) and/or multiscale hierarchical scaffolds according to step b).

An embodiment of the present invention is a process for preparing ring-like clusters of nanofibers (ring bundles) comprising the following steps:

a) electrospinning on a ground collector shaped like a drum rotating at different speeds according to the wished alignment level, a plurality of nanofibers;

b) cutting peripheral strips of membrane of nanofibers obtained by the electrospinning according to step a);

c) rolling-up the peripheral strips of membrane of nanofibers obtained according to the step b) according to the drum axis;

d) pulling out the drum the ring-like clusters of nanofibers (ring bundles) obtained according to step c).

In particular the process for preparing multiscale hierarchical scaffolds with ring-like clusters of nanofibers (ring bundles) will provide the following steps:

a) preparing by electrospinning a plurality of clusters of axially aligned nanofibers (bundles) and/or clusters of twisted nanofibers (yarns) and/or ring-like clusters of nanofibers (ring bundles);

b) positioning said plurality of clusters of axially aligned nanofibers (bundles) and/or clusters of twisted nanofibers (yarns) and/or clusters of ring-like nanofibers (ring bundles) prepared according to step a) so as to form one single group of clusters of axially aligned nanofibers (bundles) and/or clusters of twisted nanofibers (yarns) and/or ring-like clusters of nanofibers (ring bundles);

c) clamping the group obtained according to step b) on grip capable of axially rotating rigidly and in line, thus keeping the group of clusters of nanofibers and/or axially aligned nanofibers (bundles) and/or clusters of twisted nanofibers (yarns) and/or ring-like clusters of nanofibers (ring bundles), clamped in a suitable position for the coating process with electrospun sheath;

d) implementing an outer sheath on the group of clusters of axially aligned nanofibers (bundles) and/or clusters of twisted nanofibers (yarns) and/or ring-like clusters of nanofibers (ring bundles) clamped at step c) by electrospinning, in particular by controlling the rotation parameters of the clamped group of clusters of axially aligned nanofibers (bundles) and/or clusters of twisted nanofibers (yarns) and/or ring-like clusters of nanofibers (ring bundles), the geometrical parameters of the setup, and process parameters, by obtaining a multiscale hierarchical structure or scaffold.

e) implementing an additional outer sheath on the group of structures or multiscale hierarchical scaffolds obtained according to step d) and clamped as according to step c) by electrospinning, in particular by controlling the rotation parameters of the clamped group of structures or multiscale hierarchical scaffolds, the geometrical parameters of the setup, and process parameters.

According to an embodiment the nanofibers of the clusters of axially aligned nanofibers (bundles) and/or clusters of twisted nanofibers (yarns) and/or ring-like clusters of nanofibers (ring bundles) and/or of the sheath could be prepared by electrospinning a solution of PLLA dissolved in suitable solvent, for example in dichloromethane (DCM) and N,N-dimethylformamide (DMF). The solution could be prepared for example with 10-30% (weight/volume) of PLLA for example in 65/35 (volume/volume) (DCM/DMF).

According to an embodiment the nanofibers of the clusters of axially aligned nanofibers (bundles) and/or clusters of twisted nanofibers (yarns) and/or ring-like clusters of nanofibers (ring bundles) and/or of the sheath could be prepared by electrospinning a solution of nylon 6,6 dissolved in suitable solvent, for example in trifluoroacetic acid (TFA) and acetone (AC). The solution could be prepared with 10-30% (weight/volume) of nylon 6,6 for example in 50/50 (volume/volume) (TFA/AC).

According to an embodiment the spinning conditions of the clusters of axially aligned nanofibers (bundles) and/or of the clusters of twisted nanofibers (yarns) and/or of the ring-like clusters of nanofibers (ring bundles) provide the application of an electrical field having a voltage comprised between 10 and 30 kV, preferably 18 kV for an electrospinning time period of at least 5 min, and in particular at least 15 min, preferably one hour, by depositing the fibres on a collector rotating at high speed allowing an alignment degree of the nanofibers. The nanofibers deposited on the collector are subsequently collected together to form clusters of axially aligned nanofibers (bundle) and/or clusters of twisted nanofibers (yarn) and/or a ring-like clusters of nanofibers (ring bundles) with an alignment degree.

According to an embodiment the electrospinning conditions on the rotating machine for the production of the outer sheath of nanofibers provide the application of an electrical field having a voltage comprised between 10 and 30 kV, for an electrospinning time period of at least 2 hours, preferably 3 hours.

Advantageously for preparing the sheath the following process parameters will be applied:

- distance between the group of clusters and the flat collector smaller than 5 mm;
- a rotation speed of the group of clusters of about 20-25 rpm;

- stillness periods of the group of clusters of about 3-5 min;
- rotation periods of the group of clusters 1-2 min.

The process for preparing the multiscale hierarchical scaffold according to the present invention has important advantages, in particular the development of the sheath around the clusters of axially aligned nanofibers (bundles) and/or clusters of twisted nanofibers (yarns) and/or ring-like clusters of nanofibers (ring bundles), which is produced without inserting anything in the body of a multiscale hierarchical scaffold to guide the deposition of fibers.

Such result is obtained by modulating the shape, the sizes and the position of the collector placed nearby, but not in contact with the group of clusters of axially aligned nanofibers (bundles) and/or clusters of twisted nanofibers (yarns) and/or ring-like clusters of nanofibers (ring bundles) to be coated and modulating the rotation and stasis time periods of the same, for example it could be positioned at a distance comprised between 1 and 50 mm.

Making this way, during the stillness time periods the clusters of axially aligned nanofibers (bundles) and/or clusters of twisted nanofibers (yarns) and/or ring-like clusters of nanofibers (ring bundles) will be surrounded by a layer of nanofibers which will have its own ends deposited on the collector. By putting in rotation the group of clusters, the detachment of one end of the layer of nanofibers from the flat collector will take place, by wrapping the group of clusters of nanofibers, favouring the compaction and the pretensioning. Once the whole layer of nanofibers is rolled up around the group of clusters of nanofibers, the end still attached to the flat collector will detach, in turn. Once the detachment is completed, thanks to the combined action of rotation and electrostatic field even the remaining portion of the layer of nanofibers will deposit on the surface of the clusters of nanofibers. The repetition of this process progressively leads to the compaction with consequent reduction in the section of the group of clusters of nanofibers and to the complete formation of the sheath to obtain the complete multiscale hierarchical scaffold.

Similarly, by repeating the process for producing the sheath of nanofibers on a plurality of multiscale hierarchical scaffolds, produced as previously described, and joined together to form one single group, it will be possible to obtain a multiscale

hierarchical scaffold in turn constituted by a plurality of multiscale hierarchical scaffolds, all of them coated and compacted by an electrospun sheath of nanofibers.
According to an embodiment, the grips for fixing the clusters of axially aligned nanofibers (bundles) and/or twisted nanofibers (yarns) and/or ring-like clusters of nanofibers (ring bundles), capable of rotating rigidly and in line thus keeping the group of clusters of nanofibers, clamped in suitable position for the coating process with electrospun sheath, could be made of metallic material, preferably stainless steel and/or aluminium. According to an embodiment such grips could have a shape which facilitates the fixing of clusters of nanofibers, for example structures with cylinder arms from 1 to 100, preferably 6, having different and/or equal diameter, preferably between 0.5 and 30 mm of diameter. Such grips could be electrically connected to the ground potential to ease the covering of the ends of the multiscale hierarchical scaffold, during the spinning process, by the sheath of nanofibers according to any embodiments of the herein described process.
In the state of art, in fact, with such homogeneity level there were implemented 1) sheaths electrospun on clusters of twisted nanofibers (yarns) fixed around a drum put in rotation, or 2) sheaths produced apart, inside thereof in a second moment the clusters of axially aligned nanofibers (bundles) and/or clusters of twisted nanofibers (yarns) are inserted or 3) sheaths produced on groups of clusters of axially aligned nanofibers (bundles) and/or clusters of twisted nanofibers (yarns) fixed with each other by a filler such as for example resins. These procedures do not allow high levels of compaction of the final scaffold, which is fundamental to increase the mechanical properties of the construct, and poses serious design constraints on the number of usable clusters of axially aligned nanofibers (bundles) and/or clusters of twisted nanofibers (yarns) and/or ring-like clusters of nanofibers (ring bundles).
The present invention also relates to the ring-like clusters of nanofibers (ring bundles) obtainable according to any one of the embodiments of the herein described process and the production method thereof.
The present invention also relates to a multiscale hierarchical scaffold which can be obtained according to anyone of embodiments of the herein described process.
The herein described multiscale hierarchical scaffold could be used in different applications for example in the biomedical sector in orthopaedic or veterinary field

as implantable prosthetic device, in particular if made of biostable material, or for the cellular proliferation and tissue regeneration, in particular if made of bioresorbable material.

If made of biostable synthetic material it could also be applied in robotics and in the production of actuators and guides or in the production of tendons and/or ligaments and/or muscles and/or synthetic nerves for simulating in vitro surgical procedures.

A method for the regeneration or replacement of tissues, in particular of the tendinous and/or ligamentous and/or muscular and/or nervous tissue is also herein described, comprising a step of implantation in a subject requiring a multiscale hierarchical scaffold according to anyone of herein described embodiments.

The herein described multiscale hierarchical scaffold could be used in an ex vivo method for the production of in vitro tendons and/or ligaments and/or muscles and/or nerves, for example a method wherein cells are cultured in vitro with the multiscale hierarchical scaffold.

According to an embodiment the present invention also relates to a multiscale scaffold for the replacement, repair, reconstruction or simulation of a tissue, in particular of the tendinous and/or ligamentous and/or muscular and/or nervous tissue comprising:

- a plurality of clusters obtained by electrospinning consisting of axially aligned nanofibers (bundles) and/or clusters of twisted nanofibers (yarns) and/or ring-like clusters of nanofibers (ring bundles) and wherein said plurality of clusters are arranged in order to form one single group;
- a porous sheath obtained by electrospinning consisting of randomly arranged and/or aligned nanofibers, wherein said sheath externally coats and compacts said plurality of clusters keeping them aligned with each other.

The scaffold according to anyone of herein described embodiments advantageously could also be used as sensor implantable in vivo or in vitro, for example for acquiring and/or transmitting mechanical or physiological signals.

* * *

B.3 Examples

B.3.1 Example 1

8 prototypes of multiscale hierarchical scaffolds were developed, made of Poly-(L)-lactic acid (PLLA) having length of 100 mm (average diameter 5-6 mm) constituted by 100 clusters of axially aligned nanofibers (bundles) consisting of nanofibers aligned in the direction of the cluster of axially aligned nanofibers (bundle) itself (average diameter of cluster of axially aligned nanofibers (bundles) 550-650 μm, average diameter of nanofibers 500-600 nm).

The sheath was produced thereon by electrospinning the same solution of PLLA used to produce the clusters of axially aligned nanofibers (bundles). The composition is prepared with 13% (weight/volume) of PLLA dissolved in a solvent system of Dichloromethane (DCM) and Dimethylformamide (DMF) in percentage 65/35 (volume/volume). The sheath was produced by electrospinning for 3 hours and by alternating stasis periods of the group of clusters of axially aligned nanofibers (bundles) with rotation periods.

Spinning conditions for the production of one single cluster of axially aligned nanofibers (bundle):

- spinning with 2 metal needles Gauge 20;
- syringe pump delivery 1.2 ml/h;
- electrical field voltage 18 kV;
- rotating collector rotation speed 2900 rpm;
- needle-collector distance 200 mm;
- useful thickness of produced cluster of axially aligned nanofibers (bundle) 550-650 μm

Once the clusters of axially aligned nanofibers (bundles) are cut into samples, each one having length of 100 mm, they were aligned and fixed on the rotating machine for the production of the outer sheath of random nanofibers, by applying the following conditions:

- spinning with needle Gauge 20;
- syringe pump delivery 1.2 ml/h;

- electrical field voltage 18 kV;
- metal collector;
- collector-needle(s) distance 200 mm;
- distance between group of clusters of axially aligned nanofibers (bundles) and flat collector smaller than 5 mm;
- rotation speed of the group of clusters of axially aligned nanofibers (bundles) about 20-25 rpm;
- stillness periods of the group of clusters of axially aligned nanofibers (bundles) 2-5 min;
- rotation periods of the group of clusters of axially aligned nanofibers (bundles) 1-2 min;
- useful thickness of the sheath: 5-10 μm

B.3.2 Example 2: mechanical tests of the produced clusters of axially aligned nanofibers (bundles) obtained in example 1

Single clusters of axially aligned nanofibers (bundles) were then tested mechanically with a tensile test.

Synthetically the test was performed by using a tensile breaking test with a strain rate of 100% sec-1 for simulating physiological conditions of strain rate compatible to breaking of the tendinous tissue:

- tested samples: 10
- gauge length 16 mm
- crosshead speed 16 mm/sec (strain rate: 1/sec);
- monotonic ramp to break;
- displacement control;
- hydration of the samples before the test for 2 min in 0.9% NaCl saline solution;

The single clusters of axially aligned nanofibers (bundles) resisted to breaking up to 4-5 N with a ductile behaviour and deformations in the order of 90%, with an elastic modulus of about 80 MPa.

B.3.3 Example 3: mechanical tests on produced multiscale hierarchical scaffolds obtained in example 1

The complete multiscale hierarchical scaffolds were tested mechanically, too, with a tensile test even in this case with a strain rate of 100% sec-1 for simulating physiological breaking conditions of the tendinous tissue:

- useful tract 50 mm for 5 tested samples;
- the ends of the samples before the test had been cemented in polymethylmethacrylate (PMMA) for a better clamping. Such casts had tapered shape to minimize the stress concentration.
- crosshead speed 50 mm/sec (strain rate:1/sec);
- monotonic ramp to break;
- displacement control;
- hydration of the samples before the test for 2 min in 0.9% NaCl saline solution;

The five multiscale hierarchical scaffolds reached force values between 230 and 380 N, with deformations of about 30% and an elastic modulus of about 130 MPa. The breaking of samples took place at the interface between a multiscale hierarchical scaffold and cement: this involves that a stress concentration comes up due to the grips which involved a considerable underestimation of the breaking force value of the multiscale hierarchical scaffold.

B.3.4 Example 4

3 prototypes of multiscale hierarchical scaffolds made of nylon 6,6 with length 230 mm (average diameter 4-5 mm) were developed, constituted by 25 ring-like clusters (ring bundles) consisting of nanofibers aligned in the direction of the axis of the ring-like cluster (ring bundle) (average diameter of bundles 550-650 μm, average diameter of nanofibers 200-300 nm).

The ring-like clusters (ring bundles) were fixed at the ends to the rotating system for the production of sheath, through two grips made of stainless steel constituted by 6 symmetrical cylindrical arms with 8 mm diameter.

On the multiscale hierarchical scaffolds the sheath was produced by electrospinning the same solution of nylon 6,6 used to produce the ring-like clusters (ring bundles).

The composition is prepared with 15%(weight/volume) of nylon 6,6 dissolved in a solvent system of Trifluoro-acetic acid (TFA) and Acetone (AC) in percentage 50/50 (volume/volume). The sheath was produced by electrospinning for 12 hours and alternating stasis periods of the group of ring-like bundles (ring bundles) with rotation periods.

Spinning conditions for the production of the single ring-like clusters (ring bundles):

- spinning with 2 metal needles Gauge 20;
- syringe pump delivery 0.5 ml/h;
- electrical field voltage 20 kV;
- rotating collector rotation speed 2900 rpm;
- needle-collector distance 160 mm;
- useful thickness of produced ring-like bundles (ring bundles) 550-650 μm
- length of the ring-like bundles (ring bundles): about 470 mm (deriving from the deposition on a drum with 150 mm diameter)

Once obtained the ring-like clusters (ring bundles), 25 thereof were aligned and fixed at the ends to the arms of the above-described metal grips, on the rotating machine for the production of the outer sheath of random fibers,

by applying the following conditions:

- spinning with 2 needles Gauge 20;
- syringe pump delivery 0.5 ml/h;
- electrical field voltage 18 kV;
- ground flat metal collector;
- collector-needle(s) distance 160 mm;
- distance between group of ring-like clusters of nanofibers (ring bundles) and flat collector smaller than 5 mm;
- rotation speed of the group of ring-like clusters of nanofibers (ring bundles) about 20-25 rpm;
- stillness periods of the group of ring-like clusters of nanofibers (ring bundles) 2-5 min;
- rotation periods of the group of ring-like clusters of nanofibers (ring bundles) 1-2 min;

- useful thickness of the sheath: 5-10 μm
- after 10 hours of sheath spinning on flat collector electrically connected to the ground as previously described, even the two metal grips positioned at the ends of the group of ring-like clusters of nanofibers (ring bundles) were placed to ground potential, so as to coat with the sheath of randomly arranged nanofibers (random) even the ends themselves. The spinning parameters are the same shown above.

B.3.5 Example 5: mechanical tests of the produced ring-like clusters (ring bundles) obtained in example 4

The single ring-like clusters of nanofibers (ring bundles) were then tested mechanically with a tensile test.
Synthetically the test was performed by using a tensile breaking test with a strain rate of 100% sec-1 to simulate physiological conditions of strain rate compatible to breaking of the tendinous and/or ligamentous and/or muscular and/or nervous tissue:
- tested samples: 5
- gauge length 230 mm
Crosshead speed 230 mm/sec (strain rate: 1/sec);
- monotonic ramp to break;
- displacement control;
- hydration of the samples before the test for 2 min in 0.9% NaCl saline solution;
The single ring-like clusters of nanofibers (ring bundles) resisted to breaking until 20-24 N with a ductile behaviour and deformations in the order of 9-12%, with an elastic modulus of about 600-900 MPa.

B.3.6 Example 6: mechanical tests on produced multiscale hierarchical scaffolds obtained in example 4

The complete multiscale hierarchical scaffolds, too, were tested mechanically with a tensile test even in this case with a strain rate of 100% sec-1 to simulate breaking physiological conditions of the tendinous and/or ligamentous and/or muscular and/or nervous tissue:
- gauge length 230 mm per 3 tested samples;

- As grips of the samples for the mechanical test, the same metal grips were used therewith the samples were fixed to the machine for the sheath production. Such grips had been planned suitably to deconcentrate the tensions.
- crosshead speed 230 mm/sec (strain rate: 1/sec);
- monotonic ramp to break;
- displacement control;
- hydration of the samples before the test for 2 min in 0.9% NaCl saline solution;

The 3 multiscale hierarchical scaffolds reached force values between 300 and 350 N, with deformations of about 9% and an elastic modulus of about 300 to 400 MPa. The breaking of the samples took place both at the interface between a multiscale hierarchical scaffold and grips and in the gauge length: this involves that a partial stress concentration comes up due to the grips which involved an underestimation of the breaking force value of the multiscale hierarchical scaffold.

* * *

The present invention has been so far described with reference to some preferred embodiments. It is to be meant that other embodiments belonging to the same inventive core may exist, as defined by the protective scope of the here below reported claims.

B.4 Claims

1. A multiscale hierarchical scaffold for replacing, repairing, regenerating, reconstructing or simulating a tissue, in particular the tendinous and/or ligamentous and/or muscular and/or nervous tissue comprising:
- a plurality of clusters obtained by electrospinning each one consisting of nanofibers, wherein said plurality of clusters are arranged in order to form one single group;
- a porous sheath obtained by electrospinning consisting of nanofibers, wherein said sheath externally coats and compacts said plurality of clusters keeping them aligned with each other.

2. The scaffold according to claim 1 comprising:
- a plurality of clusters of axially aligned nanofibers (bundles) and/or of clusters of twisted nanofibers (yarns), obtained by electrospinning, consisting of axially

aligned and/or twisted nanofibers, respectively, axially arranged so as to form one single group;

- a porous sheath obtained by electrospinning consisting of nanofibers, wherein said sheath externally coats and compacts said plurality of clusters keeping them aligned with each other.

3. The scaffold according to claim 1 or 2 comprising:

- a plurality of ring-like clusters of nanofibers (ring bundles), obtained by electrospinning, consisting of axially aligned and/or axially twisted nanofibers, respectively, and/or arranged randomly so as to form one single group;

- a porous sheath obtained by electrospinning consisting of nanofibers, wherein said sheath externally coats and compacts said plurality of clusters keeping them aligned with each other.

4. The scaffold according to any one of claims 1 to 3 having a mechanical resistance comprised between 2 and 10000 N, in particular between 10 and 5000 N and an elastic modulus comprised between 20 and 100000 MPa, in particular between 30 and 20000 MPa.

5. The scaffold according to any one of claims 1 to 4 having a mechanical resistance comprised between 200 and 500 N and/or an elastic modulus comprised between 30 and 20000 MPa.

6. The scaffold according to any one of claims 1 to 5 having a mechanical resistance comprised between 2 and 10000 N and an elastic modulus comprised between 20 and 100000 MPa.

7. The scaffold according to any one of the preceding claims wherein said scaffold has a length comprised between 10 and 1000 mm, in particular between 10 and 500 mm, and an average diameter comprised between 1 and 100 mm.

8. The scaffold according to any one of the preceding claims wherein said scaffold has a length comprised between 20 and 200 mm and an average diameter comprised between 5 and 50 mm.

9. The scaffold according to any one of the preceding claims wherein said nanofibers constituting said clusters and/or said sheath have an average diameter comprised between 10 and 10000 nm.

10. The scaffold according to any one of the preceding claims wherein said nanofibers constituting said clusters and/or said sheath have an average diameter comprised between 200 and 1000 nm, in particular between 300 and 1000 nm.

11. The scaffold according to any one of the preceding claims wherein the average diameter of said clusters is comprised between 1 and 10000 μm, in particular between 20 and 10000 μm.

12. The scaffold according to any one of the preceding claims wherein the average diameter of said clusters is comprised between 500 and 650 μm.

13. The scaffold comprising a plurality of inner scaffolds according to any one of claims 1 to 12, in turn joined by a second porous sheath obtained by electrospinning consisting of nanofibers, wherein said sheath externally coats and compacts said plurality of scaffolds.

14. The scaffold according to claim 1 to 13 wherein said porous sheath and/or sheaths consists/consist of randomly arranged nanofibers.

15. The scaffold according to claim 1 to 13 wherein said porous sheath and/or sheaths consists/consist of nanofibers arranged aligned axially with respect to the scaffold axis.

16. The scaffold according to claim 1 to 13 wherein said porous sheath and/or sheaths consists/consist of nanofibers arranged with circumferential alignment with respect to the scaffold axis.

17. The scaffold according to claim 1 to 13 wherein said porous sheath and/or sheaths consists/consist of nanofibers arranged according to a combination of claims 14 to 16.

18. The scaffold according to any one of claims 13 to 17 wherein said inner scaffolds are axially aligned with one another.

19. The scaffold according to any one of claims 13 to 17 wherein said inner scaffolds are twisted with one another (twisting) and/or arranged randomly.

20. The scaffold according to any one of the preceding claims wherein the number of said clusters in said scaffold is comprised between 40 and 1000.

21. The scaffold according to any one of the preceding claims wherein said scaffold is made of bioresorbable or biostable and/or inert material.

22. The scaffold according to any one of the preceding claims wherein said scaffold is made of a synthetic material selected from polyesters, polyurethanes, polyamides, polyolefins and fluorinated polymers and copolymers thereof or of natural material selected from polysaccharides, proteins, polyesters, polypeptides and copolymers thereof and/or mixtures thereof.

23. The scaffold according to any one of the preceding claims wherein poly-(L)-lactic acid (PLLA), polyamides and/or nylon 6,6 is used for preparing the nanofibers.

24. The scaffold according to any one of the preceding claims wherein said scaffold and/or said nanofibers are loaded and/or functionalized with organic and/or inorganic components apt to perform a biological action and/or change in the chemical-physical and/or mechanical properties of said tissue.

25. The scaffold according to claim 24 wherein said organic and/or inorganic components are selected from drugs, growth factors, antibacterial agents, peptides, hydroxyapatites, phosphates, bio-glasses, metal oxides, graphene, carbon nanotubes or mixtures thereof.

26. The scaffold according to any one of the preceding claims wherein gel or hydrogel are injected into said scaffold.

27. The scaffold according to any one of the preceding claims wherein said nanofibers are monophasic.

28. The scaffold according to any one of claims 1 to 26 wherein said nanofibers are multiphasic.

29. The scaffold according to any one of the preceding claims wherein said nanofibers are of core-shell type and/or hollow-shell type and/or porous and/or combinations thereof.

30. The scaffold according to any one of the preceding claims wherein the nanofibers are of piezoelectric type.

31. The scaffold according to any one of the preceding claims wherein said bundles have an axial cavity inside thereof.

32. An implantable prosthetic device comprising a scaffold according to any one of claims 1 to 31.

33. A synthetic tendon and/or ligament comprising a scaffold according to any one of claims 1 to 31.

34. A synthetic muscle comprising a scaffold according to any one of claims 1 to 31.

35. A synthetic nerve comprising a scaffold according to any one of claims 1 to 31.

36. A process for preparing a multiscale hierarchical scaffold according to any one of claims 1 to 31 comprising the following steps:

a) preparing by electrospinning a plurality of clusters of axially aligned nanofibers (bundles) and/or clusters of twisted nanofibers (yarns) and/or ring-like clusters of nanofibers (ring bundles);

b) electrospinning nanofibers so as to coat said clusters with a porous sheath consisting of nanofibers so as to provide an external coating and to compact the plurality of clusters prepared according to step a).

37. The process for preparing a multiscale hierarchical scaffold according to any one of claims 1 to 31 comprising the following steps:

a) preparing by electrospinning a plurality of clusters of axially aligned nanofibers (bundles) and/or clusters of twisted nanofibers (yarns) and/or ring-like clusters of nanofibers (ring bundles);

b) positioning said plurality of clusters prepared according to step a) so as to form one single group;

c) clamping the group of clusters obtained according to step b) on a grip, capable of axially rotating rigidly and in line, thus, by keeping the clamped group of clusters in a position suitable for the process of coating with electrospun sheath;

d) making by electrospinning a sheath external to the group of clusters clamped at step c), in particular by controlling the rotation parameters of the clamped group of clusters, the geometrical parameters of the setup, and process parameters.

38. The process according to claim 36 or 37 wherein the nanofibers of the clusters and/or of the sheath are prepared by electrospinning a solution of PLLA dissolved in dichloromethane (DCM) and/or N,N-dimethylformamide (DMF) or nylon 6,6 dissolved in trifluoro-acetic acid (TFA) and/or acetone (AC).

39. The process according to any one of claims 36 to 38 wherein during the step of electrospinning the nanofibers an electrical field having a voltage comprised

between 10 kV and 30 kV, preferably 18 kV, is applied for a time period of at least 5 min, and in particular at least 15 min.

40. The process according to any one of claims 36 to 39 wherein during the step a) of electrospinning the nanofibers, said nanofibers are deposited on a collector so as to allow the alignment thereof.

41. The process according to any one of claims 36 to 40 wherein during the step of implementing the sheath the nanofibers are deposited on a collector positioned close to the group of clusters to be coated but having no contact with said group of clusters, in particular it is positioned at about 2-5 mm away from the group of clusters to be coated.

42. The process according to any one of claims 36 to 41 wherein in said step for preparing the sheath the following process parameters are used:

- distance between group of clusters and the collector smaller than 5 mm;
- rotation speed of the group of clusters comprised between about 20 and 25 rpm;
- stillness periods of the group of clusters comprised between about 3 and 5 minutes;
- rotation periods of the group of clusters comprised between 1 and 2 minutes.

43. The process according to any one of claims 36 to 42 wherein the grips are made of conductive metallic material, for example stainless steel and/or aluminum and positioned at ground potential to improve the deposition of the sheath of nanofibers arranged randomly on the ends of the scaffold itself.

44. The process according to any one of claims 36 to 43 wherein during the step of implementing the sheath the ground collector has a plane geometry.

45. The process according to any one of claims 36 to 43 wherein during the step of implementing the sheath the ground collector is a concave, convex or prismatic plate.

46. The process according to any one of claims 36 to 43 wherein during the step of implementing the sheath the ground collector consists of two parallel metal rods and/or plates.

47. The process according to any one of claims 36 to 46 comprising the following steps:

a) spinning on rotating drum collector of a plurality of electrospun nanofibers;

b) circumferential winding on the drum of sections of the membrane of electrospun nanofibers to obtain ring-like bundles (ring bundles);

c) removal of the ring-like clusters of nanofibers (ring bundles) from the drum.

48. The process for preparing a multiscale hierarchical scaffold comprising a plurality of inner scaffolds comprising:

a) preparing a plurality of scaffolds according to any one of the preceding claims;

b) electrospinning nanofibers so as to coat said plurality of scaffolds with a porous sheath consisting of nanofibers so as to provide an external coating and to compact the plurality di scaffolds prepared according to step a).

49. The scaffold which can be obtained according to the process of any one of claims 36 to 48.

50. The scaffold according to any one of claims 1 to 31 to be used as sensor for acquiring and/or transmitting mechanical or physiological signals.

51. A use of a scaffold according to any one of claims 1 to 31 as in vitro sensor for acquiring and/or transmitting mechanical or physiological signals.

B.5 Figures

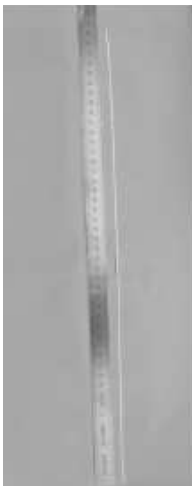

Figure 1

Figure 2

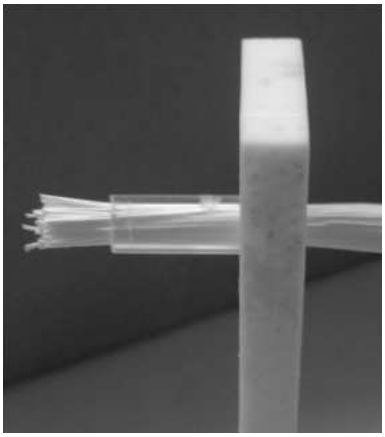

Figure 3

Figure 4

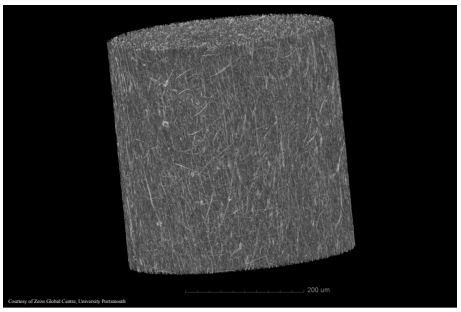

Figure 5

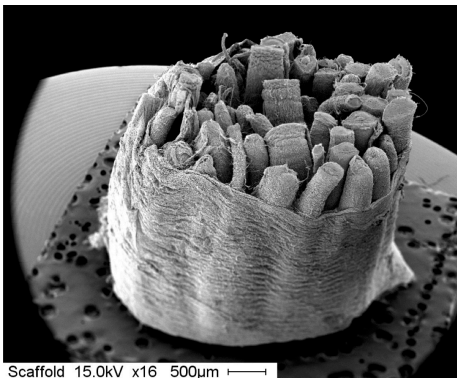

Figure 6

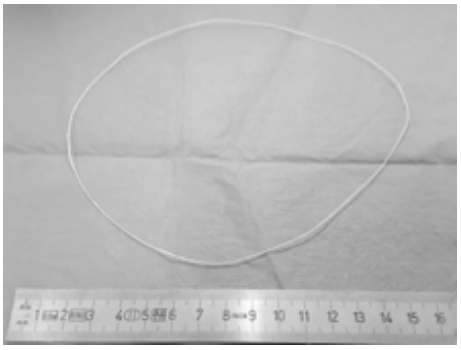

Figure 7

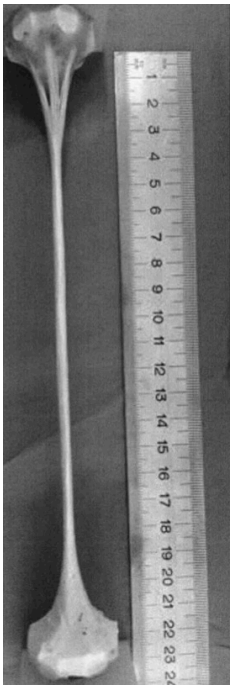

Figure 8

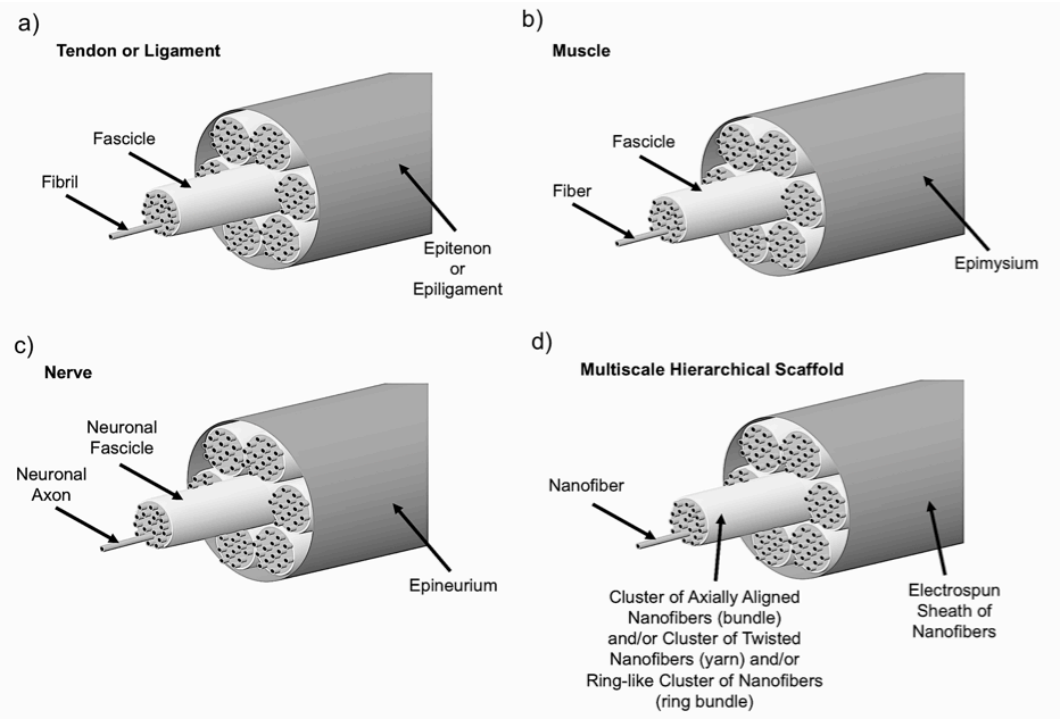

Figure 9

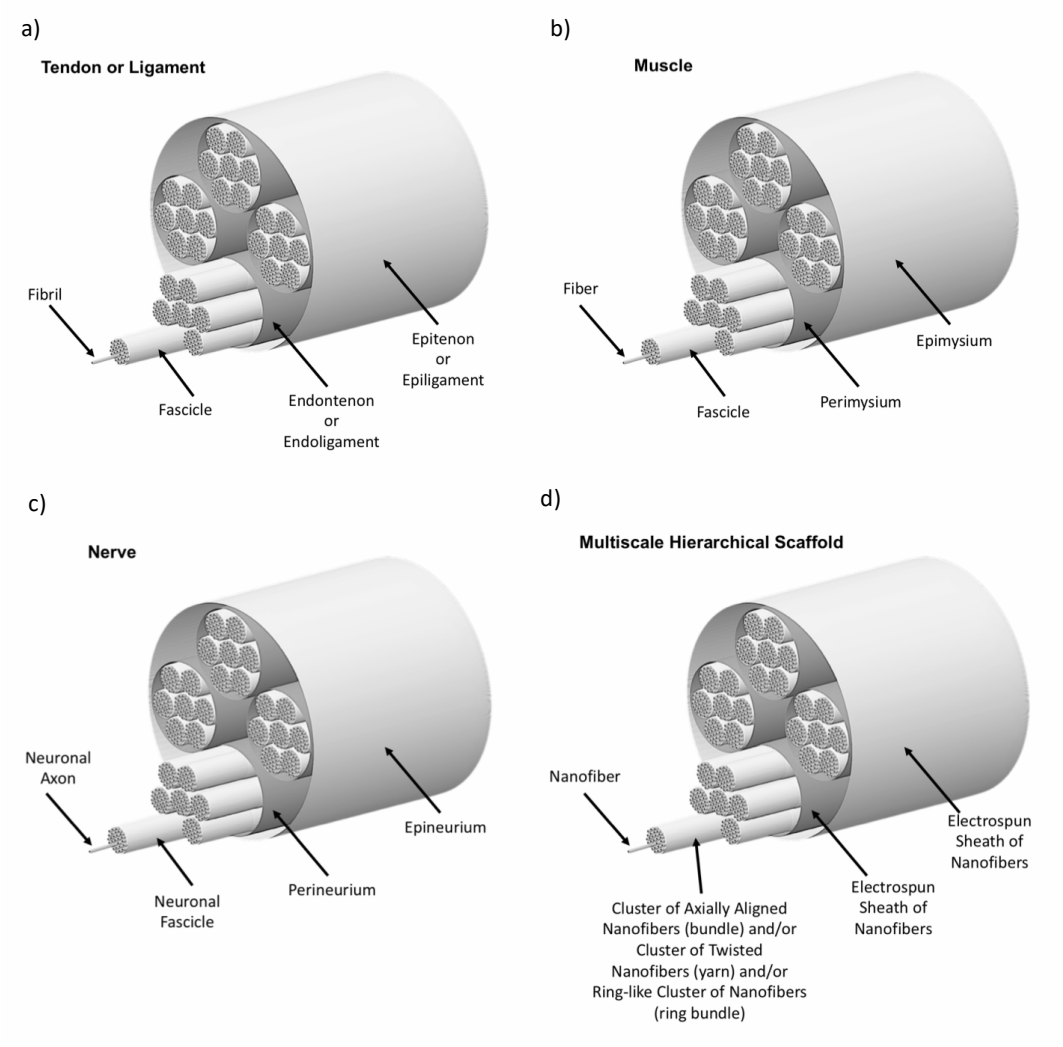
a)
Tendon or Ligament
Fibril
Fascicle
Endontenon
or
Endoligament
Epitenon
or
Epiligament
b)
Muscle
Fiber
Fascicle
Perimysium
Epimysium
c)
Nerve
Neuronal
Axon
Neuronal
Fascicle
Perineurium
Epineurium
d)
Multiscale Hierarchical Scaffold
Nanofiber
Cluster of Axially Aligned
Nanofibers (bundle) and/or
Cluster of Twisted
Nanofibers (yarn) and/or
Ring-like Cluster of Nanofibers
(ring bundle)
Electrospun
Sheath of
Nanofibers
Electrospun
Sheath of
Nanofibers

Figure 10

Appendix C: Scaffold multiscala gerarchico elettrofilato per la rigenerazione e/o sostituzione del tessuto tendineo/legamentoso e metodo di produzione

Alberto Sensini[1], Luca Cristofolini[1,3], Chiara Gualandi[2], Maria Letizia Focarete[2,3], Juri Belcari[1], Andrea Zucchelli[1]

1 Department of Industrial Engineering, Alma Mater Studiorum—University of Bologna, I-40131 Bologna, Italy

2 Department of Chemistry 'G. Ciamician' and National Consortium of Materials Science and Technology (INSTM, Bologna RU), Alma Mater Studiorum—University of Bologna, I-40126 Bologna, Italy

3 Health Sciences and Technologies—Interdepartmental Center for Industrial Research (HST-ICIR), Alma Mater Studiorum—University of Bologna, I-40064 Ozzano dell'Emilia, Bologna, Italy

International publication number: WO2018/229615 A1

The candidate was the first name of the PCT patent. This appendix is the Italian version of the patent.

Patent filed 8 June 2018

C.1 Riassunto

La presente invenzione si riferisce ad un supporto o scaffold gerarchico multiscala per la rigenerazione tissutale, in particolare per la rigenerazione o sostituzione del tessuto tendineo e/o legamentoso e/o muscolare e/o nervoso. La presente invenzione si riferisce inoltre ai procedimenti per ottenere tale supporto ed ai suoi usi.

C.2 Descrizione

C.2.1 Campo tecnico dell'invenzione

La presente invenzione si riferisce ad un supporto (scaffold) caratterizzato da una struttura tridimensionale gerarchica e multiscala per la rigenerazione tissutale, in particolare per la rigenerazione o sostituzione del tessuto tendineo e/o legamentoso. La presente invenzione può anche essere applicata per la rigenerazione e/o sostituzione e/o simulazione del tessuto muscolare e/o nervoso.
La presente invenzione si riferisce inoltre ai procedimenti per ottenere tale supporto ed ai suoi usi.

C.2.2 Stato della tecnica

Nel campo dell'ingegneria dei tessuti, lo scaffold svolge un ruolo importante nel fornire un ambiente ideale per l'adesione, proliferazione e migrazione delle cellule. La morfologia e la struttura dei supporti per ingegneria tissutale sono fondamentali per la forma e la struttura definitiva dei tessuti e degli organi da ricostruire o sostituire. Pertanto, ci sono alcuni requisiti specifici nella struttura, nella morfologia ed in altri aspetti delle proprietà fisiche e chimiche dello scaffold che lo rendono ideale per la ricostruzione e/o sostituzione dei tessuti.
In particolare gli *scaffold* per la ricostruzione del legamento o del tendine dovrebbero essere biodegradabili, porosi, biocompatibili, presentare una sufficiente resistenza e rigidezza meccanica, e favorire la formazione di tessuti del legamento o del tendine.

Dawei et al. in *J. Mater. Chem* B 2015, 3, 8823 descrivono un supporto *(scaffold)* per la rigenerazione di lesioni nervose periferiche preparato mediante elettrofilatura di nanofibre di poli(L-lattide-co-caprolattone) (P(LLA-CL)) e acido polilattico (PLLA). Tale scaffold presenta una camicia esterna formata da nanofibre elettrofilate senza una orientazione preferenziale, che riveste un certo numero di fasci di nanofibre attorcigliate (yarns) precedentemente realizzati. Appaiono evidenti i limiti di applicabilità di questo costrutto nel campo della ingegneria tissutale del tessuto tendineo e/o legamentoso e/o muscolare e/o nervoso.

In primo luogo infatti se per la filatura della camicia esterna viene utilizzato un collettore di terra a rullo attorno al quale vengono fissati manualmente i fasci di nanofibre attorcigliate (yarns) che comporranno lo scaffold completo tale soluzione tecnologica non consente il buon compattamento di tali fasci di nanofibre attorcigliate (yarns) nello scaffold completo, limitandone evidentemente le proprietà meccaniche finali; inoltre questo approccio richiede una successiva rimozione del collettore di terra dal costrutto finale, operazione che potrebbe compromettere la struttura dello scaffold stesso. In ultimo la soluzione tecnologica adottata da Dawei at al. consente di rivestire un numero limitato di fasci di nanofibre attorcigliate (yarns) elettrofilati con la camicia esterna: all'aumentare del numero di fasci di nanofibre attorcigliate (yarns) e/o il diametro dei fasci di nanofibre attorcigliate (yarns), o eventualmente riducendo il diametro del collettore a rullo, vi è il forte rischio che l'effetto di terra del collettore venga drasticamente indebolito, rendendo impossibile la deposizione delle fibre elettrofilate che costituiscono la camicia esterna.

Inoltre in letteratura ad oggi non vengono fornite valide soluzioni in grado di poter efficacemente suturare e/o fissare tali fasci nanofibre attorcigliate (yarns) e/o fasci di nanofibre con allineamento assiale (bundles) all'interfaccia col tessuto lesionato e/o con l'interfaccia muscolare e/o ossea.

Jackson et al. (WO 2010/062297 A1) descrivono un supporto (scaffold), per la rigenerazione di alcuni tessuti come quello nervoso, ottenuto attraverso la tecnologia dell'electrospinning composto da una camicia porosa di nanofibre disposte in maniera casuale (random), la quale contiene una parte interna composta da singole nanofibre, anch'esse ottenute attraverso la tecnologia

dell'electrospinning, allineate assialmente allo scaffold stesso. Secondo la descrizione degli autori, per elettrofilare lo scaffold vengono utilizzati come collettori di terra, due cilindri rotanti all'unisono, e che presentano tra di essi uno spazio vuoto (gap). Durante la fase iniziale del processo di electrospinning le nanofibre, attratte dai due collettori di terra, si fissano sui due lati affacciati dei rulli andando a riempire lo spazio vuoto tra i rulli stessi ed allineandosi. Una volta ricoperte le facce interne dei rulli con nanofibre allineate, proseguendo il processo, le nanofibre si disporranno in maniera casuale (random), costituendo una camicia che riveste le nanofibre allineate (attirate dalla zona assiale dei due rulli). Al termine del processo si ottiene uno scaffold poroso composto da singole nanofibre allineate assialmente al suo interno, rivestite da una camicia di nanofibre disposte in maniera casuale. La prima limitazione risiede nell'impossibilità di poter modulare la lunghezza finale dello scaffold. È noto infatti che aumentando la distanza tra i rulli progressivamente l'effetto di terra tra i due rulli diminuisce fino a perdersi completamente, permettendo alle nanofibre di depositarsi solamente sui due rulli separatamente, rendendo impossibile la produzione dello scaffold e/o l'allineamento delle nanofibre. Morfologicamente inoltre tale scaffold presenta una struttura assai differente rispetto al tessuto nervoso, il quale si caratterizza per una complessa struttura fibrosa compatta, gerarchica e multiscala, organizzata in sottostrutture che si uniscono in differenti livelli per dare vita al tessuto completo. Nella struttura gerarchica multiscala dei nervi, gli elementi fondamentali di tali tessuti risiedono negli assoni mielinizzati neuronali. Gli assoni neuronali si allineano ed uniscono in gruppi, i fascicoli neuronali; gruppi di fascicoli neuronali sono uniti e compattati l'un l'altro da una guaina fibrosa chiamata epineurium per ottenere il nervo completo. Inoltre in alcuni nervi, singoli sottogruppi di fascicoli neuronali sono uniti tra loro da guaine chiamate perineurium, ed a loro volta, queste strutture vengono legate assieme dalla guaina epineurium. Tutte le strutture appena citate non vengono riprodotte morfologicamente dallo scaffold proposto dagli autori che si configura invece con una struttura tridimensionale né gerarchica né multiscala. Tale mancanza di organizzazione gerarchica nello scaffold proposto dagli autori, compromette inoltre le proprietà meccaniche dello scaffold stesso che, contenendo al suo interno solamente nanofibre allineate ma senza organizzazione

in sottostrutture e con nessun grado di compattamento, non possono offrire soddisfacente resistenza meccanica per poter sopportare i carichi fisiologici a cui tali tessuti vengono sottoposti in vivo.

Sensini et al. (Biofabrication. 2017 Mar 8;9(1):015025) descrivono un metodo per produrre attraverso la tecnologia dell'electrospinning fasci di nanofibre allineate assialmente (bundles). Per la loro realizzazione, sono elettrofilate nanofibre polimeriche su di un rullo collettore, rotante ad alta velocità. Al termine del processo di electrospinning sono tagliate strisce circonferenziali di membrana di nanofibre sul rullo, e sono arrotolate formando dei fasci di nanofibre allineate assialmente (bundles) (di diametro circa 500 micrometri ciascuno) che vengono poi tagliati e rimossi dal rullo. Gli autori tuttavia presentano questi fasci di nanofibre allineate assialmente (bundles), come scaffolds che mimano la morfologia e le proprietà meccaniche di singoli fascicoli tendinei di collagene, senza proporre nessuna metodologia per poter produrre uno scaffold gerarchico multiscala in grado di riprodurre un intero tendine.

Da ciò si riscontra una enorme lacuna nella letteratura per la produzione di scaffolds gerarchici multiscala in grado di riprodurre in ogni suo elemento la struttura gerarchica di tendini e/o legamenti e/o muscoli e/o nervi.

Lo stato della tecnica come sopra ricostruito indica quindi la necessità di fornire nuovi supporti e metodi per la loro produzione che non presentino gli svantaggi di quelli della tecnica nota.

C.2.3 Sommario dell'invenzione

Gli inventori sono riusciti ad ottenere un supporto *(scaffold)* che permette di sostituire e/o ricostruire il tessuto tendineo e/o legamentoso e/o muscolare e/o nervoso attraverso un costrutto con struttura tridimensionale gerarchica e multiscala (scaffold gerarchico multiscala) in grado di riprodurre le caratteristiche meccaniche, morfologiche e fisiologiche di tendini e legamenti e/o di muscoli e/o di nervi.

Nella presente descrizione per costrutto e/o scaffold gerarchico multiscala si intende ogni dispositivo o struttura, composta da sottostrutture, di scale dimensionali differenti, che si uniscono a vicenda in un ordine gerarchico. Questa

configurazione è tipica dei tessuti connettivi come tendini e/o legamenti, ed anche dei muscoli e dei nervi. Infatti i tessuti tendinei e/o legamentosi e/o muscolari e/o nervosi sono composti da una struttura gerarchica multiscala composta da diverse caratteristiche (elencate di seguito a partire dal livello molecolare fino all'intero tendine e/o legamento e/o muscolo e/o nervo):

Nella struttura gerarchica multiscala di tendini e/o legamenti, gli elementi fondamentali di tali tessuti risiedono nelle molecole di tropo-collagene che sono unite l'una con l'altra producendo una fibrilla di collagene; le fibrille di collagene sono allineate in gruppi differenti, chiamate fascicoli; gruppi di fascicoli sono uniti e compattati l'un l'altro da una guaina di fibrille di collagene, chiamata epitenon/epiligament, per formare l'intero tendine o legamento. Inoltre in alcuni tendini e/o legamenti, singoli sottogruppi di fascicoli sono uniti tra loro da guaine chiamate endotenon/endoligament ed a loro volta, queste strutture vengono legate assieme dalla guaina epitenon/epiligament.

La struttura gerarchica multiscala naturale di tendini e/o legamenti è perfettamente mimata dallo scaffold gerarchico multiscala oggetto della presente invenzione: le nanofibre elettrofilate (fibre del diametro di nanometri, paragonabili alle fibrille di collagene di tendini e/o legamenti) sono costituite da macromolecole di polimero (ad una scala dimensionale simile al tropo-collagene); una pluralità di nanofibre elettrofilate sono allineate a formare un fascio di nanofibre con allineamento assiale (bundle) e/o attorcigliate a formare un fascio di nanofibre attorcigliate (yarn) (simile al fascicolo di tendini e/o legamenti); la pluralità di fasci di nanofibre con allineamento assiale (bundles), e/o la pluralità di fasci di nanofibre attorcigliate (yarns), sono unite e compattate l'una con l'altra da una camicia elettrofilata di nanofibre (imitando la guaina epitenon/epiligament di tendini e/o legamenti) che forma lo scaffold gerarchico multiscala oggetto della nostra invenzione. Inoltre più scaffolds gerarchici multiscala oggetto di invenzione, possono essere uniti, a loro volta, tra loro in un ulteriore livello gerarchico, da una ulteriore camicia elettrofilata prodotta similmente alla precedente. In questo caso la camicia che riveste i singoli scaffolds gerarchici multiscala simulerà le guaine l'endotenon/endoligament di tendini e/o legamenti, mentre la camicia esterna che li unisce, simulerà l'epitenon/epiligament di tendini e/o legamenti.

Nella struttura gerarchica e multiscala dei muscoli, gli elementi fondamentali di tali tessuti risiedono nelle molecole di actina e miosina, unite l'una con l'altra producendo strutture filamentose dette fibre muscolari. Le fibre muscolari si allineano ed uniscono in gruppi, i fascicoli muscolari; gruppi di fascicoli muscolari sono uniti e compattati l'un l'altro da una guaina fibrosa chiamata epimisio, formando il muscolo completo. Inoltre in alcuni muscoli, sottogruppi di fascicoli muscolari sono uniti tra loro da guaine dette perimiso, ed a loro volta queste strutture vengono legate assieme dall'epimisio.

La struttura gerarchica multiscala naturale dei muscoli è perfettamente mimata dallo scaffold gerarchico multiscala oggetto della presente invenzione: le macromolecole del polimero (ad una scala dimensionale paragonabile ad actina e miosina dei muscoli), formano le nanofibre elettrofilate (paragonabili alle fibrille muscolari); una pluralità di nanofibre elettrofilate sono allineate a formare un fascio di nanofibre ad allineamento assiale (bundle), e/o attorcigliate a formare un fascio di nanofibre attorcigliate (yarn) (simile al fascicolo muscolare); la pluralità di fasci di nanofibre con allineamento assiale (bundles), e/o di la pluralità di fasci di nanofibre attorcigliate (yarns), sono unite e compattate l'una con l'altra da una camicia elettrofilata di nanofibre (imitando la guaina epimisio) che forma lo scaffold gerarchico multiscala, oggetto della presente invenzione. Inoltre più scaffolds gerarchici multiscala oggetto di invenzione, possono essere uniti, a loro volta, tra loro in un ulteriore livello gerarchico da una ulteriore camicia elettrofilata prodotta similmente alla precedente. In questo caso la camicia che riveste i singoli scaffolds gerarchici multiscala, simulerà le guaine perimiso dei muscoli, mentre la camicia esterna che le unisce, simulerà la guaina epimisio del tessuto muscolare.

Nella struttura multiscala dei nervi, gli elementi fondamentali di tali tessuti risiedono negli assoni mielinizzati neuronali. Gli assoni neuronali si allineano ed uniscono in gruppi, i fascicoli neuronali; gruppi di fascicoli neuronali sono uniti e compattati l'un l'altro da una guaina fibrosa chiamata epineurium per ottenere il nervo completo. Inoltre in alcuni nervi, singoli sottogruppi di fascicoli neuronali sono uniti tra loro da guaine chiamate perineurium, ed a loro volta, queste strutture vengono legate assieme dalla guaina epineurium.

La struttura gerarchica multiscala naturale dei nervi è perfettamente mimata dallo scaffold gerarchico multiscala oggetto della presente invenzione: una pluralità di nanofibre elettrofilate (per guidare la crescita dei germogli neuronali e delle cellule di Schwann) sono allineate e raggruppate in fasci di nanofibre con allineamento assiale (bundles) e/o attorcigliate in fasci di nanofibre (yarns) (simili ai fascicoli dei nervi); la pluralità di fasci di nanofibre con allineamento assiale (bundles) e/o la pluralità di fasci di nanofibre attorcigliate (yarns), sono unite e compattate l'una con l'altra da una camicia elettrofilata di nanofibre (che imita la guaina epineurium dei nervi) che forma lo scaffold gerarchico multiscala, oggetto della nostra invenzione. Inoltre più scaffolds gerarchici multiscala oggetto di invenzione, possono essere uniti, a loro volta, tra loro in un ulteriore livello gerarchico da una ulteriore camicia elettrofilata prodotta similmente alla precedente. In questo caso la camicia che riveste i singoli scaffold gerarchici multiscala simulerà le guaine perineurium dei nervi, mentre la camicia esterna che li unisce, simulerà la guaina epineurium del tessuto nervoso.

Il procedimento usato per la produzione di tale scaffold gerarchico multiscala permette di produrre una camicia esterna elettrofilata, che può anche essere utilizzata per compattare sottogruppi di fasci di nanofibre con allineamento assiale (bundles) e/o di fasci di nanofibre attorcigliate (yarns) all'interno dello scaffold gerarchico multiscala, senza l'utilizzo di collettori di terra interni al corpo dello scaffold gerarchico multiscala. Inoltre tale camicia conferisce protezione, e compattamento meccanico dei fasci di nanofibre con allineamento assiale (bundles) e/o fasci di nanofibre attorcigliate (yarns) al suo interno, permettendo al contempo il passaggio delle cellule.

Lo scaffold gerarchico multiscala ottenuto dagli inventori riesce a replicare vari livelli di aggregazione del tessuto tendineo/legamentoso, dalle fibrille di collagene, ai fascicoli tendineo/legamentosi, fino a raggiungere il tendine/legamento completo. Inoltre gli inventori sono riusciti a sviluppare un procedimento per poter elettrofilare una camicia di nanofibre sulla superficie dei fasci di nanofibre con allineamento assiale (bundles) e/o fasci di nanofibre attorcigliate (yarns), simile per morfologia alla guaina che riveste i tendini/legamenti (epitenon), riuscendo eventualmente a rivestirne anche sottogruppi (endotenon), in modo tale da

permettere il compattamento dei fasci di nanofibre con allineamento assiale (bundles) e/o fasci di nanofibre attorcigliate (yarns) e favorirne la resistenza meccanica da un lato, ma permettere anche il passaggio delle cellule attraverso la camicia e la colonizzazione dei fasci di nanofibre con allineamento assiale (bundles) e/o fasci di nanofibre attorcigliate (yarns).

Un ulteriore vantaggio dello scaffold gerarchico multiscala qui descritto risiede nella possibilità di includere al proprio interno un numero qualsiasi di fasci di nanofibre con allineamento assiale (bundles) e/o fasci di nanofibre attorcigliate (yarns) di qualsiasi diametro, compattati e riuniti attraverso una camicia elettrofilata porosa in grado di garantire da un lato protezione ai fasci di nanofibre con allineamento assiale (bundles) e/o fasci di nanofibre attorcigliate (yarns) al suo interno, dall'altro il passaggio delle cellule attraverso di essa al fine di potersi depositare sui fasci di nanofibre con allineamento assiale (bundles) e/o fasci di nanofibre attorcigliate (yarns) e ricostruire la matrice extracellulare tendineo/legamentosa e/o muscolare e/o nervosa. La camicia elettrofilata viene prodotta senza l'utilizzo di collettori interni allo scaffold gerarchico multiscala ed è in grado di compattare ed eventualmente attorcigliare (twisting) i fasci di nanofibre con allineamento assiale (bundles) e/o fasci di nanofibre attorcigliate (yarns) al proprio interno. Tale camicia può anche essere utilizzata per rivestire sottogruppi di fasci di nanofibre con allineamento assiale (bundles) e/o fasci di nanofibre attorcigliate (yarns) all'interno dello scaffold gerarchico multiscala incrementando ulteriormente le proprietà meccaniche e il livello gerarchico di aggregazione.

È quindi un primo oggetto della presente invenzione uno scaffold gerarchico multiscala per la sostituzione e/o riparazione e/o rigenerazione e/o ricostruzione e/o simulazione di un tessuto, in particolare del tessuto tendineo e/o legamentoso e/o muscolare e/o nervoso comprendente:

-una pluralità di fasci ottenuti per elettrofilatura costituiti ciascuno da nanofibre, in cui detta pluralità di fasci sono disposti in modo da formare un singolo gruppo;

-una camicia porosa ottenuta per elettrofilatura costituita da nanofibre, in cui detta camicia riveste esternamente e compatta detta pluralità di fasci mantenendoli allineati tra loro.

Tale camicia è anche in grado di unire gruppi di scaffolds gerarchici multiscala tra loro, incrementando il livello gerarchico di aggregazione.

Detta camicia quindi riesce a compattare i fasci di nanofibre allineamento assiale (bundles) e/o attorcigliate (yarns) mantenendoli contemporaneamente allineati tra loro, senza la necessità di doverli intrecciare, attorcigliare e senza l'eventuale utilizzo di riempitivi compattanti per ottenere il medesimo effetto, a differenza del caso dei costrutti precedentemente sviluppati, garantendo di conseguenza proprietà meccaniche simili a quelle proprie del tessuto tendineo e/o legamentoso e/o muscolare e/o nervoso corporeo, consentendo contemporaneamente di mimare in maniera assolutamente fedele l'organizzazione gerarchica del tessuto tendineo e/o legamentoso e/o muscolare e/o nervoso stesso.

Tale caratteristica risulta di fondamentale importanza per uno scaffold pensato per la rigenerazione del tessuto tendineo e/o legamentoso e/o muscolare e/o nervoso: variando infatti la struttura morfologica dello scaffold da quella del tessuto nativo, è forte il rischio dell'insorgere di tessuto cicatriziale con conseguente impoverimento delle proprietà meccaniche e morfologiche finali del tessuto rigenerato. Detta camicia permette inoltre il passaggio delle cellule che dovranno colonizzare l'intera struttura gerarchica multiscala; altresì permette la corretta vascolarizzazione della componente cellulare e l'eliminazione delle componenti di scarto prodotte dalle cellule durante la ricostruzione dei tessuti in oggetto. Lo scaffold che ne consegue ha caratteristiche meccaniche (resistenza e rigidezza) elevate, dello stesso ordine di grandezza dei tessuti tendinei e/o legamentosi e/o muscolari e/o nervosi umani.

Un secondo oggetto della presente invenzione è un procedimento per la preparazione di uno scaffold gerarchico multiscala per la sostituzione, riparazione o ricostruzione di un tessuto, in particolare del tessuto tendineo e/o legamentoso e/o muscolare e/o nervoso, comprendente i seguenti passaggi:

a) preparare mediante elettrofilatura una pluralità di fasci di nanofibre con allineamento assiale (bundles) e/o fasci di nanofibre attorcigliate (yarns);

b) elettrofilare nanofibre in modo da rivestire detta pluralità di fasci di nanofibre con allineamento assiale (bundles) e/o fasci di nanofibre attorcigliate (yarns) con una camicia porosa costituta da nanofibre in modo tale da fornire un rivestimento

esterno e compattare la pluralità di fasci di nanofibre con allineamento assiale (bundles) e/o fasci di nanofibre attorcigliate (yarns) preparati con il passaggio a).
In particolare secondo una forma di realizzazione tale procedimento prevede i seguenti passaggi:
a) preparare mediante elettrofilatura una pluralità di fasci costituiti ciascuno da nanofibre allineate assialmente (bundles) e/o fasci di nanofibre attorcigliate (yarns);
b) posizionare detta pluralità di fasci di nanofibre con allineamento assiale (bundles) e/o fasci di nanofibre attorcigliate (yarns) preparati al punto a) in modo da formare un singolo gruppo;
c) afferrare il gruppo di fasci di nanofibre con allineamento assiale (bundles) e/o fasci di nanofibre attorcigliate (yarns) ottenuto al passaggio b) su un afferraggio capace di ruotare rigidamente e in asse mantenendo così il gruppo di fasci di nanofibre con allineamento assiale (bundles) e/o fasci di nanofibre attorcigliate (yarns) afferrato in posizione idonea per il processo di rivestimento con camicia elettrofilata;
d) realizzare una camicia esterna del gruppo di fasci di nanofibre con allineamento assiale (bundles) e/o fasci di nanofibre attorcigliate (yarns) afferrato al punto c) mediante elettrofilatura, in particolare controllando i parametri di rotazione del gruppo di fasci di nanofibre con allineamento assiale (bundles) e/o fasci di nanofibre attorcigliate (yarns) afferrato, i parametri geometrici del setup, e parametri di processo.
La camicia che si genera ha l'effetto di compattare i fasci di nanofibre con allineamento assiale (bundles) e/o attorcigliate (yarns), minimizzando gli spazi vuoti tra i diversi fasci e minimizzando quindi la sezione globale dello scaffold gerarchico multiscala. Tale effetto permette di ottenere un costrutto capace di esprimere proprietà meccaniche paragonabili a quelle tessuti naturali che deve imitare, ed omogenee per tutta la sua sezione.
Sostituendo il gruppo di fasci di nanofibre con allineamento assiale (bundles) e/o fasci di nanofibre attorcigliate (yarns), di cui al punto b), con un gruppo di scaffolds gerarchici multiscala, e ripetendo i passaggi c) e d), sarà inoltre possibile ottenere uno scaffold gerarchico multiscala con un livello gerarchico di aggregazione

ulteriormente incrementato, in quanto composto a sua volta da una pluralità di scaffolds gerarchici multiscala.

Un terzo oggetto di invenzione riguarda un nuovo costrutto elettrofilato chiamato fascio ad anello di nanofibre (ring bundle). Tale costrutto, si configura morfologicamente come un anello chiuso, composto di nanofibre disposte in modo casuale (random) e/o con un grado di allineamento lungo la direzione assiale dell'anello. Tali fasci ad anello di nanofibre (ring bundles) non saranno necessariamente utilizzati nella forma circolare originaria, ma potranno essere stirati secondo una direzione per ottenere una forma oblunga chiusa. In particolare tale fascio ad anello di nanofibre (ring bundle), se usato singolarmente e/o affiancato ad una pluralità di fasci ad anello di nanofibre simili a questo, potrà essere impiegato per costruire scaffolds gerarchici multiscala elettrofilati simili a tendini e/o legamenti e/o muscoli e/o nervi. In particolare se sostituiti i fasci di nanofibre con allineamento assiale (bundles) e/o fasci di nanofibre attorcigliate (yarns), di cui al punto a), con un singolo fascio ad anello di nanofibre (ring bundle) e/o con una pluralità di fasci ad anello di nanofibre (ring bundles), e ripetendo la procedura per la produzione della camicia di cui dal punto b) al punto d), la camicia elettrofilata compatterà la zona centrale dei fasci ad anello di nanofibre elettrofilate (ring bundles), conferendo ad esse una forma oblunga, e generando dei cappi all'estremità dello scaffold gerarchico multiscala. Tali cappi risulteranno, ad esempio utili alla sutura e/o al fissaggio, dello scaffold gerarchico multiscala così ottenuto, all'interfaccia con il tendine e/o legamento e/o muscolo e/o nervo e/o osso di interesse. Inoltre tali fasci ad anello di nanofibre (ring bundles) potranno trovarsi disposti internamente agli scaffolds gerarchici multiscala, sia allineati assialmente gli uni agli altri e/o attorcigliati (twisted) gli uni agli altri e/o singolarmente attorcigliati ed affiancati assialmente gli uni agli altri e/o attorcigliati (twisted) singolarmente ed a loro volta attorcigliati (twisted) tra loro e/o trovarsi nel medesimo scaffold assieme ad uno o più fasci di nanofibre con allineamento assiale (bundles) e/o uno o più fasci di nanofibre attorcigliate (yarns).

Tali fasci ad anello di nanofibre elettrofilate (ring bundles) potranno essere a loro volta composti di nanofibre disposte in maniera casuale (random) e/o con allineamento assiale e/o attorcigliate.

Altri vantaggi, caratteristiche e le modalità di impiego della presente invenzione risulteranno evidenti dalla seguente descrizione dettagliata di alcune forme di realizzazione, presentate a scopo esemplificativo e non limitativo.

C.2.4 Descrizione breve delle figure

-La Figura 1 è una fotografia di un singolo fascio di nanofibre con allineamento assiale (bundle) dello scaffold gerarchico multiscala secondo una forma di realizzazione preferita della presente invenzione.
-la Figura 2 è una fotografia che mostra lo scaffold gerarchico multiscala per intero, costituito da una pluralità di fasci di nanofibre con allineamento assiale (bundles) (Figura 1) tenuti insieme da una camicia esterna di fibre disposte in modo casuale secondo una forma di realizzazione preferita della presente invenzione.
-la Figura 3 è una fotografia del set-up sperimentale che consente di fissare i fasci di nanofibre con allineamento assiale (bundles) e/o fasci di nanofibre attorcigliate (yarns) parallelamente uno all'altro e uno di fianco all'altro nella fase precedente alla filatura della camicia secondo una forma di realizzazione preferita della presente invenzione.
-la Figura 4 è una fotografia del set-up sperimentale che consente di rivestire i fasci di nanofibre con allineamento assiale (bundles) e/o fasci di nanofibre attorcigliate (yarns) con una camicia esterna di nanofibre secondo una forma di realizzazione preferita della presente invenzione.
- la Figura 5 è una immagine tomografica delle nanofibre di un singolo fascio di nanofibre con allineamento assiale (bundle) in acido poli(L)lattico (PLLA).
- la Figura 6 è una immagine SEM della sezione di uno scaffold gerarchico multiscala in PLLA composto da 100 i fasci di nanofibre con allineamento assiale (bundles) e con camicia esterna elettrofilata.
- la Figura 7 è una fotografia di un singolo fascio ad anello di nanofibre (ring bundle) secondo una forma di realizzazione preferita della presente invenzione.
- la Figura 8 è una fotografia che mostra lo scaffold gerarchico multiscala per intero, costituito da una pluralità di fasci ad anello di nanofibre (ring bundles) (Figura 7) tenuti insieme da una camicia esterna di nanofibre disposte in modo casuale

secondo una forma di realizzazione preferita della presente invenzione, mostrando i cappi per la sutura e/o il fissaggio alle proprie estremità.

-la Figura 9 è una rappresentazione schematica dei livelli di aggregazione gerarchici multiscala del tessuto tendineo e/o legamentoso, muscolare e nervoso, confrontati con la struttura gerarchica dello scaffold gerarchico multiscala oggetto della presente invenzione. In particolare: a) Struttura gerarchica multiscala di tendini e/o legamenti; b) Struttura gerarchica multiscala di muscoli; c) Struttura gerarchica multiscala di nervi; d) Struttura scaffold gerarchico multiscala.

-Figura 10 è una rappresentazione schematizzata dei livelli di aggregazione gerarchici multiscala del tessuto tendineo e/o legamentoso, muscolare e nervoso secondo la quale più sotto unità gerarchiche del medesimo tessuto si uniscono assieme incrementando il livello gerarchico multiscala degli stessi. Tali livelli vengono confrontati con la struttura gerarchica dello scaffold gerarchico multiscala oggetto della presente invenzione secondo la forma in cui gruppi di scaffolds gerarchici multiscala vengono uniti assieme da una ulteriore camicia di nanofibre elettrofilate, formando uno scaffold gerarchico multiscala con un livello maggiore di organizzazione gerarchica. In particolare: a) Struttura gerarchica multiscala di tendini e/o legamenti; b) Struttura gerarchica multiscala di muscoli; c) Struttura gerarchica multiscala di nervi; d) Struttura scaffold gerarchico multiscala composto a sua volta da gruppi di scaffolds gerarchici multiscala.

C.2.5 Descrizione dettagliata dell'invenzione

La presente invenzione si riferisce ad uno scaffold gerarchico multiscala, ai procedimenti per la sua produzione e ai suoi usi.

Nella presente descrizione con gerarchico e multiscala si intende: ogni dispositivo o struttura, composta da sottostrutture, di scale dimensionali differenti, che si uniscono in un ordine gerarchico.

Nella presente descrizione con l'espressione "supporto o scaffold gerarchico multiscala" s'intende: un costrutto tridimensionale anisotropo poroso composto da biomateriali assemblati a livello morfologico a diversi livelli di scala dimensionale (da nanometrica a micrometrica e millimetrica), gerarchicamente organizzati in una struttura multiscala (come precedentemente definita), per mimare il più fedelmente

possibile la matrice extracellulare del tessuto che si vuole ricostruire nel suo stato nativo. Gli scaffold sono tipicamente progettati per eseguire le seguenti funzioni: (i) promuovere l'interazione cellula-biomateriale, l'adesione cellulare e la proliferazione cellulare, (ii) consentire il trasporto di ossigeno, anidride carbonica, e nutrienti, (iii) se bioassorbibili, biodegradare ad una velocità che approssimi il tasso di rigenerazione tissutale sotto le condizioni di coltura di interesse, (iv) non provocare infiammazione o tossicità in vivo e (v) avere proprietà meccaniche simili al tessuto che si vuole ricostruire.

Potrà essere scelto anche un materiale non bioriassorbibile, ma in questo caso non dovrà provocare infiammazione o tossicità in vivo ed avere proprietà meccaniche e morfologiche simili al tessuto che si vuole ricostruire e/o simulare e/o sostituire.

Nella presente descrizione per "fascio di nanofibre con allineamento assiale (bundle)" si intende una struttura elettrofilata, di estensione e/o sezione variabili, composta di nanofibre che si dispongono con un grado di allineamento secondo l'asse del bundle stesso, ovvero lungo la direzione di sviluppo maggiore di questi costrutti.

Nella presente descrizione per "fascio di nanofibre attorcigliate (yarn)" si intende una struttura elettrofilata, di estensione e/o sezione variabili, composta di nanofibre che si dispongono con un grado attorcigliamento secondo l'asse dello yarn stesso, ovvero lungo la direzione di sviluppo maggiore di questi costrutti.

Nella presente descrizione per "fascio ad anello di nanofibre (ring bundle)" si intende una struttura elettrofilata a forma di anello, di estensione e sezione variabili, composta di nanofibre, con un grado di allineamento secondo l'asse del fascio ad anello o ring bundle stesso.

Nella presente descrizione con l'espressione "formare un singolo gruppo" s'intende formare un singolo fascio.

In una ulteriore forma di realizzazione le nanofibre che compongono il fascio ad anello o ring bundle potranno essere disposte in maniera casuale (random) e/o attorcigliate (twisted) e/o con un grado di allineamento assiale all'interno del corpo del fascio ad anello o ring bundle stesso.

Lo scaffold gerarchico multiscala secondo la presente invenzione comprende inoltre una camicia porosa ottenuta per elettrofilatura che riveste esternamente i

fasci di nanofibre con allineamento assiale (bundles) e/o fasci di nanofibre attorcigliate (yarns) e/o fasci ad anello di nanofibre (ring bundles), ottenuti per elettrofilatura. Detta camicia esterna (involucro) è costituita anch'essa da nanofibre. La porosità della camicia viene generata dalla sovrapposizione di strati di nanofibre continue che si depositano nel tempo di processo su uno stesso piano, formando una struttura tridimensionale come quella di un tessuto-non-tessuto. La porosità della camicia è quindi interconnessa, nel senso che i pori mettono in comunicazione lo strato esterno della camicia di fibre con lo strato più interno, a contatto con i fasci di nanofibre con allineamento assiale (bundles) e/o fasci di nanofibre attorcigliate (yarns) e/o fasci ad anello di nanofibre (ring bundles) e/o sottogruppi di scaffolds gerarchici multiscala. L'interconnessione tra i pori consente alle cellule di filtrare attraverso la camicia esterna per raggiungere gli strati interni dello scaffold gerarchico multiscala.

Le nanofibre della camicia potranno essere disposte in maniera casuale (random) e/o con un grado di allineamento assiale e/o un grado di allineamento circonferenziale.

Il diametro medio delle nanofibre che compongono lo scaffold gerarchico multiscala potranno essere compre tra i 10 e i 100000 nm.

La lunghezza dello scaffold gerarchico multiscala potrà essere compresa tra 10 e 1000 mm, in particolare tra 10-500 mm, preferibilmente 20-200 mm e avrà un diametro medio compreso tra 1 e 100 mm, preferibilmente compreso tra 2 e 50 mm.

Secondo una forma di realizzazione lo scaffold gerarchico multiscala sarà in materiale bioriassorbibile o biostabile e/o inerte.

Esempi di materiali bioassorbibili o biostabili di origine sintetica sono poliesteri, poliuretani, poliammidi, poliolefine, polimeri fluorurati e loro copolimeri. Esempi di materiali bioassorbibili o biostabili di origine naturale sono polisaccaridi, proteine, poliesteri, polipeptidi e loro copolimeri. Esempi preferiti di materiali per la preparazione delle nanofibre sono acido poli-(L)-lattico (PLLA) e/o collagene e/o nylon 6,6, potranno essere usate anche altre poliammidi biocompatibili note al tecnico del settore.

Secondo una forma di realizzazione lo scaffold gerarchico multiscala e/o le nanofibre di cui esso si compone, potranno essere caricate e/o funzionalizzate con

componenti di natura organica e/o inorganica che svolgano un'azione biologica e/o di cambiamento delle proprietà chimico-fisiche e/o meccaniche del tessuto in cui potrà essere usato lo scaffold gerarchico multiscala. Ad esempio componenti di natura organica e/o inorganica che potranno essere usati sono farmaci, fattori di crescita, sostanze antibatteriche, peptidi, idrossiapatiti, fosfati, biovetri, ossidi metallici, grafene, nanotubi di carbonio.

In una forma di realizzazione delle nanofibre che compongono lo scaffold gerarchico multiscala e/o la camicia e/o i fasci di nanofibre con allineamento assiale (bundles) e/o i fasci di nanofibre attorcigliate (yarns) e/o i fasci di nanofibre ad anello (ring bundles) potranno essere, dal punto di vista della morfologia, classiche nanofibre composte da una singola fase (costituita da un singolo materiale e/o da una miscela di materiali e/o materiali caricati e/o funzionalizzati) e/o nanofibre composte da due o più fasi (ad esempio nanofibre core-shell, dove per core-shell si intendono nanofibre composte da materiali differenti tra parte centrale ed esterna della nanofibra stessa) e/o nanofibre hollow-shell (dove per hollow-shell si intendono nanofibre composte da una cavità centrale interna lungo l'asse delle nanofibre stesse) e/o nanofibre porose (per nanofibre porose si intendono nanofibre che presentano pori lungo la loro superficie e/o nel loro volume interno).

Le procedure di caricamento e/o funzionalizzazione e/o produzione di nanofibre a diversa morfologia sono note al tecnico del settore.

Le nanofibre che costituiscono i singoli fasci di nanofibre con allineamento assiale (bundles) e/o fasci di nanofibre intrecciate (yarns) e/o fasci di nanofibre ad anello (ring bundles) e/o la camicia e/o le camicie avranno un diametro medio compreso tra 10 e 10000 nm, preferibilmente compreso tra 200 e 1000 nm, ed in particolare tra 300 e 1000 nm, mentre il diametro medio dei fasci di nanofibre con allineamento assiale (bundles) e/o fasci di nanofibre intrecciate (yarns) e/o fasci di nanofibre ad anello (ring bundles) potrà essere compreso tra 10 e 10000 μm, in particolare compreso tra 20 e 10000 μm, preferibilmente tra 500 e 650 μm. Il numero di fasci di nanofibre con allineamento assiale (bundles) e/o fasci di nanofibre intrecciate (yarns) e/o fasci di nanofibre ad anello (ring bundles) sarà ad esempio compreso tra 2 e 1000, preferibilmente tra 40 e 200, ad esempio 100.

Gli scaffolds gerarchici multiscala secondo la presente invenzione avranno vantaggiosamente un valore di resistenza meccanica compreso tra 10 e 5000 N preferibilmente tra 200 e 500 N e/o un modulo elastico compreso tra 20 e 100000 MPa, preferibilmente di circa 30-20000 MPa. Tali caratteristiche meccaniche sono state misurate tramite prova a trazione monoassiale con afferraggi a cabestano (capstan grips) e cementando le estremità come descritto negli esempi.

Un ulteriore oggetto della presente invenzione è un procedimento per la preparazione di uno scaffold gerarchico multiscala per la sostituzione e/o riparazione e/o rigenerazione e/o ricostruzione e/o simulazione di un tessuto, in particolare del tessuto tendineo e/o legamentoso e/o muscolare e/o nervoso comprendente i seguenti passaggi:

a) preparare mediante elettrofilatura una pluralità di fasci di nanofibre con allineamento assiale (bundles) e/o di fasci di nanofibre attorcigliate (yarns)

b) elettrofilare nanofibre in modo da rivestire una pluralità di detti fasci di nanofibre con allineamento assiale (bundles) e/o fasci di nanofibre attorcigliate (yarns) con una camicia porosa costituta da nanofibre in modo tale da fornire un rivestimento esterno e compattare la pluralità di fasci di nanofibre con allineamento assiale (bundles) e/o fasci di nanofibre attorcigliate (yarns) preparati con il passaggio a) ottenendo un supporto o scaffold gerarchico multiscala;

c) elettrofilare nanofibre in modo da rivestire una pluralità di detti supporti o scaffolds gerarchici multiscala di cui al punto b) con una ulteriore camicia porosa costituita da nanofibre in modo tale da fornire un rivestimento esterno e compattare la pluralità di fasci di nanofibre con allineamento assiale (bundles) e/o fasci di nanofibre attorcigliate (yarns) e/o scaffolds gerarchici multiscala di cui al punto b).

Una forma di realizzazione della presente invenzione è un procedimento per la preparazione di fasci ad anello di nanofibre (ring bundles) comprendente i seguenti passaggi:

a) elettrofilare su di un collettore di terra a forma di rullo rotante a differente velocità a seconda del grado di allineamento desiderato, una pluralità di nanofibre;

b) tagliare strisce circonferenziali di membrana di nanofibre ottenute dall'elettrofilatura secondo il passaggio a);

c) arrotolare le strisce circonferenziali di membrana di nanofibre ottenute secondo il passaggio b) secondo l'asse del rullo;

d) sfilare dal rullo i fasci ad anello di nanofibre (ring bundles) ottenuti secondo il passaggio c).

In particolare il procedimento per la preparazione di scaffolds gerarchici multiscala con fasci ad anello di nanofibre (ring bundles) prevedrà i seguenti passaggi:

a) preparare mediante elettrofilatura una pluralità di fasci di nanofibre con allineamento assiale (bundles) e/o fasci di nanofibre attorcigliate (yarns) e/o fasci ad anello di nanofibre (ring bundles);

b) posizionare detta pluralità di fasci di nanofibre con allineamento assiale (bundles) e/o fasci di nanofibre attorcigliate (yarns) e/o fasci ad anello di nanofibre (ring bundles) preparati al punto a) in modo da formare un singolo gruppo fasci di nanofibre con allineamento assiale (bundles) e/o fasci di nanofibre attorcigliate (yarns) e/o fasci ad anello di nanofibre (ring bundles);

c) afferrare il gruppo ottenuto al passaggio b) su afferraggio capace di ruotare rigidamente e in asse mantenendo così il gruppo di fasci di nanofibre e/o con allineamento assiale (bundles) e/o fasci di nanofibre attorcigliate (yarns) e/o fasci ad anello di nanofibre (ring bundles), afferrato in posizione idonea per il processo di rivestimento con camicia elettrofilata;

d) realizzare una camicia esterna sul gruppo di fasci di nanofibre con allineamento assiale (bundles) e/o fasci di nanofibre attorcigliate (yarns) e/o fasci ad anello di nanofibre (ring bundles) afferrato al punto c) mediante elettrofilatura, in particolare controllando i parametri di rotazione del gruppo di fasci di nanofibre con allineamento assiale (bundles) e/o fasci di nanofibre e/o attorcigliate (yarns) e/o fasci ad anello di nanofibre (ring bundles) afferrato, i parametri geometrici del setup, e parametri di processo, ottenendo una struttura o scaffold gerarchico multiscala.

e) realizzare una ulteriore camicia esterna sul gruppo strutture o scaffolds gerarchici multiscala ottenuti al punto d) ed afferrato come al punto c) mediante elettrofilatura, in particolare controllando i parametri di rotazione del gruppo di strutture o scaffolds gerarchici multiscala afferrato, i parametri geometrici del setup, e parametri di processo.

Secondo una forma di realizzazione le nanofibre dei fasci di nanofibre on allineamento assiale (bundles) e/o fasci di nanofibre attorcigliate (yarns) e/o fasci ad anello di nanofibre (ring bundles) e/o della camicia potranno essere preparate elettrofilando una soluzione di PLLA sciolto in idoneo solvente, ad esempio in diclorometano (DCM) e N,N-dimetilformammide (DMF). La soluzione potrà essere preparata ad esempio con 10-30% (w/v) di PLLA in ad esempio 65/35 (v/v) (DCM/DMF).

Secondo una forma di realizzazione le nanofibre dei fasci di nanofibre con allineamento assiale (bundles) e/o fasci di nanofibre attorcigliate (yarns) e/o fasci ad anello di nanofibre (ring bundles) e/o della camicia potranno essere preparate elettrofilando una soluzione di nylon 6,6 sciolto in idoneo solvente, ad esempio in acido trifluoroacetico (TFA) e acetone (AC). La soluzione potrà essere preparata ad esempio con 10-30% (w/v) di nylon 6,6 in ad esempio 50/50 (v/v) (TFA/AC).

Secondo una forma di realizzazione le condizioni di filatura dei fasci di nanofibre con allineamento assiale (bundles) e/o dei fasci di nanofibre attorcigliate (yarns) e/o dei fasci ad anello di nanofibre (ring bundles) prevedono l'applicazione di un campo elettrico con un voltaggio compreso tra 10 e 30 kV, preferibilmente 18 kV per un tempo di elettrofilatura di almeno 5 min, ed in particolare almeno15 min, preferibilmente di un'ora, depositando le fibre su un collettore rotante ad alta velocità che consenta un grado di allineamento delle nanofibre. Le nanofibre depositate sul collettore vengono successivamente raccolte insieme per formare fasci di nanofibre con allineamento assiale (bundle) e/o fasci di nanofibre attorcigliate (yarn) e/o un fascio ad anello di nanofibre (ring bundles) con un grado di allineamento.

Secondo una forma di realizzazione le condizioni di elettrofilatura sulla macchina rotante per la produzione della camicia esterna di nanofibre prevedono l'applicazione di un campo elettrico con un voltaggio compreso tra 10 e 30 kV, per un tempo di elettrofilatura di almeno 2 ore, preferibilmente di 3 ore.

Vantaggiosamente per la preparazione della camicia saranno applicati i seguenti paramenti di processo:

- distanza tra ii gruppo di fasci e il collettore piano minore di 5 mm;
- una velocità rotazione del gruppo di fasci di circa 20-25 rpm;

- periodi di immobilità del gruppo di fasci di circa 3-5 min;
- periodi di rotazione del gruppo di fasci 1-2 min.

Il procedimento per la preparazione dello scaffold gerarchico multiscala secondo la presente invenzione ha importanti vantaggi, in particolare lo sviluppo della camicia attorno ai fasci di nanofibre con allineamento assiale (bundles) e/o fasci di nanofibre attorcigliate (yarns) e/o fasci ad anello di nanofibre (ring bundles), che viene prodotta senza inserire nulla nel corpo dello scaffold gerarchico multiscala per guidare la deposizione delle fibre.

Tale risultato è ottenuto modulando la forma, le dimensioni e la posizione del collettore posto nelle vicinanze, ma non a contatto con il gruppo di fasci di nanofibre con allineamento assiale (bundles) e/o fasci di nanofibre attorcigliate (yarns) e/o fasci ad anello di nanofibre (ring bundles) da rivestire e modulando i tempi di rotazione e di stasi degli stessi, ad esempio potrà essere posizionato ad una distanza compresa tra 1 e 50 mm.

Così facendo durante i tempi di stasi i fasci di nanofibre con allineamento assiale (bundles) e/o fasci di nanofibre attorcigliate (yarns) e/o fasci ad anello di nanofibre e (ring bundles) saranno circondati, da uno strato di nanofibre che avrà le proprie estremità depositate sul collettore. Mettendo in rotazione il gruppo di fasci, si verificherà il distaccamento di una estremità dello strato di nanofibre dal collettore piano, avvolgendo il gruppo di fasci di nanofibre, favorendone il compattamento ed il pretensionamento. Una volta arrotolato tutto lo strato di nanofibre attorno al gruppo di fasci di nanofibre, l'estremità ancora adesa al collettore piano si staccherà a sua volta. A distacco avvenuto, grazie all'azione combinata di rotazione e di campo elettrostatico anche la parte restante dello strato di nanofibre si depositerà sulla superficie dei fasci di nanofibre. La ripetizione di questo processo porta progressivamente alla compattazione con conseguente riduzione della sezione del gruppo di fasci di nanofibre ed alla completa formazione della camicia per ottenere lo scaffold gerarchico multiscala completo.

Similmente, ripetendo il processo di produzione della camicia di nanofibre su di una pluralità di scaffolds gerarchici multiscala, prodotti come precedentemente descritto, ed uniti assieme a formare un unico gruppo, sarà possibile ottenere uno scaffold gerarchico multiscala composto a sua volta da una pluralità di scaffolds

gerarchici multiscala, tutti rivestiti e compattati da una camicia elettrofilata di nanofibre.

Secondo una forma di realizzazione, gli afferraggi di fissaggio dei fasci di nanofibre con allineamento assiale (bundles) e/o attorcigliate (yarns) e/o fasci ad anello di nanofibre (ring bundles), capaci di ruotare rigidamente e in asse mantenendo così il gruppo di fasci di nanofibre, afferrato in posizione idonea per il processo di rivestimento con camicia elettrofilata, potranno essere di materiale metallico, preferibilmente in acciaio inossidabile e/o alluminio. Secondo una forma di realizzazione tali afferraggi potranno avere una forma che facilita il fissaggio dei fasci di nanofibre, ad esempio strutture a bracci cilindrici da 1 a 100, preferibilmente 6, di diverso e/o medesimo diametro, preferibilmente tra gli 0.5 e 30 mm di diametro. Tali afferraggi potranno essere collegati elettricamente al potenziale di terra per facilitare la copertura delle estremità dello scaffold gerarchico multiscala, durante il processo di filatura, dalla camicia di nanofibre secondo una qualsiasi delle forme di realizzazione del procedimento qui descritto.

Allo stato dell'arte infatti, sono state realizzate con un tale livello di omogeneità, 1) camicie elettrofilate su fasci di nanofibre attorcigliate (yarns) fissati attorno ad un rullo messo in rotazione, oppure 2) camicie prodotte a parte, al cui interno in un secondo momento vengono inseriti i fasci di nanofibre con allineamento assiale (bundles) e/o fasci di nanofibre attorcigliate (yarns) oppure 3) camicie prodotte su gruppi di fasci di nanofibre con allineamento assiale (bundles) e/o fasci di nanofibre attorcigliate (yarns) fissati tra loro da un riempitivo come ad esempio resine. Questi procedimenti non permettono alti livelli di compattamento dello scaffold finale, fondamentale per aumentare le proprietà meccaniche del costrutto, e pone seri vincoli progettuali sul numero di fasci di nanofibre con allineamento assiale (bundles) e/o fasci di nanofibre attorcigliate (yarns) e/o fasci ad anello di nanofibre (ring bundles) utilizzabili.

Sono anche oggetto della presente invenzione i fasci ad anello di nanofibre (ring bundles) ottenibili secondo una qualsiasi delle forme di realizzazione del procedimento qui descritto ed il loro metodo di produzione.

È anche oggetto della presente invenzione lo scaffold gerarchico multiscala ottenibile secondo una qualsiasi delle forme di realizzazione del procedimento qui descritto.

Lo scaffold gerarchico multiscala qui descritto potrà essere usato in diverse applicazioni ad esempio nel settore biomedicale in ambito ortopedico o veterinario come dispositivo protesico impiantabile, in particolare quando preparato in materiale biostabile, o per la proliferazione cellulare e la rigenerazione tissutale, in particolare quando preparato in materiale bioriassorbibile.

Quando preparato in materiale sintetico biostabile potrà inoltre essere applicato anche in robotica e nella produzione di attuatori e guide o nella produzione di tendini e/o legamenti e/o muscoli e/o nervi sintetici per la simulazione di pratiche chirurgiche in vitro.

È anche qui descritto un metodo per la rigenerazione o sostituzione di tessuti, in particolare del tessuto tendineo e/o legamentoso e/o muscolare e/o nervoso comprendente un passaggio d'impiantare in un soggetto che necessita di uno scaffold gerarchico multiscala secondo una qualsiasi delle forme di realizzazione qui descritte.

Lo scaffold gerarchico multiscala qui descritto potrà essere usato in un metodo ex vivo per la produzione di tendini e/o legamenti e/o muscoli e/o nervi in vitro, ad esempio un metodo in cui cellule sono coltivate in vitro con lo scaffold gerarchico multiscala.

Secondo una forma di realizzazione è oggetto della presente invenzione anche uno scaffold multiscala per la sostituzione, riparazione, ricostruzione o simulazione di un tessuto, in particolare del tessuto tendineo e/o legamentoso e/o muscolare e/o nervoso comprendente:

-una pluralità di fasci ottenuti per elettrofilatura costituiti da nanofibre con allineamento assiale (bundles) e/o fasci di nanofibre attorcigliate (yarns) e/o fasci ad anello di nanofibre (ring bundles) e in cui detta pluralità di fasci sono disposti in modo da formare un singolo gruppo;

-una camicia porosa ottenuta per elettrofilatura costituita da nanofibre disposte in modo casuale e/o allineate, in cui detta camicia riveste esternamente e compatta detta pluralità di fasci mantenendoli allineati tra loro.

Lo scaffold secondo una qualsiasi delle forme di realizzazione qui descritte potrà anche essere vantaggiosamente usato come sensore impiantabile in vivo o in vitro, ad esempio per l'acquisizione e/o trasmissione di segnali meccanici o fisiologici.

* * *

C.3 Esempi

C.3.1 Esempio 1

Sono stati sviluppati 8 prototipi di scaffold gerarchici multiscala in Acido poli-(L)-lattico (PLLA) di lunghezza 100 mm (diametro medio 5-6 mm) composti da 100 fasci di nanofibre con allineamento assiale (bundles) costituiti da nanofibre allineate nella direzione fascio di nanofibre con allineamento assiale (bundle) stesso (diametro medio fasci di nanofibre con allineamento assiale (bundles) 550-650 μm, diametro medio nanofibre 500-600 nm).
Su di essi la camicia è stata prodotta elettrofilando la medesima soluzione di PLLA utilizzata per produrre i fasci di nanofibre con allineamento assiale (bundles). La composizione è preparata con il 13%(w/v) di PLLA disciolto in un sistema solvente di Diclorometano (DCM) e Dimetilformammide (DMF) in percentuale 65/35 (v/v).
La camicia è stata prodotta elettrofilando per 3 ore ed intervallando periodi di stasi del gruppo di fasci di nanofibre con allineamento assiale (bundles) con periodi di rotazione.
Condizioni di filatura per la produzione di un singolo fascio di nanofibre con allineamento assiale (bundle):
- filatura con 2 aghi metallici Gauge 20;
- portata pompa a siringa 1,2 ml/h;
- voltaggio campo elettrico 18 kV;
- velocità rotazione collettore rotante 2900 rpm;
- distanza ago-collettore 200 mm;
- spessore utile fascio di nanofibre con allineamento assiale (bundle) prodotto 550-650 μm

Una volta tagliati i fasci di nanofibre con allineamento assiale (bundles) in campioni da 100 mm di lunghezza ciascuno sono stati allineati e fissati sulla macchina rotante per la produzione della camicia esterna di nanofibre random, applicando le seguenti condizioni:

- filatura con ago Gauge 20;
- portata pompa a siringa 1,2 ml/h;
- voltaggio campo elettrico 18 kV;
- collettore metallico;
- distanza collettore-ago/i 200 mm;
- distanza tra gruppo di fasci di nanofibre con allineamento assiale (bundles) e collettore piano minore di 5 mm;
- velocità rotazione del gruppo di fasci di nanofibre con allineamento assiale (bundles) circa 20-25 rpm;
- periodi di immobilità del gruppo di fasci di nanofibre con allineamento assiale (bundles) 2-5 min;
- periodi di rotazione del gruppo di fasci di nanofibre con allineamento assiale (bundles) 1-2 min;
- spessore utile della camicia: 5-10 μm

C.3.2 Esempio 2: test meccanici dei fasci di nanofibre con allineamento assiale (bundles) prodotti ottenuti nell'esempio 1

Sono stati poi testati meccanicamente fasci di nanofibre con allineamento assiale (bundles) singoli con un test a trazione.

Sinteticamente il test è stato eseguito utilizzando un test a trazione a rottura con velocità di deformazione del 100% sec-1 per simulare condizioni fisiologiche di velocità di deformazione compatibili a rottura del tessuto tendineo:

- campioni testati: 10
- tratto utile 16 mm
- velocità traversa 16 mm/sec (velocità di deformazione: 1/sec);
- rampa monotona a rottura;
- controllo di spostamento;

- idratazione dei campioni prima della prova per 2 min in soluzione salina allo 0,9% NaCl;

I singoli fasci di nanofibre con allineamento assiale (bundles) hanno resistito a rottura fino a 4-5 N con un comportamento duttile e deformazioni nell'ordine del 90%, con un modulo elastico di circa 80 MPa.

C.3.3 Esempio 3: test meccanici su scaffolds gerarchici multiscala prodotti ottenuti nell'esempio1

Gli scaffold gerarchici multiscala completi sono anche essi stati testati meccanicamente con una prova a trazione anche in questo caso con velocità di deformazione del 100% sec-1 per simulare condizioni fisiologiche di rottura del tessuto tendineo:

- tratto utile 50 mm per 5 campioni testati;
- le estremità dei campioni prima della prova erano state cementate in polimetilmetacrilato (PMMA) per un migliore afferraggio. Tali colate avevano forma rastremata per minimizzare la concentrazione di tensioni.
- velocità traversa 50 mm/sec (velocità di deformazione: 1/sec);
- rampa monotona a rottura;
- controllo di spostamento;
- idratazione dei campioni prima della prova per 2 min in soluzione salina allo 0,9% NaCl;

I cinque scaffold gerarchici multiscala hanno raggiunto valori di forza compresi tra i 230-380 N, con deformazioni circa del 30% ed un modulo elastico di circa 130 MPa.

La rottura dei campioni è avvenuta all'interfaccia tra scaffold gerarchico multiscala e cemento: ciò implica l'insorgere di una concentrazione di tensioni a causa degli afferraggi che ha comportato una notevole sottostima del valore di forza a rottura dello scaffold gerarchico multiscala.

C.3.4 Esempio 4

Sono stati sviluppati 3 prototipi di scaffold gerarchici multiscala in nylon 6,6 di lunghezza 230 mm (diametro medio 4-5 mm) composti da 25 fasci ad anello (ring bundles) costituiti da nanofibre allineate nella direzione dell'asse del fascio ad anello (ring bundle) (diametro medio fasci 550-650 μm, diametro medio nanofibre 200-300 nm).

I fasci ad anello (ring bundles) sono stati fissati alle estremità, al sistema di rotazione per la produzione della camicia, tramite due afferraggi in acciaio inossidabile composti da 6 bracci cilindrici simmetrici di diametro 8 mm.

Sugli scaffolds gerarchici multiscala la camicia è stata prodotta elettrofilando la medesima soluzione di nylon 6,6 utilizzata per produrre i fasci ad anello (ring bundles). La composizione è preparata con il 15%(w/v) di nylon 6,6 disciolto in un sistema solvente di Acido Trifluoroacetico (TFA) e Acetone (AC) in percentuale 50/50 (v/v). La camicia è stata prodotta elettrofilando per 12 ore ed intervallando periodi di stasi del gruppo di fasci ad anello (ring bundles) con periodi di rotazione.

Condizioni di filatura per la produzione dei singoli fasci ad anello (ring bundles):

- filatura con 2 aghi metallici Gauge 20;
- portata pompa a siringa 0.5 ml/h;
- voltaggio campo elettrico 20 kV;
- velocità rotazione collettore rotante 2900 rpm;
- distanza ago-collettore 160 mm;
- spessore utile fasci ad anello (ring bundles) prodotti 550-650 μm
- lunghezza dei fasci ad anello (ring bundles): circa 470 mm (derivanti dalla deposizione su un rullo di 150 mm di diametro)

Una volta ottenuti i fasci ad anello (ring bundles), 25 di essi sono stati allineati e fissati alle estremità ai bracci degli afferraggi metallici, sopra descritti, sulla macchina rotante per la produzione della camicia esterna di fibre random,

applicando le seguenti condizioni:

- filatura con 2 aghi Gauge 20;
- portata pompa a siringa 0.5 ml/h;
- voltaggio campo elettrico 18 kV;
- collettore metallico piano di terra;

- distanza collettore-ago/i 160 mm;
- distanza tra gruppo di fasci ad anello di nanofibre (ring bundles) e collettore piano minore di 5 mm;
- velocità rotazione del gruppo di fasci ad anello di nanofibre (ring bundles) circa 20-25 rpm;
- periodi di immobilità del gruppo di fasci ad anello di nanofibre (ring bundles) 2-5 min;
- periodi di rotazione del gruppo di fasci ad anello di nanofibre (ring bundles) 1-2 min;
- spessore utile della camicia: 5-10 μm
- dopo 10 ore di filatura della camicia su collettore piano elettricamente connesso alla terra come precedentemente descritto, sono stati posti a potenziale di terra anche i due afferraggi metallici posti alle estremità del gruppo di fasci ad anello di nanofibre (ring bundles), in modo tale da rivestire con la camicia di nanofibre disposte in modo casuale (random) anche le estremità stesse. I parametri di filatura sono i medesimi riportati sopra.

C.3.5 Esempio 5: test meccanici dei fasci ad anello (ring bundles) prodotti ottenuti nell'esempio 4

Sono stati poi testati meccanicamente i fasci ad anello di nanofibre (ring bundles) singoli con un test a trazione.
Sinteticamente il test è stato eseguito utilizzando un test a trazione a rottura con velocità di deformazione del 100% sec-1 per simulare condizioni fisiologiche di velocità di deformazione compatibili a rottura del tessuto tendineo e/o legamentoso e/o muscolare e/o nervoso:
- campioni testati: 5
- tratto utile 230 mm
velocità traversa 230 mm/sec (velocità di deformazione: 1/sec);
- rampa monotona a rottura;
- controllo di spostamento;
- idratazione dei campioni prima della prova per 2 min in soluzione salina allo 0,9% NaCl;

I singoli fasci ad anello di nanofibre (ring bundles) hanno resistito a rottura fino a 20-24 N con un comportamento duttile e deformazioni nell'ordine del 9- 12%, con un modulo elastico di circa 600-900 MPa.

C.3.6 Esempio 6: test meccanici su scaffolds gerarchici multiscala prodotti ottenuti nell'esempio 4

Gli scaffold gerarchici multiscala completi sono anche essi stati testati meccanicamente con una prova a trazione anche in questo caso con velocità di deformazione del 100% sec-1 per simulare condizioni fisiologiche di rottura del tessuto tendineo e/o legamentoso e/o muscolare e/o nervoso:

- tratto utile 230 mm per 3 campioni testati;
- Come afferraggi dei campioni per la prova meccanica, sono stati utilizzati gli stessi afferraggi metallici coi quali i campioni erano fissati alla macchina per la produzione della camicia. Tali afferraggi erano stati progettati in modo idoneo a deconcentrare le tensioni.
- velocità traversa 230 mm/sec (velocità di deformazione: 1/sec);
- rampa monotona a rottura;
- controllo di spostamento;
- idratazione dei campioni prima della prova per 2 min in soluzione salina allo 0,9% NaCl;

I 3 scaffold gerarchici multiscala hanno raggiunto valori di forza compresi tra i 300-350 N, con deformazioni circa del 9% ed un modulo elastico di circa 300-400 MPa. La rottura dei campioni è avvenuta sia all'interfaccia tra scaffold gerarchico multiscala e afferraggi sia nel tratto utile: ciò implica l'insorgere di una parziale concentrazione di tensioni a causa degli afferraggi che ha comportato una sottostima del valore di forza a rottura dello scaffold gerarchico multiscala.

* * *

La presente invenzione è stata fin qui descritta con riferimento ad alcune forme preferite di realizzazione. È da intendersi che possano esistere altre forme di realizzazione che afferiscono al medesimo nucleo inventivo, come definito dall'ambito di protezione delle rivendicazioni qui di seguito riportate.

C.4 Rivendicazioni

1. Scaffold gerarchico multiscala per la sostituzione, riparazione, rigenerazione, ricostruzione e/o simulazione di un tessuto, in particolare del tessuto tendineo e/o legamentoso e/o muscolare e/o nervoso comprendente:
-una pluralità di fasci ottenuti per elettrofilatura costituiti ciascuno da nanofibre, in cui detta pluralità di fasci sono disposti in modo da formare un singolo gruppo;
-una camicia porosa ottenuta per elettrofilatura costituita da nanofibre, in cui detta camicia riveste esternamente e compatta detta pluralità di fasci mantenendoli allineati tra loro.
2. Scaffold secondo la rivendicazione 1 comprendente:
- una pluralità di fasci di nanofibre con allineamento assiale (bundles) e/o di fasci di nanofibre attorcigliate (yarns), ottenuti per elettrofilatura, costituiti rispettivamente da nanofibre con allineamento assiale e/o attorcigliate assialmente disposti in modo da formare un singolo gruppo;
-una camicia porosa ottenuta per elettrofilatura costituita da nanofibre, in cui detta camicia riveste esternamente e compatta detta pluralità di fasci mantenendoli allineati tra loro.
3. Scaffold secondo la rivendicazione 1 o 2 comprendente:
-una pluralità di fasci ad anello di nanofibre (ring bundles), ottenuti per elettrofilatura, costituiti rispettivamente da nanofibre allineate assialmente e/o attorcigliate assialmente e/o disposte in modo casuale (random) disposti in modo da formare un singolo gruppo;
-una camicia porosa ottenuta per elettrofilatura costituita da nanofibre, in cui detta camicia riveste esternamente e compatta detta pluralità di fasci mantenendoli allineati tra loro.
4. Scaffold secondo una qualsiasi delle rivendicazioni da 1 a 3 avente una resistenza meccanica compresa tra 2 e 10000 N, in particolare tra 10 e 5000 N e un modulo elastico compreso tra 20 e 100000 MPa, in particolare tra 30 e 20000 MPa.
5. Scaffold secondo una qualsiasi delle rivendicazioni da 1 a 4 avente una resistenza meccanica compresa tra 200 e 500 N e/o un modulo elastico compreso tra 30 e 20000 MPa.

6. Scaffold secondo una qualsiasi delle rivendicazioni da 1 a 5 avente una resistenza meccanica compresa tra 2 e 10000 N e un modulo elastico compreso tra 20 e 100000 MPa.

7. Scaffold secondo una qualsiasi delle rivendicazioni precedenti in cui detto scaffold ha una lunghezza compresa tra 10 e 1000 mm, in particolare tra 10 e 500 mm, ed un diametro medio compreso tra 1 e 100 mm.

8. Scaffold secondo una qualsiasi delle rivendicazioni precedenti in cui detto scaffold ha una lunghezza compresa tra 20 e 200 mm ed un diametro medio compreso tra 5 e 50 mm.

9. Scaffold secondo una qualsiasi delle rivendicazioni precedenti in cui dette nanofibre che costituiscono detti fasci e/o detta camicia hanno un diametro medio compreso tra 10 e 10000 nm.

10. Scaffold secondo una qualsiasi delle rivendicazioni precedenti in cui dette nanofibre che costituiscono detti fasci e/o detta camicia hanno un diametro medio compreso tra 200 e 1000 nm, in particolare tra 300 e 1000 nm.

11. Scaffold secondo una qualsiasi delle rivendicazioni precedenti in cui il diametro medio di detti fasci è compreso tra 1 e 10000 μm, in particolare tra 20 e 10000 μm.

12. Scaffold secondo una qualsiasi delle rivendicazioni precedenti in cui il diametro medio di detti fasci è compreso tra 500 e 650 μm.

13. Scaffold comprendente una pluralità di scaffold interni secondo una qualsiasi delle rivendicazioni da 1 a 12, uniti a loro volta da una seconda camicia porosa ottenuta per elettrofilatura costituita da nanofibre, in cui detta camicia riveste esternamente e compatta detta pluralità di scaffold.

14. Scaffold secondo la rivendicazione da 1 a 13 in cui detta camicia e/o camicie porosa/e è/sono costituita/e da nanofibre disposte in modo casuale.

15. Scaffold secondo la rivendicazione da 1 a 13 in cui detta camicia e/o camicie porosa/e è/sono costituita/e da nanofibre disposte con allineamento assiale rispetto l'asse dello scaffold.

16. Scaffold secondo la rivendicazione da 1 a 13 in cui detta camicia e/o camicie porosa/e è/sono costituita/e da nanofibre disposte con allineamento circonferenziale rispetto l'asse dello scaffold.

17. Scaffold secondo la rivendicazione da 1 a 13 in cui detta camicia e/o camicie porosa/e è/sono costituita/e da nanofibre disposte secondo una combinazione delle rivendicazioni da 14 a 16.

18. Scaffold secondo una qualsiasi delle rivendicazioni da 13 a 17 in cui detti scaffold interni sono allineati assialmente gli uni agli altri.

19. Scaffold secondo una qualsiasi delle rivendicazioni da 13 a 17 in cui detti scaffold interni sono attorcigliati (twisting) gli uni agli altri e/o disposti in modo casuale.

20. Scaffold secondo una qualsiasi delle rivendicazioni precedenti in cui il numero di detti fasci in detto scaffold è compreso tra 40 e 1000.

21. Scaffold secondo una qualsiasi delle rivendicazioni precedenti in cui detto scaffold è realizzato in materiale bioriassorbibile o biostabile e/o inerte.

22. Scaffold secondo una qualsiasi delle rivendicazioni precedenti in cui detto scaffold è realizzato in un materiale di origine sintetica scelto tra poliesteri, poliuretani, poliammidi, poliolefine e polimeri fluorurati e loro copolimeri o di origine naturale scelto tra polisaccaridi, proteine, poliesteri, polipeptidi e loro copolimeri e/o loro miscele.

23. Scaffold secondo una qualsiasi delle rivendicazioni precedenti in cui per la preparazione delle nanofibre è usato acido poli-(L)-lattico (PLLA), poliammidi e/o nylon 6,6.

24. Scaffold secondo una qualsiasi delle rivendicazioni precedenti in cui detto scaffold e/o dette nanofibre sono caricate e/o funzionalizzate con componenti di natura organica e/o inorganica atte a svolgere un'azione biologica e/o di cambiamento delle proprietà chimico-fisiche e/o meccaniche di detto tessuto.

25. Scaffold secondo la rivendicazione 24 in cui detti componenti di natura organica e/o inorganica sono scelti tra farmaci, fattori di crescita, sostanze antibatteriche, peptidi, idrossiapatiti, fosfati, biovetri, ossidi metallici, grafene, nanotubi di carbonio o loro miscele.

26. Scaffold secondo una qualsiasi delle rivendicazioni precedenti in cui all'interno di detto scaffold sono iniettati gel o idrogel.

27. Scaffold secondo una qualsiasi delle rivendicazioni precedenti in cui dette nanofibre sono monofasiche.

28. Scaffold secondo una qualsiasi delle rivendicazioni da 1 a 26 in cui dette nanofibre sono multifasiche.

29. Scaffold secondo una qualsiasi delle rivendicazioni precedenti in cui dette nanofibre sono di tipo core-shell e/o hollow-shell e/o porose e/o loro combinazioni.

30. Scaffold secondo una qualsiasi delle rivendicazioni precedenti in cui le nanofibre sono di tipo piezoelettrico.

31. Scaffold secondo una qualsiasi delle rivendicazioni precedenti in cui detti fasci presentano al loro interno una cavità assiale.

32. Dispositivo protesico impiantabile comprendente uno scaffold secondo una qualsiasi delle rivendicazioni da 1 a 31.

33. Tendine e/o legamento sintetico comprendente uno scaffold secondo una qualsiasi delle rivendicazioni da 1 a 31.

34. Muscolo sintetico comprendente uno scaffold secondo una qualsiasi delle rivendicazioni da 1 a 31.

35. Nervo sintetico comprendente uno scaffold secondo una qualsiasi delle rivendicazioni da 1 a 31.

36. Procedimento per la preparazione di uno scaffold gerarchico multiscala secondo una qualsiasi delle rivendicazioni da 1 a 31 comprendente i seguenti passaggi:

a) preparare mediante elettrofilatura una pluralità di fasci di nanofibre con allineamento assiale (bundles) e/o fasci di nanofibre attorcigliate (yarns) e/o fasci ad anello di nanofibre (ring bundles);

b) elettrofilare nanofibre in modo da rivestire detti fasci con una camicia porosa costituta da nanofibre in modo tale da fornire un rivestimento esterno e compattare la pluralità di fasci preparati con il passaggio a).

37. Procedimento per la preparazione di un scaffold gerarchico multiscala secondo una qualsiasi delle rivendicazioni da 1 a 31 comprendente i seguenti passaggi:

a) preparare mediante elettrofilatura una pluralità di fasci di nanofibre con allineamento assiale (bundles) e/o fasci di nanofibre attorcigliate (yarns) e/o bundles ad anello di nanofibre (ring bundles);

b) posizionare detta pluralità di fasci preparati al punto a) in modo da formare un singolo gruppo;

c) afferrare il gruppo di fasci ottenuto al passaggio b) su afferraggio capace di ruotare rigidamente e in asse mantenendo così il gruppo di fasci afferrato in posizione idonea per il processo di rivestimento con camicia elettrofilata;
d) realizzare una camicia esterna al gruppo di fasci afferrato al punto c) mediante elettrofilatura, in particolare controllando i parametri di rotazione del gruppo di fasci afferrato, i parametri geometrici del setup, e parametri di processo.
38. Procedimento secondo la rivendicazione 36 o 37 in cui le nanofibre dei fasci e/o della camicia sono preparate elettrofilando una soluzione di PLLA sciolto in diclorometano (DCM) e/o N,N-dimetilformammide (DMF) o nylon 6,6 sciolto in acido trifluoroacetico (TFA) e/o acetone (AC).
39. Procedimento secondo una qualsiasi delle rivendicazioni da 36 a 38 in cui durante il passaggio di elettrofilatura delle nanofibre è applicato un campo elettrico con un voltaggio compreso tra 10 kV e 30 kV, preferibilmente 18 kV, per un tempo di almeno 5 min, ed in particolare di almeno 15 min.
40. Procedimento secondo una qualsiasi delle rivendicazioni da 36 a 39 in cui durante il passaggio di elettrofilatura delle nanofibre a), dette nanofibre sono depositate su un collettore in modo da consentirne l'allineamento.
41. Procedimento secondo una qualsiasi delle rivendicazioni da 36 a 40 in cui durante il passaggio della realizzazione della camicia le nanofibre sono depositate su un collettore posto in prossimità del gruppo di fasci da rivestire ma senza alcun contatto con detto gruppo di fasci, in particolare è posto a circa 2-5 mm dal gruppo di fasci da rivestire.
42. Procedimento secondo una qualsiasi delle rivendicazioni da 36 a 41 in cui in detto passaggio per la preparazione della camicia sono applicati i seguenti paramenti di processo:
- distanza tra gruppo di fasci e il collettore minore di 5 mm;
- velocità rotazione del gruppo di fasci compresa tra circa 20-25 rpm;
- periodi di immobilità del gruppo di fasci compreso tra circa 3-5 min;
- periodi di rotazione del gruppo di fasci compreso tra 1-2 min.
43. Procedimento secondo una qualsiasi delle rivendicazioni da 36 a 42 in cui gli afferraggi sono composti di materiale metallico conduttivo, ad esempio acciaio inossidabile e/o alluminio e posti a potenziale di terra per migliorare la deposizione

della camicia di nanofibre disposte casualmente sulle estremità dello scaffold stesso.

44. Procedimento secondo una qualsiasi delle rivendicazioni da 36 a 43 in cui durante il passaggio della realizzazione della camicia il collettore di terra ha una geometria piana.

45. Procedimento secondo una qualsiasi delle rivendicazioni da 36 a 43 in cui durante il passaggio della realizzazione della camicia il collettore di terra è una piastra concava, convessa o prismatica.

46. Procedimento secondo una qualsiasi delle rivendicazioni da 36 a 43 in cui durante il passaggio della realizzazione della camicia il collettore di terra è costituito da due aste e/o piastre metalliche parallele.

47. Procedimento secondo una qualsiasi delle rivendicazioni da 36 a 46 comprendente i seguenti passaggi:

a) filatura su collettore a rullo rotante di una pluralità di nanofibre elettrofilate;

b) arrotolamento circonferenziale sul rullo di sezioni della membrana di nanofibre elettrofilate per ottenere fasci ad anello (ring bundles);

c) rimozione dei fasci ad anello di nanofibre (ring bundles) dal rullo.

48. Procedimento per la preparazione di uno scaffold gerarchico multiscala comprendente una pluralità di scaffold interni comprendente:

a) preparare una pluralità di scaffold secondo una qualsiasi delle rivendicazioni precedenti;

b) elettrofilare nanofibre in modo da rivestire detta pluralità di scaffold con una camicia porosa costituta da nanofibre in modo tale da fornire un rivestimento esterno e compattare la pluralità di scaffold preparati con il passaggio a).

49. Scaffold ottenibile secondo il procedimento di una qualsiasi delle rivendicazioni da 36 a 48.

50. Scaffold secondo una qualsiasi delle rivendicazioni da 1 a 31 per uso come sensore per l'acquisizione e/o trasmissione di segnali meccanici o fisiologici.

51. Uso di uno scaffold secondo una qualsiasi delle rivendicazioni da 1 a 31 come sensore *in vitro* per l'acquisizione e/o trasmissione di segnali meccanici o fisiologici.

C.5 Figure

The figures of this section are the same of Appendix B. Here are listed just the figures 9 and 10 translated.

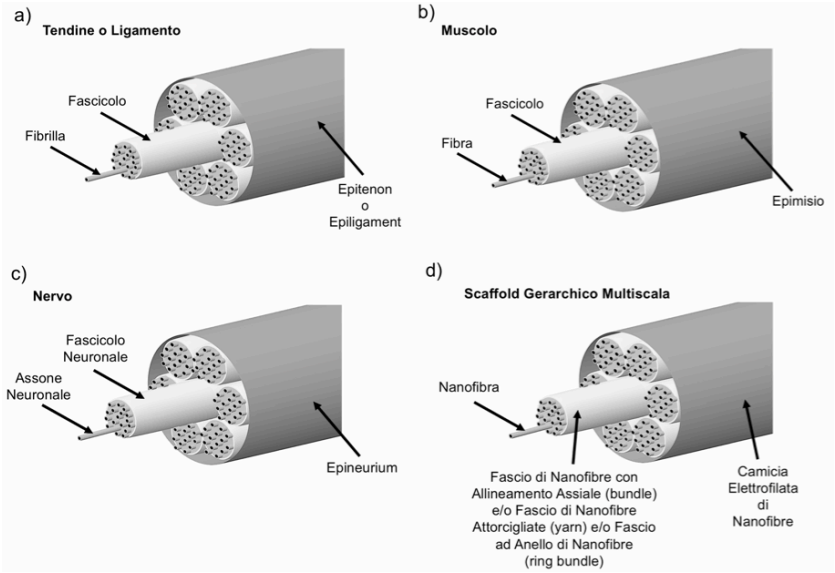

Figura 9

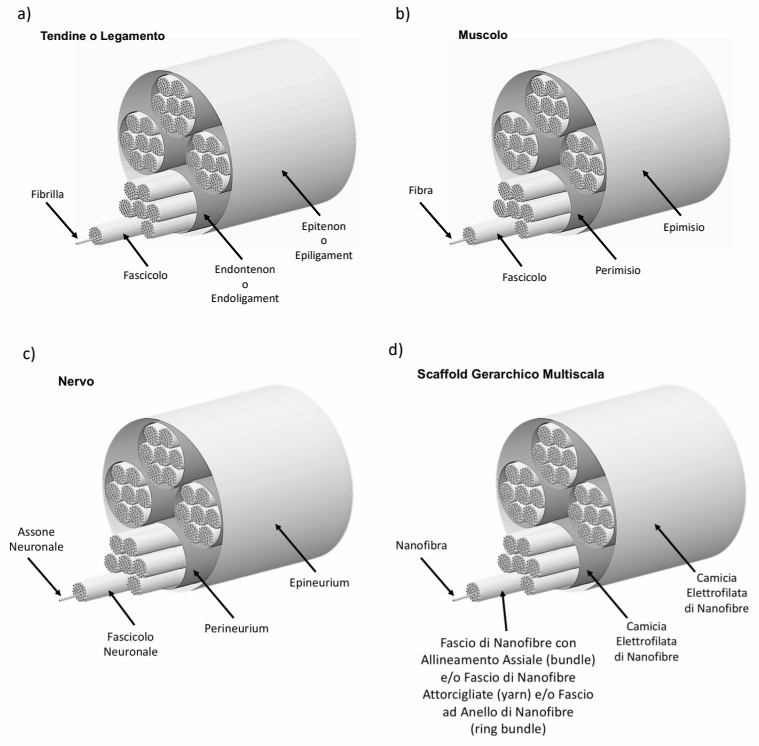

Figura 10

Acknowledgments

Before ending this long work, I would like to spend few lines to acknowledge all the people who supported me during these years and contributed to the realization of this thesis. I want of course to start from my Ph.D. supervisor Professor Luca Cristofolini: thank you very much Luca.

Thank you, Luca, for all the incredible possibilities that you offered me, thank you to have showed and explained me every day how to try to turning ideas and curiosity into research, and the research into results. Thank you to have trusted in me also when unfortunately, some situations changed in the past… and thanks also for your patience when I text you a lot of e-mails or I arrive in your office asking you hundreds of questions. But, most of all, thank you to have permitted me to meet my other two Ph.D. co-supervisors: Professor Maria Letizia Focarete and Professor Andrea Zucchelli.

Professor Focarete, thank you to have trusted in me several times and especially when, about four years ago, before starting my Master thesis, without knowing anything about the electrospinning technique, I asked you and Luca: "Why don't we electrospin a tendon?". Thank you for all the research opportunities that you have offered me and you are continuing offering me every day.

Professor Andrea Zucchelli, thank you to have teach me the enthusiasm in doing research and thinking every day new ideas. Thanks to have showed me that electrospinning is not just chemistry but also engineering and design, and to offer me everyday new projects and opportunities.

I want say thank you to Doctor Chiara Gualandi to have teach me everything about electrospinning, and to be always available when I need her help to solve a problem.

Thanks also to Juri Belcari to have introduced me the engineering side of the electrospinning, and to have helped me when I arrived three years ago in the electrospinning laboratory at the Department of Industrial Engineering.

Many thanks to Professor Gianluca Tozzi to have permitted me to discover the amazing world of the x-ray tomography and always support me in trying to develop my ideas. Thank you to make me feel at home on every research period at the University of Portsmouth, definetly my second home in United Kindom. Thanks to

have permitted me to start working with Professor Marta Roldo and Professor Gordon Blunn, incredibles researchers and Professors. I want aknowledge my friend and collegue Doctor Alexander Kao for the grat teamwork that we did, and I hope we will do, in the x-ray tomography laboratory. Thanks also to all my colleagues and friends at the University of Portsmouth Marta, Katerina, Timmy, Haider, Hamed, Saul, Roxane, Arianna, Robin and Doctor Martino Pani to have helped me and have taught me a lot of things during my stay.

Among my friends in Portsmouth, I want to acknowledge in particular, my colleague and friend Doctor Marco Curto for the hospitality first, but most of all for the amazing teamwork, the friendship, and the brainstormings and the reseach activities that we had together during my stays.

Thanks to Professor Gwendolen Reilly and Liam Boyle of the University of Sheffield for the great collaborations and the fundamental suggestions that you have offered me during these years of work.

Thank you also to all my colleagues of the University of Bologna: Marco Palanca, Kavin Morellato, Federico Morosato, Maria Luisa Ruspi, Valentina Danesi, Andrea Merlettini, Roberto di Gesù, Tommaso Brugo, Emanuele Maccaferri, Davide Cocchi, Luca Raimondi, Johnnidel Tabucol and Gregorio Pisaneschi to stand me and help me every day. It is a pleasure and an honor work with you.

Thank you very much to all the students that I have co-supervised during their theses: Michele, Chiara, Elisa, Tugce, Alessandra, Martina and Carlo Gotti. Everyone of you have given a fundamental contribution to reach these results and so a part of this thesis is for sure yours.

Thank to all my family, my parents, my grandmother Doria, my grandfather Dalmazio and Annalaura to always support me, stand me, and trust in me and in my choices every day. For sure without you all this work would not have been possible.

Finally, I want to dedicate this thesis to two people: my grandfather Bruno and my uncle Massimo. They are definitely my most important sources of inspiration during my life, and even in the choice of the topic of this work, a special merit is yours.

Ringraziamenti

Prima di concludere questo lungo lavoro, vorrei spendere poche righe per ringraziare tutte le persone che mi hanno sostenuto durante questi anni e hanno contribuito alla realizzazione di questa tesi. Ovviamente voglio iniziare dal mio supervisore di dottorato il Professor Luca Cristofolini: grazie mille Luca.

Grazie, Luca, per tutte le incredibili possibilità che mi hai offerto, grazie per avermi mostrato e spiegato ogni giorno come provare a trasformare idee e curiosità in ricerca e la ricerca in risultati. Grazie per esserti fidato di me anche quando, sfortunatamente, alcune situazioni sono cambiate in passato... e grazie anche per la tua pazienza quando ti mando un sacco di e-mail o arrivo nel tuo ufficio chiedendoti centinaia di domande. Ma, soprattutto, grazie per avermi permesso di incontrare i miei altri co-supervisori di dottorato: la Professoressa Maria Letizia Focarete e il Professor Andrea Zucchelli.

Professoressa Focarete, grazie di aver avuto fiducia in me più volte e soprattutto quando, circa quattro anni fa, prima di iniziare la mia tesi di laurea Magistrale, senza sapere nulla della tecnica di elettrofilatura, ho chiesto a lei e Luca: "Perché non proviamo un elettrofilare un tendine?". Grazie per tutte le opportunità di ricerca che mi ha offerto e continua a offrirmi ogni giorno.

Professor Andrea Zucchelli, grazie per avermi insegnato l'entusiasmo nel fare ricerca e a pensare ogni giorno nuove idee. Grazie ad avermi mostrato che l'elettrofilatura non è solo chimica, ma anche ingegneria e design, e per offrirmi ogni giorno nuovi progetti e opportunità.

Voglio ringraziare la Dottoressa Chiara Gualandi per avermi insegnato tutto sull'elettrospinning e per essere sempre disponibile quando ho bisogno del suo aiuto per risolvere un problema. Grazie anche a Juri Belcari per avermi presentato il lato ingegneristico dell'elettrospinning e per avermi aiutato quando sono arrivato tre anni fa nel laboratorio di elettrofilatura del Dipartimento di Ingegneria Industriale.

Mille grazie al Professor Gianluca Tozzi per avermi permesso di scoprire il fantastico mondo della tomografia a raggi X e supportarmi sempre nel tentativo di sviluppare le mie idee. Grazie per farmi sentire a casa in ogni periodo di ricerca presso l'Università di Portsmouth, sicuramente la mia seconda casa a nel Regno

Unito. Grazie per avermi permesso di iniziare a lavorare con la Professoressa Marta Roldo e il Professor Gordon Blunn, ricercatori e professori incredibili. Voglio ringraziare il mio amico e collega Dottor Alexander Kao per il grande lavoro di squadra che abbiamo fatto, e spero ancora faremo, nel laboratorio di tomografia a raggi X. Grazie anche a tutti i miei colleghi e amici dell'Università di Portsmouth Marta, Katerina, Timmy, Haider, Hamed, Saul, Roxane, Arianna, Robin e il Dottor Martino Pani per avermi aiutato e insegnato molte cose durante il mio soggiorno.

Tra i miei amici a Portsmouth, voglio riconoscere in particolare, prima dell'ospitalità, la mia collega e amico Dottor Marco Curto, ma soprattutto per lo straordinario lavoro di squadra, l'amicizia, i brainstorming e le attività di ricerca che abbiamo avuto durante i miei soggiorni.

Grazie alla Professoressa Gwendolen Reilly e Liam Boyle dell'Università di Sheffield per le grandi collaborazioni e i suggerimenti fondamentali che mi avete offerto durante questi anni di lavoro.

Grazie anche a tutti i miei colleghi dell'Università di Bologna: Marco Palanca, Kavin Morellato, Federico Morosato, Maria Luisa Ruspi, Valentina Danesi, Andrea Merlettini, Roberto di Gesù, Tommaso Brugo, Emanuele Maccaferri, Davide Cocchi, Luca Raimondi, Johnnidel Tabucol e Gregorio Pisaneschi per sopportarmi e aiutarmi ogni giorno. È un piacere e un onore lavorare con voi.

Grazie mille a tutti gli studenti che ho co-supervisionato durante le loro tesi: Michele, Chiara, Elisa, Tugce, Alessandra, Martina e Carlo Gotti. Ognuno di voi ha dato un contributo fondamentale per raggiungere questi risultati e quindi una parte di questa tesi è sicuramente la vostra.

Ringrazio tutta la mia famiglia, i miei genitori, mia nonna Doria, mio nonno Dalmazio e Annalaura per supportarmi sempre, sopportarmi e fidarsi di me e delle mie scelte ogni giorno. Di sicuro senza di voi tutto questo lavoro non sarebbe stato possibile.

Infine, voglio dedicare questa tesi a due persone: mio nonno Bruno e mio zio Massimo. Sono sicuramente le mie più importanti fonti di ispirazione durante la mia vita, e anche nella scelta dell'argomento di questo lavoro, un merito speciale è vostro.